

2014

# Proceedings of the 2014 Coal Operators' Conference

Naj Aziz

*University of Wollongong, naj@uow.edu.au*

---

## Publication Details

Naj Aziz, Bob Kininmonth, Jan Nemcik, Dennis Black, John Hoelle and Ismet Cunbulat (editors), Proceedings of the 2014 Coal Operators' Conference, University of Wollongong - Mining Engineering, Australasian Institute of Mining and Metallurgy and the Mine Managers Association of Australia, 12-14 February 2014, University of Wollongong, 433p.

# PROCEEDINGS OF THE 2014 COAL OPERATORS' CONFERENCE



**UNIVERSITY OF WOLLONGONG, NSW**

12 - 14 FEBRUARY 2014

## **ORGANISERS**

UNIVERSITY OF WOLLONGONG - MINING ENGINEERING  
AUSTRALASIAN INSTITUTE OF MINING AND METALLURGY- ILLAWARRA BRANCH  
MINE MANAGERS ASSOCIATION OF AUSTRALIA

Typeset by

**Zhongwei Wang**

School of Civil, Mining and Environmental Engineering, University of Wollongong

**PRINTED IN AUSTRALIA BY**  
The University Of Wollongong Printery

**ISBN: 978 1 925100 02 0**

**All papers in these proceedings are peer reviewed**

**Published on line:** <http://ro.uow.edu.au/coal>

**Or via:** <http://research.uow.edu.au/coal>

No paper in these proceedings is to be re-published unless with written permission from the conference organisers and/or the original authors who maintain the copyright for their work.

## EDITORIAL BOARD

NAJ AZIZ  
BOB KININMONTH  
JAN NEMCIK  
DENNIS BLACK  
JOHN HOELLE  
ISMET CUNBULAT

## ORGANISING COMMITTEE

<i>Naj Aziz, University of Wollongong</i>	<i>John Hoelle, AngloAmerican Coal, Australia</i>
<i>Bob Kininmonth, Illawarra Outburst Committee</i>	<i>Kevin Marston- Aus IMM –Illawarra Branch</i>
<i>Jan Nemcik, University of Wollongong</i>	<i>Lei Zhang, University of Wollongong</i>
<i>Abouna Saghafi, CSIRO, North Ryde</i>	<i>Mark Colwell, Colwell Geotechnical Services</i>
<i>Basil Beamish, B3 Mining Services, Australia</i>	<i>Paul Hagan, UNSW, Australia</i>
<i>Dennis Black, PacificMGM, NSW</i>	<i>Peter Craig, Jennmar Australia</i>
<i>Brad Elvy, BHPBilliton- Illawarra Coal</i>	<i>Peter Hatherly, University of Sydney</i>
<i>Dan Payne, BMA, Queensland</i>	<i>Peter Vrahas, Eventico Pty Ltd</i>
<i>Darren Brady, Simtars Queensland</i>	<i>Ray Tolhurst, AusIMM Illawarra Branch</i>
<i>David Cliff, University of Queensland</i>	<i>Steve Mackaway, DSI Australia</i>
<i>Frank Hungerford, University of Wollongong</i>	<i>Terry Medhurst, PDR Engineers</i>
<i>Hani Mitri, McGill University, Canada</i>	<i>Ting Ren, University of Wollongong</i>
<i>Ismet Canbulat, AngloAmerican Coal, Australia</i>	<i>Zhongwei Wang, University of Wollongong</i>
<i>James Walker, WellDog, Australia</i>	

## REVIEWERS

The organising committee would like to thank the following referees for technically reviewing the papers included in these proceedings

<i>Naj Aziz, University of Wollongong</i>	<i>Kevin Marston- Aus IMM Illawarra Branch</i>
<i>Bob Kininmonth, Illawarra Outburst Committee</i>	<i>Ray Tolhurst, AusIMM Illawarra Branch</i>
<i>Basil Beamish, B3 Mining Services, Australia</i>	<i>John Hoelle, AngloAmerican Coal, Australia</i>
<i>Jan Nemcik, University of Wollongong</i>	<i>Steve Tadolini, Orica International</i>
<i>David Cliff, University of Queensland</i>	<i>Peter Craig, Jennmar Australia</i>
<i>Ismet Canbulat, Anglo American Coal, Australia</i>	<i>Chris Lukey, Orica Australia</i>

## SPONSORS

The mining engineering group of the University of Wollongong, the Illawarra Branch of The AusIMM and the Mine Managers Association of Australia gratefully acknowledge the financial assistance of the following organisations which have sponsored the COAL2014 Conference

### Diamond Sponsors



### Gold Sponsors

**GLENCORE**



**Faculty of Engineering  
and Information Sciences**

### Silver Sponsors



---

# FOREWORD

On behalf of the organising committee I welcome you to the 14<sup>th</sup> Coal Operators Conference (Coal2014). The duration of the conference has been extended for three days because of the increasing number of good quality and innovative papers presented. 42 papers out of a total of 49 will be presented on topics covering both surface and underground mining, and includes papers on geology, geophysical logging, geotechnical engineering, rock fracture mechanics, general ground control, heading development, longwall mining, pillar design, information technology, rock cutting and rock bolting, mine ventilation, mine gases and fugitive gas emissions, outburst control, mine safety and risk management. A number of Australian mine operators, consultants, research organisations and academics are show-casing their cutting edge research findings in the conference.

This year there is a special interest on rock bolting and in particular cable bolting, with industry wide interest on the performance of cable bolts particularly under shear. Also of interest is the methodology of determining chemical resin and cementitious grout strength properties evaluation with the objective of establishing a set of guidelines for the Australian coal mining industry. There will be a number of ACARP funded project presentations, and a number of papers will focus on various aspects of surface mining.

Some of the high quality international papers include those from Czech Republic, Iran, Japan, Turkey, UK, Germany, and South Africa. The Conference is sponsored by various leading mining companies, mine services, product suppliers, various research organisations and universities.

All papers published in the Coal Operators' Conference series are also available online via the University of Wollongong online research website <http://ro.uow.edu.au/coal>, currently holding 431 records, which have been accessed by a total of 63 000 since January 2013, a monthly access of about 8 000 hits. This access is not confined to Australia alone, other countries making frequent access include USA, China, UK, Germany Iran and others. More than 130 countries have accessed the conference publications since the papers went online in 2008. I would therefore, like to take this opportunity of extending a special thanks to Michael Organ, Manager - Repository Services of the UOW Library for his help in organising and uploading all past conference papers on the University websites as well as providing all the statistics necessary for the benefit of the conference.

For a number of years, the International Longwall News (ILN) website has been providing publicity coverage for the conference. This support is deeply appreciated and thanks to Lou Caruana for maintaining support for the conference. I look forward to the continuation of this support.

Special thanks to the editorial panel members, the paper reviewers; Zhongwei Wang for typesetting the conference proceedings; Peter Vrahas of Eventico for his conference general management and efficient administration of the conference website; The University of Wollongong printery staff Gerard Toomey for designing the conference proceedings cover page, Garry Piggott for printing the conference proceedings.

All papers are independently peer reviewed and edited to maintain the highest quality.



Professor Naj Aziz  
Conference chairman and convenor

# TABLE OF CONTENTS

Organising Committee .....	ii
Reviewers .....	ii
Sponsors.....	iii
Foreword.....	iv
<b>Technical Papers</b>	
Drilling Induced Fractures in Coal Core from Vertical Exploration Wells: a Method to Determine Cleat Azimuth, and the Angle Between Cleat and Maximum Horizontal Stress, and its Application <b>D. Titheridge</b> .....	8
Mapping Techniques for Determining Sandstone Roof Channel Paleodrainage Direction in Coal Mines <b>L. Daigle</b> .....	18
Geotechnical Data from Geophysical Logs: Stress, Strength and Joint Patterns in NSW and QLD Coalfields <b>S. Pell, R. Seedsman and K. Straub</b> .....	25
Roof Support Control in Longwall Technology <b>P. Novák and J. Babjak</b> .....	34
Development of a Method for Longwall Top Coal Caveability Assessment <b>T. Medhurst, R. Rankine and M. Kelly</b> .....	42
Investigation into the Relationship Between Strata Characteristics and Longwall Caving Behaviour <b>T. Medhurst, P. Hatherly and D. Hoyer</b> .....	51
Investigation into Temporary Roof Support Principles <b>W. Gale and C. Stemp (paper withdrawn)</b> .....	63
Implementing a Suspension Design for Coal Mine Roadway Support <b>R. Seedsman</b> .....	70
New Fracture Model for the Progressive Failure of Rock Slopes <b>G. Venticinque and J. Nemcik</b> .....	82
Prediction of <i>In Situ</i> Rock Strength using Sonic Velocity <b>N. Butel, A. Hossack and M. S Kizil</b> .....	89
Effect of Different Curing Conditions on The Compressive and Flexural Properties of Plaster of Paris <b>Z. Shan, I. Porter, J. Nemcik and Q. Qiao</b> .....	103
Evaluating Methods of Underground Short Encapsulation Pull Testing in Australian Coal Mines <b>P. Craig, N. Aziz, J. Nemcik and A. Moslemi</b> .....	109
The Borehole Sleeving Test Method of Resin Anchored Roof Bolt Installations <b>K. McTyer, D. Evans, G. Reed and R. Frith</b> .....	118
The Size Effect of Rock Sample Used in Anchorage Performance Testing of Cable Bolts <b>M. Holden and P. Hagan</b> .....	128

The Load Transfer Mechanism of Fully Grouted Cable Bolts under Laboratory Tests <b>P. Hagan, J. Chen and S. Saydam</b> .....	137
<i>In Situ</i> Bond Strength Testing of Australian Cable Bolts <b>P. Craig and M. Holden</b> .....	147
Shear Strength Properties of Hilti Plain and Indented Strand Cable Bolts <b>N. Aziz, K. Heemann, J. Nemcik and S. Mayer</b> .....	156
Suggested Methods for the Preparation and Testing of Various Properties of Resins and Grouts <b>N. Aziz, J. Nemcik, A. Mirzaghobanali, S. Foldi, D. Joyce, A. Moslemi, H. Ghojavand, S. Ma, X. Li and H. Rasekh</b> .....	163
Next Generation Technology for Corrosion Protection in Ground Support Elements <b>D. Evans</b> .....	177
An Assessment of the Correlation Between the Strength and Cuttability of Rock <b>J. Langham-Williams and P. Hagan</b> .....	186
Full Scale Tests to Compare the Strength of Polymer Liners with High Tensile Steel Mesh <b>I. Porter, Z. Shan, J. Nemcik and E. Baafi</b> .....	193
Effects of Shearing Direction on Shear Behaviour of Rock Joints <b>A. Mirzaghobanali, H. Rasekh, N. Aziz and J. Nemcik</b> .....	202
A Study on the Shear Behaviour of Infilled Rock Joints under Cyclic Loading and Constant Normal Stiffness Conditions <b>A. Mirzaghobanali, J. Nemcik and N. Aziz</b> .....	210
Alternative Excavation Methods in Underground Coal Mining <b>C. Donnelly, G. Ramage and M. Donghi</b> .....	216
Minimising Mucking Time by Prediction of Muckpile Top Size in Tunnel Blasting: A Case Study <b>M. F. Hossaini, M. Mohammadi, B. Mirzapour and N. Hajiantilaki</b> .....	224
Underground Mine Ventilation Air Methane (VAM) Monitoring – an Australian Journey towards Achieving Accuracy <b>B. Belle</b> .....	230
Leveraging Gas Reservoir Data <b>R. Williams</b> .....	243
Changes in Gas Composition during Coal Seam Drainage and Laboratory Testing <b>D. Black and N. Aziz</b> .....	252
Gas Wettability of Coal and Implications for Gas Desorption and Drainage <b>A. Saghafi, K. Pinetown and H. Javanmard</b> .....	266
Concurrent <i>In Situ</i> Methods for Measuring Permeability, Gas Content and Saturation <b>Q. Morgan, J. Pope and P. Ramsay</b> .....	274
Classification of Coal Seams for Coal and Gas Outburst Proneness in the Zonguldak Coal Basin, Turkey <b>O. Esen, S. C. Ozer and A. Fisne</b> .....	285
Poly-crystalline Diamond Drill Bit Development <b>F. Hungerford and T. Ren</b> .....	293

Fluid Pressure Monitoring in Deep Cement Grouted Boreholes <b>B. Neels and I. Gray</b> .....	301
Assessment of an Environmental Sustainability Index for the Underground Coal Gasification Process by Using Numerical Analysis <b>V. F. N. Torres, A. S. Atkins and R. N. Singh</b> .....	309
Commissioning Adiabatic Oven Testing – an Inter-Laboratory Comparison <b>B. Beamish, J. Theiler, J. Saurat and T. Levi</b> .....	324
Developments in the Management of Spontaneous Combustion in Australian Underground Coal Mines <b>D. Cliff, D. Brady and M. Watkinson</b> .....	330
Measurement of Critical Self-Ignition Temperatures of Low Rank Coal Piles <b>Y. Wang, K. Sasaki, Y. Sugai and X. Zhang</b> .....	339
Numerical Modelling of Low Rank Coal for Spontaneous Combustion <b>K. Sasaki, Y. Wang, Y. Sugai and X. Zhang</b> .....	344
Active Barrier Performance Preventing Methane Explosion Propagation <b>J. J. L. d. Plessis and H. Späth</b> .....	350
Is Carbon Monoxide Sensing an Effective Early Fire Detection Option for Underground Coal Mines? <b>F. Mendham, D. Cliff and T. Horberry</b> .....	360
Development and Utilisation of Fibre Optic-based Monitoring Systems for Underground Coal Mines <b>S. M. Aminossadati, M. Amanzadeh, M. S. Kizil and T. Liu</b> .....	369
Belt Road Segregation and Escapeways - Compliance or Risk Management? <b>M. Olsen</b> .....	381
Riskgate and Australian Coal Operations <b>P. Kirsch, J. Harris, D. Sprott and D. Cliff</b> .....	389
Comparative Analysis of Coal Fatalities in Australia, South Africa, India, China and USA, 2006-2010 <b>J. Harris, P. Kirsch, M. Shi, J. Li, A. Gagrani, A. K. ES, A. Tabish, D. Arora, K. Kothandaraman and D. Cliff</b> .....	399
Open Risk - an Update on the Use of a Pit Highwall Risk Rating System <b>J. Hoelle</b> .....	408
Optimisation of Overburden Blasts at Glencore Ulan Surface Coal Operations <b>D. Thorn, B. Cediél, S. Esen and M. Nagarajan</b> .....	413
Optimisation of Waste-Dump Lift Heights for Pre-strip Operations <b>R. Lucas and M. S. Kizil</b> .....	427
<b>Index of Authors</b> .....	437

# DRILLING INDUCED FRACTURES IN COAL CORE FROM VERTICAL EXPLORATION WELLS: A METHOD TO DETERMINE CLEAT AZIMUTH, AND THE ANGLE BETWEEN CLEAT AND MAXIMUM HORIZONTAL STRESS, AND ITS APPLICATION

David Titheridge

**ABSTRACT:** Drilling induced fractures that have been described from cored sandstone, mudstone and limestone, also occur in many coal cores. This paper outlines a method of using petal and related fractures in coal core to determine the angle between face cleat and the principal horizontal stresses. The method also enables determination of the azimuth of cleat, in wells in which the apparent dip of cleat on a scanner image is vertical. As the angle between face cleat and the principal horizontal stresses can have a major influence on initial permeability, the method has application in coal bed, coal mine, and enhanced coal bed methane.

## INTRODUCTION

The value of interpreting stress azimuth from induced fractures in the bore wall is well known to the petroleum industry. The angle between (effective) principal horizontal stresses ( $S_H$ ,  $S_h$ ), and the strike of natural fractures is an important one in petroleum production, for those fractures close or parallel to  $S_H$  (and perpendicular to  $S_h$ ), have the widest oil-filled apertures and dominate permeability pathways. The same principle has applications for Coal Mine Methane (CMM; production/utilization and/or drainage/ventilation to atmosphere), Coal Bed Methane (CBM) production, and Enhanced Coal Bed Methane (ECBM; combined methane production with concurrent sequestration of  $CO_2$  in coal).

In recent years there has been increasing reliance on image logs from sonic and resistivity scanners to obtain orientation and dip of fractures and sedimentary structures with low to high dip. However, in the case of near vertical exploration drill-holes, the apparent dip of cleat in a scanner image may be vertical, and if so, it is not possible to obtain the azimuth of cleat.

This paper offers a geometrical method to determine the angle between cleat and  $S_H$  (and  $S_h$ ) as well as their azimuths. It is based on the presence of drilling induced petal (and related) fractures in coal core, and breakout azimuth from a scanner log.

## STRESS, CLEAT AND PERMEABILITY

### Stress regimes

The state of stress in rocks can be described by three orthogonal principal stress directions. The maximum, intermediate and minimum principal stress directions ( $S_1 > S_2 > S_3$ ) in rocks can be either vertical ( $S_V$ ) or horizontal ( $S_H$ ,  $S_h$ ). There are three stress regimes associated with fault formation (Figure 1). The type of fault formed in the geological past may not have any relationship to the present day stress. The nature of drilling induced tensile fractures has some dependence on stress regime.

### Cleat, stress, the angle between $S_H$ and cleat, and permeability

The stress that acts on cleat has both tectonic and pore pressure components (Figure 1). It is well established that minimum principal effective stress,  $S_h$ -Pore Pressure (PP, Figure 1) plays a major role in the initial permeability of coal prior to production/drainage (review by Bell, 2006 with examples from Australia). Matrix shrinkage and increase in cleat aperture during desorption (production) is associated with an increase in permeability (Gray, 1987; Levine, 1996).

Face cleat is the main permeability pathway in coal, though butt cleat and other fractures may contribute. In some coals there is not a dominant face cleat, and both sets may abut the other (Figure 2). Cleat properties of coals, and particularly those that contribute to interconnectedness of cleat, (spacing, height, width, aperture, development of butt or secondary face cleat, and paucity or abundance of mineralisation), all contribute to permeability.

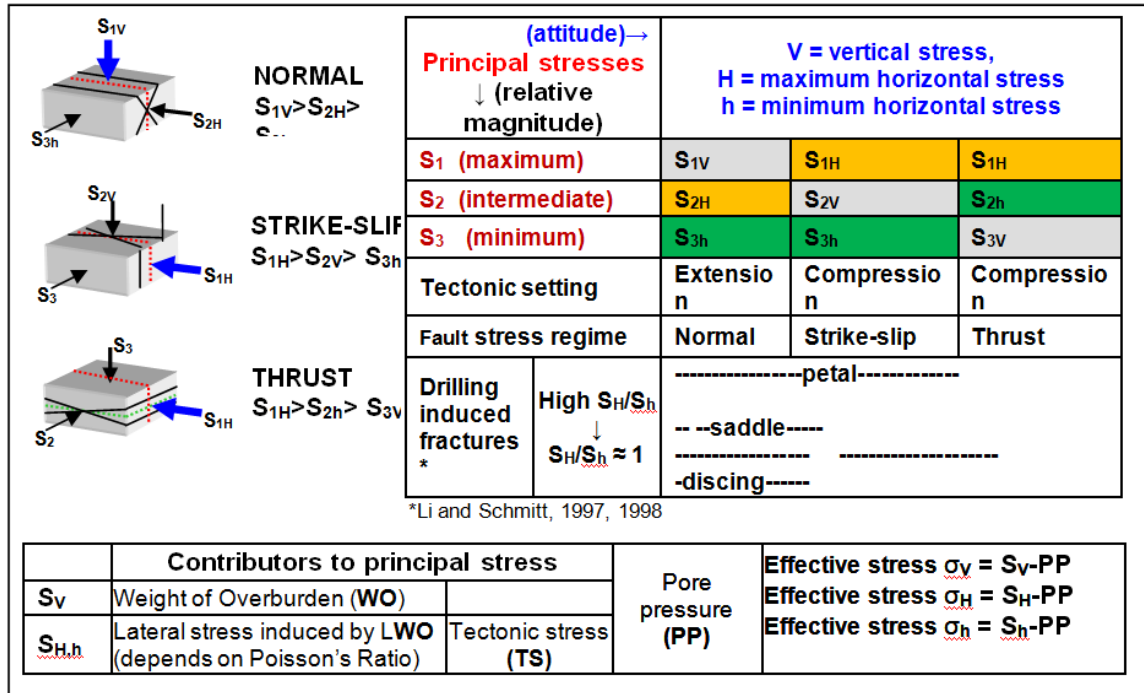


Figure 1 - Stress, shear structures (faults), and natural and drilling induced tensile fractures

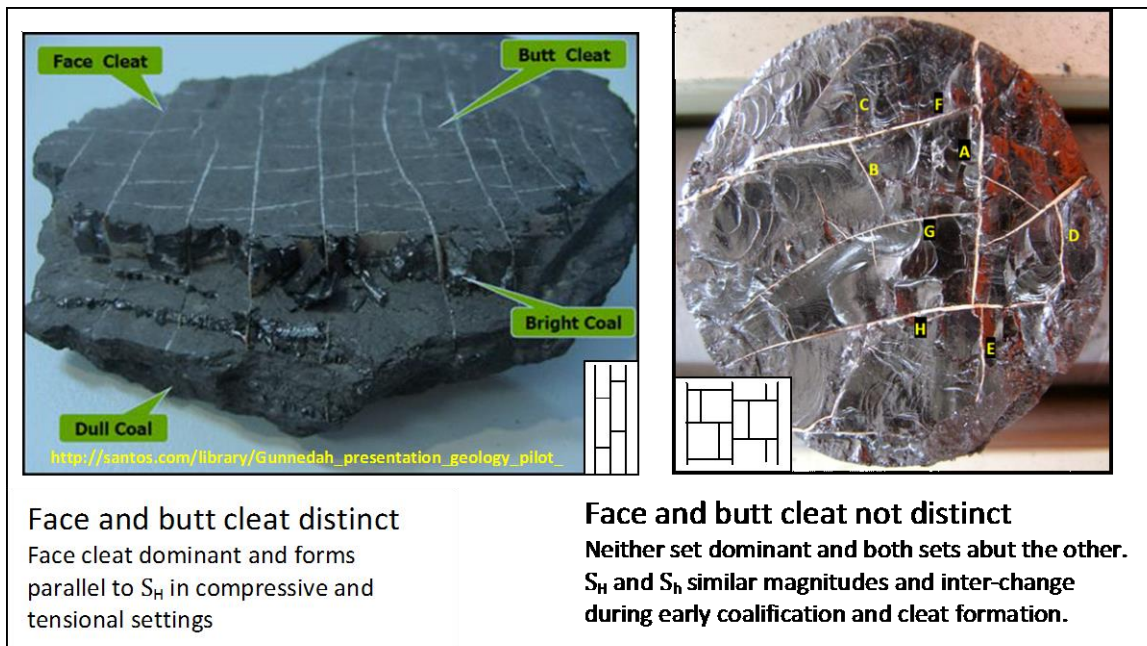
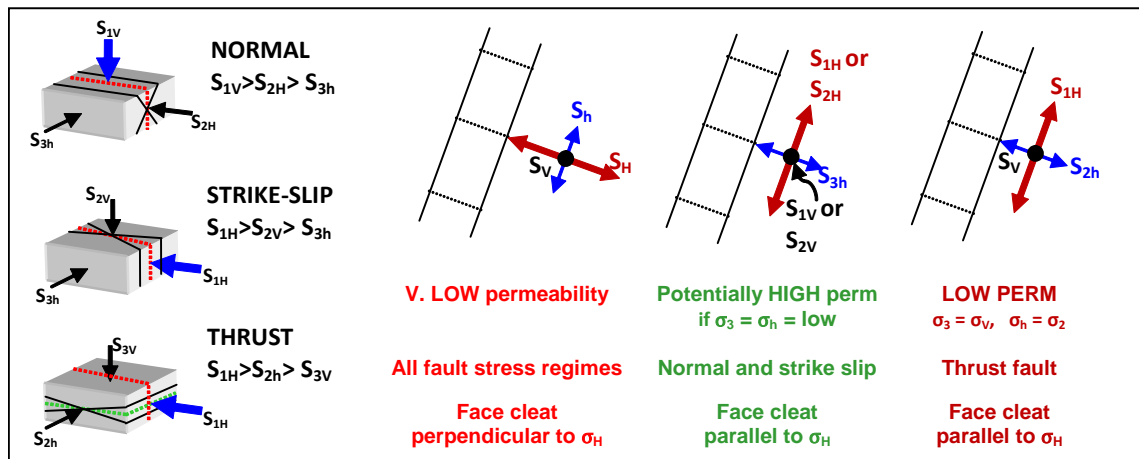


Figure 2 - Two types of cleat systems

It is self-evident from a horizontal 2D perspective that if face cleat is perpendicular to S<sub>H</sub> (and parallel to S<sub>h</sub>), initial permeability will be low. Recent measurements of coal permeability under laboratory triaxial stress conditions have confirmed this (Massarotto, *et al.*, 2003). On the other hand, also from a 2D perspective, if face cleat is parallel to S<sub>H</sub> (and perpendicular to S<sub>h</sub>), initial permeability is likely to be relatively high. However when the three 3D states of stress are considered, this is only true for normal and strike slip fault regimes, and only if S<sub>h</sub> is small. In a thrust fault regime, even if face cleat is

parallel to  $S_H$  (and perpendicular to  $S_h$ ), permeability is unlikely to be high, as  $S_3$  is vertical (Figure 3). In general, the prevailing stress regime in Eastern Australian coal basins at coal mining depths, is the thrust fault stress regime. It is invariably associated with low permeability. Normal and strike slip fault regimes with horizontal minimum stress ( $S_{3h}$ ), are a prerequisite for high permeability. Their presence is related to local geology.



**Figure 3 - Angle between face cleat and  $S_H$ , and predicted permeability based on relative magnitudes of fault stress regimes**

If face cleat is parallel or orthogonal to the principal horizontal stress, then the magnitude of normal stress acting on cleat is the orthogonal principal horizontal stress magnitude. If cleat is at an acute angle to  $S_H$  and  $S_h$ , then the normal stress magnitude acting on cleat is between that for  $S_H$  and  $S_h$ . Permeability can be expected to reflect the normal stress magnitude acting on cleat.

#### Origins of variation between the azimuths of $S_H$ and face cleat

It is widely accepted that cleat is a tensional joint in coal, and that its development occurs during early coalification, with loss of moisture and other volatiles. Face cleat generally develops parallel to  $S_H$  and perpendicular to  $S_h$  at the time of early coalification. This applies to normal, strike-slip and thrust fault regimes (Figure 1). There are many basins world-wide where the azimuth of  $S_H$  has remained the same since early coalification so that face cleat and principal horizontal stress have the same orientation e.g. SW Alberta, Canada (Bell and Bachu, 2003).

However there are also many instances where the relationship between face cleat and stress azimuths departs from this situation of similarity, as a result of regional changes in stress direction over time since cleat formation, or local perturbations of the regional stress field in the vicinity of folds and faults (Barton and Zoback, 1994; Rippon, *et al.*, 2006; Yale, 2003). A more comprehensive review is in Titheridge, 2012.

#### Orientation of core and determining azimuths of cleat

Prior to recent developments in acoustic and resistivity scanner imaging, determination of the orientation of core for sedimentary fabrics, tectonic structures and stress and strain states was entirely via retrieval of oriented core (Nelson, *et al.*, 1987). Orientation of core has also been achieved by paleo-magnetic methods (e.g. Lackie and Schmidt, 1993; Van Alstine and Butterworth, 2002).

Analysis of bore wall images from acoustic and resistivity measurements is now the prevalent means of obtaining directional data of sedimentary and structural features. The basis of determining dip and strike of planar inclined bedding and faults, is the sinusoidal trace of a planar feature on a circular image of the bore wall. The amount of dip is determined from the amplitude of the sinusoidal trace, and the dip azimuth is the minima of the sinusoidal trace. The latter can be read off the horizontal axis of a scanner log scaled from 0 to 360 degrees (Figure 4).

The azimuth of cleat in coal can also be determined where the apparent dip of cleat is not vertical from a full sinusoidal trace, or interpolation of a maxima or minima if the full trace is truncated (Figure 4b-4d). However if the apparent dip of cleat is vertical, or very near vertical, as is common for many exploration

wells, there is no sinusoidal trace, or maxima or minima to determine dip and strike (Figure 4e-4k). In this instance cleat azimuth needs to be determined from a combination of core and scanner data.

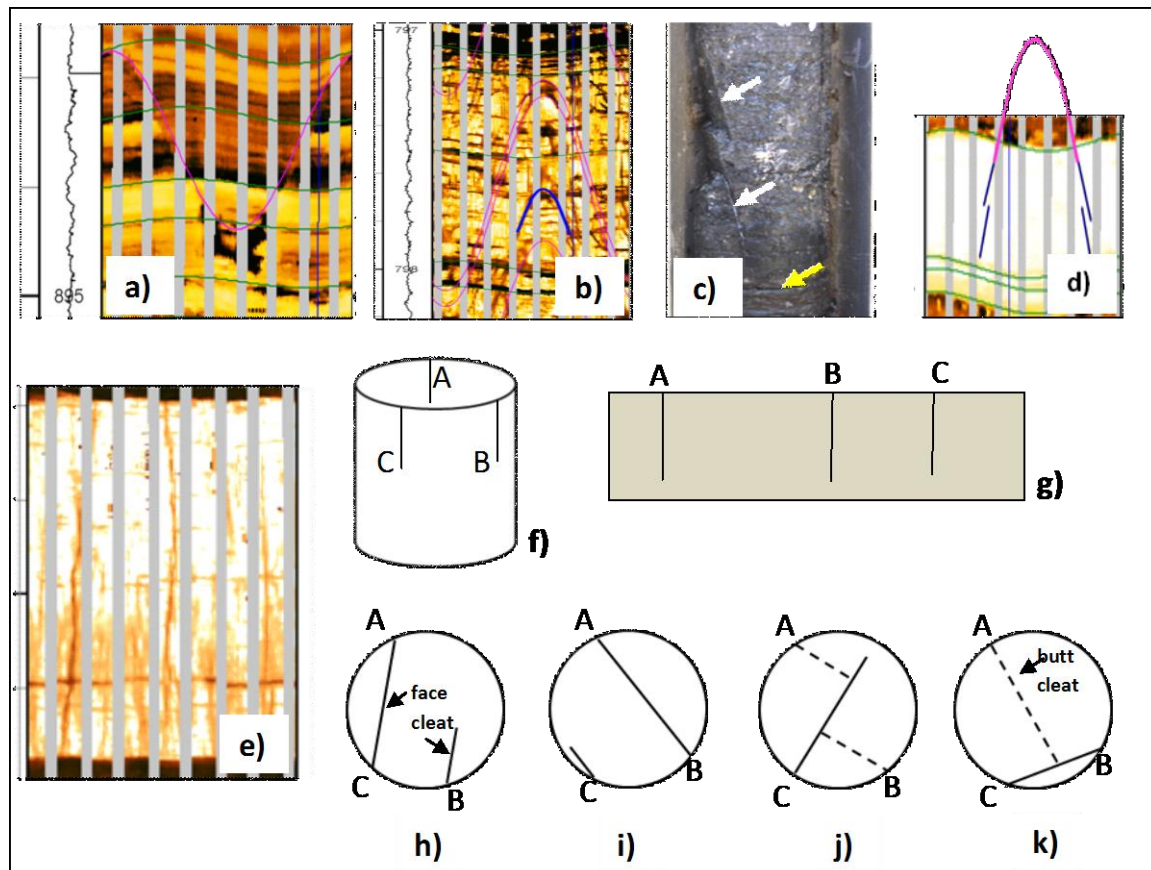


**Figure 4 - Examples where cleat can and cannot be determined from a scanner log: a) small scale fault b) and c) cleat with apparent dip and full sinusoidal trace on scanner image, and in core (same well within 8m) d) cleat with maxima only (due to truncation of cleat), maxima of sinusoidal trace can be interpolated e) apparent dip of cleat is vertical on scanner image, cleat azimuth cannot be determined f) and g) hypothetical cleat on bore wall and on scanner image h,i,j,k) four interpretations of "g" indicating no unique solution without sinusoidal trace where apparent dip of cleat on scanner image is vertical**

#### Drilling induced failures (breakout) and tensile fractures in the borewall

Borehole breakout is due to localised failure of rock around a bore wall. It forms as a result of local concentration of horizontal hoop stress exceeding the strength of the rock (Bell, 1996; McGregor, 2003). It manifests as two zones of borehole enlargement at 180 degrees to each other that can be detected on an image from an acoustic or resistivity bore-hole scanner image. Breakout has the same azimuth as  $S_H$  and the apex of petal fractures on the core perimeter, and is at 90 degrees to  $S_H$ . Breakout is often a common feature of bore wall images at coal mining depths.

Drilling induced tensile fractures may also occur in the bore-wall. They form parallel to  $S_H$  and at 90 degrees to breakout. They form when circumferential tensile stress exceeds the tensile strength of the well-bore wall. They are common in deep petroleum wells and often present at 90 degrees to breakout. They have the same orientation as centre-line fractures seen in sandstone core.

#### Drilling induced tensile fractures in coal core

Drilling induced tensile planar and curvi-planar fractures in coal core include petal, core edge, and saddle fractures, as well as discing (Figure 5). A new descriptive category, namely incipient core edge fractures, is recommended for those small fractures confined to the core perimeter. They may be present when none of the other fractures listed above, are not.

Curvi-planar drilling induced fractures are known as “petal fractures”. The origin of the name arises from their resemblance to petals attached to a stem when they coalesce with centreline fractures.

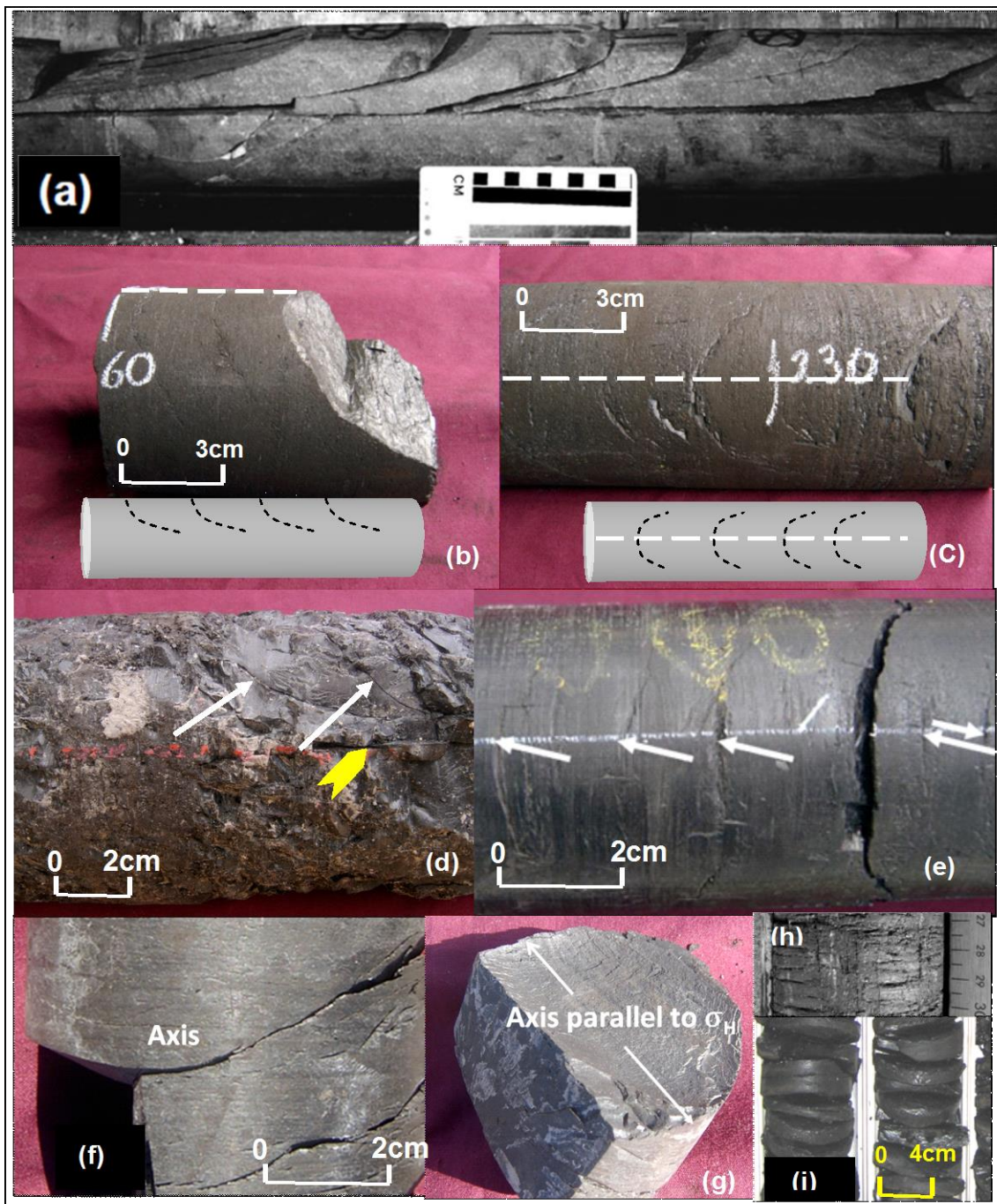


**Figure 5 - Drilling induced fractures in coal core and sandstone: a) Petal-centreline fractures (from Lacazette, 2000) in sandstone. b,c) Petal fractures top and side views d) Curved petal fractures in side view (white arrows), cleat with calcite (yellow pointer) e) Incipient core edge fractures f,g) Saddle fractures, same core h,i) Discing in coal**

Petal fractures in coal have not been observed in association with centreline fractures (cf. sandstone, Figure 5a). Curvature of petal fractures in coal occurs in their upper part (cf. the lower part of some sandstones, Bell, 1996). Petal fractures generally enter coal core at relatively low angles and steepen downwards towards the centre of the core where they become planar or near planar. In other instances, petal fractures only penetrate about a third of the core diameter from the core exterior and commonly terminate before becoming vertical. The trace of the top of petal fractures in a bore wall scanner image is flattened as a result of their curvi-planar shape (Lacazette, 2000; cf. the sinusoidal maxima of planar

features intersecting the bore wall). Curvi-planar petal fractures are rarely observed in coal on scanner images of the bore wall.

Petal fractures appear as linear features in bedding plane sections but curved when observed perpendicular to the long axis of core. The relationship of the azimuths of borehole break-out,  $S_H$ , centre-line fractures, petal fractures, and the location of petal fracture apices, in a horizontal bore-hole cross section is illustrated in Figure 6. Observations to date indicate that petal fractures only form in the more competent dull coal lithotypes with sparse bright bands and sparse cleat.

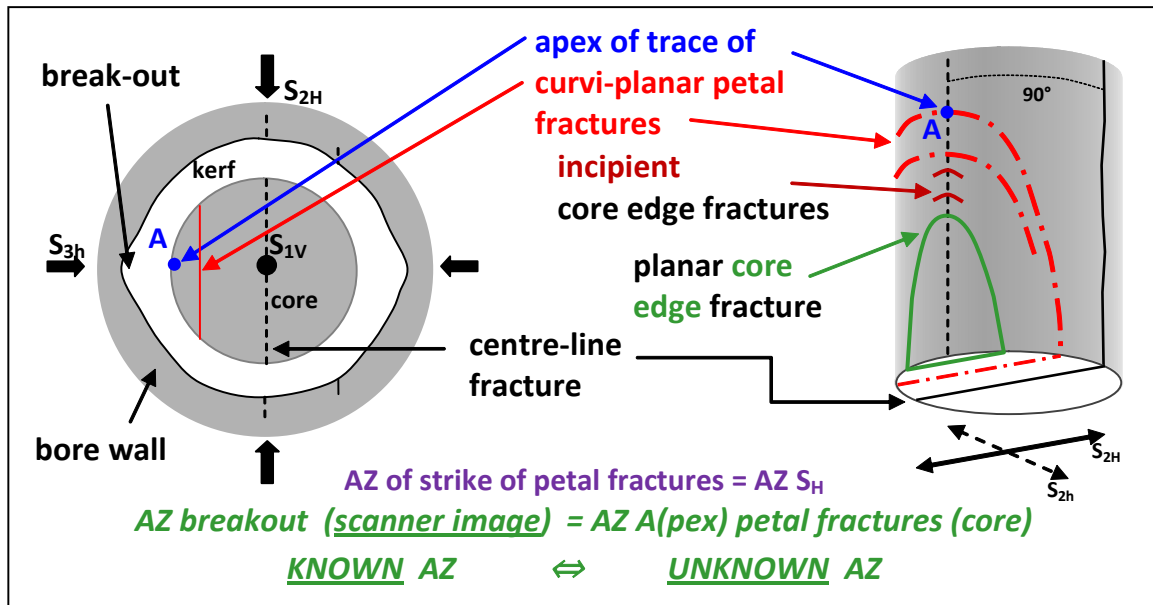


Figure 6 - Petal and related fractures in core (RHS) and on the bore wall (LHS)

The orientation of apices and strike of petal fractures are very consistent and measurable to about  $\pm 2^\circ$ . This contrasts with the wide azimuthal range of breakout, where it is necessary to visually estimate the central position of breakouts 180 degrees apart. In some instances, petal fractures in coal occur on diametrically opposite sides of the core; if that is the case the apices of petal fractures on the core perimeter are always at 180 degrees.

The axes of saddle fractures are parallel to  $S_H$  (Bell, 1996; Figures 5f and 5g). Whilst no directional stress information can be obtained from discing in core (Figures 5h, 5i) it is likely that their presence indicates the principal horizontal stresses are similar in magnitude and greater than the vertical stress (thrust fault regime). Transitional forms between saddle fractures and discing exist.

The origin of petal and saddle fractures and discing of core (Figure 5), has been attributed to the re-distribution and concentration of compressive stresses around the cutting edge of a drill bit. Finite Element Method (FEM) modelling of stress trajectories indicates that petal (and saddle-shaped) fractures strike in the direction of maximum horizontal compression (Lorenz, *et al.*, 1990; Li and Schmitt, 1997, 1998). Drill bit pressure ( $= S_V$  at the core bit) produces tensile fractures in core ahead of the drill bit. The orientation and type of tensile fractures (petal, saddle and discing) induced by drilling, shows some dependence on the type of fault stress regime and the  $S_H/S_h$  ratio (Li and Schmitt, 1998). Petal fractures develop in normal and strike-slip fault stress regimes. Saddle shaped fractures are most likely to develop in strike-slip fault stress regimes. Discing of core can form in any of the fault stress regimes but is most likely to occur in a thrust fault stress regime (Figure 1).

## METHOD AND PROCEDURE

### Preparation

It is essential to be able to restore sections of the core to their original orientation with respect to each other. The best way to do this is to paint parallel lines of different colour on the core, and parallel to the axis of the core after removal of one of the inner tube splits, prior to placement of core in a core tray or

gas desorption canister. Consistent use of different colours will indicate up and down directions of the core. This is generally standard practice for exploration drilling. It is often possible to restore core from different drill runs by matching ends but where coal has been purposefully broken to fit coal core into a canister or core box, this is often impossible. If core has petal fractures, the angle between the arbitrary lines and the petal fracture apices in the same drill run can be determined. The notional location of petal fracture apices can then be transferred to adjacent lengths of core without petal fractures where cleat is to be measured (Titheridge, 2012).

**Overview of calculation**

The process from data collection/input to azimuth and angle results is summarised in Figure 7a.

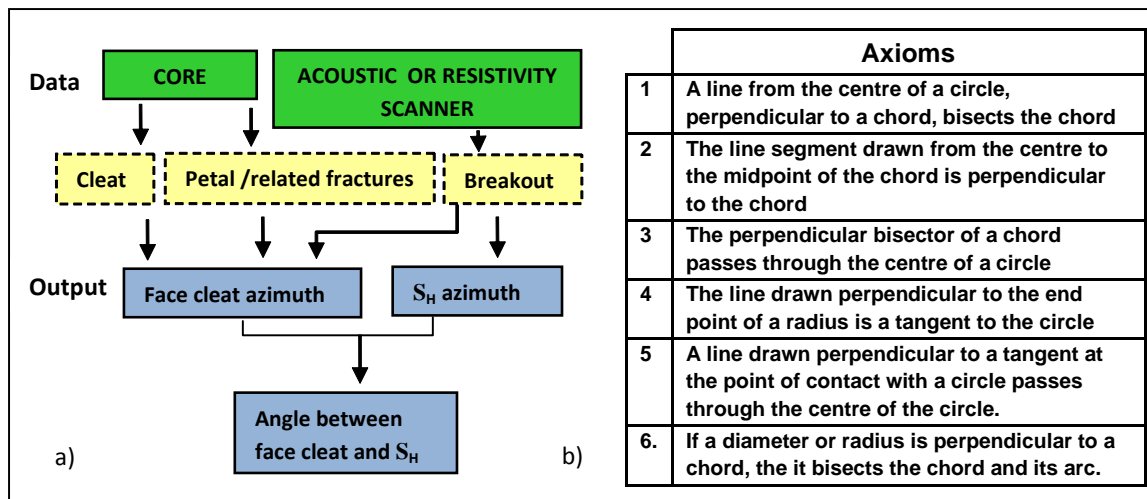


**Figure 7 - (a) Data source and output and (b) axioms to support calculation**

It is impractical and cumbersome for many reasons to measure cleat and stress directions and angles on the bedding plane of core (Titheridge, 2012). The reasons include the existence of incipient core edge fractures that develop on the core perimeter, that are a useful source of information when none of the other types of drilling induced fractures are present. The solution is to use the location of the apex of petal fractures and cleat intersections on the core parameter. The basis of the method of determination is that the azimuth of apices of curvi-planar drilling induced petal (and related) fractures on the core perimeter is the same as the azimuth of breakout on the borewall (Figure 6). S<sub>H</sub> is transposed to the notional centre of the core as it is orthogonal to breakout and the apex of petal fractures. The cleat chords are transposed to the centre of the core. The transposition is based on six axioms of geometry (Figure 7b). This procedure reduces the task of measurement, to obtaining two angles between a petal fracture apex and each of the two intersections of a cleat chord with the core circumference. Angular measurements around the perimeter of the core can be made clockwise or anti-clockwise but must be consistently recorded as positive or negative looking down-hole.

**Measurement**

The angle between petal fracture apices and cleat intersections of the core perimeter can be measured with a circular protractor that fits the diameter of the core, or a flexible wrap around protractor. Circumferential distances obtained with dress makers tape can easily be converted to degrees. On many occasions it will be necessary to extrapolate a cleat on a bedding plane to the core perimeter with a straight edge and china-graph pencils. It will also be necessary to extrapolate the location of petal fracture apices along the same piece of core (or same drill run) to a bedding plane section with cleat to be measured.

**Geometrical construction and calculation**

The steps involved in calculation are: (i) transpose S<sub>H</sub> to the centre of the core (90 degrees to the apex of the petal fracture), and (ii) transpose cleat to the centre of the core (Figure 8).

**Limitations of the method**

The limiting factor of the method is that petal and related drilling induced fractures are often rare or absent from some coal cores. For example in the Southern Coalfield, NSW, the Bulli Seam, has abundant drilling induced fractures (predominantly dull coal). In contrast, in the working section of Wongawilli Seam about 30 metres below the Bulli Seam, drilling induced fractures in coal are absent. The Wongawilli Seam contains abundant bright bands and abundant cleat.

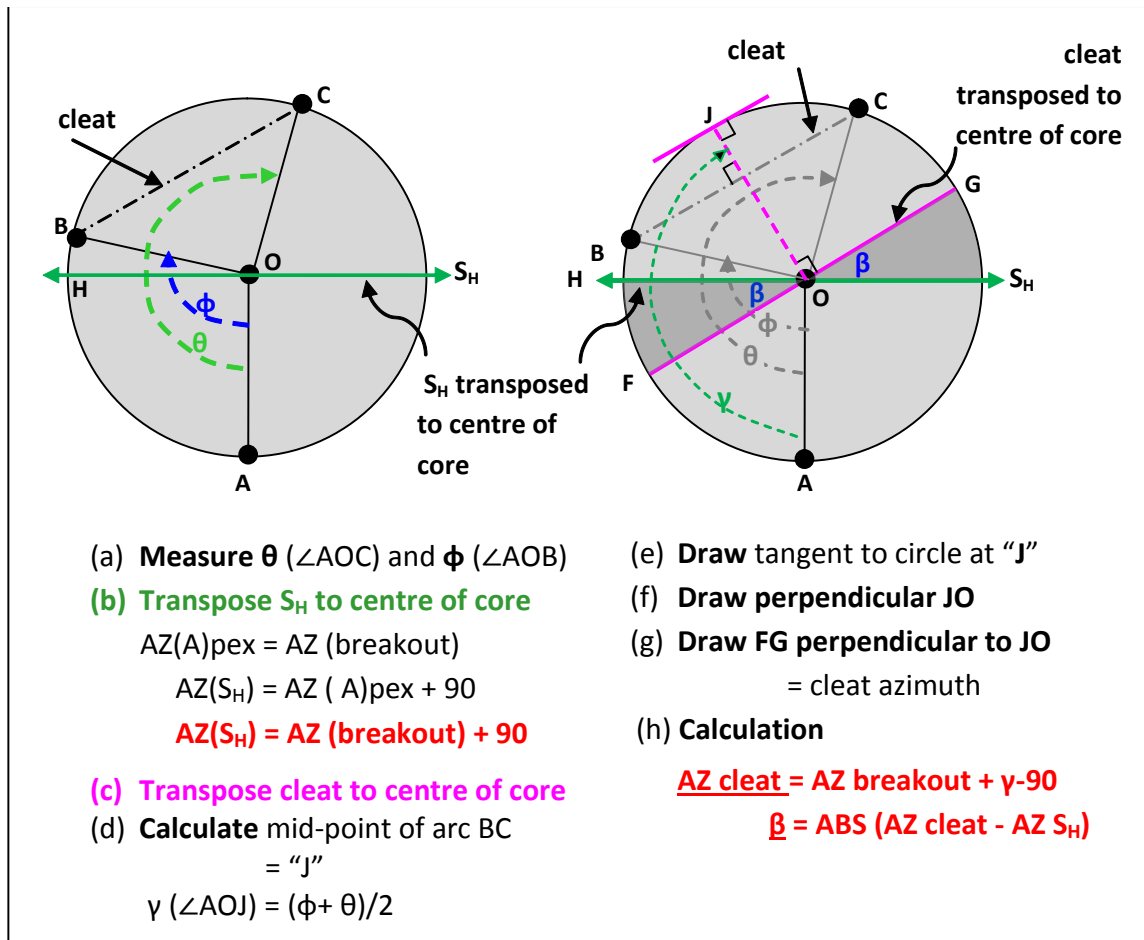


**Figure 8 - Calculation of cleat azimuth and the angle between  $S_H$  and (face) cleat**

**Application**

Knowledge of face cleat/stress angles can also assist with  $CO_2$  sequestration via the ECBM method. This may determine placement of injection and production holes depending on production objectives (Figure 9a).

Knowledge of the angle between stress and cleat is critical to planning the orientation of hydro-fracs in areas of low permeability due to unfavourable face cleat/stress angle (Figure 9b).

The method can also potentially improve the interpretive value of plots of log permeability vs effective stress (Figure 10). Traditionally the stress plotted has been  $S_{3h-PP}$  ( $\sigma_3$ ). This assumes that  $S_{3h}$  is perpendicular to face cleat. However, if at any location,  $S_H$  is perpendicular, or at a moderate to high acute angle to (face) cleat, the plotted effective stress parameter needs to be  $S_{N-PP}$ . The calculated effective normal stress is based on the magnitudes of both  $S_H$  and  $S_h$ , and the angle between cleat and  $S_H$ . If  $S_{3h-PP}$  is plotted, any outliers (assuming valid permeability and magnitude tests) could include data where  $S_H$  is perpendicular or at a high acute angle to face cleat. If  $S_{N-PP}$  is plotted, any outliers are most likely to have geological causes (Figure 10).

SUMMARY

- i) The presence of petal and related drilling induced fractures in coal core, and breakout information from scanner logs, can be used to determine the angle between  $S_H$  and face cleat direction, as well as cleat azimuth (where this cannot be obtained from a scanner log).
- ii) Whilst face cleat is often parallel to  $S_H$ , there are many instances where it is not due to post-cleat rotation of the regional stress field, or local perturbations of the regional stress field, that is often related to faulting and folding.
- iii) A knowledge of the angle between face cleat and  $S_H$  (and  $S_h$ ), together with stress magnitude measurements, assists the interpretation of anomalies on permeability vs stress plots.
- iv) The method can be applied to CMM, CBM, and ECBM/CO<sub>2</sub>.

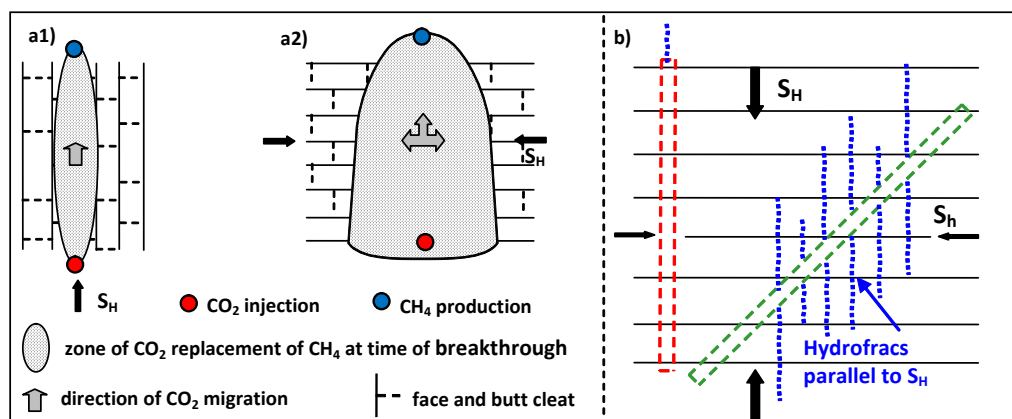


Figure 9 - Conceptual CO<sub>2</sub> migration in coal and optimal direction for in-seam fracturing when  $S_H$  is perpendicular to cleat. (a1)  $S_H$  and CO<sub>2</sub> migration parallel to face cleat. Short time to CH<sub>4</sub> production with small extent of CO<sub>2</sub> replacement. (a2)  $S_H$  parallel to face cleat but CO<sub>2</sub> migration perpendicular to face cleat. Longer time to CH<sub>4</sub> production with large extent of CO<sub>2</sub> replacement. (b)  $S_H$  is perpendicular to face cleat direction, hence low permeability. Red hole: optimal hole stability and maximum intersection of cleats but fracs same orientation as hole. Green hole: RHS may have wall failure but fracturing achievable

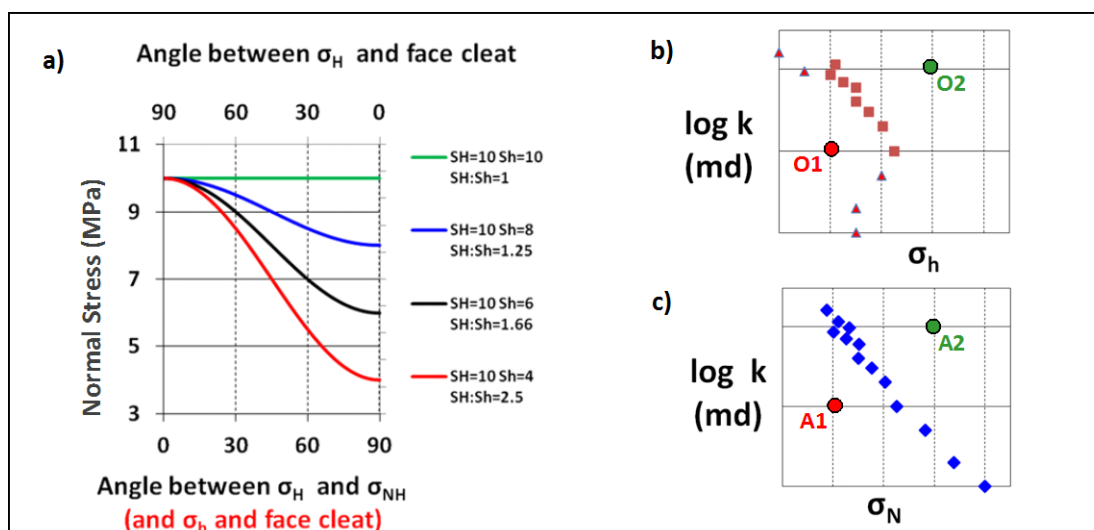


Figure 10 - Application of stress/cleat angle and stress magnitude data in detecting permeability anomalies. a) Calculated normal stress acting on face cleat at all angles with constant  $S_H$  and variable  $S_h$ . b) Hypothetical  $\log k$  vs effective minimum principal stress ( $\sigma_h$ ). Numerous outliers. c) Same hypothetical permeability data with  $\log k$  vs effective normal stress ( $\sigma_N$ ). Many outliers from plot above now fall on general trend leaving two residual anomalies, A1(?mineralisation of cleat, very high CO<sub>2</sub> % and gas content) and A2(? zone of secondary tectonic fracture)

## REFERENCES

- Barton, C A and Zoback, M D, 1994. Stress perturbations associated with active faults penetrated by boreholes: Possible evidence for near-complete stress drop and a new technique for stress magnitude measurement. *Journal of Geophysical Research*, 19: 9373-9390.
- Bell, J.S., 1996. *In Situ* stresses in sedimentary rocks (Part 1): Measurement Techniques: *Geoscience Canada*, 23:85-100.
- Bell, J.S., 2006. *In-situ* stress and coal bed methane potential in Western Canada. *Bulletin of Canadian Petroleum Geology*, 54:197-220.
- Bell, J.S. and Bachu, S., 2003. *In-situ* stress magnitude and orientation estimates for Cretaceous coal-bearing strata beneath the plains of central and southern Alberta. *Bulletin of Canadian Petroleum Geology*, 51:1-28.
- Gray, I, 1987. Reservoir Engineering in Coal Seams: Part 1. The physical process of gas storage and movement in coal seams. *SPE Reservoir Engineering*, 2:28-34.
- Lacazette, A, 2000. Distinguishing natural from induced fractures in image logs. <http://www.naturalfractures.com/5.3.htm#petcent> [Accessed:19 November 2013].
- Lackie, MA and Schmidt, PW, 1993. Drill core orientation using paleomagnetism. *Bulletin of Australian Society of Exploration Geophysics*, 24:609-614.
- Levine, J.R., 1996. Model Study of the Influence of Matrix Shrinkage on Absolute Permeability of Coal Bed Reservoirs in *Coalbed Methane and Coal Geology* (eds: R Gayer R and I Harris), pp 197-212 (Geological Society of London Special Publication, 109).
- Li, Y. and Schmitt. DR, 1997. Well-Bore Bottom Stress Concentration and Induced Core Fractures. *AAPG Bulletin*, 81(11):1909-1925.
- Li, Y. and Schmitt. D.R., 1998. Drilling induced fractures and *in situ* stress. *Journal of Geophysical Research*, 103:5225-5239.
- Lorenz, J C, Finley, S J., and Warpinski, N R., 1990. Significance of coring induced fractures in Mesaverde Core, Northwestern Colorado. *AAPG Bulletin*. 74:1017-1029.
- MacGregor, S, 2003. Definition of stress regimes at borehole, mine and regional scale in the Sydney Basin through breakout analysis in *Proceedings of the 35<sup>th</sup> Sydney Basin Symposium "Advances in the study of the Sydney Basin September 29-30, 2003, University of Wollongong, Australia* (eds. Hutton, A C, Jones B G, Carr, P F, Ackerman, B, and Switzer, A D) pp 223-227.
- Massarotto, P, Rudolph, V, Golding, S D, and Iyer, R, 2003. The effect of directional net stresses on the directional permeability of coal, in *International Coalbed Methane Symposium* (University of Alabama).
- Nelson, R.A., Lenox, L.C. and Ward, B.J., 1987. Oriented core: Its Use, Error and Uncertainty. *AAPG Bulletin*, 71:357-367.
- Rippon, J.H., Ellison, R.A. and Gayer, R.A., 2006. A review of joints (cleats) in British Carboniferous coals: indicators of paleo-stress orientation. *Proceedings of the Yorkshire Geological Society*, 56:15-30.
- Titheridge, D G, 2012. Drilling induced petal fractures in coal core: A simple method of using these features in conjunction with bore-wall breakout to determine the angular relationship between cleat and maximum horizontal stress as well as cleat azimuth in vertical drill-holes, in *Eastern Australasian Basins Symposium IV [CD ROM]* (ed: T Mares) pp 89-111 (Petroleum Exploration Society of Australia, Special Publication).
- Van Alstine, D. R, and Butterworth, J. E., 2002. [Paleomagnetic core orientation helps determine the sedimentological, paleostress, and fluid-migration history in the Maracaibo Basin, Venezuela](#) [Accessed 19 November 2013] *Core Workshop for I Congreso Virtual de Sedimentología, 11 de Febrero al 08 de Marzo de 2002*.
- Yale, D.P., 2003. Fault and stress magnitude controls on variations in the orientation of *in situ* stress, in *Fracture and In-Situ Stress Characterization of Hydrocarbon Reservoirs* (ed: M Ameen) pp17-26 (Geological Society, London, Special Publication, 209.).

# MAPPING TECHNIQUES FOR DETERMINING SANDSTONE ROOF CHANNEL PALEODRAINAGE DIRECTION IN COAL MINES

Luc Daigle

**ABSTRACT:** Sandstone channels are constant hazards to coal mining operations, the presence of a channel over a seam can result in thinning of the seam, changes in stress orientations, variation in stress intensity, abrasive cutting, roof hangup, faulting, jointing, loading of the face and even wind blasts. Prediction of the trend of a channel is usually difficult as channels tend to meander and follow complex orientations. However, geological mapping of development roadways can provide very good information on where to expect channels.

Mapping paleodrainage indicators at Yancoals' Ashton Coal Mine in the Hunter valley demonstrates channel trends can be projected through analysis of these indicators. Recognising and recording oriented indicators on hazard plans can assist in forewarning where channels may be anticipated. The experience at the Ashton Coal Mine shows how recording these features provide a means of predicting channel trends. Drainage pattern interpretation of the sandstone channels was possible due to excellent exposure of coarse grain channel sediment, levee, and overbank facies deposition. Comparison of the plotted drainage trends with paleodrainage direction indicated by oriented plant debris demonstrates direct correlation, using paleodrainage indicators in the absence of an exposure of the channel base can be used to predict the trend of the channel at a specific location.

## INTRODUCTION

Coal seams are the fossil remains of peat deposits formed through the thick accumulation of plant debris in very low energy sedimentary conditions. These former swamps and forests can be compared to modern analogies that are used as models for understanding the distribution and formation of coal seams and their associated sedimentary deposits forming their stone roof and floor. The enclosing sediments forming these roof and floors are critical to mining and the anticipated conditions. Each seam represents a unique depositional event; the pattern of sedimentation and type of sediment present is completely dependent on the conditions that existed at the time the deposits were formed.

Increased sediment load and higher energy deposition characterises the formation of sandstone channels and associated levee and overbank deposits of silt and clay. Geological mapping of the roadways excavated into coal seams can provide detail on these enclosing sediments if the roadways expose the coal seam roof. It is possible to predict sediment trends through mapping the contact changes and analysis of recorded trend indicators whenever possible. Trend indicators at this locality consisted of oriented plant debris present as imprints in the roadway roof and also the orientation of channel edges. Comparison of the mapped sediment distribution pattern to modern analogies provides a basis for interpreting the patterns observed. This paper will look at the mapping completed at the Ashton Coal Mine in the Hunter Valley of New South Wales. At this location the mine has developed and extracted the Pikes Gully Seam and is now moving into a deeper seam to continue mining, this paper examines the data collected from the Pikes Gully Seam. Both geological trends of channel sandstone sediments and analysis of paleodrainage trend indicators were compiled to determine the paleodrainage. Paleodrainage can be described as the drainage distribution channels existing at the time of deposition of the coal seams and their enclosing roof and floor sediments.)

## PALEODRAINAGE

Paleodrainage mapping is an important component of basin analysis and is carried out as part of sedimentary rock mapping of coal, oil and gas deposits. Modern channel systems are easily delineated by direct plotting of the recognised facies distribution, as can be viewed in aerial photos and satellite images, the examples used in this paper are images published by Google Earth, the modern Mississippi

---

Senior Engineering Geologist, SCT Operations Pty Ltd, Email: l.daigle@sct.gs, Tel: +61 2 4222 2777

River and delta (Figures 1, 2) provides a very good analogy for the distribution of sediment deposits found in many coal basins such as the Sydney Coal Basin and Hunter Valley deposited in the Permian geological period approximately 240 million years ago.



**Figure 1 - Main channel, meandering river deposit of the Mississippi River basin**

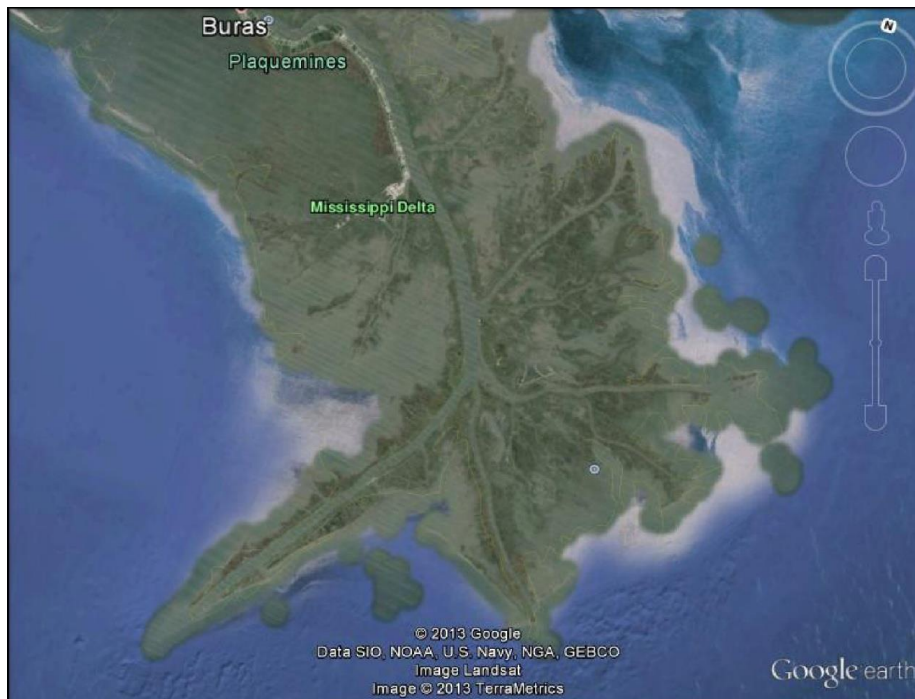


**Figure 2 - Deltaic facies channel distribution in a delta Mississippi Delta**

Coal forming peat swamps allowing the thick accumulations of organic matter necessary for coal seam formation was a recurring environment within the sedimentary basins of the Hunter Valley, The Ashton Coal Mine has numerous repetitive cycles of peat swamp separated by intervals of coarse sediment burial exhibiting the characteristics of meandering river channels, levees, overbank flood plain deposits of sediment and organic debris.

Channel sedimentation seen in the modern analogies demonstrate recognisable trends can be anticipated in the buried sediments of the coal basins. A main channel can be hundreds of metres across with well developed levee deposits and extensive overbank deposit, yet a flood breach (Crevasse splay) in the levee can result in deep cutting channel deposits at right angles to the true sedimentary drainage direction only tens of metres wide (Figure 3).



**Figure 3 - Detail of levee and overbank distribution**

Recognition of the sediment deposit types in underground mapping requires piecing together the limited exposures of the depositional facies mapped along the extensive network of roadways developed to extract the coal. Subtle indicators are exposed in the roadways which can be recognised and documented as part of the geological mapping conducted along the roadways. In surface geological mapping of sedimentary basins, the most frequently recognised indicators of flow direction include:

- Ripple marks.
- Cross beds.
- Oriented plant debris.
- Parting lineation.
- Channel edges.
- Scours and flutes.
- Imbricated clasts.
- Mapped extent of channel deposits.

Where these features can be recognised in underground mapping, the observer must understand the depositional nature and geometry of these indicators to be able to successfully interpret the drainage trends. Analysis of these data provides a means to recognise the ancient sediment deposition pattern.

## MAPPING

This paper looks at geological mapping methods that can be utilised to determine distribution of sandstone channels in the roof strata through direct observation and recording of paleodrainage indicators.

Distribution of sediment channels can prove relatively easy to identify where sufficient exposures of the channel base is exposed in the underground workings or where sufficient drilling from the surface and underground can provide information. Where direct exposure of sediment channels may not be found, additional indicators of the presence of a channel include recognition of paleodrainage direction, distribution of depositional facies, changes in stress direction and intensity, flexure of the seam and other clues such as an increase in water dripping can be noted. The thickness and extent of an individual channel determines how great an impact it may have on mining, this also determines how easily the channel system may be mapped and projected.

**Table 1 - Oriented Plant Debris (Tree trunks/Logs) (Measured from grid north) Longwall 2**

Azimuth	Azimuth	Azimuth	Azimuth
047	157	142	152
032	045	043	052
163	152	164	121
157	052	153	158
145	022	149	057
138	070		

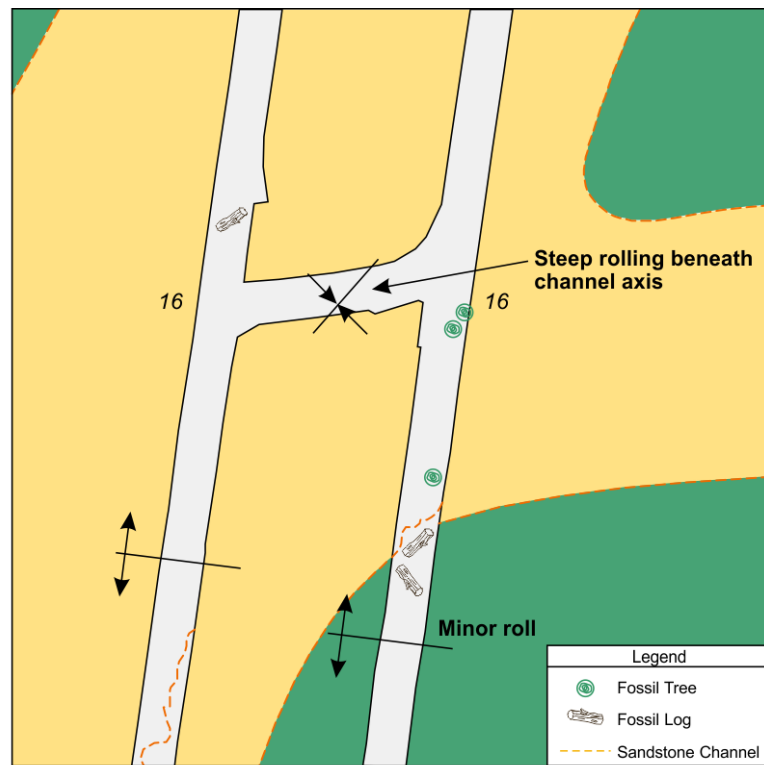


**Figure 4 - Typical roadway mapping detail from Ashton Coal Mine**

Most well developed channels are bounded by levee and overbank deposits. Levee deposits are often characterised underground by the abundance of fossil tree bases, root systems and hummocky layering within the deposit. The overbank deposits can exhibit a variety of sub facies, with drier overbanks having abundant siderite cement, siderite nodules, plant imprints and rootlets while wetter overbank deposits may have greater amounts of carbonaceous plant debris and oxbow filled deposits. Logs and any other long linear plant debris may be found as imprints in all these deposits, in nature plant debris with a long axis is found oriented either parallel to the direction of flow, or at right angles to the flow direction. These features are recorded directly as a mapped oriented feature on the mine plan, or as a compass azimuth reading. Statistical analysis of oriented plant debris is completed by plotting groups of recorded data in rosette diagrams for a specific location and thus represent the direction a channel trends through that area of observation.

At Ashton Coal Mine, since the mine opened to extract the Pike Gully Seam, geological mapping has been completed systematically Geological detail mapped includes rock type, contact trends,

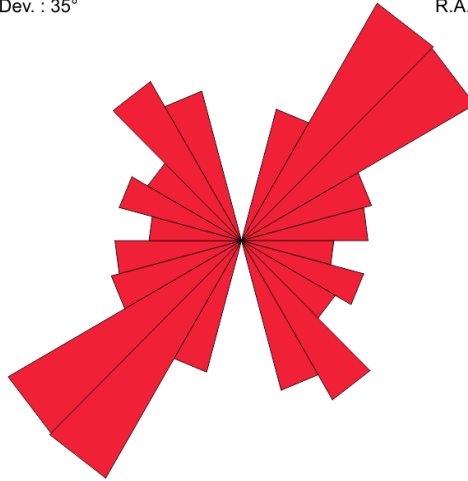
geotechnical condition, and features such as oriented plant debris, and tree stumps (Figure 4). Compilation of the data progressed as mining progressed and was provided to the mine for their running operations, mining is now nearly complete in this seam. Paleodrainage was progressively determined through the analysis of channel edge alignment and oriented plant debris which can be found throughout the workings particularly adjacent channels and mainly in the adjoining levee deposits. Analysis was accomplished by direct plotting the location and orientation of these features onto the mine geological plan (Figure 5). Oriented features can be located and read directly from the mine geological map as an azimuth reading (Table 1), an area of the workings can be selected and the associated data within that area plotted as a rosette graph (Figure 6). This creates a representation of drainage direction at that specific locality, complete analysis of the indicators mapped throughout the completed mapping of the Pike Gully Seam, results in a full analysis of drainage distribution that shows a very positive correlation between the mapped channel distribution and the paleodrainage indicated orientation of the channel (Figure 7).



**Figure 5 - Distribution of mapped channel exposures and distribution of levee deposits in Ashton underground roadway development headings**

Resultant : 112  
 Ang. Dev. : 35°

Area Scaling  
 R.A. Window : 20



Total Data : 13  
 Largest Freq : 12.64%

Figure 6 – Analysis of orientated plan debris forming a paleodrainage rosette

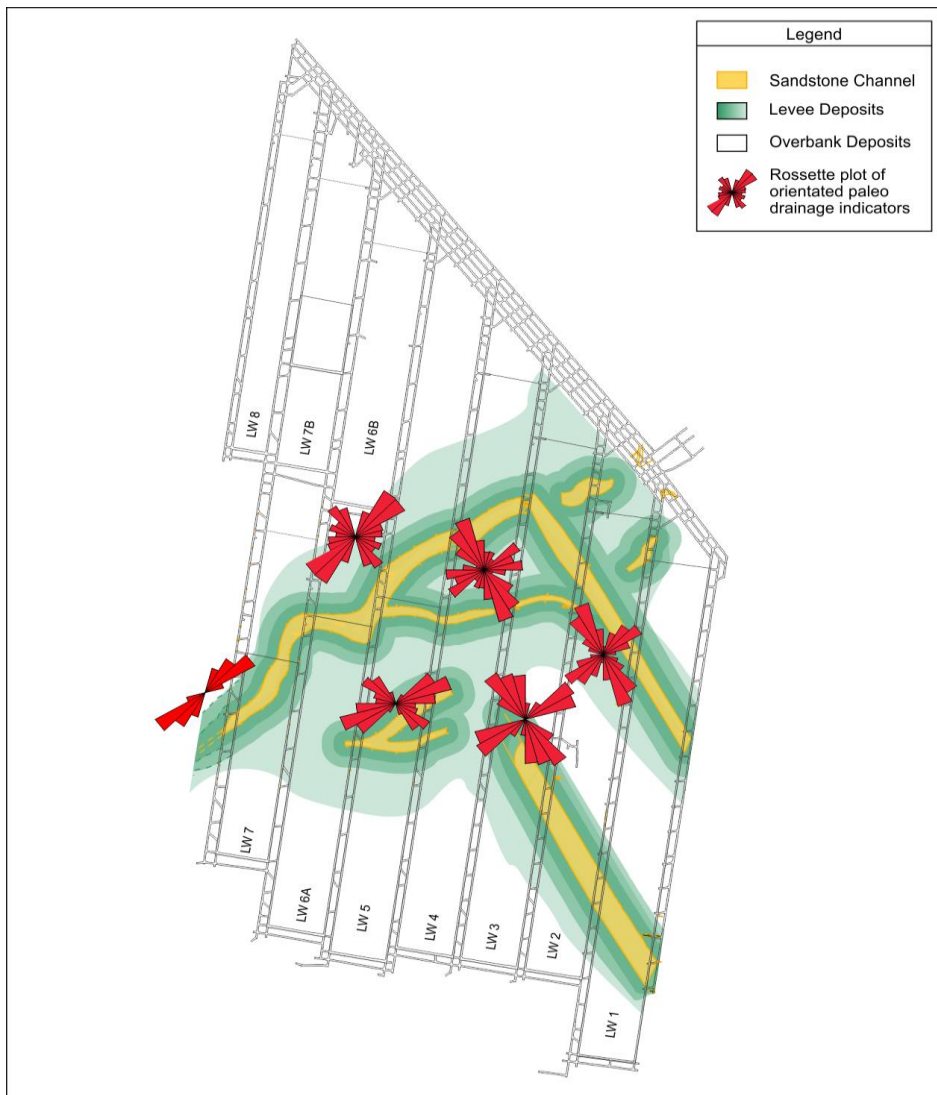


Figure 7 – Completed drainage analysis for the Pike Gulley Seam Ashton Coal Mine

A total of 74 oriented paleodrainage indicators were used to characterise the drainage at seven locations within the Pikes Gulley Seam at Ashton Coal Mine. These were identified in the gateroads within the interpreted levee deposits adjacent sandstone channel exposures.

From the analysis completed, rosette plots of oriented paleodrainge indicators usually show two distinct trends, typically oriented at approximately 90<sup>0</sup> to each other. The two oriented sets show there is a dominant trend and a lesser secondary trend. Comparison with the mapped distribution of the sandstone channel exposures, the dominant trends are found to correlate with the trend of the main channel while the lesser trends correlate to smaller channels which likely represent flood breaches (Crevasse splays) of the levee facies as seen in modern drainages (Figure 3).

### **CONCLUSIONS**

Exposures of sandstone channel within Yancoals' Ashton Coal Mine, Pikes Gulley Seam development roads was sufficient to project the paleodrainage drainage distribution and permit comparison with the mapped oriented drainage direction indicators. Mapping sedimentary facies types and paleodrainage analysis of oriented plant debris defined the sediment deposition trends at Ashton Coal Mine. These are useful methods for projecting the location of sandstone channels and for determining main channel trends and secondary channels. Comparison with modern analogies such as the Mississippi River Basin provides the ability to recognise depositional patterns. Understanding the nature of the channels identified and their distribution can provide valuable information for risk evaluation of the potential impact of the channels on mining and the resultant conditions that may be encountered.

# GEOTECHNICAL DATA FROM GEOPHYSICAL LOGS: STRESS, STRENGTH AND JOINT PATTERNS IN NSW AND QLD COALFIELDS

Stacey Pell<sup>1</sup>, Ross Seedsman<sup>2</sup> and Kim Straub<sup>3</sup>

**ABSTRACT:** In order to appreciate the geotechnical regimes operating at any mine site a comprehensive database accessing all available borehole data is crucial. An extensive geotechnical database across the mine site area must be considered for mine planning and design. Some geotechnical parameters can be defined through the analysis of an appropriate suite of geophysical logs, including the acoustic scanner and sonic velocity logs and by incorporating a strict hybrid logging classification system. The acoustic scanner tool is becoming part of the standard geophysical logging suite used today in all stages of exploration drilling. Analysis of the acoustic scanner log can provide accurate and reliable geotechnical orientation data including joint and horizontal stress orientations. Rock strength data, including massive unit identification, can be calculated using the sonic velocity, gamma and neutron log responses. The study of patterns across three separate sites in eastern Australia shows lateral stress, strength and joint set variability brought about by variations in the geological domain. While vertical variability in rock strength downhole is often observed, the range of downhole variation in borehole breakout orientation and joint set patterns is usually minor.

## INTRODUCTION

In the Australian coal sector, geophysical logs are routinely run in both cored and non-core holes. The primary use of the logs is the identification of coal seams, for which the density and gamma logs are particularly useful. The sonic velocity log is also used to provide estimates of the uniaxial compressive strength (UCS) of the rock and the coal. The acoustic scanner log has replaced the dipmeter and caliper logs in providing information on bedding dips and borehole breakout and has the additional capability to provide orientation information on the joints and other discontinuities that are able to be identified. ASIMS was established in the late 1990's to focus on the interpretation of geophysical logs for geotechnical purposes with the objective of providing reliable estimates of the orientation of horizontal stresses from borehole breakout, the strength of the rock and coal, massive unit identification and the orientation of the dominant joint sets. To date, in excess of 1500 holes have been examined by ASIMS from coalfields throughout the Hunter Valley, Central Queensland, Western Australia and the Southern Highlands, as well as several overseas deposits.

The details of the logging tools and responses have been extensively discussed by others (Weatherford, 2012, 2013). The acoustic scanner tool provides extremely valuable orientation data and there is a strong preference to run this tool in the vertical holes that are typical of coal exploration. The acoustic scanner needs a reasonably smooth borehole wall, and the borehole must be water-filled where the fluid medium is reasonably clear.

Images from the acoustic scanner tool can be used to identify discontinuities within the borehole. The acoustic scanner tool transmits ultrasonic pulses and records both the amplitude and travel time of the returned signal. The amplitude represents the properties of the rock, which is useful for identifying changes in lithology, texture or structure. The travel time represents the shape of the borehole when viewed transversely, and assists in recognising caving due to weaker lithologies, structures or stress.

Vertical holes, both non-core and cored, are of primary interest, where in most cases both the stone and coal intervals produce clear and reliable images. Generally data is interpreted without direct reference to the core, although in many cases core has been available. It is logistically more efficient and cost effective to analyse the scanner data independently as analysis occurs off site. However, a hybrid logging system (Gwynn, *et al.*, 2013) utilising additional data obtained from the core can facilitate a greater understanding of the discontinuities identified.

<sup>1</sup> McElroy Bryan Geological Services Pty Ltd, NSW, stacey.pell@mbgs.com.au, Tel: +61 2 9958 1455

<sup>2</sup> Seedsman Geotechnics Pty Ltd, NSW, sgplross@bigpond.com, Tel: +61 417 279 556

<sup>3</sup> McElroy Bryan Geological Services Pty Ltd, NSW, kim.straub@mbgs.com.au, Tel: +61 2 9958 1455

Analysis of the sonic velocity log produces rock strength data that is extracted via a standard sonic velocity/strength regression relationship. Additionally, massive unit identification is possible utilising the sonic velocity, gamma and neutron logs. Massive overburden units are of particular interest for longwall and pillar extraction.

The full suite of geophysical logs is used to extract reliable stress, strength and joint orientation data. Incorporating the acoustic scanner tool within the suite of geophysical logs used in an exploration program is a relatively inexpensive method of obtaining accurate orientation data, important for both open cut and underground mine planning and development.

### STRESS MEASUREMENTS

#### Borehole breakout versus drilling induced fractures

Stress conditions around a borehole may induce compressive or tensile failure in the rock or coal in the hole wall. For compressive failure, the drill fluids may dislodge the failed material and the resulting deformation is referred to as Borehole Breakout (BBO) and appears as two rounded zones 180° apart. It has a distinct elongated or lemon shaped appearance in cross section. If tensile stresses develop, it may be possible to observe Drilling Induced Fractures (DIF). For BBO, the major principal stress is normal to the plane defined by the axis of the lemon, while for DIF the major principal stress direction is parallel to the axis of the fractures (Figure 1). Zoback *et al.* (2003) suggest they can be readily differentiated, where DIF appears as an open crack and BBO as a zone. BBO is accepted as a very good indicator of the direction of the major principal horizontal stress.

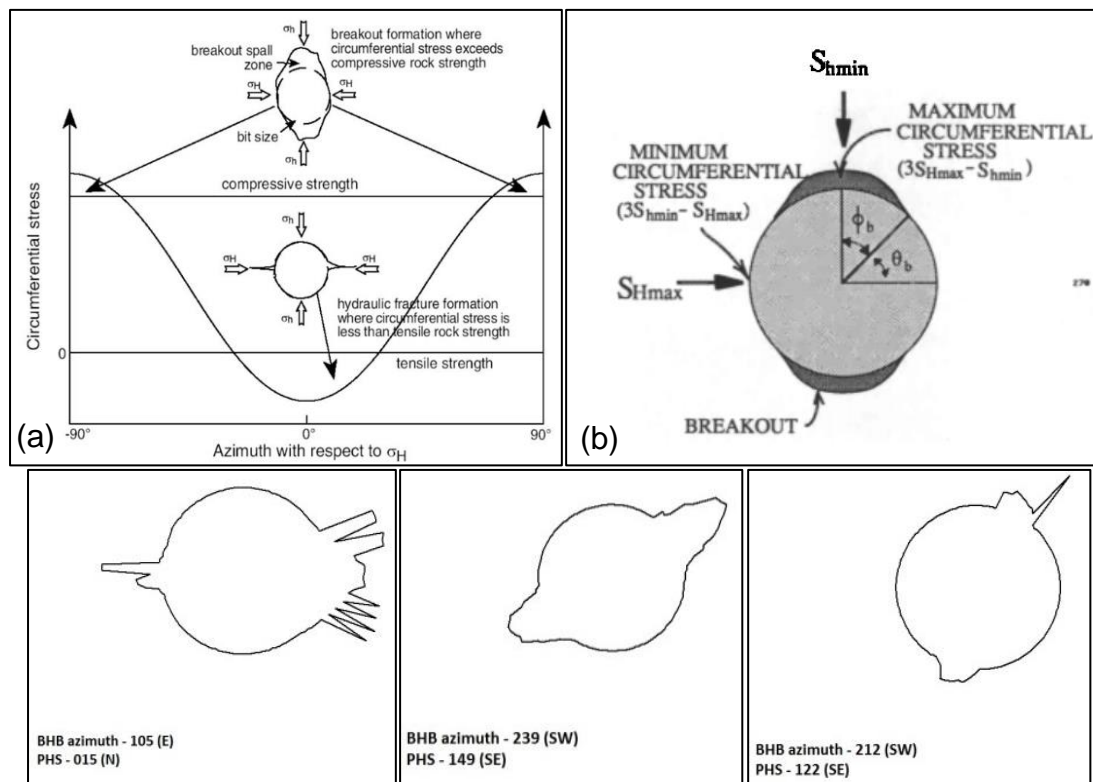


Figure 1 - Borehole Breakout and Drilling Induced Fractures ((a) Tingay, *et al.*, 2008; (b) Barton *et al.*, 1998) and examples from NSW and QLD coalfields

Determining stress magnitudes from BBO has been discussed extensively in the oil sector (Zoback, *et al.*, 2003). The elastic stress redistribution about a hole leads to compressive and shear stresses that can exceed the rock strength. The magnitude of the shear stresses is a function of the stress magnitudes and also the difference between the major and minor horizontal principal stresses. The lemon shape is not reproduced in either elastic or plastic analysis and Zoback *et al.* (2003) suggests that the depth is the result of erosion of failed rock by the drilling fluids. Zoback *et al.* (2003) further suggests that the width of the breakout is the appropriate parameter to use in a simple elastic analysis and defines

the angle of breakout initiation ( $\theta_b$ , Figure 1b). Ignoring temperature effects and assuming the vertical stress is a principal stress, the major principal horizontal stress ( $\sigma_{hmax}$ ) can be estimated as:

$$\sigma_{hmax} = [(UCS + H \cdot 0.0098) - \sigma_{hmin}(1 + 2 \cos 2\theta_b)] / (1 - 2 \cos 2\theta_b)$$

UCS = uniaxial compressive strength, H = depth,  $\theta_b$  = angle from the major principal horizontal stress to start of breakout,  $\sigma_{hmin}$  = minor principal horizontal stress.

It is noted that this model does not include consideration of brittle behaviour (Martin, *et al.*, 1999). It can be seen that independent estimates of the UCS and  $\sigma_{hmin}$  are needed if the major horizontal stress is to be estimated. To demonstrate the sensitivities, if the angle of breakout initiation is  $55^\circ$  in 50 MPa rock at 400m depth, the inferred major principal horizontal stress is 24 MPa if the minor horizontal stress is assumed to be 12.5 MPa or 22.7 MPa if the minor horizontal stress is assumed to be 15 MPa. More significantly, if the UCS is 40 MPa, the major principal horizontal stresses are 18.3 MPa and 17.8 MPa respectively. A 25% change in the assumed strength gives a 25% change in the stress magnitude and a 25% change in the assumed minor stress gives a 6% change in stress magnitude.

### Borehole breakout in Australian coal mines

To demonstrate patterns, sites have been selected in the Southern, Hunter, and Bowen Basin coalfields. Client confidentiality prevents revealing the locations. In some cases the depth and/or orientation data has been transformed to further disguise the sites. The purpose is to discuss the extent of variation at a site, and not to discuss absolute directions. One direction is reported for each depth recorded, being the orientation of a line drawn to the maximum extent of the identified breakout. In some cases the lemon shape is difficult to detect due to other damage to the borehole (Figure 1) possibly associated with additional breakout along joints or small faults.

### Variation within a borehole

The World Stress Map (WSM) project (Tingay, *et al.*, 2008) suggests the highest quality breakout data has a standard deviation of no more than  $12^\circ$ . In Figure 2 and Table 1 it can be seen that the stress direction is generally consistent down the hole for the Hunter and Bowen Basin examples with a standard deviation of  $12^\circ$  in the Hunter hole and  $15^\circ$  in the Bowen Basin hole. This suggests that the horizontal stress direction in these two holes is well defined.

**Table 1 - Orientation data from a single hole and a number of holes in three Australian coalfields**

	Hunter	Southern	Bowen Basin
Single hole			
Number of readings	62	24	9
Direction	$133^\circ$	$143^\circ$	$30^\circ$
Standard deviation	$12^\circ$	$37^\circ$	$15^\circ$
WSM quality ranking	A : within $\pm 12^\circ$	D: questionable	B: within $\pm 20^\circ$
All holes			
Number of holes	19	31	21
Number of readings	350	248	93
Average	$136^\circ$	$119^\circ$	$38^\circ$
Standard deviation	$28^\circ$	$45^\circ$	$41^\circ$
WSM quality ranking	D: questionable	E: not reliable	E: not reliable

### Areal variation of stress direction

When all the orientation data are combined from all holes in a project/lease area (Table 1, Figure 3), the average direction for the Hunter and Bowen Basin cases remains very similar although the standard deviation is higher. For the Southern Coalfield example, the variation within the borehole extends across the project area. In both of the NSW sites, the strike of the major joint set was the same as the direction of the major principal horizontal stress. In the Bowen Basin site, the strike of the major joint set was perpendicular to the direction of the major principal horizontal stress.

No relationship was found between the onset of breakout, the sonic derived UCS (see later) and the estimated vertical stress. It was concluded that the accuracy of the sonic derived UCS and the variation

in the ratio of the major to minor principal horizontal stress for the Australian coalfields (Figure 4) masks any patterns. ASIMS does not provide estimates of the horizontal stress magnitudes.

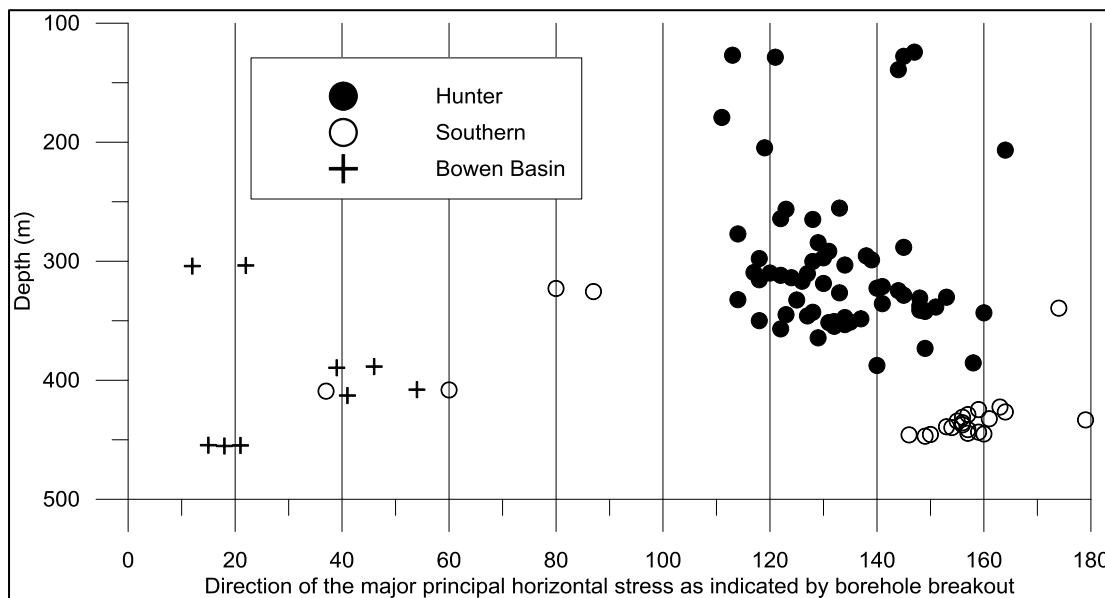


Figure 2 - Variation of direction of the major principal horizontal stress in selected boreholes in three coalfields

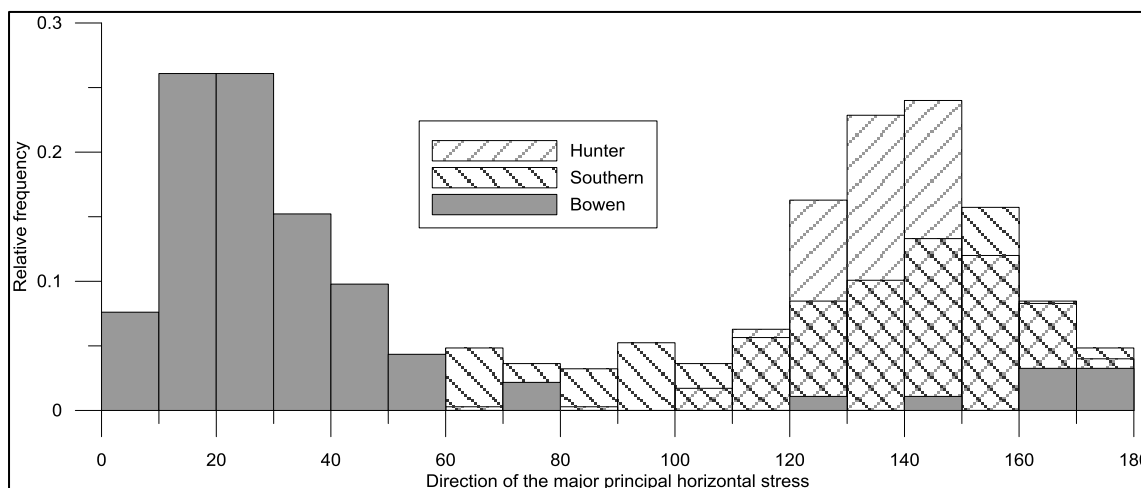


Figure 3 - Areal variation in the direction of the major principal horizontal stress

No DIF has been seen in logs from Australian coalfields. Tensile conditions only generate if the ratio of the major to minor horizontal stresses is greater than 3.33 which is not shown in the Australian data in the WSM (Figure 4). The controversial stress field proposed for coal (Seedsman, 2004) does not produce DIF in a horizontal plane, but could produce BBO in a very low strength coal.

**DISCONTINUITIES**

**Acoustic scanner image**

It is important to emphasise that the acoustic images are differences in false colour in digital images. There needs to be a significant amount of judgement in interpreting the digital image in terms of their geological and particularly their geotechnical significance. Geotechnically, the interest is in discontinuities defined as features in a rock mass with zero or negligible tensile strength. This translates to bedding partings (not textures) and joints/cleats that are not healed or cemented.

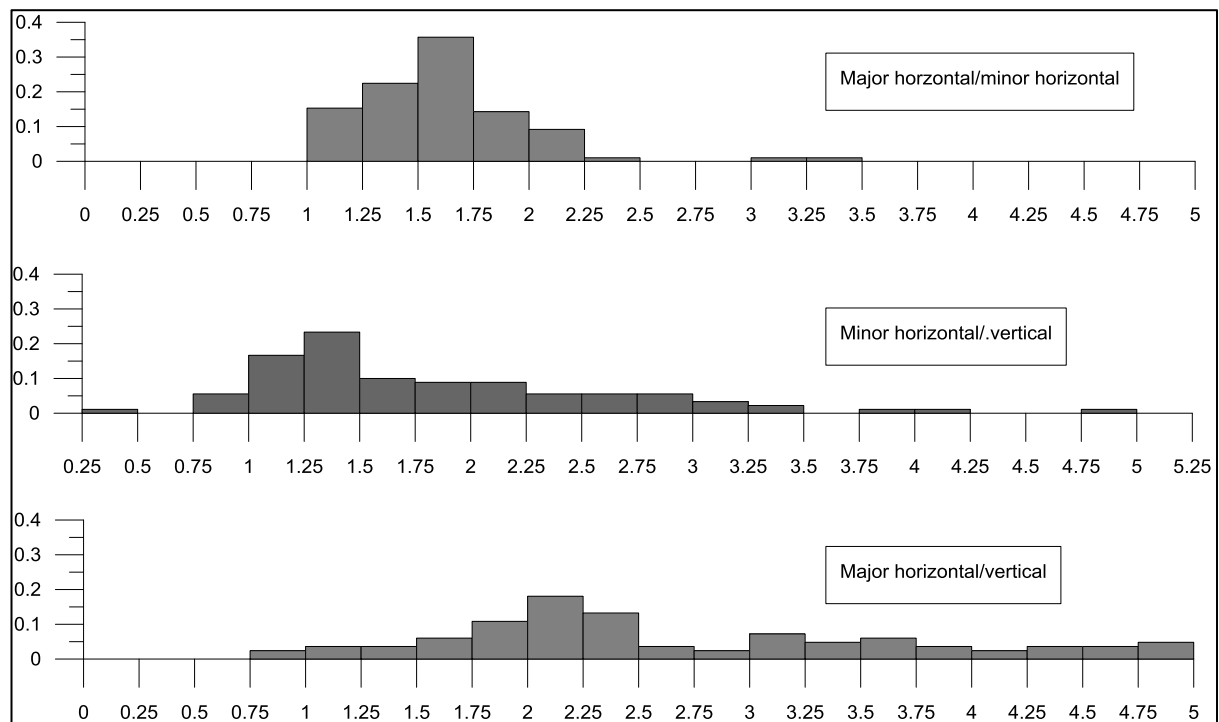


**Figure 1 - Summary of horizontal to vertical stress ratios for NSW and QLD Coalfields (extracted from World Stress Map, 2008)**

Without core, it is necessary to use all the geophysical logs to determine changes in rock properties and lithology, and to identify possible discontinuities in the scanner image. Density is useful for determining stone/coal interfaces and gamma can be used to identify clay units.

There should be an emphasis on picking quality data, where the focus is on identifying small, meaningful data sets from features that fit a strict classification system. By adhering to this system, between one and four major joint set directions can usually be identified within each borehole, using 20 or more features. The most frequent number of joint sets identified is two. Occasionally, these occur as conjugate sets.

Bedding is identified along coal/stone boundaries, such as the top and base of a coal seam or the claystone bands within a seam. Reliable bedding orientations can be identified along these prominent boundaries. Other bedding partings may have textural interest but they are not of geotechnical significance.

Joints and other structures, such as faults, are distinguished by looking at contrast either side of the trace, smoothness and continuity of the trace, and caving in the travel time image.

Coaly bands and siderite can be determined by the colour of the scanner image and the density log.

Another aspect of acoustic scanning that warrants highlighting is the advantage over oriented core. Most oriented core boreholes require angled holes so that the bottom of the hole can be identified by a system relying on gravity. Orientation data collected via this method tends to produce a much larger database, where small insignificant discontinuities are difficult to screen from the larger defects so that meaningful data sets are difficult to obtain (Fowler, 2013).

In Australia most of the coal seams of interest dip at less than  $10^{\circ}$  to  $15^{\circ}$ . With the joints dominantly being normal to bedding there is a bias against intersection of joints in vertical holes. Fortunately the observation that joint spacing in slightly deformed sedimentary rocks tends to be equal to the spacing of the dominant bedding (Price and Cosgrove, 1990) appears to lessen the impact of the orientation bias. Generally, a joint can be identified within the scanner image on average every 10 m to 20 m. Applying the Terzaghi (1965) correction to a 15m spacing and a  $5^{\circ}$  dip this apparent spacing implies a joint spacing of 1.3m, which is a reasonable value for typical bedding spacing within an Australian coal deposit.

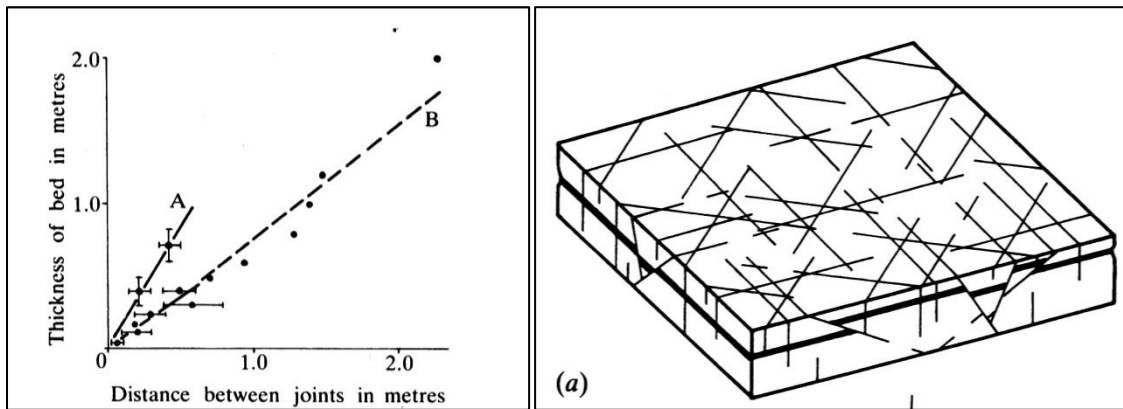


**Figure 5 - Joint models in slightly deformed sedimentary formations (after Price and Cosgrove, 1990)**

### Hybrid logging versus traditional logging

The acoustic scanner image is analysed by experienced geologists who have an understanding of the geotechnical implications of the quality and type of discontinuities picked. The quality of data interpreted is further enhanced where additional detailed geological data collected from the core has been made available. This is known as a hybrid logging system (Gwynn, *et al.*, 2013).

When available, detailed examination of lithology logs, geotechnical logs and core photographs provide further clarity to the discontinuities identified in the scanner image.

For example, a significant horizontal defect such as a fault identified in the geotechnical and lithological logs can be correlated against the scanner image and assigned an accurate orientation. Orientations can be easily obtained for horizontal features in the scanner image. However displacement or truncation of bedding, both indicators of faulting, may not always be readily visible to the examining geologist. In this case without the availability of the additional core data this feature may not be classified as a fault. The hybrid logging system further enhances the identification process such that significant discontinuities are not misinterpreted.

### Joints in Australian coal measures

Price and Cosgrove (1990) define four joint sets over large areas of weakly deformed horizontal sedimentary deposits, two strongly developed, two weakly developed (Figure 5). On borehole to borehole basis, very good data can be obtained, with generally two major joint sets with no rotation down the hole (Figure 6). But over the whole deposit, there is more variation (Figure 7) possibly reflecting the presence of the other sets in the Price and Cosgrove model.

## STRENGTH AND MASSIVENESS

### Estimating compressive strength

For Australian coalfields, it is preferable to use a standard sonic velocity/strength regression line, and one originally developed by BMA and ANGLO for Queensland's Moranbah and German Creek Coal Measures which has a particular focus on the lower strength rocks, has been chosen and is depicted by:

$$\text{UCS (MPa)} = 5785 e^{(-17374/\text{vel})}, \text{ where vel = sonic velocity (m/s)}$$

The method is unlikely to give an accuracy of better than +/-10 MPa at all strength ranges.

This equation has wide applicability and can be used in the Hunter and Southern coalfields of the Sydney Basin. In fact, it is recommended that rock strength testing should be conducted to justify the continued use of this standard rather than to develop a site specific relationship. If developing a site specific line a few points of advice are offered. Firstly the trend lines available in Excel are not adequate to fit over the full range of data. There is a need to assess the engineering application – for roof support

design better accuracy at the low strength range is required, for excavatability better accuracy over the high strength range is preferred.

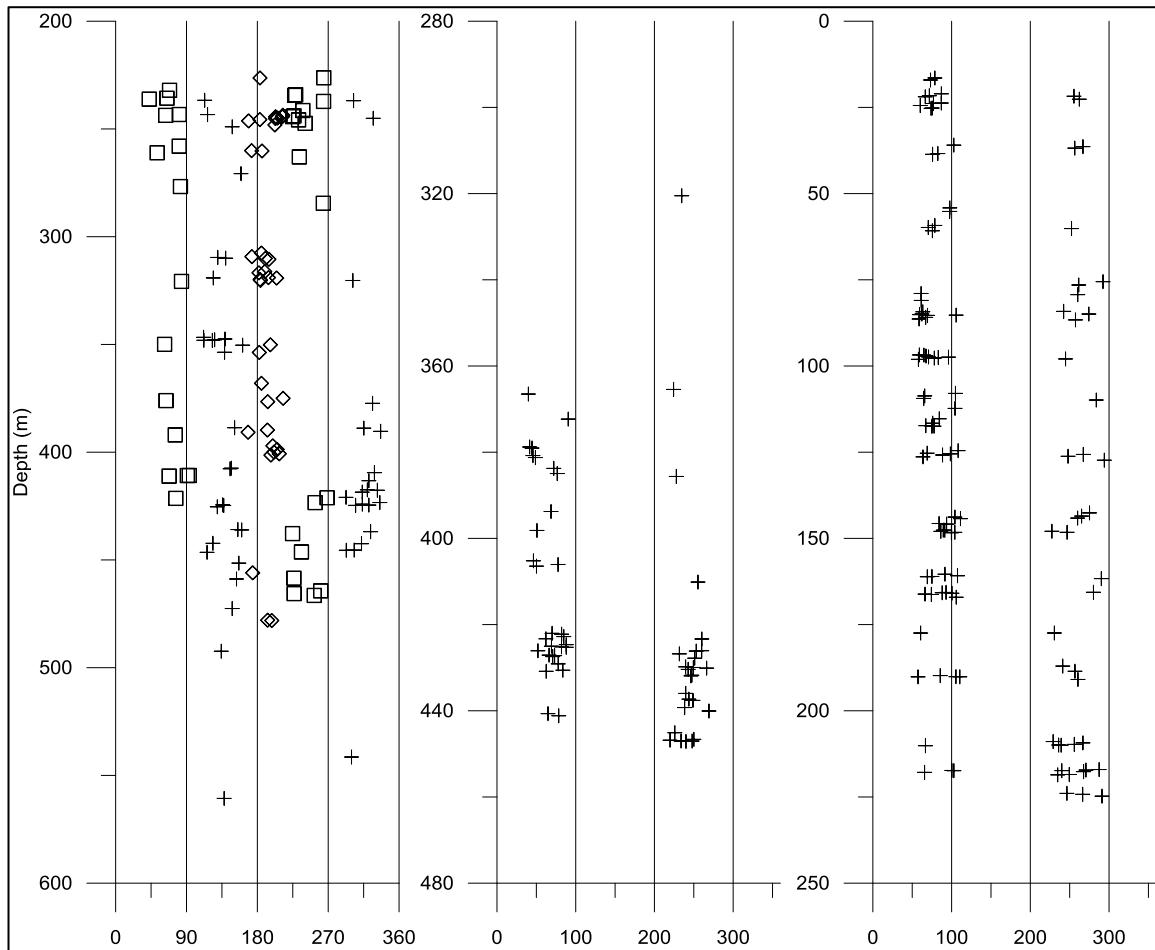


Figure 6 - Typical orientations on a hole by hole basis

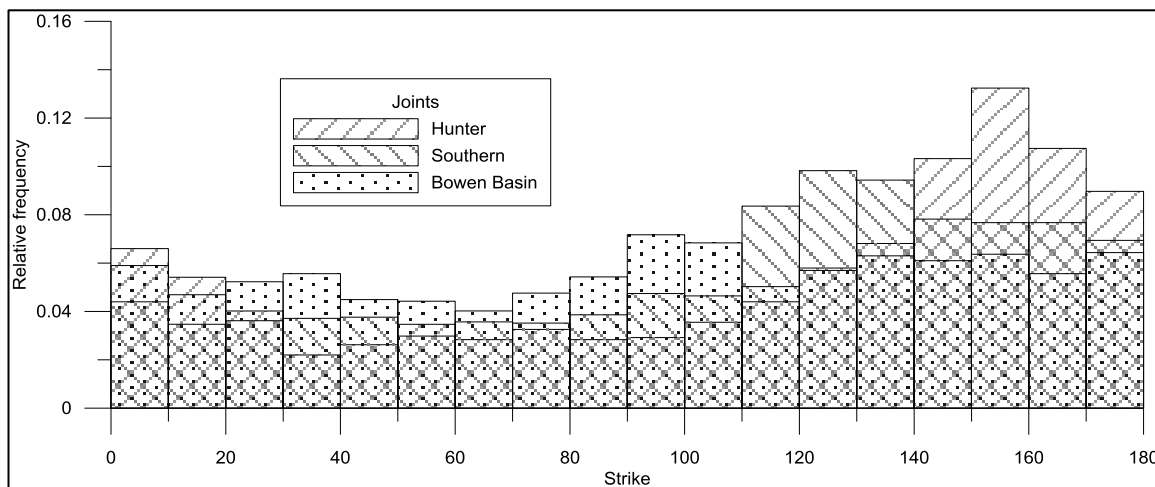
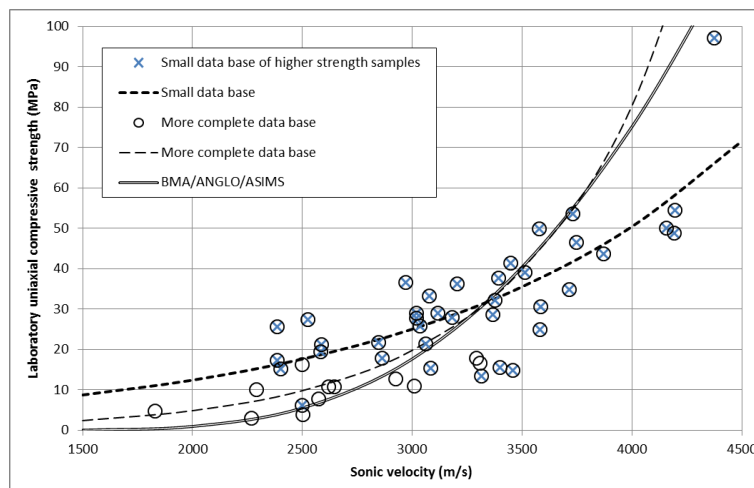


Figure 7 - Compilation of joint orientation over a large area

The data in Figure 8 is provided as a case study on some of the dangers in a site specific line (note that data has been randomised to some extent to maintain confidentiality). In this case study, a small database of high quality testing results had been established which had no low strength rocks. This site specific relationship was used to extrapolate in the lower velocity/strength range. It was apparent that the inferred strengths were much higher than those from the standard line so more testing was conducted. The larger database resulted in a relationship much closer to the standard. There were

potentially very large errors introduced into the engineering design by extrapolating the site specific line for roof support and floor strength purposes (where the concern is with low strength strata).



**Figure 8 - Modified data from a case study on the perils of developing a site specific sonic velocity/strength equation**

### Identifying potential massive units

Of interest for longwall and pillar extraction is the possibility of massive overburden units which can be distant from the target seams and so are often not cored. The presence of massive units may be identified from a uniform sonic velocity (suggesting no change in lithology), or a high energy sandstone/conglomerate unit separated by laterally persistent thinly bedded units. A combination of sonic velocity, natural gamma, and neutron logs can be used to provide an initial estimate of such ground conditions.

For the sonic trace, there are key thresholds in signal noise that can be empirically related to massive units previously identified in core. Coal slivers (for example remnants of trees/branches in a coarse grained sandstone channel deposit) can disrupt the sonic velocity although they do not represent a laterally continuous surface that could disrupt a spanning unit. Also noted, finely interbedded units can produce a consistent sonic trace if the lithological variability is at a scale much less than the spacing of the source and detector in the sonic tool. Fortunately the gamma log can identify this possibility and can be used to dismiss sonic units if they have a high gamma response.

The gamma log can be used to identify laterally persistent bedded units. Here the assumption is made that the bedded units contain the clay mineral illite and that the massive units have negligible illite. In coal measure rocks, illite is one of the very few minerals that contain potassium so its presence can be identified by the gamma daughter product of the potassium to argon decay. As a geotechnical aside it is highlighted that a gamma log will not identify the presence of the other main clay minerals – kaolinite or montmorillonite. In some cases the neutron log is also used to assess massiveness and in this case the assumption is made that the massive unit has a low porosity and low clay content so that there is little hydrogen in the system. The neutron response in the thinly bedded units is assumed to be associated with hydration of any clay minerals.

### CONCLUSIONS

Understanding the geotechnical domain of a deposit is crucial for both open cut and underground mine planning and design. It is clear that extensive and quality geotechnical data is necessary for this understanding to occur. The acoustic scanner log facilitates the collection of this valuable data from all open and vertical holes. It is imperative to use a rigorous classification system to extract only reliable and quality data. Evaluating the nature of the stress, strength and joint patterns within a deposit using the acoustic scanner is further enhanced when incorporating a hybrid logging system. Rock strength and massive unit identification gives extended detail to the geotechnical parameters operating within a mine site.

Identifying patterns on a borehole by borehole basis for an individual site will yield a good range of data but given the broad lateral variation between boreholes will not represent the mine site as a whole. Understanding the geotechnical parameters can only be achieved with a comprehensive database that encompasses the total area to be mined. This approach takes into account lateral variability caused by various geological dynamics.

## REFERENCES

- Barton, A, Zoback, M D and Burns, K L, 1988. In-situ stress orientation and magnitude at the Fenton geothermal site, New Mexico, determined from wellbore breakouts, *Geophysical Research letters*, Vol. 15, No. 5, pp 467 - 470.
- Fowler, M J, 2013. Structural data bias in the digital age, *International Symposium on Slope Stability in Open Pit Mining and Civil Engineering*, Brisbane, Australia, 25 – 27 September 2013, pp 219 - 225.
- Gwynn, X P, Brown, M C and Mohr, P J, 2013. Combined use of traditional core logging and televiewer imaging for practical geotechnical data collection, *International Symposium on Slope Stability in Open Pit Mining and Civil Engineering*, Brisbane, Australia 25 – 27 September, 2013, pp 1 - 13.
- Heidbach, O, Tingay, M, Barth, A, Reinecker, J, Kurfelß, D and Müller, B, 2008. The World Stress Map database release 2008 [online]. Available from: <http://dc-app3-14.gfz-potsdam.de/> [Accessed: 11 November 2013].
- Martin, C D, Kaiser, P K and McCreath, D R, 1999. Hoek Brown parameters for predicting the depth of brittle failure around tunnels, *Canadian Geotechnical Journal*, Vol. 36, pp136-151.
- Price, N J and Cosgrove, J W, 1990. *Analysis of geological structures*. (Cambridge University Press: Cambridge, New York) p 55, p 213.
- Seedsman, R W, 2004. Failure modes and support of coal roof. Ground support in mining and underground construction, *Proceedings 5th International Symposium on Ground Support*, Perth, Australia, September 2004, pp 367 - 374
- Terzaghi, R D, 1965. Sources of error in joint surveys, *Geotechnique*, Vol. 15, pp 287 – 304.
- Tingay, M, Reinecker, J and Müller, B, 2008. Borehole breakout and drilling-induced fracture analysis from image logs. World Stress Map Project [online]. Available from: [http://dc-app3-14.gfz-potsdam.de/pub/stress\\_data/stress\\_data\\_frame.html](http://dc-app3-14.gfz-potsdam.de/pub/stress_data/stress_data_frame.html) [Accessed 11 November 2013].
- Weatherford, 2012. WFT146430 – Slimline logging services [online]. Available from: <http://www.weatherford.com/weatherford/groups/web/documents/weatherfordcorp/wft146430.pdf> [Accessed 11 November 2013].
- Weatherford, 2013. Slimline Services: coal mining and exploration, answer products [online]. Available from: <http://www.weatherford.com/dn/WFT244840> [Accessed 11 November 2013].
- World Stress Map, 2008 [online]. Available from: [http://dc-app3-14.gfz-potsdam.de/pub/introduction/introduction\\_frame.html](http://dc-app3-14.gfz-potsdam.de/pub/introduction/introduction_frame.html) [Accessed 11 November 2013].
- Zoback, M D, Barton, C A, Brudy, M, Castillo, D A, Finkbeiner, T, Grollmund, B R, Moos, D B, Peska, P, Ward, C D and Wiprut, D J, 2003. Determination of stress orientation and magnitude in deep wells, *International Journal of Rock Mechanics and Mining Sciences*, Vol. 40, pp 1049 – 1076.
- Zoback, M D, Moos, D, Mastin, L and Anderson, R N, 1985. Well bore breakouts and *in situ* stress, *Journal of Geophysical Research*, Vol. 90, No. B7, pp 5523 - 5530.

# ROOF SUPPORT CONTROL IN LONGWALL TECHNOLOGY

Petr Novák and Jan Babjak

**ABSTRACT:** The article describes the structure of the selected Support Control System subsystems belonging to the automated longwall equipment complex. It shows some singularities resulting from the application conditions that must be taken into consideration while designing the particular control system, especially power restriction. It demonstrates how the relevant standards of ATEX regulation – coal mine with methane and coal dust explosion hazard – are taken into consideration. The structure of the automated longwall equipment complex is mentioned, emphasizing Support Control Unit (SCU) and meeting the intrinsic safety requirements. The article also describes the external module watch-dog, a communication subsystem, including the solution meeting the intrinsic safety requirements. The technical solution of low-input energizing of electro-hydraulic valves within the limited power conditions is presented.

## INTRODUCTION

Modern technologies of black coal mining have necessitated application of automation in this area of human activity. One of the possibilities in mining is longwall technology. It involves a system of automated mining support consisting of a line (up to a few hundred) of hydraulic roof supports. This line forms a longwall where the mining equipment (shearer or coal plough) moves (see Figure 1). At the same time, the hydraulic roof supports ensure safe movement of persons operating and servicing the equipment. In connection with work in explosion-hazard areas (methane in the case of coal mines), increased requirements are placed on this equipment.

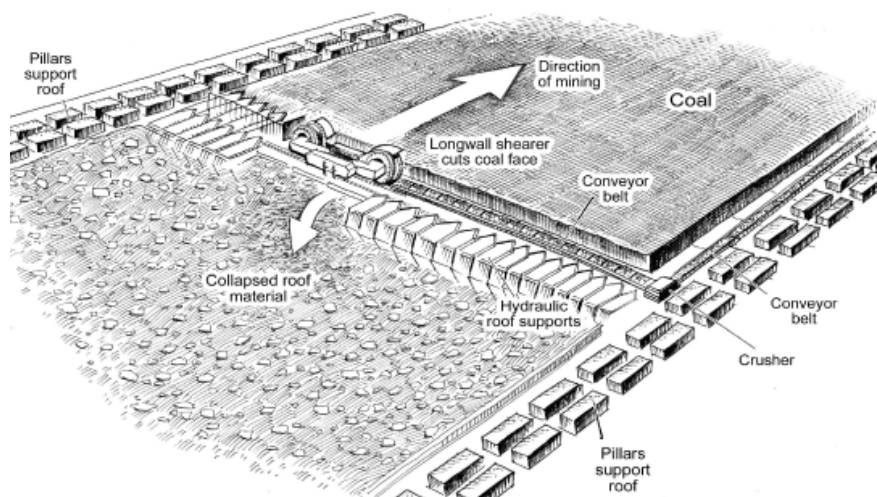


Figure 1 - A typical underground mining operation using longwall mining techniques

## AUTOMATION

Automation is primarily based on the fact that by means of their hydraulic drives, hydraulic roof supports can move the track of the conveyor to the space left after drawing coal, and subsequently, the support can be pulled to the conveyor. Thus, the whole mine excavation (longwall) is gradually shifted in the direction of mining and simultaneously there is controlled caving at the back of the longwall.

For the operator of individual supports, the hydraulic medium is used and it is conveyed by arterial line to the individual parts of the support. Each support is equipped with electro-hydraulic valves controlling individual support functions (their number differs with respect to the facilities and the customer's

particular needs and ranges from 8 to 32 functions). For automated control of these electro-hydraulic valves, each support has its own embedded control module - Support Control Unit (SCU).

### CONTROL SYSTEM OF AUTOMATED MINING SUPPORT

The control system for longwall mining technology consists of three parts. In the aboveground part of the mine there is a central computer, a Surface Monitoring System (SMS) intended for remote monitoring and administration of the equipment located underground. In the main gallery near the longwall (usually as a part of power-train) there is Headgate Control Unit (HCU), synchronizing the work of individual supports and the mining equipment itself. The last part of the control system is formed by Support Control Unit (SCU), one for each support – see Figure 2.

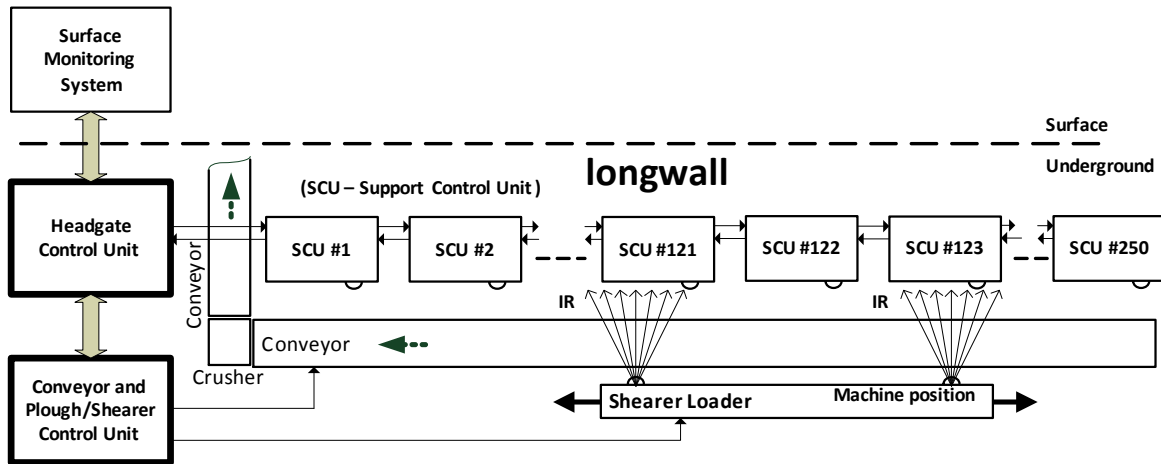


Figure 2 - Longwall – the control system hierarchy

These SCUs are designed in accordance with the relevant standards for work in the environment with explosion hazard based on ATEX Directive.

Described control system SCU is intended for use in environments with potentially explosive methane atmospheres – mines with “I M2 Ex ib I Mb” classification.

- I - Group I: Mines where methane may be present
- M2 (Mb) - Electrical parameters. These products are intended to be de-energised in the event of an explosive atmosphere.
- Ex - Explosive gas atmosphere
- ib - Apparatus - which is adequately safe with one fault and a factor of safety of 1.5 is considered safe for use in less frequently hazardous areas (Zone 1).
- Nothing - For normal thermal conditions (-20 to +40°C) – not marked.

The type of protection “Intrinsic Safety” is based on the principle of current and voltage limitation within an electric circuit/unit. The energy from a power circuit capable of causing an explosive atmosphere to ignite is thus limited to such an extent that the surrounding explosive atmosphere cannot ignite as a result of sparks or inadmissible surface heating of the electrical components.

The type of protection “Intrinsic Safety” is particularly used in measurement and control technology, as no high currents, voltage and capacities are required here.

Intrinsic safety permits the use of conventional instrumentation cables and cases, thus reducing costs. The intrinsic safety technique is the only technique that permits live maintenance within the hazardous area without the need to obtain ‘gas clearance’ certificates. This is particularly important for instrumentation, since fault-finding on de-energised equipment is difficult.

Many international standards for intrinsic safety exist throughout the world. The most influential of these is the European Committee for Electrotechnical Standardization (CENELEC). There are several test laboratories authorized to issue approvals of intrinsic safety equipment to CENELEC standards. In North America, these regulations must be verified in each province, state or city since individual locations can differ in their installation and/or application of intrinsic safety. The same is true in Europe where

regulations are subdivided into European (EU) and national requirements. The European standards define the general specifications and the detailed guidelines for methods of protection against explosion. The national requirements primarily contain installation requirements. Control module supply for the individual supports is realized by means of a mining power-supply unit in a flame proof enclosures. One unit is able to supply a group of 3-4 intrinsically safe SCUs, connected to a 12V supply branch in parallel - through internal barriers created by imbedded Zener diodes.

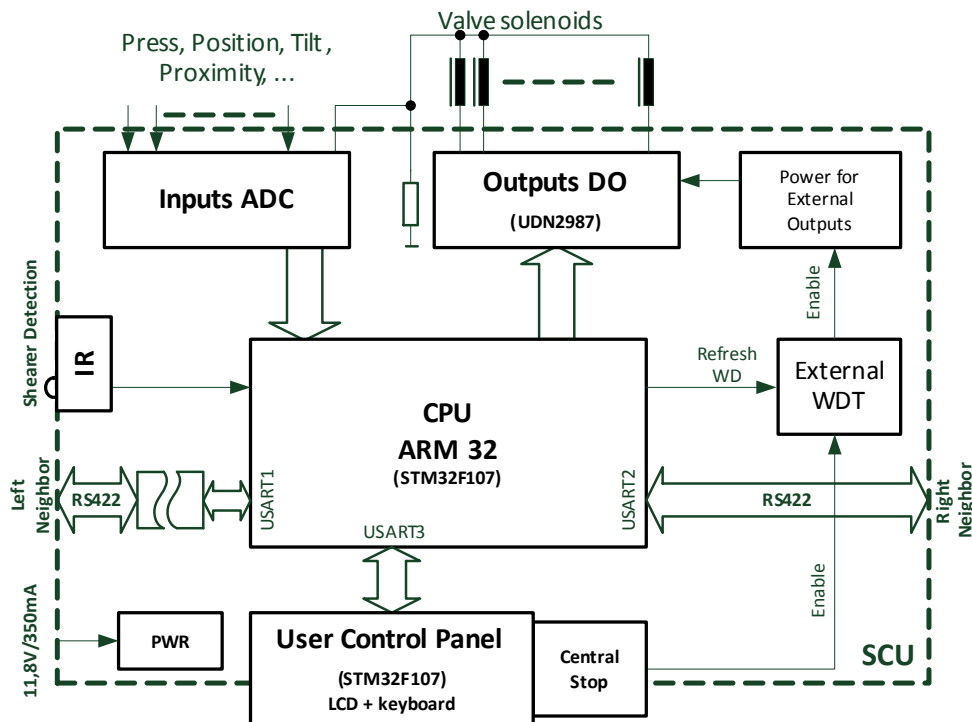


Figure 3 - Schematic diagram of the SCU

Maximum power take-off on each of these devices is defined by standards EN 60079-11 and EN 60079-25 and for a developed system it corresponds to the current of 350 mA at supply voltage 12V (11,8V). This current is limited by a fuse in the unit, which ensures that even in case of the particular device failure, power take-off will not reach the value that could cause thermal impact with a hazard of initiating ignition or explosion. It is necessary to realize that this current supplies both the SCU control system itself and all the action members (solenoids of electro-hydraulic valves) and sensors. This must be considered while selecting them, and also in the way the action members (up to 32) with power take-off approx. 120/60 mA a piece are controlled (see below). Typically used sensors are: absolute sensor monitoring the movable cylinder position, hydraulic pressure sensors, IR sensor for detecting the plough in front of the particular SCU, inclinometer(s), induction contactless position sensors and possibly SCU wireless receiver remote control.

### CONTROL SYSTEM SAFETY

Safety of intrinsically safe devices is ensured by several different means. On the supply side, the device is equipped with protective fuse and intrinsically safe barrier. Mutual data communication between individual sections is realized by means of metallic interface RS422 with opto-isolation of individual sections, which eliminates potential fault currents, equalizing the differences in potential in individual parts of the longwall with separate power supply – see Figure 4. If an appropriate technical device (jumper wire) is used, the conception of the power supply system enables to distribute supply voltage from the neighbouring device (on the left). One source thus typically supplies 3 – 4 SCUs.

The control system is also equipped with local stop button for the corresponding part of the longwall, which ensures that within the defined area of the button activation, all support motion functions will be immobilized. This action on a particular support(s) cuts off supply of an individual action members. This shutdown will be realized both through the control logic (by means of activating the corresponding

control microprocessor subroutine) and independently – by activating logical circuits outside the control processor. This enables safe shutdown also in case of a control processor fault in the particular section.

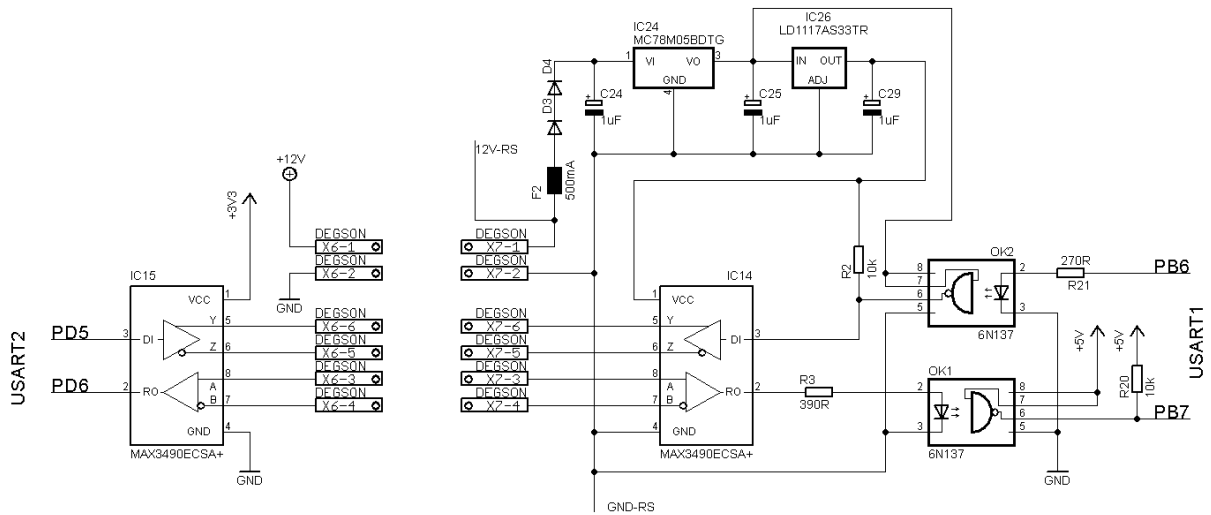


Figure 4 - Circuit of communication subsystem between SCU (optical isolation)

Information on emergency out activation is also transferred by data line to adjacent supports, whose shutdown is, however, only ensured by the SCU logic of the corresponding support.

Another safety element is a set of separate monitoring circuits (Watchdog), which monitors proper function of SCU control processor and in the case of a fault, it can deactivate support also without the need to press the local stop button – see Figure 5.

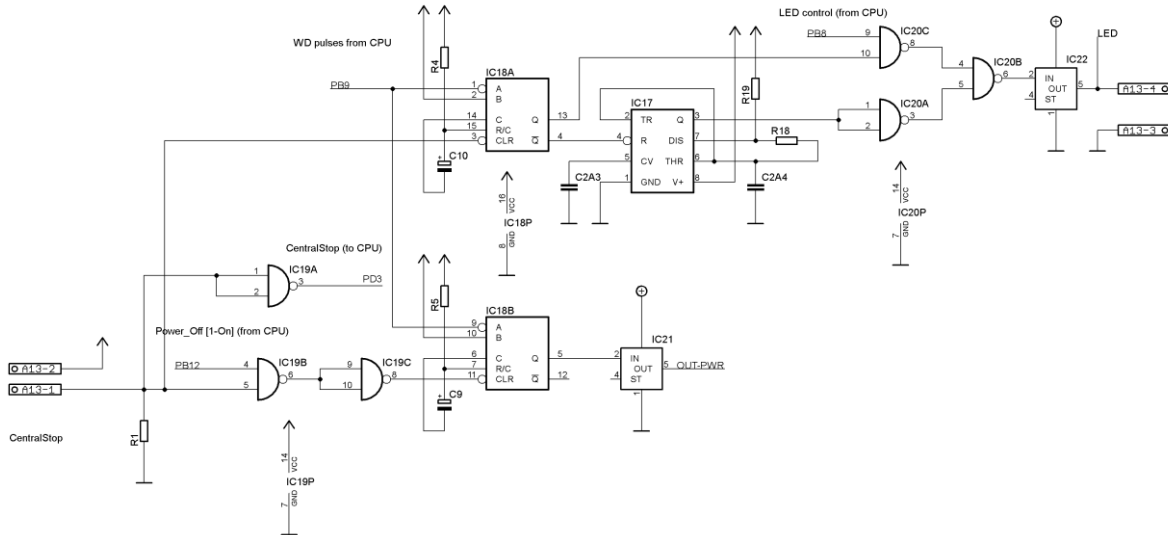


Figure 5 - Example of the external independent watchdog and warning light controller

COMMUNICATION

Communication between the longwall HCU and the SCU's (up to 250 units), and mutual communication among SCUs is realized by means of a full duplex galvanically separated bus with the interface RS422, brought from one SCU to the adjacent one, each SCU forming a transparent reciprocal communication bridge.

Each SCU has its own 1-byte address (ID) and for the sake of simplicity, it is assumed that it forms a regular line from 1 to 250 for the purpose of this text. (However, for operational reasons, it is not always the case in practice). The basic structure of the telegram is showed and explained in Figure 6. The

telegram heading is the telegram type: order, request, and reply. The listener corresponds to SCU ID address, where the telegram is sent. The talker corresponds to the sender of the telegram. It is followed by detailed information concerning the message type - message code and possibly data message 4 – 32 bytes long (it depends on message code). The whole telegram is finished by a 4-byte checksum CRC-32 (Ethernet). If the accepted telegram is not related to it (Listener ≠ ID) – it will simply start forwarding it to the adjacent SCU – see Figure 7.

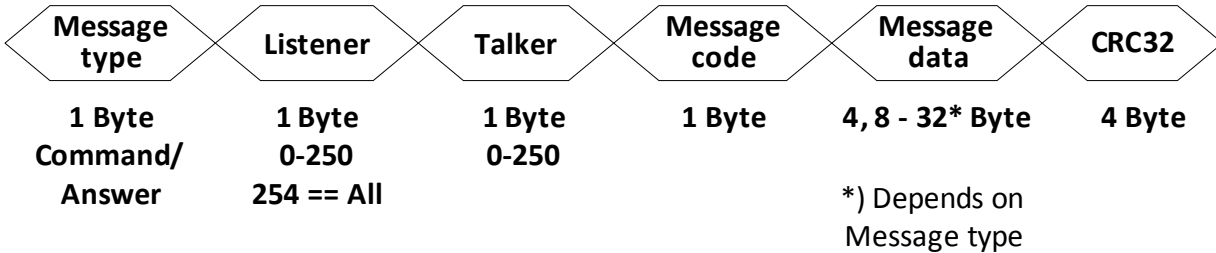


Figure 6 - Telegram structure

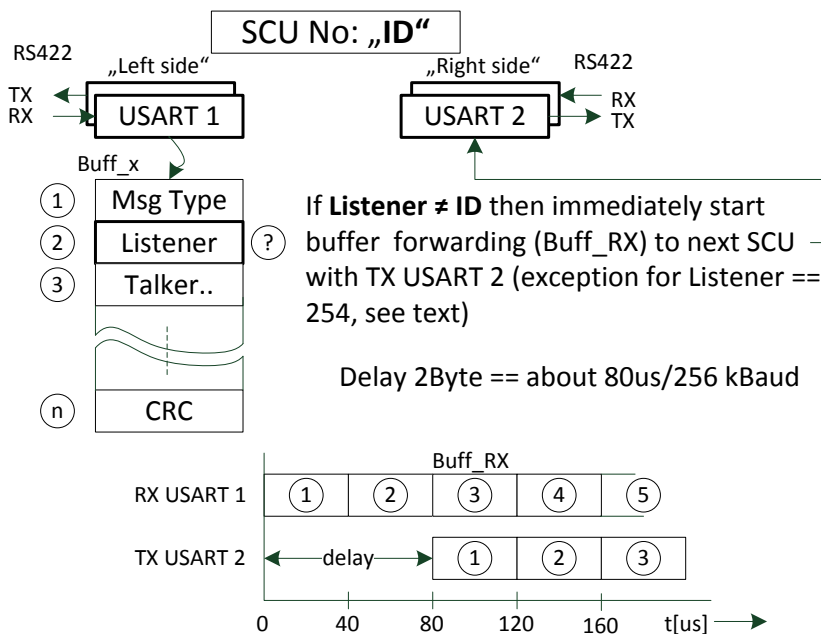


Figure 7 - Communication (only one direction is illustrated)

If the particular telegram concerns this SCU, it is processed after having been completely accepted and according to its type, it responds or forwards the message like in the above mentioned case. The address Listener == 254 is assigned for addressing all SCUs simultaneously – e.g. at the request concerning the current position and direction of the shearer loader machine.

In reality, e.g. in the longwall with 250 SCUs, the longwall HCU can communicate with the 250<sup>th</sup> SCU by gradually transferring the telegram from the 1st SCU to the last, the 250<sup>th</sup> one. The potential response to the particular order/request will proceed in the opposite direction. At the same time, SCUs can communicate mutually (typically in an automated mode).

For communication speed of 256 kBauds, the time lag in forwarding the telegram within one SCU is 2Byte, which corresponds to about 80µs – see Figure 7. The maximum time lag between sending by the talker and accepting by the listener will be in the situation when the telegram/message from HCU is sent to the last one, e.g. 250<sup>th</sup> SCU. In this case, the time lag is compliant with the necessary control dynamics and it is 250 x 80µs = about 20ms.

### CONTROLLING SOLENOID FOR THE ELECTRO-HYDRAULIC VALVE

The significant element of the hydraulic roof support control system is a group of electro-hydraulic valves which are energized from the SCU. In some phases, the mining technology requires simultaneous function of several of these electromagnetic units, therefore it is necessary to ensure their minimum consumption. For this purpose, it is possible to use the solenoid coil property; the coil requires multiple-higher current for bringing the coil core closer, compared to the current which is sufficient for keeping it in an active position.

Electronic circuit realizing the above mentioned current limitation is usually integrated directly in the solenoid body. The principle of the solution is based on using series resistance in the batch with the coil; when it is switched on, the resistance is spanned by a semiconductor element for a moment. This interval can be determined by changing the value of R-C member parts for the used timing circuit of the 555 type – see Figure 8. As the graph below shows, this procedure enables the value of the necessary current to be lower for the active valve up to one half (from the initial value 115mA to 56mA) – see Figure 9.

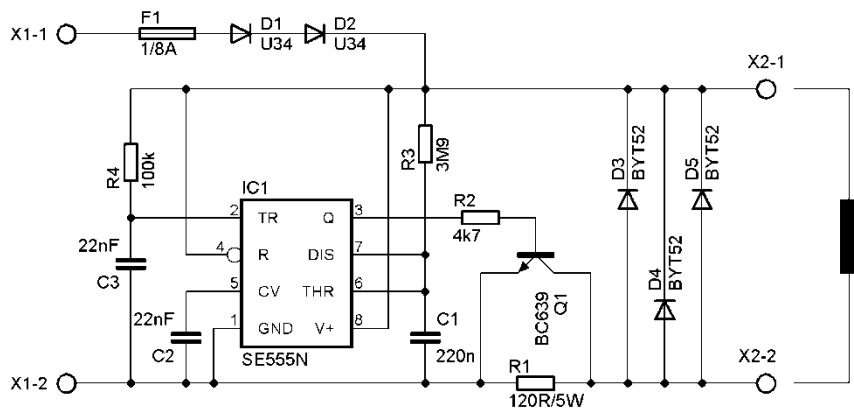


Figure 8 - Electronics of the solenoid

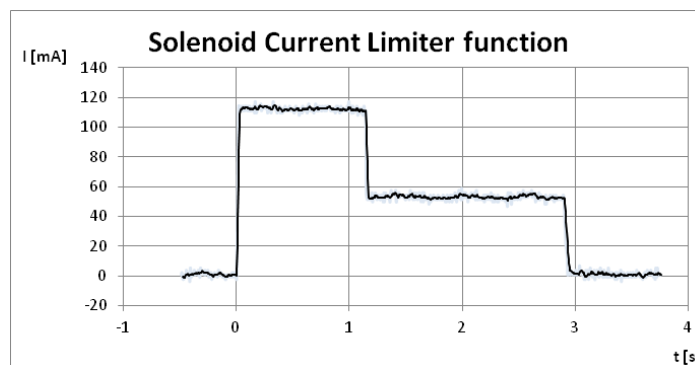


Figure 9 - Current time response of the energised solenoid

This time is necessary for safe mechanical repositioning of the valve and its stabilization in an active position. Owing to this, it is technically possible to energize 3-4 solenoids simultaneously from an intrinsically safe system with limited power; the solenoids are switched gradually with a time lag approx. 1.2 s.

### SOFTWARE SAFETY

While developing software for mining equipment control systems, it is necessary to consider and respect safety requirements and requirements for functioning in all the possible conditions and failure states. The programmers have a number of recommendations at their disposal on how to proceed while creating and subsequently testing the control application. One of the universally accepted standards (however, not required by the regulations) includes a set of rules, originally issued by "Motor Industry Software Reliability Association" under the title MISRA-C. It is a set of guidelines for the programmer

resulting in code safety, transferability and reliability within the context of integrated systems programmed mainly in the ISO C language (There is also a set of guidelines for MISRAC++).

Microprocessor control systems and their software are also considered in the IEC60335 standard, dividing the equipment reliability into three categories:

- Class A – the equipment safety does not depend on software
- Class B – the equipment safety depends also on software
- Class C – software also ensures prevention from special risks (e.g. explosion)

For the development of the mining section control system, it is necessary to consider the requirements for Class B category (Class C category safety is intended for special applications and, besides other things, it is ensured e.g. by redundant check while using more CPUs and it is not necessary for support control applications).

If the application safety depends on electronic components, it must stay safe even after two consecutive defaults. The software is not taken into account for the first failure: the application must be safe with one hardware failure and MCU not operating under reset or CPU not operating properly. Annex Q of IEC60335 defines precisely in which conditions a class B software is required (see Figure 10)

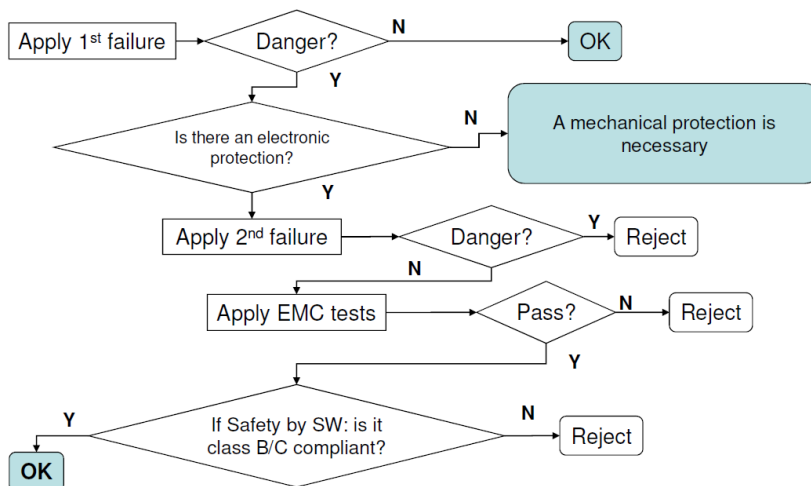


Figure 10 - IEC60335 test flow diagram (simplified)

For developing control system in compliance with these requirements, the producer of the microcontroller usually offers both software and hardware tools.

- Hardware standpoint – Dual watchdog architecture on chip (one has its own independent clock (Resistor - Capacitor oscillator based), the other is windowed). Both are started by hardware (option byte in flash, not depend on software). Dual internal RC oscillators and versatile clock circuitry allows frequency deviations detection.
- Software standpoints – Class B self-diagnostics routines for microcontroller (RAM, Flash and core integrity testing).

Application of these tools enables the creation of a control system which can ensure defined behaviour (mainly safe shutdown) after detecting various faults in the equipment electronics, like the CPU programmed memory damage and other problems (interference, power supply drop, processor hourly signal failure). Testing can be carried out in two modes:

- At power-up
  - CPU registers self-test
  - Watchdog self-test (even if not directly required by the standard)
  - Flash integrity check with a 16-bit CRC
  - RAM function test (using March C –algorithm)

- External clock frequency measurement
- A "self-test start up" including function calls and logical sequence monitoring
- During run-time
  - CPU registers self-test
  - Transparent RAM functional test (March C and March X algorithm available)
  - External Clock frequency measurement
  - Stack overflow monitoring (even if not directly required by the standard)

A number of these tests are supported by some ARM processors from both a technical and a software standpoint. Safe software must be able to detect the above mentioned problems and respond in a defined, programmed way, to ensure safe shutdown, to alert the operators or possibly to carry out automatic restart and assess whether the problem lingers on.

## CONCLUSIONS

The article described the construction of the control system intended for the hydraulic roof support control used in longwall mining techniques – see Figure 1. It specified the ATEX requirements for a coal mine with methane and coal dust explosion hazard. The SCU control system is designed as intrinsically safe. It also characterized the conception of the external Watchdog Timer (WDT) circuit monitoring SW run and controlling the action members – electro-hydraulic solenoids – supply. As far as energising electro-hydraulic valves is concerned, the article described how they are controlled with reduced consumption. It also characterised the communication subsystem on the basis of the bus RS422, including the telegram format with CRC securing. The telegrams are transferred among up to 250 SCUs with emphasis on minimisation of time lags.

## REFERENCES

- Paul S. Babiarz *Intrinsic Safety Circuit Design*. 19 p. <[www.omega.com](http://www.omega.com)>.  
ARCH COAL, INC., Annual report 2010.  
MTL Instruments Pty Ltd, *AN9003 - A Users Guide to Intrinsic Safety*. 20p.  
R. STAHL SCHALTGERÄTE GMBH, *Basics of Explosion Protection – Introduction to Explosion Protection for Electrical Apparatus and Installations*. 36p, S-SD-02-E-07/99 · Printed in Germany.  
STI Scientific Technologies GmbH *Applying Intrinsic Safety*. 9p.  
EN 60079-0 Explosive atmospheres - Part 0: Equipment - General requirements.  
EN 60079-11 Explosive atmospheres - Part 11, Equipment protection by intrinsic safety "i".  
EN 50271:2010 Electrical apparatus for the detection and measurement of combustible gases, toxic gases or oxygen - Requirements and tests for apparatus using software and/or digital technologies.  
ATEX - Directive 94/9/EC on equipment and protective systems intended for use in potentially explosive atmospheres (ATEX)  
<http://ec.europa.eu/enterprise/sectors/mechanical/documents/legislation/atex/>.

# DEVELOPMENT OF A METHOD FOR LONGWALL TOP COAL CAVEABILITY ASSESSMENT

Terry Medhurst<sup>1</sup>, Rudd Rankine<sup>2</sup> and Michael Kelly<sup>3</sup>

**ABSTRACT:** Prediction and assessment of caveability for Longwall Top Coal Caving (LTCC) operations remains problematic. Whilst operating effectively in China for some years and having recently been introduced into Australia, there remains limited information and methods for predicting optimal coal recovery and productivity under Australian conditions. This paper describes the development of a novel approach to LTCC assessment. This involved the development of a coal failure and breakage model and then simulation of the LTCC process using a hybrid FLAC/PFC model. In order to establish key parameters for coal fracture, a Synthetic Rock Mass (SRM) modelling process was used to examine a range of variables such as particle size, clumping logic, contact strength, and fracture energy and how they relate to the strength, stiffness and dilation behaviour of the coal. This was processed was calibrated using triaxial test data. Simulation of the LTCC process used a Particle Flow Code (PFC) model of coal behaviour based on the SRM results embedded within a FLAC model to allow simulation of both far field and near field effects. This allows the influence of depth, mining induced stresses, goaf behaviour, weak and strong overlying strata, to be superimposed on the near field caving response. The main outputs from this modelling process include a measure of caveability or recovery and draw profile; and the effect of operating controls upon them.

## INTRODUCTION

BHP Billiton Mitsubishi Alliance (BMA) is currently in the process of implementing the Longwall Top Coal Caving (LTCC) mining method at Broadmeadow Mine (BRM). As part of studies on various aspects of the proposed operation, BMA commissioned MineCraft Consulting Pty Ltd (MineCraft) and PDR Engineers Pty Ltd (PDR) to develop a caving and materials handling model for input into their productivity assessments. The project had two broad aims, namely:

- To develop a generic modelling tool for LTCC extraction that provides an ability to assess potential mining reserves and production capacity for current and future projects;
- Undertake an analysis of the proposed Broadmeadow operation as a starting point for model development and productivity assessment, thereby providing the opportunity for further calibration and ongoing improvement.

LTCC extraction is heavily dependent on the behaviour of the top coal itself followed by the manner in which the caving sequence is managed. Distinct Element (DEM) analysis was identified as a one of the few methods in which to address caving behaviour via simulation of rock failure and breakage, then the subsequent gravity flow of broken material. These methods however are highly computationally intensive, which require the problem to be separated into two parts, namely:

- Coal Failure and Breakage Model– which is designed to simulate the caving process over the selected range of mining conditions and cover depths; with a corresponding estimate of the volume and size of material delivered to the rear AFC;
- Materials Handling Model– which is designed to simulate the rear door sequencing process over a selected range of door opening times; with a corresponding estimate of throughput.

The project was aimed at addressing several key feature of LTCC extraction. In particular, a suitable combination of cutting height and support geometry is required to maintain face stability whilst achieving the desired caving behaviour. It is commonly accepted that caveability depends on several factors including coal strength characteristics and cleating, mining induced stresses, cut height and seam

<sup>1</sup> Principal Engineer, PDR Engineers Pty Ltd, tmedhurst@pdrengineers.com.au, Tel: (07) 4051 5599

<sup>2</sup> Senior Geotechnical Engineer, PDR Engineers Pty Ltd

<sup>3</sup> Senior Manager – Directional Studies, BHP Billiton Mitsubishi Alliance

thickness as well the influence of the overlying strata. Moreover, the sequence and timing of rear door caving operations will also affect the development of the drawzone.

One major question is how much the drawzone will influence face stability, associated support load and ultimately coal recovery. In order to establish the size of the cave zone, a means to assess the level of fracturing within the coal seam is needed. This paper describes the development of the coal breakage and failure model and key results arising from the analyses.

### CHALLENGES FOR CAVE MODELLING

Cave prediction and modelling present one of the most challenging areas of analysis in geomechanics today. At the heart of these predictions is the ability to capture the right failure mechanisms and to estimate the rock mass properties that govern this behaviour. Failure of rock masses at low confining stress, as is the case for LTCC, is a complex process in which the role of both joints and cleat as well as the strength of the coal blocks itself plays a role.

Tensile cracking leads to a unique failure process (slabbing) that is inconsistent with conventional shear based failure criteria. In this case rock mass strength is controlled by damage initiation mechanisms that are relatively insensitive to confinement and by fracture propagation (extension) mechanisms that dominate at low confinement. For brittle rock, the strength envelope can be represented by a multiphase linear failure envelope illustrated in Figure 1.

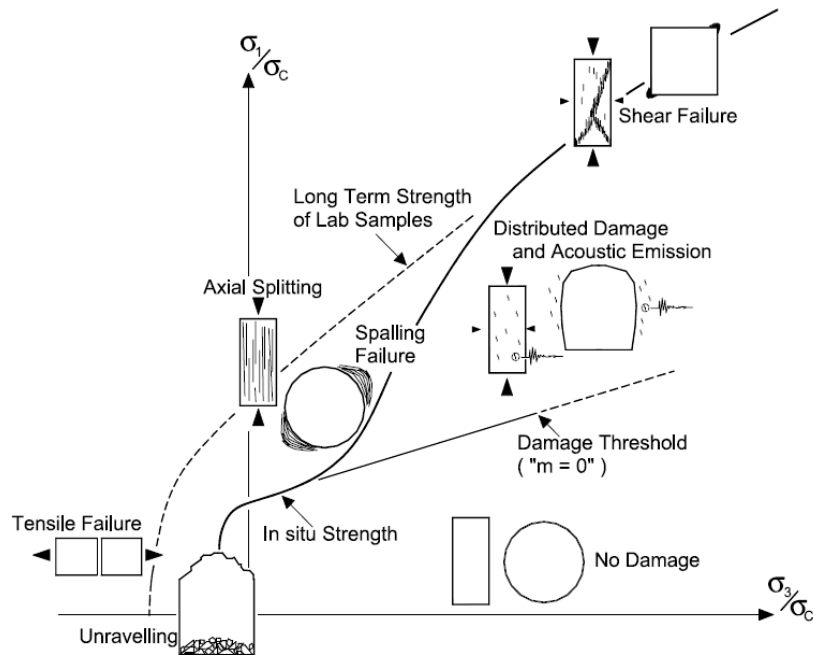


**Figure 1 - Schematic failure envelope for brittle failure (Diederichs, 2003)**

The most important aspect of this representation of failure behaviour is that different failure mechanisms reflect different estimates of rock mass properties. These properties depend on the stress path leading to failure and the role the discontinuities might play in the failure process.

The process of LTCC extraction can involve several failure mechanisms involving gravity driven failure such as unravelling or tensile failure at the cave boundary, axial splitting due to abutment loading above the longwall supports and shearing at seam contacts and along bedding in the overlying strata. This requires models that can capture these processes. The use of DEM analysis is one of the few methods that can be used to simulate rock failure and breakage under conditions of differing stress paths (or loading conditions). The basic concept of DEM is to model the rock mass as an assemblage of particles, which are bonded together. Joints or cleats can also be inserted into the assemblage to form preferred weakness planes. The general concept is shown in Figure 2 (Itasca, 2012).

It can be appreciated that a Bonded Particle Model (BPM) is a powerful technique in which any possible rock failure scenario might be simulated. However such an approach with its ability to model the

relative movements of particles, or blocks of particles will suffer from the ability to reliably calibrate performance under a range of different loading scenarios.

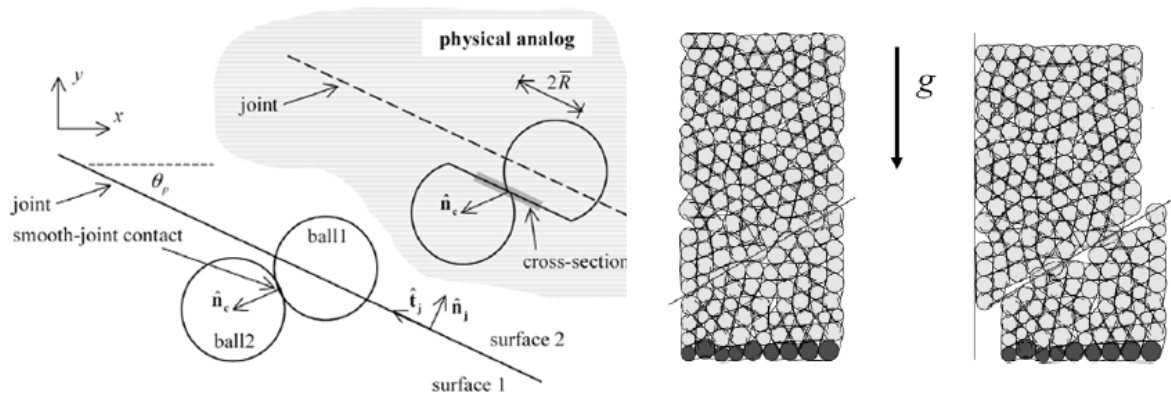


Figure 2 - Schematic bonded particle model with smooth joints

### COAL BREAKAGE AND FAILURE MODEL

#### Effect of scale

In order to build a framework for LTCC extraction an important consideration is to recognize the scale effect present, i.e. to capture the effects of fractures, joints or cleats on the geomechanical properties of the coal when transitioning from small samples to larger field scales. Figure 3 shows the transition from intact coal to a typical cleated coal seam. It can be seen that the influence and variation of cleating needs to be considered in assessing the seam's mechanical properties. If laboratory testing is undertaken, core samples from the seam may exhibit a different cleat distribution from that of the entire seam.

The problem of size dependency on the strength and stiffness of rock is a well-known problem and is present in most all rock masses that contain joints and fractures. In general the strength of rock reduces with increasing sample size due to the greater number of fracture per unit volume that is present. For coal, this problem was addressed via a detailed experimental study of the strength and deformation behaviour of coal in the mid 90's, sponsored by BHP Australia Coal, in order to establish the relationship between coal type, strength and scale. An experimental program was conducted to measure the change in coal properties by triaxial testing of 61 mm, 101 mm, 146 mm and 300 mm diameter coal samples (Medhurst and Brown, 1998).

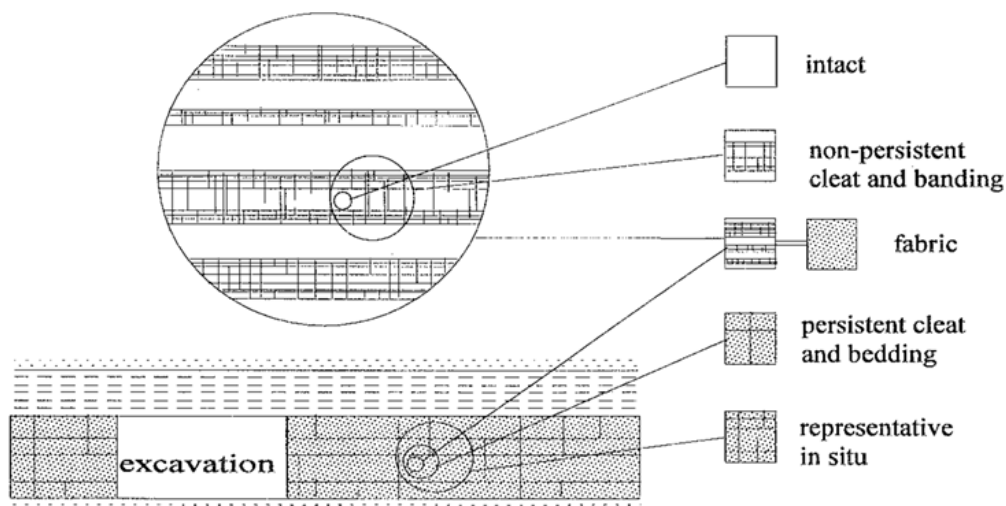


Figure 3 - Idealised diagram showing the appearance of coal at different scales

Figure 4 shows the effect of sample size on the peak strength of coal at various confining pressures. The important point to note is that the mechanical properties reach a constant minimum value. This limit is known as the Representative Element Volume (REV) and is thought to be at the point where the density of fractures within a given volume of rock becomes constant. This particular aspect of rock behaviour allows the properties of rock to be predicted masses from laboratory measurements of rock samples.

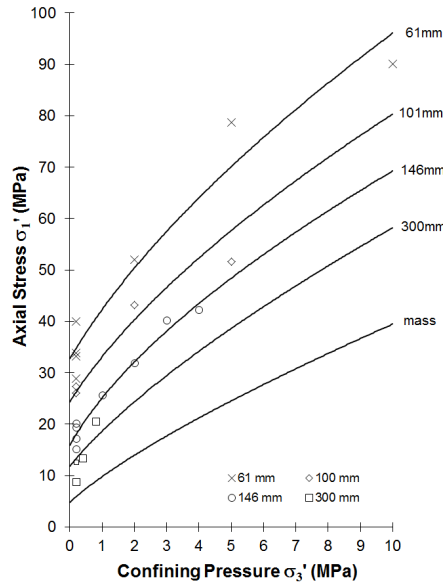


Figure 4 - Influence of sample size on peak strength of coal

The ability to predict the strength of coal seams becomes viable provided some measure of cleat density can be undertaken and matched against laboratory and field performance. Underground pillar strength tests were undertaken some years ago in South Africa suggesting that the REV for coal was about 1 to 2 m<sup>3</sup>. Further work undertaken in the Bowen and Sydney Basins based on experiences for highwall mining pillar design has allowed the experimental work outlined above to be extended across a range of Australian coal seam condition (Medhurst, 1999). This work provides the foundation in which the coal breakage and failure model is developed.

**Synthetic rock mass model**

The Synthetic Rock Mass (SRM) approach was developed to determine the main factors influencing the rock mass behaviour in block cave mines such as caveability, fragmentation, gravity flow and draw control (Mas Ivars, *et al.*, 2011). The process involves the generation and testing of synthetic rock mass samples by combining the bonded particle models of rock and discrete fracture network modelling. Figure 5 shows the SRM components.

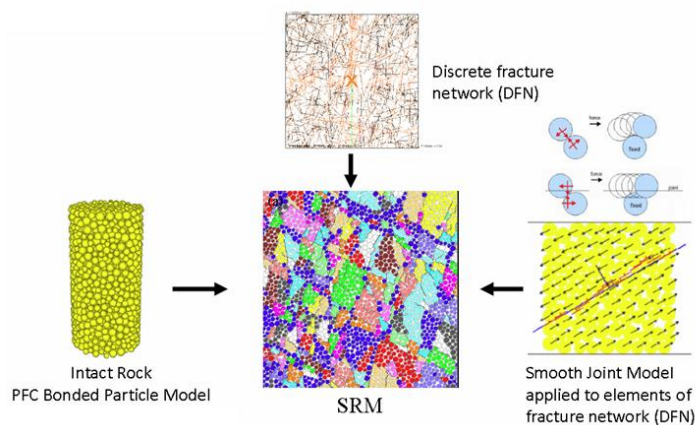


Figure 5 - Development of synthetic rock mass model

Using these concepts SRM models can be generated that represent samples of the rock mass at small scale up to large scale. This process therefore allows the development of a coal failure and breakage model based on simulation of the experimental triaxial test data. In particular, the experimental study revealed some fundamental aspects of coal behaviour that are important to caving. Figure 6 shows volumetric/axial strain measurements from triaxial testing of the 101, 146 and 300 mm diameter samples at various levels of confinement. The results show that when confining stress is low, coal fails along cleats resulting in expansion or dilation of the coal. When confining stress is high, cleating has minimal influence on the coal response and shearing across cleats is the dominant failure mechanism and the volume change of coal is small.

The experimental data shows how the coal will behave at the cave front. Under low confining stress, cleating has a dominant role and results in a weakening effect on the coal (this effect is similar to rib spall). Further into the coal mass, confining stresses are higher and shearing is more predominant. The caving model needs to be able to mimic the expansionary effect of coal at low confining stress, whilst adequately reflecting the effect of scale on strength.

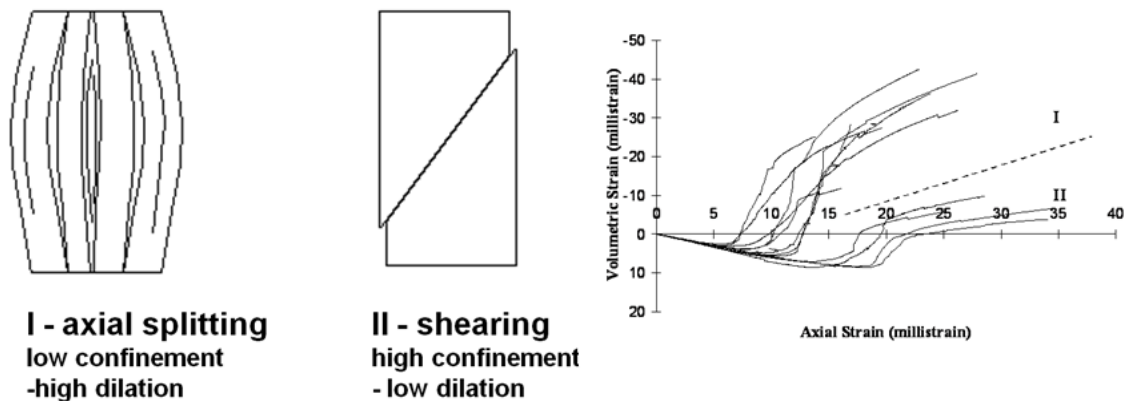


Figure 6 - Mechanisms of coal failure

Figure 7 shows the SRM workflow used in the project. The SRM consists of the Bonded Particle Model (BPM) and the fracture network represented by a smooth joint contact model. The BPM represents the intact or matrix of the SRM and is calibrated against laboratory test data. The joints and cleats are then inserted into the numerical model using smooth joints and the assigned its relevant properties. The BPM and fracture network can then be created at any scale and tested against the available data.

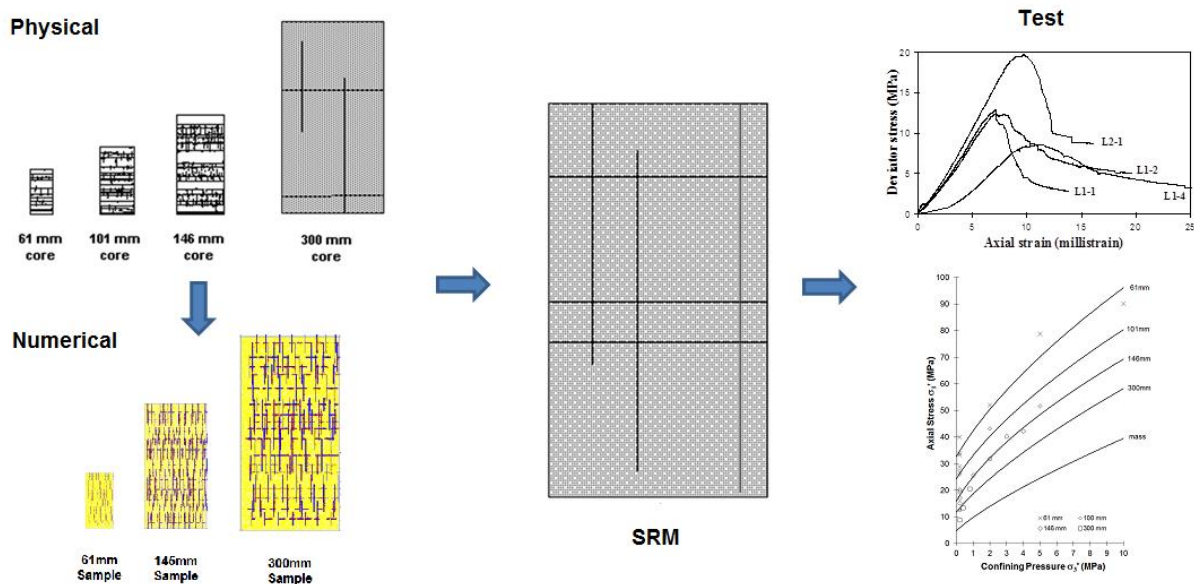


Figure 7 - SRM workflow for characterisation of coal seam properties

## LONGWALL TOP COAL CAVING MODEL

### Mechanics of caving

The process of cave development requires an understanding of what is required to carry a rock mass from peak to residual strength (i.e. post-peak behaviour). To be able to predict caving, the modelling process requires the prediction of four distinct zones:

- Elastic zone: where rock mass behaviour and properties are undisturbed;
- Seismogenic zone: where discontinuity damage (discontinuities going from peak to residual strength) and the initiation of new fractures develops;
- Yielded zone: the rock mass is fractured and has lost some or all of its cohesive strength and provides minimal support to the overlying rock mass;
- Mobilized zone: the rock mass has caved and may be recoverable with continued draw.

In the case of LTCC extraction, all of these factors need to be considered. One of the key geotechnical risks is potential for the cave line developing over the canopy resulting in poor face stability and uncontrolled caving. Fragmentation is another important factor which has to be evaluated together with the ability to maintain a consistent top coal caving sequence. The model must therefore be able to investigate the inter-relationship between roof stability, fragmentation and dilution under variable overlying strata conditions.

In an effort to simulate the LTCC process, the model must be able to adequately capture the transition from intact to completely broken material. The preceding discussion outlines several key challenges to develop these models including adequately addressing the geometry of the problem; representation of differing strata conditions; modelling the fracture process and finally, simulating the longwall retreat and draw sequence. At the core of this problem is the need to capture the mechanical behaviour of the coal under various stages of loading and its impact on its failure behaviour. For this reason a coupled model is required. In the near field, a detailed particle based model of the coal caving process is developed. Surrounding this model is a continuum FLAC model, which captures the necessary far field influences such as cover depth, different overlying strata and abutment stresses. Figure 8 shows the modelling architecture used for the development of the FLAC-PFC hybrid model. It consists in a PFC2D inclusion embedded in a rectangular FLAC grid with a fine mesh resolution. This inner FLAC grid is itself then embedded in a coarser FLAC grid.

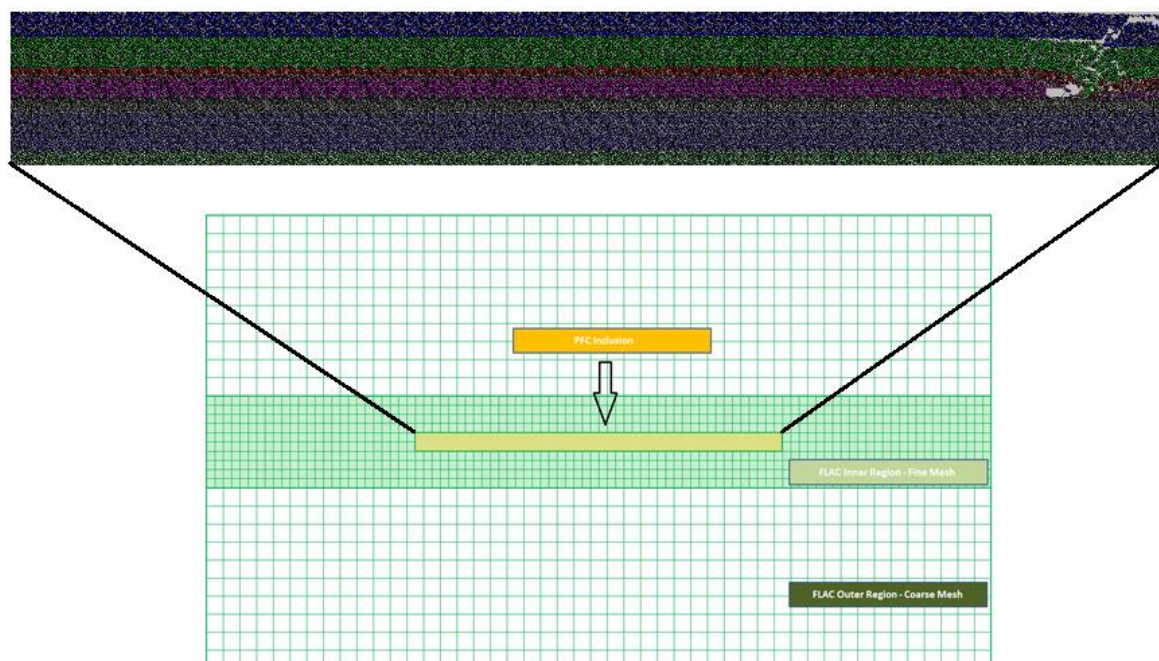


Figure 8 - Modelling architecture of FLAC-PFC model

## Caving analysis

Modelling was completed for a range of conditions including depths set at 150 m, 250 m and 350 m with the coal strength being defined as 'low' or 'high' and the overburden material strength being represented as either 'weak' or 'strong'. A weak overburden represents the case where predominantly siltstones are present and the strong case where heavier sandstones predominate. Of particular interest in this study were:

- The particle size distribution of coal and overburden material;
- Recovery rates of the top coal when using the LTCC process.

Figure 9 shows a snapshot of the caving behaviour for a siltstone roof at 350 m depth. In this case the caving is regular, reflecting a frequent periodic cycle often noted in LTCC operations. In general the model shows that the coal caves regularly and moves readily down the rear of the shield, typically with a significant movement of coal when the support moves forward. It is notable that occasionally a fracture forms just ahead of the face line as a result of the draw sequence. For modelling purposes the draw sequence was set to "draw to dilution" to enable an estimate of recovery and to help determine the effects of LTCC extraction at "full" recovery.

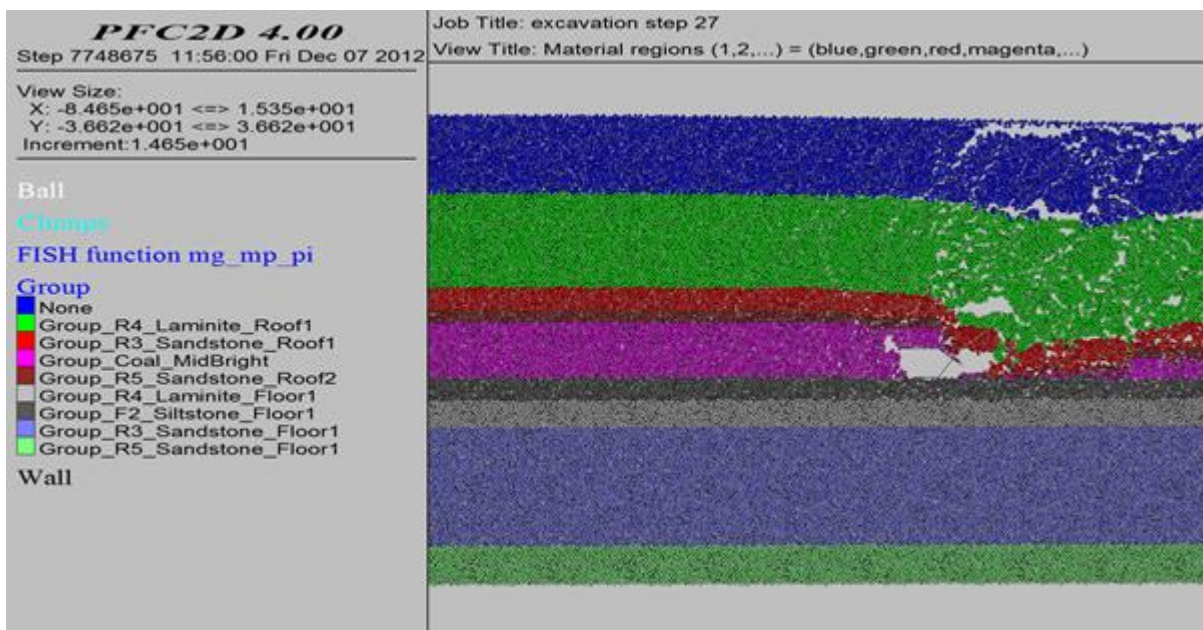


**Figure 9 - Caving behaviour under siltstone roof at 350 m depth**

Another aspect of caving response is the periodic behaviour of both support loading and coal recovery. A close examination of the models shows how, depending on the fracture pattern, some shears are associated with large recoveries as the support moves forward, and others less so, since a significant proportion of the top coal has been recovered on the previous shear. This is a common observation on LTCC faces, and from the results of the modelling, suggests this becomes pronounced under a scenario of drawing to dilution.

The FLAC-PFC caving model was developed to allow for the detection and extraction of materials entering into a cluster detection window as depicted by the square at the rear of the longwall in Figure 10. Any particle or clusters with a particle contained in, or touching the boundaries of the window were then removed from the model. This sequential removal material is referred to as a 'draw' within the modelling environment. The number of draws taken was set by considering the amount of top coal which would become available after each longwall advance. The width of the top coal rectangle was set to be the same as the distance covered by each longwall advance and the height as the difference between the seam thickness and cut height. In doing so, algorithms were developed to measure the number of particles, size and type entering the detection window.

The ability to report the finer fraction of top coal particle size distribution was limited to the minimum particle radius ( $R_{min}$  in the caving model was 150 mm for computational purposes). Nevertheless the model provided an ability to determine the maximum size of particles as well as to estimate the percentage of particles detected that would be less than the minimum detected particle size. A typical result at 250 m depth for example indicated a maximum particle size of around 2 m and approximately 73% of caved coal would be less than the about of 450 mm and 84% would be less than 700 mm. It is important to note that model results represent primary breakage of top coal from the overlying seam and do not include secondary breakage effects that may occur in the goaf zone or on the rear AFC.

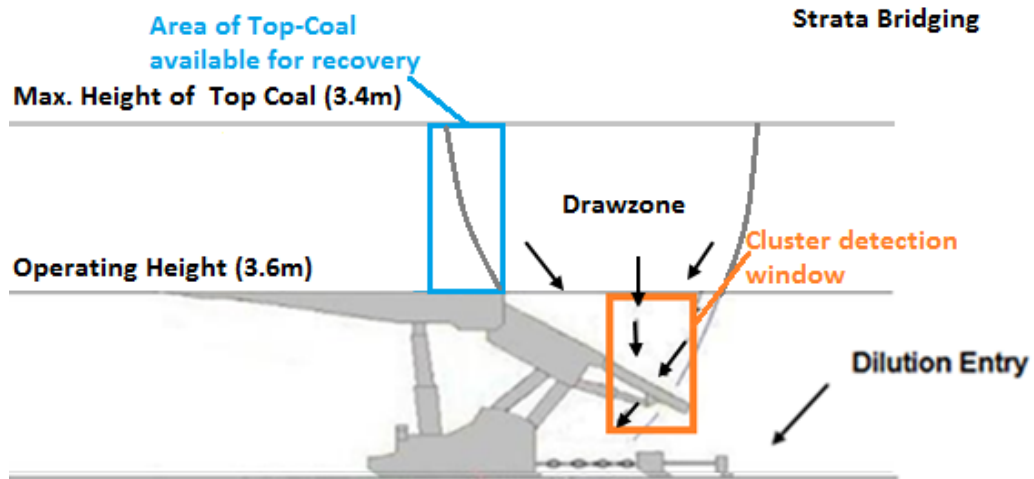


Figure 10 - Model setup for top coal recovery

A typical cumulative recovery profile arising from the analysis is shown in Figure 11. For example, the expected range of top coal recovery at 250 m depth based on a strategy of drawing to dilution is between 65% and 81% depending upon the roof conditions and coal parameters used.

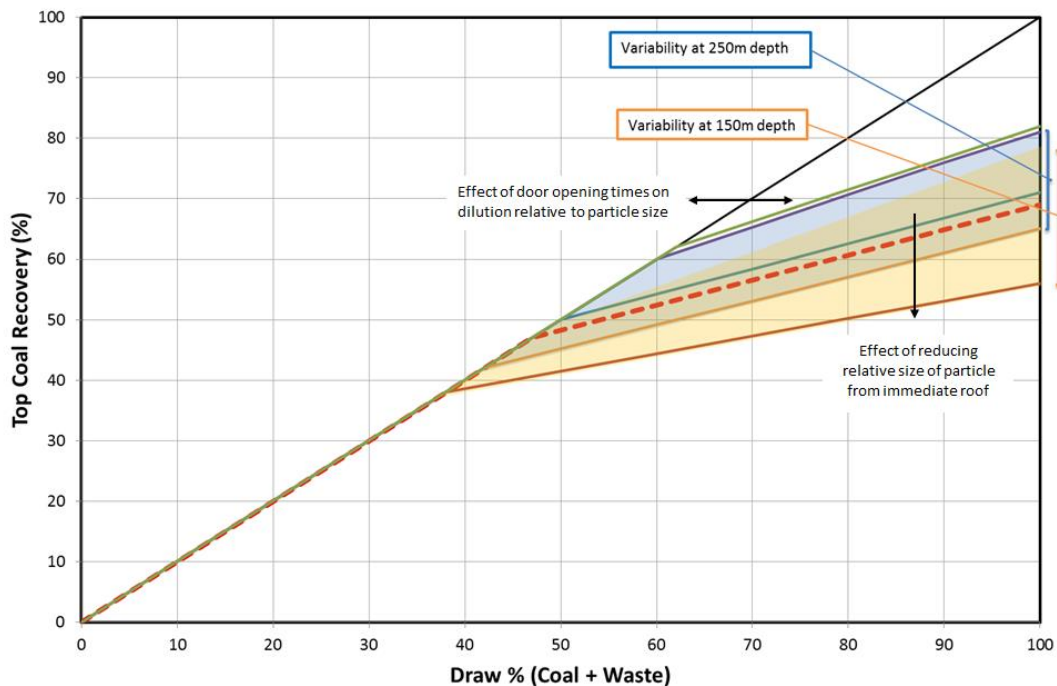


Figure 11 - Top coal recovery profile

The 45 degree line is the upper limit of coal recovery and represents the idealised case where 100% of the material that is drawn from the rear AFC is coal. The effect of increasing door opening times may increase recovery, but potentially also increase dilution. If the goaf material from the immediate roof has

a relatively small particle size, then it is more likely to migrate through the caved coal and report to the rear AFC, thereby reducing recovery and increasing dilution.

## CONCLUSIONS

The development of the caving models has provided a range of outcomes including several theoretical aspects concerning the behaviour of coal and modelling of the fracture process; the failure mechanics and what influences any given outcome; and from this an ability to understand what is governing the caving process and what factors can affect it. From this perspective the key outcomes obtained from the caving models were as follows:

- The coal properties are of primary importance in caveability and top coal recovery estimates. For a given depth and overburden condition, up to a 16% range in coal recovery may be present depending upon the *in situ* roof conditions and coal properties.
- Increased particle sizes for both the coal and overburden are expected at the shallower depths as is the variability of recovery of top coal. Periodic events are expected to be more frequent at shallower depth;
- Caving conditions are expected to improve with increased cover depth, as the cover loads increase the level and extent of fracturing. Particle sizes are expected to be finer, and the top coal recoveries higher and more consistent than in shallower parts of the mine;
- The modelling process was directed towards “drawing to dilution” as is commonly practiced in LTCC operations. Examination of caving behaviour under this scenario revealed that the well-known periodicity experienced in LTCC operations is a function of this draw strategy. This affects both support loading and coal recovery. A close examination of the models shows how, depending on the fracture pattern, some shears are associated with large recoveries as the support moves forward and others less so, since a significant proportion of the top coal has been recovered on the previous shear;
- In some instances drawing to dilution can result in what has been termed “overdraw”, which can result in excessive face loading and cavity development under weak strata conditions or creation of goaf voids under strong strata conditions leading to caving in large blocks;
- There is obviously a trade-off between the percentage draw and coal recovery and the risks associated with overdraw under maximum coal recovery. The balance of these risks is difficult to estimate other than that based on the recovery trend.

## ACKNOWLEDGEMENTS

The opportunity and financial support provided by BMA to undertake this work is greatly appreciated. The assistance and input provided by Minecraft Consulting and in particular Monica Lagos is also acknowledged.

## REFERENCES

- Diederichs, M.S. 2003. Rock fracture and collapse under low confinement conditions. *Rock Mech. Rock Engng.* 36 (5), 339–381.
- Itasca Consulting Group Inc., 2012. PFC user manual.
- Mas Ivars, D., Pierce, M.E., Darcel, C., Reyes-Montes, J., Potyondy, D., Paul Young, R. and Cundall, P. 2011. The synthetic rock mass approach for jointed rock mass modelling, *Int. J. Rock Mech. Min. Sci.*, Vol. 48, pp219-244.
- Medhurst, T.P. 1999. Highwall mining: practical estimates of coal seam strength and the design of slender pillars. *Trans. Instn Min. Metall. (Sect. A: Min. industry)*, Vol. 108, A161-71.
- Medhurst, T.P. and Brown, E.T., 1998. A study of the mechanical behaviour of coal for pillar design. *Int. J. Rock Mech. Min. Sci.*, Vol. 35, pp1087-1105.

# INVESTIGATION INTO THE RELATIONSHIP BETWEEN STRATA CHARACTERISTICS AND LONGWALL CAVING BEHAVIOUR

Terry Medhurst<sup>1</sup>, Peter Hatherly<sup>2</sup> and David Hoyer<sup>3</sup>

**ABSTRACT:** This paper outlines the results of a study to analyse various longwall operations using the Geophysical Strata rating (GSR) to characterize the strata, assess the likelihood of weighting and then correlate this with the various outputs that can be provided by longwall support monitoring analyses. A significant advantage of integrating GSR and longwall datasets is to allow a 3D spatial understanding to be developed between strata characteristics and various support loading related parameters. A caving chart has been developed based on a combination of previous experience in longwall support assessment, strata characterisation, leg pressure data analysis and caving behaviour. The chart provides a link between strata conditions, stresses, panel layout and anticipated support loads via design thresholds that are related to roof convergence. The intent is to provide a means to assess the risk of cavities in the immediate roof and/or the risk of heavy weighting from the overlying roof units.

## INTRODUCTION

Massive strata overburden units are known to influence support loading on longwall faces. Past studies of the conglomerates in New South Wales and sandstones in Queensland have identified factors such as unit thickness, proximity to coal seam, immediate roof strength and panel width that may all play a role in support loading and in the development of adverse ground conditions. Other controls such as cut height, cutting method, hydraulic supply, leg pressure control parameters and pressure settings can also influence ground behaviour.

The interaction between longwall supports and the surrounding strata is a complex phenomenon. At present neither empirical nor numerical models can adequately capture the critical factors required to predict strata response. However, recent advances in the ability to analyse longwall monitoring data such as that developed by Longwall Visual Analysis (LVA) provide a potentially large and valuable data source to quantify time related factors. It also provides a means by which to assess how operational practice can influence shield behaviour. There is a need to develop a view to understanding the relative changes in behaviour from one set of conditions to the next. The aim of the ACARP study described here (Medhurst, *et al.*, 2013) was therefore to produce a set of tools and/or indicators that can be used for interpreting key strata caving mechanisms and quantifying its impact on longwall support performance.

Through previous ACARP projects an approach to characterise ground conditions using borehole geophysical logs has been developed. One aspect of this is the Geophysical Strata Rating (GSR), a rating scheme devised for coal bearing strata. Using geophysics data provides a high density and cost effective means of gathering geotechnical information that enables development of 2D and 3D models of strata characteristics. This study aimed to take advantage of GSR estimates to provide a practical means to classify or identify features that affect caving behaviour. Data from three sites were used for the study namely, Moranbah North, Dendrobium and Newlands Mines as they represented a range of conditions and locations. Anecdotal evidence and experience from other sites was also used in the formulation of the outcomes of the study.

## LONGWALL EXTRACTION BELOW MASSIVE STRATA

Caving mechanics and the ability to predict caving events in rock strata remains as one of the key challenges in mining geomechanics practice. In massive strata the problem is not only one of predicting caving behaviour, but also of assessing if such behaviour can potentially lead to periodic weight and/or windblast events. In the late 90's a series of well documented studies were undertaken to examine the

<sup>1</sup> PDR Engineers Pty Ltd, tmedhurst@pdrengineers.com.au, Tel: (07) 4051 5599

<sup>2</sup> Coalbed Geoscience Pty Ltd

<sup>3</sup> LVA Pty Ltd

caving behaviour of massive strata. This experience was captured in the empirical chart based on Voussoir beam principles (Frith and Creech, 1997), shown in Figure 1.

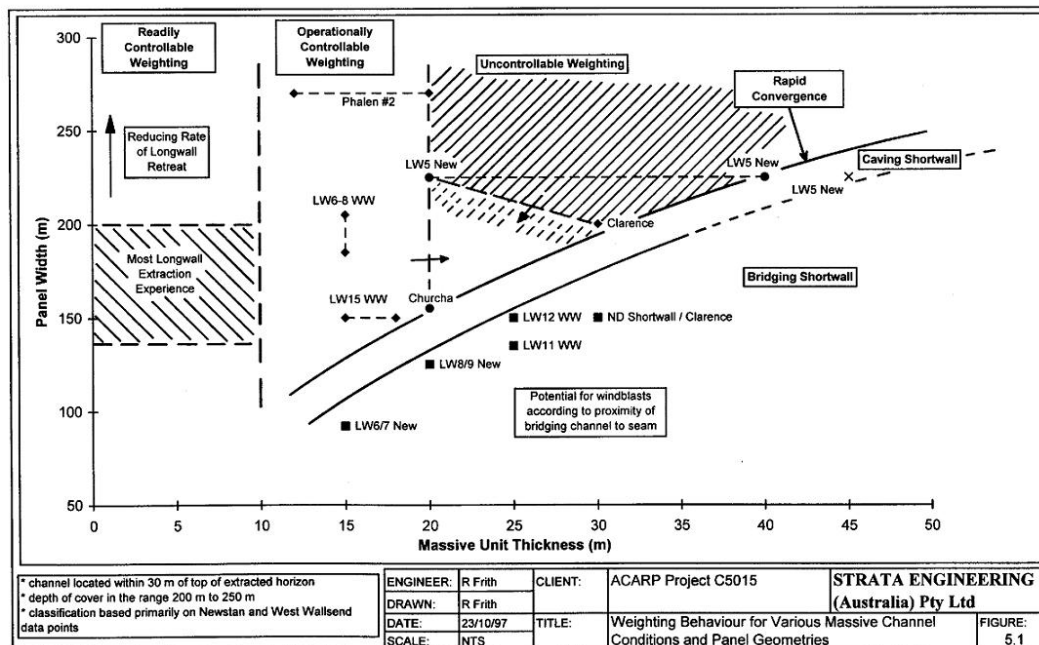


Figure 1 - Empirical caving chart under conglomerate roof

The concept of fracturing ahead of the face under longwall conditions and behind the face under shortwall conditions, potentially leading to windblast conditions, provides the basis for the design chart shown in Figure 1. In general, this concept remains valid and has served the industry well. However the intensity of periodic weighting, or in some cases a lack of events when anticipated, suggests that a more detailed understanding of the controlling factors at play is required. It is important to note that limited work on the issue of conglomerates has been done since that time. Since then longwall panel dimensions, equipment and operating practices have changed. More recent observations suggest that weighting is not just a function of thickness and width, but also location of units within the sequence and surrounding strata conditions.

Frith (1996) provides a detailed discussion of the classic periodic weighting mechanism in which tensile fracturing occurs ahead of the face due to self-weight cantilever loading. The discussion is extended to show the potential of bedding plane shear on underlying laminated material as a result of the tensile fracturing via a mechanism of the lowering of the neutral axis of the overlying massive strata beam. Albeit somewhat academic it raises the question of whether bedding plane shear occurs before or after the development of tensile failure leading to weighting events. The short answer to this question is that both scenarios can occur and in fact, leads to the heart of understanding the interplay between strata conditions, support characteristics and operating practice.

Experience in the weaker, thick seams of the Bowen Basin show that weighting issues are most prominent where "soft" forward abutments can develop via shear ahead of the face due to factors such as excessive horizontal stress conditions, high cut heights and significant face spall, stress relaxation due to prolonged face stoppages and/or poor longwall operating performance. The potential for periodic weighting is not only dependent upon thickness and strength of massive roof units, but also the thickness and character of interburden, including position of weakness planes. In other words this might be a case where bedding plane shear due to the presence of unfavourable strata conditions is a key factor in the damage of overlying laminates and the main source of cavities.

The rate of retreat is also critical. Where conditions might have otherwise been considered reasonable, a slow retreat rate or lack of adequate set pressure may allow excessive convergence of overlying strata leading to tensile fracturing. In this case, the classical mechanism may be relevant in which the development of poor immediate roof conditions are essentially mining induced. A typical scenario might be that shown in Figure 2.

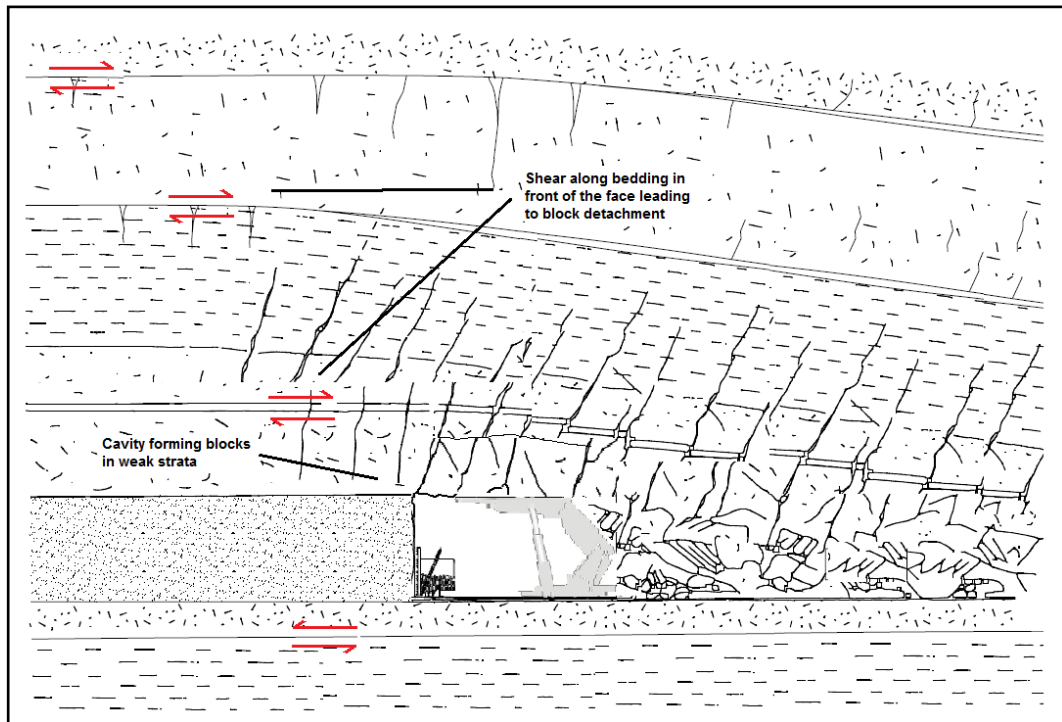


**Figure 2 - Caving mechanism under slow retreat and/or poor roof conditions**

Previous studies show that shearing and cavity development often occurs in the presence of a weak layer within the lower 2 m to 3 m of the roof horizon (Medhurst, 2005). This is related to how far the influence of active pressure from the supports is able to extend into the roof. The background rate of roof convergence is also important in controlling roof stability and can sometimes be related to the impact of a slow retreat rate or the effect of soft roof.

At Moranbah North, microseismic monitoring showed that shear events had occurred up to 40 m ahead of the face (Strawson and Moodie, 2007). Up to 40 m of overlying sandstones were also present, but in this case the presence of a weak immediate roof provided an area of high propensity for cavity development. Comparison of examples from the conglomerates in NSW and sandstones such as at Moranbah North show how different outcomes can occur despite relatively similar massive unit characteristics and panel dimensions. In essence, a one size fits all solution to longwall ground control problems is an elusive goal without due consideration of strata and operating conditions.

## SHIELD MONITORING

### Leg pressures

Longwall leg pressure monitoring has in various forms been used in Australia for over 20 years. Peng (1998) characterised pressure changes within a mining cycle into three major types: increasing, steady and decreasing types, shown in Figure 3. The increasing type was described to be representative of a relatively intense roof loading. The steady type is denoted as relatively weak roof loading, and the decreasing type being of extremely weak roof and/or the presence of too much rock/coal debris between the canopy/roof, base/floor or due to leg leakage.

An inherent characteristic of the support loading cycle is its relationship to the overlying roof conditions. In general, whilst variations on this behaviour exist, the plots show an initial high load rate period where the supports are seated against the roof; which will depend on the set pressure applied. A second long period of constant load rate that reflects the stiffness and load transfer capacity of the overlying roof, and a third, high load rate component, which in most cases is normally associated with the cutting cycle, increase in tip-to-face span and lowering of the adjacent shield.

The time weighted average leg pressure represents the most common and traditional means of assessing support resistance over a load cycle. Several features of longwall support response can usually be identified such as whether there is adequate set pressure or if the support is being

overloaded due to a number of repeated yield cycles (Trueman, *et al.*, 2005). One key aspect however, is the change in load over a given time span. A measure of loading rate provides a measure of roof stability as it reflects the rate of strata movement.

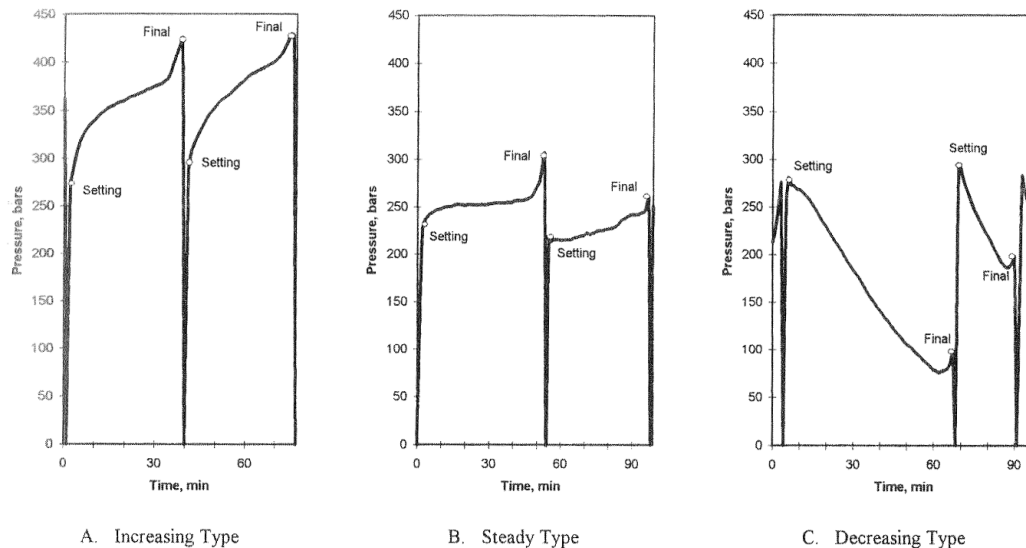


**Figure 3 - Pressure changes in a shield supporting cycle**

One difficulty in assessing load rates is setting criteria for the calculation of initial load rate, steady state load rate or final load rate. For each case, a change in state in the pressure record has to be estimated or a time cut-off has to be defined, e.g. initial rate over 10 mins. This cut-off is an arbitrary measure and to various extents can produce significant variation depending upon the consistency of operating characteristics between operators, panels or even different mines.

Another aspect is that when calculating load rates longwall data are inherently “noisy”. Crisafulli and Medhurst (1994) have addressed this issue by developing a continuous load rate estimation algorithm that takes account of sharp changes in the pressure record due to operational influences or measurement errors. A comparison is shown in Figure 4.

The top plot shows the pressure record. The time difference calculation is shown at the bottom. This represents the standard calculation that would be done in excel, in which the difference between pressure measurements at each minute is calculated. Notice how extremely high load rates are estimated ( $> 50$  bar/min) due to the support resets and other signal discontinuities, producing a “noisy” estimate. The centre plot shows the continuous load rate calculation. This method removes the signal discontinuities and provides a smoothed estimate of load rate that is reflected by the rate of overlying strata movement. In this case load rates in the order of 4 bar/min are shown which is more representative of the pressure record.

Estimation of load rates provides a measure of strata response and reflects the rate of overlying roof convergence. In a pre-yield condition load rates can be directly related to convergence rates. However if the support is in yield, measures such as yield counts have been used since they present an indirect measure of load rate and hence convergence rates.

Convergence based triggers are routinely used for strata control purposes. Until recently however, such measurements have been difficult to obtain in a longwall environment. In the absence of direct convergence measurements, estimation of critical load rates or yield counts or combinations thereof have provided the most useful stability measures as they reflect the potential to reach the point of critical roof convergence.

### Roof convergence

The typical response in a strata control environment is to install more support when a trigger is reached. This is generally not an option in a longwall environment leaving only the ability to keep moving or lowering cut height to alter the loading conditions. In this case a greater reliance on a predictive model of

longwall ground response is required in order to take preventive action. This is an important consideration for support design and operational planning.

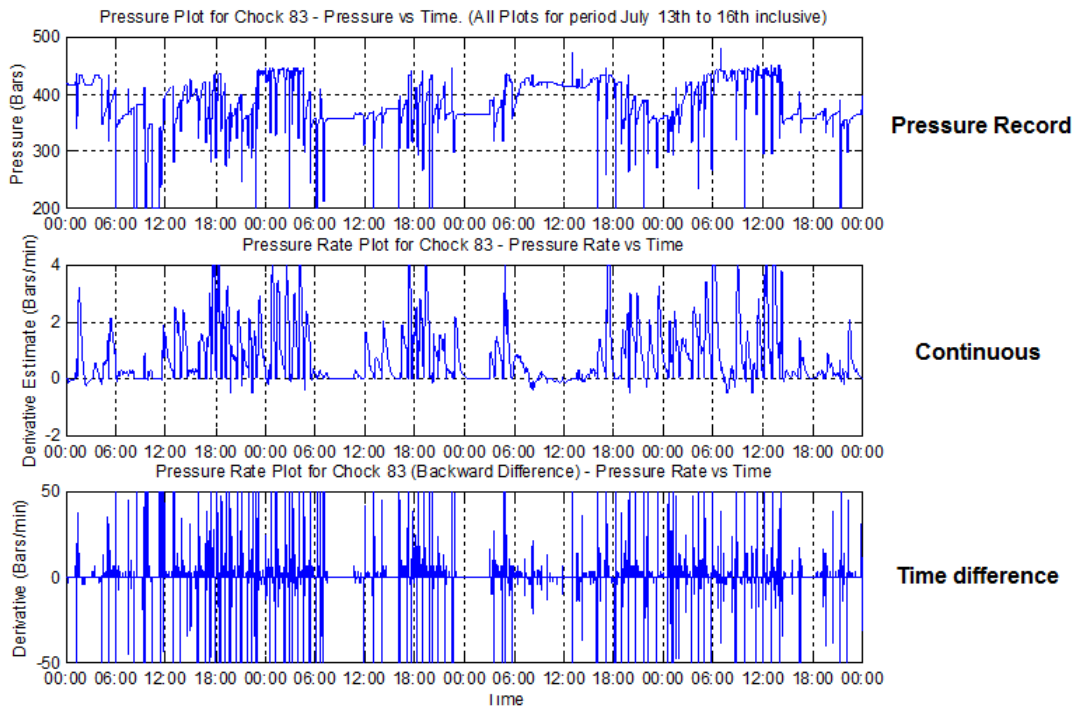


**Figure 4 - Load rate estimation using continuous and time difference methods**

One approach used to assess roof support response requires introduction of the Ground Response Curve (GRC) concept (Medhurst and Reed, 2004). The GRC was originally developed by the civil tunnelling industry to optimise ground support practices in weak ground. The advantage of this approach is that ground behaviour and support set-to-yield characteristics can be assessed together. The general concept is illustrated in Figure 5.

It is important to note that total roof convergence is made of two components, initial roof convergence before the support is set in each the Lower-Advance-Set (LAS) cycle and the roof convergence during the cutting cycle as demonstrated in Figure 5. An estimate of initial roof convergence is important for understanding the impact of the LAS cycle on roof stability. A high level of initial roof convergence gives a lower margin for controlling the roof and more demand on support load to limit the roof reaching critical convergence levels.

Unfortunately, initial convergence cannot be measured directly, even via convergence monitoring, as it occurs at the faceline as part of the LAS cycle. However an estimate can be made if there is some measure of the convergence rate of the overlying strata and a timeframe in which to estimate the amount of movement. As previously mentioned a high load rate spike is often detected at the end of the cutting cycle as shown in Figure 3. This pressure increase provides an indirect measure of initial convergence.

A measure of the set-to-yield convergence for a nominated set pressure is normally provided with the technical specification of the supports. An analysis of leg stiffness from several modern support designs shows a typical set-to-yield leg closure ranging from 1.1 to 1.5 mm for every 10 bar of pressure increase. This equates to an average leg stiffness of about 8 bar/mm resulting in leg closures of 6.5 mm to 13 mm for a 50 bar to 100 bar set-to-yield pressure range. Any given pressure change can then be equated to a value of roof convergence from the longwall monitoring data.

A typical example might be a pressure spike of 20 bar over a period of 45 s after the shearer goes past and the support is advanced. This equates to a pressure increase of up to 30 bar/min or 200 mm/hr. At a nominal shear speed of 10 m/min and an exposed roof of say 10 supports (20 m), this suggests an unsupported roof area (after the cut) for about 2 mins. At 200 mm/hr this gives about 7 mm of roof movement. Analyses of this type over several sites suggests about 50% of initial roof convergence

occurs due to seam compression and the other 50% from the LAS cycle. In this example, the total initial roof convergence would be about 15 mm.

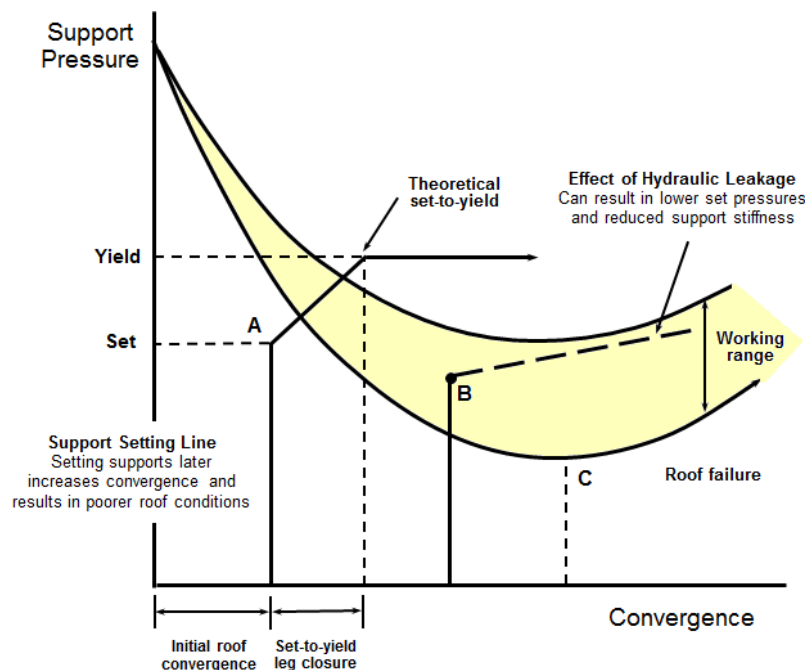


Figure 5 - Ground response curve

The second aspect is set-to-yield convergence. For an 80 bar set-to-yield range this might result in an additional 10mm of roof movement. However if a low set pressure is applied, e.g. giving say a 160 bar set to-yield range, the convergence will double to 20 mm. Combined with an estimate of initial convergence this shows how low set pressure can result in a significant amounts of roof movement.

The third aspect is post-yield roof convergence. Obviously direct convergence measurement will provide the best answer. But if such information is not available, a minimum value of roof convergence can be estimated via the pressure drop in each yield cycle. For example a 10 bar pressure drop during yield and then an increase back to yield pressure equates to  $2 \times 1.5$  mm; or a minimum of 3 mm leg closure for every 10 bar yield cycle. Depending upon the flow rate in the yield valve and the convergence rate of the strata, the roof convergence may be greater. Nevertheless the preceding discussion shows why combined measures of set pressure, load rate and yield cycles such as the Cavity Risk Index (Hoyer, 2012) give some measure of roof stability, since they all indicators of reaching some level of critical roof convergence.

## LONGWALL CAVING ASSESSMENT

### Strata characterisation

Through ACARP projects C15019 (Hatherly, *et al.*, 2008) and C17009 (Medhurst, *et al.*, 2010) an approach for characterising ground conditions using borehole geophysical logs has been developed. One aspect of this is the GSR, a rating scheme devised to allow coal bearing strata to be quantitatively assessed in every borehole that is geophysically logged. Table 1 shows an indicative range of rock quality as it relates to GSR.

The GSR allows a full analysis of overburden characteristics to provide 2D and 3D models of strata conditions. This provides the opportunity to correlate strata conditions with longwall support response. Each longwall face will operate over a given set of panel dimensions, stresses and ground conditions, which can be represented in the ground response plot in Figure 6. The ability to develop a cave prediction model therefore relies upon the active zones defined by four variables namely, strata conditions (GSR), support behaviour/characteristics, support load/stresses and convergence limits. It then becomes feasible to define a relationship between these variables for assessing caving and roof stability.

Table 1 - GSR applied to Australian coal measures

GSR Range		Description
0	15	Very poor
15	30	Poor
30	45	Fair
45	60	Good
60	80	Very good
80	100	Extremely good

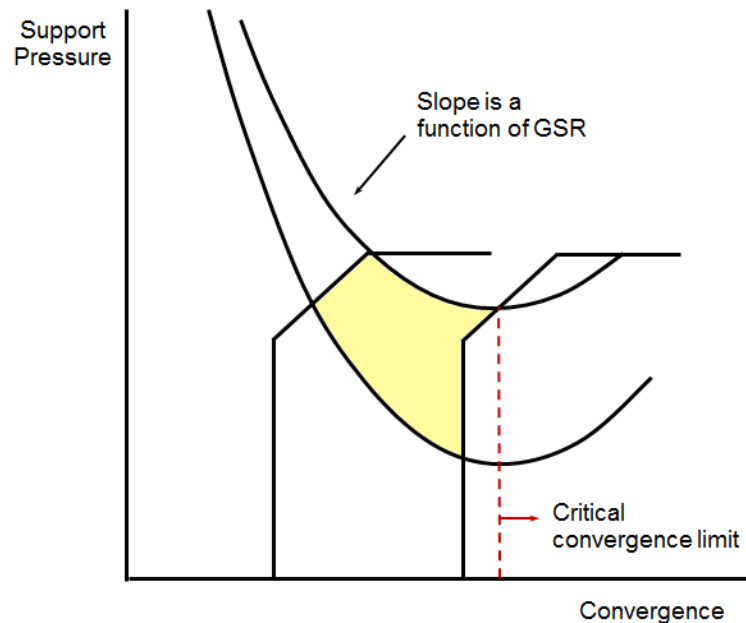


Figure 6 - Ground response over active longwall panel

The first task in providing an assessment of the caveability of overlying strata is to establish suitable parameters for strata characterisation. In accepting GSR as a measure of changing strata conditions, it then becomes a question of how it is to be used. Australian experience shows that severe periodic weighting effects tend to develop where massive strata units are present, i.e. where a single unit or series of combined units are greater than 15 m to 20 m thick as reflected in Figure 1. This can lead to heavy weighting, windblasts and/or face stability issues.

There is significant evidence to suggest that the potential for cavity development at the faceline is more pronounced in the presence of weak immediate roof conditions. This can be due to the inherent conditions, or by mining induced shear or fracturing from localised mining induced stresses or periodic weighting effects. As discussed previously, the potential for cavity development is particularly high in the presence of massive strata overlying a weak immediate roof unit.

Shearing and cavity development often occurs in the presence of a weak layer within the lower 2 m to 3 m of the roof horizon. The influence of poor roof conditions can also often be observed to reach up to 5 m under failure conditions. The overall zone of influence for caving assessment therefore could be separated into two basic zones comprising the immediate roof above the supports and the main roof that may contain massive units from 15 m up to 50 m thick. In keeping with industry experience, a 30m interval has been selected to represent the main roof and a 3m interval for the immediate roof as shown in Figure 7. Median values are chosen in preference to averages since they are less prone to the influence of outliers.

The presence of coal roof can shield the face from high stresses and influence roof stability. A stress correction factor is proposed to account for the additional stability provided by a coal roof. In this case, where the thickness of coal is at least 1m thick above the cutting horizon, the median GSR value for the proportion of coal in the roof should be multiplied by a factor of 1.4. This factor relates to the stress transfer capability of a fixed end beam in a low stress environment.

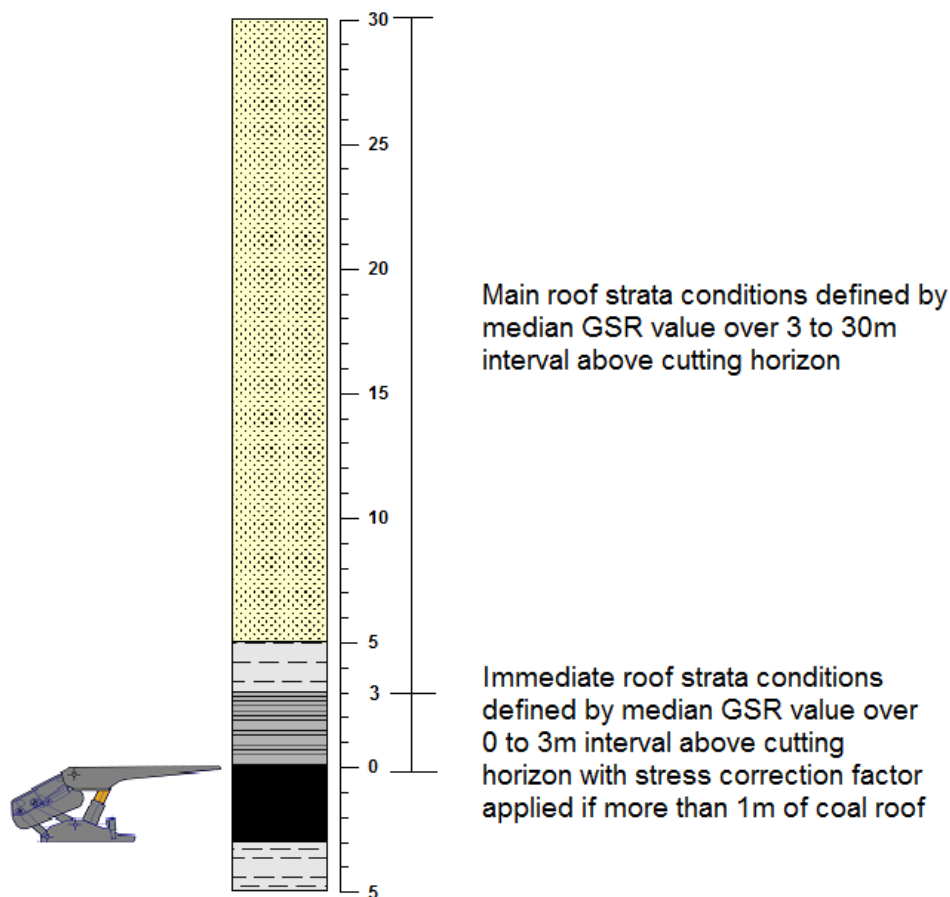


**Figure 7 - Basis of strata characterisation for caving assessment**

### Caving assessment

A critical aspect for caving assessment is the influence of panel dimensions and stress. For sub-critical panel layouts longwall supports are unlikely to experience full cover depth conditions. The ability of a massive unit to create a cantilever or the ability of a weak immediate roof to become unstable will be related to both the depth and panel width. This introduces the concept of Equivalent Depth (ED) in which a reduction in full depth conditions can be used to account for sub-critical panel layouts.

Using the concept shown in Figure 6, an analysis was undertaken of longwall support loads, critical convergence levels, ground conditions, panel dimensions and cover depth using data from a large proportion of longwall operations in Australia. A corresponding relationship between GSR and ED for a range of longwall support conditions was subsequently determined. This is shown in Figure 8.

Figure 8 is based on a combination of previous experience in longwall ground response, GSR analysis, analysis of leg pressure data and caving behaviour. The stable to transitional boundary represents a zone of increasing roof convergence and can vary locally, hence "transitional". Longwall support capacity thresholds are also shown and represent the yield density (before the cut) in  $t/m^2$  required to maintain acceptable levels of roof convergence.

The ED can be estimated using the formula shown in the bottom right hand corner of Figure 8; and takes account of the effect of panel width and depth on support loading. The GSR is chosen as the median value over a given roof interval. This can be used to assess the risk of cavities in the immediate roof and/or the risk of heavy weighting from the overlying roof units as defined in Figure 7.

The majority of Australian operations present data in the lower half of the design curves, although several proposed operations are planning to mine at considerable depths. In order to obtain some representative guidelines for the greater depths, data for several proposed operations were used along with some international data where available. In particular, a useful dataset from a colliery in Canada was provided for the study that included longwall mining beneath massive strata at depths greater than

700m (Payne, 2013). Such data provided additional information for defining curves where the ED was in excess of 300 m.

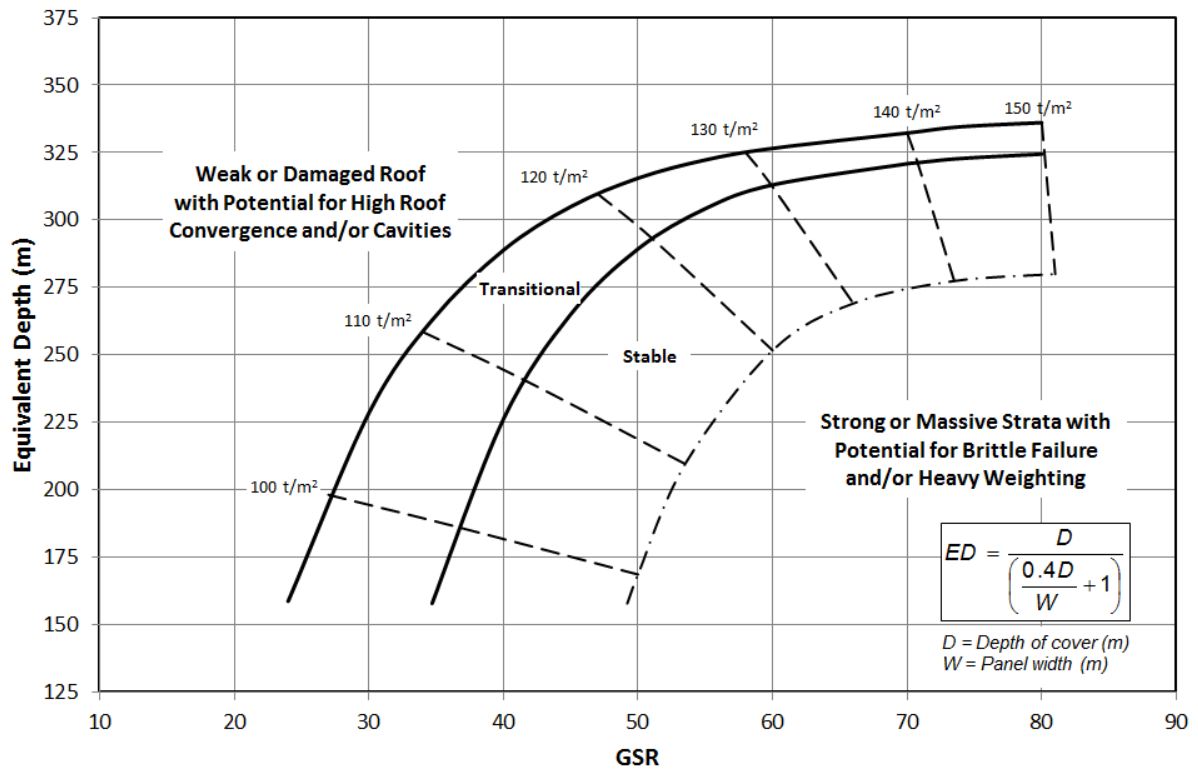


Figure 8 - Summary of caving response for Australian longwall operations

### Assessing risk

Longwall face cavities generally develop as a result of excessive roof convergence, which can be caused by several inter-related factors including:

- Poor setting loads, canopy contact and/or horizon control during operation of supports
- Presence of weak, sheared, faulted ground and/or damaged roof from overlying weighting behaviour and/or mining induced behaviour such as increased loading due to stress notching
- Increased tip-to-face roof spans due to excessive face spall due to high abutment loading from overlying weighting behaviour, poor face alignment and/or other mining induced factors
- Inability to support the roof due to non fit-for-purpose support characteristics or inadequate hydraulic supply system attributes
- Insufficient support capacity leading to excessive yielding during operations

A one size fits all solution to assessing risk is therefore a challenging task. Nevertheless on the basis of the summary design chart an assessment can be made. For the purposes of cavity risk analysis, it is suggested that the chart may be used in a staged process, namely

1. Plot immediate roof GSR vs ED to assess stability
2. Plot main roof GSR vs ED to assess stability
3. A first pass assessment can then be based on thresholds of immediate roof and main roof.

An example is shown in Figure 9. This represents a typical weak roof, strong overlying strata scenario of typical panel dimensions and depth with a median GSR of 30 for the immediate roof and a main roof GSR of 60. Assuming an installed support density of 110 t/m<sup>2</sup>, the chart suggests that the immediate

roof will be prone to cavities and the overlying strata may cause some periodic weighting that could overload the supports.

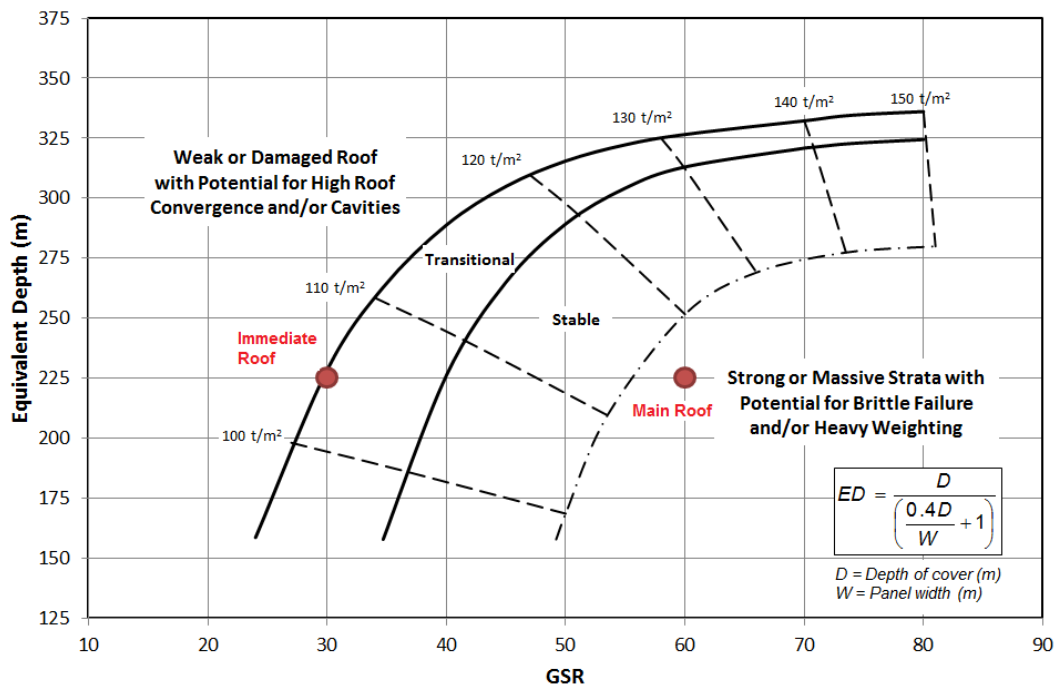


Figure 9 - Caving chart example

As roof conditions and/or stresses change as a panel is mined different points may be plotted on the chart. The chart can therefore be used as a broad scale assessment of the potential for cavities and/or periodic weighting. Table 2 provides a guideline for undertaking a first pass risk assessment based on a point plotted on the caving chart.

Table 2 - Summary of caving risk

Threshold	Main Roof < Transitional	Transitional < Main < Heavy	Main Roof > Stable
Immediate Roof < Transitional	Cavity High, Weighting Low	Cavity Moderate, Weighting Low	Cavity High, Weighting High
Transitional < Immediate < Heavy	Cavity Moderate, Weighting Low	Cavity Low, Weighting Low	Cavity Moderate, Weighting High
Immediate Roof > Stable	Cavity Low, Weighting Low	Cavity Low, Weighting Low	Cavity Low, Weighting High

The caving chart provides a link between support load, roof conditions and support requirements via design thresholds that are related to roof convergence. The risk matrix is useful as a first pass but does not address variation in support loading across the face and/or high/low loading or convergence rate of the supports and its effect on roof stability during operations. It therefore provides a guide and starting point for site based analysis and the use of real-time longwall monitoring data.

**Site-based analysis**

As per the example outlined one approach that can be used to assess cavity risk is to superimpose the effect of changing roof conditions on the caving chart as a function of longwall retreat. Figure 10 shows an example from Moranbah North.

In this case GSR values plotted from the model at every 25 m are superimposed on the chart. The results show the variation in cavity risk and reflect the potential for increased roof convergence in the weaker roof zones.

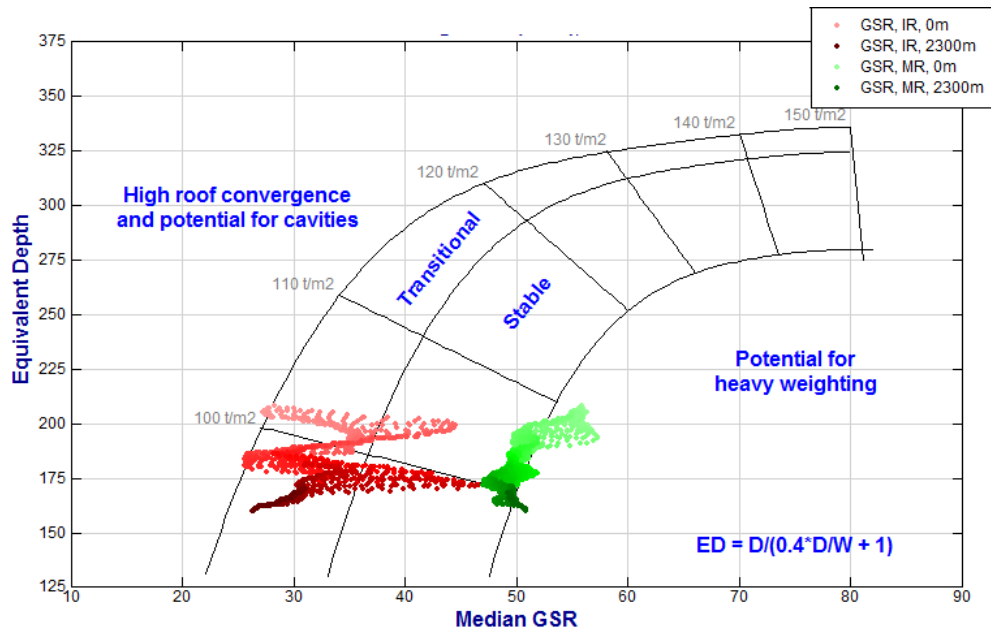


Figure 10 - Caving chart showing change in roof conditions

An alternative is direct roof convergence measurement and/or estimates of roof convergence and convergence rates using leg pressure data as discussed previously. Past experience suggests that cavity development starts to occur when roof convergence is in the range of 30 mm to 50 mm at most operations. Examples are provided in the ACARP study (Medhurst, *et al.*, 2013) that outline the use of loading rate and convergence rate analysis for estimating time related strata relaxation and critical convergence thresholds. Each requires site specific considerations.

The collective theme and key consideration through various methods is a measure of convergence. The caving chart is a broad scale measure that reflects the impact of roof conditions on support response. The CRI method as it applies to existing operations is an index measure of convergence obtained from leg pressure data combined with some basic parameters that relate to support load and continuity of prevailing conditions across the face. A third approach considers convergence more directly from leg pressure data through conversion from leg stiffness data.

The direct convergence estimate approach will be augmented in future by convergence monitoring. This will be a useful advancement. It is likely however, that accuracy of convergence monitoring may be limited and leg pressure conversions will be useful for estimating to the 1 mm accuracy required.

## CONCLUSIONS

Longwall face stability depends upon a range of geotechnical conditions, operational factors and the mechanical constraints of the longwall system. It is therefore sometimes difficult to determine the relative importance of these three main influences and their degree of interaction when assessing risk of instability. In this regard "a one size fits all" solution to longwall ground control problems is an elusive goal without due consideration of strata conditions and operating practice.

A caving chart has been developed based on a combination of previous experience in longwall support assessment, strata characterisation, leg pressure data analysis and caving behaviour. The chart provides a link between strata conditions, stresses, panel layout and anticipated support loads via design thresholds that are related to roof convergence. The intent is to provide a means to assess the risk of cavities in the immediate roof and/or the risk of heavy weighting from the overlying roof units.

Measures of convergence/convergence rate either directly or indirectly combined with a measure of load cycle times provides a mean to estimate convergence over a shear or multiple shears. This leads to the ability to determine whether the roof strata are near critical convergence levels.

Whilst achievable, continuous load rate analysis requires sophisticated smoothing algorithms to remove pressure spikes and other data discontinuities commonly present in longwall data. However when

measures of continuous load rate become available various parts of a shield's load cycle can be interrogated to help define support response.

The caving chart can provide the broader setting for design, risk assessment and planning whilst longwall monitoring data can be used to disseminate key parameters from the daily records. A direct convergence estimate using leg pressure data will obviously be augmented in future by convergence monitoring.

Convergence estimates from any particular shield alone however is unlikely to provide the necessary detail for a reliable real-time cavity risk indicator. A more sophisticated algorithm that uses each part of the load cycle in conjunction with continuous load rate and direct convergence measurement will be required for short-term longwall face stability assessment. Future algorithms will also need to incorporate factors such as the influence of load sharing from adjacent supports, standing time and the influence of varying set pressure on each load cycle. This is likely to require site-specific assessments that take account of operating practice, longwall support configuration and prevailing ground conditions in order to provide a reliable quantitative outcome.

### ACKNOWLEDGEMENTS

This paper outlines the geotechnical aspects of a broader study into the relationship between GSR characterisation, longwall monitoring analysis and caving behaviour funded by ACARP (Project C20032), which includes examples from a number of minesites. The reader is directed to this report for further information. The collaboration of the companies that provided data, in particular Anglo American Metallurgical Coal, BHP Billiton and Glencore is greatly appreciated.

### REFERENCES

- Crisafulli, S. and Medhurst, T.P, 1994 Robust on-line digital differentiation techniques with an application to underground coal mining. *Control Eng. Practice*, Vol. 2, pp210-209.
- Frith, R, 1996. Development and demonstration of longwall monitoring system for operational decision making. ACARP Project Report No. 4017, July 1996.
- Frith, R. and Creech, M, 1997. Face Width Optimisation in both Longwall and Shortwall Caving Environments, ACARP Report C5015, October, 1997.
- Hatherly, P., Medhurst, T. and MacGregor, S., 2008. Geophysical strata rating. ACARP end of grant report C15019.
- Hoyer, D, 2012. Early warning of longwall roof cavities using LVA software. In *Proceedings of 12th Underground Coal Operators Conference*, Wollongong, February 16/17, ISBN 978-1-921522-57 -4 (Eds. N Aziz, B Kininmonth, Jan Nemcik, Ting Ren), pp 70-78. <http://ro.uow.edu.au/coal/392/>.
- Medhurst, T.P, 2005. Practical considerations in longwall support behaviour and ground response. *Proc. 6th Australasian Coal Operators Conference*, AusIMM, pp 49-57. <http://ro.uow.edu.au/coal/72/>.
- Medhurst, T, Hatherly, P, and Hoyer, D, 2013. Dynamic response of longwall systems and their relationship to caving behaviour, ACARP Report C20032, September 2013.
- Medhurst, T, Hatherly, P, Zhou, B and Ye, G, 2010. Application of the Geophysical Strata Rating in production settings. ACARP end of grant report C17009.
- Medhurst, T.P and Reed, K, 2004. Ground response curves for longwall support assessment, *Trans. Instn. Min. Metall. (Sect. A: Min. industry)*. 2005, Vol. 114, A81-8.
- Payne, D, 2013. Personal communication.
- Peng, S.S, 1998. What can a shield leg pressure tell us? *Coal Age*, 103(3), March, 41-43.
- Strawson, C. and Moodie, A, 2007. Moranbah North tests the critical caving theories. *Proc. 26th Int. Conf. on Ground Control*, Morgantown, 180-187.
- Trueman, R. Lyman, G. Callan, M. and Robertson, B., 2005. Assessing longwall support-roof interaction from shield leg pressure data. *Journal of Mining Technology (Trans. Inst. Min. Metall. A)*. September 2005 Vol. 114.

# INVESTIGATION INTO TEMPORARY ROOF SUPPORT PRINCIPLES

Winton Gale and Craig Stemp

[Paper withdrawn at the request of the authors]

# IMPLEMENTING A SUSPENSION DESIGN FOR COAL MINE ROADWAY SUPPORT

Ross Seedsman

**ABSTRACT:** Suspension of the immediate roof is one of fundamental ground control strategies available to a coal mine engineer. Correctly implemented suspension offers the greatest improvement in roof stability and greatest reduction in longwall risk. In some circumstances an alternative strategy based on the reinforcement of bedding parting may be more appropriate. For the control of maingates ahead of retreating longwall faces the ideal suspension support (if required) consists of angled, partially debonded, medium-length tendons installed as far behind the development face as possible. For situations where the roof may be subjected to tensile horizontal stress, immediate support by equally spaced short vertical tendons is required. The step away from fully-grouted tendons improves their survivability during the onset of compressive failure in the roof, minimises the risk of isolated loading, and allows a more robust TARP for roof movement. All suspension systems require a sling or truss between the suspension elements.

## BACKGROUND

Typically the immediate roof of a coal mine roadway consists of a regular assemblage of rectangular prisms of rock or coal defined by bedding and joints (Figure 1), with an important exception if the joints are not aligned normal to bedding such as near faults. With the joints normal to bedding, the roof horizon has a finite compressive strength but zero tensile strength. The logical framework identifies suspension as the appropriate response to disordered roof, compressive failure and tensile failure (Seedsman, 2012). As alternatives, prop support cannot be used if the roadways are to be used for traffic flow and beam reinforcement cannot be used if the rocks within the beam have undergone compressive failure, the immediate roof is in tension, or if there are discontinuities dipping at less than about 70°. Recently, suspension design has been dismissed as fundamentally flawed (Frith, 2011, Frith and Colwell, 2011) on the basis that roof collapses have occurred even though calculations based on a suspension design give installed capacities in excess of the dead weight of the collapsed volume. This paper examines the details of a suspension design and highlights where engineering skills and judgement are required.

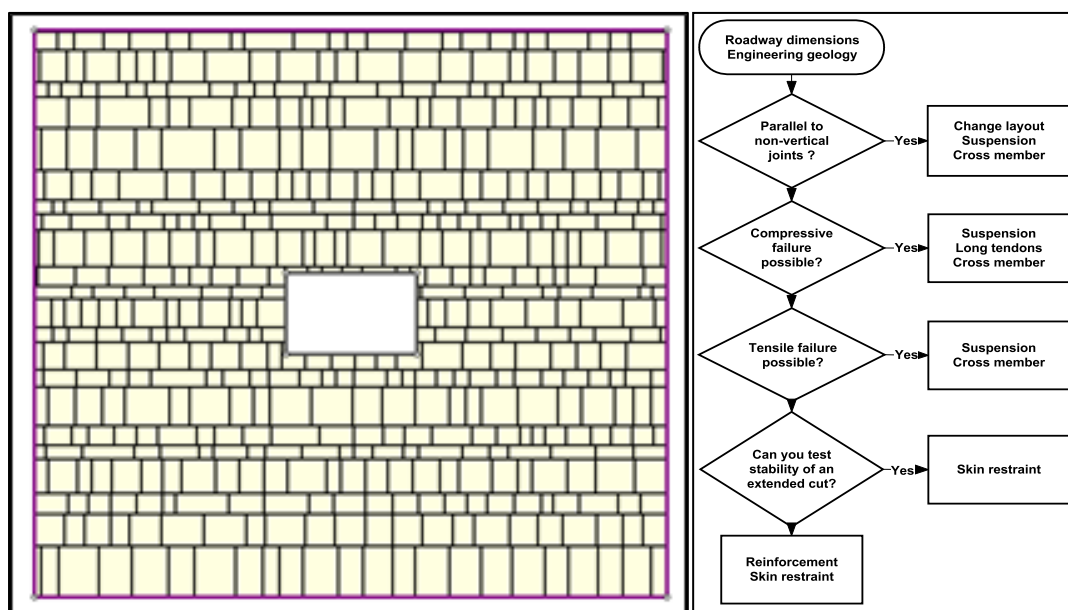


Figure 1 - Representative coal mine roof geology and the logical framework for coal mine roof control

There are two distinct applications for suspension designs in underground coal mines (Figure 2):

- Onset of compressive or tensile failure in the immediate roof, requiring that the broken and de-stressed rock mass be suspended from the intact rock that is arching over the roadway (Figure 2a).
- A possibly unstable immediate roof with a spanning unit within the bolted horizon (Figure 2b). This application requires determination of what is in fact a spanning unit.

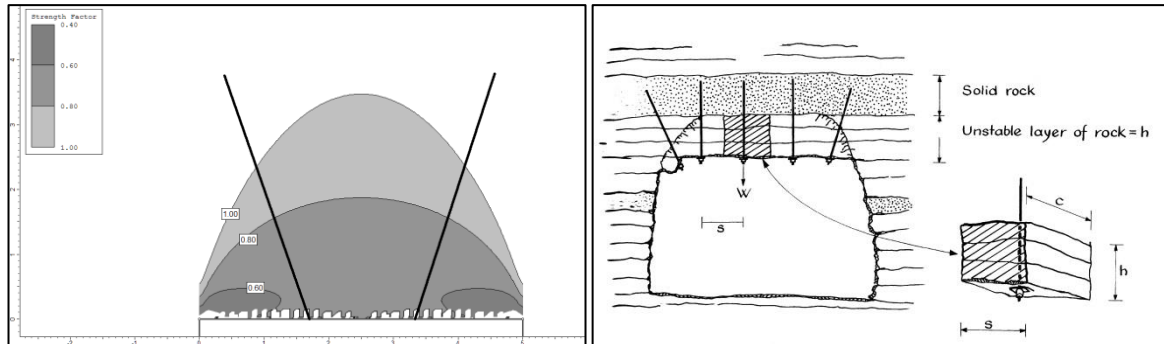


Figure 2 - Two suspension conditions (a) from a stable stress arch (b) from a strong bed (Stillborg, 1994)

## DESTRESSED ZONE AFTER COMPRESSIVE FAILURE

### Extent of compressive failure

Seedsman (2011) proposed a method to predict the height of compressive failure consistent with recent developments in the understanding of brittle rock strength and calibrated to mining experiences. In the method, the height of compressive failure is used as a proxy for the “height of softening” as determined by extensometry, with the conservative assumption that the height of softening represents the height to which the roof would collapse if it were to be unsupported. The rock strength criterion is further discussed in Seedsman (2013). Combined with an elastic analysis of stress in a transversely isotropic (bedded) material, the method allows the calculation of the maximum height of failure above any shaped opening as a function of the Uniaxial Compressive Strength (UCS), the vertical and horizontal stresses (Figure 3)<sup>1</sup>. Figure 3 shows how the height of compressive failure can increase substantially between roadway development and subsequent longwall retreat. At the development face, normal bolting lengths (1.5 m - 1.8 m) may be adequate but at the maingate longer tendons would be required. Close inspection of Figure 3 reveals lower strength factors towards the roof/rib corners which can be interpreted to be a reflection of stress guttering reported in underground roadways.

The height of the zone in the roof with a strength factor less than unity depends on the ratio of the UCS to the pre-mining vertical stress (Roof Strength Index – RSI), the ratio of the horizontal to vertical stress and the roadway span (Figure 4). Very high values of the RSI are required for the failure zone to disappear, and it is noteworthy that the zone needs to be in excess of 0.5m before it extends fully across the roadway.

### Mining context

It is important to note that these are elastic analyses, such that the numerical model does not redistribute the stresses after failure. It is assessed that more sophisticated models are not required for practical roof support design. Seedsman (2009) presented a conceptual model for stress redistributions in the immediate roof for conditions where the rock strength index would lead to the onset of large-scale compressive failure (Figure 5). In this model, horizontal stresses are not present within the immediate roof – these have been transferred to the stress arch as seen in the data reported by Mark *et al.* (2007) and the earlier work of Gale and Mathews (1992). This redistribution of stresses is

<sup>1</sup> In this paper Examine2D is used for simplicity to demonstrate concepts. For specific design, it is possible to use the same elastic parameters but should include different rock strength layers as appropriate in other numerical techniques.

not recognised in AMCMRR (Analytical Method – Coal Mine Roof Rating, Colwell and Frith 2010) which relies on the maintenance of elevated stress in the immediate roof line.

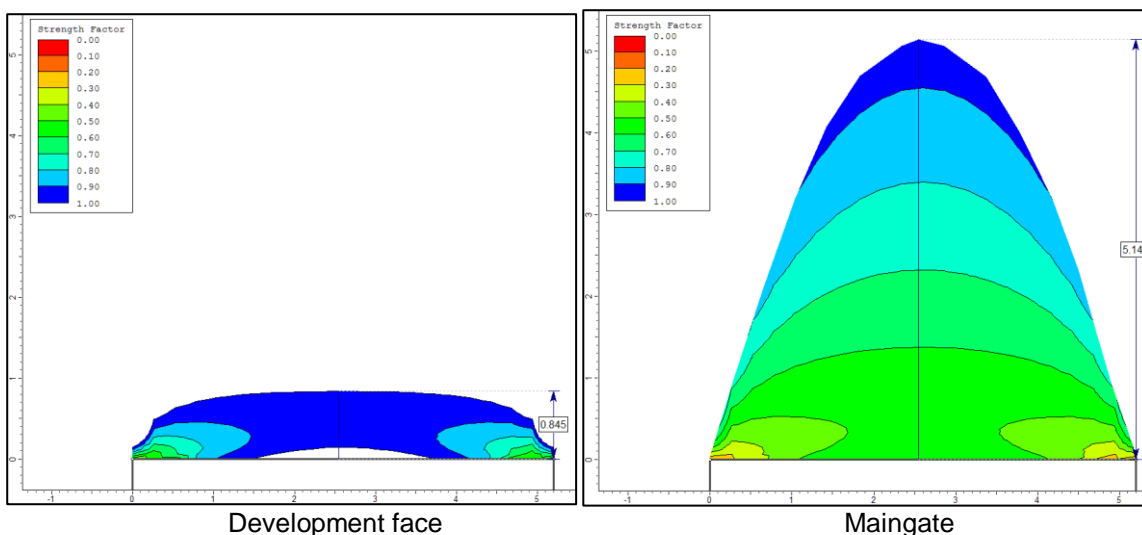


Figure 3 - Extent of compressive failure on development and at the maingate corner (depth = 300m, UCS = 45 MPa, frictional limit = 33°, K=1.5, reducing to 1.4 at maingate)

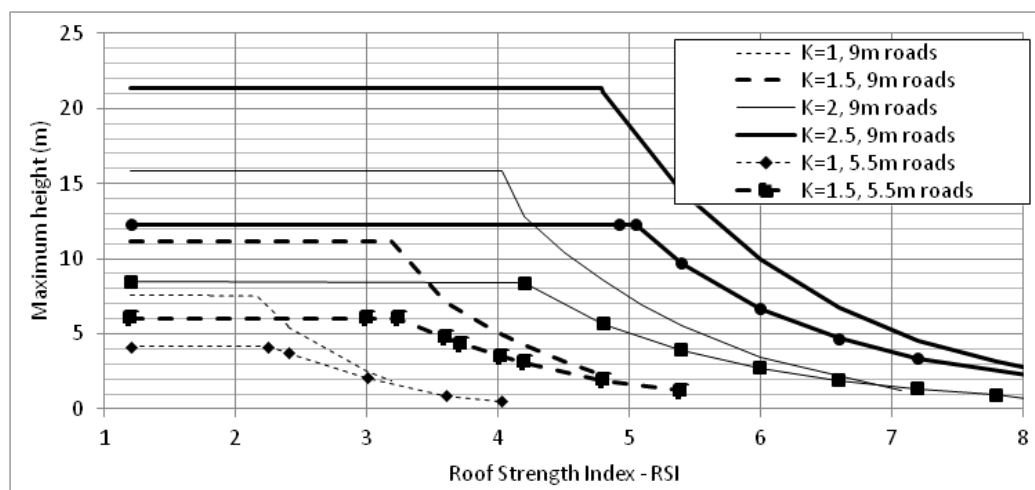


Figure 4 - Height of the zone with a strength factor less than 1.0 as a function of the roof strength index and the ratio of the horizontal to vertical stress

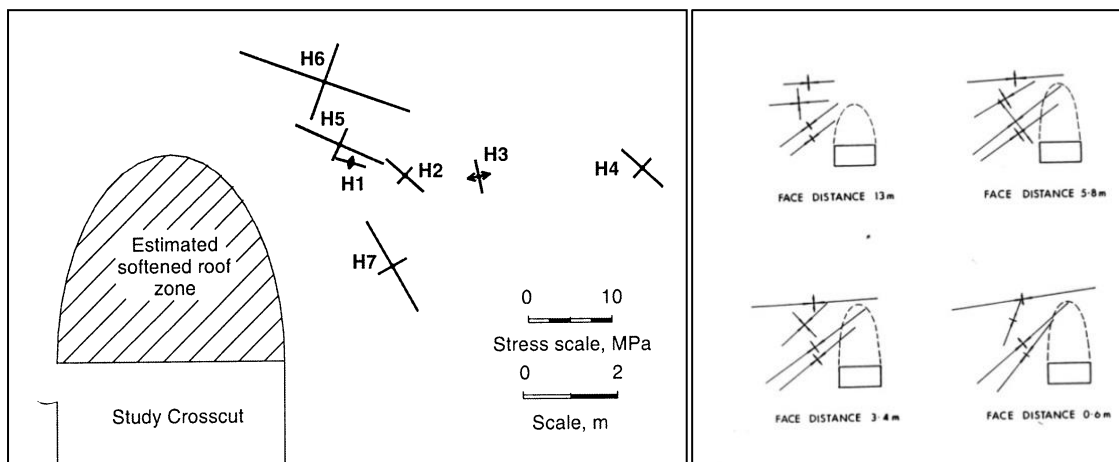


Figure 5 - Stress redistribution about softened zones (Mark, et al., 2007; Gale and Mathews, 1992)

### DESTRESSED ZONE AFTER TENSILE FAILURE

For the design of any ground control strategy at the roadway scale, the default assumption should be that the roof has zero tensile strength as a result of the presence of joints and bedding (Figure 1). This is totally consistent with the recommendations not to use the Generalised Hoek Brown criterion (Hoek and Brown, 1997) if there are only two discontinuity sets (joints and bedding). An important implication for numerical modellers is the need to use a tensile cut-off in a Mohr Coulomb criterion if continuum behaviour is assumed.

It is of interest to examine the height of failure (tensile or compressive) above the centreline of a typical development roadway for a rock mass with zero tensile strength and a Roof Strength Index (RSI) of 3.2 (Figure 6). Equally high zones may develop at very low horizontal to vertical stress ratios as at high stress ratios.

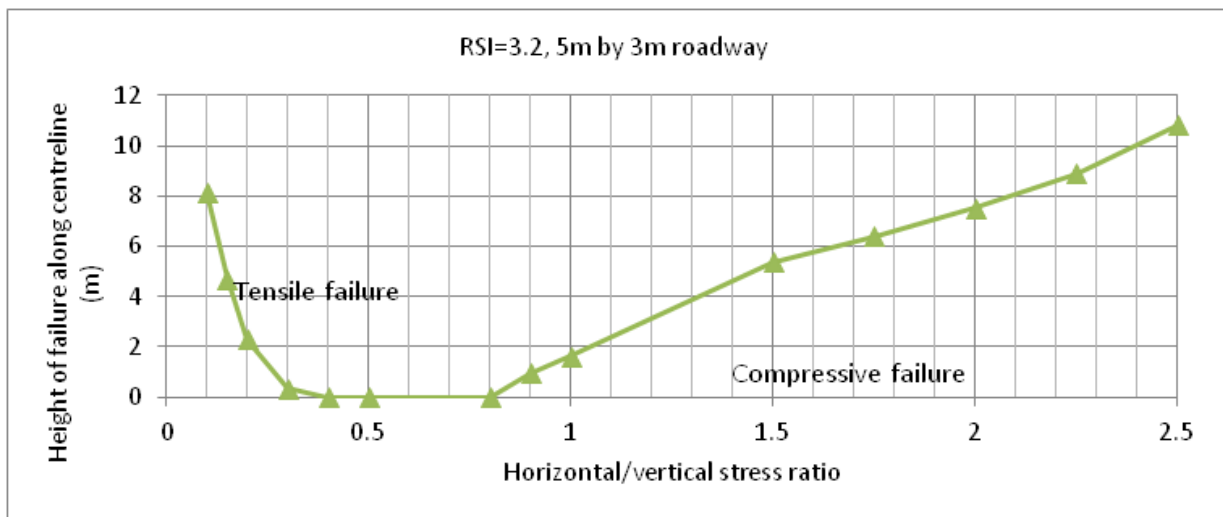


Figure 6 - Height of failure (strength factor = 1.0) varies with the ratio of the horizontal to vertical stress

#### Horizontal tensile stresses

If zero tensile strength is assumed, the extent of any tensile failure is the same as the zone of tensile stress. The discontinuity set of interest for roof collapse are the joints that are normal to the bedding and hence effectively vertical. These joints will contribute to roof collapse if the horizontal stress is either zero or tensile. Whether shear failure along joints leads to roof collapse will depend on the kinematics of the joint-bounded blocks which is related to the amount of dilation of the joints. Small dilations may allow block interaction and the formation of a voussoir beam. Larger dilations may mean blocks simply fall. Figure 7 shows the distribution of tensile horizontal stress for isotropic and a simple implementation of transversely isotropic ( $E_1=E_2$ ,  $E_1/G=15$ ) cases and three horizontal to vertical stress ratios. It is noted that the dimensions of the tension zones are independent of the magnitude of the applied stresses, and that the magnitudes of the tensile stress within the zones and the associated dilation increase as the stress magnitudes increase. The height of the tensile zones at the centreline decreases with an increase in stress ratio. The "ears" in  $K=0.1$  do not define kinematically acceptable blocks that could collapse.

#### Mining context

Elastic stress analyses, as well as closed-form solutions of stress around holes (Poulos and Davis, 1974, Brady and Brown, 1985) all indicate a reduction of roof stress as the vertical stress increases compared to the horizontal stress. This is opposite to that proposed by Frith (2000) who invoke the so called Poissons Ratio effect, although the fundamental requirement for absolute zero lateral strain when invoking this effect cannot be satisfied at or near an excavation boundary given that the roadway itself deforms.

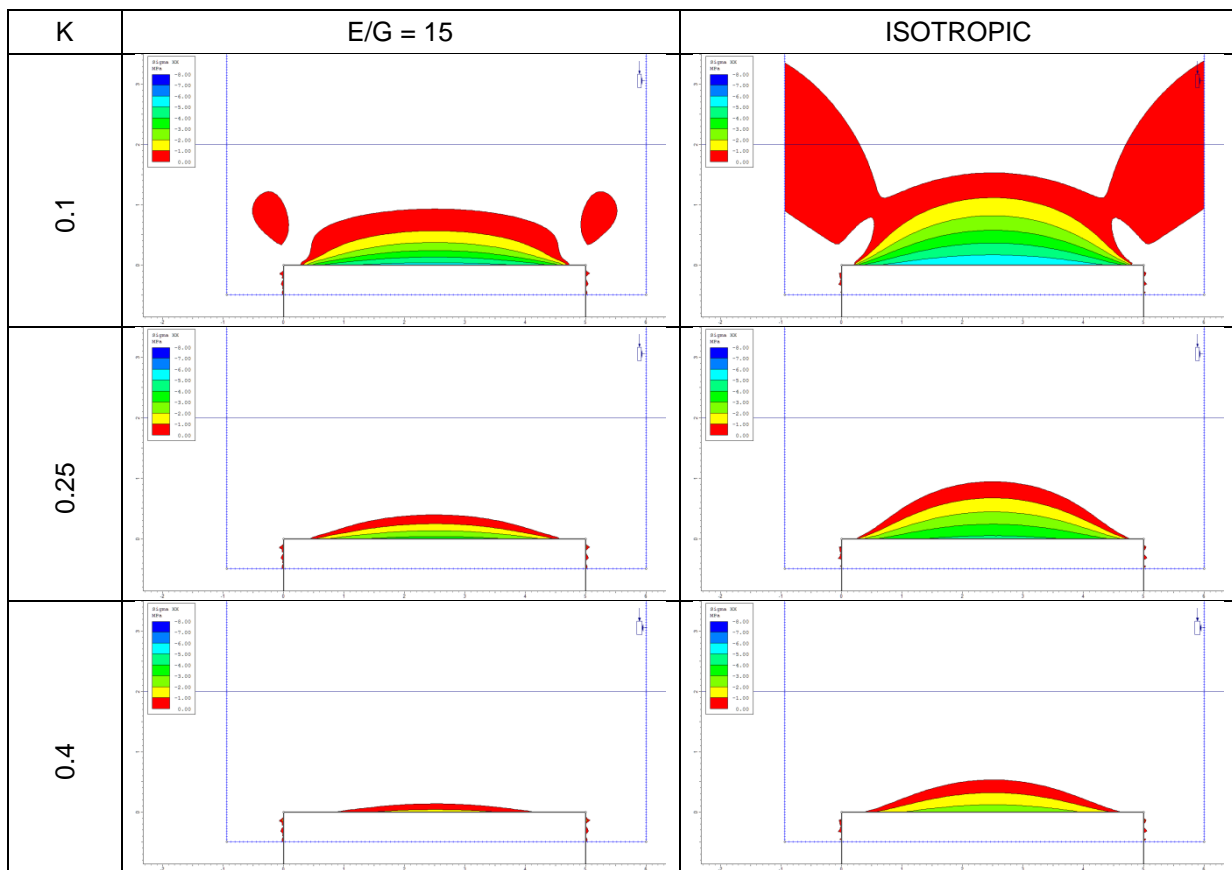


**Figure 7 - 2D Continuum tensile horizontal stresses in the roof of a roadway**

The key to anticipating the onset of tensile roof stress is to consider the situation where the vertical stresses are higher than the horizontal stress. The compilations of international stress data (Hoek and Brown, 1980) and Australian coal measures stress data (Nemcik, *et al.*, 2006) suggest that this is relatively rare. However in the coal mining sector, there are a number of specific environments where a low stress ratio should be anticipated as the “base-case”:

- thick coal seams where the immediate roof is coal (Seedsman, 2004). Very low horizontal to vertical stress ratios have been uniquely measured in coal and this is possibly related to shrinkage of the coal as it is dewatered by underground mining (gas may be of secondary importance). It is noted that lower stress ratios may result as the joint spacing in the coal reduces. A consequence is the need to be particularly vigilant when forming wide roadways with a coal roof.
- undermining of pillars in multiple seam operations. Transverse isotropy induced by bedding appears to result in a columnisation of the vertical stress (Suchowerska, *et al.*, 2013) and this is consistent with the author’s observations and simple analyses (Figure 8). The spread of vertical stresses implied by the simple Boussinesq models may not be appropriate for coal mine pillars.

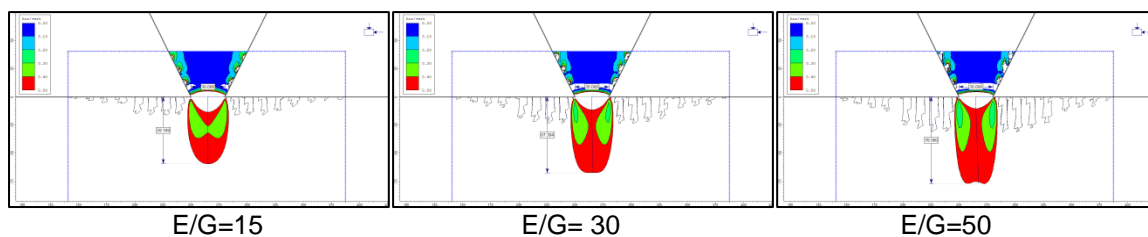


**Figure 8- Columnisation of vertical stress below a 30m wide chain pillar with 250m wide extraction**

- tailgates. The impact of yielding pillars and floor failure is discussed by Diederichs and Kaiser, 1999). Based on the author’s observations and an interpretation of the ALTS method (Colwell,

1998), on the other side of an adequately-sized chain pillar, the stress reduction associated with the adjacent longwall is not sufficient to lead to adverse stress ratios and the onset of tensile relaxation in the tailgate. Adequately sized in this context is one that is behaving elastically. If the pillar is designed to yield, then the additional vertical deflections in the pillar will lead to tangential relaxation in the roof line. This is considered to be the fundamental mechanism behind ALTS: the pillar strength equation is a criterion and roofs with low CMRR are those that are more closely bedded, more closely jointed and hence more susceptible to tensile failure. A bearing failure of weak layers in the floor of a pillar system may lead to sufficient vertical deflection to mobilise this mechanism as well.

**IDENTIFYING A SPANNING UNIT**

In this case the key question to be asked is “What defines a spanning unit?”. Voussoir beam theory presumes jointed rock and so removes the theoretical difficulty in applying elastic beam equations to a no-tension material. There are several solutions to the statically indeterminate analytical formulation of a voussoir beam and the method of Sofianos and Kapensis (1998), with the low value for the fractional loaded section (n) has been found to be appropriate. Although not strictly rigorous, it is possible to examine the effect of an axial stress applied to a voussoir beam by reducing the UCS value without changing the modulus. The impact of an applied axial loading on the required beam thickness is not significant until the applied stress is about 80% of the UCS (Figure 9).

An interesting aspect of voussoir beam analysis is the recognition that the deflection of a beam at the onset of compressive failure is independent of its span or its thickness, but is a function of the UCS (and by implication its modulus) and the surcharge carried (Figure 10). This may be of value when developing Trigger Action Response Plans (TARPS) based on roof deformations.

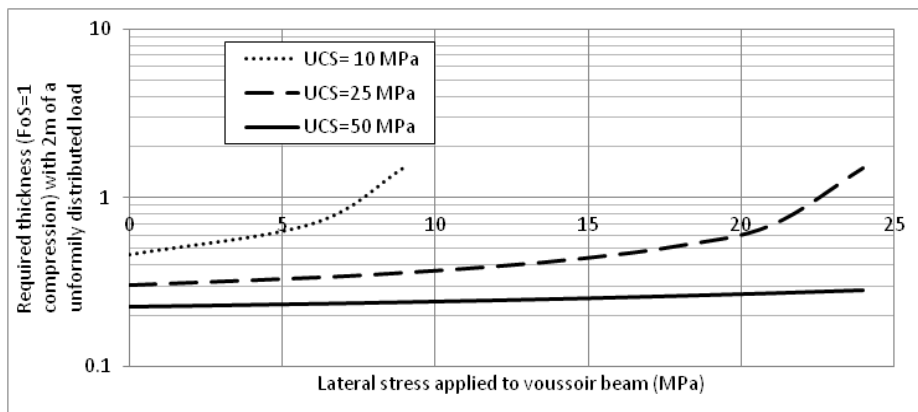


**Figure 9 - The sensitivity of the required thickness of a voussoir beam with a 5 m span to an applied axial stress**

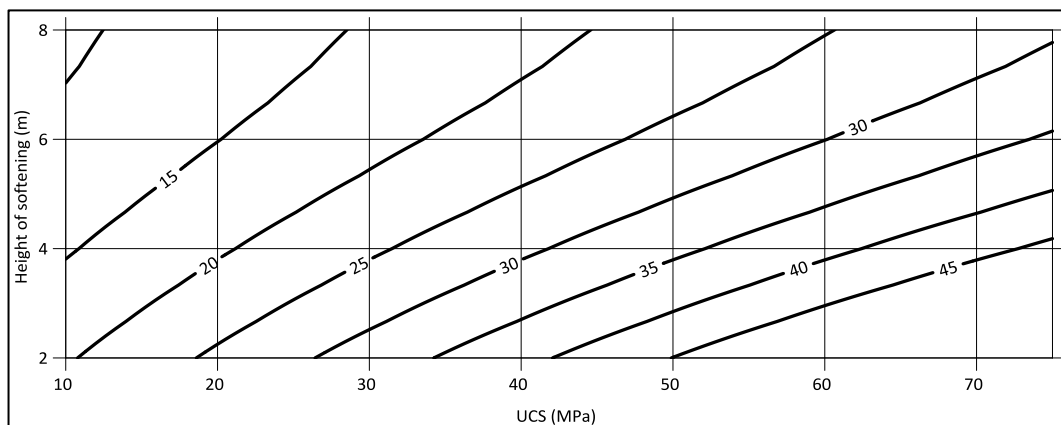


**Figure 10 - Centreline deflection (mm) of a voussoir beam at the onset of failure (E=250 UCS)**

## Mining context

Inspection of Figure 9 suggests that the thickness of a spanning unit needs to be in the order of 300 mm. As defined, the spanning unit in this context is similar to the minimum of 300 mm for the "strong bed adjustment" referenced in the CMRR system and the requirements of the US regulations - 30 CFR 75.204(f)(1) which states that "roof bolts that provide support by suspending the roof from overlying stronger strata shall be long enough to anchor at least 12 inches into the stronger strata".

A note of warning is important: a high degree of confidence in the sedimentary geology of the strong bed is required or it will be necessary to commit to reinforce potential layers within the strong bed. The base of coal measure units such as sandstones and conglomerates may be locally thinly bedded, unlike limestones that often form the strong beds in the US mines.

## SPECIFYING THE SUSPENSION PATTERN

In the circumstances outlined above and if there is a need to keep the roadway open for access or egress, then a suspension design is required. The design model is simple and involves the dead weight of volume of rock or coal with no imposed horizontal stresses. Some horizontal stress may be induced by subsequent block rotations within the fractured volume but these cannot be relied on in a robust support design. It is noted that these assumptions rule out the use of ground reaction curves – the model invokes gravity dead weight so there is no arching of loads or stresses.

The parameters to be considered are the height and weight of the suspended block, the length of the anchorage, the capacity of the tendon, the location of the tendons, the "sling" between tendons, the mode of installation, and the resultant improvement in the stability of the roof.

### Height and weight to be suspended

The density of the material to be suspended is usually well known (1.4 - 1.6 t/m<sup>3</sup> for coal, 2.5 t/m<sup>3</sup> for rock) so the design quickly focussed on the height and shape of the collapse volume. For compressive failure the height ( $H_{max}$ ) can come from an analysis similar to Figure 4 and the shape can be assumed to be a parabola (cross sectional area = 2/3 base\*height). For tensile failure, the height can come from analyses like Figure 7 with the shape assumed to be a rectangle.

### Tendon capacity

Assuming the anchorage is adequately designed (see below), the capacity to use is either the tensile strength of the tendon or the collar assemblage if the tendon is point-anchored. There is an important question about whether the tendons will be equally loaded. This is likely to be the case for the spans being considered but it is good practice to have some ductility in the cables so that there is an increased ability to redistribute loads evenly between them.

### Length

The anchorage can be estimated using the methods of Littlejohn (1993), viz:

$$L_a = M^2 \cdot \cos\Phi \cdot T / (\pi \cdot d \cdot UCS \cdot (1 - \sin\Phi))$$

Where  $L_a$  = required anchorage length,  $T$  = tendon capacity, UCS of the rock or grout (MPa) and  $\Phi$  = friction angle, and  $M$  is a confidence factor.

Analyses should be conducted for the cable/grout interface and at the grout/rock interface, with the former considering the maximum diameter of bulbed or nutcaged cables.

### Location

The vertical height of a parabolic shaped collapse zone is given by:

$$L_{vh} = H_{max} - 4x^2 H_{max} / W^2$$

Where  $L_{vh}$  = vertical height,  $W$  = roadway width, and  $x$  is distance from the centreline. The algebra for angled cables is more complex and it may be better to determine the length with a scale drawing.

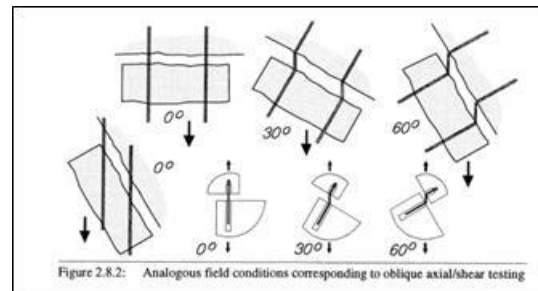
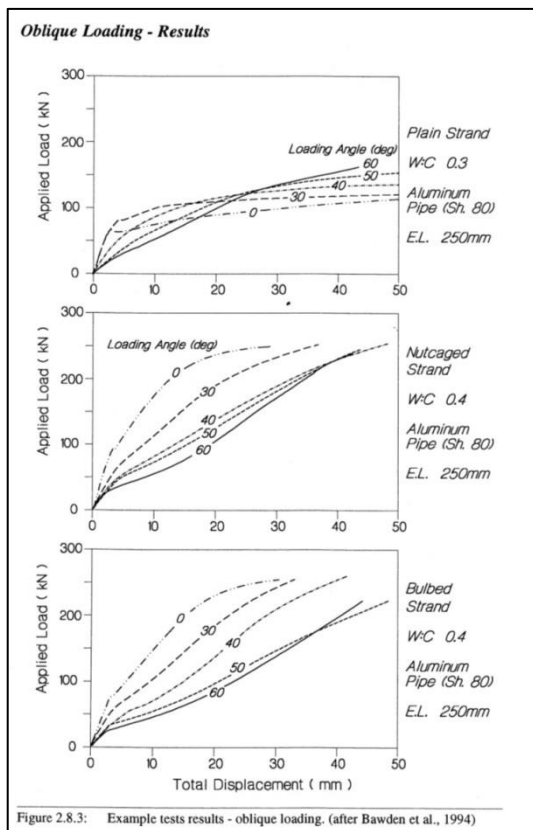
For compressive failure, an optimum design is obtained by locating the anchorages angled away from centreline to reduce the exposure of the design to uncertainties in the height of failure that could lead to the anchorage being over-ridden (there may be little if any deformation warning of this). The collars should not be located within 1 m of the rib corner as the extent of damage may be too great to allow the

transfer of loads from the tendon to the roof. Routinely pairs of cables are used spaced 1/3 and 2/3 across a development roadway and angled at no more than about 15° from the vertical.

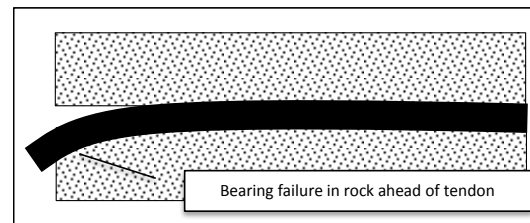
For tensile failures and suspension from a spanning unit, evenly spaced tendons are probably the best.

**Inclined tendons**

Hutchinson and Diederichs (1996) present a discussion on the capacity of angled tendons based on a series of laboratory tests of plain, nutcaged and bulbed cables. The results for the plain cable were anomalous and are the result of the cables slipping at the cable/grout interface. For the other cable types, where the effective diameter of the cable is much greater, the experimental design was valid, and the results show no significant difference in the peak loads. The decrease in capacity proposed by Frith (2011) and Frith and Colwell (2011) by referencing structural engineering is not observed and this has been attributed by many researchers to the yielding of the grout/rock ahead of the tendon (Holmberg and Stille, 1992).



Experimental design



Yielding of rock in front of tendon

**Figure 11 - Combined axial and tensile loading of tendons (reproduced from Hutchinson and Diederichs, 1996)**

The angled cables show greater deformation which is advantageous for a roadway suspension system in that it allows a greater opportunity to redistribute the loads between the cables and also provides a level of deformation that can be used in a TARP.

**Stiffness - Post installation shear**

The conventional view is that a stiff installation is required to limit the development of the height of softening. This view may have developed as a consequence of the way in which the empirical data has been presented (Figure 12). It is equally valid to plot the height of softening as the independent variable (abscissa) and the roof deflection as the dependent variable or ordinate. With this presentation an alternative interpretation is possible - that roof deflection is a response to failure in the roof, possibly in response to the dilation that occurs at failure. This interpretation leads to a conclusion that it is futile to seek to limit deflections given the very high stresses that drive failure. In rock masses, the ground stresses can arch above a roadway so the ground control approach is to seek to control unacceptable deflections until the stresses are redirected into the arch.

This interaction between deflection and stress redistribution is the basis of the ground reaction concept, and the classic discussion of this concept involves the early installation of stiff support. Referring back to Figure 3, installation of roof support at the development face or even in front of the longwall abutment front is "early" in the context of the stress changes that are about to impact the maingate corner. A stiff installation will not be able to prevent the onset of failure in the roof and more importantly may not be able to sustain the deformation. Test data on the shear stiffness of fully-grouted and point-anchored cables has not been found, but data on double-embedment tension tests (Clifford, *et al.*, 2001) has a fully grouted cable failing at 7 mm to 8 mm of opening of a joint compared to in excess of 40 mm for a point anchored cable (Figure 13)

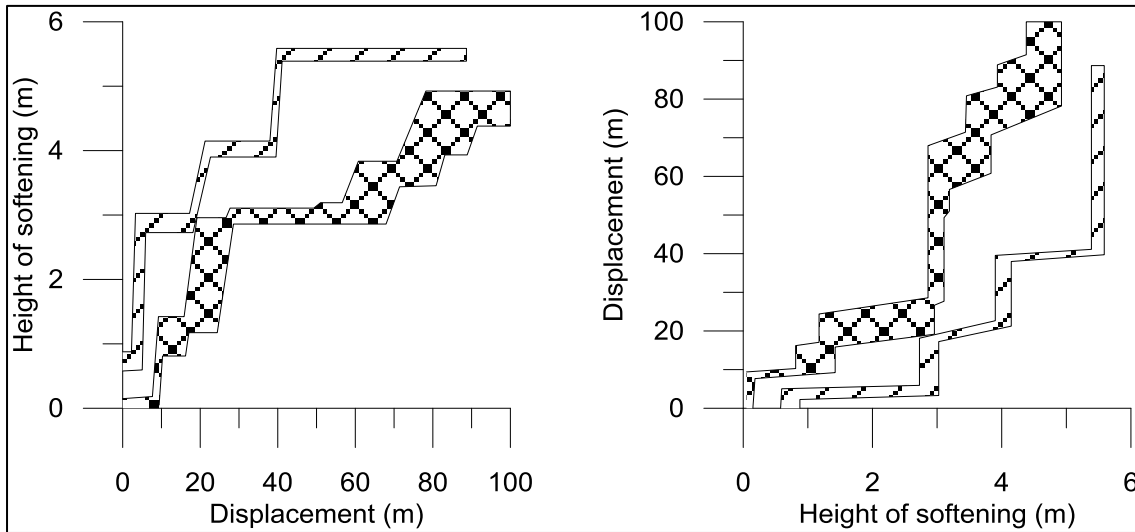


Figure 12 - Replotting of height of softening and roof deflection data changes interpretation of empirical data (after Gale, *et al.*, 1992)

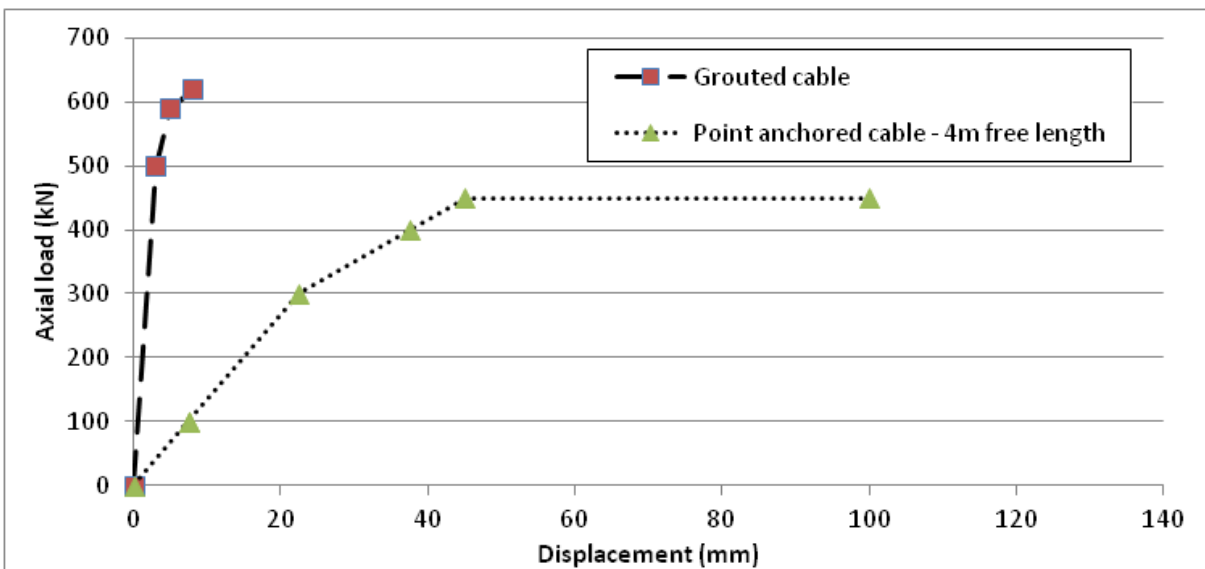
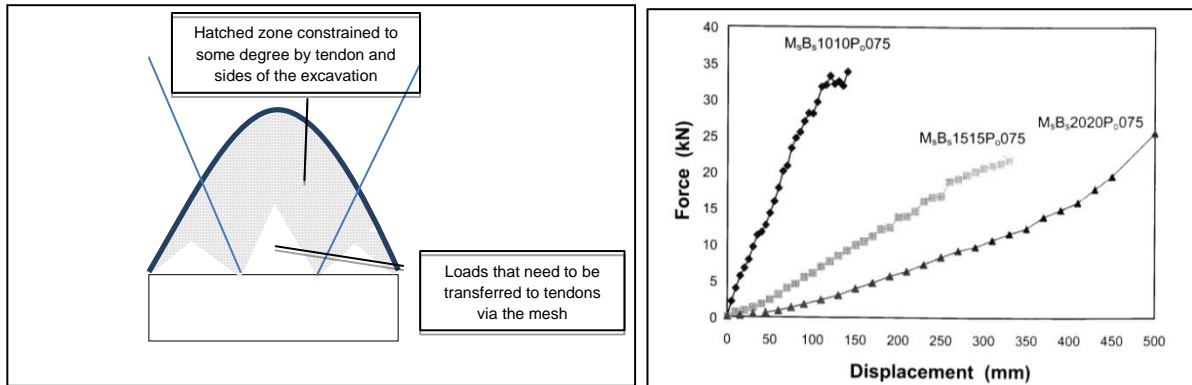


Figure 13 - Comparison of double embedment test on a grouted cable (after Clifford, *et al.*, 2001) and calculated deformation of a 4m free length of cable

Under simple direct loading, a point-anchored cable has lower capacity than a fully grouted cable and this is the result of yielding and failure of the collar assembly. To address the stiffness concerns while still being able to mobilise the full tensile capacity of the cable it should be possible to fully grout the tendon but to decouple the middle section. As well as increasing the survivability of the tendon, the roof deflections before failure will be greater and this will allow a more robust deflection trigger for any TARP. However there would be no deformation at the collar assembly itself.

## Mesh/sling

If a broken de-stressed rock mass is assumed, there may be zones within the immediate roof that are not directly restrained by the tendons (Figure 14). If these zones were to collapse, the roof would unravel around the long tendons leading to total collapse. Depending on the load distribution angle beneath the collar and the spacing of the tendons, loads of up to 3 to 5 tonnes can be reasonably expected and these need to be retained by the roof mesh, W strap or a truss. Laboratory tests on standard mesh panels (Thompson, 2004) indicate a capacity of 2 to 3.5 tonnes depending on the bolt spacing. It is concluded that any suspension strategy must also include specific measures to ensure that collapse of the roof between the tendons does not lead to unravelling of the roof. Closer spaced, lower capacity tendons may be preferable despite the greater installation time.



**Figure 14 - Zones which need to be supported to transfer loads to the tendons and the capacity of typical mesh panels**

## Design factors

The term “Factor of Safety” is still commonly used although its misuse and incorrect application is now being recognised. At its simplest arithmetic level, a factor of safety is the ratio of the estimated strength to the estimated load. In the real world, there may be uncertainty in the estimates. A design is then considered acceptable if the likelihood of the strength being exceeded by the load is acceptable given the consequences. In some industries, for example aerospace, the factors of safety can be relatively low compared to geotechnical designs because the uncertainties in the strength and load estimates are low even though the consequences of failure are high - high factors of safety could lead to planes that are too heavy to fly. In geotechnical designs, the factors may be high because of the difficulties in estimating strengths. From a design perspective, confidence in these estimates determines the factor of safety that is acceptable.

With this use of the term in geotechnical engineering, factors of safety should not be pre-determined although it is recognised that mining regulation is tending to move that way. It is meaningless to apply factors of safety from other industries, for example crane cables. If a factor of safety value is mandated on a mine geotechnical engineer, it should be used to determine the required site investigation to reduce the uncertainties to the implied level.

When finalising the design, the mine geotechnical engineer should consider:

- Height factor – how reliable is the estimate of height? How reliable are the estimates of rock strength and the in-situ stresses, what have back analyses suggested, is there a precedent at your mine or close by? Lower bound strength values and any available stress data should be used when accepting the heights given by Figure 4. This parameter leads directly to the loads to be suspended, with little uncertainty regarding width or density.
- Loading factor - will the tendons be loaded equally? Given the general industry expectations regarding “Factors of Safety” it may be appropriate wise to add about 20% to calculated loads.
- Survivability factor - could they fail due to deformation incompatibility? An arbitrary 50% reduction in the mobilised strength of fully grouted cables can be considered used but it should be recognised that this is without technical justification – clearly more research is required.

- Anchorage length – The civil engineering literature suggests a doubling of the calculated length to address uncertainties about installation quality, values between 1.25 and 1.5 have been used.

## CONCLUSIONS

Correctly designed, suspension is a very robust roof support design approach. There are some important subtleties in the design which conflict with some of the incorrect concepts that have been published in the last decade. A suspension design accepts that it is not possible to prevent tensile or compressive failure of the roof and that what is needed is a support regime that can survive the onset of failure and then prevent the subsequent gravity-driven collapse. A corollary of this is that deformations are inevitable and can be utilised in a TARP process, recognising that the triggers will be related to deformations of flexible systems. Suspension systems are installed proactively, in that they anticipate the onset of failure and are ready to prevent collapse. In better ground where compressive or tensile failure is not likely, it may be efficient and economic to prevent the deterioration of a bedded roof by reinforcing against shear.

## REFERENCES

- Brady, B H G and Brown, E T, 1985. *Rock mechanics for underground mining*. London, UK: George Allen and Unwin.
- Clifford, B, Kent, L, Altounyan, P and Bigby, D, 2001. Developments in the long tendon systems used in coal mining reinforcement. *In Proceedings, 20<sup>th</sup> International Conference on Ground Control in Mining*. Morgantown WV August 7-9, 235-241.
- Colwell, M G, 1998. *Chain Pillar Design – Calibration of ALPS*. Final Report – ACARP Project C6036, 67p.
- Colwell, M G and Frith, R, 2010. AMCMRR – an analytical model for coal mine roof reinforcement. *10<sup>th</sup> Underground Coal Operators' Conference*. University of Wollongong and the Australasian Institute of Mining and Metallurgy, 73-83. <http://ro.uow.edu.au/coal/302/>.
- Diederichs, M S and Kaiser, P K, 1999. Tensile strength and abutment relaxation as failure control mechanisms in underground excavations. *International Journal of Rock Mechanics and Mining Sciences*: 36, 69-96.
- Frith, R. 2000. The use of cribless tailgates in longwall extraction. *Proceedings 19<sup>th</sup> International Conference on Ground Control in Mining*. Morgantown, 84-92.
- Frith, R, 2011 Why Dead Load Suspension Design For Roadway Roof Support Is Fundamentally Flawed Within A Pro-Active Strata Management System. *11<sup>th</sup> Underground Coal Operators Conference*. University of Wollongong and the Australasian Institute of Mining and Metallurgy, 73-82. <http://ro.uow.edu.au/coal/341/>.
- Frith, R and Colwell, M G, 2011 Why Dead Load Suspension Design For Roadway Roof Support Is Fundamentally Flawed Within A Pro-Active Strata Management System. *Proceedings 30<sup>th</sup> International Conference on Ground Control in Mining*. <http://icgcm.conferenceacademy.com/papers/detail.aspx?subdomain=icgcm and iid=890>.
- Gale, W J, Fabjanczyk, M W, Tarrant, G C and Guy, R J, 1992, Optimisation of reinforcement design of coal mine roadways. *11<sup>th</sup> International Conference Ground Control in Mining*. Wollongong, 7-10 July 1992. pp272-292. <http://icgcm.conferenceacademy.com/papers/detail.aspx?subdomain=icgcm and iid=2001>.
- Gale, W J and Matthews, S M, 1992. *Stress control methods for optimised development and extraction operations*. Report to National Energy Research Development, and Demonstration (NERD and D) Program, Project 1301.
- Hoek, E and Brown, E T, 1980. *Underground Excavations in Rock*. The Institution of Mining and Metallurgy, London.
- Hoek, E and Brown, E T, 1997. Practical estimates of rock mass strength. *International Journal of Rock Mechanics and Mining Sciences*, 34 (8), pp1165-1186.
- Holmberg, M and Stille, H, 1992. The mechanical behaviour of a single grouted rock bolt. *In Rock Support in Mining and Underground Excavation*, Edited by Kaiser and McCreath, Balkema. Rotterdam, pp473-481.
- Hutchinson, D J and Diederichs, M S, 1996. *Cable bolting in underground mines*. Vancouver: Bitech, Richmond British Columbia.
- Littlejohn, S, 1993. Overview of rock anchorages. *Comprehensive Rock Engineering*, 4:413-450. Oxford: Pergamon.

- Mark, C, 1990. Pillar Design Methods for Longwall Mining. *United States Bureau of Mines Information Circular* 9247, 53p.
- Mark, C and Molinda, G M, 2005. The coal mine roof rating (CMRR): A decade of experience. *Coal Geology*, 64, pp85-103.
- Mark, C, Gale, W, Oylar, D and Chen, J, 2007. Case history of the response of a longwall entry subjected to concentrated horizontal stress. *International Journal of Rock Mechanics and Mining Sciences*, 44, pp210-221.
- Martin, C D, Kaiser, P K and McCreath, D R, 1991. Hoek-Brown parameters for predicting the depth of brittle failure around tunnels. *Canadian Geotechnical Journal*, 36: 136-151.
- Nemcik, J A, Gale, W J and Fabjanczyk, M W, 2006. Methods of interpreting ground stress based on underground stress measurements and numerical modelling. *Proceedings Coal 2006, 7<sup>th</sup> Underground Coal Operators Conference*. pp104-112. <http://ro.uow.edu.au/coal/39/>.
- Poulos, H G and Davis, E H, 1974. *Elastic solutions for soil and rock mechanics*. John Wiley and Sons Inc. New York.
- Seedsman, R W, 2004. Failure modes and support of coal roof. *Ground Support in Mining and Underground Construction, Proceedings 5<sup>th</sup> International Symposium on Ground Support*. pp367-374.
- Seedsman, R W, 2009. Stresses in the immediate roof of a coal mine roadway. *9th Australasian Coal Operators' Conference*, University of Wollongong and the Australasian Institute of Mining and Metallurgy, pp62-69. <http://ro.uow.edu.au/coal/80/>.
- Seedsman, R W, Brisbane, P and Mitchell, G. 2002. Strata management at the Goonyella Exploration Adit Project. *Coal 2002 3<sup>rd</sup> Australian Coal Operators' Conference*, pp193-202. <http://ro.uow.edu.au/coal/210/>.
- Seedsman, R W, 2011. Application of the brittle failure criterion to the design of roof support in the soft rocks of coal mines. *Coal 2011 - 11th Australasian Coal Operators' Conference*, University of Wollongong and the Australasian Institute of Mining and Metallurgy, pp60-72. <http://ro.uow.edu.au/coal/342/>.
- Seedsman, R W, 2012. The development and application of a logical framework for specifying roof and rib support/reinforcement in Australian underground coal mines. *7th International Symposium on Rock bolting and Rock Mechanics in Mining*. Aachen 30-31 May.
- Seedsman, R W, 2013. A practical strength criterion for coal mine roof support design in laminated soft rocks. Accepted by Mining Technology. <http://dx.doi.org/10.1179/1743286313Y.0000000044>.
- Sofianos, A and Kapensis, A P, 1998. Numerical evaluation of the response in bending of an underground hard rock voussoir beam roof. *International Journal of Rock Mechanics and Mining Sciences*, 35(8), pp1071-1086.
- Stillborg, B, 1994. *Professional Users Handbook for Rock Bolting*. Series on Rock and Soil Mechanics, Vol 18, Trans Tech Publications.
- Suchowska, A M, Merifield, R S and Carter, J P, 2013. Vertical stress changes in multi-seam mining under supercritical longwall panels. *International Journal of Rock Mechanics and Mining Sciences*, 61, pp306-320.
- Thompson, A G, 2004. Rock support action of mesh quantified by testing and analysis. *Paper presented in Surface Support in Mining*. (Eds. Potvin, Y., Stacey, D., and Hadjigeorgiou, J.) Australian Centre for Geomechanics, pp391-398.

# NEW FRACTURE MODEL FOR THE PROGRESSIVE FAILURE OF ROCK SLOPES

Gaetano Venticinque and Jan Nemcik

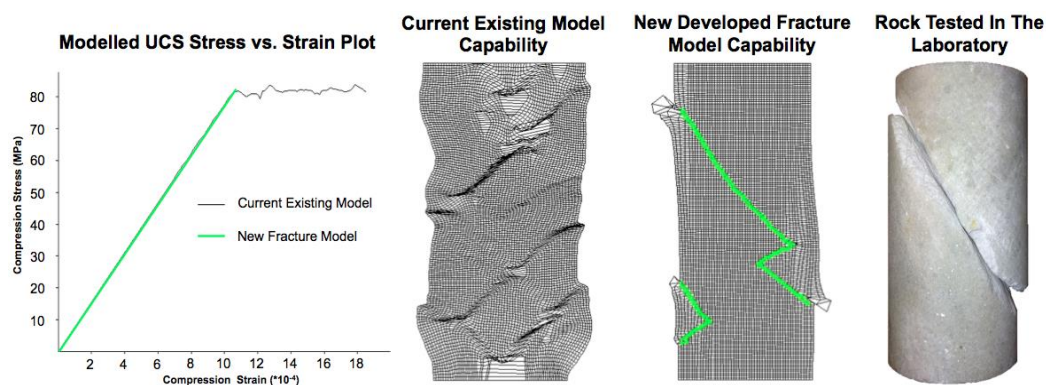
**ABSTRACT:** An improvement to previously developed constitutive FISH User-Defined-Model subroutine by Venticinque (2013) is demonstrated here to simulate the initiation and progressive propagation of fractures through rock structures. This model is based on the amalgamating failure and fracture mechanics theory applied to the finite difference FLAC code. The prior validation of fracture propagation in isotropic rock has been modified to simulate fracture propagation in anisotropic rock. It is shown that the model is capable to accurately simulate fracture distributions in both isotropic and anisotropic rock mass. Furthermore, application of the model to study rock slope stability highlights several characteristics relevant to the progressive failure process of hard rock dry wall slopes. Moreover the model introduces new potential insight towards the effectiveness of rock and cable bolt supports. This work contributes towards improving safety in mines through an increased understanding of key fracture and progressive failure characteristics within geological structures.

## INTRODUCTION

In open cut mines the failure of high wall rock slopes is regarded as a non-simultaneous occurrence. Instead massive shear failure events are recognised as being a progressive consequence of local fracture propagation from one area to another within the slope, (Bertoldi, 1988). The knowledge of when fractures initiate and how they may propagate through a rock mass is fundamental to the safety and efficiency of stable mine design. During simulation it is often useful to determine if and more importantly how a structure will fail. This paper presents an example to further demonstrate the capability of the recently developed model by Venticinque (2013).

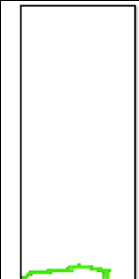
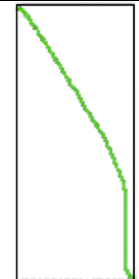
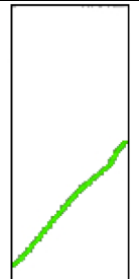
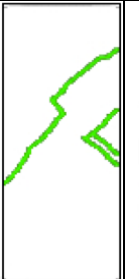
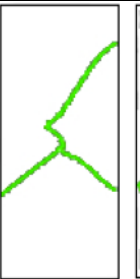
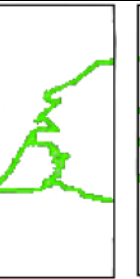
The fracture model is a constitutive FISH subroutine driving the FLAC 2D geotechnical software by Itasca (2005). It offers independent simulation of rock fracture initiation and propagation behaviour. This model has been previously verified for isotropic rocks where it was proved to offer more realistic solution of the brittle fracture propagation and post failure response of rock as illustrated in Figure 1. The modelled fractures exactly matched the fracture geometry that developed in the isotropic marble rock tested in the laboratory. It also shows the difference between the brittle fracture propagation and the unrealistic plastic-like failure akin to rock at critical stress modelled without the FISH subroutine.

Furthermore in its current form, the model incorporates all three combinations of fractures described by: Mode I tensile, Mixed Mode I-II and Mode II pure shear. This was verified through simulated application over the entire brittle-to-ductile transitional failure range of rock and shown in Table 1.



**Figure 1 - Comparison of current existing and newly developed modelled failure against real isotropic marble rock tested in the laboratory (Venticinque, *et al.*, 2013)**

**Table 1 - Simulated brittle-to-ductile transitional failure range of isotropic marble rock (Venticinque, et al., 2013)**

Confining Pressure	0 MPa*	0 MPa	3 MPa	5 MPa	10 MPa	25 MPa	50 MPa
$\sigma_1$ Theory	-3.5 MPa	80 MPa	99 MPa	111 MPa	137 MPa	199 MPa	283 MPa
$\beta$ ° Theory	0°	64°	-	-	-	-	-
$\sigma_1$ Modelled	-3.3 MPa	80 MPa	99 MPa	115 MPa	138 MPa	202 MPa	283 MPa
$\beta$ ° Modelled	0°	64°	55°	55°	50°	50°	45°
Fracture Distribution							

\*Under Tensile Loading Condition

**VALIDATION OF FRACTURE MODEL FOR ANISOTROPIC ROCK**

A FLAC model driven by the FISH fracture subroutine was constructed to simulate uniaxial compression failure in anisotropic marble rock. In FLAC anisotropic rocks are modelled with an isotropic continuum exhibiting reduced strength properties in the direction of existing joints. Simulated results have been validated against theoretical failure criteria for anisotropic rock by Jaeger and Cook (1971).

**Validation model**

The model used identical model geometry, intact rock properties and loading procedure as in previous verification reported in Venticinque *et al.* (2013) for isotropic rock. The anisotropy was introduced by altering FLAC joint properties to include weakly oriented joints at 40° to the sample vertical axis. The geometry of the modelled cylindrical rock core and the rock properties are shown in Figure 2 and Table 2 respectively.

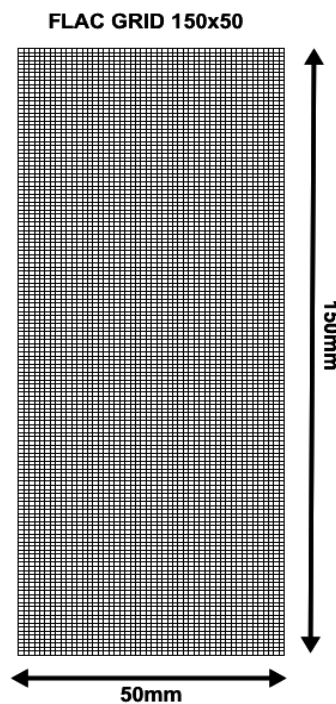


**Figure 2 - FLAC model geometry for cylindrical rock**

**Table 2 - Anisotropic modelled rock properties**

Isotropic Marble Rock Properties	Properties	Introduced Anisotropic Marble Rock Properties	
Bulk Modulus (GPa)	58.5	Joint Angle (°)	40
Shear Modulus (GPa)	27	Joint Friction (°)	32
Cohesion (MPa)	19.3	Joint Cohesion (MPa)	1
Tension (MPa)	3.5	Joint Tension (MPa)	3.5
Internal Friction (°)	38.5		
Density (kg/m <sup>3</sup> )	2700		

**Validation results**

The modelled fracture distribution presented in Figure 3 closely aligned expected slip failure along weakly bound joints oriented at 40°. In addition from the respective stress-strain plot, compressive strength was indicated at 8MPa. This value is identical to the theoretical derived value from Jaeger and Cook (1971) equations for anisotropic rock strength, Figure 4. In this way predicted fracture distributions of anisotropic rock in the fracture model are verified.

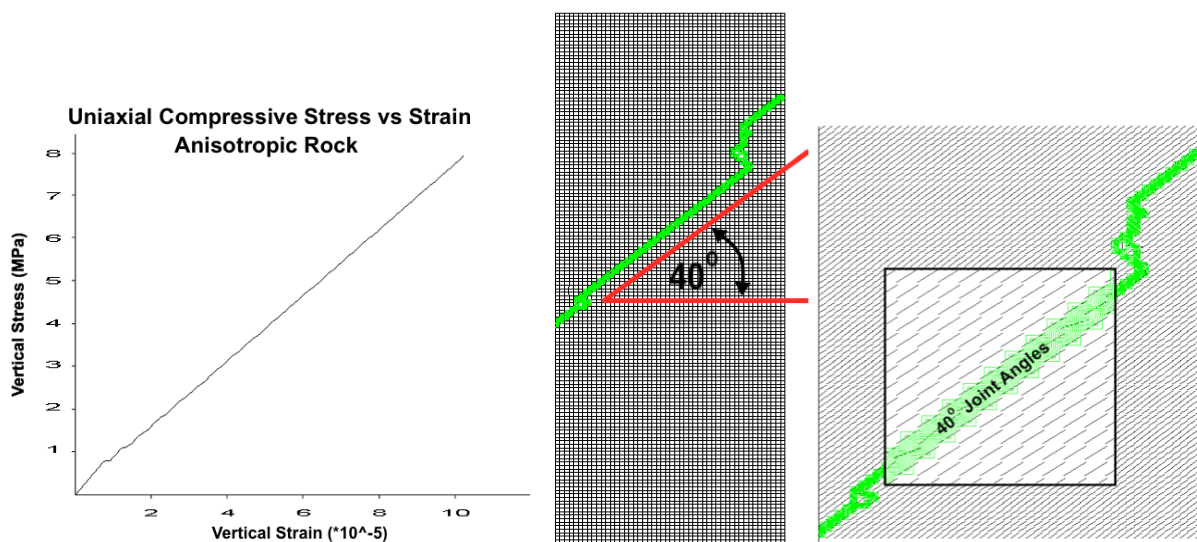


**Figure 3 - Interpretation of simulated failure plane produced for anisotropic rock**

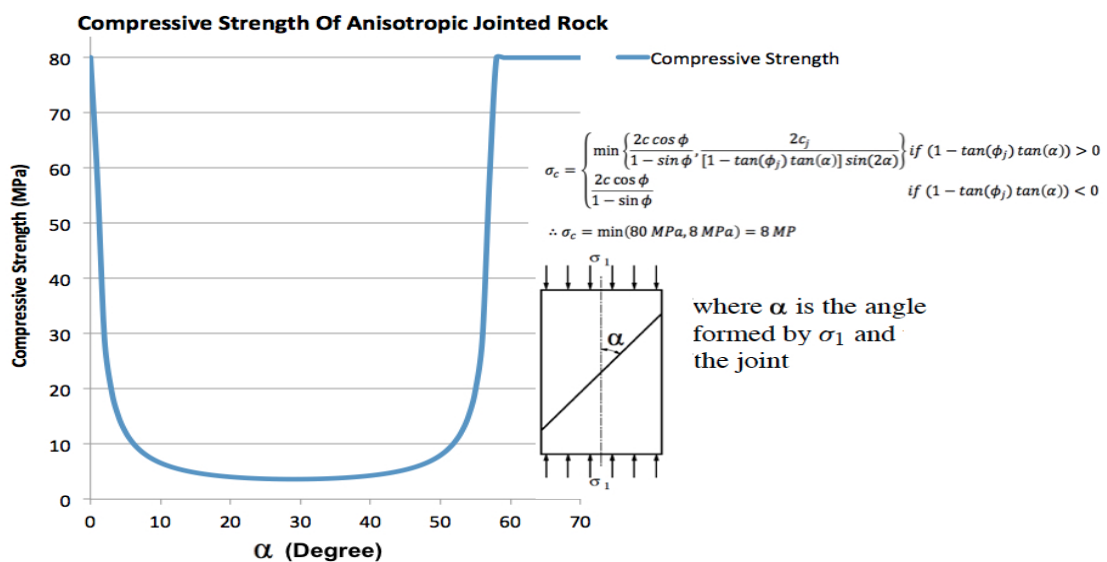


**Figure 4 - Comparison of uniaxial compressive strength values for anisotropic rock**

## SIMULATION OF ROCK SLOPE FAILURE

The application of the FISH subroutine fracture model for progressive failure simulation of hard rock slopes is demonstrated here. Two examples make the advantages of this developed model apparent, in particular the ability to perform comparative analysis between both fracture distribution and progressive failure of unsupported or supported rock slope designs.

### Rock slope model

The FLAC model used in these simulations reflected a hypothetical layered rock slope mined at 60° batter angle. In-situ stresses were equalised in models and progressive mining simulation undertaken through incremental excavations of 1m strips. Fractures and localised failures were produced independently throughout this entire process. Geological section of the model had a simple stratigraphy illustrated in Figure 5. The strata consisted of two coal seams overlain by claystone and weathered sandstone unit. Rock properties applied to this geology are listed in Table 3. Mechanical properties of rock and cable bolts can also be found in Table 4 representing the typical values experienced in the field.

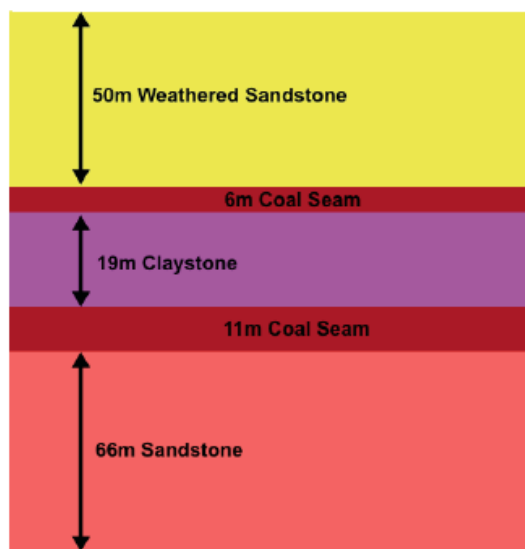


Figure 5 - Geologic stratigraphy of modelled rock units

Table 3 - Modelled rock unit properties

Property	Weathered Sandstone	Coal Seam	Claystone	Sandstone
Bulk Modulus (GPa)	6	2.5	4	6.7
Shear Modulus (GPa)	3	1.1	4.8	4
Cohesion (MPa)	.1	.1	.25	2
Tension (MPa)	.1	.1	.5	1
Internal Friction (°)	32	25	30	35
Density (kg/m <sup>3</sup> )	2500	1380	2500	2500

Table 4 - Modelled rock bolt and cable bolt properties

Property	Rock Bolt	Cable Bolt
Youngs' Modulus (GPa)	200	200
Yield Strength (MPa)	340	1380
Cross Sectional Area (mm <sup>2</sup> )	370	380
Installed Length (m)	2	10-20m
Tensioned Force (kN)	-	100

### Example 1 - Simulation of unsupported rock slope

The FLAC results plotted in Figure 6 reveals the dominating fracture produced at failure for the 60-degree batter design. Maximum depth following failure for the unsupported slope is reported as 49m.

Following all fracture initiation and propagation the FLAC model was iterated once again to establish the effect that newly formed fractures would have on the overall model structure. For the FLAC model with the FISH subroutine an immediate failure was simulated through increasing rotational displacement shown in Figure 7. This is compared to FLAC model without application of the FISH subroutine with negligible unchanged displacement. In this way the FISH subroutine demonstrates ability to simulate failure initiated through multiple fracturing that previous FLAC modelling was incapable performing.

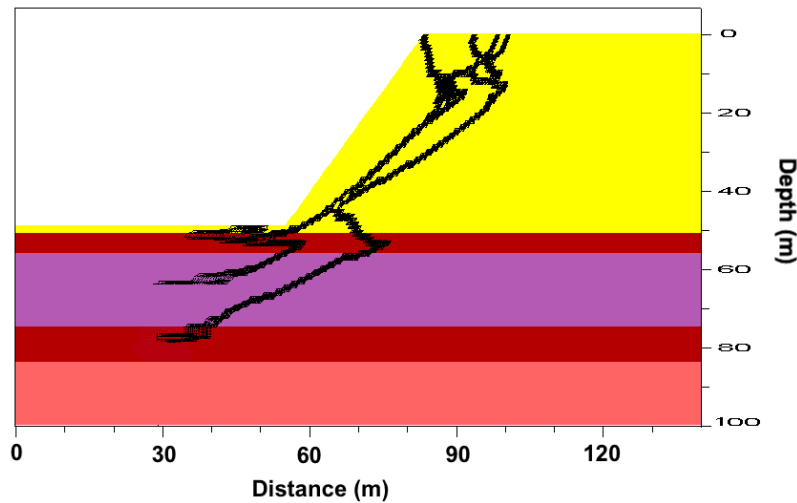


Figure 6 - Simulated failure in unsupported rock slope

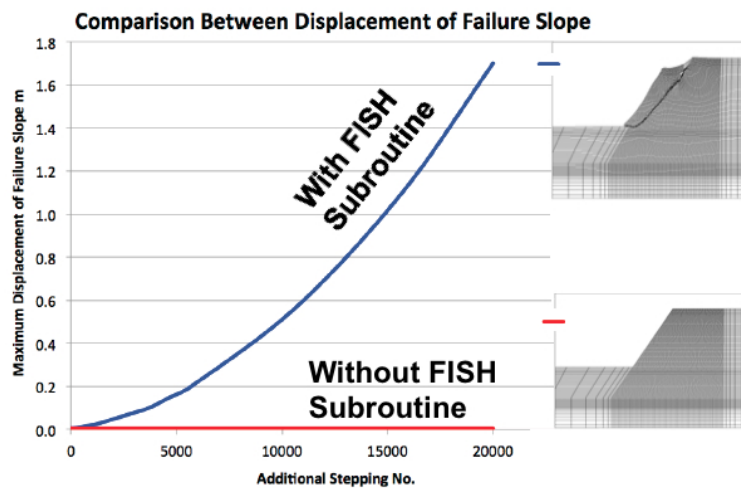


Figure 7 - Comparison between slope displacement at failure for FLAC model with and without application of FISH subroutine

### Example 2 - Simulation of supported rock slope

The progressive failure and fracture distribution of rock slope designs reinforced with rockbolts and cable bolts are presented in Figure 8.

In the case of rock slope reinforced with 2m rockbolts at 3m depth intervals, slope failure propagated at 49m. Whilst this may seem indifferent to the previous unsupported result, comparison between fracture distributions reveals otherwise. It is shown that application of rock bolts produced a reinforced capping over the slope face increasing the existing rock strength close to the slope surface. During progressive failure large bulky rock pieces remained intact generating a resistance to material flow. This effectively reduced the large rotational failure size with combination of rotation and plane failure. This was further observed to change from an initially occurring circular failure plane into a non-circular one.

In contrast to rock bolts, 10m-20m cable bolts tensioned to 100kN at 4m depth intervals proved to be significantly more effective, reinforcing an 82m high slope before failure was observed. Reason for this was a deeper penetration by the cable bolts.

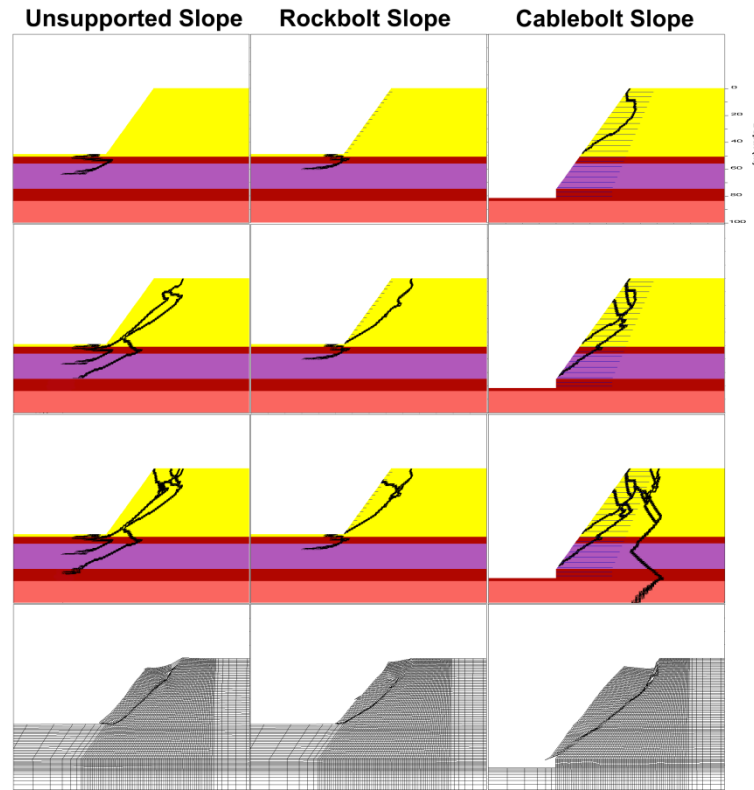


**Figure 8 - Comparison of simulated rock slope progressive failure**

Through assessing the progressive failure between supported and unsupported rock slope designs several important observations became apparent:

- New fractures that daylight from slope faces are active signs of continuing failure and fracturing deeper into the slope. Fracturing and heaving at the base of the slope toe are signal of a major failure formation.
- Additional signs of progressive slope failure activity is spall like fracture or failure of rock at the slope face. In mining communication of any such observation from haul truck drivers is both first and most important potential warning of a larger potential event and should be inspected accordingly. This reflects already encouraged practice in training haul truck drivers to be able to identify and report suspect out-of-place debris.
- Following any major slope failure event, further fractures behind the failed slope face should not be discounted from triggering additional failure events. As both models have shown, formation of large loose wedges behind the rubble is commonly generated during the progressive failure and relief process. This highlights an active risk of secondary slope failure during the removal of failed debris confining concealed failures.

In summary, the newly developed fracture model is offering new approach to simulate progressive fracture zones within geological structures.

## CONCLUSIONS

This study extends verification of a recently developed fracture model to anisotropic rocks. As demonstrated through the analysis of different rock slope controls, such analysis would not have been possible using any previous conventional modelling approach. Through continued validation of other complex problems the new model is envisaged to offer safer and more realistic predictions of rock slope failure for the mining and wider geotechnical industries.

**REFERENCES**

- Bertoldi, C E, 1988. Computer simulation of progressive failure in soil slopes, Doctor of Philosophy thesis, Department of Civil and Mining Engineering, University of Wollongong.
- Itasca Consulting Group, I., 2005. FLAC - Fast Lagrangian Analysis of Continua. *Version 5.0, User Manual*. Minneapolis.
- Jaeger, J.C. and N.G.W. Cook, 1971. *Fundamentals of Rock Mechanics*, Chapman and Hall, London.
- Venticinque, G A, 2013. *Advanced Numerical Modelling of Fracture Propagation in Rock*, Honours Thesis, Department of Engineering, School of Mining Engineering, University of Wollongong.
- Venticinque, G A, Nemcik, J A and Ren, T, 2013. New fracture model For the prediction of longwall caving characteristics, *6th International Symposium on Green Mining (ISGM)*, 2013. University of Wollongong, pp 63-68.

# PREDICTION OF *IN SITU* ROCK STRENGTH USING SONIC VELOCITY

Nicholas Butel<sup>1</sup>, Alex Hossack<sup>2</sup> and Mehmet S Kizil<sup>1</sup>

**ABSTRACT:** Uniaxial Compressive Strength (UCS) and sonic velocity correlations are used widely in the Australian coal mining industry to predict *in situ* rock strength. These models are cheap, fast and easy to produce, as well as easy to understand and have a number of practical applications in mine planning and design. The major downfall of these models is that there is a large variation in UCS values at high sonic velocities limiting their predictive ability. The aim of this research project is to improve the reliability of UCS/Sonic velocity correlations by reducing the variability in the underlying data. This is performed by identifying and eliminating sources of error affecting the data and looking at the impact of certain factors on the quality of the correlations. Results show that improved models can be obtained by filtering the datasets to remove samples with high length-to-height ratios, conglomerate or pebbly lithologies, and large sonic velocity ranges.

## INTRODUCTION

Uniaxial Compressive Strength (UCS) testing is a common method for estimating *in situ* rock strength in Australian coal mines, either as a standalone measure or within one of the many rock mass rating systems. Researchers in the mining industry have been investigating alternatives to UCS testing that are cheaper and faster at predicting *in situ* rock strength (Hatherly, *et al.*, 2007; Lawrence, *et al.*, 2013; Sharma and Singh, 2008). One option currently adopted in a number of Australian coal mines is to correlate sonic velocity, a geophysical measurement of compression waves travelling through rock, and laboratory UCS results to obtain an equation to predict rock strength (McNally, 1990; Oyler, *et al.*, 2010). This method has the potential to be cheaper and faster to develop compared to measured UCS modelling, and is easy to create and understand. It is also useful where rock is highly fractured and the ability to collect suitable UCS samples is difficult. The main disadvantage is the significant variability in measured UCS values for a given velocity. These models currently produce low quality correlations, which reduces their reliability for use in planning and design applications.

Prediction of UCS from sonic velocity logs has been a widely accepted practice in the Australian coal mining industry for over 20 years. The first study was conducted by McNally (1987) who derived a general expression for all Australian sites, which has been widely recognised in the mining industry. Today most mines employ site-specific correlations rather than the generalised McNally equation, which has resulted in more accurate and reliable prediction of rock strength for sites (Oyler, *et al.*, 2010).

At Rio Tinto Coal Australia (RTCA), site-specific correlations have previously been created for several mines. The most recent and comprehensive analysis was performed by Stam *et al.*, (2012) at Kestrel Mine. As a result of the Kestrel investigation, correlations have been produced for all other RTCA sites (Butel, 2012). It was found that site wide models were better predictors of rock strength compared to lithotype and regional models. However, the overall quality of the correlations was below the industry standard. The low quality was due to a number of uncontrolled sources of error in the data sets. It was recommended that the sources of error in the underlying data be identified and removed from the datasets to improve the correlations.

The goal of this project is to increase the reliability of UCS/Sonic correlations for use in mine planning and design applications by reducing the amount of spread in the data. To achieve this, sources of error present in the underlying data were investigated and removed. Factors causing the spread in UCS values at high sonic velocities were investigated by filtering the datasets and creating subset correlations based on these factors. Site wide and subset correlations were compared to determine if any improvement has occurred. This analysis is performed using data from eight RTCA sites, including six operating mines and two development projects. A case study of RTCA's Hunter Valley Operations

<sup>1</sup> School of Mechanical and Mining Engineering, The University of Queensland, St Lucia Qld 4072, m.kizil@uq.edu.au  
Tel: +61 07 3365 4499

<sup>2</sup> Rio Tinto Coal Australia, 123 Albert Street, Brisbane Qld 4000; Tel (H) +61 07 3878 7612 +M: 04 5090 6307,

(HVO) mine in the Hunter Valley (NSW) is presented in this paper as it is the best representation of overall results from all the sites.

### UCS TESTING

The UCS of an intact rock sample is the amount of compressive force per unit area applied in a single direction required to induce failure. UCS is calculated by dividing the compressive load at failure by the cross sectional area of the sample, as shown in Equation 1. The UCS test is also called the unconfined compressive test as there is no confining pressure applied to rock samples (Peng and Zhang, 2007). The uniaxial compressive test can also measure the Poisson's ratio and Young's modulus of an intact rock sample.

$$\text{UCS (MPa)} = \frac{\text{Compressive Load at Failure (kN)}}{\text{Cross Sectional Area (mm)}} \quad (1)$$

This test is carried out according to the International Society for Rock Mechanics (ISRM) suggested method ISO9001 and Australian Standards under controlled laboratory conditions (Bieniawski, *et al.*, 1979). This standard specifies that cylindrical shaped specimens of intact rock core must be compressed parallel to their longitudinal axis. Sample dimensions must be within a height to diameter ratio of 2.5-3:1 and free from discontinuities or defects to be valid. Figure 1 shows a diagram of the UCS test setup and the direction of loading.

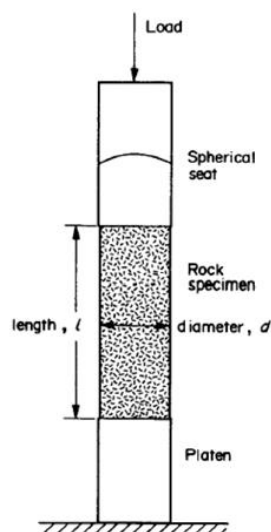


Figure 1 - Diagram of UCS test setup (Brown, 1981)

A geophysical log is a continuous record of measurements made by a probe able to respond to variations in some physical property of a rock mass (Firth, 1999). They are commonly presented as a line graph with depth on the vertical axis and the geophysical log type on the horizontal axis. Geophysical methods are divided into land and borehole, based on the location of the measurement device (Takahashi, *et al.*, 2006). Land geophysics is measured from the ground surface, while borehole geophysics places the measuring device down the borehole. Borehole geophysical methods are the focus of this discussion.

Sonic (acoustic) velocity logging is a form of borehole geophysical logging that measures the transit time of compression (P-wave) waves travelling through the rock mass surrounding the borehole (McNally, 1987). Sonic logging tools contain a transmitter which generates high frequency sound waves that travel through fluid in the borehole and rock mass in the wall. These waves are generated by an ultrasonic source, typically operating at about 20 kHz and firing at about 0.1s intervals (McNally, 1990). An uncased water or mud filled hole is required to ensure adequate acoustic coupling is achieved. These frequencies are detected by multiple receivers located on the logging tool. Measuring the time difference between arrivals at two receivers eliminates the common time spent by the signal in the borehole, leaving the time spent in the rock. This produces an interval transit time, or delta-t log. When divided by

the receiver separation, the log becomes an inverse velocity or slowness log. Inverting the slowness log will produce the sonic velocity log shown in Equation 2 (Firth, 1999).

$$\text{Sonic Velocity (m/s)} = \frac{\Delta d_{R_i \rightarrow R_j} \text{ (m)}}{\Delta t_{R_i \rightarrow R_j} \text{ (s)}} \quad (2)$$

where,

$R_{i,j}$  = Receiver  $i, j$

$\Delta d$  = distance between receivers  $i$  and  $j$

$\Delta t$  = change in time between receivers  $i$  and  $j$  detecting signal.

The most commonly used down hole sonic logging tool is the multi-channel P-wave compensated series (MS). Figure 2 illustrates the basic setup and principles of this tool. It has four receivers spaced 20 cm apart and is capable of measuring multiple sonic velocity values on four separate channels. Borehole data can be presented for 0.2, 0.4 and 0.6 m thick strata intervals on channels 1, 2 and 3 (McNally, 1990). The different velocities are determined by the change in signal times between combinations of receiver pairs. Table 1 shows the available velocity measurements on the MS2 multi-channel sonic tool. The short-spaced option, VL2F, measures the transit time between receiver 1 and 2. It is the most commonly used log in UCS/Sonic correlations, since the interval length is approximately the same as a UCS specimen, and it is least affected by spiking (McNally, 1990).

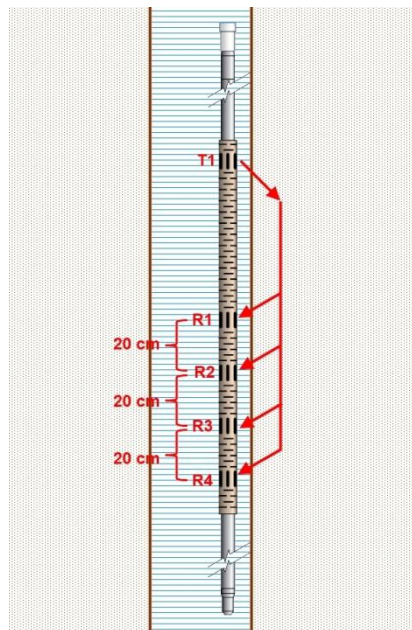


Figure 2 - MS logging tool in a water filled hole and wave propagation in the rock mass

Table 1 - Velocity logs available on a MS2 logging tool

Channel	Velocity Log	1 <sup>st</sup> Receiver	2 <sup>nd</sup> Receiver	Receiver Spacing
1	VL2F	R1	R2	20cm
2	VL4F	R2	R4	40cm
3	VL6F	R1	R4	60cm
4	VL2A	R3	R4	20cm

### UCS/SONIC CORRELATIONS

According to Oyler *et al.*, (2010) sonic logging has been routinely used for many years in Australia to obtain UCS estimates in coalfield strata. This is performed by collecting sonic log measurements of the compression P-wave velocity (m/s) and then correlating these with UCS measurements made on core samples from the same holes at the same depth. The sample points are plotted and an exponential regression line is fitted to determine the correlation for that dataset. An example of sonic velocity correlation from RTCA's Kestrel Mine is shown in Figure 3. The generalised formula for UCS/Sonic

velocity correlations is shown in Equation 3. The constants  $K$  and  $r$  are derived from the regression line fitted to the data set. Only VL2F sonic velocity values are shown in this paper, although VL4F and VL2A values were also modelled but did not produce improved correlations.

$$UCS = K \times e^{a \times VL2F} \quad (3)$$

where  $K$  and  $a$  = site specific constants.

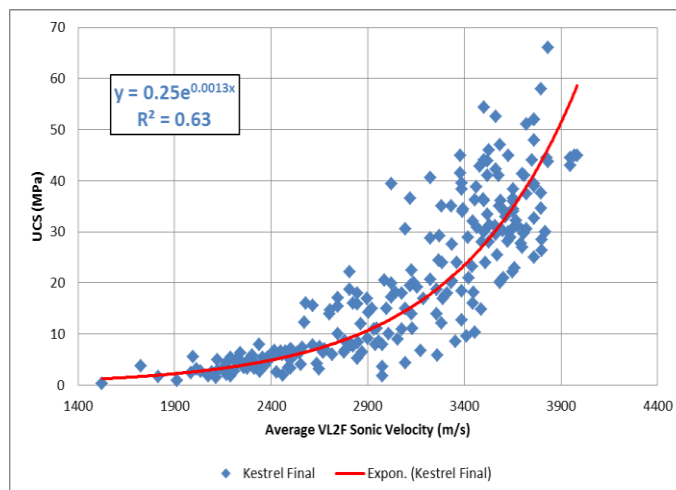


Figure 3 - Kestrel Mine UCS/Sonic correlation (Stam, *et al.*, 2012)

The quality of a correlation is determined by the coefficient of determination ( $R^2$ ) value, the size of the dataset, and the visual fit of the regression curve. The coefficient of determination is a measure of how well a regression curve fits a data set. This value ranges from 0 to 1, with zero showing no relationship, and one being a perfect correlation. The commonly accepted  $R^2$  in the Australian mining industry for a good UCS/Sonic correlation is greater than 0.7 (Oyler, *et al.*, 2010). This value was used as a benchmark for determining the quality of the correlations throughout this project. For descriptive purposes in this analysis, an  $R^2$  of 0.5-0.7 is average, 0.3-0.5 is low, and  $<0.3$  is poor quality. The minimum required dataset size to produce a reliable correlation was set at 30 sample points to assume a normal distribution under the Central Limit Theorem.

### Classic studies

Research into the relationship between dynamic rock mass properties and sonic logs was first performed by Carroll (1969). He identified that there were empirical relationships between rock characteristics including Young's Modulus, shear modulus, bulk modulus and sonic logs in volcanic rocks. He recommended that this could be extended to siliceous rock types, as well as estimation of other rock parameters using sonic logs.

Based on this research, McNally conducted two classic studies, in 1987 and updated in 1990, in which sonic velocity logs and drill cores were obtained and correlated from 16 mines throughout Australia's coalfields. The first study in 1987 concluded that a single generalised correlation was sufficient for estimating *in situ* rock strength at all sites. The 1990 study indicated that these models may be lithology dependent. The findings from the 1990 study were used to predict geomechanical properties of various coal measures rock types (McNally, 1990). McNally (1987) derived a general correlation for sonic transit time and UCS, which is shown in Equation 4. This correlation has been extensively adopted in the Australian mining industry, and is still regularly quoted in literature (Oyler, *et al.*, 2010; Hatherly, *et al.*, 2001; Hatherly, *et al.*, 2005).

$$UCS = 1000 \times e^{-0.035t} \quad (4)$$

where,

UCS = Uniaxial Compressive Strength (MPa);

t = interval travel time of the P-wave ( $\mu$ s/ft).

One of the major problems identified by McNally (1987) is the level of error in the input variables, which subsequently reduces the overall accuracy of the models. He suggested that these correlations may be improved by carefully hand-picking sample locations to correspond with peaks or troughs on logs, and avoiding depths where the log gradient is steep. Samples should also be located at the centre of uniform (flat) log segments. McNally concluded that sonic logs provide a reliable and continuous record of rock strength in coal measures strata. He also commented that correlations can vary with lithology, as conglomerates appear to specifically overestimate UCS values. Sonic velocity also appears to increase with confining pressure. Importantly, he commented that sonic logs appeared not to be site-specific.

### Current research

Current research in this area has separated into two schools of thought. One side supports the traditional method suggested by McNally, correlating sonic logs to UCS (Oyler, *et al.*, 2010; Lawrence, 1999; Zhou, *et al.*, 2001; Stam, *et al.*, 2012; Sharma and Singh, 2008; Kelessidis, 2011; Peng and Zhang, 2007). However, other researchers suggest that this does not adequately account for variations in sonic velocity due to rock mass parameters (Hatherly, *et al.*, 2009; Medhurst, *et al.*, 2010; Barton, 2006).

Sharma and Singh (2008) support the traditional theory of correlating sonic velocity directly with UCS on a regional basis. However, they believe a linear relationship is most appropriate for this relationship. Oyler *et al.* (2010) also support the use of the traditional correlation established by McNally. They created UCS and sonic travel time correlations for a number of coal mines across the USA, aimed at increasing awareness and adoption of these models in the US coal industry. It was concluded that this correlation can also be adopted in US coalfield strata to estimate UCS. According to Oyler *et al.* (2010), it is not certain that site specific correlations would give better results than a generalised model such as McNally's. They also highlighted that high-quality sonic logs are essential if the technique is to be used successfully.

A number of recent papers have identified that site-specific UCS and sonic velocity correlations produce more accurate and reliable correlations than generic models such as the McNally equation (Zhou, *et al.*, 2001; Stam, *et al.*, 2012; Butel, 2012). This is due to the fact that these models are able to more effectively account for variations in the local geology than generalised models. Today, mining operations are deriving their own correlations to suit local conditions. For example, at Kestrel Mine, German Creek Mine and Crinum Mine in central Queensland, where there is a well-defined and consistent geological environment, specific correlations have been derived (Zhou, *et al.*, 2005; Hatherly, *et al.*, 2009; Stam, *et al.*, 2012).

Some researchers believe lithology, or rock type, specific correlations are most appropriate for *in situ* strength modelling (Lawrence, 1999; McNally, 1990). In McNally's paper in 1990, he identified that the generalised correlation curve steepens rapidly below 60 MPa UCS, indicating sonic logs are sensitive to low strength rocks. Lawrence (1999) produced linear correlations for individual rock types with reasonable success. This research indicated that the correlation gradient increases with grain size. For coarse grain rock types such as sandstone, there is expected to be a large range in rock strength values over a small range of sonic transit time. In contrast, finer grained material such as siltstone exhibits a smaller strength range, but a much larger range in sonic transit times. Peng and Zhang (2007) recognised that lithology specific models for a particular site can be effective estimators of rock strength, and that generalised lithology models across a region may produce less accurate results.

A second school of thought suggests that UCS and sonic velocity correlations are inadequate account for all of the variation in sonic velocity logs. According to this group, the broad scatter exhibited by UCS/Sonic correlations is due to the fundamental difference between static UCS and dynamic sonic log properties (Zhou, *et al.*, 2005). When the rock mass is homogenous and isotropic, sonic velocity will match the rock strength. However when structures and defects are present in the rock mass, sonic velocity can vary substantially from the UCS value due to its sensitivity to changes in conditions (Hatherly, *et al.*, 2007). This has led to the development of several alternative models to estimate *in situ* rock strength incorporating rock mass parameters influencing sonic velocity (Barton, 2006; Hatherly, *et al.*, 2007; Zhou, *et al.*, 2005; Hatherly, *et al.*, 2001). These models correlate sonic velocity to rock mass properties such as rock quality, joints or fractures per metre, rock composition, or a combination of these with varying degrees of success.

The main alternative model to McNally's generalised UCS/Sonic correlation is the Geophysical Strata Rating (GSR) developed by Hatherly *et al.*, (2005). It is derived solely from geophysical log data to

develop a more complete strata characterization than the UCS/Sonic correlation (Hatherly, *et al.*, 2009). It is designed to provide a measure of strata properties on a linear scale from 0 to 100. The model takes into account moisture sensitivity, bedding and other factors besides rock strength (Oyler, *et al.*, 2010). This model was developed using data from the Australian coalfields, so it is suited to coal measures rock types at depths less than 500 m. The major problems associated with this model are the amount of input data required and the processing involved. Purchase of the required software and training is also required. However, this model is showing signs of acceptance in the Australian Coal Mining industry, and is increasingly being quoted in related literature (Stam, *et al.*, 2012).

## CASE STUDY

To determine the effectiveness of UCS/Sonic correlations for *in situ* rock strength estimation, models were created using data collected from six RTCA open cut mines and two development projects. The sites are located in the Bowen Basin in Queensland and the Hunter Valley in New South Wales. The geographic spread of the sites provides a good basis for determining the robustness of these correlations in a number of different geological environments. Creation of the models for each site and their analysis were conducted in a number of successive stages. The five stages were:

1. Data collection and compilation;
2. Review of datasets;
3. Creation of site specific correlations;
4. Creation of subset correlations; and
5. Comparison of correlations.

### Data collection

Data was obtained from existing repositories on the RTCA Brisbane computer network, as well as site specific networks. The two fundamental values required to create a valid sample point are the laboratory UCS test result and the average VL2F sonic velocity value over the same depth in the same borehole. Additional criteria were collected to identify potential sources of error, as well as a means of separating the full dataset into subsets for analysis of additional factors. Additional information collected included UCS test result information to identify any violations of ISRM Standards, the sample lithology, the minimum, maximum and range for each average VL2F velocity value, as well as the VL4F and VL2A velocities for comparison. Using the collected information, several values were calculated including the sample length, which is the difference between the depths of the top and base of the sample; Length-to-Height (L: H) Ratio, the ratio of the core sample length to the UCS sample height; and the Height to Diameter (H: D) Ratio.

### Review of datasets

One of the major problems identified in the previous RTCA study was that underlying error in the data had not been identified and removed from the datasets (Butel, 2012). To reduce the impact of identifiable errors on the correlations, a review of the data was performed. Only sources of error in the UCS test procedure and the sonic velocity log were targeted in this review, as these were the only factors able to be adequately investigated from the data available. Importantly, during the project only samples containing identified errors were able to be removed according to the information provided. This limited the analysis significantly as only errors related specifically to the UCS test and spiking in sonic logs could be thoroughly measured. Major sources of error identified and removed from the datasets in this analysis included:

- UCS Testing;
  - Non-compliant sample dimensions;
  - Defect or bedding in sample;
  - Failure mechanism indicating problem with test – end failure, conical; and
  - Test significantly different to ISRM standards;
- Sonic Logging;

- Cycle skipping or spikes;
- Problems associated with the water level downhole;
- Measurement error, including poor vertical resolution (10 cm increments);
- Other;
  - Lithology - conglomerate, pebbly, schist;
  - Outliers; and
  - Suspicious Legacy data – missing information.

### Subset correlations

Subset correlations were created for each site to determine if factors other than UCS were affecting sonic velocity values, and therefore the quality of the correlations. This was performed by dividing the dataset into subsets based on the factor being analysed and creating new correlations from these. A factor was deemed to have a significant impact on the dataset if a strong correlation was able to be produced from the subset models. The factors analysed in this project included:

- Lithology (rock type);
- Overburden pressure (depth);
- Mining horizon;
- Velocity range;
- L/H ratio;
- Drilling program;
- Regional location; and
- Laboratory.

Several factors were obtained from previous research including lithology, velocity range and overburden pressure (depth) (Lawrence, 1999; McNally, 1990). Other factors were identified as potential sources of error in the data review stage.

### Comparison of models

Site-wide and subset correlations were compared at each site to determine which model was the best predictor of *in situ* rock strength. The criteria for determining whether the subset models were an improvement on the site wide models included:

1. The coefficient of determination ( $R^2$ ) increased;
2. The size of the subset was > 30 sample points; and
3. Strong correlations were able to be obtained for all models within a subset where there were multiples (i.e. lithology)

Site-wide and subset models were also compared across sites to determine if there were recognizable trends.

## RESULTS

The figures shown are only for the site wide and subset correlations which showed significant impacts on the data spread. These factors included lithology, L/H ratio and sonic velocity range. The sonic velocities shown in all figures are VL2F although both VL4F and VL2A models were also produced. No significant improvements in quality were identified in the VL4F and VL2A models.

Figure 4 shows the site wide correlation for HVO. The  $R^2$  value for this correlation is 0.54, which is below the industry benchmark of 0.7. The initial dataset contained 406 samples. After the data review, 58 points were removed due to errors, leaving 348 points in the final dataset. The data shows a regular

trend for this type of model with few points in the low velocity range, and becoming broadly spread in the high velocity range. The confidence interval is close to the regression line indicating the line fits the data well, although it does deviate above 4500 m/s. The data spread indicates that there is a  $\pm 30$  MPa variation around the regression line in the high velocity range ( $>3000$  m/s), and  $\pm 10$  MPa in the low range ( $< 3000$  m/s). This indicates that there is high variability in the predictive confidence of this model at high velocities.

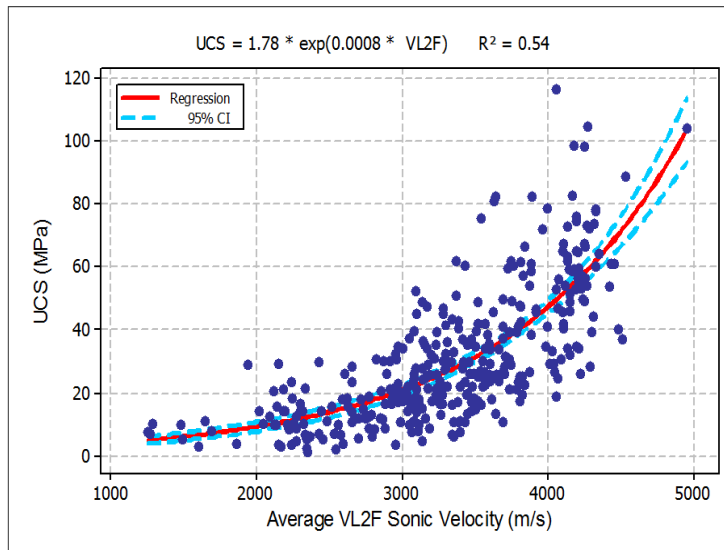


Figure 4 - HVO site wide correlation

Two correlations have been created for sample points with velocity ranges less than 100 m/s and 250 m/s (Figure 5). The correlations have very similar trend line equations and moderate  $R^2$  values. The 100 m/s model has an  $R^2$  of 0.64 for a dataset of 99 points. The 250 m/s model contains 203 sample points and has an  $R^2$  of 0.62. These present a significant increase in  $R^2$  compared to the site wide model.

The HVO dataset has been filtered by L/H ratios of less than 1.5 and 2 (Figure 6). The equations for the two models are similar to the site wide model. The L:H  $< 1.5$  model has a fair correlation at 0.58 using a small dataset of 39 points, compared to a correlation of 0.51 using 139 points for the L:H  $< 2$  model. The L:H $<1.5$  model presents a slight increase in  $R^2$  compared to the site wide model, and the L:H $<2$  shows a slight decrease.

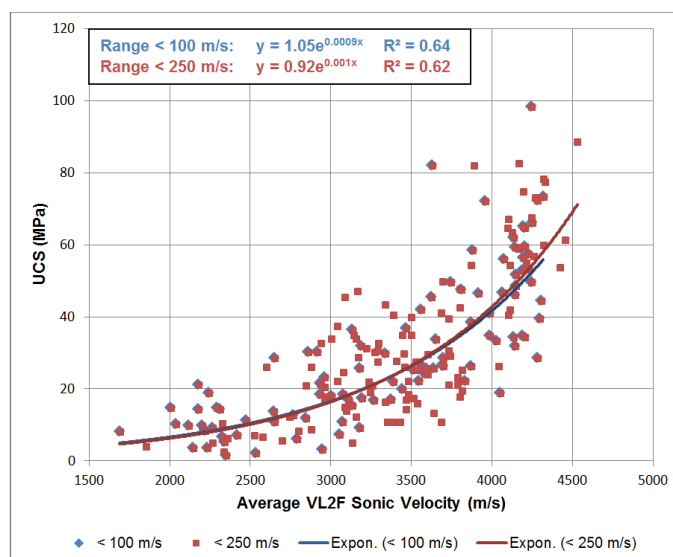


Figure 5 - HVO velocity range correlations

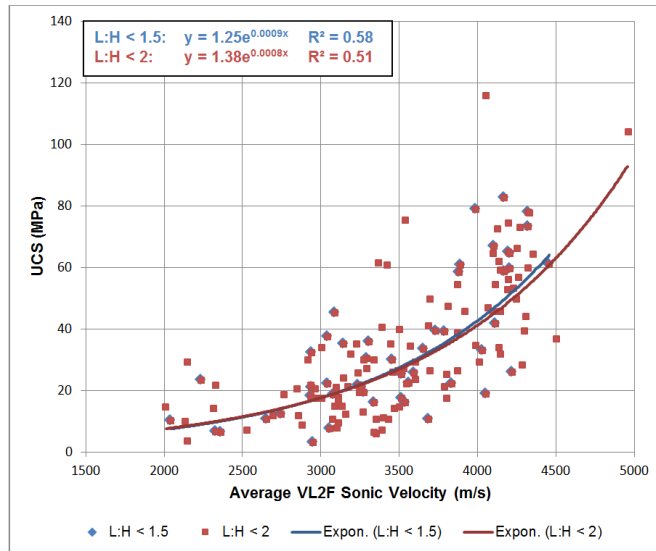


Figure 6 - HVO L:H ratio correlations

Lithology models have been produced for Interbedded Sandstone/Siltstone, Siltstone, Sandstone, and Shale (Figure 7). Sandstone displays a reasonable correlation with an  $R^2$  of 0.59 for a dataset of 180 points. This represents an improvement compared to the site wide model. The other correlations are generally poor, with  $R^2$  values below 0.4. The siltstone, interbedded siltstone/sandstone, and shale models contain 73, 35 and 18 sample points respectively.

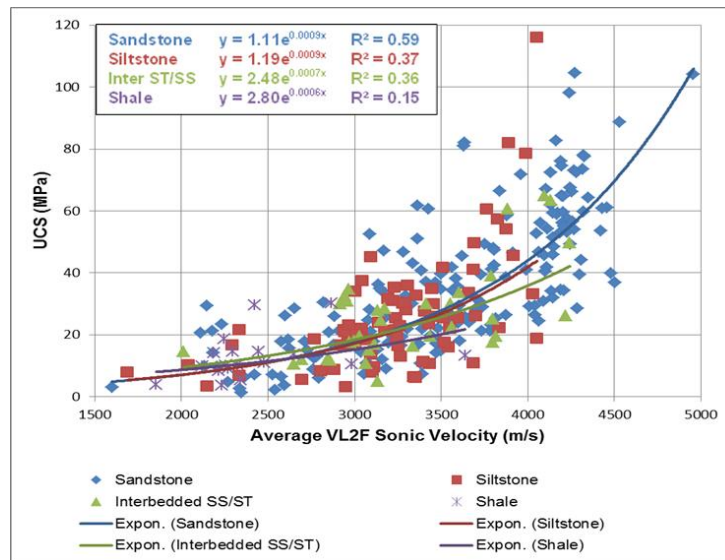


Figure 2 - HVO lithology correlations

**Comparison of subset and site-wide models**

Tables 2 and 3 show comparisons of  $R^2$  values and dataset sizes between the L:H Ratio and Velocity Range models to the site-wide model for all sites reviewed in this project. In most cases there is a reasonable increase in  $R^2$  for subset models compared to the site-wide model. However, the datasets for the L:H < 1.5 and range < 100 m/s models are generally too small to be reliable, containing less than 30 sample points.

**Table 2 - Comparison of L:H and site models**

Model	L:H < 1.5		L:H < 2		Site-Wide	
	R <sup>2</sup>	n	R <sup>2</sup>	n	R <sup>2</sup>	n
BA	0.82	14	0.69	36	0.64	49
HCK	0.64	55	0.55	156	0.57	257
WIN	0.73	15	0.75	36	0.73	52
CLM	0.32	22	0.12	129	0.14	279
HVO	0.53	49	0.51	148	0.54	348
BMC/MTP	0.3	38	0.36	73	0.35	84
MTW	0.23	46	0.25	219	0.15	387

**Table 3 - Comparison of range and site models**

Model	< 100 m/s		< 250 m/s		Site-Wide	
	R <sup>2</sup>	n	R <sup>2</sup>	n	R <sup>2</sup>	n
BA	0.85	8	0.69	22	0.64	49
HCK	0.46	41	0.48	146	0.57	257
WIN	0.16	7	0.67	22	0.73	52
CLM	0.02	46	0.09	147	0.14	279
HVO	0.64	99	0.62	203	0.54	348
BMC/MTP	0.23	18	0.49	51	0.35	84
MTW	0.13	49	0.17	209	0.15	387

## ANALYSIS

### Site wide

The overall results show that most of the site-wide models produced an R<sup>2</sup> value below the industry benchmark for a good correlation of 0.7. Some of the site models are of such poor quality that they cannot be used in their current form with confidence. These site models include MTW, Clermont and Bengalla. Other sites show reasonable trends although they still do not meet the 0.7 benchmark. These include HVO, Hail Creek, Blair Athol, Mt Pleasant, and BMC/MTP Combined. These models can be used for *in situ* rock strength prediction but with caution. Winchester South is the only site-wide model that exceeds an R<sup>2</sup> of 0.7 indicating that it is a good quality correlation. The main cause of these low values is the large spread in UCS values for sonic velocities greater than 4000 m/s. This indicates that there is a large amount of variability in UCS not being accounted for in these models.

A number of subset correlations based on potential sources of error in the data were created to determine if these are affecting the spread in the data. The results indicate that lithology, velocity range and L/H ratio have the most significant impact on the data spread. In most cases correlations with stronger R<sup>2</sup> values compared to the site wide models were able to be produced from the subsets. This analysis indicates that these factors are contributing to the spread in the data shown in the site wide models.

### L / H ratio

One major source of potential error found during the data review was that the sample depth quoted in UCS test result sheets did not correspond to the height or position of the sample tested. The sample depths were generally much larger than the actual sample height. This was up to four times in some samples. This is because the core lengths sent to the laboratory needs to be large enough to ensure a good quality sample of sufficient height and without defects. However, the location at which the test sample is taken from along this length is not recorded. The problem is that average sonic velocity values must be taken over the entire sample depth range, which introduces a large amount of uncertainty into sample points where the ratio of sample length to sample height is high. Furthermore, it is speculated that where a large core length has been provided, this may indicate that the core was fractured or poor quality, which would also cause problems for the sonic log measurement at this depth.

To determine whether this discrepancy was having a major impact on the models, the datasets were filtered by sample points with L:H ratios of less than 1.5 and 2. For L:H less than 2, this typically resulted

in a reduction in the size of the dataset by approximately 40%, and for less than 1.5 the dataset was reduced by 80%. The reduction in the dataset size for the L:H < 1.5 model generally made them unusable as there were less than 30 sample points. The improvement created by filtering the dataset using L:H can be seen in Hail Creek and for MTW, as well as for Blair Athol, Winchester South, Bengalla, Mt Pleasant, and HVO. Table 2 highlights the differences in  $R^2$  between the site-wide model and subset models for all sites. The largest improvement was shown by MTW, with a 0.10 increase in  $R^2$  by applying the L:H < 2 filter. This indicates that L:H ratio does have an impact on the variability in the data, and that by filtering the dataset using this factor the correlation can be improved.

### Sonic velocity range

A second source of error in the correlations is large velocity ranges in sample points. These points are likely to be affected by fractures in the rock, or changes in lithology, which skew the average velocity value. These velocity values are probably not representative of the corresponding UCS sample, as UCS samples are intact rock core without bedding or changes in lithology. McNally (1990) suggested that correlations may be improved by choosing samples corresponding with flat sections on logs, and avoiding sections where the log gradient is steep. McNally's recommendation has been applied to this research and it has been found to improve the quality of correlations. Site datasets were filtered by sample points with sonic velocity ranges of less than 100 m/s and 250 m/s. These filters reduced the size of the dataset by on average 50% for 250 m/s and 80% for 100 m/s. These correlations generally produced higher  $R^2$  values than the full dataset models (Table 3). The HVO velocity range < 250 m/s correlation showed a significant increase in  $R^2$  to 0.62, compared to 0.54 for the site-wide model (Figure 4). The largest increase occurred in the combined Bengalla and Mt Pleasant model, which showed a 14% increase in  $R^2$  (Table 3). This indicates that this filter can help to reduce some of the underlying variability in the data.

### Lithology

Lithology correlations showed varying levels of success in explaining the spread in the data. At most sites reasonable sandstone models were able to be produced, such as Blair Athol, Winchester South, and HVO. At some sites strong siltstone and interbedded sandstone/siltstone models were also able to be produced, including Blair Athol, Winchester South and Bengalla/Mt Pleasant combined. Other lithologies were not able to be adequately modelled due to the small size of the subsets. One observation that was noted is that Clermont Mine dataset contains a significant amount of samples points with conglomerate, basalt and schist lithologies. From the Clermont dataset, a strong correlation for Basalt was able to be created with an  $R^2$  of 0.74. However conglomerate data correlated very poorly, with an  $R^2$  of only 0.22. The quality of lithology correlations is due to the composition of the rock. Conglomerate consists of high strength clasts (pebbles, rock or boulders) within a low strength fine grained matrix. This causes high sonic velocities as compression waves reflect off the clasts, but low UCS due to failure in the matrix. This effect was also noted in other lithologies containing a significant 'pebbly' component, such as pebbly sandstone. Other rock types which have a more consistent grain size have been shown to correlate much better. To improve the quality of correlations, sample points with conglomerate or pebbly components should be removed from the dataset.

A significant limitation of adopting lithology correlations over a site-wide correlation is the added complexity in applying these models to UCS contour mapping. Different models must be used in different zones where the geology changes, and then they must be amalgamated into a single map to be useful. This increased complexity makes the models less attractive and therefore less likely to be used in mine planning and design. Although strong correlations can be produced for some lithologies, overall these models are impractical and do not include all lithologies present on mine sites.

### Legacy data

A third source of error identified in the analysis was that legacy data introduced a moderate degree of uncertainty into the datasets. For a number of sites, most of the additional information that would normally be used to identify errors was not available. This limited the ability to review the data for errors, so these sample points were treated with caution during the analysis. Attempts were made to identify irregularities by looking for significantly different trends in the drilling program and laboratory correlations. In the Hail Creek drilling program correlations, the 200 and 400 series sample points showed distinct trends from the rest of the dataset and had very little additional information available on the UCS test results. Therefore these sample points were removed from the dataset for all other correlations.

Another issue arising from the legacy data is that in some cases it has already been highly filtered. The Hail Creek Laboratory correlations show a very strong model for the Mackay laboratory, which includes legacy data from 2005. It appears that this data has already been filtered to produce the strong correlation shown by this model. Therefore this introduces bias into the dataset as the spread in the historical data is not fully represented. The unfiltered datasets for these holes were unable to be located during the data collection stage.

### Measurement error

A major issue identified during the completion of this project was that where the site wide model showed a very low correlation, it was very difficult to produce significantly improved subset correlations. This was particularly evident in the Mount Thorley Warkworth models, which produced an  $R^2$  of 0.30 in the best subset correlation. This is likely to be due to sources of error in the main dataset being unable to be filtered out in the subset correlations due to a lack of available identifying information. Based on previous research conducted in this field, these unidentified sources may include measurement error, rock density, composition, porosity, and the impact of discontinuities on sonic logs.

A key limitation of this research is that the cause of errors in sonic logs was unable to be identified from the data provided. Measurement error has been recognized at several sites which may have contributed to the poor quality of correlations (Guy and Bamberry, 2011; Turner, 2009). In the MTW dataset, a large number of the removed sample points had problems with the sonic velocity value caused by cycle skipping or spikes in the log. Two holes in particular contained a large number of issues in the sonic log. Although this cannot be confirmed based on the information available, it is suspected that these problems are associated with measurement error. Implementation of a standardised sonic velocity logging manual is expected to reduce the amount of measurement error present in samples in the future.

### Standardised sonic logging procedure document

Currently there is no standardised procedure for sonic velocity logging across all RTCA sites. Furthermore, no comprehensive and informative international or Australian standards exist for sonic velocity logging. The quality and reliability of these models depends on the accuracy of sonic velocity data collected from site. This has been raised as a major potential source of measurement error, as different logging companies or individual loggers may use different standards (Guy and Bamberry, 2011). Another problem is that it is very difficult to identify this error in the sonic logs. To address this problem at RTCA sites, a draft version of a standardised sonic logging procedure was created as part of this project. This document is to be reviewed and potentially implemented at all RTCA sites in the future. The purpose of this document is to ensure adequate calibration, measurement, quality control, and data presentation is achieved for all sonic logs, so that the best possible quality data can be collected.

## CONCLUSIONS

The aim of this project was to create improved UCS/Sonic correlations that can be used with confidence for mine planning and design. Analysis of the correlations created for RTCA sites has shown that improved models can be obtained by filtering the datasets to remove samples with high L/H ratios and large sonic velocity ranges. There is some evidence indicating that lithology specific models could produce stronger correlations than site-wide models. However, it was concluded that these models should not be used in replacement of the site-wide models because of the increased complexity required to create UCS contour maps based on these models. Sample points containing conglomerate and pebbly components should be removed from datasets to improve the quality of correlations. Similarly, mining horizon, depth, localised, lease, and lab models did not show significant improvements compared to the site-wide model. Therefore the site-wide correlation filtered by length-to-height ratio and sonic velocity range is considered to be the most appropriate model for the purpose of *in situ* rock strength prediction for this dataset. If good quality data already exists for a site, UCS/sonic correlations can be used as effective predictors of *in situ* rock strength with confidence at virtually no cost. Sonic derived UCS contour maps can be easily created from these models, which can be used in a number of important mine planning and design applications such as:

- High/low wall slope stability analysis;
- Open cut blast design optimization;

- Underground principal hazard management plans;
- Underground roof support design; and
- Drill performance optimization.

The overall quality of the models shown in this analysis has been significantly below the industry benchmark for a good correlation. The main reason for this is that a component of the variability in UCS has not been accounted for in the model. A source of this variability is believed to be measurement error from sonic velocity logging, which was difficult to identify and remove with the information available. This problem was particularly noticeable at NSW sites including MTW, HVO and BMC. This has previously been identified as a major issue in the sonic logs at these sites (Guy and Bamberly, 2011; Turner, 2009). A draft standardised procedure for sonic velocity logging has been developed to reduce measurement error in data collected in the future. Other factors not accounted for in UCS/Sonic models are also contributing to the large spread in the data plots and low correlation quality. Research suggests these factors include rock density, porosity, composition, shale content and discontinuities.

### RECOMMENDATIONS

To improve the quality of UCS and sonic velocity correlations, six key recommendations have been made based on this research. These include:

1. Record the exact depth of UCS samples after cutting at the lab to reduce error associated with L/H ratio;
2. Remove sample points with large velocity ranges affected by changes in lithology or discontinuities;
3. Identify and remove suspicious legacy data skewing the data trend;
4. Utilise a standardised sonic velocity logging procedure proposed as part of this research to reduce the amount of measurement error, and ensuring it is consistent across all samples;
5. Develop Australian standards for geophysical logging to allow accurate UCS prediction to be undertaken, and for better comparison of data between sites; and
6. Perform laboratory sonic velocity logging as a form of quality control by comparing lab and field results.

This is expected to significantly reduce the amount of error currently present in the models, and improve confidence in applying these models to mine planning and design.

### ACKNOWLEDGEMENTS

The authors would like to thank the members of the Rio Tinto Coal Australia Orebody Knowledge team who contributed to the project. The authors gratefully acknowledge Mark Sjoberg for his geotechnical expertise and advice provided throughout the project. Andrew Dawes assisted in the creation of the sonic derived UCS contour maps. Sabine Stam provided advice regarding *in situ* strength modelling which was greatly appreciated.

### REFERENCES

- Barton, N, 2006. Relationships between rock quality, depth and seismic velocity, in *Rock Quality, Seismic Velocity, Attenuation and Anisotropy*, pp 69-96 (Taylor and Francis).
- Bieniawski, Z T, Franlin, J A, Bernede, M J, Duffaut, P, Rummel, F, Horibe, T, Broch, E, Rodrigues, E, van Heerden, W L, Vogler, U W, Hansagi, I, Szlavin, J, Brady, B, Deere, D U, Hawkes, I and Milovanovic, D, 1979. Suggest Methods for Determining the Uniaxial Compressive Strength and Deformability of Rock Materials, in *The complete ISRM suggested methods for rock characterization, testing and monitoring: 1974-2006* (ed: R Ulusay, J A Hudson), pp 151-155 (Commission on Testing Methods, International Society of Rock Mechanics: Ankara).
- Brown, E T, 1981. Rock Characterisation Testing and Monitoring, in *ISRM Suggested Methods*, (Pergamon: Oxford).

- Butel, N, 2012. UCS and Sonic Velocity Correlation Report, Rio Tinto Coal Australia, Brisbane.
- Carroll, R D, 1969. The determination of the acoustic parameters of volcanic rocks from compression velocity measurements, *International Journal of Rock Mechanics and Mining Sciences and Geomechanics Abstracts*, 6(6):557-579.
- Firth, D E, 1999. *Log Analysis for Mining Applications* (ed: P Elkington), pp 5-47, (Reeves Wireline Services).
- Guy, G and Bamberry, J, 2011. Groundsearch – Weatherford Logging Trial. Internal Memorandum, Rio Tinto Coal Australia.
- Hatherly, P, Medhurst, T, Sliwa, R and Turner, R, 2005. A rock mass assessment procedure based on quantitative geophysical log analysis of coal measure sequences, *Exploration Geophysics*, 36(1):112.
- Hatherly, P, Medhurst, T, Ye, G and Payne, D, 2009. Geotechnical evaluation of roof conditions at Crinum Mine based on geophysical log interpretation, in *Proceedings Coal 2009: Coal Operators' Conference*, Wollongong Australia (ed: N Aziz) (Australasian Institute of Mining and Metallurgy). <http://ro.uow.edu.au/coal/67/>.
- Hatherly, P, Medhurst, T and MacGregor, S, 2007. A rock mass rating scheme for clastic sediments based on geophysical logs, paper presented to *Proceedings of the International Workshop on Rock Mass Classification in Underground Mining*, NIOSH Publication.
- Hatherly, P, Medhurst, T, Zhou, B and Guo, H, 2001. Geotechnical evaluation for mining – assessing rock mass conditions using geophysical logging, ACARP Project C8022B.
- Kelessidis, V C, 2011. Rock drillability prediction from *in situ* determined unconfined compressive strength of rock, *The Journal of The Southern African Institute of Mining and Metallurgy*, 111(June 2011):7.
- Lawrence, W, 1999. Interpreting and understanding strata behaviour, paper presented to 2nd Annual Longwall Mining Summit, Yeppoon.
- Lawrence, W, Emery, J and Canbulat, I, 2013. Geotechnical roof classification for an underground coal mine from borehole data, in *Proceedings of the 13th Coal Operators' Conference*, Wollongong, 16-20 February. <http://ro.uow.edu.au/coal/433/>.
- McNally, G H, 1987. Estimation of Coal Measures Rock Strength using Sonic and Neutron Logs, *Geoexploration*, 24:14.
- McNally, G H, 1990. The prediction of geotechnical rock properties from sonic and neutron logs, *Exploration Geophysics*, 21(2):65.
- Medhurst, T, Hatherly, P and Zhou, B, 2010. 3D geotechnical models for coal and clastic rocks based on the GSR, in *Proceedings of the 10th Coal Operators' Conference*, Wollongong, 16-20 February. <http://ro.uow.edu.au/coal/301/>.
- Oyler, D C, Mark, C and Molinda, G M, 2010. *In situ* estimation of roof rock strength using sonic logging, *International Journal of Coal Geology*, 83(4):484-490.
- Peng, S and Zhang, J 2007. Rock properties and mechanical behaviors, in *Engineering Geology for Underground Rocks*, pp 1-26 (Springer Berlin Heidelberg).
- Sharma, P and Singh, T, 2008. A correlation between P-wave velocity, impact strength index, slake durability index and uniaxial compressive strength, *Bulletin of Engineering Geology and the Environment*, 67(1):17.
- Stam, S, Guy, G and Gordon, N, 2012. Back analysis of roof classification and roof support systems at Kestrel North, in *Proceedings of the 12<sup>th</sup> Coal Operators' Conference Wollongong*, Wollongong Australia (ed: N Aziz) pp 42-51 (Australasian Institute of Mining and Metallurgy). <http://ro.uow.edu.au/coal/389/>.
- Takahashi, T, Takeuchi, T and Sassa, K, 2006. ISRM Suggested Methods for borehole geophysics in rock engineering, *International Journal of Rock Mechanics and Mining Sciences*, 43(3):337-368.
- Turner, R, 2009. Progress Report: Groundsearch Data Review DDH407; WD410; WD411; WD413; WD437; WD439. Consultant's Report, Borehole Logging Consultancy Services (Redhill, QLD).
- Zhou, B, Fraser, S, Borsaru, M, Aizawa, T, Sliwa, R and Hashimoto, T, 2005. New approaches for rock strength estimation from geophysical logs, paper presented to *Bowen Basin Symposium The Future For Coal-Fuel For Thought*, Yeppoon, 12-14 October.
- Zhou, B, Hatherly, P, Guo, H and Poulsen, B, 2001. Automated geotechnical characterisation from geophysical logs: Examples from Southern Colliery, Central Queensland, *Exploration Geophysics*, 32(4):336.

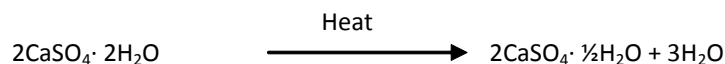
# EFFECT OF DIFFERENT CURING CONDITIONS ON THE COMPRESSIVE AND FLEXURAL PROPERTIES OF PLASTER OF PARIS

Zhenjun Shan, Ian Porter, Jan Nemcik and Qiuqiu Qiao

**ABSTRACT:** Gypsum plaster is often used when modelling rock and rock structures. As such, it is important that the mechanical properties of the plaster models are known and are consistent. In this study, uniaxial compressive tests (UCS) and 3-point bending tests were conducted to investigate the effect of different curing conditions on the compressive and flexural properties of Plaster of Paris specimens. The variations in curing condition consisted of curing time (1 day, 3 days, 5 days, 1 week, 2 weeks, 3 weeks, 4 weeks, 8 and 12 weeks) and curing environment (room temperature and in a 45°C oven). It was found that the plaster placed in the oven possessed greater overall uniaxial compressive strength than its room condition counterpart, and both groups experienced an increase in UCS over time, reached a maximum but then weakened with further cure time. In a similar finding the plaster cured in the oven had greater flexural strength than the plaster cured under room conditions.

## INTRODUCTION

Plaster of Paris is manufactured by heating gypsum to about 150°C:



When the dry plaster powder is mixed with water, hydration of the calcium sulphate hemihydrate occurs (Çolak, 2006):



Dry cured plaster behaves in a linear elastic manner. A number of researchers have investigated the properties of plaster. Coquard and Boistelle (1994) found that drying and wetting significantly affects the mechanical strength of plaster. Specifically, a 50% decrease in the mechanical strength will occur if the cured plaster absorbs 2% water, but will regain the strength if the water evaporates. A possible reason for this phenomenon is that water contributes to a reduction in the interfacial free energy of the gypsum crystals. It was confirmed in the study of Taylor, Vardy and MacDougall (2006) that moisture content also has an adverse influence on the strength of earthen plasters.

Plaster, which is a polycrystalline material made of intricate gypsum needles, is often used as a rock mechanics modelling material in rock mechanics (Coquard and Boistelle, 1994), thus, it is important to understand the factors that affect the mechanical properties of the plaster. One particular problem is determining how long plaster models should cure for before testing and under what environment should the plaster be cured. This study is an attempt to evaluate the influence of different curing times and environments on the compressive and flexural properties of cured plaster specimens.

## UNIAXIAL COMPRESSIVE TEST

### Samples preparation and test procedure

Water and a plaster powder were mixed with a weight ratio of 1 : 3.5 respectively. After it became homogeneous the mixture was cast into a cylindrical mould 54 mm in diameter and 120 mm in height. The samples were divided into two groups; while one group was placed in a room environment with the

relative humidity recorded the other one was placed in a 45°C oven. The samples were then cured for various lengths of time, 1 day, 3 days, 5 days, 1 week, 2 weeks, 3 weeks, 4 weeks, 8 and 12 weeks.

After cure uniaxial compressive tests were conducted in accordance with the International Society for Rock Mechanics (ISRM) 'Suggested Method for Determining the Uniaxial Compressive of Rock Materials'. As the top end of the plaster cylinder may not be perfectly flat all the samples were cut to 109 mm in height and then polished using a lapping machine to make sure the ends were flat and parallel as per the standard. Figure 1 shows the final dimensions of the sample. The test set-up is shown in Figure 2.

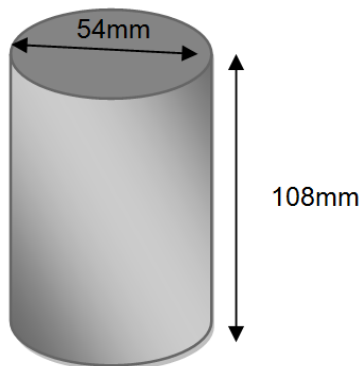


Figure 1 - Final dimensions of the sample



Figure 2 - Uniaxial compressive test set-up

**Test results**

Statistics on the detailed uniaxial compressive test results are recorded elsewhere, the averages of the test results at each curing time and environment are illustrated in Figure 3. As expected the oven cured plaster samples exhibited a more rapid increase in strength than the corresponding room cured samples, but possibly not so intuitive was that the peak strength of the oven cured samples was greater than the room cured samples at 75.5 MPa and 62.4 MPa respectively. It is evident that the oven cured samples underwent a rapid increase in UCS in the first three days from 38.8 MPa to 63.2 MPa, rapid strengthening stage, but there was not much change in the UCS of the room cured samples, slow strengthening stage. The UCS of both the room and oven samples reached a peak after two weeks, the oven having undergone slow strengthening from day 3 to week 2, while the room samples underwent rapid strengthening from week 1 to week 2.

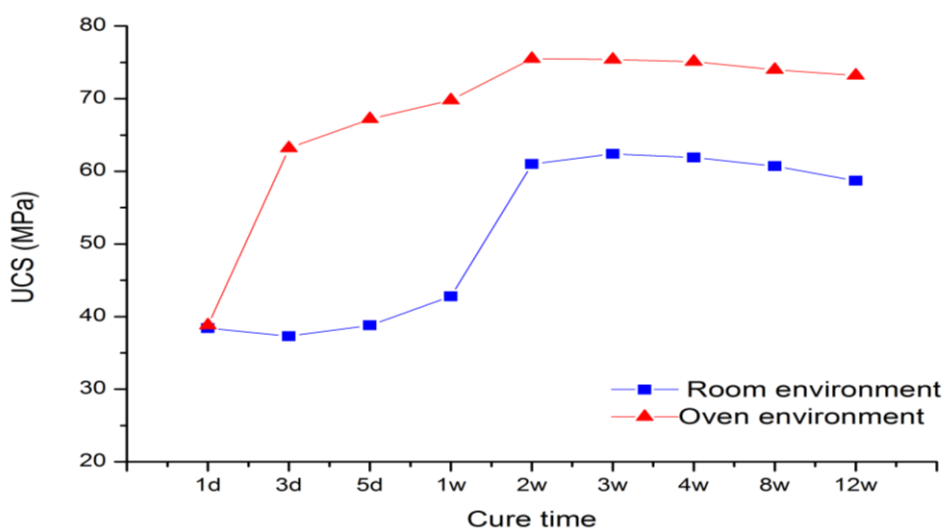


Figure 3 - Uniaxial compressive test results. Note: 1d=1 day, 2w=2 weeks.

After week 2 all samples remained stable during the period from week two to somewhere between weeks four and eight, but then experienced a slight decrease, a weakening stage. This suggests that

samples should not be used for modelling after around six weeks of curing. No matter what the curing conditions all samples exhibited brittle failure in compression.

### THREE-POINT BENDING TEST

#### Samples preparation and test procedure

As before plaster and water were mixed with a weight ratio of 3.5 : 1 and rectangular blocks of 160 mm × 40 mm × 40 mm were cast, Figure 4. One group of samples was placed in a 45°C oven and the another was placed in the room environment for the predetermined curing times. An Instron servo-hydraulic system was employed to conduct the experiments. The plaster blocks were supported by two rollers located 20 mm from the edge of each sample and a vertical load was applied at a rate of 0.1 mm/min rate to the centre of the sample as shown in Figure 5. Load versus displacement behaviour of the plaster was recorded during the test.

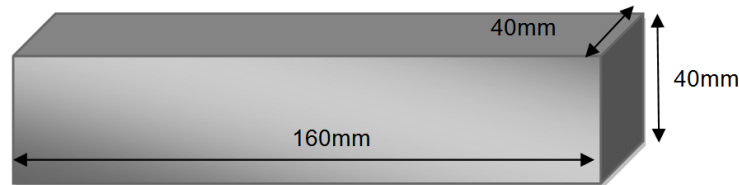


Figure 4 - Geometry of the sample for a three-point bending test

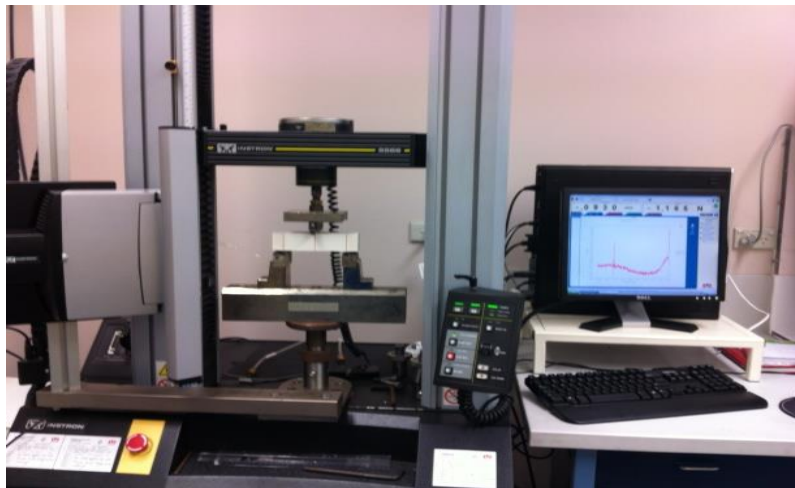


Figure 5 - Three-point bending test set-up

#### Test results

Figure 6 illustrates a typical load versus displacement curve of a three-point bending test on plaster. Initially, the displacement driven load increased very gently. When the displacement reached 2.8 mm, the load increased dramatically. This was probably caused by insufficient roller contact at the top plaster surface that occurred during the initial setup. The effective load versus displacement line, as shown in Figure 6, is proposed to describe the deformability of the plaster. The slope of this line is calculated from Equation (1):

$$k = \frac{l_p - l_{50}}{d_p - d_{50}} \quad (1)$$

Where  $k$  is the slope,  $l_p$  is the peak load and  $d_p$  is the corresponding displacement,  $l_{50}$  is 50% of the peak load and  $d_{50}$  is the displacement at  $l_{50}$ . The displacement offset  $d_0$  is defined as the point where the effective load versus displacement line intersects the displacement axis, representing the displacement needed to activate the load carrying capacity of the plaster block. The effective displacement equals the difference between  $d_p$  and  $d_0$ .

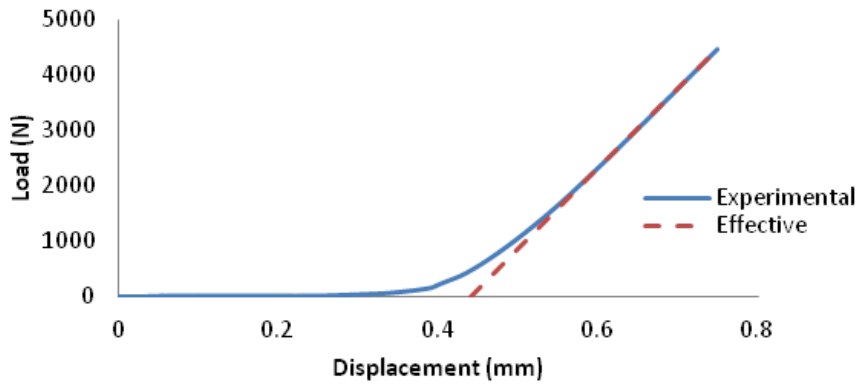


Figure 6 - Typical load versus displacement curve of three-point bending test of plaster

The flexural strength of the plaster ( $\sigma_f$ ) was calculated using Equation (2):

$$\sigma_f = \frac{3fl}{2bh^2} \tag{2}$$

where: f = load at failure, l = span length, b = sample width, h = sample thickness.

The average results of the three-point bending tests are shown in Figures 7 and 8. Generally, the displacement at failure of the plaster increased as its flexural strength rose. Plasters cured in the oven had greater flexural strength and displacement at failure than their room cured samples, the peak flexural strength of the oven group was 15.6 MPa with a corresponding displacement at failure of 0.39 mm while the room cured samples were 11.9 MPa and 0.30 mm respectively.

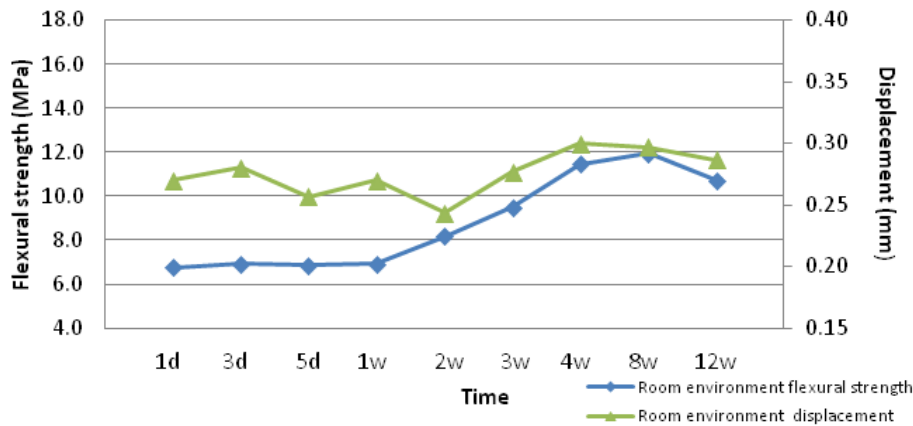


Figure 7 - Flexural properties of room cured plasters

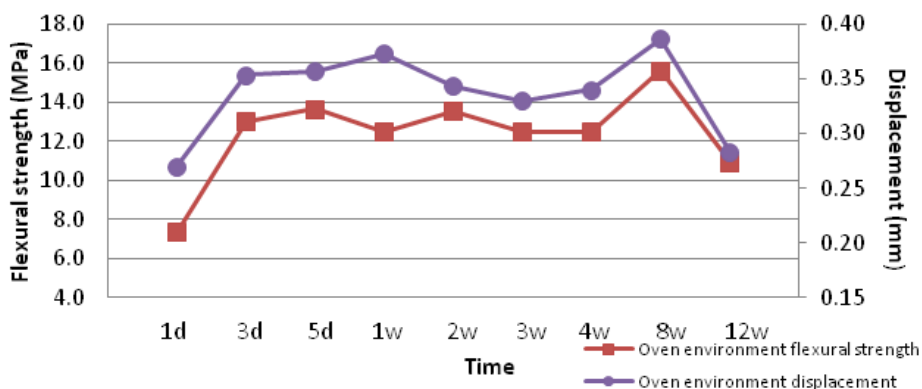


Figure 8 - Flexural properties of oven cured plasters

For the oven group, the flexural strength of the plaster increased significantly from day one at 7.4 MPa to day three at 13.0 MPa, from then till week four it held at around 13 MPa. The peak flexural strength came up in week eight with a value of 15.6 MPa, and after that the plaster experienced a significant decrease in flexural strength. For the room cured plasters, the flexural strength kept stable at about 6.9 MPa during the first week and then started to grow, reaching a peak at 11.9 MPa in week eight. As before the plaster became weaker from then on. It is important to note that although different curing times and environments affected the flexural properties of the plaster, as with the compression test, the material still experienced brittle failure.

As with the compression test samples, the change of flexural strength of the plasters can be divided into different stages, Figure 9. Unlike the compression samples four stages, the room cured samples exhibited only three stages; a stable stage, a slow strengthening stage and a weakening stage. The stable stage occurred in the first week of curing, then followed a slow strengthening stage which lasted to the eighth week and, from the eighth on, the weakening stage. For the oven cured samples, as with the compression samples, there were four stages: a fast strengthening stage for the first three days, a stable stage which lasted to week four, a slow strengthening stage in the following four weeks and finally a weakening stage.

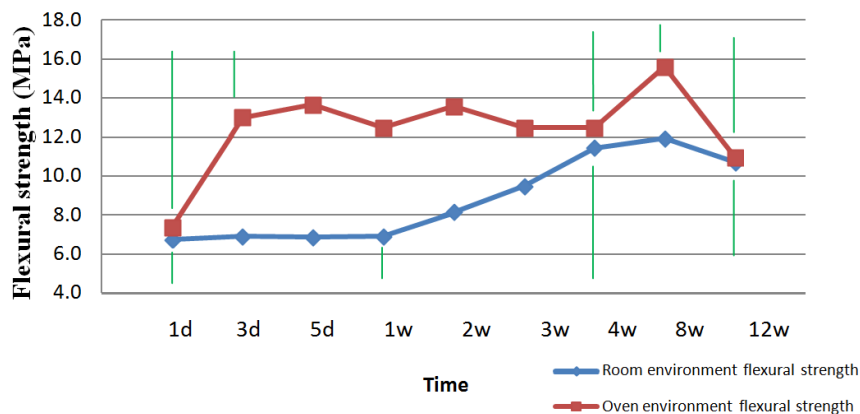


Figure 9 - Flexural strength at various stages of curing

## DISCUSSION

It is common knowledge that higher curing temperatures result in faster curing times for Plaster of Paris, providing that temperatures are not so high as to cause calcination. In this study an oven temperature of 45°C was used to cure one set of samples, while another set was cured at room temperature. The tests indicate that while it took two weeks for the room temperature cured samples to achieve a significant increase in mechanical resistance the oven cured samples increased dramatically in both UCS and flexural strength in the first three days. In addition, results from the laboratory tests demonstrate that plaster samples stored (extended curing) in the 45°C oven had a greater peak strength, both in compression and flexure, than those stored under room conditions. The peak UCS of the oven samples was 75 MPa, which was about 20% greater than that of room samples, and the peak flexural strengths of the two groups were around 16 MPa and 12 MPa respectively. This suggests that higher temperature contributes positively to the hydration reaction, resulting in a 20% increase in both compressive and flexural strength.

No matter under which of the above conditions the plaster was stored it initially increased in UCS and flexural strength over a limited time, but then experienced a decrease owing to degradation of the cured sample over extended time periods. Specifically, the UCS of the plasters started to reduce slightly after week four, from 75.4 MPa to 73.2 MPa for the oven group and 61.9 MPa to 58.7 MPa for the room group. The two groups of samples decreased by 4.6 MPa and 1.2 MPa in flexural strength respectively from week eight to week twelve. The reason for this degradation in strength may be as suggested by Palha *et al.* (2012), who, when reporting various researchers (Henriques, 1992; Pühringer, 1983; Arnold and Zehnder 1987; Goudie and Viles 1997), stated that water movement in gypsum plaster may transport soluble salts which can crystallize and damage the mechanical resistance. Thus it is important that curing conditions are optimised.

The curing times to reach the stable stage of the mechanical properties of plaster samples are different with respect to different curing conditions. It is important to make sure the plaster samples are in the stable stage when they are employed as a rock simulation material, otherwise sub-optimum results may be obtained.

### CONCLUSIONS

Multiple tests were performed for each cured state to investigate the change of UCS and flexural properties of Plaster of Paris samples as a function of curing time and environment. It can be concluded that:

- Higher temperature makes the plaster cure quicker and produces stronger samples in both compression and flexure;
- The plaster increased in UCS and flexural strength over time to a limit, and then experienced a degradation of strength after around 6 to 8 weeks;
- When plaster is utilized to simulate rock materials it is important to make sure they are tested in the stable stage.

### REFERENCES

- Arnold, A and Zehnder, K, 1987. Monitoring wall paintings affected by soluble salts, in Proceedings *the conservation of wall paintings* (ed: S Cather) pp 103–135 (Symp. of the Courtauld Institute of Art and the Getty Conservation Institute: London).
- Coquard, P and Boistelle, R, 1994. Water and solvent effects on the strength of set plaster, *International Journal of Rock Mech. Min. Sci. and Geomech*, 31(5): 517-524.
- Çolak, A, 2006. Physical and mechanical properties of plaster-polymer composites, *Journal of Materials Letters*, 60: 1977-1982.
- Goudie, A and Viles, H A, 1997. Salt weathering hazard, (John Wiley: Chichester, UK).
- Henriques, F, 1992. Action of moisture in walls: Types of defects quantification criteria and repair solutions, Ph.D. thesis, Instituto SuperiorTécnico, Technical Univ. of Lisbon, Lisbon, Portugal (in Portuguese).
- International Society for Rock Mechanics 1979, ISRM Suggested Methods for Determining the Uniaxial Compressive strength and Deformability of Rock Materials, ISRM.
- Palha, F, Pereira, A, Brito, J and Silvestre, D, 2012. Effect of water on the degradation of Gypsum plaster coatings: inspection, diagnosis, and repair, *Journal of performance of constructed facilities*, 26: 424-432.
- Pühringer, J, 1983. Salt disintegration, salt migration and degradation by salt - A hypothesis, Document D15, Swedish Council for Building Research (Stockholm).
- Taylor, B, Vardy, S and MacDougall, C, 2006. Compressive Strength Testing of Earthen Plasters for Straw Bale Wall Application, in Proceedings of *International Conference on Advances in Engineering Structures, Mechanics and Construction*, pp 175-183 (Springer: Waterloo).

# EVALUATING METHODS OF UNDERGROUND SHORT ENCAPSULATION PULL TESTING IN AUSTRALIAN COAL MINES

Peter Craig<sup>1</sup>, Naj Aziz<sup>2</sup>, Jan Nemcik<sup>2</sup> and Arash Moslemi<sup>3</sup>

**ABSTRACT:** In May 2012, an Australian Coal Association Research Program (ACARP) funded project C21011 commenced to develop coal industry standard test methods for assessing resin chemical anchors. The project was run by the University of Wollongong with assistance from Australia's two resin anchor manufacturers, J-Lok and Orica. A program of field and laboratory studies was undertaken to examine various factors influencing effective the load transfer mechanism between the bolt/resin and rock to ensure test methods represented field performance.

This paper discusses the field component of the research project. A series of Short Encapsulation Pull Tests (SEPT) were carried out in three mines with different geological conditions to determine the most representative and practical method of SEPT. Additional field work included installation of bolts into threaded steel tubes for subsequent laboratory evaluation. Factors of importance considered to affect bolt installation and the subsequent SEPT representing the fully encapsulated bolt performance included; borehole diameter, resin annulus thickness, installation time (including bolt spin to the back and "spin at back"), the effect of gloving and its impact on installation quality of the bolt and load transfer variation along the length of the installed bolt.

## INTRODUCTION

The resin bond between rock bolt and the strata is one of the critical elements of a roof bolting system, yet the Australian coal industry does not have an agreed standard for bolting system evaluation. Australia continues to rely on other country's standards, notably British, South African, and USA to evaluate its bolting systems even though material components are significantly different to those other countries. The Australian usage of bolting systems is much more homogeneous with similar diameter bolts and with little diversity in the use of resin until now. In light of the recent increases in various resin types in Australian coal mines, there is a need for setting up a practical method of testing, by the end users

Mark, *et al.*, (2002) described the US study by NIOSH aimed at developing a US standard Short Encapsulation Pull Tests (SEPT) method. The non-reamed and reamed hole methods described by Mark *et al.*, (2002) are illustrated in Figure 1. These methods form the basis of the Australian study using M24 threaded rebar bolts and oil based catalyst resin most commonly used by the Australian industry.

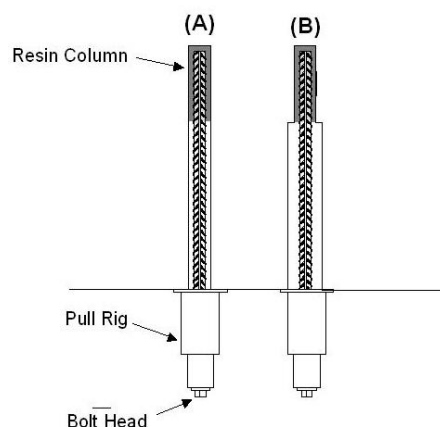


**Figure 1 - The Short Encapsulation Pull Test. (A) Normal hole; (B) Reamed hole (Mark, *et al.*, 2002)**

<sup>1</sup> Jennmar Australia, Email: PCraig@jennmar.com.au, Tel: 0419 018 998

<sup>2</sup> University of Wollongong, Email: naj@uow.edu.au, Tel: 02 42 213 449

<sup>3</sup> J-Lok Reins Australia Pty Ltd, Tel: 0431 219 338

The Australian study used the most common 21.7 mm core diameter, M24 threaded X-grade bolt as illustrated in Figure 2. The most common oil based catalyst fast set polyester resin was used, containing a 5-7% catalyst component.

Hillyer(2012) highlighted that Australia's M24 bolts fully encapsulated in 28 mm diameter threaded pipes gave a variable bond strength performance along their length due to variable mixing of the resin and gloving from the plastic capsule film. The new ACARP study considered that pull testing the very top 200 – 300 mm of encapsulated bolt may not be representative of the entire fully encapsulated bolt, and that changes in the SEPT method should be explored.

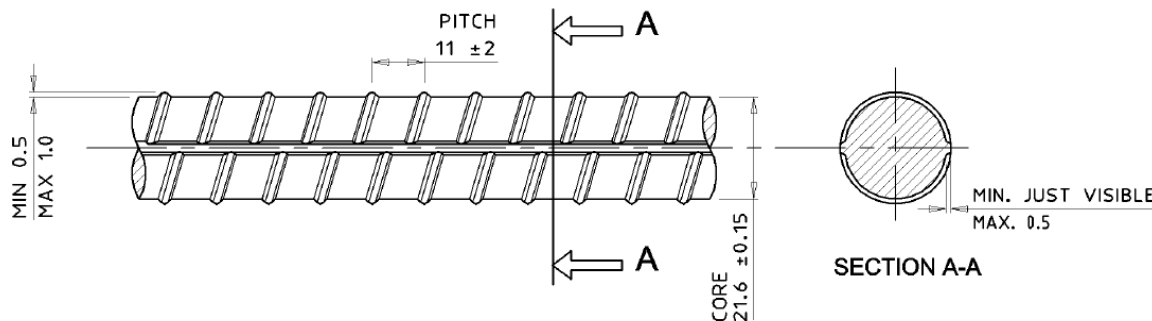


**Figure 2 - Australia's most common profile X grade bolt**

Testing was carried out at three different mine sites. Baal Bone Colliery mines the Lithgow seam and roof bolts were anchored into a moderate strength mudstone. Tahmoor Colliery mines the Bulli seam and roof bolts were anchored into a strong siltstone, whilst NRE Colliery, Russell Vale, the Wongawilli seam with roof bolts being anchored through a weak coal roof. All testing was done in a selected outbye area with no significant fracturing of the strata. The installation equipment used at all three sites were Alminco Goaffer hand-held compressed air rotary bolters operating at 600 – 700 rpm.

The underground SEPT were carried out by researchers from the University of Wollongong alongside Jennmar mine service technicians who are experienced operators of both the hand-held bolting installation and hydraulic pull testing equipment.

### DIFFERENT SEPT METHODS TESTED

Drill bits used at the sites were twin-wing rotary water flush 'angle' bits. The first test site included 28 mm and 27 mm diameter drill bits for comparison, whilst the remaining study sites used 27 mm bits only. Hillyer *et al.* (2013) identified the variability in load transfer from mixing. A SEPT only involves mixing through 200 – 300 mm of resin capsule which would be significantly different to mixing through a full length resin capsule typically 1000 – 1400 mm long. The underground tests included the following variable mix times for investigation;

1. The manufacturers recommended mix time of 10 seconds. Taking 5 s to spin through the capsule and 5 s when the bolt was at the back of the hole
2. Under-mixing with a total of 5 seconds. Taking 3 s to spin through the capsule and 2 seconds at the back of the hole
3. Over mixing with a total over 30 s

The reamed and non-reamed SEPT was used at Baal Bone and NRE Russel Vale test sites due to being weaker types of rock. The reamed test was used exclusively at Tahmoor mine with both 200 mm and 300 mm bond length due to the known stronger rock.

The issue of gloving has been identified by many previous studies, and has been found to be most likely at the top of the bolt. The SEPT only tests the top of the bolt and is therefore more likely to be prone to gloving reducing the bond strength results. It was decided to trial 50 mm of overdrill to provide a space for the plastic film to accumulate and not interfere with the bolt/resin/rock interface. This overdrill method was trialed at all test sites and is illustrated in Figure 3.

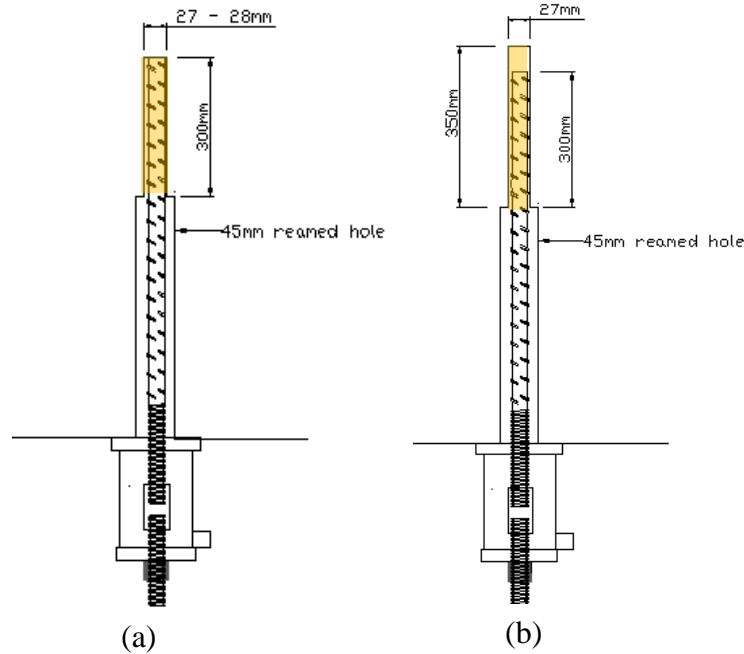


Figure 3 - (a) Reamed standard and (b) Reamed overdrill

## RESULTS

### Baal Bone Colliery

The first SEPT field investigation was carried out at Glencore's Baal Bone Colliery. The mine ceased production in 2011 but has been kept open as a training facility for Glencore employees.. A total of 24 short encapsulation bolts were installed at Baal Bone. All bolts were installed in the Triassic mudstone/shale immediate formation above the Lithgow seam, with known typical strength of 35 MPa.

Table 1 shows the summary of retrieved data of the bolt pull testing with subsequent analysis. The bond strength (kN/mm) was determined as the peak (maximum) pull load divided by the encapsulation length. Figure 4 shows the average pull test load-displacement profiles of the different set of test methods.

Bolts 5, 6, 7 and 8 installed in smaller diameter holes of 27 mm achieved better load transfer capacity than the bolts installed in 28 mm diameter boreholes (1, 2, 3 and 4). It is envisaged that the top 200 mm bond strength of most bolts, was significantly reduced, because of the accumulation of the capsule plastic film remnants in the over-drilled length. Thus the 50 mm over-drilled space allows resin skin shredding to accumulate in the over drill space above the bolt end and away from the area between the bolt and the reamed section of the borehole. Consequently, the results showed an extremely significant improvement. Thus, it is reasonable to conclude that the current short encapsulation pull test method used to study bond strength appears to demonstrate the effectiveness of hole over drill in Australian mines.

The non-reamed installations used a borehole micrometer and encapsulation chart to calculate the length of capsule required to target 300 mm of bond length. Table 1 shows that the bond lengths achieved varied between 368 mm and 419 mm which demonstrate the difficulty of the method with variables of capsule preparation and borehole micrometer error a significant problem.

In summary, it can be inferred from the pull testing at Baal Bone that:

1. Bolt installation time of around 10 s constitutes an acceptable time for effective bolt installation as is normally recommended for use with Minova/Orica fast setting resin of 14 s,
2. The results of the over spinning at back was inconclusive, because the spin times to shear the pin were too extreme in the 300 mm limited bolt encapsulation length,

3. The use of 300 mm long encapsulation length may be the maximum acceptable length for pull testing, but this depends on the type of the rock formation, which has some bearing on load transfer capability of the installation. This finding is in agreement with the study carried out by Wilkinson and Canbulat (2005),
4. In-line reamer drill rod saved time for drilling reamed holes and provided repeatable accurate bond lengths.
5. Hole over drilling contributed to increased load transfer capacity of the installed bolt and thus became the accumulation zone for the gloving material.

**Table 1 - Analysed data from the short encapsulation pull tests-Baal Bone Mine**

Bolt No.	Peak Load (kN)	Bond Strength (kN/mm)	Displacement at Peak (mm)	Spin to Back (sec)	Spin at Back (sec)	Total Spin Time (sec)	Bond Length (mm)	Average Hole Dia. (mm)	Borehole Type
1	117.7	0.39	4.7	3	7	10	300	28	reamed
2	98.1	0.33	5.9	3	7	10	300	28	reamed
3	117.7	0.39	10.0	3	7	10	300	28	reamed
4	107.9	0.36	1.3	3	7	10	300	28	reamed
5	137.3	0.46	3.5	5	5	10	300	27	reamed
6	176.6	0.59	1.6	5	5	10	300	27	reamed
7	166.8	0.56	2.2	5	5	10	300	27	reamed
8	147.2	0.49	2.6	5	5	10	300	27	reamed
9	147.2	0.49	1.8	3	2	5	300	27	reamed
10	137.3	0.46	1.8	3	2	5	300	27	reamed
11	157.0	0.52	2.0	3	2	5	300	27	reamed
12	137.3	0.46	4.0	3	2	5	300	27	reamed
13	94.2	0.31	3.3	3	22	25 (NB)	300	27	reamed
14	95.2	0.32	3.2	3	31	34 (NB)	300	27	reamed
15	73.6	0.25	5.5	3	47	50 (NB)	300	27	reamed
16	29.4	0.10	3.5	3	39	42 (NB)	300	27	reamed
17	215.8	0.59	2.4	5	5	10	368	28	NOT reamed
18	215.8	0.56	4.4	5	5	10	385	28	NOT reamed
19	215.8	0.54	2.7	5	5	10	402	28	NOT reamed
20	215.8	0.52	1.7	5	5	10	419	28	NOT reamed
21	215.8	0.72	4.6	5	5	10	300	27	reamed + 50 mm OD
22	206.0	0.69	2.8	5	5	10	300	27	reamed + 50 mm OD
23	157.0	0.52	2.5	5	5	10	300	27	reamed + 50 mm OD
24	215.8	0.72	2.3	5	5	10	300	27	reamed + 50 mm OD

- Bolt: JBX, Core diameter: 21.7 mm, Length: 1200 mm, Installed horizon: 1100 mm; Resin: Orica, fast-setting, RA33025F.
- Un-reamed holes encapsulation length was achieved by wrapping tape around the end of the first 300 mm length of the bolt.
- Bond strength is defined as the maximum pull load/encapsulation length.

## Tahmoor Colliery

The next round of pull testing was carried out at Glencore's Tahmoor Colliery in late November 2012. The Bulli seam roof is relatively stronger than the Lithgow measures of Baal Bone mine and comprises mudstone, shale and sandstone. Therefore, the mine roof at the test site can be described as moderately competent. Similar to Baal Bone, a total of 24 bolts were installed in intersection 5/1 near the pit bottom. The process of drilling and installation of 24 rock bolts as well as the equipment used was similar to the bolt installation operation at Baal Bone mine.

Two encapsulation lengths of 200 mm and 300 mm were trialled at Tahmoor, with and without the additional 50 mm of over drilling. The installation time of the bolts was mostly in accordance with the normal standard time of 10 s, however, there were some variations, mostly at lower installation times as shown in Table 2.

Table 2 highlights the summary of test results and analysis. The 200 mm long short encapsulation pull tests for the first eight bolts (1- 8) showed a variation in bond strength between the standard hole length and the 50 mm over-drilled holes. The over-drilled holes pull test values were, in most cases, higher

than the standard installations. The influence of over drilling is also evident with bolts installed at short installation times in bolts 22 and 24. Similar to the Baal Bone Mine study, the over-drilled holes generally showed a significant improvement in the load bearing capacity of the bolts.

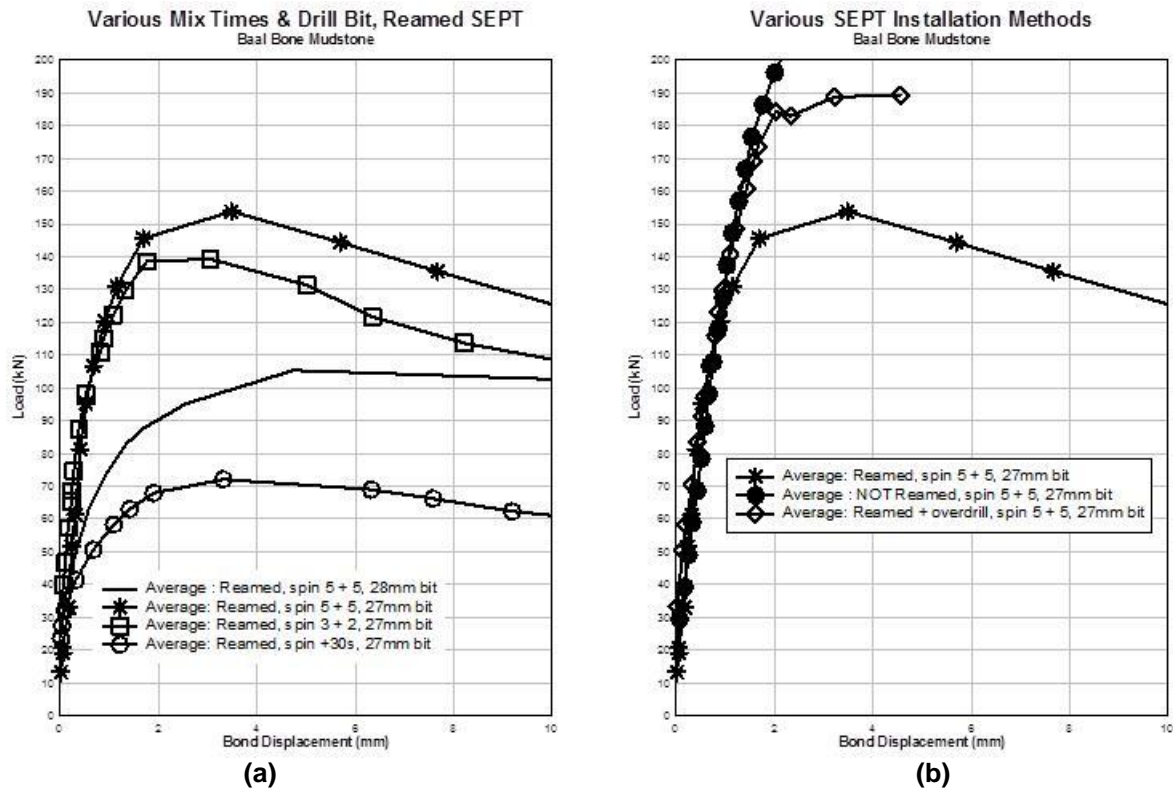


Figure 4 - Baal Bone Colliery: Variation in load transfer capacity by SEPT method

Table 2 - Analysed data from the short encapsulation pull tests- Tahmoor Mine

Bolt No.	Peak Load (kN)	Bond Strength (kN/mm)	Displacement at Peak (mm)	Spin to Back (sec)	Spin at Back (sec)	Total Spin Time (sec)	Bond Length (mm)	Borehole Type
1	98.1	0.49	2.6	5	5	10	200	reamed
2	127.5	0.64	4.3	5	5	10	200	reamed
3	127.5	0.64	2.3	5	5	10	200	reamed
4	127.5	0.64	3.9	5	5	10	200	reamed
5	166.8	0.83	2.6	5	5	10	200	reamed + 50 mm OD
6	137.3	0.69	2.4	5	5	10	200	reamed + 50 mm OD
7	147.2	0.74	3.4	5	5	10	200	reamed + 50 mm OD
8	107.9	0.54	1.8	5	5	10	200	reamed + 50 mm OD
9	235.4	Long encapsulation	4.6	5	5	10	300	reamed
10	201.1	0.67	6.3	5	5	10	300	reamed
11	235.4	Long encapsulation	3.2	5	5	10	300	reamed
12	235.4	Long encapsulation	4.4	5	5	10	300	reamed
13	186.4	0.62	3.2	5	5	10	300	reamed + 50 mm OD
14	225.6	Long encapsulation	4.0	5	5	10	300	reamed + 50 mm OD
15	225.6	0.75	6.5	5	5	10	300	reamed + 50 mm OD
16	215.8	0.72	3.3	5	5	10	300	reamed + 50 mm OD
17	78.5	0.39	1.3	3	2	5	200	reamed
18	63.8	0.32	5.3	3	2	5	200	reamed
19	98.1	0.49	2.0	3	2	5	200	reamed
20	34.3	0.17	2.2	3	2	5	200	reamed
21	107.9	0.54	11.7	3	2	5	200	reamed + 50 mm OD
22	137.3	0.69	2.4	3	2	5	200	reamed + 50 mm OD
23	98.1	0.49	1.5	3	2	5	200	reamed + 50 mm OD
24	147.2	0.74	1.9	3	2	5	200	reamed + 50 mm OD

NB: OD – over drill. All encapsulated holes diameter: 27mm. All holes reamed. Bond strength (kN/mm) is the peak (maximum) pull load divided by the encapsulation length

Within the over-drilled bolts with 200 encapsulation length, bolt 5 had the highest bond strength at around 167 kN, with mixing time of 5 s “spin to back” plus 5 s “spin at back”.

As expected, the pull test results for 300 mm long encapsulation length yielded significantly stronger bond strength, which, at times, exceeded the 22 – 24 t yield strength of the bolt.

It is not possible to draw any realistic and comparative conclusion between the standard 300 mm long encapsulation with and without over drilling (bolts 9 to 16) as pull test loads were close to bolt yield strength. However, the narrow and higher margins in pull loads were evident in over-drilled hole bolt installations, hence it is reasonable to assume that the over drill installation pull load values were better than the standard bolt installations. The profiles of the load-displacement graphs are shown in Figure 5.

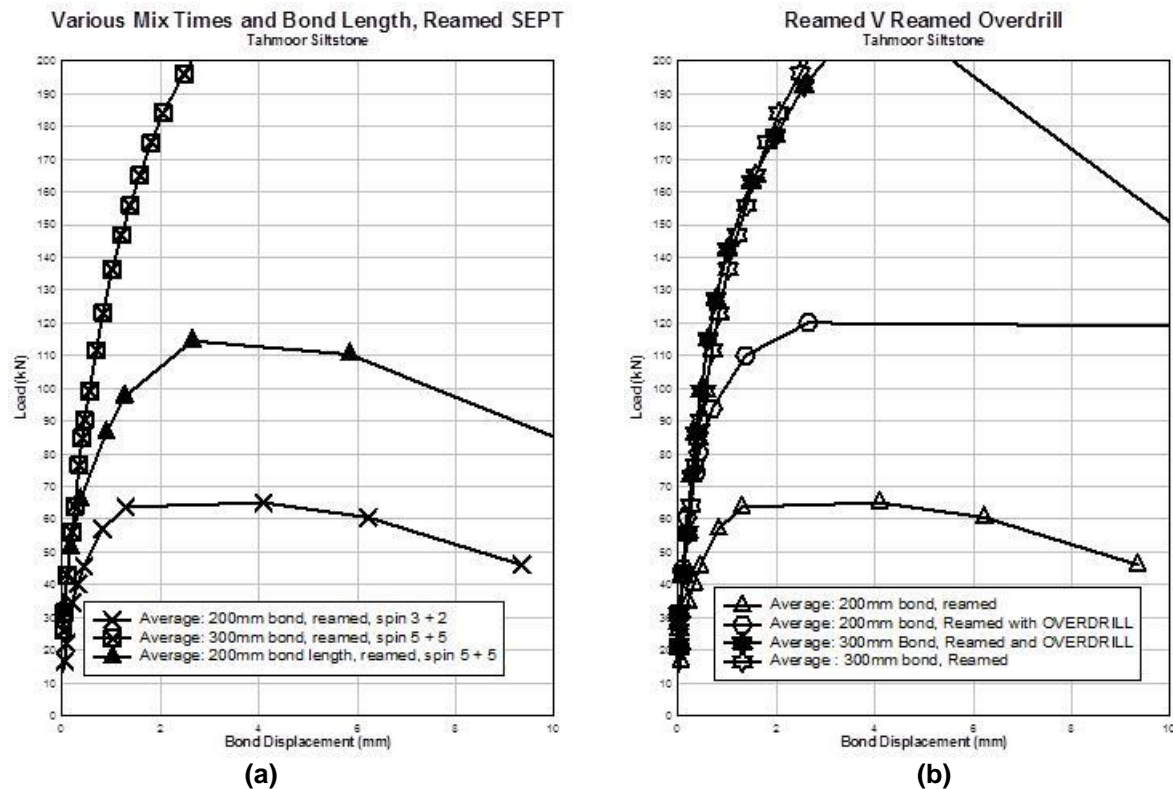


Figure 5 - Tahmoor (a) 200 mm V 300 mm Bond Length, (b) Reamed V Reamed Over-drill

With regard to short installation times, it is clear that shorter installation spin times of less than 10 s were inadequate for proper resin mixing to allow effective anchorage and hence a relatively lower peak pull load strength. Again over drilling appears to yield relatively superior bond strength.

Thus, it can be inferred from the tests carried out at Tahmoor Colliery that:

- bolts installed in over-drilled holes had superior load transfer capacity
- as expected, the 300 mm encapsulation length yielded greater load transfer capacity (higher pull force values) leading to yield strength, and
- shorter mixing time of half the recommended 10 sec was counter-productive for an effective load transfer mechanism. Prolonged “spin time at back” and shorter “spin time to back” is also counter-productive.

### NRE Colliery, Russell Vale

The third and final round of field tests was carried out in mid-December 2012 at NRE Rusell Vale Colliery within the Wongawilli Seam. The test site was located in C heading, between CT20 and 21 of the Wongawilli Seam East main headings. The selected stratification above the working part of the Wongawilli Seam was a soft formation of mainly coal layers and clay bands.

In a similar manner to the previous field studies, an even and flat roof area was selected at the CT20 intersection for bolt installation. A total of 16 bolts, 1200 mm long, were installed in 1100 mm long holes using a handheld and compressed air operated Alminco Gopher drill. Table 3 shows the details of pull testing results.

- Encapsulation length of the first 12 holes were constant at 300 mm and the encapsulation lengths of holes 13 to 16 holes were variable as indicated in Table 3.
- Bolts 1 to 4 were installed in 50 mm long over-drilled holes with a reamed 200 mm bottom section. The installation time was consistent at standard time of ten seconds (5 s "spin to back" and 5 s "spin at back").
- Bolts in holes 9 to 12 were installed at the total spin time of five seconds (2 s "spin to back and 3 s "spin at back").
- In the unreamed holes 13-16, the desired anchorage lengths of holes 13 to 16 were accomplished by wrapping an insulation tape of sufficient thickness around the bolt to the determined length, thus preventing the resin from spreading down the length of the bolt.

**Table 3 - Analysed data from the short encapsulation pull test-NRE No.1**

Bolt No.	Peak Load (kN)	Bond Strength (kN/mm)	Displacement at Peak (mm)	Spin to Back (sec)	Spin at Back (sec)	Total Spin Time (sec)	Bond Length (mm)	Average Hole Dia. (mm)	Borehole Type
1	215.8	0.72	2.8	5	5	10	300	27	reamed + 50 mm OD
2	137.3	0.46	2.1	5	5	10	300	27	reamed + 50 mm OD
3	147.2	0.49	3.4	5	5	10	300	27	reamed + 50 mm OD
4	137.3	0.46	2.9	5	5	10	300	27	reamed + 50 mm OD
5	73.6	0.25	2.7	5	5	10	300	27	reamed
6	127.5	0.43	3.9	5	5	10	300	27	reamed
7	107.9	0.36	1.5	5	5	10	300	27	reamed
8	78.5	0.26	1.0	5	5	10	300	27	reamed
9	117.7	0.39	2.6	2	3	5	300	27	reamed
10	157.0	0.52	7.0	2	3	5	300	27	reamed
11	127.5	0.43	5.0	2	3	5	300	27	reamed
12	103.0	0.34	6.0	2	3	5	300	27	reamed
13	196.2	0.61	3.6	3	7	10	320	28	NOT reamed
14	157.0	0.56	2.7	3	7	10	280	28	NOT reamed
15	98.1	0.34	2.5	3	7	10	290	28	NOT reamed
16	157.0	0.68	1.4	3	7	10	230	28	NOT reamed

NB: BH encapsulated length diameter 27 mm, using twin-wing bit  
Holes 1-12 were reamed using a 45 mm diameter in-line reamer

With regard to the non-reamed holes, using the average diameter of holes the length of resin capsules were calculated and resin capsules were cut and re-sealed accordingly. The length of the resin capsules was 250 mm for bolt installation in 300 mm anchorage.

Table 3 shows the current 300 mm short encapsulation pull test for the first 12 rock bolts. As can be seen the un-reamed holes with variable encapsulation length have a better load bearing capacity of up to 196 kN in comparison with the performance of reamed holes with 300 mm encapsulation lengths. Figure 6 shows the load displacement graphs of all the bolts. It is clear that the performance of the first four bolts installed in over-drilled holes was better than the bolts installed with the standard methods without over drilling.

The following were inferred from the pull tests at NRE Russel Vale installations in the Wongawilli formation:

1. Bolts installed in the over-drilled holes (bolts 1-4) had relatively higher pull loads than the ones installed in holes 5 and 8 without over drilling.
2. The pull load of bolts installed at shorter installation spin time was, in general greater than the standard 10 s time.

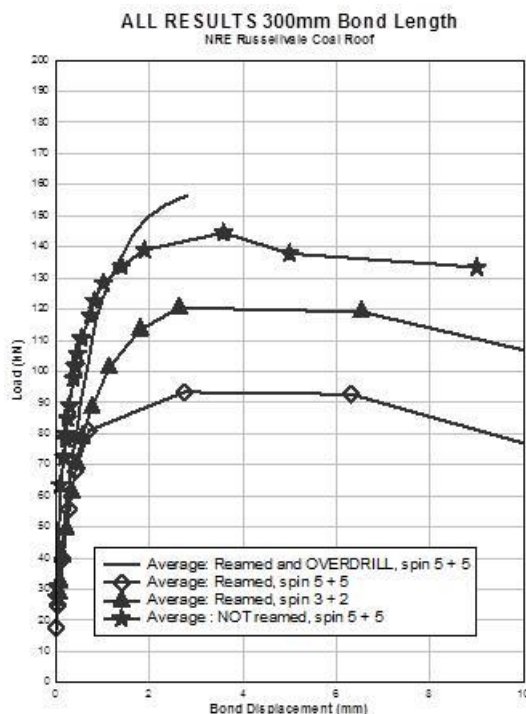


Figure 6 - All results NRE Colliery, Russell Vale

### CONCLUSIONS AND RECOMMENDATIONS

Given the limited number of bolts installed at three sites of varying geological formations, it is clear that over drilling of the bolts by 50 mm has led to load transfer capacity improvement. This increase in bolt resin rock bonding can be attributed to the resin capsule film being pushed upwards and accumulating in the over drill space above the bolt end. The removal of the film from the main body of the resin mixture has permitted increases in bonding strength between the bolt, resin and rock. This finding is being further analysed in the ACARP Project.

The following conclusions were inferred from the field SEPT study:

- Bolt installation time of approximately 10 s constitutes an acceptable time for effective bolt installation as is normally recommended for use with Minova/Orica fast setting resin of 14 s,
- The results of the over spinning at back was inconclusive because of the limited bolt encapsulation length
- The use of 300 mm long encapsulation length may be the maximum acceptable length for pull testing. This may also depend on the type of the rock formation, which has some bearing on load transfer capability of the installation. This finding is in agreement with the study carried out by Wilkinson and Canbulat (2005).
- Over drilling contributed to increased load transfer capacity of the installed bolts and thus became the accumulation zone for the gloving material.
- Non-reamed methods are not repeatable and accurate due to the errors in borehole measurement and capsule preparation.

### ACKNOWLEDGEMENTS

The research project has been funded by the Australian Coal Association Research Program (ACARP), project C21011. We are grateful for the cooperation of the personnel of Baal Bone, Tahmoor and NRE Russel Vale. Also many thanks to Jennmar Australia for providing bolts and assistance in the field trials, and Minova /Orica Australia in providing resins.

**REFERENCES**

- Hillyer, J, 2012. Influence of installation method and resin properties on rock bolt performance in underground coal mines. Undergraduate thesis, UOW, 110p.
- Hillyer, J, Craig, P, Shuqi Ma, Aziz, N, Nemcik, J and Ren, T, 2013. Variation in load transfer along the length of fully encapsulated rock bolts, based on the installation mixing parameters, in *Proceedings of 4<sup>th</sup> Underground Coal Operators Conference, Coal 2013, February 14-15, Wollongong*, (eds: N. Aziz and Kininmonth), pp137-143. <http://ro.uow.edu.au/coal/447/>.
- Mark, C., Compton, C.S., Oyler, D.C., Dolinar, D.R., 2002, Anchorage Pull Testing for Fully Grouted Roof Bolts, in *Proceedings of the 21st International Conference on Ground Control in Mining*, Morgantown, WV, West Virginia University, pp. 150-113.
- Wilkinson, A and Canbulat, I, 2005. Investigations into support systems in South African Collieries, in *Proceedings of 24<sup>th</sup> International Conference on Ground control in Mining*, August 2-5, Morgantown, WV, USA, pp 263-269.

# THE BOREHOLE SLEEVING TEST METHOD OF RESIN ANCHORED ROOF BOLT INSTALLATIONS

Kent McTyer<sup>1</sup>, David Evans<sup>2</sup>, Guy Reed<sup>1</sup> and Russell Frith<sup>1</sup>

**ABSTRACT:** Resin anchored roof bolts are the basis for the primary roof support system of every underground coal mine in Australia. However, the negative influences of uncured resin and resin loss due to installation pressure are common problems despite more than 30 years of product development. The current study details a surface testing method that installs a commonly used roof bolt into lengths of PVC pipe. Results were gathered in two ways, instrumentation measured bolt displacement and rotation speed and back-pressure during installation. The PVC was then cut open to assess the quality of the resin anchor. Comparative testing was undertaken on two resin cartridges commonly used in Australia: 2:1 mastic-to-catalyst resin and 15:1 mastic-to-catalyst resin. The tests were performed in 28 mm and 30 mm internal diameter PVC pipes to simulate a range of underground roof conditions. Data analysis shows the influence of borehole diameter, mastic-to-catalyst ratio and insertion pressure development on resin anchor reliability.

## INTRODUCTION

Resin-anchored roof bolts are used for primary roof support in every Australian underground coal mine. However, the efficacy of the resin-anchored roof bolt system has been found to be compromised in many Australian and New Zealand underground operations (Campbell and Mould, 2003; Craig, 2012).

A number of studies from Australia, New Zealand and the United States of America (US), as outlined below, have been conducted into the various limitations of resin-anchored roof bolts over the past 25 years. These include: gloving (where the polyester film cartridge wrapper remains intact around significant sections of the bolt and resin); uncured resin (particularly in the upper section of bolt); and the development of very high pressure in the uncured resin during installation. This paper describes recent ACARP-funded research into two factors: the proportion of uncured resin and the development of pressure in the resin during installation.

## PREVIOUS RESEARCH - INSTALLATION PRESSURE

Inserting a length of roof bolt through a resin cartridge into a drill hole can create significant pressure in the resin system. The pressure developed is a function of a number of factors including drill hole diameter, rebar diameter, drill hole depth, resin length and viscosity, insertion rate, and the maximum thrusting force that can be delivered by the bolting rig. Research has shown that this pressure can cause both hydraulic fracturing of the roof strata and resin injection into pre-existing strata voids, potentially damaging the roof strata. Pressure can also lead to a reduction in the length of the bolt that is encapsulated in resin, thereby comprising the bolt's effectiveness.

In US studies, the measured peak installation pressure ranged from 27-34 MPa (Compton and Oyler, 2005) and 24-48 MPa (Giraldo, *et al.*, 2006). Giraldo found that as annulus area was increased - by increasing borehole diameter for a given bolt diameter - the peak pressure reduced. Pettibone (1987) found that the installation pressure developed in the resin was sufficient to split (hydraulic fracture) 31 MPa concrete. Research using bolts recovered by overcoring (Campbell and Mould, 2003; Compton and Oyler, 2005; Craig, 2012) found evidence of the hydraulic injection of resin into the strata surrounding the drill hole. This resin injection was observed to a distance of 100 mm from the drill hole in the Campbell and Mould (2003) study. The underground trial by Compton and Oyler (2005) found that resin losses - averaging 40% of the total resin volume - occurred in weak roof strata. These losses were inferred to result from resin injection into either existing fractures or fractures created by the installation pressure. Underground studies of full resin encapsulated bolts found that increasing the annulus area resulted in a reduction in resin loss from 30% (Giraldo, *et al.*, 2006) and 27% (Craig, 2012) to 0%.

<sup>1</sup> Mine Advice Pty Ltd, Newcastle, NSW 2302; kentmctyer@mineadvice.com.au, Tel: 0400262818

<sup>2</sup> Dywidag Systems International Pty Ltd, Bennetts Green, NSW 2290; David.Evans@dywidag.com.au, Tel: +61408 475 568

A conflict becomes apparent because minimising the resin annulus has been shown to increase the load-transfer properties of an encapsulated roof bolt. However, this also directly reduces the amount of bolt encapsulation via the mechanisms just described. Therefore, a solution to maximise load transfer and resin encapsulation along the bolt will represent a significant improvement in roof bolting effectiveness.

### PREVIOUS RESEARCH - UNCURED RESIN

Adequate resin mixing relies on both the satisfactory shredding of the polyester film that contains the mastic and catalyst compartments and sufficient mixing of the two components to promote a uniform resin and mastic compound. When this occurs the resulting resin compound is typically fully cured, hard and homogeneous. Conversely, inadequate resin mixing results in a partially cured, soft and non-uniform resin.

The integrity of resin-anchored roof bolts relies on the quality and consistency of the cured resin. Uncured resin offers no load transfer to the strata (Campbell and Mould, 2003). The 15:1 mastic:catalyst resin cartridges, used commonly in Australia, have been found to be susceptible to uncured resin in the upper portion of the bolt. Campbell and Mould (2003) found that of 79 overcored "run of mine" bolts, the average uncured resin length was 245 mm (with a range from 0 - 750 mm).

The high incidence of uncured resin was found to be caused by the radial expansion of the resin cartridge as the installation pressure increased. This forces the catalyst section hard against the wall of the bolt hole and allows the bolt to pass through the resin without piercing the small catalyst compartment. In the USA, Compton and Oyler (2005) tested 24 overcored bolts using the 2:1 mastic:catalyst resin cartridges commonly used in the US market. They found no evidence of uncured resin, and concluded that both mastic and catalyst compartments of the 2:1 resin are more likely to be torn during bolt installation than the 15:1 resin used in Australia.

### CURRENT ACARP STUDY (PROJECT C21023)

The ACARP study aims firstly, to develop a new, highly controlled, surface-testing method designed to simulate underground resin bolt installations while also allowing rapid, multiple tests. Underground field trials are subject to both the naturally occurring geological variability present in the bolted interval, and the variability in the installation process caused by different drilling hardware, machinery and operators. The method aims to both remove these sources of variability and to provide a larger, and therefore more robust, data set than has been possible with previous methods.

Secondly, instrumentation was used to accurately record the bolt displacement, bolt rotation, and installation pressure over time. The data was collected following manufacturers specifications using typical Australian bolts, resin cartridges and drill hole diameters. This study aims to add to the research previously undertaken on US roof support hardware by providing data that is more relevant to Australian bolting practices.

Thirdly, this study aims to observe and compare 15:1 and 2:1 resin systems during bolt installation to further understand the degree of uncured resin present in fully encapsulated roof bolts used in Australian underground coal mines. The method design aimed to allow observation of the degree of uncured resin in test bolts under controlled conditions for the first time.

### SURFACE TESTING

The testing used a commonly available 1.8 m long M24 bolt with a core bar diameter of 21.7 mm and major bar diameter of 23.2 mm. Two resin types were tested: the catalyst-to-mastic ratio was either 15:1 or 2:1. Resin length was 1000 mm and resin diameter was 23 to 24 mm in all tests. Both resins were two-speed 50% fast- and 50% slow-set cartridges. These products were chosen to compare the 15:1 resin-anchored roof bolt system commonly used in Australian coal mines, with an alternative (2:1 resin) that could readily be brought into use without major changes in bolting hardware or installation practices.

Two drill hole diameters were assessed: 28 mm and 30 mm. This was made possible by using PVC pipe sleeves with different wall thickness. These diameters were chosen to represent the drill hole

diameters found underground that typically form when drilling with 27 mm and 28 mm drill bits. The 30 mm internal diameter is considered representative of coal mines with either weak roof lithologies such as claystone or coal, or immediate roof strata subject to elevated horizontal stress conditions that can cause substantial drill hole overbreak.

Bolts were installed according to manufacturer's recommendations on a specially devised hydraulic bolting rig, albeit one that may not be as powerful hydraulically as those commonly available on underground continuous miners' in Australian operation. The rig was fitted with instrumentation to measure bolt rotation, bolt travel, and pressure generated during bolt insertion. A total of 91 bolt installations were undertaken as part of the surface installation testing program.

### **RESIN MIXING EXPERIMENTATION BACKGROUND**

Traditionally, the simulation of resin roof bolt installations has been conducted into media such as sandstone core samples, internally grouted steel pipes, or into heavy walled steel tubing. For sandstone cores and grouted pipes, a pilot guide hole and then a final bore hole are pre-drilled to provide the desired test hole diameter. For steel tubing, often a crude thread or rifling is cut along the internal wall of the bore to simulate surface roughness commonly associated with underground drilling. There was often great focus on the surface properties and compressive strength of the media used in an effort to simulate underground lithology and performance. These traditional methods are useful for laboratory trials involving load transfer tests, where the steel element of the roof bolt was loaded and the resin bond strength was tested between the steel element and the media.

However, to visually assess the effectiveness of resin mixing, these traditional methods are in fact a hindrance. For sandstone and grouted pipes, the media has to be progressively removed to manually expose the outer surface of the resin annulus. The outer resin surface is mechanically damaged during removal of the media and the true interface can be difficult to precisely determine. As a result of this damage, visibility of the outer resin annulus was unclear and it was difficult to fully assess the effectiveness of resin mixing. The removal process was also laborious and time-consuming.

### **BOREHOLE SLEEVING – A NEW EXPERIMENTAL METHODOLOGY**

In order to overcome these issues, a new methodology was developed which provides a comprehensive visual assessment of resin curing under realistic bolt installation conditions. The new methodology involved internal sleeving of the test borehole, where the sleeve was readily removable after each resin installation test was completed. The internal sleeve was neatly constrained within a dimensionally rigid, heavy walled steel pipe to prevent any swelling of the sleeve during the test. As such, comparatively weak plastic materials such as PVC could be used for the internal sleeve, with bolt insertion and resin mixing pressures constrained by the outer heavy walled steel pipe. A closed-end cap assembly at the top of the sleeve prevented any resin loss from the test pipe system, and therefore, allowed resin backpressures to be developed. An open end cap at the bottom of the jig retained the sleeve in position prior to insertion of the bolt.

### **BENEFITS OF THE NEW EXPERIMENTAL METHODOLOGY**

The benefits of the new methodology were two-fold. The first was the ability to conduct rapid, multiple test installations, which produced a large data set of test results under controlled, repeatable and measureable conditions. As each test was completed, the end caps containing the sleeve were removed and the completed test specimen - sleeve and resin bolt assembly - were readily removed as a single piece from within the steel outer pipe. A new sleeve was then inserted, the end caps were replaced and a new test was ready to be conducted. Using this method, up to 49 installations were conducted in a day.

The second major benefit was the ability to conduct a comprehensive visual inspection of the resin annulus for each completed test sample. The PVC was cut with an angle-grinder along the length of the bolt. The PVC and resin were cut through to the rebar to facilitate removal of the bolt and resin intact from the sleeve. This method allowed for observation of the degree of resin curing through the entire thickness of the resin annulus within the saw cuts. The remainder of the resin visual examination can be made around 360 degrees of annulus surface and along the full length of the bolt. Areas of poor resin curing were therefore immediately exposed.

## RESULTS - INSTALLATION PRESSURE

The instrumentation used here produced accurate measurements of installation force, bolt displacement and rotation speed. Together with a known bore diameter, these measurements reduce the number of unknown factors that exist when installing a resin-anchored roof bolt in an underground setting.

Table 1 shows that the peak pressure measured in the two previous US studies were higher than those measured in the current study. This could be due to a number of factors, including typically higher resin viscosity used in US resins (Craig, 2012), installation method (i.e. push to back rather than spin during insertion) and the greater hydraulic capacity of the drill rigs in the US studies.

**Table 1 - Resin-anchored roof bolt insertion pressure results from this study and previous studies**

STUDY	Major Bar Diameter	Hole Diameter	Annulus	Insertion Rate	Peak Pressure	Installation Method
Compton and Oyler (2005)	18 mm	27 mm	4.5 mm	127 mm/s	34.5 MPa	Push to back then spin
	21.5 mm	27 mm	2.75 mm	Stalled	N/A	
Giraldo <i>et al.</i> (2006)	21.5 mm	27 mm	2.75 mm	180 mm/s	45 MPa	Push to back then spin
	21.5 mm	27 mm	2.75 mm	115 mm/s	43 MPa	
	21.5 mm	32 mm	5.25 mm	180 mm/s	45 MPa	
	21.5 mm	32 mm	5.25 mm	115 mm/s	33 MPa	
	24 mm	35 mm	6 mm	180 mm/s	34 MPa	
	24 mm	35 mm	6 mm	115 mm/s	24 MPa	
McTyer <i>et al.</i> (2014)	23 mm	28 mm	2.5 mm	145 mm/s	18 MPa	Spin during insertion
	23 mm	30 mm	3.5 mm	170 mm/s	14 MPa	

In this study, the maximum available thrust force of the drill rig was achieved for both 28 mm and 30 mm diameter pipe tests. The average insertion rate was found to be slower during the 28 mm tests, with a slowing rate of insertion being found to coincide with the period over which elevated pressure was recorded. A "dry run" without resin was measured to take approximately 5 seconds to travel 1000 mm (i.e. 200 mm/s). When resin was used, the insertion rate slowed to 170 mm/second for a resin bolt in a 30 mm diameter pipe and to 145 mm/second in a 28 mm diameter pipe (Table 1). These results indicate that the drill rig used was not able to maintain the same insertion rate throughout the full bolt insertion stage, probably because of its limited hydraulic capacity. This finding was not significant to the results but does suggest that higher peak insertion pressures (similar to those found in the US studies) would inevitably be reached with a more powerful drill rig.

For the 28 mm internal diameter pipe samples (Figure 1), an average of 18 MPa of pressure was maintained for a period of approximately 4 seconds. Most importantly, this elevated magnitude of pressure occurred during the final 500 mm of the bolt insertion.

The samples in the larger 30 mm internal diameter pipe (Figure 2) had a lower average pressure of 13 - 14 MPa but were observed to have a fundamentally different trajectory. Specifically, the period of peak pressure was considerably shorter, approximately 0.5 seconds, and was only present during the final 100 mm of bolt insertion.

## RESULTS - RESIN CURING

Observation of resin curing was made along the entire resin encapsulation length. Individual areas of uncured resin were measured and a total recorded along the axial length of the bolt. The total length of uncured resin was recorded for three sections of the bolt. The three sections of bolt were the upper (0 - 300 mm), middle (300 - 800 mm), and lower (800 - 1700 mm). The amount of uncured resin was recorded for both all the way around the bolt circumference and partially around the circumference. Two distinct uncured resin types were observed.

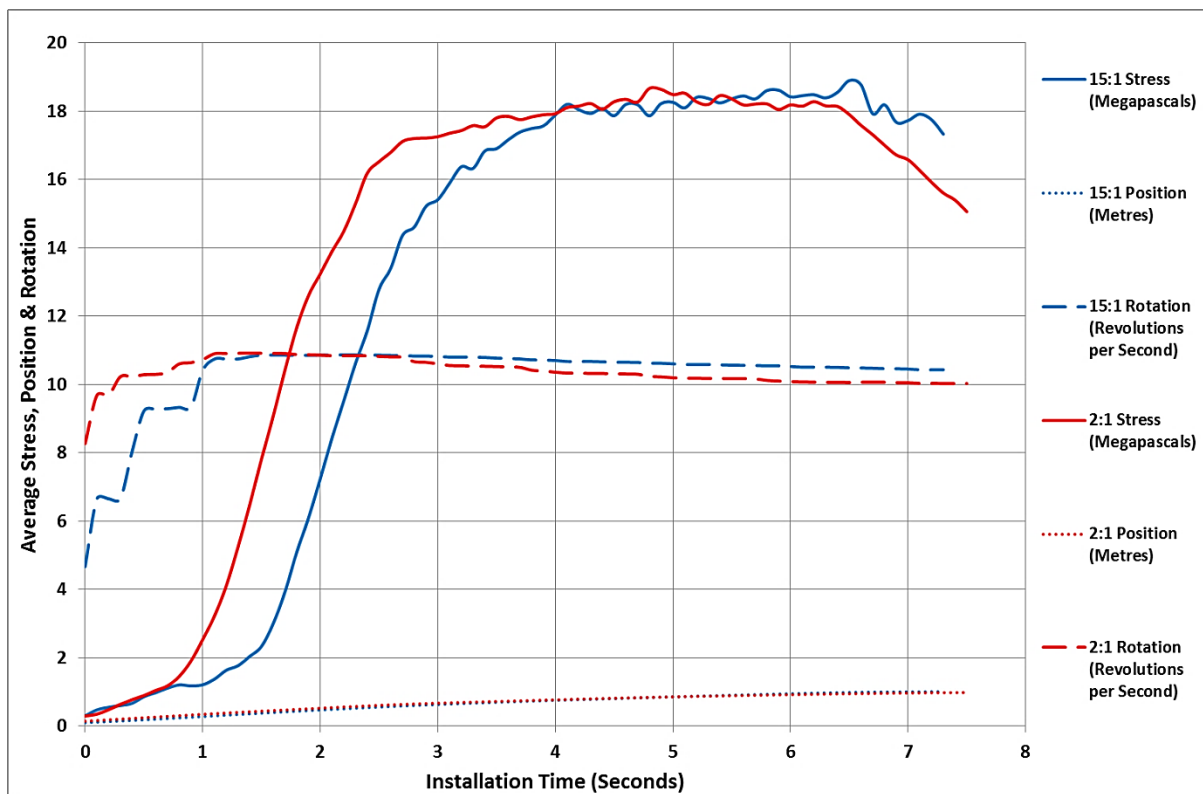


Figure 1 - Stress, position and rotation averages from 28 mm internal diameter pipe installations

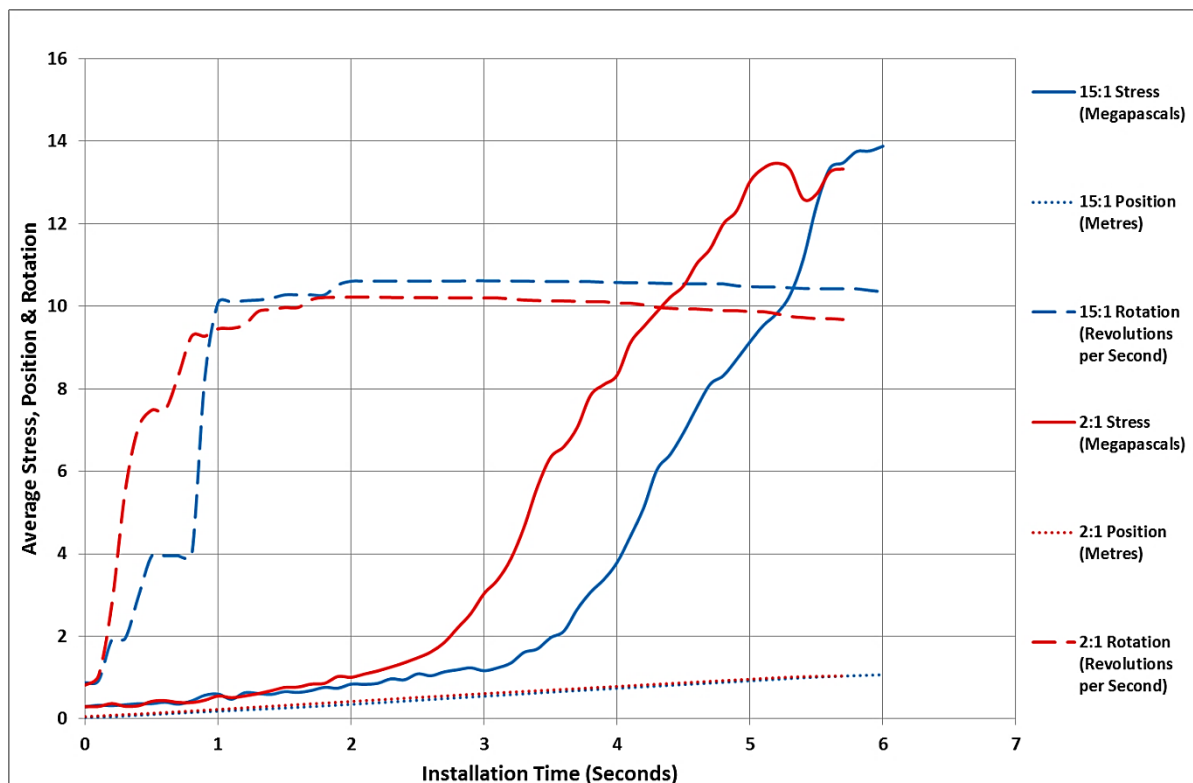


Figure 2 - Stress, position and rotation averages from 30 mm internal diameter pipe installations

The first was wet mastic found throughout the entire thickness of the resin annulus. This appears to occur when the bolt does not pierce the catalyst compartment. There were no examples of this observed in the 2:1 resin. Full-annulus uncured resin was not observed in the 2:1 resin because it is a geometric impossibility for the bolt to not pass through both the mastic and the catalyst compartment during bolt insertion. However, four examples of this type of uncured resin were observed in the 15:1

resin samples (approximately 8% of samples). This may be possible because of the mechanism of radial expansion of the resin cartridge (Campbell and Mould, 2003). This mechanism allows the bolt to reach the back of the hole without piercing the catalyst compartment. The result was typically wet mastic around the full circumference of the bolt (Figure 3).



**Figure 3 - 15:1 resin installed in a 30 mm ID pipe (above) and in a 28 mm ID pipe (below)**

Secondly, uncured resin was observed in the channels cut through the PVC and resin to the rebar. The cuts were made more than 24 hours after bolt installation. Uncured resin was found to flow out from the annulus beneath a hard cured "crust" of resin (Figure 4). While the impact of these uncured sections under a hard crust has not been quantified in terms of load transfer, it is reasonable to assume that load transfer properties would be negatively affected.



**Figure 4 - Resin "flow" into the saw-cut channel of 15:1 resin (above) and 2:1 resin (below)**

Analysis of the results was undertaken on a total of 91 installations: 15:1 resin in 28 mm diameter pipe (n=34); 15:1 resin in 30 mm diameter pipe (n=14); 2:1 resin in 28 mm diameter pipe (n=30); and 2:1 resin in 30 mm pipe (n=13). The data collected was further separated into three categories representing the upper (0-300 mm), middle (300-800 mm), and lower (800-1700 mm) section of the total encapsulation length. The results are reported as the average percentage of uncured resin.

Figure 5 shows the average uncured resin percentage for 2:1 and 15:1 resins measured along the encapsulated length of the bolt for both 28 mm and 30 mm internal diameter pipe installations.

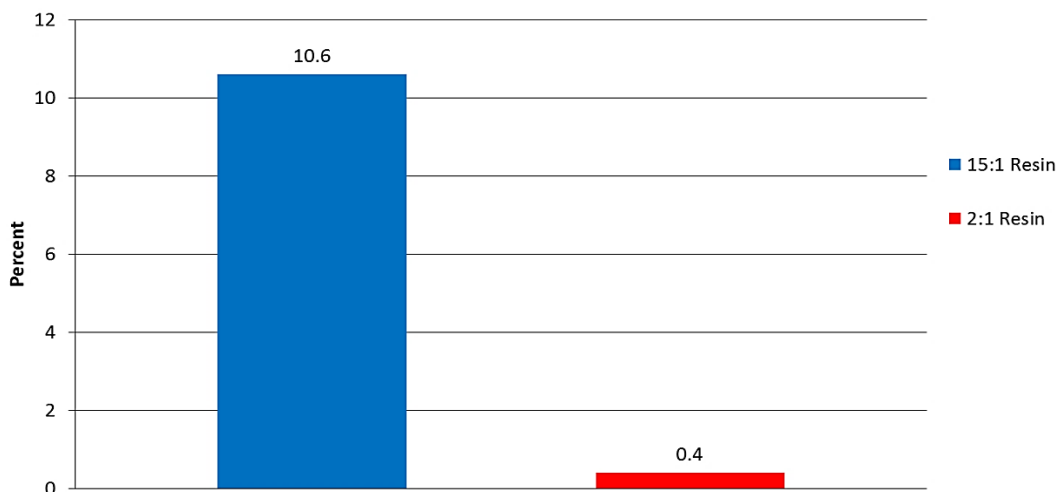


Figure 5 - Average percentage uncured resin observed for 15:1 and 2:1 resins

Figure 6 shows the average uncured resin percent for 2:1 and 15:1 resins measured in the lower, middle and upper sections of the bolt for both 28 mm and 30 mm internal diameter pipe installations. The highest proportion of uncured resin was observed in the upper 300 mm of both resin types. The results show a higher average percentage of uncured resin in the 15:1 resins across the entire length of the resin anchor. The results also show a trend of an increasing proportion of uncured resin toward the upper portion of the bolt.

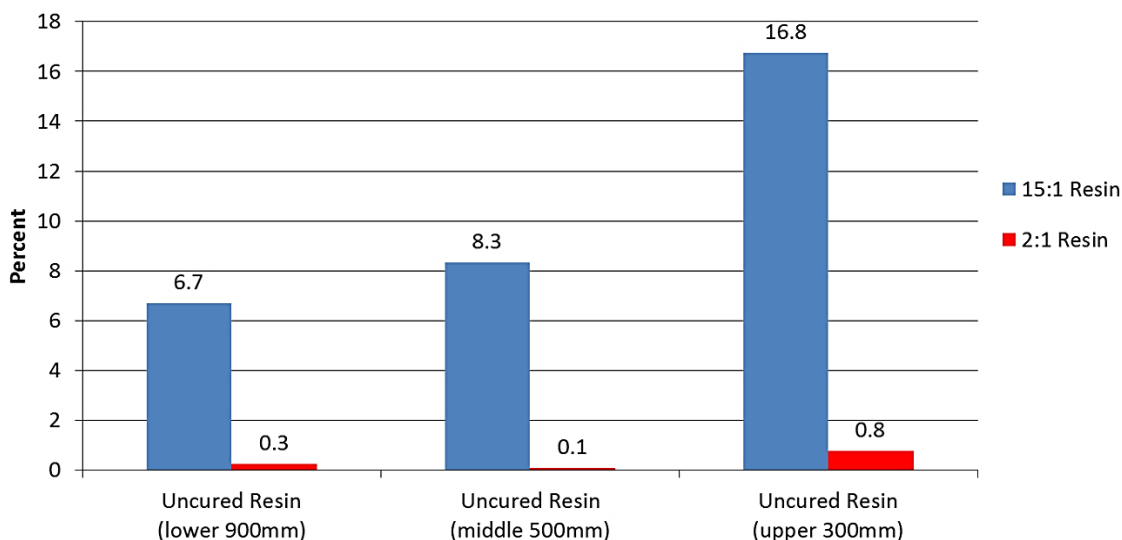
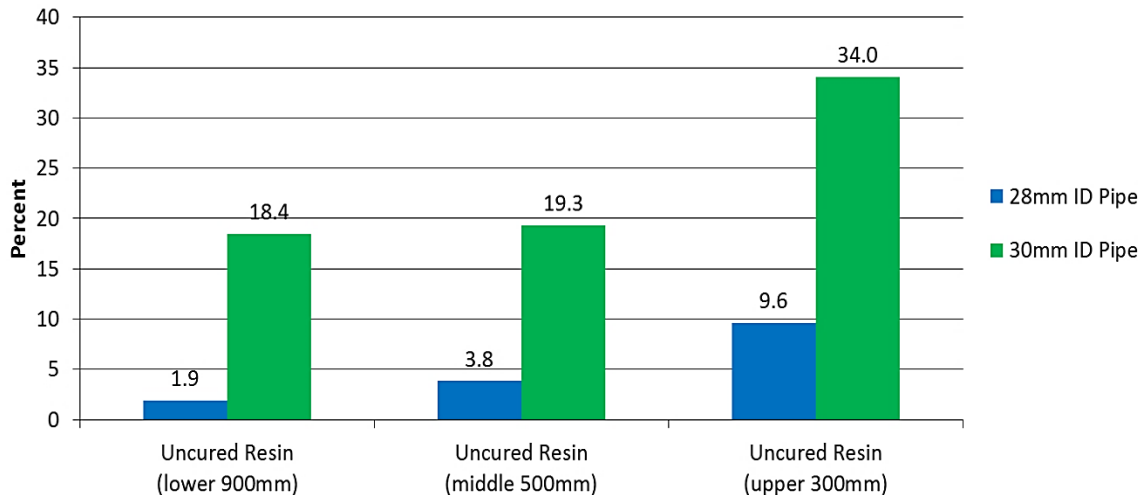


Figure 6 - Average percentage uncured resin observed for 15:1 and 2:1 resins by lower, middle and upper bolt sections

Figure 7 shows the separation of the 15:1 data into 28 mm and 30 mm internal diameter pipe installations. The averages show an increasing percentage of uncured resin toward the upper end of the pipe in both 28 mm and 30 mm pipe. Significant variability was found in the range of uncured resin in the upper 300 mm. The maximum length of uncured resin was 170 mm in 28 mm pipe, and 240 mm

in 30 mm pipe. Uncured resin was observed in 50% of 28 mm pipes, and 86% of 30 mm pipes. This data shows that 15:1 resin systems become increasingly susceptible to uncured resin as the hole diameter was increased.



**Figure 7 - Average percentage uncured resin observed for 15:1 resins by lower, middle and upper bolt sections in 28mm and 30mm ID pipes**

## DISCUSSIONS AND CONCLUSIONS

The surface installation method of borehole sleeving was found to allow reliable, repeatable and standardised testing of resin-anchored bolt installations. A large number of tests was possible during a day of testing and the removal of the PVC sleeve allowed a comprehensive visual inspection of the resin annulus. The method was found to be relatively inexpensive compared with both underground installation trials, and tests using grout-filled pipes.

The primary purpose of the new methodology was to provide a highly visual analysis of resin mixing effects. However, two constraints arose. Firstly, the new methodology could not be used for load transfer assessments – due to the comparatively weak mechanical properties inherent with plastic materials. However, load transfer was not the intended purpose of this experiment.

The second constraint was that of borehole-surface effects during resin mixing. A rougher borehole will naturally enhance fluid shear in resin mixing due to the micro turbulence created by the relative roughness in the borehole surface. The plastic sleeve has a comparatively smooth surface, so theoretically, micro turbulence effects would be reduced at the borehole wall. However, the greater contribution to mixing turbulence was actually from the bolt rib profile, due to the high speed cyclic pumping action generated by rotation of the ribs at approximately 600 rpm. The test results inherently confirmed the substantial contribution of the bolt ribs in generating mixing turbulence. While the plastic sleeve might not be fully representative of borehole roughness underground, the sleeve provided a standardised and repeatable environment for comparative testing.

The implications of high insertion pressure are significant for a mining operation. Results of the current study confirmed that high pressure was developed during resin bolt installation, but was subject to varying resin annulus thickness. The maximum installation pressure was approximately 18 MPa in a 28 mm diameter pipe and was present during the upper 500 mm of the bolt travel. The results also indicate a reduction in the peak pressure to 14 MPa in 30 mm diameter bore, which was only generated during the upper 100 mm of bolt travel. The installation pressure results were very similar for both the 15:1 and 2:1 resin types tested.

The magnitude of pressure in each case would theoretically be sufficient to cause hydraulic fracturing of weak roof types, and to initiate crack development along existing planes of weakness such as bedding planes, coal cleat or rock joints. This finding supports the evidence of hydraulic fracturing and resin injection found in previous studies that used overcoring (Campbell and Mould, 2003; Compton and Oyler, 2005; Craig, 2012).

The implications of hydraulic fracturing are significant and include artificial damage to the roof and increased resin loss. Both Giraldo *et al.*, (2006) and Craig (2012) found that increasing the annulus area resulted in a reduction in resin loss. Although each mine site is subject to individual factors, the results indicate that the potential for hydraulic fracturing and resin loss is reduced by using a larger diameter bore. This is reasonable because the drill hole volume is larger for the same volume of resin. Hence, the onset of elevated pressure is delayed until later in the bolt travel toward the back of the hole. Further, the larger bolt annulus allows the resin to pass along the bolt more readily, this being the effective "relief valve" that limits peak back pressure development.

The use of a larger resin annulus has two potential benefits. Firstly, more resin will remain in the borehole with an associated greater likelihood of achieving theoretical full resin encapsulation. Secondly, a smaller area of the bolted interval will be subject to the potentially negative effects of elevated resin back pressures and associated potential for hydraulic fracturing damage. While the load transfer downside of a larger diameter hole is duly noted, it is offset to a large degree if a substantial portion of the bolt is not encapsulated. This finding provides an incentive for industry to develop a bolting system that combines high load transfer properties with the reduction in pressure inherent in using a slightly larger annulus.

Occurrence of uncured resin were observed on 1.8 m long roof bolts installed with 1000 mm long resin cartridges in both 28 mm and 30 mm diameter bores. The results show that the average percentage of uncured resin along the entire encapsulated length of both 28 mm and 30 mm bores was 10.6% for 15:1 resins, and 0.4% for 2:1 resins. Based on this finding, the use of 2:1 resins could offer a significant improvement in roof bolt effectiveness.

A potential reason for the broad difference in uncured resin percentages was the size of the limestone filler. The 15:1 resin was characterised by smaller limestone fragments than the 2:1 resin. The larger limestone filler in the 2:1 resin was clearly observed to scour the internal surface of the PVC pipe. This scouring was not seen on the inside of the 15:1 resin pipes. It is reasonable to suggest that the larger filler particles cause a greater degree of friction and shearing of the fluid during bolt rotation, contributing to a more uniform resin mix. In combination with the higher proportion of catalyst, the difference in filler may explain the reduced potential for uncured resin observed in the annulus of 2:1 resins.

For both resin types in both bore diameters, the highest percentage of uncured resin was observed in the upper 300 mm of the bolt. The percentage of uncured resin was 16.8% in the 15:1 resin samples, and 0.8% in the 2:1 resin samples. Therefore, the 2:1 resin can be concluded to be a more robust resin anchor with regard to curing in the critical top 300 mm for both 28 mm or 30 mm bore diameters, in the context of this study. This finding has substantial implications for the development and use of roof bolt pre-tensioning. Pre-tensioning is highly reliant on a consistent anchor being generated at the top of the bolt as soon as the fast set resin cures. With a highly reliable anchor at the top of the bolt, the theoretical strata control improvements of increasing roof bolt pre-tension can be investigated with greater confidence.

When the 15:1 resin was assessed by bore diameter, a higher percentage of uncured resin was found in the lower, middle and upper portion of the bolt in the 30 mm diameter bores. Further, it was found that 9.6% of the resin was uncured in the upper 300 mm of 28 mm bores, while 34% of resin was uncured in the upper 300 mm of 30 mm bores. These findings demonstrate the sensitive link between increasing hole diameter and uncured resin for the 15:1 resins. This relationship between borehole size, resin type and installation pressure indicates further investigation is required to optimise roof bolting systems.

It is noted that there is less control available on the actual bolt hole diameter in underground conditions because of factors such as strata conditions and installation variables. Consequently, "run of mine" installations may be subject to higher percentages of uncured resin than the equivalent surface trials performed under controlled test conditions. The results of this study suggest that 2:1 resin cures more reliably over the entire encapsulated length for the two bore diameters assessed.

## REFERENCES

- Giraldo L., Cotton, S. and Farrand J., 2006. Characterisation of internal insertion pressure during installation of fully grouted bolts, *In Proceedings of 25<sup>th</sup> International Conference on Ground Control in Mining, Morgantown, WV*. pp 395-399.  
<http://icqcm.conferenceacademy.com/papers/detail.aspx?subdomain=icqcm and iid=484>

- Campbell R. and Mould R., 2003. Investigation into the extent and mechanism of gloving and un-mixing resin in fully encapsulated roof bolts, *In Proceedings of 22<sup>nd</sup> International Conference on Ground Control in Mining*, Morgantown, WV. pp 256-262.  
<http://icgcm.conferenceacademy.com/papers/detail.aspx?subdomain=ICGCM and iid=632>
- Compton C. and Oylar D., 2005. Investigation of fully grouted roof bolts installed under *in situ* Conditions, *In Proceedings of 24<sup>th</sup> International Conference on Ground Control in Mining*, Morgantown, WV, pp 302-312.  
<http://icgcm.conferenceacademy.com/papers/detail.aspx?subdomain=icgcm and iid=534>.
- Pettibone H., 1987. Avoiding anchorage problems with resin-grouted roof bolts, *Report of Investigations (United States Bureau of Mines) 9129*.
- Craig P., 2012. Addressing resin loss and gloving issues at a mine with coal roof, *In Proceedings of Coal Operators Conference 2012*, Wollongong. pp 120-128. <http://ro.uow.edu.au/coal/399/>.

# THE SIZE EFFECT OF ROCK SAMPLE USED IN ANCHORAGE PERFORMANCE TESTING OF CABLE BOLTS

Matthew Holden and Paul Hagan

**ABSTRACT:** This paper outlines the results of a study into the effect of rock specimen size on the anchorage performance of a hollow strand bulbed cable bolt. As part of the design of a Laboratory Short Encapsulation Pull Test (LSEPT) facility, a question arose as to the appropriate size of the rock sample in which the cable bolt is embedded and whether size might affect the pull out strength of the cable bolt. An analysis of previous research revealed little information regarding the rationale for the sample size used in previous test work. Many of pull out tests in the past had made use of either a rigid encasement such as steel, aluminium, or PVC casing or a biaxial pressure cell to apply a constant stress to model the *in situ* rock mass conditions.

A test arrangement was developed to assess whether there was any appreciable change in anchorage performance with varying diameter of the rock sample. Cable bolts were embedded into the rock sample using a polyester resin grout having diameters of 150 mm, 215 mm, 300 mm and 450 mm with a constant embedment length of 280 mm. A hollow hydraulic ram was used to load the cable bolts to failure.

The results indicate there was a size effect albeit only marginal whereby an increase in the diameter resulted in increased anchorage capacity of the cable bolt.

## INTRODUCTION

Cable bolting is widely utilised in ground support of surface and underground excavations in both mining and civil engineering applications. Since they were first used in the 1970s, a wide variety of cable bolt configurations and geometries have been developed. The performance of cable bolts has been found to be affected by parameters that include:

- borehole diameter;
- embedment length;
- borehole radial confinement conditions;
- cable bolt configurations and geometry; and
- grout type and quality (Hutchinson and Diederichs, 1996).

The failure mechanism of cable bolting systems is complex and a function of loading conditions and the interaction between the cable bolt, grout and rock mass. There are four general mechanisms of cable bolt failure each of which is illustrated in Figure 1.

Failure at the cable-grout interface, indicated as Mode (ii) in Figure 1, is considered the most common failure mechanism identified in the field (Hyett, *et al.*, 1996; Hyett, *et al.*, 1995; Hutchinson and Diederichs, 1996; Rajaie, 1990; Singh, *et al.*, 2001). This usually results from insufficient frictional resistance between the ridges on the cable strands and the grout material. A combination of poor ground conditions and lack of quality control at the time of installation may also affect the bond strengths at the interfaces that in turn can lead to premature failure of the system before the capacity of the cable bolt is actually achieved. Hence a standardised testing methodology should be designed such that failure of the system is more likely to occur at the cable-grout interface (Rajaie, 1990; Hutchinson and Diederichs, 1996).

A comprehensive review of the testing methodologies revealed that while there are a number of testing methods that have the potential to become the standard for pull out tests, there is no standardised or universally accepted suggested method with which to assess the strength of the wide range of cable

bolts that are available to industry. Essentially there are two approaches that have been adopted in the past in the design of a testing facility these being either a constant stiffness system where the material in which the cable bolt is embedded is encased in a steel or other rigid tube or pipe such as the double-embedment test or, a constant load system where the material is placed within a pressurised biaxial cell.

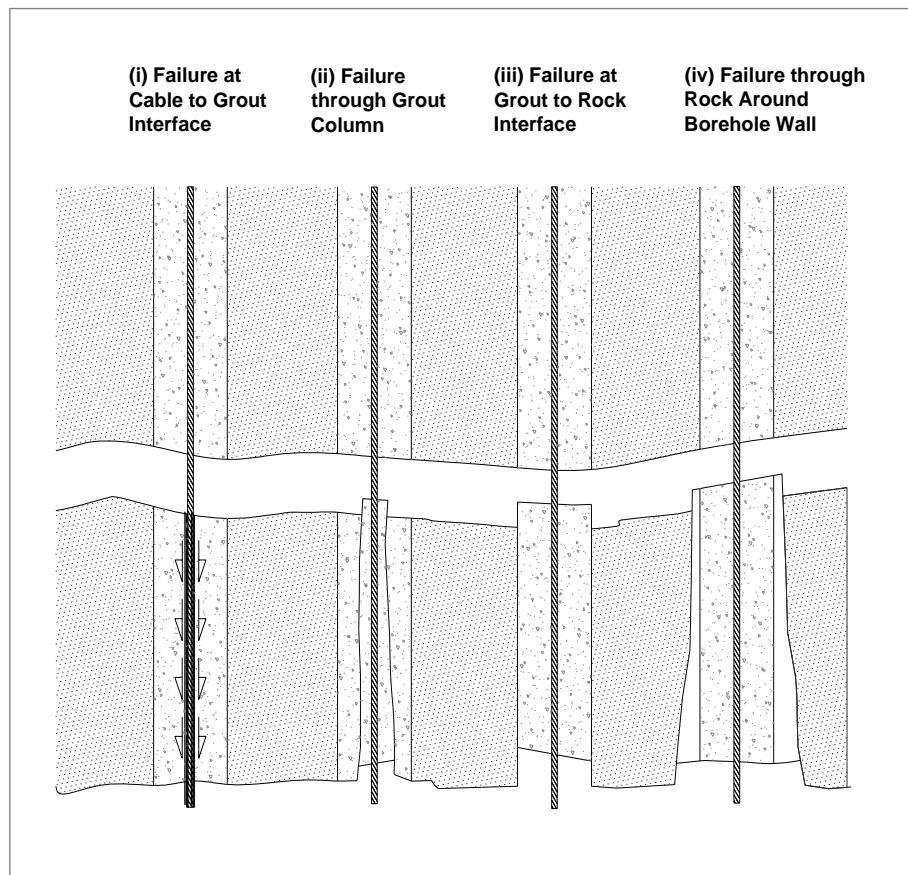


**Figure 1 - Schematic illustration of the four modes of load transfer related failure in cable bolts (Thomas, 2012)**

Following a recent analysis of various pull out testing arrangements it was concluded the Laboratory Short Encapsulation Pull Test (LSEPT) as developed by Clifford *et al.* (2001) and reported by Thomas (2012) is the most appropriate method to test the extensive range of cable bolts available. One of the key advantages of the LSEPT is that one end of the cable bolt is embedded in a cylinder of material as can be seen in Figure 2. In other tests the cable bolt is embedded in a rigid or semi-rigid casing such as a steel tube in the double embedment test which acts to constrain any lateral dilation. On axial loading, cable bolts activate some level of lateral dilation stress in a rock mass as part of the load transfer process which can influence the magnitude and distribution of stress within the rock mass. The level of this dilation varies with the different cable bolt designs. There is little published information however about the size effects of the material cylinder at the cable bolt/grout, grout/rock and rock containment interfaces during testing and consequently on the load/deformation characteristics and ultimate load achieved by the cable bolt. Hence in developing a standard test method it is important to determine the minimum size of cylindrical block that will not affect the anchorage performance of a cable bolt.

A study by Rajaie (1990) reported a link between the anchorage strength of a cable bolt and the diameter of the rock sample surrounding the grouted cable bolt. It was found that there was little change in load carrying capacity of the cable bolt with a specimen diameter in excess of 250 mm as can be seen Figure 3. This study however only involved a plain strand cable bolt that was in common use at that time. It therefore needs to be confirmed whether the same limit applies to the modified cable bolts now available such as bulbed and birdcage bolts. The newer type cable bolts are likely to induce higher lateral stresses during failure requiring a larger rock mass to deal with the dilation generated by the bolt.

In the design of a standardised pull-out test, the diameter of the rock specimen should be such as to withstand the range of stresses generated by the range of modified geometry cable bolt designs. This diameter should remain within practical limits to enable ease in logistics and sourcing such a rock sample, as well as, for compatibility with testing equipment.

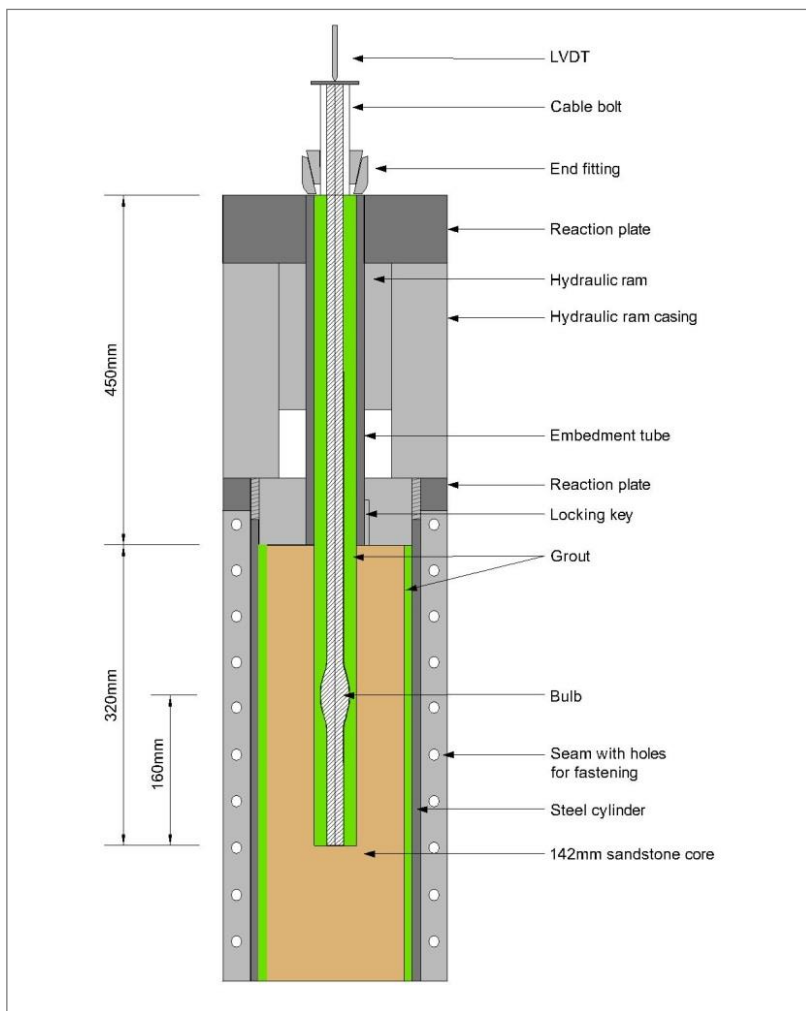


Figure 2 - Modified version of the laboratory short encapsulation pull test incorporating a steel cylinder (Thomas, 2012)

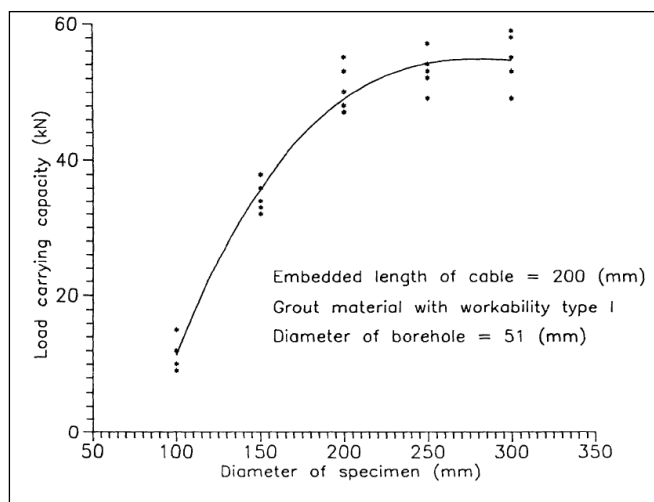
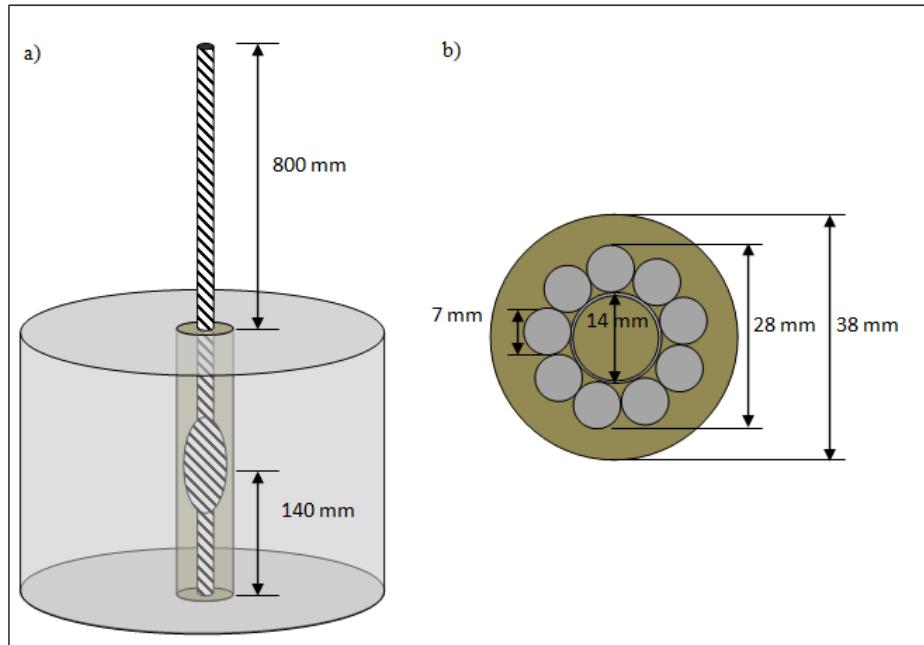


Figure 3 - Load carrying capacity for different external diameter sample (Rajaie, 1990)

## EXPERIMENTAL PROCEDURE

### Test specimen preparation

A total of 16 artificial rock cylinders were prepared, each 300 mm in length and having diameters of 150 mm, 215 mm, 300 mm and 450 mm. A 35 mm TG bolt was embedded in a 38 mm diameter hole with the centre of the bulb located close to the midpoint of the cylinder, at a constant distance of 140 mm from the cylinder end as shown in Figure 4.



**Figure 4 - a) Schematic of cable bolt installation technique; b) Cross-section of resin column and cable bolt**

Each test specimen was formed using the following four step process:

*Step 1* - Rock samples were cast in moulds made from thick-walled cardboard cylinders of the desired diameter size: 150 mm, 215 mm, 300 mm and 450 mm. Water was added to super strength grout and mixed to a water to cement ratio of 0.3 and then poured into the moulds to a height of approximately 300 mm. Vibration of the samples occurred post-pouring to remove excess air bubbles entrained in the grout during the mixing process, to create a stronger homogeneous material. The cardboard cylinders were lined with casting oil prior to pouring the grout mixture to minimise water seepage that could create shrinkage cracking along the sides of the sample. The oil also allowed for ease in removing the rock cylinders from the mould after curing.

*Step 2* - The samples were left to cure for two weeks. Boreholes were then drilled with a diamond core drill to create a 38 mm hole, in accordance with the manufacturer's specification (Jennmar, 2010). This produced relatively smooth side walls compared with field drilling techniques which create hole rifling and roughened walls. Ideally the boreholes should be drilled using a twin wing or finger bit creating a hole rifling effect. Attempts were made post drilling to mimic hole rifling conditions and roughen the wall surface of one of the 300 mm diameter samples, however no consistent method of creating such conditions was achieved. As a result, all the holes were left untreated for the pull out tests.

*Step 3* - The cable bolts were grouted into each rock cylinder using a slow set resin with a setting time of 20 to 25 minutes. The resin and oil based catalyst were mixed for 13 minutes. An electric mixer was employed to combine the two components to ensure a thorough and even distribution of catalyst throughout the resin, which is imperative for the ultimate strength of the cured resin. The mixed resin was poured into the boreholes to a height 50 mm below the top of the borehole. This allowed room for displacement of the resin after the cable bolt was installed into the borehole. Excess resin spilled out around the rim of the borehole.

*Step 4* - Immediately following pouring of the resin into the hole, the cable bolt was spun, by hand, into the borehole to ensure complete encapsulation of the bolt, and particularly to infuse the bulb and hollow strand with resin. To ensure centrality of the bolt in the borehole and to maintain a constant embedment length of 280 mm, with the bulb located 140 mm from the top of the borehole, a simple frame was attached to the bolt using L-shaped brackets. Later examination of the samples showed the low viscosity of the resin enabled it to penetrate inside the bulb of the cable bolt as well as the central hollow strand. A cross-sectional schematic of the 5 mm thick resin annulus surrounding the bolt can be seen in Figure 4b. The final specimen with embedded cable bolt can be seen in Figure 4a, with the free end of the cable bolt extending 800 mm from the face of the rock cylinder to enable sufficient length to be secured by the loading machine.

### Pull out test arrangement

The cable bolt in each cylindrical sample was axially loaded to failure to determine the failure characteristics and anchorage capacity. The equipment arrangement used in each test is shown in Figure 5.

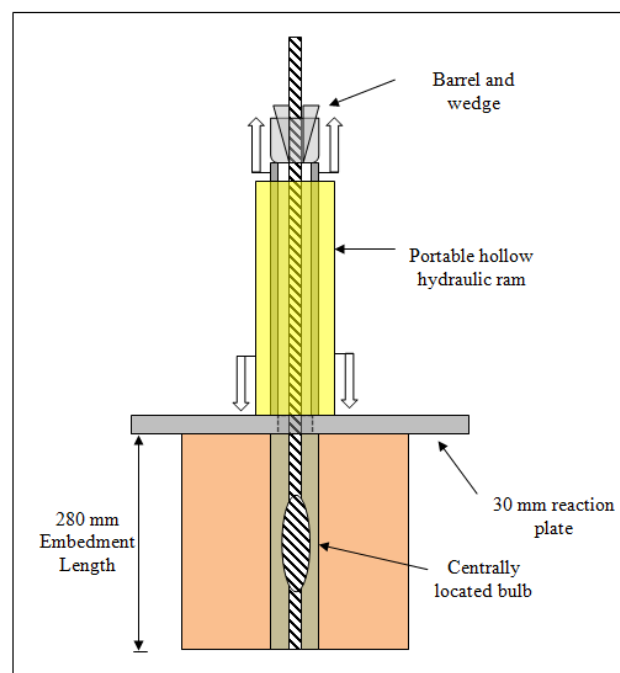


**Figure 5 - Schematic of pull testing arrangement using hydraulic cylinder**

The test arrangement employed a 600 kN capacity RCH606 hollow hydraulic cylinder to load the cable bolt specimen. One end of the cylinder acted against a barrel and wedge attached to the free end of the cable bolt while the other end reacted against a plate placed on top of the cylindrical sample as shown in Figure 5.

This loading arrangement is similar to the setup designed by Ito *et al.* (2001). The displacement of the cable bolts under load was measured using a Linear Variable Differential Transformer (LVDT) attached to the outer casing of the hydraulic cylinder, while the axial load was measured using a pressure transducer attached to the hydraulic pump.

## EXPERIMENTAL RESULTS

Results from the pull out tests are summarised in Table 1 showing the maximum load recorded for each cylinder diameter.

The results fall into one of two categories of failure:

- Type 1 failure that occurs at the grout/rock interface; and
- Type 2 failure that occurs at the bolt/grout interface.

The majority of the samples failed at the grout/rock interface with only three specimens failing at the cable bolt/grout interface as indicated in Table 1. Also identified in the table is one 300 mm sample which had a roughened borehole wall as a result of rifling the borehole post-coring.

The 13 specimens that failed at the rock-grout boundary showed detachment between the grout column and the borehole walls, which was clearly visible during later examination of the test samples. Despite this debonding between the resin column and the cylindrical sample, high loads were attained before failure occurred.

**Table 1 - Summary of pull out loads for TG bolts embedded in cylindrical block samples (All samples failed at grout/rock interface unless otherwise indicated)**

Cylinder diameter (mm)	Peak Load (kN)					mean $\pm$ s.d.
	Test Number					
	1	2	3	4		
150	55	-	107*	109*	90.3 $\pm$ 30.6	
215	45	116	56	46	65.8 $\pm$ 33.9	
300	61	58	125**	86	82.5 $\pm$ 31.0	
450	61	131	142*	165	124.8 $\pm$ 44.8	

\* Sample failed along the bolt/grout interface; \*\* Roughened borehole wall

Figure 6 shows a graph of the ultimate pull out load against rock cylinder diameter. Over the range of diameters examined there is an increasing relationship in the load capacity of the cable bolts with diameter. This would suggest that the range of diameters tested was not sufficient for a limiting relationship to become apparent.

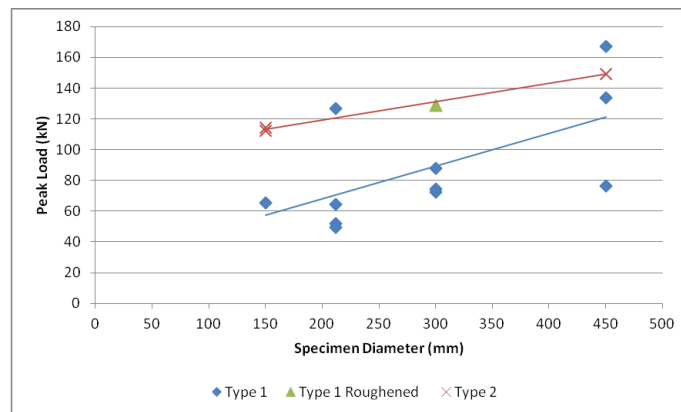


**Figure 6 - Variation in peak load with cylinder diameter**

### INTERPRETATION OF EXPERIMENTAL RESULTS

Initial interpretation of the results from the pull out tests suggests the forces were within the predicted loading range and the load versus displacement relationships were consistent with previous pull out test results (Thomas, 2012; Rajaie, 1990; Hyett, *et al.*, 1996). Subsequent analysis of the measured results together with observational evidence indicates there may have been other contributing factors. Inspection of the relatively intact resin-grout column and smooth borehole walls of the 13 samples that failed at the rock/grout interface suggest these samples should have failed at lower loads.

However, this was not the case as the measured loads were markedly higher for the larger diameter samples which reached loads in excess of 150 kN when compared to 60 kN with the smaller diameters. If bolt/grout failure had occurred as opposed to the weaker rock-grout failure, this relationship would have been valid.

The radial tension cracking that developed in all of the samples suggest there is some form of dilation in the system, stressing the sidewalls of the borehole, examples of which can be seen in Figure 7. This seems to contradict the lack of evidence for dilation, with the relatively smooth condition of the borehole, the intact resin column and minimal cable bolt displacement suggesting otherwise. All this suggests that

the shear forces at the artificial rock-grout interface could not have generated the level of stresses necessary to fracture the samples.



**Figure 7 - Evidence of radial tension cracking across all rock cylinder diameters**

Further analysis of these findings revealed two possible mechanisms that might be responsible for the inconsistency between the observed peak failure loads as well as the apparent contradiction of observed radial tension cracking and the lack of evidence for radial dilation:

1. The resin-grout column slowly failed along the smooth rock-grout interface, requiring relatively low loads to overcome shear resistance along this boundary. However, the grout column's movement is constrained by the small size of hole in the steel reaction or bearing plate placed between the top of the cylinder and hydraulic ram, this being smaller than the diameter of the borehole.

This resulted in the grout being compressed causing dilation of the grout due to the Poisson effect and thereby increasing the radial stress in the surrounding rock. This caused the sample to fail in a manner similar to the pull out tests revealed in previous research through radial tension cracking (Rajaie, 1990; Ito, *et al.*, 2001). A schematic of arrangement is illustrated in Figure 8.

2. The resin grout column failed in a similar manner described in 1) however the induced stresses in the surrounding rock are generated by moment forces being transferred through the grout column.

Eccentric loading conditions at the point of contact between the hole in the steel plate and the grout annulus are generated by slight misalignment of the resin column and the hole.

This results in moment forces acting on the borehole walls as the grout column pivots around the steel plate contact point on the edge of the hole. This is illustrated in Figure 9.

## CONCLUSIONS

The single embedment length unconstrained pull out tests found a slight increase in cable bolt anchorage capacity with size of the cylindrical block sample containing the cable bolt.

In three tests where there was failure at the cable bolt/grout interface, which included two 150 mm diameter specimens and one 450 mm sample, anchorage capacity of the cable bolt increased with diameter of the cylinder used in the tests. The peak load achieved with the two smaller diameter cylinders was approximately 110 kN while the larger cylinder achieved a peak load of 140 kN.

Of the remaining tests, 13 samples failed along the rock/grout interface. It is unlikely that the failure mechanisms in this instance is representative of the expected *in situ* failure conditions due in part to the

relatively smooth surface of the borehole and confinement of the grout caused by the steel loading plate during loading.

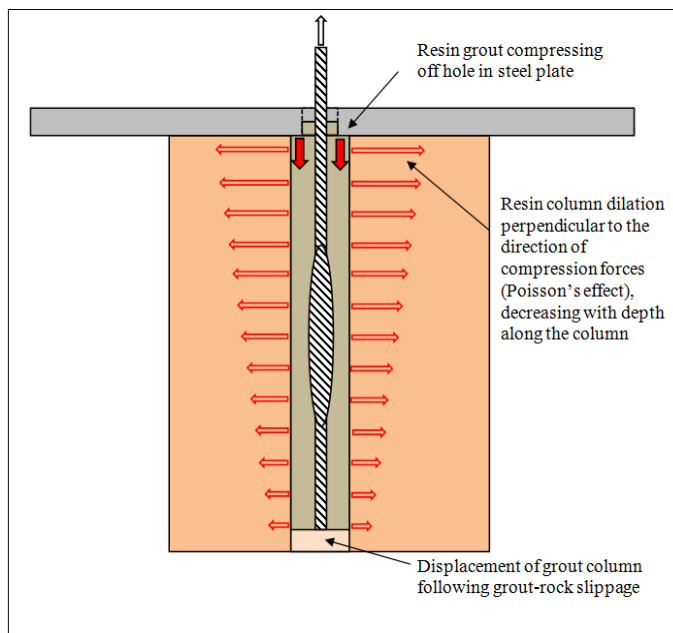


Figure 8 - Schematic of resin column dilation inducing sample failure

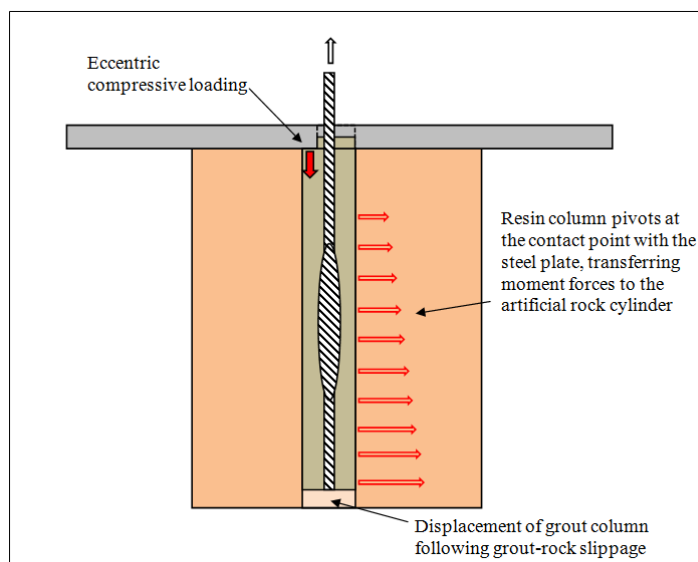


Figure 9 - Schematic of eccentric loading failure mechanism

**ACKNOWLEDGEMENTS**

The authors would like to thank Peter Craig and Jenmar for supplying the cable bolts tested in the investigation and providing much valued consultation, Lynda Laidler and JLoK for supplying the slow set polyester resin and Kanchana Gamage for his assistance in the laboratory.

**REFERENCES**

Clifford, B, Kent, L, Altounyan, P and Bigby, D, 2001. Systems used in coal mining development in long tendon reinforcement, in *Proceedings 20th International Conference on Ground Control in Mining*, 7-9 August, Morgantown, USA.

- 
- Hutchinson, D J and Diederichs, M S, 1996. *Cablebolting in Underground Mines*, Richmond, Canada, (BiTech Publishers).
- Hyett, A J, Bawden, W F, Macsporrán, G R and Moosavi, M, 1995. A constitutive law for bond failure of fully-grouted cable bolts using a modified Hoek cell, *International Journal of Rock Mechanics and Mining Sciences and Geomechanics Abstracts*, 32(1):11-36.
- Hyett, A J, Moosavi, M and Bawden, W F, 1996. Load distribution along fully grouted bolts, with emphasis on cable bolt reinforcement, *International Journal for Numerical and Analytical Methods in Geomechanics*, 20(7):517-544.
- Ito, F, Nakahara, F, Kawano, R, Kang, S and Obara, Y, 2001. Visualization of failure in a pull-out test of cable bolts using x-ray CT, *Construction and Building Materials*, 15(5–6):263-270.
- Jennmar, 2010, TG bolt features, Jennmar [online]. Available from: <<http://www.jennmar.com.au/>> [Accessed: 12 September 2013].
- Rajaie, H, 1990. Experimental and numerical investigations of cable bolt support systems, PhD thesis, Montreal, Canada, McGill University.
- Singh, R, Mandal, P K, Singh, A K and Singh, T N, 2001. Cable-bolting-based semi-mechanised depillaring of a thick coal seam, *International Journal of Rock Mechanics and Mining Sciences*, 38(2):245-257.
- Thomas, R, 2012. The load transfer properties of post-groutable cable bolts used in the Australian coal industry, in *Proceedings 31st International Conference on Ground Control in Mining*, 12 July, Morgantown, USA.

# THE LOAD TRANSFER MECHANISM OF FULLY GROUTED CABLE BOLTS UNDER LABORATORY TESTS

Paul Hagan, Jianhang Chen and Serkan Saydam

**ABSTRACT:** The load transfer mechanism of fully grouted cable bolts plays an important role in the performance of cable reinforcement systems. In order to better understand this behaviour, researchers have utilised a number of approaches including theoretical analysis, laboratory tests and numerical simulation. However, laboratory experiments are more often used because it offers a more direct and relatively accurate way to understand the physical and mechanical behaviour of cable bolts. This paper outlines the major developments and evolution in understanding the load transfer mechanism of fully grouted cable bolts under axial loading conditions through laboratory testing. The advantages and some of the shortcomings arising from previous tests are also presented. The major influencing factors that have been studied include embedment length, cable surface geometry and confinement of surrounding rock. A number of theoretical equations have been proposed based on these experiments. In conclusion, a roadmap for future research has been outlined that is necessary to better understand and improve the performance of cable bolts in stabilising underground excavations.

## INTRODUCTION

A cable bolt is a flexible tendon consisting of a quantity of wound wires that are grouted in boreholes at certain spacings in order to provide ground reinforcement of excavations (Hutchinson and Diederichs, 1996). They were first introduced into the mining industry in the 1960s (Thorne and Muller, 1964) and since the early 1970s have been used in both hard rock and coal mining operations. Over time, cable bolts have become the dominant form of ground support particularly in highly stressed ground conditions.

Originally, cables were only used as a temporary reinforcement element. This was due to the fact that many earlier cables were made from discarded steel ropes which had very poor load transfer properties as a consequence of their smooth surface profile. Over subsequent years a number of modifications have been made to the basic plain strand cable such as buttoned strand (Schmuck, 1979), double plane strand (Matthews, *et al.*, 1983), epoxy-coated strand (Dorsten, *et al.*, 1984), Fiberglass Cable Bolt (FCB) (Mah, 1990), birdcaged strand (Hutchins, *et al.*, 1990), bulbed strand (Garford, 1990), and nutcaged strand cable bolts (Hyett and Bawden, 1993). These changes to the cable surface geometry have been undertaken in an effort to improve the load transfer efficiency and anchorage capacity that has resulting in the more widespread use of cable bolts for permanent reinforcement.

Despite these development in design, failure of cable reinforcement systems still occur. Rupture of the cable strands rarely occurs as it requires the shear resistance between the cable strand and the grouted surface of the strand being larger than the cable's maximum tensile capacity (Mitri and Rajaie, 1992). Potvin *et al.* (1989) stated that it is more likely for a cable bolt to fail at either of the cable/grout or grout/rock interfaces but more likely the cable/grout interface which is a function of the load transfer between the cable bolt and rock mass.

In order to evaluate load transfer efficiency, both peak shear stress capacity and system stiffness need to be determined. Although values for these can be estimated, most researchers tend to use the load versus displacement curves obtained from laboratory tests to study and compare the load transfer characteristics of cable bolts. More recently Thomas (2012) proposed the Load Transfer Index to evaluate the cable load transfer efficiency.

Hartman and Hebblewhite (2003) stated there are three sets of factors that have an impact on the cable load transfer, including the reinforcing element, rock mass and loading conditions. The following sections outline results of the effect of relevant parameters on cable load transfer together with the evolution in design of testing facilities showing the development in understanding the load transfer mechanism of cable bolts with respect to axial loading.

## LOAD TRANSFER BEHAVIOUR OF CABLE BOLTS UNDER AXIAL LOADING

### “Split-pull/push” tests

The earliest “split-pull” testing equipment as shown in Figure 1 was designed by Fuller and Cox (1975) and used in a study of the load transfer mechanism of cable bolts. In this design, steel split pipes were used to represent the rock mass and provide confinement to the grouting material surrounding the cable bolt. Within this facility, although the rotating behaviour of cables was constrained, the steel tube provided a level of confinement that was markedly different from that of a rock mass as evident by the stress-strain relationship. The consequence of this was very high peak loads being achieved, much greater than was achieved in field measurements.

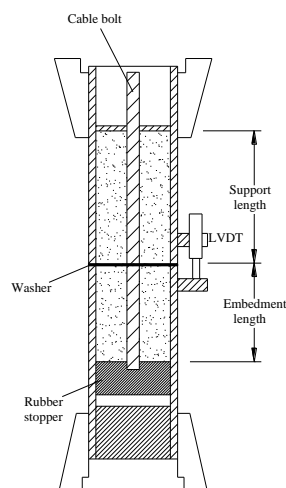


Figure 1 - Split-pulling rig (after Fuller and Cox, 1975)

The facility was used to evaluate the effect of surface geometry on the performance of cables and they found the shape and conditions of the cable had a critical impact on the load transfer. Any protrusion such as surface rust on the wire strands improved the load transfer whereby the location of each protrusion would influence the characteristic of the residual load but it had little impact on the peak load. Following that, the effect of wire indentations on the performance of cables was reported by Cox and Fuller (1977). They found that the indentations have a positive effect on load transfer for mill-finished wires. However, for rusted wires, indentations reduced the effective rusted surface area and thereby the change in load transfer capacity. Thus, it was suggested, the wire surface should be slightly rusted and non-indented. They also showed that high grout strength had a positive impact on load transfer.

Goris and Conway (1987) went on to use a similar test rig design to investigate the impact of epoxy coating, showing that epoxy-coated cables had a larger bearing capacity compared with conventional cables. In addition with respect to the position of steel buttons along the cable bolt in a grout column they found that an increase in the distance between the button and joint significantly enhanced the performance of the cable bolts. Finally the impact of birdcage node location with respect to rock fractures was investigated. Here if the node was located at the pipe discontinuity, the bearing capacity of cables was nearly 31% higher than that of strands in which the anti-node was located at the discontinuity, indicating the birdcage node if located near a rock joint would degrade, the load transfer efficiency. However, this effect is only suitable for single birdcage cables whereas double birdcage cables were less sensitive to the location of nodes or antinodes with respect to rock joints (Goris, 1991). Comprehensive experiments were carried out by Goris (1990) to investigate the axial performance of cable bolts. The ultimate bearing capacity of plain cables improved linearly with embedment length from 203.2 to 812.8 mm. The bearing capacity was also found to increase with the presence of two wound cables, high curing temperatures, low water-cement ratios and sand-cement grouts. Furthermore the load transfer of cables was not influenced by breather tube size and the existence of a breather tube so long as the breather tube was fully filled with grout.

Strata Control (1990) paid particular attention to the effect of bulb density of twin strand Garford bulb cables. A linear relation was found between the cable bearing capacity and bulb density with bulb density frequency ranging from 3.9 to 6 bulbs per strand per metre, indicating load transfer increased with the bulb frequency and number.

Although the "split-pull" test provided much useful information on the different kinds of cable bolts, the design was defective in the extra confinement created near the pulling threads given by the the screw gripping assembly that tended to over-estimate the measured pull-out load. In order to overcome this issue, Reichert (1991) designed the "split-push" test, which was a modification of the traditional pulling test. In this arrangement, the grout column and pipe were pushed off from the cable as indicated on the right in Figure 2, rather than being 'pulled' as in the conventional sense shown on the left.

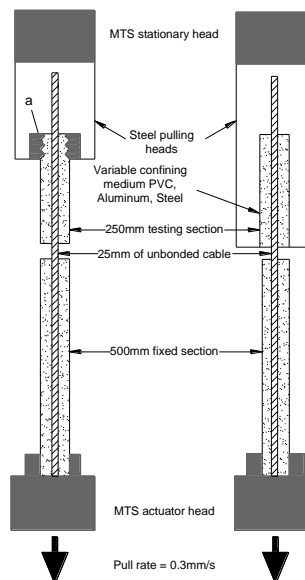


**Figure 2 - Comparison of conventional and modified test (after Reichert, *et al.*, 1992)**

Using this test arrangement aluminium, PVC and steel pipes were used to model the effect of different radial confinements or stiffness. It was reported that larger capacities were achieved with higher radial confinement. Also bearing capacity of cables increased with embedment length though not in direct proportion. Finally, cable capacity increased by 50% to 75% when using stiffer grouts having low water-cement ratios of less than 0.40.

With this "split-push" test equipment, Hyett and Bawden conducted tests on various kinds of modified cable bolts. In 1993, the impact of nutcase geometry was evaluated and they found that the nutcase cables were less sensitive to high water to cement ratios and lower confinement. As for the nutcase size the larger the nutcase, the larger the nutcase cable stiffness (Hyett and Bawden, 1993). In later follow-up work 1994, they also studied the impact of low radial confinement and low water: cement ratio on 25 mm Garford bulb cables. In this case, radial confining pressure had little impact on the load transfer capacity of this cable. As for the effect of water to cement ratio, it was found that the load carrying capacity remained largely unchanged even at a high water to cement ratio of 0.5 (Hyett and Bawden, 1994).

Further improvements to the design were made by Macsporrán (1993) when he pointed out that previous research on the performance of cable bolts was based on constant normal stiffness conditions. This was as a consequence of the use of metal pipes, concrete blocks or actual rock to provide confinement to the cable. However, load transfer under constant normal pressure conditions had not been studied. To this end he incorporated a Modified Hoek Cell (MHC) to apply constant radial pressure as shown in Figure 3.

The MHC was integrated into the "split-push" testing rig. Using this design, the effect of confining pressure and water to cement ratio on cable performance was studied. A direct link was reported between the carrying capacity of the cable bolt and confining pressure whereby carrying capacity increased with confinement. As for the impact of water to cement ratio, a low ratio resulted in larger bond capacity.

### Single embedment pull test

Stillborg (1984) had taken a different approach using concrete blocks to represent the rock mass and provide confinement to the cable bolt, carrying out both short and long single embedment length pull-out tests. This approach has several advantages, firstly concrete blocks more closely model the properties of a rock mass compared to metal tubes. Furthermore, both the borehole roughness and radial stiffness of concrete blocks better simulate that of boreholes within a rock mass. It was found that bearing capacity of the cable was not directly related to embedment length. Also the surface properties of the cable bolt, curing conditions and grout type all influenced load transfer to a large extent. But the design had the disadvantage in that a length of cable was left free which allowed rotation or unravelling of the cable bolt under load.

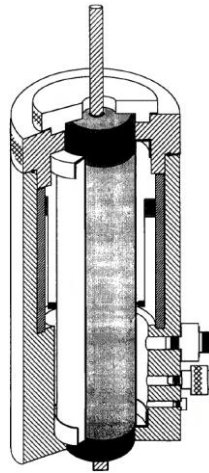


**Figure 3 - Cutaway section of a modified Hoek cell (after Macsporrán, 1993)**

Farah and Aref (1986) used a similar method to study axial behaviour of cables using a fast loading rate to simulate dynamic loading environments. They compared the effects of a mortar mix of sand, water and cement as the grout material against a concrete mix of mortar plus an aggregate. They found the cable bolts grouted with concrete had a larger ultimate bonding strength and ductility as well as higher load at bonding failure compared to mortar-based grouts. These being desirable properties in dynamic loading environments.

Hassani and Rajaie (1990) conducted tests to study the effect of shotcrete as aggregate on load transfer of cables, finding that when using grouts having shotcrete, the peak strength of cables was larger than that of cables with traditional grout materials. Furthermore, large residual bonding strength could be attained. However, the bearing capacity and bonding stiffness decreased.

Mah (1990) just used Schedule 80 pipe to confine the grouted FCB strand and conducted tests to understand the performance of FCB used in hard rock mines. After the experiment, the author indicated that three parameters including hand-mix time, embedment length as well as water to cement ratio were the most important for FCB performance.

Similar single embedment tests were reported by Hassani *et al.* (1992). In their research, PVC and steel pipes were used to represent rock mass with different stiffness. They found that rock mass with larger stiffness tended to generate more confinement, enhancing the cable load transfer capacity.

Benmokrane *et al.* (1992) used a concrete cylinder having a diameter of 200 mm to represent the rock mass and conducted tests on two kinds of reinforcing tendons including a seven-wire cable and a deformed bar, which is shown in Figure 4.

They studied the effect of grout type on bond stress-slip relationship, using six kinds of grouts. It was found that there was a difference in the load transfer mechanism between the steel bars and cable bolts, which was later verified by Ito *et al.* (2001). Further work by Benmokrane *et al.* (1995), based on a theoretical analysis approach, developed a model for the behaviour of the rock tendons the results of which are shown in Figure 5.

This model is tri-linear in nature and can be represented by Equation 1:

$$\tau = ms + n \tag{1}$$

Where,

$\tau$ : shear stress on the tendon-grout interface;

$s$ : slip between the tendon and grouts;

The coefficients of  $m$  and  $n$  for three phases in the bond stress vs. slip curve were depicted as:

In the case when  $0 \leq s \leq s_1$

$$m = m_1 = \frac{\tau_1}{s_1} \text{ and } n = 0 \tag{2}$$

When  $s_1 \leq s \leq s_2$

$$m = m_2 = \frac{\tau_1 - \tau_2}{s_1 - s_2} \text{ and } n = \frac{\tau_2 s_1 - \tau_1 s_2}{s_1 - s_2} \tag{3}$$

Finally when  $s_2 \leq s$

$$m = 0 \text{ and } n = \tau_2 \tag{4}$$

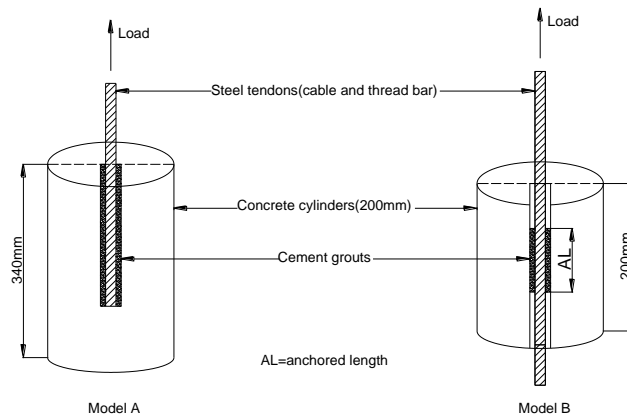


Figure 4 - Concrete cylinders reinforced with two different tendons (after Benmokrane, et al., 1992)

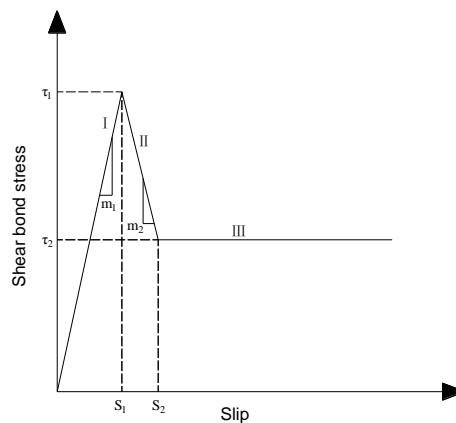


Figure 5 - Tri-linear bond stress-slippage model (after Benmokrane, et al., 1995)

During the first phase of loading (indicated as I in Figure 5), there is a linear relation between the bonding stress and slip. Immediately following the ultimate load (II), debonding takes place resulting in a reduction in stress. In the third and final phase (III) some level of residual stress was achieved due to interface friction.

Thompson and Windsor (1995) studied the impact of pretension on load transfer in an axial direction, finding that pretension did not seem to improve load transfer performance. This finding was later confirmed by Mirabile *et al.* (2010).

Martin *et al.* (1996) carried out tests using resin-grouted cable bolts to study the effect of surface buttons on load transfer. It was found that those cables that had buttons had a much greater stiffness. The effect of borehole size on Garford bulb cables was also evaluated. When the borehole diameter was within the range of 25.4 to 35 mm, there was little change in load transfer efficiency. However when testing from 42 to 106 mm there was a degradation in performance. Similar findings were reported by Mosse-Robinson and Sharrock (2010) who found that smaller borehole diameter resulted in larger load transfer capacity for bulb cables.

Hyett and Bawden (1996) conducted 75 pull-out tests to study the effect of bulb spacing on performance of Garford bulb cables. According to their research, at shorter bulb spacing and longer embedment length as well as higher radial stiffness of the confining medium, axial load increased as did bond stiffness, which is illustrated in the graph in Figure 6.

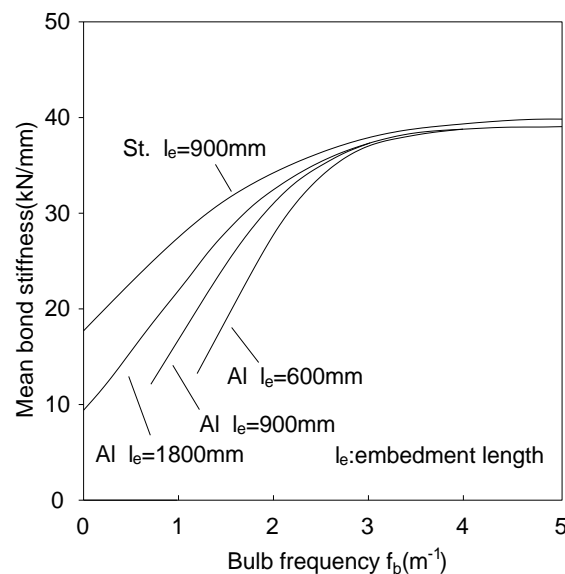


**Figure 6 - Effect of bulb spacing on bonding stiffness (after Hyett and Bawden, 1996)**

The effect of stress change on axial performance of plain and bulb cables in hard and soft rock mass was studied by Prasad (1997). He reported that the load transfer capacity of the plain cables in weaker rock was found to be more sensitive to both isotropic and anisotropic stress change compared with stronger rock. However, the effect of stress change on the bearing capacity of Garford bulb cables was negligible.

Tadolini *et al.* (2012) studied the indentation geometry impact on the behaviour of PC strands, finding the indentations had an important effect on cable load transfer whereby both cable bearing capacity and stiffness increased with indentation depth. They concluded that indentations on cable wires enhanced the mechanical interlock at the interface between the cables and grouts, which in turn improved load transfer efficiency.

### Double embedment pull test

The double embedment pulling test illustrated in Figure 7 was initially proposed by Hutchins *et al.* (1990) to investigate the load transfer features of birdcage cable bolts. This newly devised testing method differed from previous pull test methods in that it enabled the study of the effect of embedment lengths on either side of the discontinuity. However, this type of test could not properly simulate underground

conditions, particularly the grout/rock interface since the tube used in the test was specially threaded internally to prevent failing along this interface.

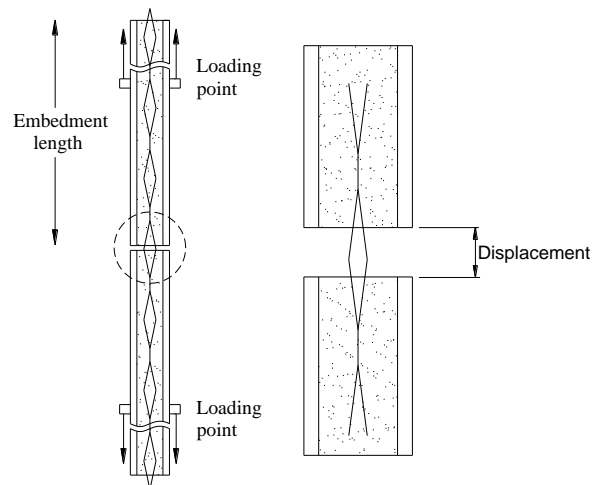


**Figure 7 - Double embedment length test set up (after Hutchins, *et al.*, 1990)**

The effect of debonding was studied whereby parts of the surface of the cable were painted. In the case of standard cables, the ultimate pull-out load decreased significantly, which was also verified by Satola (1999). This reduction in load was not repeated with birdcage cables although there was a reduction in system stiffness. There was also little effect of node location relative to the discontinuity on load transfer. Later, Satola and Aromaa (2004) designed a new double pipe test system to investigate the impact of epoxy and zinc coatings on the performance of cable bolts. In this arrangement, the embedment length was increased nearly ten-fold to 2.0 m. It was found that the corrosion protection mechanisms of epoxy coating and zinc galvanising on the cable surface increased the cable ultimate load capacity and stiffness to a large extent.

#### **Laboratory short encapsulation pull test**

Thomas (2012) reported on a modified Laboratory Short Encapsulation Pull Test (LSEPT) as originally reported by Clifford *et al.* (2001) and shown in Figure 8. Here a thick-walled steel cylinder is used to provide confinement to a sandstone core in which the cable bolt is grouted. Incorporated between the two halves of the test cell is an anti-rotation device that prevents the cable bolt from rotating or unravelling during a test.

A total of 14 different types of grouted cable bolts were tested with the aim of evaluating the effect of cable design and borehole diameter on load transfer,. As expected, there was a marked difference in load transfer with the different cable designs. The impact of borehole diameter on cables was not consistent. For bulbed and nutcaged cables, the load transfer efficiency increased with borehole diameter from 45 to 71 mm. Whereas for plain-strand cables, the load transfer efficiency decreased as borehole diameter increased from 28.5 to 61 mm.

## **DISCUSSION**

Previous studies found that load transfer mainly relies on the shear resistance at the cable/grout interface and this resistance is provided by three basic mechanisms: chemical adhesion, mechanical interlock and friction (Gambarova, 1981). However, the influence of chemical adhesion is only temporary since a small displacement of approximately 0.2 mm can damage this adhesive bond (Fuller and Cox, 1975). Hence in most instances the latter two mechanisms dominate (Stillborg, 1984). Mechanical interlock can be enhanced by the relative movement between the cable bolt and cement grout, compressing the grout within the borehole and generating extra normal pressure at the cable/grout interface. As for friction, it occurs along the cable/grout interface as a result of shear resistance, preventing the cable from slipping, which is the most important part in determining the load transfer behaviour. This also explains the reason why the load transfer efficiency of modified cable bolts is much greater than that of conventional cables. In the case of modified cable bolt designs, structures such as

the bulb on the strand, especially when they are filled with grout, increases the geometric mismatch and normal pressure at the cable/grout interface, resulting in the much higher load transfer capacity.

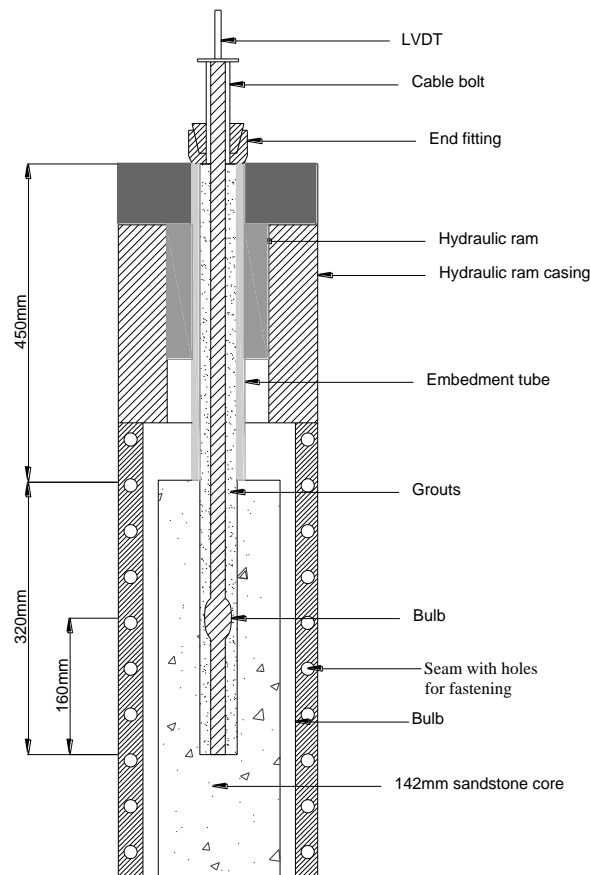


**Figure 8 - Schematic diagram of modified LSEPT (after Thomas, 2012)**

## CONCLUSIONS AND RECOMMENDATIONS

It has been found that over the past years, many different testing procedures and equipment have been developed and used to determine the influence of a wide range of parameters on the load transfer behaviour of fully grouted cable bolts in the axial direction. Based on previous research, the impacts of critical parameters including the rock mass confinement, the cable surface geometry, water: cement ratio, embedment length and so forth on the axial strength of cables are well understood. However, there is a lack of knowledge on the load transfer behaviour of the wide range of cable bolts currently available for use in ground control particularly based on a common testing methodology. A project is underway with support of the Australia Coal Association through their research funding organisation, ACARP (the Australian Coal Association Research Program) to devise a testing facility. This project focuses on studying the axial performance of some particular types of cable bolts and assessing the impacts of corresponding factors on them. The design of the new testing facility which is shown in Figure 9 is based on the recommendation design principles outlined in the British Standard with modifications that accommodate the requirements of the wider range of cable bolt designs used in Australia.

The main objectives of this project mainly include the following aspects:

- 1) To design and establish a robust axial test rig for kinds of fully grouted cable bolts;
- 2) To evaluate the behaviour of cables including the twin-strand, PC strand, indented PC strand, Sumo bolt and TG bolt.
- 3) To assess the effects of soft and medium rock confinement on those types of cable bolts.
- 4) To study the impacts of normal and larger boreholes on corresponding cable bolts.
- 5) To investigate the influences of normal and higher grout strength on the load transfer of cable bolts.

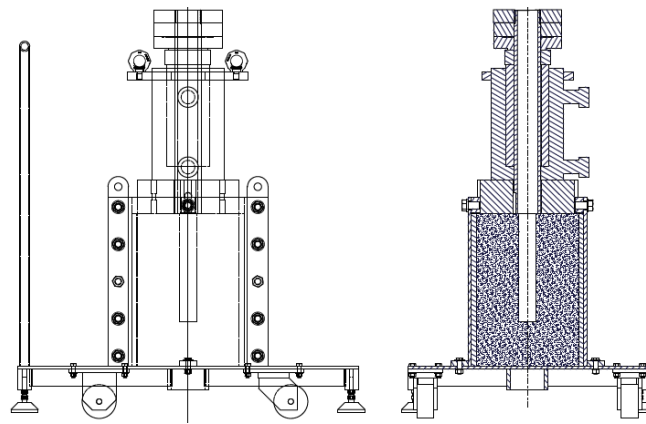


Figure 9 - Schematic of the design of proposed new LSEPT test facility

## REFERENCES

- Benmokrane, B, Chennouf, A and Ballivy, G, 1992. Study of bond strength behaviour of steel cables and bars anchored with different cement grouts, in *Proceedings Rock Support in Mining and Underground Construction* (ed: Kaiser, P K and McCreath, D R), pp 293-301 (A. A. Balkema: Rotterdam).
- Benmokrane, B, Chennouf, A and Mitri, H S, 1995. Laboratory evaluation of cement-based grouts and grouted rock anchors, *International Journal of Rock Mechanics and Mining Sciences and Geomechanics Abstracts*, 32(7):633-642.
- Clifford, B, Kent, L, Altounyan, P and Bigby, D, 2001. Systems used in coal mining development in long tendon reinforcement, in *Proceedings 20th International Conference on Ground Control in Mining Proceedings*, pp 235-241 (CSM: Morganton).
- Cox, R H T and Fuller, P G, 1977. *Load transfer behaviour between steel reinforcement and cement based grout*, pp 1-12 (Division of Applied Geomechanics, CSIRO: Australia).
- Dorsten, V, Frederick, F H and Preston, H K, 1984. Epoxy coated seven-wire strand for prestressed concrete, *Prestressed Concrete Institute*, 29(4):1-11.
- Farah, A and Aref, K, 1986. An investigation of the dynamic characteristics of cable bolts, in *Proceedings 27th U.S. Symposium on Rock Mechanics*, pp 423-428 (American Rock Mechanics Association: Tuscaloosa).
- Fuller, P G and Cox, R H T, 1975. Mechanics of load transfer from steel tendons to cement based grout, in *Proceedings Fifth Australasian Conference on the Mechanics of Structures and Materials* (ed: Grundy, P and Stevens, L K), pp 189-203 (Melbourne).
- Gambarova, P, 1981. *On aggregate interlock mechanism in reinforced concrete plates with extensive cracking*, pp 105-134.
- Garford, 1990. *An improved, economical method for rock stabilisation*, pp 1-4 (Garford, Pty Ltd: Perth).
- Goris, J M, 1990. *Laboratory evaluation of cable bolt supports (in Two Parts) 1. Evaluation of supports using conventional cables*, pp 1-23 (United States Bureau of Mines: America).
- Goris, J M, 1991. *Laboratory evaluation of cable bolt supports (in Two Parts) 2. Evaluation of supports using conventional cables with steel buttons, birdcage cables, and epoxy-coated cables*, pp 1-14 (United States Bureau of Mines: America).
- Goris, J M and Conway, J P, 1987. Grouted flexible tendons and scaling investigations, in *Proceedings 13 World Mining Congress*, pp 783-792 (Stockholm).
- Hartman, W and Hebblewhite, B, 2003. Understanding the performance of rock reinforcement elements under shear loading through laboratory testing-A 30-year history, in *Proceedings 1st Australian Ground Control in Mining Conference*, pp 151-160 (Australasian Mining Rock Mechanics Society: Sydney).
- Hassani, F P, Mitri, H S, Khan, U H and Rajaie, H, 1992. Experimental and numerical studies of the cable bolt support systems, in *Proceedings Rock Support in Mining and Underground Construction* (ed: Kaiser, P K and McCreath, D R), pp 411-417 (A. A. Balkema: Rotterdam).
- Hassani, F P and Rajaie, H, 1990. Investigation into the optimization of a shotcrete cable bolt support system, in *Proceedings 14th Congress of the Council of Mining and Metallurgical Institution*, pp 119-129 (Edinburgh).
- Hutchins, W R, Bywater, S, Thompson, A G and Windsor, C R, 1990. A versatile grouted cable dowel reinforcing system for rock, in *Proceedings The Australasian Institute of Mining and Metallurgy Proceedings*, pp 25-29.

- Hutchinson, D J and Diederichs, M S, 1996. *Cablebolting in underground mines*, pp 1-2 (BiTech Publishers Ltd.: Richmond).
- Hyett, A J and Bawden, W F, 1993. The nutcase cable bolt, in *Proceedings Innovative Mine Design for the 21st Century: Proceedings of the International Congress on Mine Design* (ed: Bawden, W F and Archibald, J F), pp 409-419 (Ontario).
- Hyett, A J and Bawden, W F, 1994. *The 25mm Garford bulb anchor for cable bolt reinforcement Part 1: laboratory results*, pp 1-16 (Garford Pty. Ltd.: Perth).
- Hyett, A J and Bawden, W F, 1996. *The effect of bulb frequency on the behaviour of fully grouted Garford bulb cable bolts*, pp 1-54 (Garford Pty Ltd: Canada).
- Ito, F, Nakahara, F, Kawano, R, Kang, S-S and Obara, Y, 2001. Visualization of failure in a pull-out test of cable bolts using X-ray CT, *Construction and Building Materials*, 15(5-6):263-270.
- Macsporrnan, G R, 1993. An empirical investigation into the effects of mine induced stress change on standard cable bolt capacity, Master thesis(Published), Queen's University, Kingston.
- Mah, G P, 1990. The development of a fibreglass cable bolt, Master thesis(Published), The University of British Columbia, Vancouver.
- Martin, L, Girard, J M and Curtin, R, 1996. Laboratory pull tests of resin-grouted cable bolts, in *Proceedings 15th International Conference on Ground Control in Mining Proceedings*, pp 455-468 (CSM: Golden).
- Matthews, S M, Tillmann, V H and Worotnicki, G, 1983. A modified cable bolt system for the support of underground openings, in *Proceedings AusIMM annual conference*, pp 243-255 (Australasian Institution of Mining and Metallurgy: Melbourne).
- Mirabile, B, Poland, R and Campoli, A, 2010. Application of tensioned cable bolts for supplemental support, in *Proceedings 29th International Conference on Ground Control in Mining*, pp 128-133 (West Virginia University: Morgantown).
- Mitri, H S and Rajaie, H, 1992. Shear bond stress along cable bolts, in *Proceedings International conference on ground control in mining*, pp 90-95 (CSM: Morgantown).
- Mosse-Robinson, S and Sharrock, G, 2010. Laboratory experiments of quantify the pull-out strength of single strand cable bolts for large boreholes, in *Proceedings Second Australasian Ground Control in Mining Conference* (ed: Hagan, P and Saydam, S), pp 201-209 (Australasian Institution of Mining and Metallurgy: Sydney).
- Potvin, Y, Hudyma, M and Miller, H D S, 1989. Design guidelines for open stope support, *CIM bulletin*:53-62.
- Prasad, K, 1997. Effect of isotropic and anisotropic stress changes on the capacity of fully grouted cable bolts, Master thesis(Published), Queen's University, Kingston.
- Reichert, R D, 1991. A laboratory and field investigation of the major factors influencing bond capacity of grouted cable bolt, Master thesis(Published), Queen's University, Kingston.
- Reichert, R D, Bawden, W F and Hyett, A J, 1992. Evaluation of design bond strength for fully grouted cables, *CIM Bulletin*, 85(962):110-118.
- Satola, I S, 1999. Testing of the yielding cable bolt achieved by debonding, in *Proceedings 9th Congress of the International Society for Rock Mechanics* (ed: Vouille, G and Berest, P), pp 1467-1470 (International Society for Rock Mechanics: Paris).
- Satola, I S and Aromaa, J, 2004. The corrosion of rock bolts and cable bolts, in *Proceedings Ground Support in Mining and Underground Construction* (ed: Villaescusa and Potvin), pp 521-528 (London).
- Schmuck, C H, 1979. Cable bolting at the Homestake gold mine, *Mining Engineering*, 31(12):1677-1681.
- Stillborg, B, 1984. Experimental investigation of steel cables for rock reinforcement in hard rock, PhD thesis(Published), Högskolan i Luleå University, Kiruna.
- Strata Control, 1990. *Testing of Garford bulb tendons*, pp 1-5 (Strata Control Technology Pty. Ltd.: Australia).
- Tadolini, S C, Tinsley, J and McDonnell, J P, 2012. The next generation of cable bolts for improved ground support, in *Proceedings 31st International Conference on Ground Control in Mining*, pp 1-7 (CSM: Morgantown).
- Thomas, R, 2012. The load transfer properties of post-groutable cable bolts used in the Australian coal industry in *Proceedings 31st International Conference on Ground Control in Mining*, pp 1-10 (CSM: Morgantown).
- Thompson, A G and Windsor, C R, 1995. Tensioned cable bolt reinforcement-An integrated case study, in *Proceedings 8th ISRM Congress* (ed: Balkema, A A), pp 679-682 (International Society for Rock Mechanics: Tokyo).
- Thorne, L J and Muller, D S, 1964. Prestressed roof support in underground engine chambers at Free Geduld Mines Ltd., pp 411-428.

# ***IN SITU* BOND STRENGTH TESTING OF AUSTRALIAN CABLE BOLTS**

**Peter Craig and Matthew Holden**

**ABSTRACT:** Testing of axial load transfer of various Australian cable bolts has been conducted in overseas laboratories within the last two years (Thomas, 2012). The comparative laboratory testing determined that nutcaged cables and indented wire cables provide stiffer and higher capacity bond strength compared to plain cable. Laboratory studies have limitations in terms of rock strength and installation practice but have the benefit of controlling the type of load applied during the test. *In situ* cable bolt tests were conducted underground using common installation equipment, resin capsules instead of cementitious grout where relevant, and in a typical coal mine roof. *In situ* testing methods included anti-twist methodology similar to that used in laboratory tests.

## **INTRODUCTION**

Research conducted by Thomas (2012) on the anchorage performance of 14 cable bolts available in Australia at the time determined that the aggressive profile of indented wire cables and modified geometry cable configurations have the potential to provide higher bond strengths. The results from the Laboratory Short Encapsulation Pull Test (LSEPT) found peak loads were up to 400% higher for nutcaged or bulbed cable designs in comparison to plain strand designs. The constant stiffness confinement conditions implemented during the LSEPT included grouting a sandstone core into a two-part steel casing to simulate a relatively strong *in situ* ground environment. Typically the weakest load transfer point in a cable bolt system, installed into competent rock, is the cable/grout interface, with slip initiating along this surface prior to degradation of the surrounding rock and/or grout. However, weaker and more variable rock masses can significantly alter the effective cable bolt strength as the load transfer between the rock/grout interface and through the strata is correspondingly weaker. *In situ* pull testing can overcome the idealised confinement conditions implemented in the laboratory and more accurately compare the performance of different cable bolt designs in typical installation conditions.

Hutchinson and Diederichs (1996) identified that constrained and unconstrained pull tests tend to give upper and lower bond strengths of cable bolts. LSEPT's by Hyett *et al.* (1995) identified that the failure mechanism of a 15.2mm diameter plain wire strand in cement was both shearing of the grout flutes and unscrewing of the cable from the cement annulus, and that the helical form of a cable bolt creates a different mechanical behaviour compared to solid deformed bar. A cable bolt will undergo torsional rotation of the wires along a free length, and the interaction of a free length adjacent to a bonded length in a SEPT would not represent the failure mechanism of a fully grouted cable bolt in service.

LSEPT typically utilise constrained methods, such as anti-rotation devices, when assessing the performance of fully encapsulated cable bolts. However, the increase in complexity between constrained and unconstrained pull test methodologies, particularly with regards to setting up anti-rotation devices, is largely prohibitive for *in situ* testing. The need for comparative testing of cable bolt performance in rock weaker than that used in LSEPTs, led to a program of *in situ* experimentation using different apparatus and methods. An anti-twist testing arrangement was subsequently developed and adapted to the common reamed hole SEPT. A selection of different diameter plain and nutcaged cable bolts were comparatively tested using the new method in moderate strength mudstone at Baal Bone Colliery to test the practicality and repeatability of the method.

## **DEVELOPMENT OF THE UNDERGROUND *IN SITU* TEST METHOD**

### **Embedment length**

A common SEPT method used for rebar rock bolts involves reaming of the hole below the target bond length to allow for excess resin to fall out of the top 27-28 mm diameter drill hole section, effectively de-bonding a free length of bolt and guaranteeing a specific bond length. This technique for solid rebar

rock bolts is described by Mark *et al.* (2008). This test typically uses a short 300 mm embedment length and an initial set of *in situ* testing was conducted using this method on 22 mm Indented and plain wire SuperStrand cable bolts. These results were compared to rebar rock bolts pull tested using the same method with 300 mm embedment length.

The length of wire lay is defined as the distance along the axial length of the cable corresponding to a full spiral rotation of an individual wire (Hutchinson and Diederichs, 1996), as depicted in Figure 1. It was surmised that an embedment length with an entire length of lay within the bond would incorporate the effect of the helical structure of the strands. The typical range of lay lengths for 22 mm SuperStrand and 28 mm hollow strand cable wires are 300-350 mm and 400-450 mm, respectively. Bigby and Reynold (2005) used 450 mm embedment length for cable bolt LSEPT and the resulting bond strength on non-modified geometry cable did not exceed the yield strength of the ~60t cable. The LSEPT method described by Thomas (2012) used 320 mm embedment length in a strong sandstone rock core. *In situ* SEPT of 28 mm Hollow strand cable by Craig and Murnane (2013) successfully used 400 mm embedment length in a weak coal roof. As a result of considering the length of cable lay, previous LSEPT embedment lengths used and that the *in situ* tests would be conducted in moderate strength mudstone; the 400 mm embedment length was adopted for the remainder of the study as opposed to the first tests using the shorter 300 mm encapsulation. It should also be noted that most Australian post groutable cables have a nutcage at 500 mm centres down the fully grouted portion of the cable bolt. The true comparison of non-modified geometry cables against nutcage cables would need to be in a bond length equivalent to the nutcage spacing.

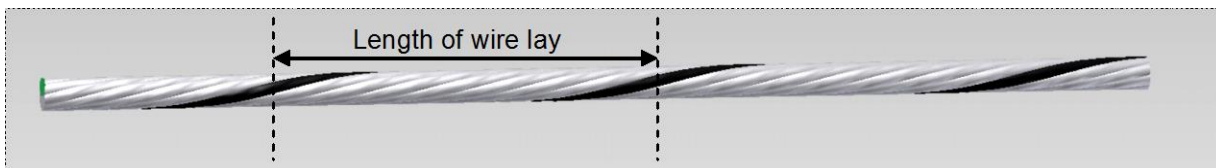


Figure 1 - Length of lay for an individual wire

### Bonding agent

The Australia coal mining industry utilises 22 mm diameter cable bolts in 28 mm drill holes exclusively with resin capsules, and it was noted that Thomas utilised non-shrink cementitious grout for all comparative laboratory tests including those in 28 mm drill holes. The benefit of *in situ* test methods is the use of normal installation equipment used in service, which allowed the use of resin capsules for the cables in 28 mm drill holes and Australian made top-down thixotropic cementitious grout for the hollow post groutable cables in 42 mm drill holes. The initial *in situ* tests aimed at developing the method used resin capsules for immediate results and to provide in service performance information. The test program using the final developed pull test method included cementitious grout in 28 mm drill holes to compare against earlier results with resin.

The top-down pumped high strength thixotropic grout used for the *in situ* testing has a typical Uniaxial UCS of 30 MPa at 1 d, 55 MPa at 7 d and 70 MPa at 28 d. The grout cure time before pull testing was six days due to mine access requirements, which gave an estimated grout UCS strength of 50 MPa. The resin capsules used in the study have a typically UCS strength of 70 MPa

### Anti-twist method

Research into load transfer of Australian cable bolts conducted by Thomas (2012), using a LSEPT methodology, utilised an anti-twist mechanism to restrict the rotation of the free length of the cable. Cable rotation was restricted during testing by grouting the free length of cable in a steel pipe which is secured by a locking key that prohibits rotation, as shown in Figure 2(b).

Axial loading of a fully grouted cable *in situ* caused by simple roof dilation would naturally have no twisting of the rock mass, so design of the *in situ* test to represent in-service cable bolt loading was sought after. A similar anti-twist concept was adopted for the *in situ* pull testing investigation, the set-up illustrated in Figure 2(a). Preparation included grouting the middle section of the 1.4 m cable into a 600 mm long thick-walled steel pipe with an exterior profile which matches the key hole in a 25 mm thick steel loading plate. The steel plate remained fixed during loading, as it was compressed against the seam roof, which in turn locked the profiled pipe as it attempted to rotate. The steel pipe within the

reamed out section of the borehole below the embedment length was covered in two layers of lubricant and plastic film to prevent excess installation grout from adhering to the pipe, which had the potential to provide additional strength to the system during loading.

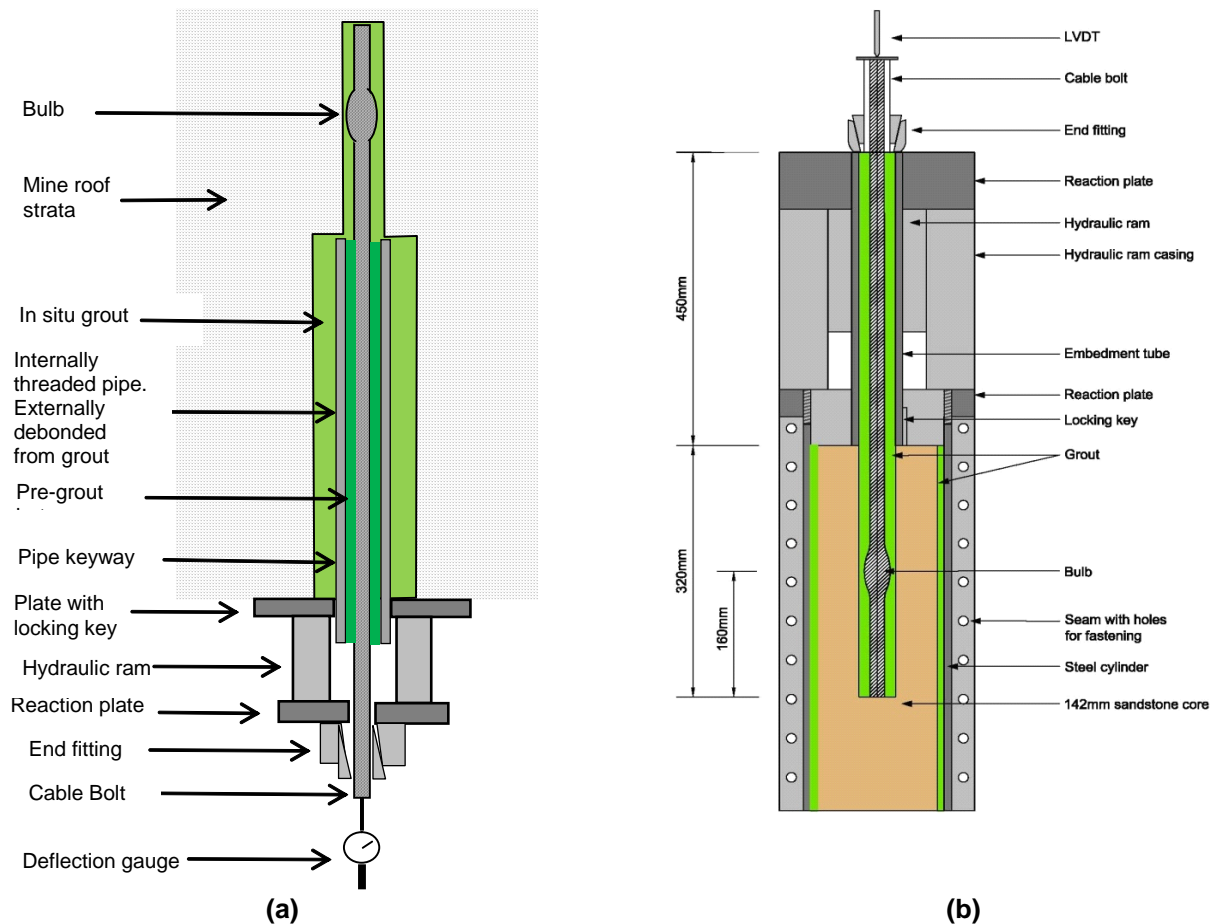


**Figure 2 - (a) Anti-twist *in situ* method developed, (b) Anti-twist laboratory pull test method (Thomas, 2012)**

The final pull test arrangement developed for *in situ* testing at Baal Bone Colliery, as illustrated in Figure 2(a), was an adaptation of the reamed hole SEPT using 400 mm embedment length and included the anti-twist grouted pipe apparatus

### Final *in situ* test program

The cable test pieces were installed 0.9 m into the mudstone roof of the Baal Bone mine. The pull test horizon location, with respect to the Lithgow coal seam, can be seen in the stratigraphy in Figure 3. The UCS of the mudstone horizon is known to be approximately 35 MPa.

Four types of cable were selected for the final test program: 1) Indented 22 mm SuperStrand; 2) Indented TG cable 28 mm hollow strand; 3) Indented SUMO 28 mm hollow strand with a 35 mm diameter nutcage; and 4) Plain wire SUMO 28 mm hollow strand with a 35 mm diameter nutcage.

The SuperStrand is a 19 wire cable with a capacity of 60 t. All three 28 mm cable configurations consist of 9 wires wound around a central hollow strand with a capacity of 63 t. The two modified geometry cables had the nutcage located half-way along the 400 mm embedment length. The 28 mm hollow strand cables were installed into holes drilled with a standard 42 mm twin-wing drill bit, while the 22 mm SuperStrand were installed using a 28 mm drill diameter.

The aim of the final larger set of tests was to ensure the pull test method gave repeatable results and that it was practical for future studies within the restrictions of underground coal mine testing.

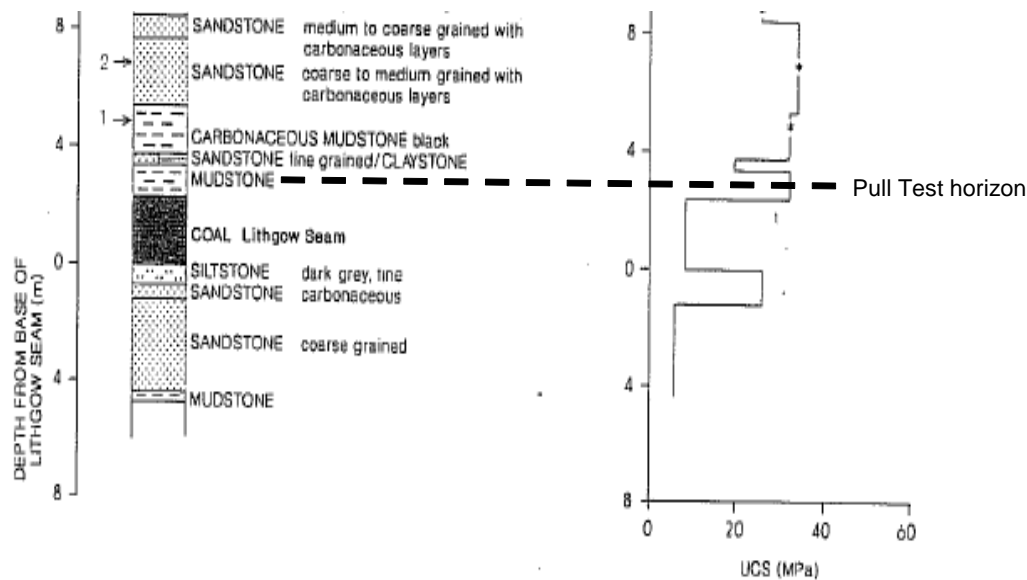


Figure 3 - Stratigraphy referenced to pull test horizon (SCT, 1997)

## RESULTS AND DISCUSSIONS

### Common reamed hole 300 mm SEPT

The load displacement results from the common reamed hole SEPT conducted on indented and plain wire 22 mm SuperStrand using resin capsules, compared to 22 mm rebar rock bolts can be seen in Figure 4(a). These tests did not include a pre-grouted pipe with anti-twist mechanism, therefore the free length of cable was able to stretch and twist. The tests did utilise a hydraulic ram with a key between the piston and body of the cylinder. The raw displacement measurements were corrected for theoretical cable stretch using the Young's modulus for the 22mm cable bolt.

The results for the plain wire cable were variable in comparison to the indented wire cable. This could be due to the indented wire offering resistance to the cable unscrewing from the resin annulus, and shear failure of the resin flutes possibly being the main failure mechanism. The plain strands are more likely to suffer unscrewing from the resin preventing shearing of the flutes and giving a variable result. The comparison of the 22mm diameter cables to a rebar rock bolt gave a higher bond strength for the cables. The reason for such results would require further investigation and should include effects of resin mixing between cables and rebar bolts.

### Anti-twist reamed hole 400 mm SEPT with resin

The indented SuperStrand was pull tested using the longer 400 mm embedment length and anti-twist method. The results plotted alongside the previous common 300mm SEPT are shown in Figure 4(b). The bond strength for the common SEPT averaged 11 t per 300 mm, while the anti-twist bond strength averaged 18 t per 400 mm bond length. Although two different bond lengths were implemented in each test method the bond strength per unit length can still be compared. Assuming a linear extrapolation for bond strength, the common 300 mm SEPT without anti-twist equates to 15 t per 400 mm bond length.

The lower bond strength of the common SEPT method is probably due to the strands of the cable unwinding along the helical grout channels that encapsulate the outer surface of the cable strands. Restricting cable bolt rotation can eradicate this unwinding effect by forcing the strands of the cable to ride up and over the grout ridges, as opposed to following the channels. This mechanism of failure induces higher radial dilation pressures in the grout which in turn increases shear resistance to axial movement along the cable length and overall bond strength (Hutchinson and Diederichs, 1996). This effect could be magnified by the length of wire lay within the bond. The 400 mm embedment length encapsulates an entire length of wire lay, creating grout channels that restrict the movement of a single wire around the entire circumference of the drill hole. This could increase resistance to cable rotation within the bond length to a greater extent, when coupled with an anti-twist device, and consequently generate even higher dilation pressures during loading.

Under such assumptions it can be reasoned that the anti-twist device, with an entire wire lay length within the bond, has the potential to increase the bond strength of the system by up to 20%. It is therefore imperative these two parameters are either controlled or understood within pull testing methodologies as the effect on bond performance can be significant.

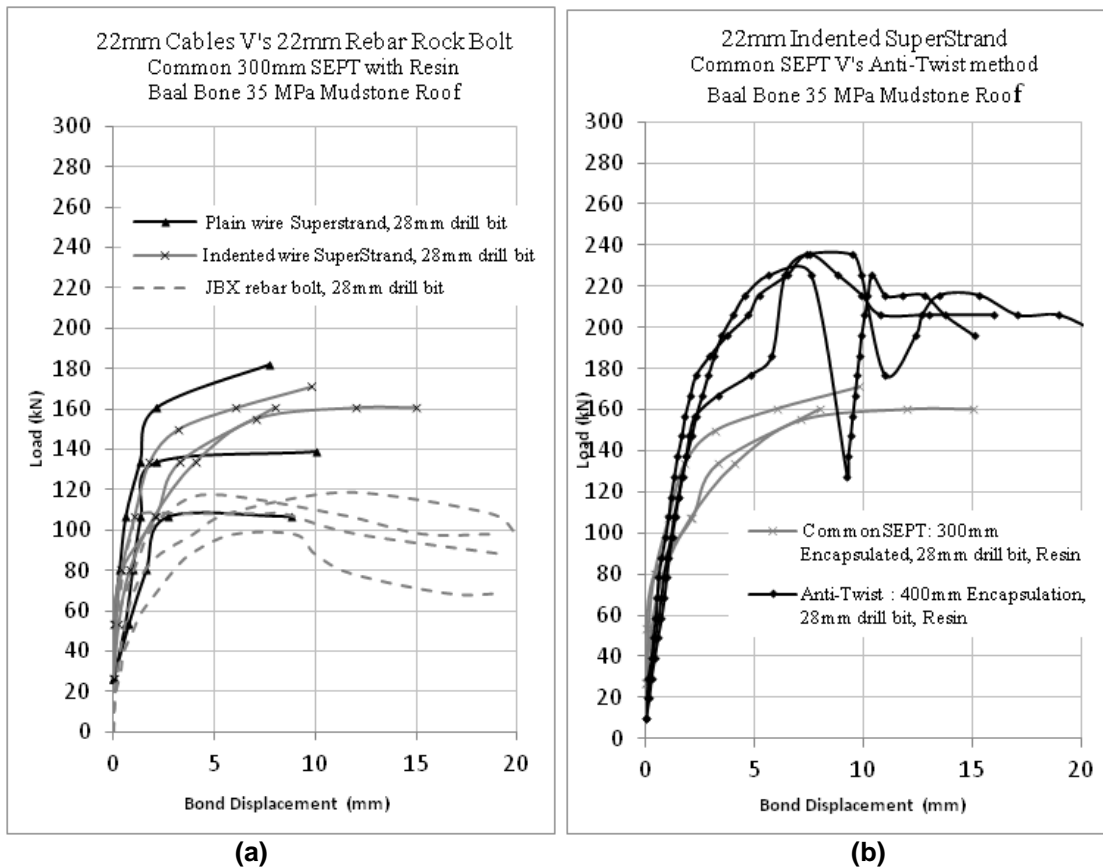


Figure 4 - Reamed hole SEPT results with resin

#### Anti-twist reamed hole SEPT with grout

The nine various configurations of 28 mm hollow strand cable bolts were installed by pumping grout through the central hollow strand to achieve full encapsulation along the 400 mm testing length. The three Indented SuperStrand cables, on the other hand, were installed using a grout and insert method (Hutchinson and Diederichs, 1996) as the diameter of the hole was too small to accommodate both cable and grouting tube. Unfortunately, complications arose during installation of one indented nutcaged cable that resulted in inadequate encapsulation of the cable. The failure load measured for this cable was significantly lower than the other samples, and as such was disregarded.

The twelve grouted cable bolts were pull tested 6d after installation using a 60 t hydraulic cylinder. The displacement measurements were corrected to account for cable elongation of the 300 mm free length between the barrel and wedge and the base of the grouted steel pipe. It was assumed that the elongation along the grouted cable in the heavy walled pipe section was negligible. In accordance with the British Standard (2007), bond strength of the cables was determined when the stiffness fell below 20 kN/mm.

The results summary for the *in situ* pull tests are contained in Table 1. The load versus displacement curves for each test are shown in Figure 5, with the nutcaged and non-modified geometry bolt results plotted on separate graphs. The plain wire SUMO cable bolt stiffness decreased rapidly after the bond strength was exceeded, displacing comparably more than all other indented cables at peak bond loads. This suggests the aggressive profile of the indented wire cables generates significantly more resistance to cable/grout slip, most likely due to interlocking along the irregular wire surface.

Comparing the bond strengths of the 28 mm nutcaged indented and plain wire cables, averaging 35 t and 34 t per 400 mm bond length respectively, revealed little difference in bond strength due to the

indentations. The indented nutcaged cables had higher bond stiffness shown by the gradient of the curves which should be attributed to the indentations. A similar mode of failure was found for all bulbed cables with a sudden drop in load corresponding to a loud pop before cable reloading. Craig and Murnane (2013) reported similar types of failure during *in situ* pull tests conducted on 28 mm hollow strand cable using injected polyurethane and cementitious grout. The sudden bond slip was suggested to have occurred at the rock/grout boundary or through the rock mass. A problem with *in situ* testing is the inability to view the failure mechanism.

**Table 1 - Summary of *in situ* pull test results**

Test No.	Cable Type	Bond Strength (kN)	Av. Bond Strength (kN)	Range of Results (max – min)
1	Plain wire SUMO	334	350	68kN (19%)
2		392		
3		324		
4	Indented wire SUMO	373	344	59kN (17%)
5		314		
6		265		
7	Indented wire TG	314	288	49kN (17%)
8		284		
9		157		
10	Indented SuperStrand (grout)	147	147	20kN (14%)
11		137		
a		157		
b	Indented SuperStrand (resin)	177	180	49 (27%)
c		206		

The load displacements graphs for the indented 28 mm TG and 22 mm SuperStrand cables, shown in Figure 5, have average bond strengths of 29 t and 15 t per 400 mm bond length, respectively. In comparison, laboratory pull tests conducted by Thomas (2012) found that plain strand 28 mm TG and 22 mm SuperStrand embedded 320 mm into sandstone cores had bond strengths of 21 t per 320 mm and 6 t per 320 mm bond length, respectively. Linearly extrapolating these results to an equivalent 400 mm bond length gives 26 t and 7.5 t bond strengths suggesting that either the indentations or test method created a significant difference in performance between the two different diameter non-modified geometry cables. Also included in Figure 5 are SuperStrand results from the investigation using resin encapsulation under the same testing configuration. The resin anchored cables had a 20% higher bond strength than the top-down high strength thixotropic grout at 6 d cure; this is most likely due to the stronger 70 MPa UCS of the resin, compared to 50 MPa for the grout.

Comparing the 28 mm nutcaged cable configurations to non-modified geometry indented 28 mm cables reveals a 20% increase in the bond strength with nutcaged cables. The percentage margin was larger between 22 mm Indented SuperStrand and nutcaged 28 mm cables at approximately 135%.

The only cable tested *in situ* which had also been tested using the same laboratory method described by Thomas (2012), was the plain wire SUMO cable. The plain wire SUMO was tested in the Golders UK laboratory and reported independently to Jennmar Australia Pty Ltd. The results from the Laboratory test plotted against the *in situ* tests are shown in Figure 6, with a summary shown in Table 2.

The average bond strength from the LSEPT was 30 t per 320 mm bond length. This extrapolates to a 37.6 t per 400 mm bond length which is comparatively higher than the *in situ* pull tests at 35 t per 400 mm bond length. This discrepancy is not considered excessive and could be attributed to the difference in rock or grout strength between the laboratory and *in situ* tests, with the former grout strength reaching an average UCS of 94 MPa at 58 d and the latter an approximate UCS of 50 MPa at 6d.

The Golder UK laboratory reported that failure occurred predominantly due to slip along the cable/grout interface and is shown in Figure 7. The corresponding load displacement curves in Figure 6 have gradual reloading characteristics, following the debonding load, which are indicative of such types of failure. This differs from the *in situ* pull test failure which possibly occurred along the rock/grout interface or through the rock mass. This difference can be attributed to the confinement conditions of the LSEP tests which incorporate a sandstone core and steel cylinder, representing a strong rock mass, while the *in situ* pull length was located in a weaker mudstone horizon. The strength of the grout could also have contributed to such a difference in failure modes.

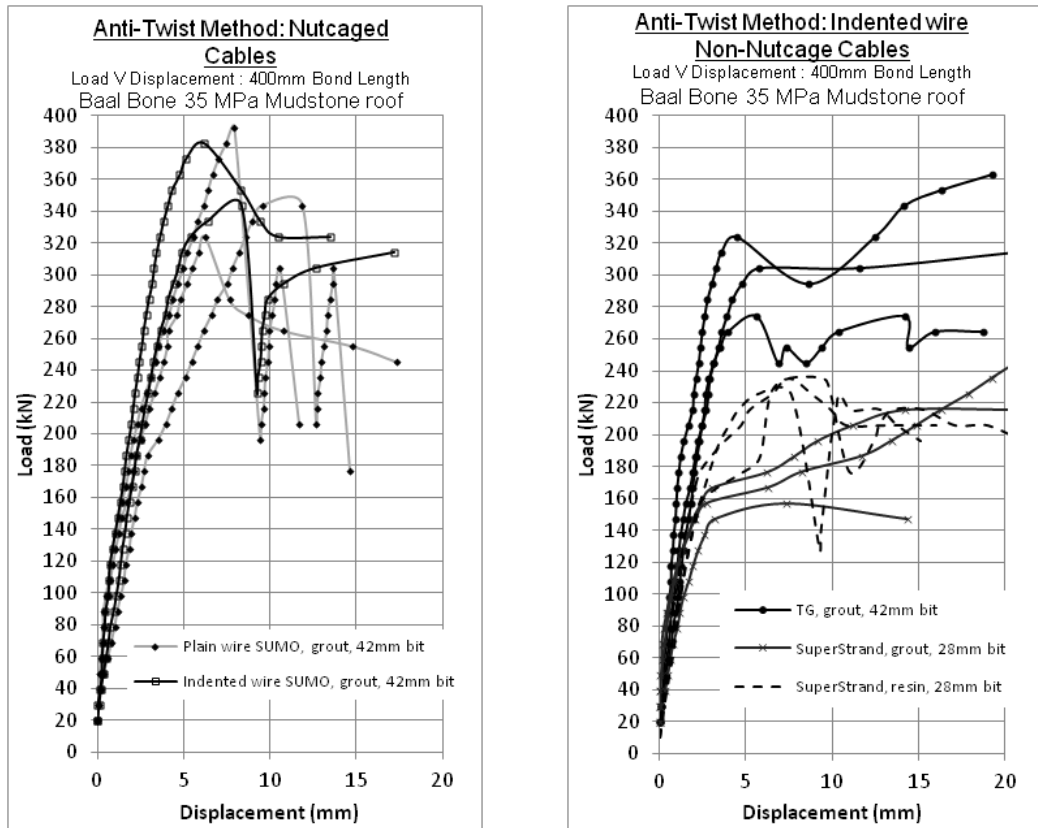


Figure 5 - *In situ* load transfer results

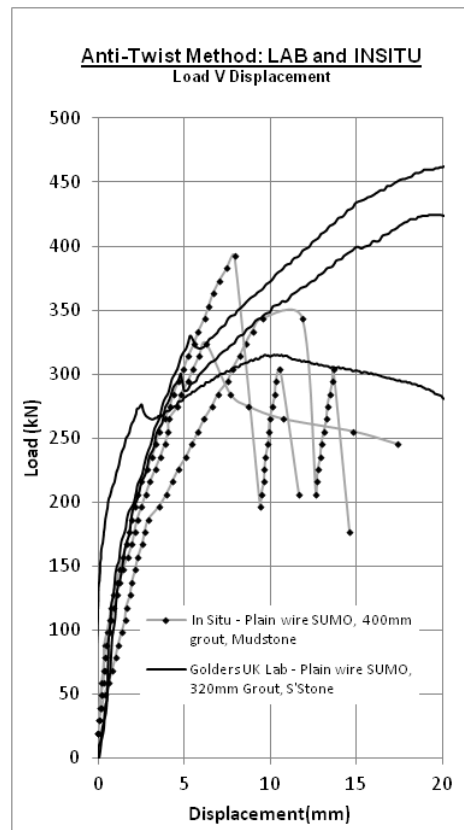


Figure 6 - Comparison of laboratory and *in situ* results

Table 2 - Summary of laboratory pull test results

Cable Type	Bond Strength (kN)	Av. Bond Strength (kN)	Range of Results (max – min)
Plain wire SUMO	276	301	54kN (18%)
	330		
	298		



Figure 7 - Test sample after pull test and splitting of the core (Golders UK)

### CONCLUSIONS

The development of an *in situ* pull testing methodology that incorporates an anti-twist device into the commonly reamed hole short encapsulation pull test was found to increase cable bolt anchorage test results by 20%. It was also found that the embedment length may have contributed to this increase as an entire length of wire lay was encapsulated within the bond length. It is recommended that these two parameters be controlled during *in situ* pull testing as they also best represent in service loading mechanisms of fully grouted cables. The anti-twist *in situ* method proved practical and as accurate as the LSEPT with the range between identical tests less than 20%.

The 28 mm hollow strand nutcaged cable bolts had comparatively higher bond performance than both types of indented wire non-modified geometry cable bolts. Within the 35 MPa mudstone rock, the average nutcage 28 mm cable bond strength was 25% higher than the indented wire 28 mm TG cable bolt and 135% higher than the Indented wire 22 mm SuperStrand cable bolt.

In the mudstone rock, the indented strands provide little benefits to the bond strength of nutcaged cable designs, which is more likely attributed to the non-collapsible bulb as opposed to the profile of the wire. The indentations, however, increased the stiffness of the system as loads approached the ultimate bond strength, with the plain strand cable displacing 50% more on average. Golders UK lab pull tests on the 28 mm plain wire SUMO cables were comparatively similar to the *in situ* test method developed.

The *in situ* test method developed is envisaged to allow further research into the parameters of embedment length and bonding material to eventually provide accurate comparative test results between different cables in the more common weak to moderate rocks found in roof strata requiring high density cable bolting.

### ACKNOWLEDGEMENTS

The authors acknowledges assistance from the following persons:

- Gary Linford and Mark Bulkeley of Baal Bone Colliery for their assistance and provision of the test site, and
- Tim Gaudry, Paul Holmes, Mark Bedford and Danny Murrill of Jenmar Australia for their assistance in preparation, installation, grouting and pull testing of the cables.

## REFERENCES

- Craig, P and Murnane, B, 2013. *In situ* pull testing of cable bolts encapsulated with injection polyurethane, in *Proceedings of 13<sup>th</sup> Coal Operators' Conference*, pp 131-136, February 14 - 15, (The University of Wollongong). <http://ro.uow.edu.au/coal/446/>.
- Bigby, D. and Reynolds, C. 2005. Development of the laboratory short encapsulation pull test for a revised British standard on rock reinforcement components used in coal mining. In *Proceedings of the 24<sup>th</sup> International Conference on Ground Control in Mining*, Morgantown, WV, August 2 - 4, pp 313-322, [http://icgcm.conferenceacademy.com/papers/detail.aspx?subdomain=icgcm\\_and\\_iid=535](http://icgcm.conferenceacademy.com/papers/detail.aspx?subdomain=icgcm_and_iid=535).
- Golder Associates (UK) Ltd. March 2013. REPORT to Jennmar: Split cylinder pull tests on three samples of the SUMO cable bolt manufactured by Jennmar.
- Hutchinson, D J and Diederichs, M S, 1996. Cablebolting in underground mines, Richmond, Canada, (BiTech Publishers).
- Hyett, A.J., Bawden, W. F., Macsporrán, G.R., Moosavi, M. 1995. A Constitutive law for bond failure of fully-grouted cable bolts using a modified Hoek cell. *Int. J. Rock Mech. Min. Sci. Geomech. Abstr.*, 32, 11–36.
- Mark, C, Compton, C S, Dolinar D R and Oyler, D C, 2008. Field performance testing of fully grouted roof bolts, [online]. Available from: <http://www.cdc.gov/niosh/mining/UserFiles/works/pdfs/fptof.pdf> [Accessed on December 30, 2013].
- Strata Control Technology (SCT), 1997. Report to Baal Bone Colliery: Development of a numerical model to simulate roadway behaviour under shallow cover.
- The British Standard BS 7861- 2007. Strata reinforcement support system components used in coal mines- Part 1. Specification for rock bolting and Part 2: Specification for flexible systems for roof reinforcement,
- Thomas, R. 2012. The load transfer properties of post– groutable cable bolts used in the Australian coal industry, In *Proceedings of the 31<sup>st</sup> International Conference on Ground Control in Mining*, Morgantown, WV, July 31- August 2, 10 p [http://icgcm.conferenceacademy.com/papers/detail.aspx?subdomain=ICGCM\\_and\\_iid=1011](http://icgcm.conferenceacademy.com/papers/detail.aspx?subdomain=ICGCM_and_iid=1011).

# SHEAR STRENGTH PROPERTIES OF HILTI PLAIN AND INDENTED STRAND CABLE BOLTS

Naj Aziz<sup>1</sup>, Kay Heemann<sup>2</sup>, Jan Nemcik<sup>3</sup> and Stefan Mayer<sup>4</sup>

**ABSTRACT:** An investigation into the performance of two 22 mm diameter, 60 tonne tensile strength capacity Hilti cable bolts in shear was conducted using the double shear testing apparatus at the laboratory of the School of Civil, Mining and Environmental Engineering Faculty of Engineering and information sciences, University of Wollongong. The tested cable bolts were (a) Hilti19 wire HTT-UXG plain strand and (b) Hilti 19 wire HTT-IXG spirally indented strand cable bolt, with indentation only on the surface of the outer strands. Both cable bolts were of sealed wire construction type, consisting of an outer 5.5 mm diameter strand layer overlying the middle 3 mm diameter wire strands. Both layers are wrapped around a single solid 7 mm diameter strand wire core. The double shearing test was carried out in 40 MPa concrete blocks, contained in concrete moulds. The cable bolts were encapsulated in concrete using Minova/ Orica FB400 pumpable grout. Prior to encapsulation, each cable bolt were pretensioned initially to 50 kN axial force. A 500 t capacity servo controlled compression testing machine was used for both tests, and during each test the vertical shear displacement was limited to 70 mm on travel. The rate of vertical shear displacement was maintained constant at 1 mm/min. The maximum shearing load achieved for the plain strand cable was 1024 kN, while the indented cable peak load was 904 kN, before the cable bolt strands began to individually snap, which lead to the cable bolt break up into two pieces. It was found that indentation of the cable bolt's outer strand weakened both the tensile and shearing strength.

## INTRODUCTION

Cable bolt usage in Australian coal mines is on the increase, because it is mostly used as A secondary support to supplement the primary support system for strata reinforcement. Several factors have contributed to the increase in cable bolt usage in mines; the most prominent of these are a better understanding of the principals of rock mechanics and strata control, and better management of difficult ground conditions. As a consequence, the reliance on Short Encapsulation Pull Testing (SEPT) of cable bolt cannot be considered as adequate alone for providing realistic answers to the credibility of the installation in given ground condition. The unwinding/unscrewing of the cable bolts from their anchorage medium, and shear behaviour across the stratified formation represent important challenges to be addressed. A number of papers have been reported on studies examining the load transfer and unscrewing characteristics of cable bolts (Clifford, *et al.*, 2001; Tadolini, *et al.*, 2001 and 2012; Thomas, 2012), and there have been significant variations in the design to include both plain and indented cable bolts of different sizes and combinations. The increased variations in cable bolt configurations and designs have also generated deep interest in shear failure of tendons'. *In situ* studies in cable bolt shear are difficult to conduct, but can carried out in laboratory simulated conditions. Goris *et al.*, (1996), carried out shear testing of cable bolts using pairs of 0.025 m<sup>3</sup> concrete blocks made from fine sand-concrete mix having an average 28 days compressive strength of 69 MPa. The concrete mixture was poured into steel moulds that contained an aluminium-cast joint surface prints. The tested cable was installed across two concrete blocks with the desired shear surface roughness produced as off prints of aluminium joint surface moulds. The study reported that a cable bolt placed across a joint more than doubled shear resistance of shear blocks having both smooth and rough joints.

Testing of the cable bolt in shear using the double embedment assembly (Figure 1) as recommended by the British Standard (BS 7861-2:2009) is an un-realistic approach. Guillotining of the cable tendon, leading to true shearing of the metal elements is not what occurs when a cable bolt is sheared across a rock joint. In reality the past laboratory experiences have shown that the failure of the cable bolt in rock or composite material is a combination of both tensile and shear failure manifested with crushing of the rock or concrete surrounding the zone of the sheared plains, (Craig and Aziz, 2010a, b). These findings were also demonstrated by numerical simulations in both rock bolts (Jalalifar, *et al.*, 2006). Accordingly,

<sup>1</sup> University of Wollongong, NSW, Australia, Email: naj@uow.edu.au, Tel: +61 (0 2) 42 213 449

<sup>2</sup> Hilti Australia, NSW. www.hilti.com

<sup>3</sup> University of Wollongong, NSW, Australia

<sup>4</sup> Hilti Australia, NSW. www.hilti.com

the application of the double shear system for testing cable and rock bolts in concrete moulds is the subject of reporting in this paper.

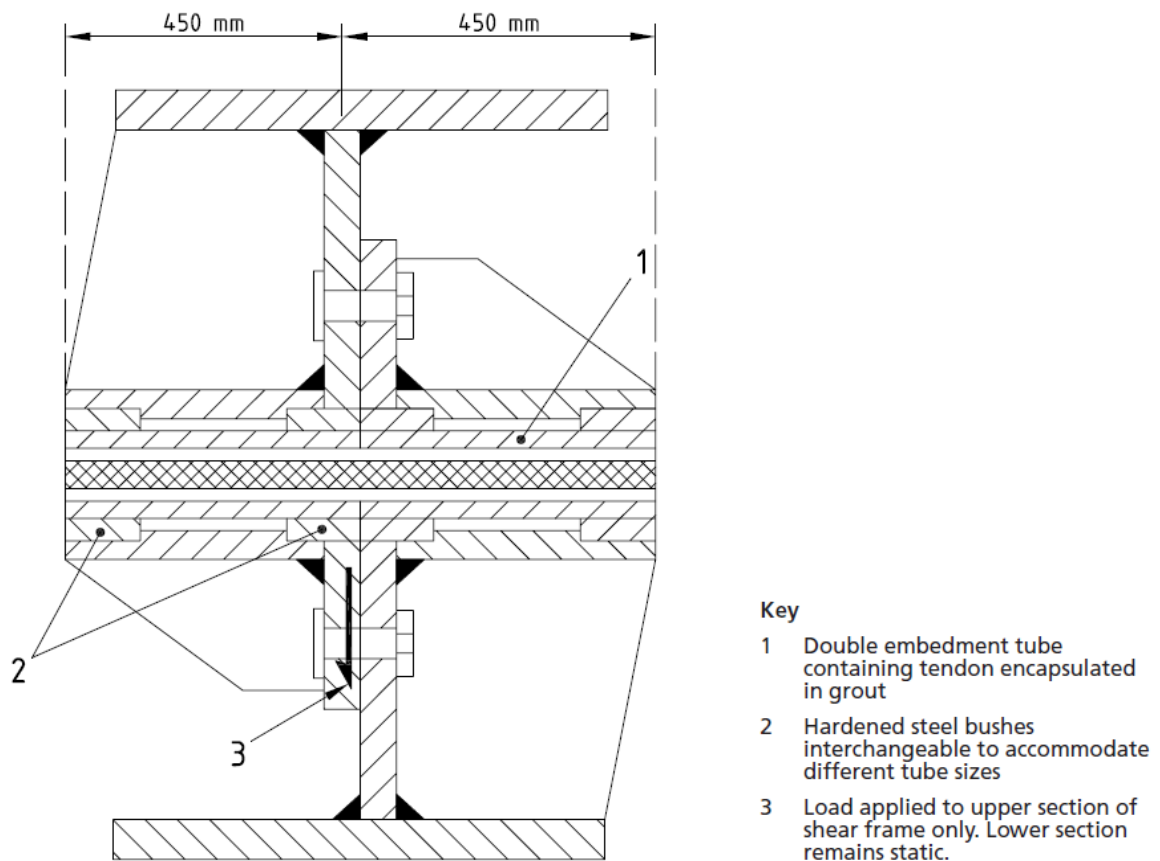


Figure 1 - Sectional diagram of double embedment shear frame (BS 7661-2: 2009)

### CABLE BOLT DESCRIPTION

The tested cable bolts were (a) Hilti 19 wire HTT-UXG plain strand and (b) Hilti 19 wire HTT-IXG spirally indented strand cable bolt, with indentation only on the surface of the outer strands. Both cable bolts were of sealed wire construction type, consisting of an outer 5.5 mm diameter strand layer overlying the middle 3 mm diameter wire strands. Both layers are wrapped around a single solid 7 mm diameter strand wire core. Both Hilti plain and indented cable-bolts shown in Figure 2 (A and B) consisted of 19 strands (9 x9x1) of seal construction wire rope as shown in Figures 2C. The cables were both 22 mm in diameter with the rope thread profiles being "Left Hand Lang's Lay" construction type. The lay length of the strands in both cables was 300 mm. Details of both cables specifications are shown in Table 1.

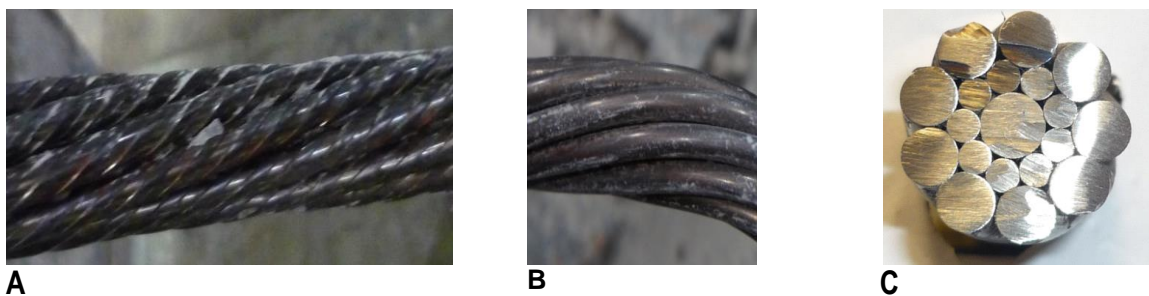


Figure 2 - Hilti 19 wire plain and indented strand cables

## CONCRETE SAMPLES PREPARATION AND CABLE BOLT INSTALLATION

### Concrete block casting

Figure 3 shows a general layout of an assembled double shear apparatus with installed cable bolt. Each double shear testing process required three cement /mortar concrete blocks with two outer 300 mm side cubes and a central rectangular block 450 mm long. The casting of the concrete blocks for the test was carried out in the steel frame of the double shear apparatus. Once mixed, the cement mortar was poured into each section of the 20 mm thick steel frame. A plastic conduit 20 mm in diameter was set through the centre of the mould lengthways to create a hole for cable installation in the concrete blocks. Once the concrete was set, the plastic conduit was removed from the center of the blocks. The center hole was subsequently reamed to a 27/28 mm diameter rifled shaped hole, using twin wing drill bits. The UCS value of the concrete used in this study was 40 MPa, determined from testing the representative 100 mm diameter cylindrical concrete samples.

**Table 1 - specification of Hilti Cable bolts**

Performance data	Hilti HTT-UXG (Plain strand)	Hilti HTT-IXG (Indented strand)
Ultimate yield load	495 kN (50 t)	425 kN (43 t)
Ultimate failure load	573 kN (58 t)	510 kN (52 t)
Bolt Diameter	21.8 mm	21.8 mm
Cross sectional Area	312.9 mm <sup>2</sup>	277 mm <sup>2</sup>
Mass	2.482 kg/m	2.2 kg/m
Outer strand diameter	5.5 mm	5.5 mm
Inner lay strand diameter	3.0mm	3.0 mm
Core strand diameter	7.0 mm	7.0 mm
Hole diameter / Collar Reaming size	28 mm/55 mm	28 mm/55 mm

### Cable bolt installation in concrete blocks

The installation of the cable bolt in a three pieces concrete mould was carried out using Minova FB400 cable bolt grout. The cable bolt was inserted into the central hole of the assembled concrete blocks. A 60 t load cell was then mounted on one side of the protruding cable bolt using a barrel and wedge assembly. This was followed by the addition of the grout injection sleeve/and bolt tensioner assembled on the other side of the assembled double shear box, and was held in place using another barrel and wedge. The cable bolt was pre-tensioned to an axial load of 50 kN by a torque wrench prior to grouting.

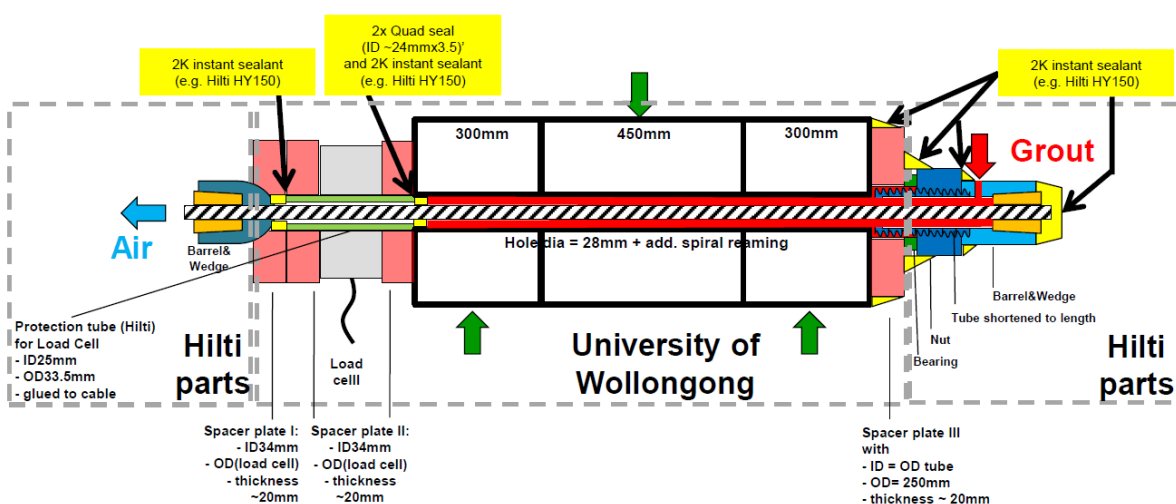


**Figure 3 - A schematic layout of the cable installation assembled in concrete blocks**

Grouting of the cable bolt in concrete was achieved by pumping Orca / Minova FB400 grout into the hole containing the cable bolt using grouting sleeve, and in accordance with the established process of grouting. Quad Seals were used to seal around the cable in the load cell side of the concrete block in order to protect the load cell from being contaminated by the grout. Special grout seals were used to

minimise grout outflow during pressure injection of the grout. Air was allowed to escape from one end of the assembled cable bolt system and along the free cable strand end as grout was pushed through the hole length.

### Testing procedure

The assembled double shear box apparatus was then placed on a carrier base frame consisting of a parallel pair of rail track sections welded to a 35 mm thick steel plate. The whole assembly was mounted between the 600 x 600 mm loading plates of the 500 t compression testing machine as shown in Figure 4. The outer 300 mm side concrete cubes were seated on 75 mm high steel blocks, leaving the central 450 mm long block free to move vertically down during the shearing process. The rate of shearing of the double shear apparatus the middle section was maintained constant at 1 mm/min for the 75 mm of vertical displacement. The rate of loading and displacement was monitored and simultaneously displayed visually on a PC monitor.

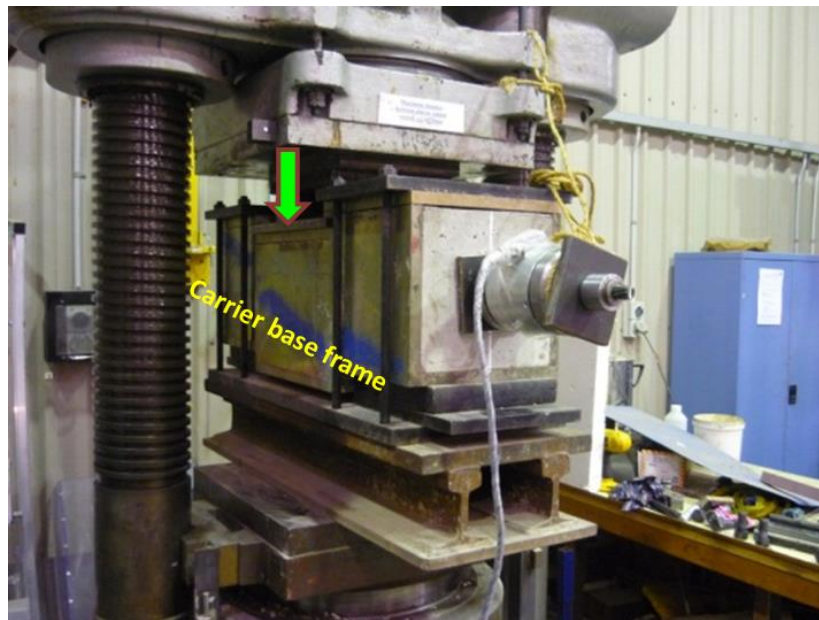


Figure 4 - Double shearing apparatus loaded in 500 t Avery compression testing machine

## RESULTS AND ANALYSIS

### Indented cable bolt

Figure 5 shows the applied shear load and axial load in the cable versus the vertical displacement of the central block of the double shear apparatus with indented cable bolt. The maximum vertical load was 904 kN, which occurred when the vertical travel of the central block reached approximately 52 mm. The maximum axial load developed at the cable bolt was 254 kN.

Various shear load that occurred beyond the vertical displacement of 52 mm were due to individual cable strand failures (strand snap). The relatively larger shear load drop, post the 904 kN maximum load, was likely due to the larger diameter (5.5 mm diameter) outer strand as well as the central core strand failures (7 mm diameter), while small drops are indicative of the small 3 mm diameter strand failure. It is interesting to note that the outer strand failures are also marked by drops in the axial load on the cable bolt, as monitored by the 60 t load cell. The number of visible sudden drops on the load displacement graph appears to be slightly less than the total number of the 19 failed strands. This is clearly evident from Figure 6a of the failed /snapped cable section as retrieved from dismantled blocks. Characteristically, the snapped cable strand ends depict strand failures as a combination of tensile and shear failures, which are what would occur in reality when the cable is sheared in a rock mass. This kind of failure is the result of bending of the cable in the vicinity of the sheared plains where the concrete has crushed for a length of up to around 60 mm from the sheared joint plains as demonstrated in Figure 6 b.

Note that the loading changes A and B shown in Figure 5 are attributed to wedge and barrel settlement / adjustment during the early start of cable bolt loading as the cable bolt begins to take extra axial load due to the central / lateral shear loading.

**Plain strand cable**

Figure 7 shows the load /displacement profiles of the second test carried out on 22 mm diameter Hilti 19 plain strand cable. The plain cable bolt reached a maximum shear load of 1024 kN for the vertical displacement of 75 mm. The maximum generated axial load on the bolt was 400 kN. Similar to the indented strand cable, there was a typical barrel and wedge adjustment axial load drop during the early part of the cable shearing process. This settlement occurred at 502 kN of vertical shear load and at the vertical shear displacement of 25 mm. No strand failure was detected during the shearing process as evident from the post- test dismantled cable bolt shown in Figure 8.

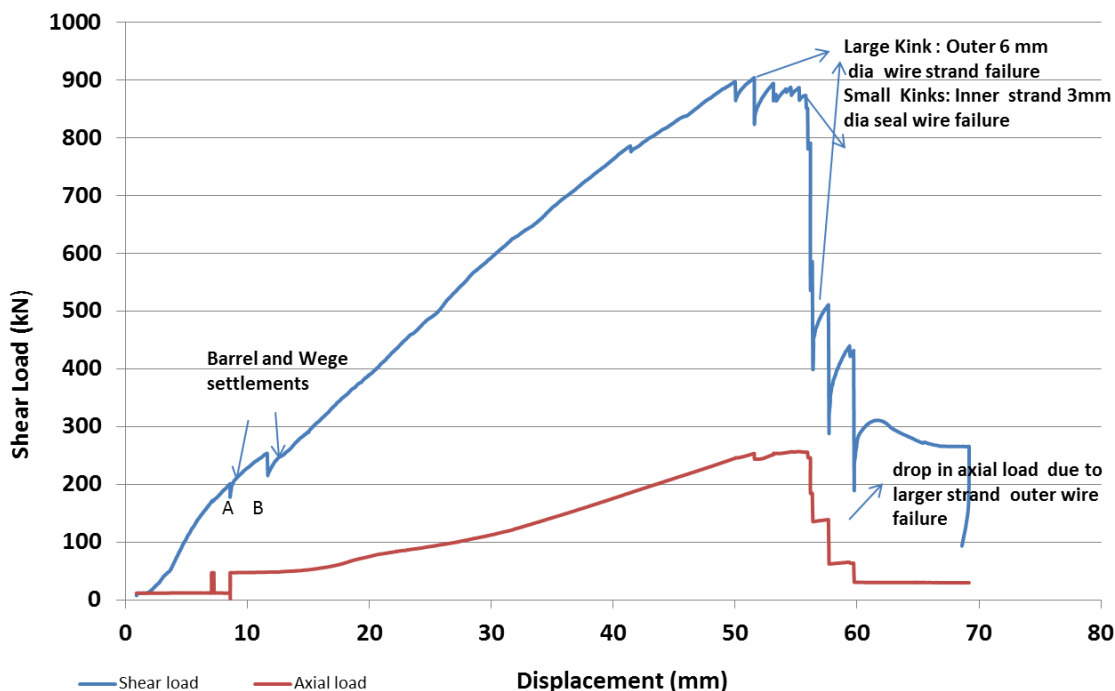


**Figure 5 - Shear load and axial load versus vertical travel of the central block of the loaded double shear apparatus**

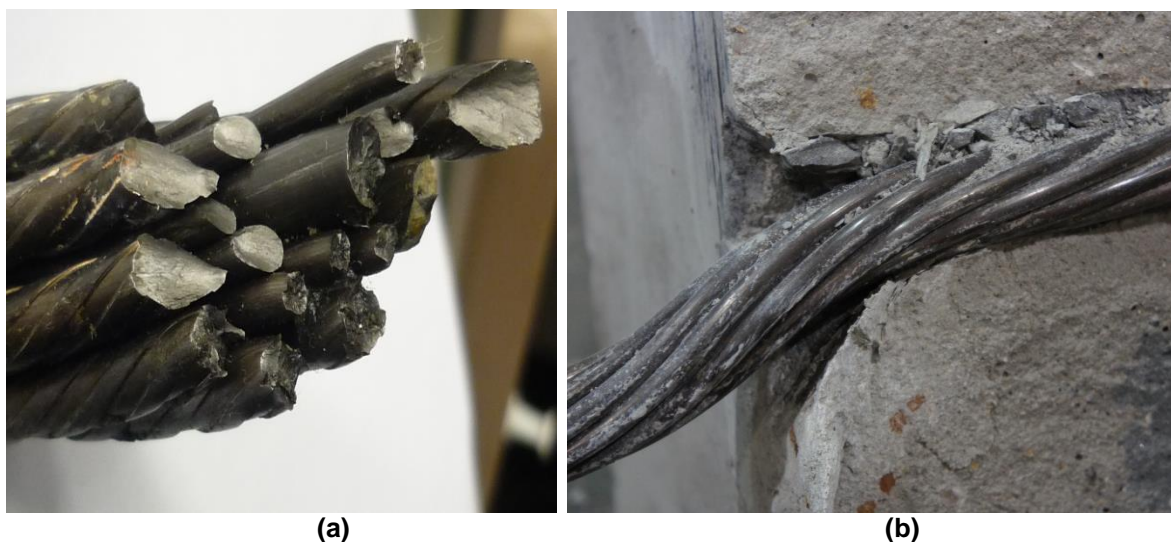


**Figure 6 - (a) failed indented strand cable bolt and (b) concrete deformation around sheared section of the bolt**

The maximum applied shear load on the UX-Strand (plain) cable of 1024 kN for vertical shear displacement of 725 mm was 13.8 % greater than the maximum shear load of 904 kN achieved from the IX strand (indented) cable. As can be seen in Table 1, the ultimate failure load of the UX-strand cable bolt of 495 kN is 70 kN more than the tensile strength of the IX -Strand cable bolt, which is an increase in the ultimate strength of 16.5% in favour of the plain strand cable bolt. Thus, the reduction of 70 kN in the ultimate tensile strength of the indented cable bolt may explain the reason as why the cable failed at much lower shearing load. This reduction in the indented cable strength was subsequently verified by tensile strength testing of cable's individual strands, which resulted in a drop in tensile strength of the indented strand by 10.0 %. Figure 9 shows typical profiles of load - elongation of both 5.5 mm plain and indented strands of cable bolts. The machining of the outer strands to create indentation may have a detrimental bearing on the strand strength, contributing to the reduced tensile and shear strength of the cable bolt. Therefore, it is fair to conclude that the strand manipulation for producing indentation may have affected the ultimate tensile strength of the intended cable bolt, as the overall cross sectional area of the indented cable bolt was reduced 13%. Finally, no cable rotation was observed in either the plain or indented strand cable bolt during the double shearing tests.

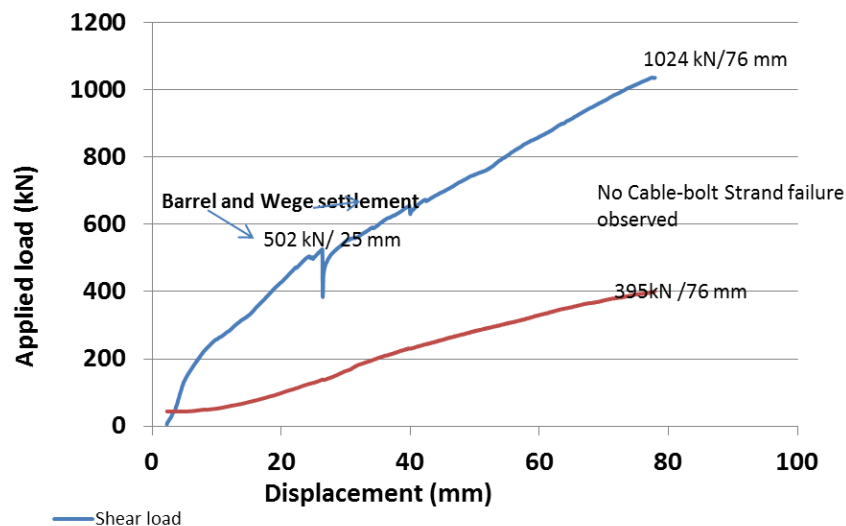


Figure 7 - Shear load and axial load versus vertical travel of the central block of the loaded double shear apparatus



Figure 8 - Post test plain strand cable. No strand failure

## CONCLUSIONS

- The shearing strength of the cable bolt is influenced by the outer strand indentation, with the reduction in shearing strength to around 13.8%. However, the tensile strength failure of the individual strand resulted in a strength reduction of 12.8 %. Thus, indentation of the cable bolt's outer strand weakens the cable bolts tensile and shearing strength.
- All strands of the indented cable bolt failed post peak shear load. No strand failures were observed in the plain strand cable bolt tested in shear.

- All strands of the IX -Strand cable bolt failed in combined tensile and shear as demonstrated by the cup and cone failures of the failed cable section strands.
- The use of the laboratory based double embedment assembly for shear test as recommended by British Standard BS 7961-2 2009 is not a realistic way of evaluating the shear strength of cable bolts *in situ*.
- No cable rotation was detected in double shear testing of either plain or indented cable bolts.

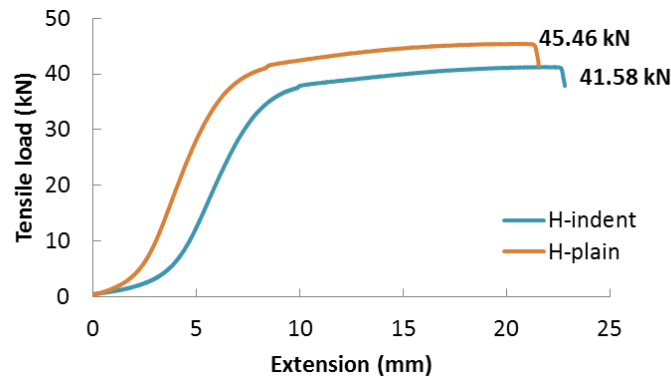


Figure 9 - Tensile load / elongation profiles of both plain and indent 5.5 mm strands of cable bolts

#### ACKNOWLEDGEMENTS

Special thanks to Alan Grant, Cole Devonshire, and Cameron Nielson of the School of Civil, Mining and environmental Engineering, University of Wollongong for their technical support during preparation and testing stages of this study.

#### REFERENCES

- British Standard BS 7861-2, 2009. Strata reinforcement support system components in coal mines Part 2. Specification for flexible systems for roof reinforcement.
- Clifford, B, Kent, Altounjan, P and Bigby, D, 2001. Systems used in coal mining development in long tandom reinforcement. in proceedings, 20<sup>th</sup> International Conference on Ground Control in Mining, Morgantown, WV, August 7-9, pp 235-241.  
<http://icgcm.conferenceacademy.com/papers/detail.aspx?subdomain=icgcm and iid=735>
- Craig, P and Aziz, N, 2010a. Shear testing of 28 mm Hollow Strand "TG" Cable Bolt, in proceedings 10<sup>th</sup> Underground Coal operators Conference, Wollongong, February 11/12, pp171-179.  
<http://ro.uow.edu.au/coal/303/>.
- Craig, P. and Aziz, N, 2010b. Shear testing of 28 mm hollow strand "TG" cable bolt. In proceedings 29th International Conference on Ground Control in Mining, ICGCM (pp. 169-174). (Publication ID=35591) <http://icgcm.conferenceacademy.com/papers/detail.aspx?subdomain=icgcm and iid=273>.
- Goris, J H, Martin, L A and Curtin, R P, 1996. Shear behaviour of cable bolt supports in horizontal, bedded deposits, in proceedings, 15<sup>th</sup> International Conference on Ground Control in Mining, Colorado school of Mines, Golden, Colorado, August 13-15, pp511-521, (Eds Ozdemir, Hanna, Haramy and Peng) <http://icgcm.conferenceacademy.com/papers/detail.aspx?subdomain=icgcm and iid=1098>
- Jalalifar, H., Aziz, N and M, Hadi, 2006. The effect of surface profile, rock strength and pretension load on bending behaviour of fully grouted bolts, *Journal of geotechnical and geological engineering*, Vol 24, pp 1203-1227.
- Tadolini, C S, Tinsly, J and McDonnell, J P, 2012. The next generation of cable bolts for improved ground control, In proceedings 31st International Conference on Ground Control in Mining, ICGCM, 7 p, <http://icgcm.conferenceacademy.com/papers/detail.aspx?subdomain=ICGCM and iid=965>.
- Thomas, R, 2012. The load transfer properties of post groutable cable bolts used in the Australian coal industry, in proceedings, 31<sup>st</sup> International Conference on Ground Control in Mining, Morgantown, WV, August, 10 P.  
<http://icgcm.conferenceacademy.com/papers/detail.aspx?subdomain=ICGCM and iid=1011>.

# SUGGESTED METHODS FOR THE PREPARATION AND TESTING OF VARIOUS PROPERTIES OF RESINS AND GROUTS

**Naj Aziz<sup>1</sup>, Jan Nemcik<sup>1</sup>, Ali Mirzaghobanali<sup>1</sup>, Stephen Foldi<sup>1</sup>, David Joyce<sup>2</sup>, Arash Moslemi<sup>3</sup>, Hooman Ghojavand<sup>1</sup>, Shuqi Ma<sup>1</sup>, Xuwei Li<sup>1</sup> and Haleh Rasekh<sup>1</sup>**

**ABSTRACT:** In the absence of bolting standards for strata reinforcement in the Australian mines, though individual mines or companies have their in house practices, there remains a visible vacuum in assessing credibly the various properties of chemical resins and cementitious grouts. Currently, all methods used in evaluating the mechanical properties of both chemical resins and other bolting reinforcement grouts are dependent on the American, British and South African standards and accordingly there is no uniform and unified methodology of testing. A simplified approach has been discussed to enable mine operators and other interested parties to determine various pertinent properties of chemical resins and grouts in the bolting system only and this paper describes the various methods used to test a set of resin properties. A special Resin Mixing Container (RMC) was developed to permit multiple resin samples to be cast with consistent resin / grout quality. Various conclusions were drawn from the study enabling a better understanding between suppliers and end users.

## INTRODUCTION

There is an increase in the variety of bolting systems used in Australian mines (rebar /cable tendons, chemical resins and cementitious grouts). Rock bolting systems constitute a major mining operation activity, particularly in underground coal mining and therefore a basic knowledge about the load transfer properties of the bolting systems must be clearly understood to enable both the suppliers of the products and end-users to maintain trust in their professional operations.

Australian mining and construction industry consumes around 7.5 m bolts (rebar and cables) annually and the installation of these supporting elements is carried out using chemical resins and cementitious grouts. In general, there are two types of resins in the market today; oil and water based resins and for each class of resin there are variations with respect to the mixing and setting times. Resins also vary in mechanical strength properties. Essentially chemical resins can be tailored to vary with respect to the setting time and curing. Some bolt installations are carried out using twin time setting, consisting of two setting time periods; the upper fast setting time of between 8-24 s, in the upper end of the bolt, and the slower setting time, of up to 90 seconds, with the latter being used in the lower section of the encapsulated bolts. Of course there are much slower resins used as pumpable products for long cable bolt installations.

The strength of the various resins can be related to the chemical composition and fillers and therefore it is useful to determine their various properties prior to use. The existing methods of evaluating various bolting system properties in Australia are still based on the established non-Australian standards, which is raising concern. Testing by double embodiments shearing of bolt in steel tube is unrealistic and therefore not applicable to shear testing of bolt in rock. Also evaluation and determination of various resin properties as specified by the American, British and South African standards guidelines may not be required for carrying out a set of tests that will be adequate for the user to gain an understanding of the strength characteristics of the resin type used. Therefore, the aim of this paper is to provide a simplified approach to determining various resin parameters, to allow both resin suppliers and end-users to make a start in the appreciation of the product availability and potential to ensure use of the correct type of resin for given ground conditions.

<sup>1</sup> School of Civil, Mining and Environmental Engineering, University of Wollongong, NSW, Australia. E-mail: naj@uow.edu.au, Tel: +61 02 42 213 449

<sup>2</sup> Orica Australia, Nowra: E-mail: david.joyce@orica.com

<sup>3</sup> J-Lok Resins Australia Pty Ltd, Smeaton Grange, NSW, 2567, M: 0467216449

## RESIN PROPERTIES EVALUTION

Based on suggested methods by various standards (British standard- BS 7861: Part 1: (1996), American Standards (ASTM- C579) (1991), South African Standard (SANS1534) (2004), and ISRM (International Society of Rock Mechanics (2007)), the evaluation of the resin properties normally include the determination of:

- Uniaxial Compressive Strength (UCS),
- Modulus of Elasticity in compression (E),
- Shear strength, ( $\tau$ ) and
- Creep or Rheological properties.

Both Uniaxial Compressive Strength (UCS) and Young's modulus (E) values were examined at the University of Wollongong laboratory in relation to resin sample shape, size, height to width or diameter ratio (H/D), resin type, resin age and cure time. 40 mm cubes, rectangular prisms of L/D 2:1 and cylindrical specimens of diameters 20, 30, 40 and 50 mm were tested with L/D ratios of 1: 1 and 2: 1. The sample shear strength was determined using the Punch Shear Box testing method.

### Uniaxial compressive strength

Traditionally in Australia resins are tested for the compressive strength using cube/prism or cylinders, H/D of 2:1. The BS 7861- part 1 Annex (M) and part 2 (Annex G) for testing resin grout uses prisms 12.5 mm x 12.5mm x 25 mm in size with respect to the fast and medium resin set time and 50 mm cubes for slow set time. On the other hand the ASTM C579 recommends testing all resins using 40 mm cubes. Opinions vary with respect to the shape and size of the tested resin sample as recommended by the British Standard of resin testing. Generally the manufacturers prefer the UCS values of the resin by testing 40 mm cubes, similar to the recommended methods for testing resin grouts according to ASTM-C579. It is a recognised fact that the strength values obtained by testing cube samples tend to be higher than the UCS values obtained by testing cylindrical samples. Also, the strength values tend to vary significantly, irrespective of the sample shape and size when samples are individually cast. The recent approach in sample preparation in bulk as reported by Aziz, *et al.*, (2013a) and Aziz, *et al.*, (2013b) provided a new methodology of sample casting thus yielding consistent test results.

### Modulus of elasticity

The determination of modulus of elasticity or Young's modulus of the resin as prescribed in BS 7861: part 1: (1996), recommends that a prism of H/D (aspect ratio) of 4 be subjected to a controlled compressive load. The axial and lateral strain to be monitored by four strain gauges mounted on the samples, or by using other means of monitoring the axial and later deformation of the tested sample, such as Linear Variable Differential Transducers (LVDTs), compression testing machines, optical devices or other suitable measuring devices. The tested sample is subjected to cyclic loading and the elastic modulus is the mean of the three-secant moduli measure between two levels of the applied load. This method of calculating the E value, through a recommended method may yield E values, which can be used for homogenous material with fractures, pores (anisotropic) and fissures such as concrete and rock or anisotropic rock. Additional benefit of sample instrumentation will include determination of the Poisson's ratio and modulus of shear, cohesion and angle of internal friction. Using the data from samples tested without instrumentation, the E value can be determined simply from the straight line extrapolation of the 20-60 kN or 40-80 kN range of the load-displacement profile as shown in Figure1. This is an average value of the compression test, which is ideal for materials such as steel with homogeneous and isotropic structure with no voids and irregularities that will cause the sample to squeeze and undergo slight displacement during the early stage of loading.

### Shear strength

Table 1 lists various apparatus used for general testing of rocks and composite material in shear. The testing for shear falls into two categories, direct and indirect methods. All listed methods are applicable for testing resins, but the resin characteristics, time and effort restrict their selection for any particular resin type.

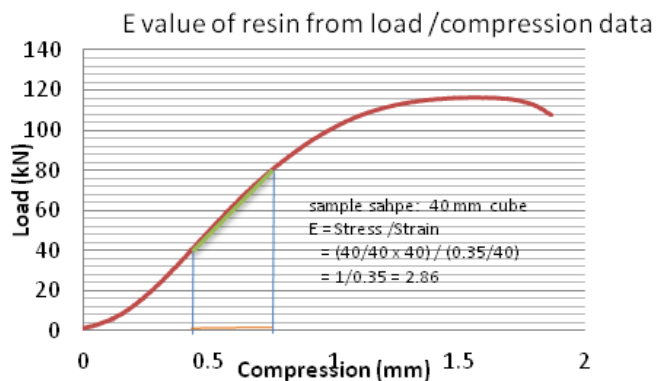


Figure 1 - Determination of E value from load–displacement (compression) testing

Table 1 - Laboratory methods of testing of shear strength of resin and grout

Method	Type	Procedure	Comments	Apparatus
Direct	Direct shear test	Resin sample in plaster or cement and shear the sample to failure peak and residual shear strength	Difficult to match resin strength with the cast medium and testing is a slow process.	
Direct	Single shear	The sample is clamped on the specimen holder and a shear force is applied perpendicular to the curved surface through a sharp edged platen. The shear strength is the force at failure divided by the area of cross-section of the failure surface	Not commonly used	
Indirect	Triaxial test	The specimen is enclosed in an airtight flexible membrane; confining pressure is applied and held constant during the test by means of a cell fluid. Apply axial load/hence stress until the sample fails. Test yields, UCS, Angle of Friction, Shear angle, failure angle	Good method of determining the shear strength of rock/resin; Requires expensive equipment, Difficult to do the test, slow, and time consuming	
Indirect	Double shear test	Lateral shearing of the sample with the samples ends supported. The specimen is sheared along two parallel planes. Shear strength = sheared failure load divided by twice the sample cross section area	Can be used for shear testing of 90 mm long and 30 mm diameter samples. Yields good results but require great quantity of resin samples cast	
Indirect	Punch shear	Shear strength carried out over a very short period of time	Easy to cast discs for testing. Several punch tests can be carried out from one large disk. Allows testing for shear strength over several weeks.	

Punch shear test method is most suited for testing resin. This method of shear strength determination is currently advocated by the South African Standards for testing of resins and grouts (SANS 1534:2004) and has been used by various resin manufacturers. Two methods are used for the preparation of the samples for the test, the 30 mm diameter disc cast in a steel ring and 65 mm discs cast in a polymer mould. Both sample types are 3 mm in thickness as shown in Figure 2. Only one test is possible from a 30 mm disc, while several tests (up to four) can be carried out on 65 mm diameter disc. The diameter of the punch rod is in the order of 12.5 mm, similar to the punch diameter specified in the SANS 1534 standard.

The test is carried out on a disc-shaped specimen at the bottom of a shear box fitted with a hollow slot of the same diameter as the punch. A disc shaped specimen is loaded by a circular punch. The shearing strength is determined using;

$$\tau = \frac{F}{\pi DT}$$

$\tau$  : Shear strength of the tested sample (MPa)

$F$ : Failure load (kN)

$T$ : Disc thickness (mm)

$D$ : Punched disc diameter (mm)

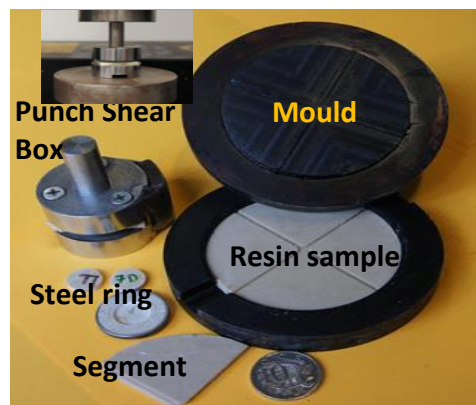
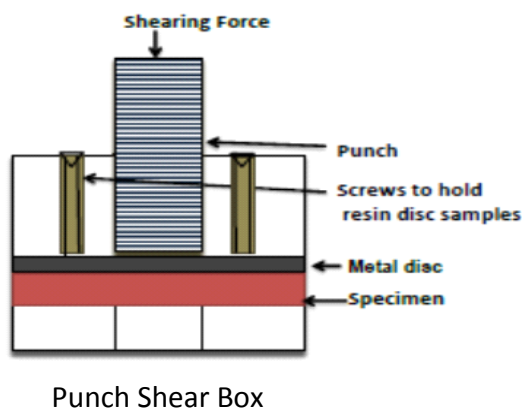


**Figure 2 - Punch shear box and mould for casting 3 mm resin samples**

Based on the experience, the punch shear test appears to be superior to other test methods because of:

1. Ability to prepare a number of samples in a very short period of time and produces a number of samples from a single resin mix with up to four sample segments being obtained from one large 65 mm cast disc. This ensures repetition of the test results for consistency.
2. Requires a small amount of resin preparation for testing, hence mixing time is not a problem.
3. Ability to test fast setting resin.
4. Consistent results for different period of times.
5. Ability to compare the resin shear strength between specifically prepared samples with results of the sections cut from the cylindrical or cube samples. This comparative study has been found to be a good indicator of the quality of the resin cast for various testings.

### Rheological properties (Creep)

The recommended approach to determine resin creep properties is to use BS-7861 (1996). During testing the sample is loaded at a stress rate of  $0.75 \text{ (N/mm}^2\text{)/s} \pm 0.25 \text{ (N/mm}^2\text{)/s}$  to a load of 5 kN for fast set resin or 20 kN for slow set resin and the load is maintained constant for a duration of 15 min. The resin strain is monitored between 0.5 and 15 min. After 15 min, the load is removed completely. The resin creep must not be more than 0.12 %, when the sample is tested 24 hours after casting.

## EXPERIMENTAL STUDY

### Sample preparation

Preparation of competent samples is an important aspect of testing resins and grouts for strength properties evaluation. The consistency of the testing results is dependent on the quality of the cast resin. Chemical resin setting time is the deciding factor in preparing competent and uniform samples. The methodology of sample casting is invariably carried out by preparing resin samples by manually mixing and casting of samples individually, particularly for fast setting resins. This method inevitably leads to less uniform or inconsistent resin grout composition and wider scatter of results. Additional drawback of manual mixing includes the difficulty of removing air bubbles from the sample, unless the sample is mechanically vibrated.

A new approach has been successfully developed for multi-sample casting of resins. The new system enables a relatively large quantity of resin to be mixed mechanically in a cylindrical container using a paint mixer. Powered by a hand held drill, the system can be used to prepare several resin samples from one mix. Both cylindrical and cube/prism samples can be cast. Once it is mixed, the resin is either poured directly into moulds as shown in Figure 3a, or the sample mould(s) are pushed into the MRC as shown in Figure 3b (Aziz, *et al.*, 2013a and 2013b). The set cast samples are then removed individually from the mould by gentle tapping. Alternatively, the whole resin block is first removed from the PVC container outer wall layer, then broken down to release individual sample moulds as shown in Figure 4.



Figure 3a - Mixed resin poured into moulds



Figure 3b - Moulds pushed into MRC

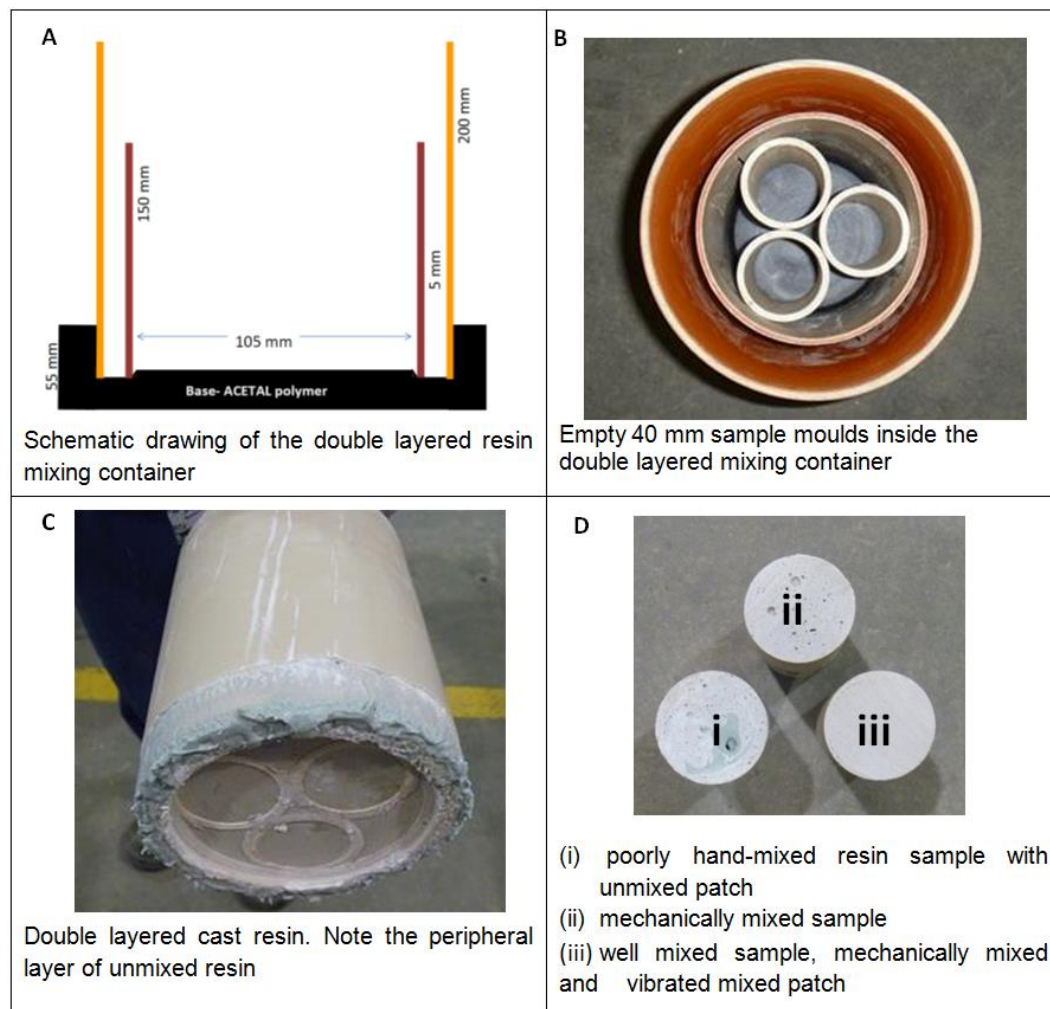


Figure 4 - The process of separating cast samples moulds and removal of individual samples

Both the mixing container and samples mould are lubricated with inert grease prior to use for ease of releasing samples once set. It is worth noting that casting resin samples using cube moulds was possible only by pouring of the resin into sample mould. Irrespective of the sample shape, preparation of the resin samples as described would invariably lead to less uniform cast resin composition resulting in inconsistent and variable strength values. To overcome this deficiency in sample preparation a new mixing container was designed, consisting of a double layered concentric PVC cylinder mounted on a black ACETAL polymer base. The base had a circular groove at the outer periphery to accommodate the concentric walls as shown in Figure 5. The outer 200 mm long concentric PVC cylindrical layer is 140 mm in diameter, while the inner 110 mm diameter PVC cylinder is 150 mm long. There is a gap of 5 mm between the concentric walls of the RMC, where the layer of the poorly-mixed resin accumulates, thus the inner circular PVC separates the well mixed resin from the poorly mixed outer layer. The occurrence of badly mixed layer between the RMC walls is clearly evident in Figure 5D. A slit in the sides of both layers allows the set resin easier to remove with minimum chance of damaging the mould.

In casting samples the resin mastic and hardener are fully mixed in the empty RMC and the sample casting moulds arranged in the inner cylinder are then pushed down into the mixed resin in the RMC. A 5 mm thick plastic circular disc 100 mm in diameter, with 10 mm tapered holes, is pressed over the resin cast moulds to permit excess resin to be forced out of the mould for easy sample-ends preparation. Once the samples have set in the predetermined time, the set resin is removed from the main inner mould holder and the cast samples released from each individual moulds as shown in Figure 4. For casting cube samples the mould can also be used for resin mixing. The mixed resin is then poured into cubes / prisms as shown in Figure 6. Normally the cube size is 40 mm<sup>3</sup>. Irrespective of the sample shape and size, the quality of the cast samples can be improved with proper vibration to remove trapped air bubbles and seal any remaining voids.

In compliance with the established standard requirements for sample end smoothness, the cylindrical samples have ends cut perpendicular to the sample axis and then subsequently lapped prior to testing.



**Figure 5 - Double layered container for mixing chemical resin mechanically and variations in resin quality due to differing mixing techniques**

### Uniaxial compressive strength

A total of 100 chemical resin samples of various shapes, sizes, set time, cure time and age as described previously were tested for UCS values. Figure 7 shows the load displacement profiles of various shaped samples prepared from the same set time resin (90 sec gel time resin and catalyst removed from a capsule)). The samples tested were prepared from Orica resin mastic and hardener (catalyst) scraped from the mine supplied sheathed capsules, as part of the overall ACARP project investigation C21011). Figure 8 shows bar charts of the variation in average UCS values with changing sample shape and size of one day old cast samples. It is obvious the UCS values determined from various shaped samples differed with respect to the sample shape and size and load to height /diameter (H/D) ratios. Typically

the UCS values were highest for 40 mm cubes and lowest for 40 mm diameter cylindrical samples with H/D ratio of two. The quality and repeatability of the tested samples are evident from Figure 9.

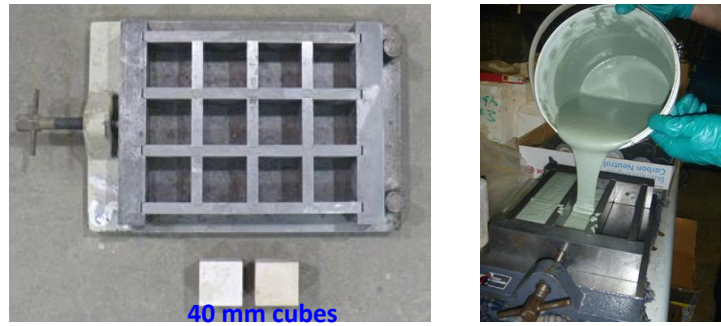


Figure 6 - Casting cube samples in cubical mould

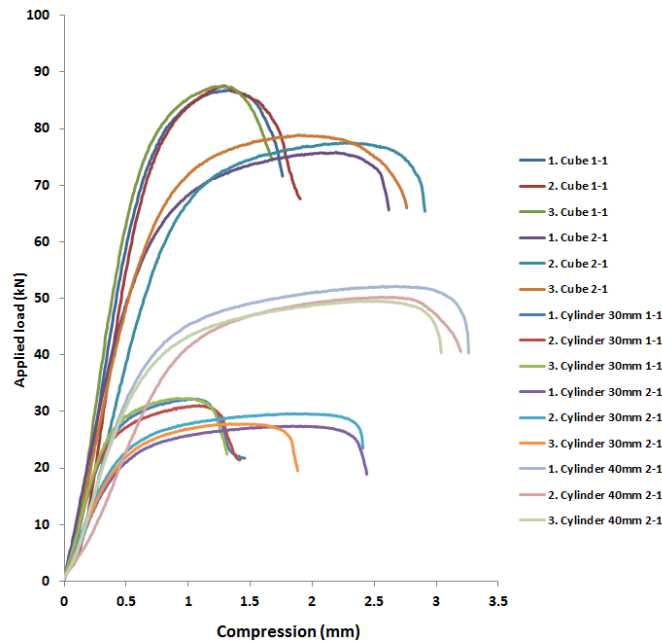


Figure 7 - Load /displacement profiles of various shaped samples prepared from the same set time resin

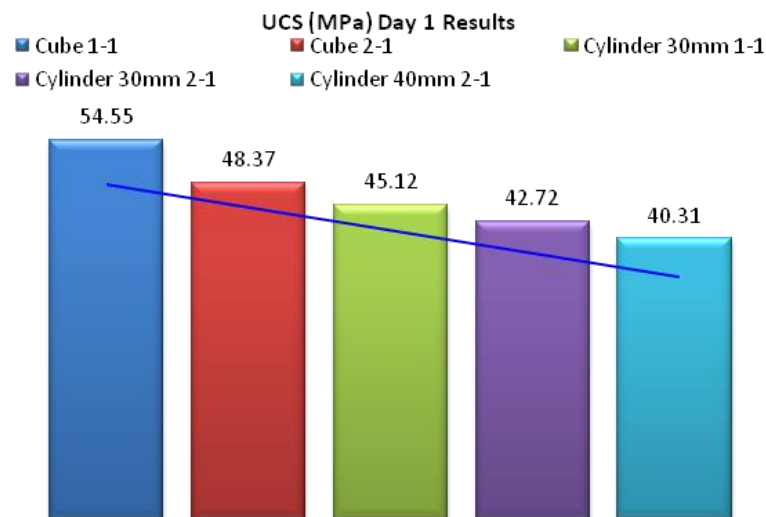


Figure 8 - Bar charts of the variation in UCS values with changing sample shape and size for one day old cast samples

The ratio between cube strength and cylinder strength varied and could be between 1.10 to 1.30. The high cube UCS value is attributed to friction between the platens of the compression machine and the specimen ends creating much more confinement (triaxial compression) than cylindrical specimens of the H/D ratio 2 and greater. The comparatively high values for cubes compared to cylinders are also the case with cementitious grouts (Minders, *et al.*, 2002). Figure 10 shows the changes in resin strength with cure time, which is expected. Figure 11 shows the variation in resin strength with respect to sample H/D ratio for cylindrical samples. As expected, the strength of the sample is influenced by the sample size and this is similar to rocks and cement grouts (Neville, 2009; Minders, *et al.*, 2002). The comparison between freshly and stored resin for various curing time is shown in Figure 12. It is observed that a higher uniaxial compressive strength is attained by using fresh resin in comparison to stored resin. It is evidently clear that the strength values of the resin used in bolt encapsulation is influenced by the above mentioned factors and in particular the shape and size of the samples used. Universality of the samples shape and size is thus an issue which requires addressing.

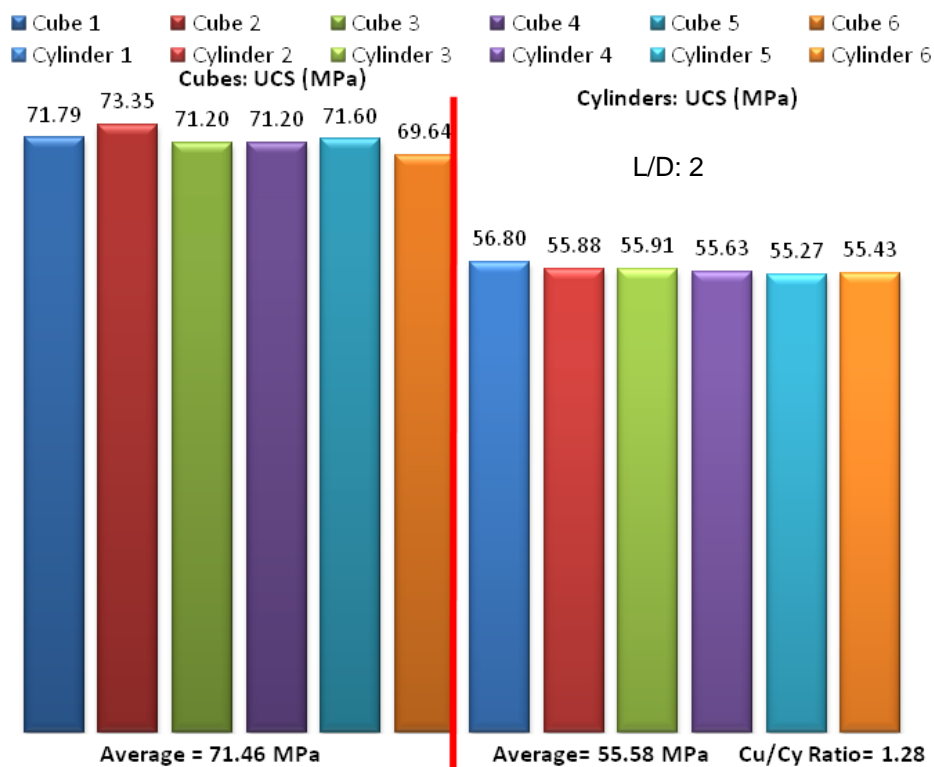


Figure 9 - Variations in UCS values between cube and cylinder resin samples (Orica slow setting resin (90 secs setting time). Note the consistency of the test results

**Modulus of elasticity**

Three methods, namely 40 kN range, tangent and secant modulus were used to make a comparative study. The use of 40 mm cube samples simplifies the determination of E value as the value of E for the 40 kN load range will be equivalent to the sample compression. However the calculated value from this approach is markedly outside the values obtained from other more credited methods.

Figure 13 shows the comparison between the E-values obtained through different ways for resin samples with various curing time ranging from 7 to 21 days. The E-values determined by the 40 kN range (manufacturers recommended) are generally higher than those obtained from ISRM recommended methods such as tangent and secant modulus for various curing intervals. Also, the E-values increased as the resin sample curing time increased from 7 to 21 days.

Figure 14 compares the E-values determined from the strained gauged samples and specimens without strain gauges. It is observed that the data extracted from strained gauged samples provide higher Elastic modulus when compared to samples without strain gauges. It should be noted that the E values obtained using strain gauges are restricted to the middle section of the tested sample and not the entire

length of the sample under compression, hence the variation in E values reflects on the condition of testing and is in line with various test standards indicated previously.

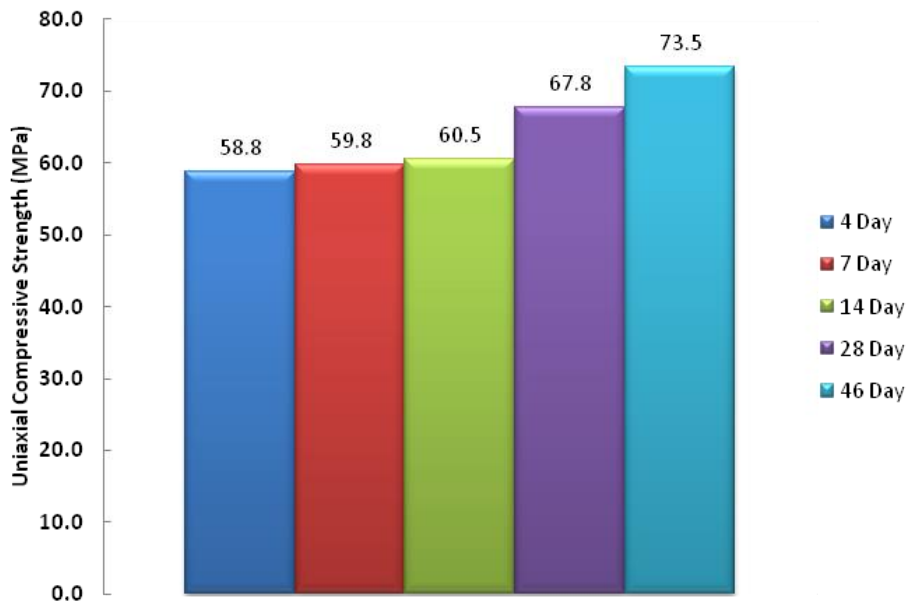


Figure 10 - Variation in resin strength with sample cure time for 30 mm diameter 2:1 ratio cylinder samples

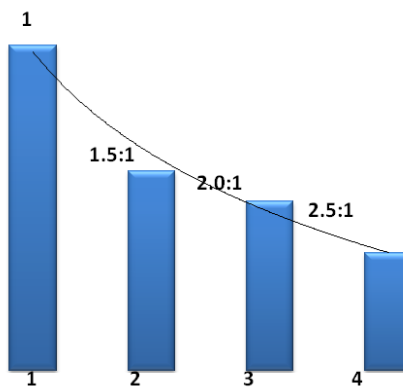


Figure 11 - Variation in UCS values with respect to sample height / diameter (H/D) for slow setting resin cylindrical samples

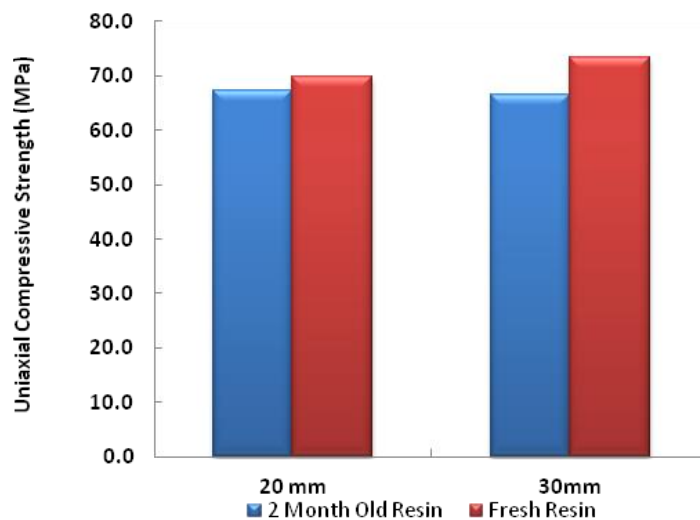
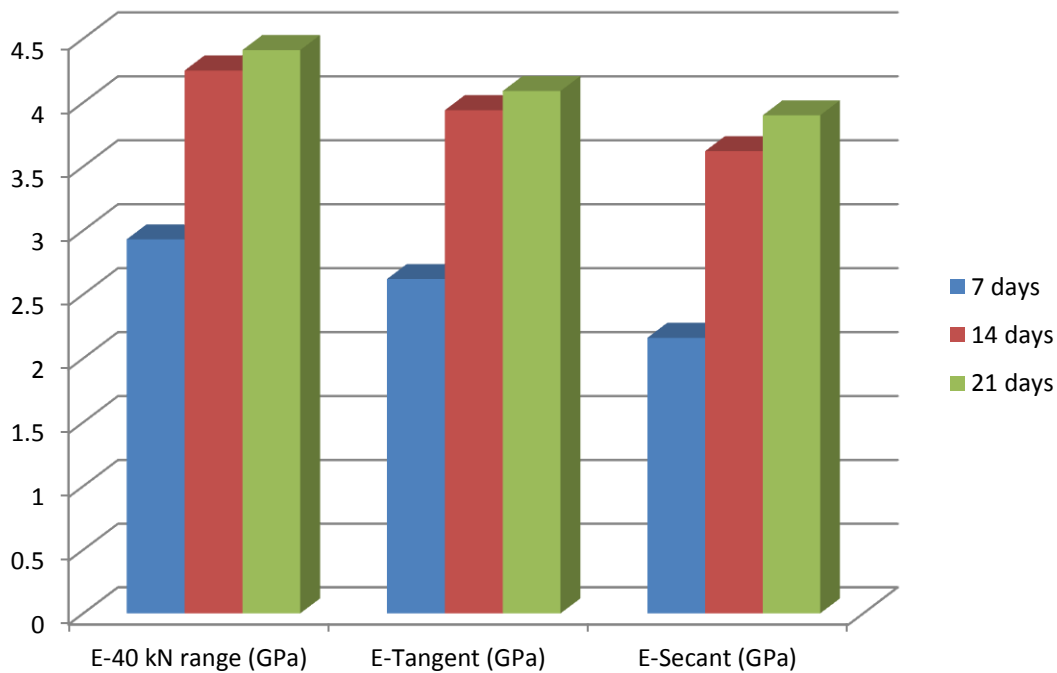
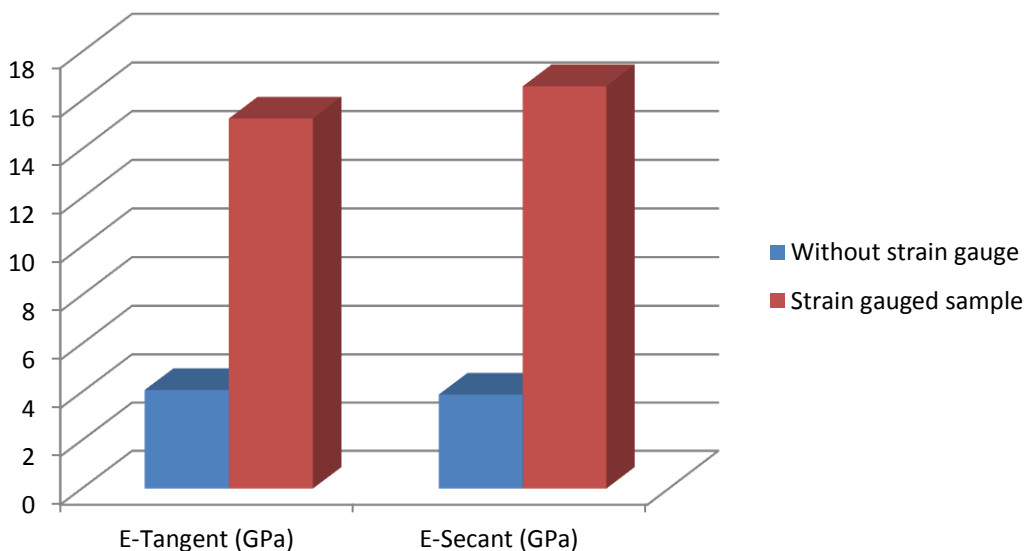


Figure 12 - Variation in resin UCS values between new supplied and stored (old) resins, for both 20 mm and 30 mm diameter samples, L/D=2



**Figure 13 - Comparison between the E-values obtained through different ways for resin samples with various curing time ranging from 7 to 21 days**



**Figure 14 - Comparison between the E-values determined from the strain gauged samples and specimens without strain gauges**

The comparison between the E- values of cubic and cylindrical samples for different curing time is shown in Figure 15. It is concluded that the cubic samples exhibit higher elastic modulus values in comparison to cylindrical specimens various curing time. However, this aspect involves further study.

**Punch shear test results**

Using the punch shear box shown in Figure 2 a series of punch shear tests were undertaken to study the shear strength of a particular resin. Each 65 mm diameter, 3 mm thick disc was cast using the new resin casting mould shown in Figure 2. Four shear tests were obtained from each disc cast. Table 2 shows typical results of punch tests carried out on several segments of one disc sample of the Orica fast setting resin, which is scraped from the resin capsules supplied to a designated mine. A number of tests from a single or several large samples prepared using the newly designed casting moulds demonstrated

the ease with which several tests can be carried out over a short time and with consistency of the results. Figure 16 shows the bar chart of variations in the average values, indicating the increase in average shear values with sample cure time, similar to UCS values. Figure 17 shows the variation of shear strength values between Mix and Pour and scraped slow setting resins respectively.

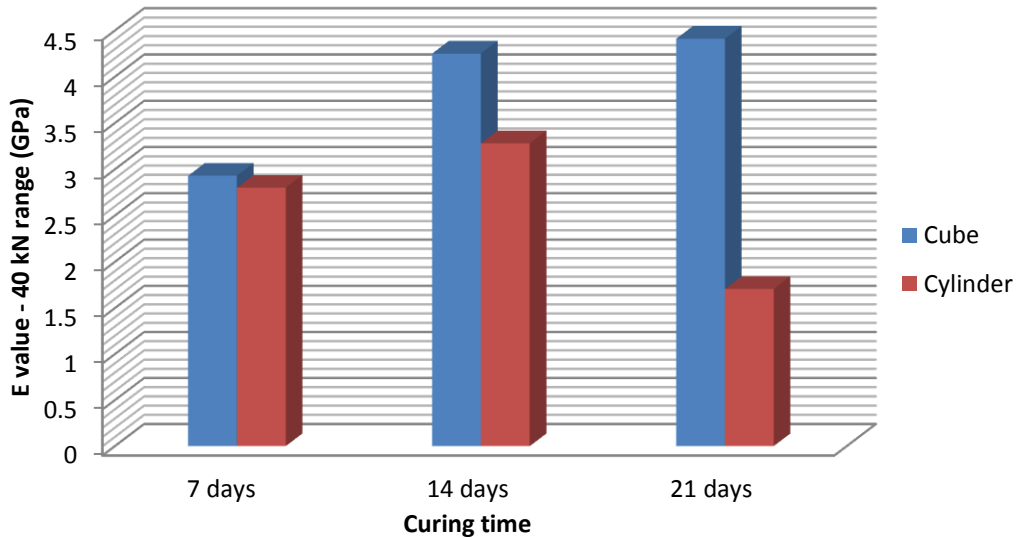


Figure 15 - Comparison between the E- values of cubic and cylindrical samples for different curing time

Table 2 - Shear strength values of resin samples tested using punch shear test. The test results are with respect to the samples cure time of 1, 7 and 14 days

	<i>MN</i>	<i>T (m)</i>	<i>D (m)</i>	$\pi$	$\tau$ (MPa)
<b>1 Day Samples</b>					
A	0.003493	0.00325	0.01258	3.142	27.1912
B	0.003455	0.00351	0.01266	3.142	24.74577
C	0.003408	0.0036	0.01264	3.142	23.83657
D	0.003706	0.00339	0.01256	3.142	27.70192
E	0.003192	0.00337	0.01261	3.142	23.90626
F	0.003493	0.00338	0.01256	3.142	26.18702
				Average	25.59479

	<i>MN</i>	<i>T (m)</i>	<i>D (m)</i>	$\pi$	$\tau$ (MPa)
<b>7 Day Samples</b>					
A	0.003983	0.00328	0.01255	3.142	30.79545
B	0.004337	0.00343	0.0126	3.142	31.9388
C	0.003447	0.0034	0.0126	3.142	25.60859
D	0.004387	0.00339	0.01264	3.142	32.58477
F	0.003821	0.00366	0.01262	3.142	26.32876
				Average	27.66446

	<i>MN</i>	<i>T (m)</i>	<i>D (m)</i>	$\pi$	$\tau$ (MPa)
<b>14 Day Samples</b>					
A	0.004148	0.0033	0.01261	3.142	31.72514
B	0.004652	0.0034	0.01264	3.142	34.45145
C	0.005442	0.00409	0.01256	3.142	33.71626
D	0.004138	0.00338	0.01263	3.142	30.85065
E	0.00344	0.0032	0.01257	3.142	27.21868
F	0.004091	0.00388	0.01254	3.142	26.76049
				Average	30.78711

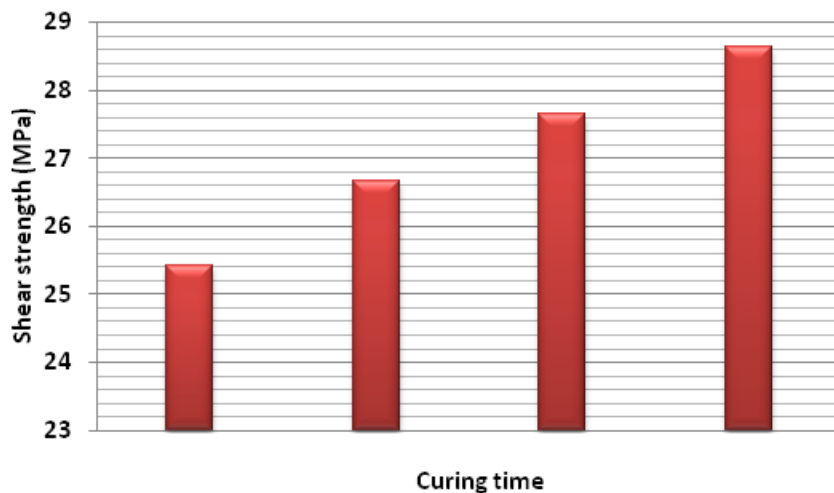


Figure 16 - Average shear strength values for various cast samples cure time

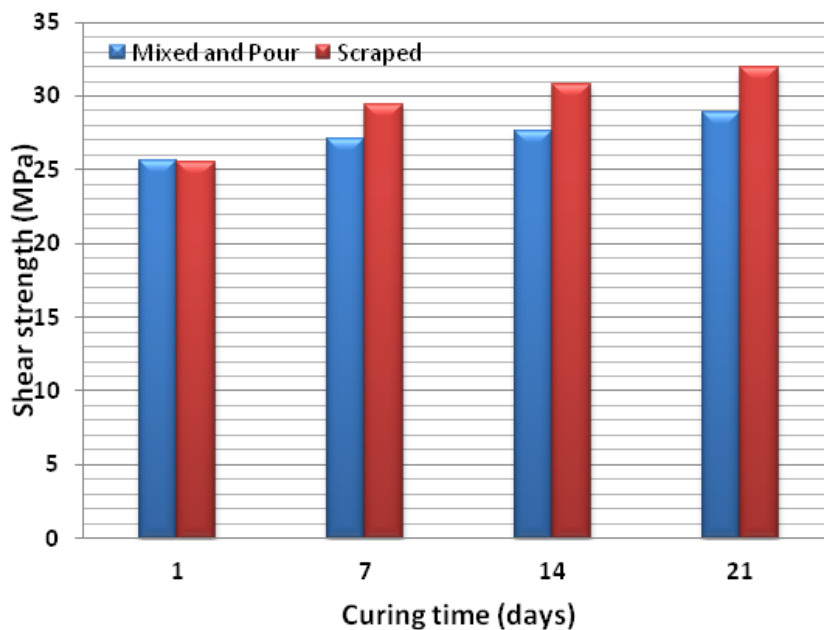


Figure 17 - Variation in resin shear strength values between new supplied and scraped resins for various curing periods

**Creep tests**

No creep tests have been carried out at this stage and will be the subject of study as part of the resin mechanical strength properties study programme for an ACARP report.

**DISCUSSION**

Cube tests are used as the normal compression test of resin and cementitious grouts in Great Britain, in Germany and in some other parts of Europe. The British standard (BS 7861-Part 1:1996) now favours 50 mm cubes for slow setting resins and much smaller sizes for fast setting resins. Similarly ASTM-C759 uses cubes and only South African standard (SANS1534) uses cylinders of H/D ratio of 2:1. In Australia the two major resin suppliers used different shapes and it was not until recently that the use of 40 mm cube has prevailed. With current methodology of resin mixing that is being described in this paper and previously by Aziz, *et al.*, (2013a), the consistency of test results for the determination of the UCS and E values and other properties can be achievable for both cube and cylindrical samples.

Normally the cube is tested at right angles to the position at which are cast; this means that the faces of the cube in contact with the bearing platens are cast against the sides of a rigid steel mould, which is an advantage.

Also the relation between the directions as cast and as tested has, however, no influence on the results since resin grout does not segregate when vibrated. Similarly, the direction away from as cast has shown not to affect appreciably the strength of cubes made with unsegregated and homogenous concrete and grouts as reported by Neville (1969). It should be remembered that the stress distribution in any compression test is such that the test is only a comparative one and the strength values obtained is dependent of the shape and size of the tested sample. The main drawback of the cube test is that the friction between the platens of the compression machine and the specimen ends creates much more confinement (triaxial compression) than cylindrical specimen of the H/D ratio of two and greater. This leads to higher strength values when measured on cubes rather than cylinders as demonstrated with the test results shown in Figures 7, 8 and 9 respectively. The ratio between cube strength and cylinder strength as tested ranges between 1.1 to 1.3. The decision on deciding whether to use cubes or cylinders for evaluating strength properties of a chemical resin relies on the following:

- How easily and consistently resin samples can be prepared and tested with a minimum of effort and extra preparation after casting, identification of the factors that contribute to the simplicity of the sample preparation and testing,
- Recognising that the UCS values obtained from testing samples will yield a relative strength and not true strength,
- Cylindrical sample ends invariably require machining to ensure the ends are smooth and perpendicular to the sample axis. Hence, labour and additional equipment for sample end preparation are required.
- The current practice adopted by the resin manufacturers, which in general use cubes is that the adoption of cubes is internationally recognised by various mining companies.

Given that the current methodology of preparation of resin mixes in bulk as described in this paper, which allow multiple samples to be readily cast irrespective of the sample shape, it is thus propitious and advantageous to use cubes, as cube samples can be easily prepared and tested without additional effort. It is thus become easier for the mine operators and other professionals that may not have access to additional sample end preparation facilities to readily conduct strength property tests. This will enable the product suppliers and end users to maintain trust and avoid unnecessary delays.

## CONCLUSIONS

The study of the suggested methods of composite material preparation and testing for strength has led to the following conclusions:

- The methodology of resin mixing and sample casting is an important aspect of evaluating the strength properties of resin. The new double wall container for mixing resin provides a practical way of thorough mixing of mastic and catalyst enabling casting of samples with minimum of unmixed patches and air bubbles.
- Cubes are the ideal and practical way of sample casting and testing as they require a minimum of time and effort of sample ends preparation after casting.
- The determination of the modulus of elasticity can best be determined by using 40 mm x 40 mm x 80 mm prisms ( H/D :2) instrumented with strain gauges. This approach will also allow the determination of Poisson's ratio, cohesion, angle of internal friction and others to be determined for analytical modelling studies for effective strata load transfer mechanism studies.
- The punch shear box test is an easy, economical and fast method of determining the shear strength of the resin. The use of 3 mm thick, large size (65 mm in diameter) sample discs enables multiple samples to be tested for repeatability and for test quality assurance. The use of vibrator during resin casting helps to produce homogeneous composition resin mix.
- More studies are currently undertaken been to examine the creep properties of the cast resin.

---

## ACKNOWLEDGEMENTS

The research project has been funded by the Australian Coal Association Research Program (ACARP), project C21011. Thanks to Orica in providing resins and on resins usage and preparation of the cast samples. Special thanks are accorded to the University of Wollongong and Faculty of Engineering for providing excellent facilities to enable the research team to undertake laboratory studies of the project. In particular the team are indebted to Alan Grant, Colin Devenish, Cameron Nielson, School of Civil, Mining and environmental Engineering and Stuart Rodd, School of Mechanical, material and mechatronics for their invaluable help.

## REFERENCES

- American Standard for Testing Materials (ASTM. C-759), 1991. Standard test method for compressive strength of chemical –resistant mortar, grouts, monolithic surfacings and polymer concretes.
- The British Standard BS 7861-1, 1996. Strata Reinforcement support system components used in Coal Mines-Part 1. Specification for rock bolting and Part 2: Specification for Flexible systems for roof reinforcement,
- South African Standard SANS1534, 2004. Resin capsules for use with tendon based support systems, published by Standards South Africa.
- International Society of Rock Mechanics, 1979. Suggested methods for determining the uniaxial compressive strength and deformability of rock materials, *Int. J. Rock Mech.Min. Sci. and Geomechanics Abstract*, 16:135-40.
- Aziz, N, Hillyer, J, Joyce, D, Shuqi Ma, Nemcik, J and Moslemi, A, 2013a. New approach to resin sample preparation for strength testing, on Proceedings, *4<sup>th</sup> Underground Coal Operators Conference, Coal 2013, February 14-15,Wollongong*, (eds: N. Aziz and Kininmonth), pp152-155. <http://ro.uow.edu.au/coal/449/>.
- Aziz, N, Namcik, J, Ren, T, Peter Craig and Hawker, R, 2013b. Development of new testing procedure for the assessment of resin performance for improved encapsulated roof bolt installation in coal mines, ACARP C21011, Part 1, September, 58 p.
- Hillyer, J, 2012. Influence of installation method and resin properties on rock bolt performance in underground coal mines. Undergraduate thesis, UOW, 110p.
- Minders, S, Young, J F, and Darwin D, 2002. Concrete, second Edition, ISBN 0130646326.
- Neville, Am, 2011. Properties of concrete, 2<sup>nd</sup> edition, published by Pitman, London, 686 p.

---

# NEXT GENERATION TECHNOLOGY FOR CORROSION PROTECTION IN GROUND SUPPORT ELEMENTS

David William Evans

**ABSTRACT:** Corrosion in ground support elements remains an important area for industry focus, given the immediate concern for mine safety and operational efficiencies, as well as the hidden cost of longer term rehabilitation work. This paper discusses emerging 'next generation' technology within the field of corrosion protection, providing new solutions for specific application areas of ground support product design.

Traditionally, anti-corrosion strategies have predominantly focussed upon Hot Dip Galvanising as a common industry solution. However, now complimenting this traditional solution, the more recent technology of Thermal Diffusion Galvanising is gaining interest within the Australian market, providing commercially viable solutions for a number of specific application areas that Hot Dip Galvanising cannot address.

Thermal Diffusion Galvanising is an alternative zinc based technology, which offers equivalent cathodic protection to that of Hot Dip Galvanising. Thermal Diffusion Galvanising has a comparatively deeper metallurgical bond to the steel substrate through various zinc-iron alloy layers, offering both increased adhesion and greater surface hardness. Beyond the capabilities of Hot Dip Galvanising, Thermal Diffusion Galvanising has specific applications of interest in high tensile steel grades, coating thickness consistency for threadforms, excellent torque / tension performance and greater flexibility with deformation. Thermal Diffusion Galvanising also continues to provide spark reduction properties on friction contact.

This paper provides a technical overview of the attributes of Thermal Diffusion Galvanising and its relative performance compared to that of Hot Dip Galvanising. Application of Thermal Diffusion Galvanising to ground support elements is then reviewed, relating the new technology to specific product design areas and field applications.

## INTRODUCTION

Ground support failure due to corrosion mechanisms is a well-known and documented phenomenon within the mining industry globally (Villaescusa, *et al.*, 2007). Earlier efforts have been made to document the prevalence of ground collapse due to corrosive mechanisms (Potvin, *et al.*, 2001), however, it is anecdotally claimed that current industry performance more reflects the effectiveness of rehabilitation efforts, rather than actual improvements in corrosion protection technology. While specific mines will have an understanding of their strata conditions and rehabilitation needs, from an industry perspective, the impact of corrosion in ground support tends to remain a hidden cost.

As such, corrosion protection continues as an important focus area in underground roof support. Technologies are now evolving that offer new solutions within this field. Specifically, Thermal Diffusion Galvanising (TDG) is an area of technology that holds increasing interest, providing a growing number of niche solutions for strata control products. While TDG is actually a maturing technology (ASTM International, 2008) (British Standards Institution, 2003) (Roads and Maritime Services, 2012a) (Roads and Maritime Services, 2012b), specific mining industry knowledge is currently in its early stages, with further potential to explore applications in this area.

This paper provides a technical introduction to TDG, including an overview of its various properties and performance. This coating technology is then related to recently developed product applications, with the system now being applied to meet the specific demands of corrosion protection in mine site strata control.

## THERMAL DIFFUSION GALVANISING

### Process history

TDG derives its technical origins from within Sherardising, also referred to as Diffusion Galvanising. The process was originally developed by the British metallurgist Sherard Cowper-Coles in 1901, based upon heating powdered zinc metal within the presence of the targeted host material and within the confines of an enclosed atmosphere (Figure 1). The zinc atoms diffuse into the surface structure of the host material, creating a specific sequence of alloyed zinc-iron layers. While the original application systems were complex and expensive, the technology has since evolved into a number of commercially viable industrial applications. TDG is the most current modern format of this technology, employing more advanced powder technologies and post application or 'top coat' treatments to provide enhanced corrosion protection performance.

Similar to sherardising, TDG involves tumbling componentry within a cylindrical drum, placed under a slow, constant axial rotation within a heated kiln. Zinc rich powders and other filler media are pre-dosed into the drum along with the targeted host material, which is then sealed to provide an air tight internal atmosphere. The zinc atoms sublime, or vaporise on the substrate surface just below their melting temperature and progressively diffuse into the targeted host material. The kiln temperature is generally around 400°C and does not exceed the melting point of zinc. The combination of constant diffusion and drum rotation results in surface coating thicknesses that are consistent and evenly applied. Controlled parameters include the constituency of the zinc powders, the dosage quantity, the applied temperature cycles and rotation time. As such, coating thickness can be readily calibrated to suit finer product geometries as well as the grade of the targeted material.

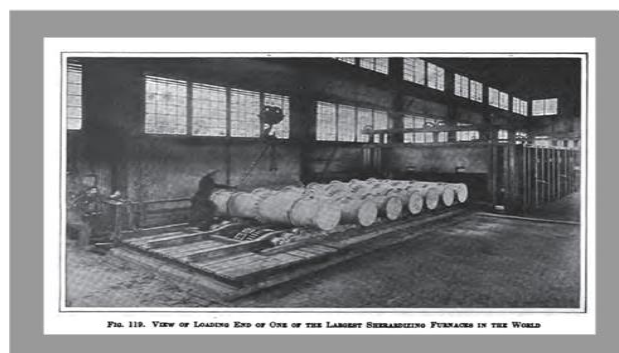


**Figure 1 - An image of an original sherardising plant, circa 1916, with processing drums and kiln visible**

Beyond the capability of earlier Sherardising processes, modern TDG consumes less zinc input, permitted by improved diffusion efficiencies. The new powder technologies can be applied at lower kiln temperatures, reducing energy requirements. Coating thicknesses can be controlled through a greater range, from 20 to 120 microns, an improvement from the original 15 to 35 microns. The new technology has been used to coat products up to 12 metres in length, rather than small batch items only, as shown in Figure 2.



**Figure 2 - A modern thermal diffusion galvanising plant, capable of handling products up to 12 metres in length**

### Technical characteristics

Both Hot Dip Galvanising (HDG) and TDG result in a specific sequence of metallurgical layers that are bonded with the host material. However, there are a number of differences in the resultant chemistries between the two galvanising methods, which produce different physical attributes.

A typical microscopic cross section for HDG is shown in Figure 3. At the surface is the Eta layer, which contains pure Zinc (Zn) and no iron alloys. The second layer is the Zeta alloy layer, containing up to 6% Iron in the form of  $\text{FeZn}_{13}$  molecules. The third layer is the Delta alloy layer, containing 7 – 11 % Iron in the form of  $\text{FeZn}_7$  molecules. The fourth layer is the thin Gamma alloy layer, at 21 – 28 % Iron - this is a solid solution of Fe and Zn atoms about 1 micron thick. The entire coating thickness is approximately 125 microns and the base steel is visible below the Gamma alloy layer. The zinc / iron alloy layers comprise 60 to 70 % of the coating.

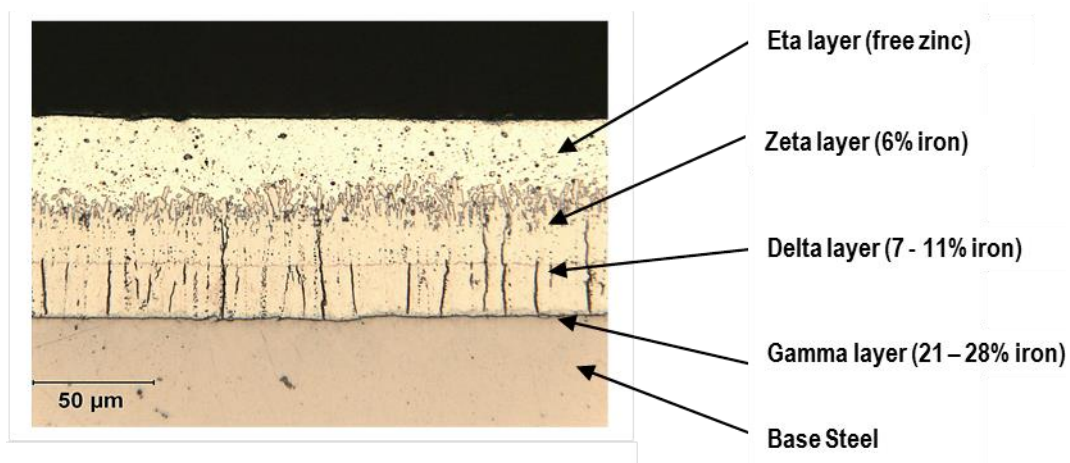


**Figure 3 - A typical hot dip galvanized coating microstructure on structural steel (Industrial Galvanizers, 2006)**

TDG is the only other coating where the zinc alloys with the iron in the steel substrate and forms the same three alloy layers as HDG, as shown in the micrograph of Figure 4. The predominant difference is the greater concentration of iron across the various alloy layers. There is no Eta or free Zinc layer – the first layer is actually the Zeta alloy layer with 7 – 10% Iron content in the form of  $\text{FeZn}_7$  molecules. The second layer is the Delta alloy layer with 25% Iron content in the form of  $\text{Fe}_{11}\text{Zn}_{40}$  molecules. The third layer is the Zn/Fe solid solution Gamma layer with 50% Iron content.

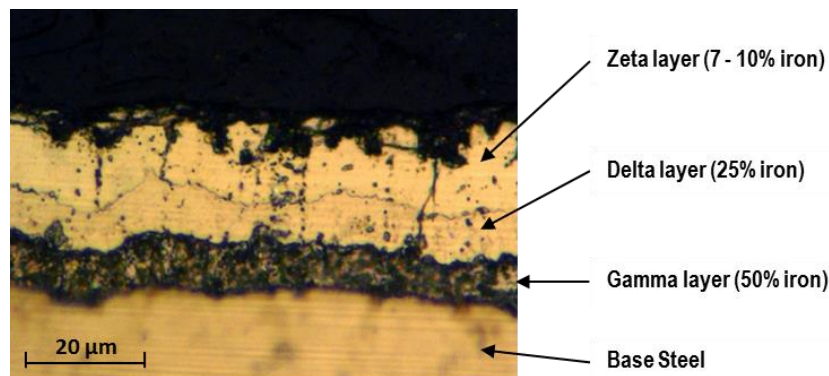


**Figure 4 - A typical thermal diffusion galvanized microstructure. Note the more fully alloyed microstructure and absence of the Eta free zinc layer (ArmorGalv, 2009)**

A HDG coating is formed in a matter of minutes, which gives the zinc atoms only a short period of time to diffuse into the steel substrate and form the required alloy layers. This results in an almost non-existent Gamma layer of about 1 micron thickness and alloy layers with very low iron content. TDG coatings are formed over a period of 60 to 120 minutes, resulting in a 10 micron Gamma layer which is diffused into the steel substrate and a Delta and Zeta layer with much higher iron contents. The crystalline Delta and

Zeta molecules have the same hexagonal structure and form the same geometric, columnar appearance, but they have more iron atoms due to the longer diffusion process.

The more heavily alloyed the zinc is with iron, the denser and more stable the alloy structure. This provides improved performance properties – corrosion resistance and increased hardness - over a greater period of time. Table 1 shows the respective chemistry differences in the layers between HDG and TDG (Industrial Galvanizers, 2006; ArmorGalv, 2009; Kainuma and Ishida, 2007).

Table 2 shows the respective physical differences in the layers between HDG and TDG (Industrial Galvanizers, 2006; Swain, 2010).

**Properties and performance**

Due to the unique surface chemistry and microstructure differences, TDG has a set of physical properties that are distinctive in comparison with HDG. These differences permit TDG to offer anti-corrosion solutions in a number of niche areas of application. The following paragraphs provide a summary of these comparative differences with reference test information.

**Table 1 - Comparative chemistry– HDG and TDG**

Alloy Layer	Hot Dip Galvanising	Thermal Diffusion Galvanising
Eta	100% Zn	None
Zeta	6% Fe (FeZn <sub>13</sub> )	7–10 % Fe (FeZn <sub>7</sub> )
Delta	7–11 % Fe (FeZn <sub>7</sub> )	25 % Fe (Fe <sub>11</sub> Zn <sub>40</sub> )
Gamma	21–28 % Fe (Solid Solution)	50 % Fe (Solid Solution)

**Table 2 - Comparative physical properties – HDG and TDG**

Alloy Layer	Hot Dip Galvanising Hardness / Microstructure	Thermal Diffusion Galvanising Hardness / Microstructure
Eta	70 HB / Spherical Nodes	None
Zeta	220 HB / Coarse Hexagonal Crystals	300 HB / Coarse Hexagonal Crystals
Delta	270 HB / Fine Hexagonal Crystals	350 HB / Fine Hexagonal Crystals
Gamma	Too Thin to measure	600 HB / Dense Diffusion Band

**Corrosion resistance**

The fundamental property of corrosion resistance for TDG coatings has been rigorously examined through laboratory tests and field trials. Neutral salt spray testing (Alvey, 2002) applied to identical base metal componentry, alternately coated in TDG and HDG, then tested in accordance with ISO9227:1990 (International Organisation for Standardisation, 1990), showed less white and red corrosion product and less corrosion overall for items coated with TDG in comparison to HDG coated items. HDG coatings had 250 hours to red rust, while TDG coatings had 1,000 hours to red rust. Salt spray testing conducted to AS2331.3.1-2001 (Standards Australia, 2001) on roof bolt material (Jeffrey, 2010) also revealed improved comparative performance for TDG, as indicated in Figure 5. The left hand image is HDG coated, while the right hand image is TDG coated - while corrosion is evident on both samples, the TDG coated roof bolt exhibited less mass loss of the original coating.



**Figure 5 - Images from 1 000 hour neutral salt spray testing, conducted on the same grade of high tensile roof bolt material (Jeffrey, 2010)**

Accelerated weather exposure testing conducted by the CSIRO at its Port Fairy facility has proven that the corrosion rate of pure zinc is more than double that of zinc-iron alloys (Fullston, *et al.*, 2004). Given that the TDG chemical structure has no free zinc, as well as a higher percentage of alloyed iron, TDG has a lower coating mass loss rate than of pure zinc under a given corrosive action. Correspondingly, a TDG surface will require less zinc and a lower coating thickness for equivalent performance. Based on this, a 50 micron TDG coating will typically offer equivalent anti-corrosion performance to a 100 micron HDG treatment, when subjected to equivalent environmental conditions.

Field trials conducted by the US Navy have also been recently completed, indicating that TDG has superior anti-corrosion performance to that of HDG (ArmorGalv, 2012). Comparative trials involving TDG, HDG and Zinc Electroplating were conducted on the cargo tie-down componentry of hovercraft landing vessels, being subjected to extreme salt spray operating conditions over a 22 week period. The positive outcomes from this trial resulted in TDG being formally approved for use by the US Navy for fasteners and hardware in Steel Grades up to 1,000 MPa in tensile strength (Department of the Navy, 2011).

#### ***Moderate acidic conditions***

A growing body of evidence suggests that TDG may outperform HDG in moderate acidic environments. Copper Accelerated Salt Spray (CASS) Tests have been conducted under ISO 9227: 2006(E) (*International Organisation for Standardisation*, 2006) by a NATA certified laboratory (Fahey, 2013), subjecting identical parent metal componentry, alternately coated in TDG and HDG, to continuous testing in an acidic salt spray environment at pH 3.1 (acetic acid). The results of this severe testing regime appear in favour of TDG over HDG, displaying less coating mass loss. However, it must be clearly noted that both TDG and HDG do not offer any long term anti-corrosion performance in low pH environments (Galvanisers Association of Australia, 2011). Validation testing is required to test the impact of site specific acidic conditions.

#### ***Coating thickness consistency / threadforms***

The process of TDG provides a uniform coating thickness that follows the contours of the componentry exactly – there is no solidifying zinc at the surface, as apparent with HDG. The consistency of the surface is produced under the diffusion action of the zinc atoms into the base metal, assisted by the slow rotation of the componentry and zinc powder within the cylindrical kiln. The coating thicknesses are governed by ASTM A1059 2008 (ASTM International, 2008). Coating classes range from 20 to 120 microns, defining the target coating thickness. For the most common coating thickness of 50 micron, thickness variance is typically between 45 and 60 micron.

#### ***Coating deformation***

The depth of diffusion of zinc atoms into the steel substrate with TDG creates a Gamma layer typically 10 microns thick. This equates to extremely high adhesion in comparison to HDG and allows very fine cracking under deformation of the parent metal observed within the Gamma layer. This fine cracking permits flexibility of the TDG layers, without impacting on the adherence of the zinc – iron alloy layers to the base metal. As a result, moderate deformation of the base metal does not reduce the cathodic protection offered by TDG, and equally does not weaken the surface structure or result in loss of the bonded zinc-iron alloy content. Under extreme deformation, a low percentage of the coating will be lost via the cracks propagating to the coating surface, with some of these fissures dislodging and falling out.

#### ***Hardness and anti-abrasion***

The layers of TDG typically exhibit hardness values greater than that of the parent material. Surface hardness results typically exceed 35 Rockwell C, as referenced within ASTM A 1059/A 1059M – 08 (ASTM International, 2008). A series of Vickers micro hardness tests conducted on a TDG treated high tensile steel grade produced 605 (HV) in the gamma phase and 375 (HV) in the delta phase, relative to a value of 327 (HV) in the parent steel (Swain, 2010). The increased surface hardness values from TDG result in excellent wear resistant properties.

#### ***Anti-galling***

Galling is defined as localised surface deformation between two solid sliding surfaces under heavy friction contact, distinguished by microscopic, usually localised, roughening and creation of protrusions

above the original surface (ASTM International, 2006). Due to increased hardness and wear resistant properties, TDG provides good anti-galling properties, predominantly facilitated by the absence of free zinc at the outer surface. Anti-galling performance has been witnessed by the long term use of TDG treatments within the componentry of hydraulic long-wall props in the United Kingdom (Bodycote, 2006). Given the corrosive, acidic and abrasive environmental conditions of coal mining under the North Sea, TDG has been employed in the main hinge pins of longwall props as a solution to also reduce galling and seizing problems.

### ***Torque / tension performance***

The uniform surface thickness of TDG, combined with good hardness and anti-galling properties, means that TDG is highly suitable for use with thread-forms. Torque / tension ratios are a significant product performance consideration - the efficiency to induce tension in the thread-form, relative to the applied torque. Testing undertaken by the NSW Roads and Maritime Services indicates that TDG provides a better torque tension performance compared to uncoated steel (Roads and Maritime Services, 2012a) (Roads and Maritime Services, 2012b).

### ***Anti-sparking***

Sparking in ferrous metals is caused under the combined action of two mechanisms. The first mechanism is friction, creating localised heat to generate a spark – dependent upon velocity, pressure, surface roughness and levels of oxidation. The second mechanism is abrasion, generating fine particles of iron, which are small enough to self-ignite in the presence of oxygen. Zinc alloys are known to provide anti-sparking properties (International Zinc Association, 2011), acting as a surface barrier to prevent both friction and abrasion of the parent ferrous metal. TDG has been used as an anti-sparking coating within coal mining applications, to meet the risk demands of this environment. Tailored anti-sparking tests should be conducted to validate the effectiveness of the application.

### ***Corrosive compatibility***

Components from TDG and HDG surface treatments are compatible when placed in direct contact and will not result in bi-metallic preferential corrosion (British Standards Institute, 1990). Such combinations have been employed frequently in civil structural applications, taking advantage of the properties of TDG for fastener components, as well as the common application of HDG for large fabricated steel sections.

### ***High tensile steel grades***

TDG is suitable for use with high tensile steel grades, as the concern for hydrogen embrittlement is removed due to the nature of the process (Roads and Maritime Services, 2012a) (Roads and Maritime Services, 2012b). Hydrogen embrittlement is caused by the adsorption of hydrogen atoms into the steel matrix, with the trapped 'H' atoms subsequently forming 'H<sub>2</sub>' gas molecules within the steel structure, resulting in extreme internal stresses. Steel grades at tensile strengths greater than 800 MPa are typically at risk of hydrogen embrittlement due to the acid pickling associated with surface preparation for HDG (Industrial Galvanizers, 2006). TDG does not employ acid pickling, but typically utilises shot blasting for surface preparation – permitted by the greater diffusion time and increased development of the TDG gamma layer.

### ***Surface adhesion to topcoats***

The TDG treatment has a porous, textured micro structure at the outer surface of the Zeta phase. This porous surface structure facilitates the adhesion of further applied topcoats over the TDG treatment, such as paint, powder coating and rubber lining. Given the absence of the Eta phase, applied topcoats penetrate directly into the porous TDG Zeta phase. The excellent bonding characteristics between TDG and applied topcoats are also referenced within ASTM A 1059/A 1059M - 08 (ASTM International, 2008) and BS EN13811:2003 (British Standards Institution, 2003).

## **APPLIED GROUND SUPPORT SOLUTIONS**

The unique attributes of TDG permit solutions for anti-corrosion in mining roof support products, specifically in a number of niche areas of application. A number of specific product applications are outlined within the following section, providing working examples of use.

## High tensile bolts

High tensile steel grades are commonly employed for mining roof support elements, more specifically in coal applications, where specialised steels have evolved to meet increased load bearing demands. For primary roof bolting in coal, steel grades are now employed with ultimate stress values typically at 920 MPa - exceeding the 800 MPa threshold where hydrogen induced stress corrosion cracking becomes a risk factor. The acid pickling process used for surface preparation prior to HDG is known to induce hydrogen embrittlement. Alternatively, TDG offers a galvanising solution that avoids the need for acid pickling – of particular interest for corrosion protection applications in high tensile bolts.

A further benefit arising from TDG in roof bolts is the increased surface adhesion associated with the gamma diffusion layer. Under shear and tensile action, roof bolts will deform – TDG provides greater adherence to the surface of the parent metal, compared to HDG having a thinner gamma layer. An additional benefit for roof bolts is the ability for TDG to conform to the surface dimensions of the bar – both to the threadform, as well as to the ribbed bar profile. The higher abrasion resistance of TDG also reduces coating damage during installation and rotation of the bolt within the bore hole. A typical coated bolt is shown in Figure 6.

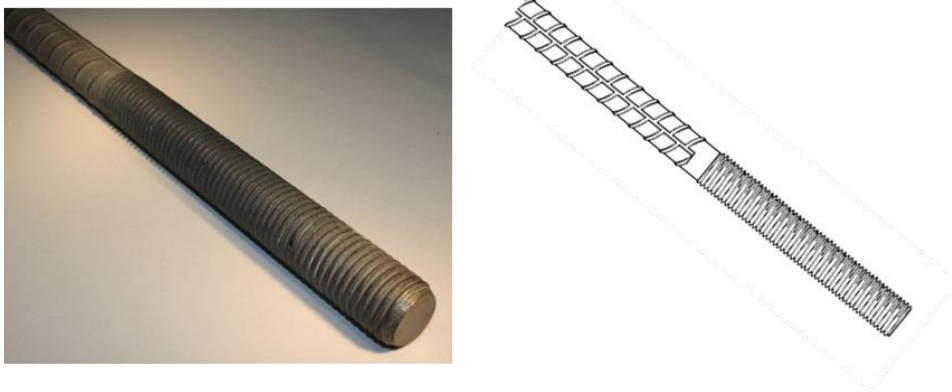


Figure 6 - TDG coated high tensile roof bolt – photographic image and product pictorial

## Meshing plates

Meshing plates, as shown in Figure 7, are secondary plates used to secure mesh sheets to pre-installed roof bolts. A common form of meshing plate incorporates a threaded fastener – in this format, the plate must be rotated to engage the fastener with the threaded roof bolt. Where black steel mesh sheets and black steel meshing plates are used, it is possible to induce sparking as the rotating meshing plate contacts and bears load against the mesh surface. Within coal mining environments, incendive sparking is a major risk which must be mitigated. TDG has been utilised to provide a solution for this risk - the TDG surface provides a barrier to friction and abrasion of the parent metal of the rotating plate. Specific testing was conducted for this application to validate the level of sparking reduction at the required rotational speed and pressure. Additionally, the presence of the threaded fastener as an integral component of the meshing plate places the requirement that the thread-form cannot be fouled by the applied coating. Again, TDG provides the correct coating thickness consistency to achieve this outcome for the thread-form.

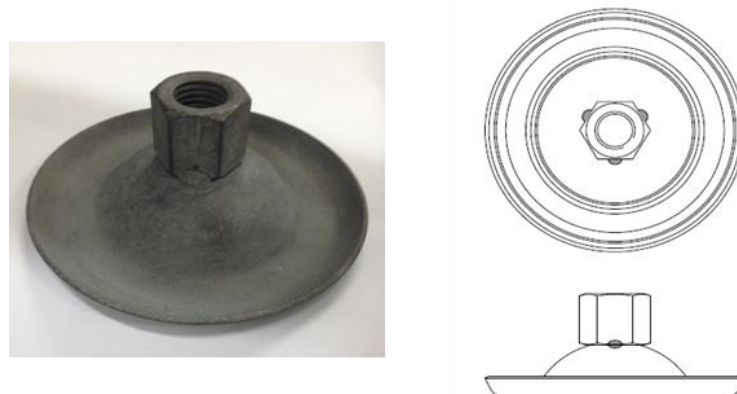


Figure 7 - TDG coated mesh express plate – photographic image and product pictorial

## Nuts and couplers

Threaded devices are an integral feature of many roof support products – in the obvious form of nuts and coupling devices. TDG provides an immediate solution for corrosion protection in nuts and couplers – with the benefit of controlled, consistent coating thickness on both the inner thread profile and the outer body of the component. HDG of female thread-forms is notoriously difficult due to the build-up of excess galvanising material on the internal form. Alternatively, the dimensional consistency of TDG coatings greatly reduces the instance of interference during engagement of the male and female threads. A further benefit is the compatibility of TDG with HDG based on bi-metallic corrosion compatibility. This means that low tensile roof bolts can be treated with HDG if desired, while the corresponding nut or coupler can be treated with TDG to improve dimensional fit. A typical arrangement is shown in Figure 8.



**Figure 8 - TDG coated M24 nut – photographic image and product pictorial**

## CONCLUSIONS

TDG is an emerging technology of great relevance and potential within the field of corrosion protection for ground support elements. Multiple test cases indicate that TDG has at least equivalent anti-corrosion performance to HDG, but also provides improved attributes in the areas of surface consistency, compatibility with high tensile steels, application with thread-forms and surface adherence under abrasion and deformation. There is some evidence to suggest that TDG may provide improved performance in mild acidic conditions, relative to HDG. However, for low pH environments, zinc based protection systems such as HDG and TDG are not suitable and will degrade rapidly.

While traditional methods of corrosion protection will continue to be employed within the industry, TDG is an area of technology that can provide solutions for a growing number of niche application areas. As knowledge of this technology is deployed across the mining industry and experience with specific product applications continues to progress, TDG has the potential to become a routine consideration within the suite of anti-corrosion solutions for mining strata control.

## REFERENCES

- Alvey, C.E, 2002. Evaluation of Distek Thermodiffusion Coating, Corrosion Advisory Technical Services, 18th December.
- ArmorGalv, 2009. Armorgalv general presentation, viewed 20 January 2013, <http://www.armorgalv.com>.
- ArmorGalv, 2012. Testing of Armorgalv protected tie downs on active LCAC starting July.12.2010, viewed 20 January 2013, <http://www.armorgalv.com>.
- ASTM International, 2006. Standard Terminology Relating to Wear and Erosion ASTM G40 (2006)
- ASTM International, 2008. Standard Specification for Zinc Alloy Thermo-Diffusion Coatings (TDC) on Steel Fasteners, Hardware and Other Products A1059/A 1059M – 08, 15<sup>th</sup> November
- Bodycote, 2006. Hinge pins for roof support systems in mining applications, viewed 20 January 2013, <http://www.bodycotemetallurgicalcoatings.com>.
- British Standards Institution, 1990. PD6484: 1979 Commentary on Corrosion at Bimetallic Contacts and Its Alleviation.
- British Standards Institution, 2003. Sherardizing – Zinc diffusion coatings on ferrous products – Specification BS EN 13811:2003, 13th May.

- Department of the Navy, 2011. Authorization to Utilize Thermo-Diffusion Zinc Process as Alternative to Electrodeposited and Hot-Dip Zinc Coatings, Naval Sea Systems Command, 2<sup>nd</sup> August.
- Fahey, A, 2013. Copper accelerated acetic acid salt spray, Bureau Veritas, 30th January.
- Fullston, D., Ganther, W.D. and Thomson, G, 2004. Zinc coating thickness effects on hot dip galvanized steel corrosion rates at a severe marine site, *Corrosion and Materials*, Vol. 29, 1, pp. 5–8.
- Galvanizers Association of Australia, 2011. Painting Galvanising, viewed 20 January 2013, <http://www.gaa.com.au>.
- Industrial Galvanizers, 2006. Specifiers manual, viewed 20 January 2013, <http://www.ingal.com.au>.
- International Zinc Association, 2011. Zinc Alloy Property Guides, viewed 20 January 2013, [http://www.zinc.org/info/zinc\\_diecastings](http://www.zinc.org/info/zinc_diecastings).
- International Organisation for Standardisation, 1990. Corrosion tests in artificial atmospheres – Salt spray tests ISO9227:1990, 12<sup>th</sup> January
- International Organisation for Standardisation, 2006. Corrosion tests in artificial atmospheres – Salt spray tests ISO 9227: 2006(E), 15<sup>th</sup> July
- Jeffrey, R, 2010. Evaluation of Corrosion Resistance of Mining Products, Pacific Testing, 4th November.
- Kainuma, R. and Ishida, K, 2007. Reactive Diffusion between Solid Fe and Liquid Zn at 723K, *ISIJ International*, Vol. 47, 5, pp. 740–744.
- Potvin, Y., Nedin, P., Sandy, M., Rosengren, K. and Rosengren, M.D, 2001. Towards the Elimination of Rockfall Fatalities in Australian Mines, Australian Centre for Geomechanics, Perth, pp. 33-34
- Roads and Maritime Services – NSW Government, 2012a. QA Specification B240 Supply of Bolts, Nuts, Screws and Washers, June 25<sup>th</sup>
- Roads and Maritime Services – NSW Government, 2012b. QA Specification R64 Soil Nails, November 21<sup>st</sup>.
- Standards Australia, 2001. Methods of test for metallic and related coatings - Corrosion and related property tests - Neutral salt spray (NSS) test AS 2331.3.1-2001.
- Swain, K, 2010 TDG Coating Hardness and Micrograph, Austpower Engineering, 21<sup>st</sup> December.
- Villaescusa, E, Hassell, R, Thompson, A, 2007. Corrosion of Rock Reinforcement in Underground Excavations, Western Australia School of Mines, Kalgoorlie, pp. 1-3.

---

# AN ASSESSMENT OF THE CORRELATION BETWEEN THE STRENGTH AND CUTTABILITY OF ROCK

Joel Langham-Williams and Paul Hagan

**ABSTRACT:** Mechanical rock excavators are widely used in the mining and civil industries. Estimating the performance of these machines can be difficult as well as a costly and time-consuming process. A number of methods exist to assess the cuttability of a rock, ranging from laboratory based cutting tests through to more convenient empirical approaches. Recent research has focussed on developing empirical relationships between rock cutting performance and rock properties involving an indirect assessment of cuttability. This paper outlines the results of a study to determine the level of correlation between the strength and cuttability for rock that is commonly associated with coal-measure formations. A reasonable correlation was found between the uniaxial compressive strength and cuttability performance of rock samples, the latter including specific energy, cutting force and normal forces.

## INTRODUCTION

Cutting machines such as shearers, roadheaders and continuous miners are used extensively throughout the world in mining and civil operations for the excavation of rock. As theory relating to the mechanical excavation of rock has evolved over time, so too has the utilisation of these machines, often substituting traditional drill and blast methods resulting in an increase in safety and performance and a reduction in operating costs.

The method by which these rock cutting machines work is highly influenced by a number of factors (Neil, *et al.*, 1994). Machine design, machine power, intact rock properties and rock mass properties all play a pivotal role in determining the efficiency of the rock cutting process (Karakas, *et al.*, 2005). As Roxborough (1987) explained, the engineer has a choice over what size and type of machine can be used for a particular excavation, however the engineer, outside of changing the designs of the project cannot influence what rock formation will be encountered in completing a given excavation. As it is the rock mass that governs cuttability and not machine selection, an investigation into the rock mass properties and what affect they have on cuttability should consequently be the focus.

It has been well documented that a number of rock strength characteristics can adversely affect cutting performance (Rostami, 2011). When rock strength increases, there is a near linear response in cutting forces (Hood and Roxborough, 1992). Similarly it has been found that abrasivity of rock tends to increase with rock strength (Jacobs and Hagan, 2009), and laboratory testing has focussed on attempting to find which rock strength properties best describe this relationship. Specific energy is extensively used to evaluate rock cuttability (Tiryaki and Dikmen, 2006). It is a measure of the force required to excavate a unit volume of rock, and hence is a measure of the relative cuttability of a particular rock. McFeat-Smith and Fowell (1977), in their well-known study, correlated rock strength properties with specific energy and found cutting performance of cutting machines diminished with specific energy.

Recent studies have focussed on an array of properties in an effort to estimate rock cuttability, with strong correlations found between the uniaxial compressive strength of rock and specific energy for a number of different rock types (Speight, 1987). Material hardness, sonic velocity, Young's modulus and other rock properties that indirectly relate to rock strength, have been correlated with specific energy, with varying degrees of statistical significance. To date, the most reliable indicator of cuttability however has been based on the uniaxial compressive strength of rock.

From a mining perspective, further investigations to confirm the validity and correlation between rock strength parameters and cuttability would be useful in the estimation of machine performance. The ability to predict cutting performance from direct and indirect rock strength measurements would be of potential benefit to the industry, especially for mining operations interested in assessing the relative cuttability of rock. The purpose of this paper is to outline the results of a study to determine the level of

correlation between rock-cutting performance and rock strength for 44 rock samples obtained from coal measures in Eastern Australia.

## METHODOLOGY

The rock cuttability test procedure was originally developed at the University of Newcastle-upon-Tyne in the UK during the 1960's and 1970's. A rock cutting test facility was established at the University of New South Wales (UNSW) in the early 1980's as part of an industry sponsored project on machine mining of rock. Since then the *UNSW Machine Cuttability Research Facility* has been used in the assessment of the cuttability of wide range of rock types ranging from coal and salt through to haematite and sulphide ores from tunnelling and mining projects around Australia.

The facility is capable of testing blocks of rock samples and diamond-cored rock specimens. The main variables in the core cuttability procedure are indicated in Figure 1.

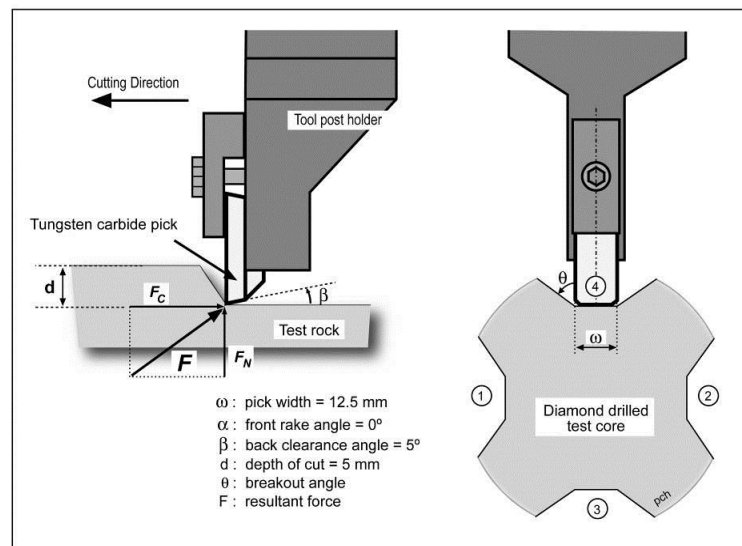


**Figure 1 - Schematic of the main variables in the core cuttability test procedure (Hagan, 1990)**

During each cutting test, a standard design tungsten carbide cutting tool is made to pass along the longitudinal axis of the core to a depth of 5 mm. Details of the cutting tool geometry are provided in Figure 1.

A tri-axial force dynamometer measures the transient forces acting on a tool during a cutting test. A data acquisition system records the forces at a sampling rate of 1000 readings per channel per second. The dynamometer resolves the resultant force into three orthogonal components of cutting ( $F_C$ ), normal ( $F_N$ ) and lateral forces ( $F_L$ ). At the end of each test cut, measurements are made of the actual length of cut and mass of excavated rock.

After each test cut the core is rotated  $90^\circ$  and another cut is made with up to four test replications made with a core as indicated by the circled numbers 1 through 4 in Figure 1.

The arrangement of equipment used in the cuttability test procedure is shown in Figure 2. The majority of the cored test specimens in this study had a diameter ranging between 54 and 59 mm and a length of approximately 200 mm.

On completion of each cutting test the following parameters are calculated.

- *Mean cutting force* ( $F_C$ ) and *mean normal force* ( $F_N$ ) (reported in units of kN) – the average resultant force acting on the cutting tool resolved into two orthogonal components.
- *Yield* ( $Q$ ) (reported in units of  $m^3/km$ ) – based on the mass of rock chippings and density of the rock sample.

- *Specific Energy (SE)* (reported in units of MJ/m<sup>3</sup>) – the amount of energy expended during cutting per unit volume of rock excavated whereby the value of SE can be calculated using Equation (1).

$$SE \text{ (MJ/m}^3\text{)} = \frac{F_c \text{ (kN)}}{Q \text{ (m}^3/\text{km)}} \quad (1)$$



Figure 2 - Cutting tool, dynamometer and data acquisition system used in the core cuttability test procedure at UNSW

### Rock strength testing methodology

The rock strength tests were based on the ISRM Suggested Methods (Brown, 1981) and conducted using cored test specimens. The tests were conducted in an MTS machine as shown in Figure 3 at a constant displacement rate of 3  $\mu\text{m/s}$ .



Figure 3 - The MTS machine setup for the compressive strength tests

## Data analysis methodology

The first step in the process to determine whether there were statistically sound correlations between rock cutting performance parameters and rock strength was to plot a graph of the test result for each parameter, examine the residuals and standard deviation and, remove any significant outliers that might tend to skew the results. In circumstances where there was a question whether it was valid to remove a value from a data set, a conservative approach was followed with the data point included. After the outliers were removed, correlations were determined. Relationships demonstrating a  $t$ -value higher than that required for a 95% confidence interval, and also possessing a strong  $R^2$  value, were considered statistically significant.

## RESULTS

### Rock samples

A total of 44 different rock samples were acquired for testing as shown in Table 1. It was found that the test specimens of many of the softer rock types disintegrated in most instances during testing as they were unable to withstand the high internal stresses induced during cutting but more important the relatively small diameter cores provided insufficient confinement to withstand the stresses. There was insufficient volume of sample available to cast it in cement or grout which is the preferred method used to provide confinement for soft rocks. A total of 23 rock samples were available for rock strength testing, with the range of strengths varying between 7 and 167 MPa.

**Table 1 - A summary of the samples and material properties included in the analysis**

Rock Type	No. of Samples	UCS (MPa)	Density (t/m <sup>3</sup> )
Sandstone	30	21-167 (21)*	2.24 – 2.66
Shale	10	-	2.23 – 2.53
Coal	2	18 (1)*	1.26 – 1.41
Grout	1	7 (1)*	1.51
Conglomerate	1	-	2.44

\* number in brackets indicates number of test samples

### Specific energy and rock strength

One of the primary parameters of interest was changes in rock strength with specific energy. As the majority of the other rock properties are related in some manner to rock strength, and can be used as an indirect method to determine rock strength, it was consequently considered to be the most important relationship to identify.

The variation in specific energy with rock strength is shown in Figure 4. It should be noted that the graph includes all the test data with none of the outliers removed in order to show the extent of the variation. As the graph indicates the majority of results were clustered within the range of 50 to 80 MPa with two rocks tested at strengths of 100 to 125 MPa and a further three rock with strengths of less than 30 MPa. As mentioned many of the the softer rock samples tended to disintegrate during cutting while there was a limited number of higher strength rocks being at the upper end of the capacity of the rock cutting facility. Despite the scatter there is a trend evident with specific energy increasing with rock strength and this is despite the range of rock types tested. In this case a linear trend is shown.

### Mean cutting force and rock strength

Figure 5 shows the variation in cutting force with rock strength. As specific energy is a function of both cutting force and yield, it would be expected that the trend in cutting force would mirror that of specific energy. The correlation coefficient ( $R^2$ ) of 0.64 is on par with that observed for specific energy of 0.63 with the latter including errors in the measurement of the rock chippings. This result is consistent with the results of Roxborough (1987).

A number of cutting tests were also conducted at 2.5 mm, that is at half of the standard depth of cut. These tests results are also included in Figure 5 and show a better correlation coefficient of 0.71. Interestingly the value for the linear regression coefficient at 5 mm depth of cut of 0.022 which is nearly

double that found for 2.5 mm. This too is consistent with the theory by Roxborough (1987) where force varies linearly with depth of cut.

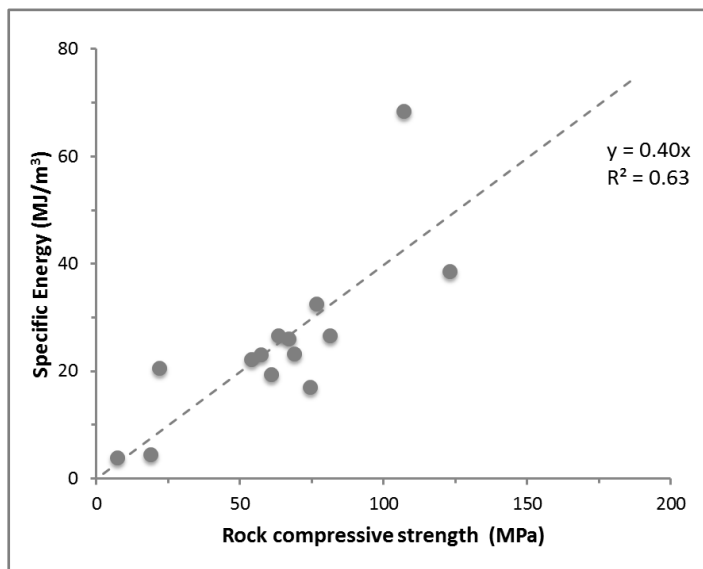


Figure 4 - Variation in specific energy with rock strength

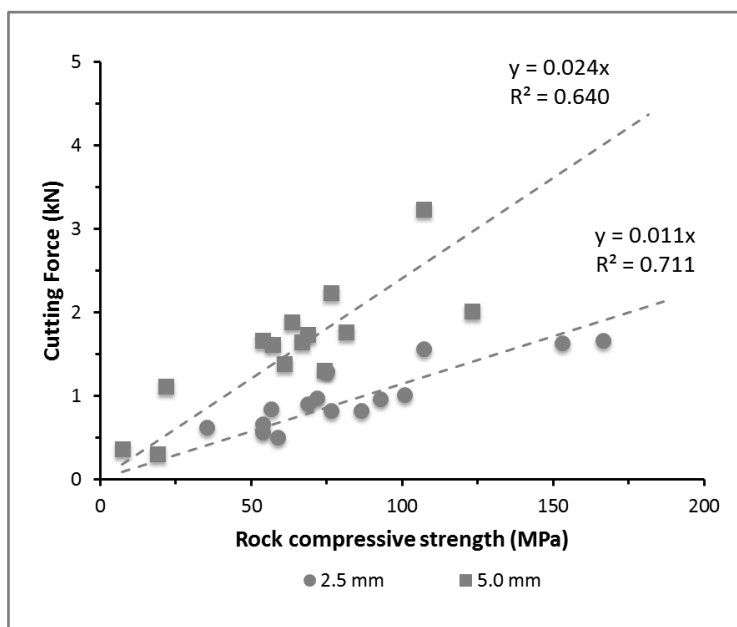


Figure 5 - Variation in cutting force with rock strength at two levels of cutting depth

**Mean normal force and rock strength**

Similar to the results for cutting force, it was found that normal force increased with rock strength as shown in Figure 6 with similar levels of correlation for both depths of cut. Based on the ratio of the gradients, for any value of rock strength, the normal force is approximately 21% higher than cutting force in this cutting configuration and for this cutting tool. Generally it is found that as the tool wears and back clearance angle reduces, the ratio of forces quickly reduces and then inverses such that the cutting force becomes much greater than normal force Roxborough (1987).

**Analysis of correlations and significance**

As mentioned, Figures 4, 5 and 6 include the test results for all samples but despite this, reasonable correlations were found. The purpose of this exercise was to demonstrate that baseline relationships were present prior to any statistical analyses and to observe the correlations of the data set as a whole.

After removing the outliers in accordance with the process detailed earlier, the intention was to provide reliable models to describe the observed trends.

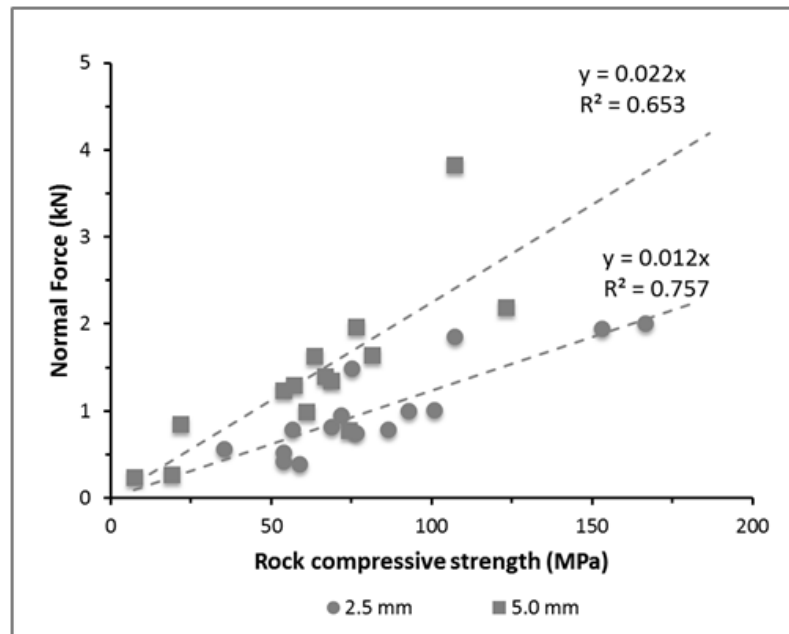


**Figure 6 - Variation in normal force with rock strength at two levels of cutting depth**

Tables 2 and 3 show the results of a linear regression analysis for the 2.5 mm and 5 mm depth of cut tests respectively. Two outliers were removed from the original 2.5 mm data set with 13 data points remaining for calculation of the regression values between rock strength and cuttability parameters. In the case of the 5 mm tests, there were a total of ten values in the data set. As a result, the correlation coefficients were significantly improved for the 2.5 mm data set and marginally improved for the 5 mm data set.

**Table 2 - Results of linear regression analysis against rock strength with outliers removed for the 2.5 mm depth of cut tests**

cutting parameter	linear regression model	$r^2$	pairs	t-value
specific energy	$y = 0.40 x$	0.93	15	13.5
cutting force	$y = 0.011 x$	0.85	13	7.86
normal force	$y = 0.013 x$	0.75	13	5.70

**Table 3 - Results of linear regression analysis against rock strength with outliers removed for the 5 mm depth of cut tests**

cutting parameter	linear regression model	$r^2$	pairs	t-value
specific energy	$y = 0.36 x$	0.85	10	6.85
cutting force	$y = 0.027 x$	0.78	9	5.01
normal force	$y = 0.021 x$	0.81	10	5.88

The values from the regression analysis are considered to be in agreement with previous studies. For example Roxborough (1987) found a linear relationship between specific energy and rock strength for Bunter sandstone in the UK, a rock that is said to have highly consistent material properties. It was in the form as shown in Equation (2), where  $c_1$  and  $c_2$  represent values for the gradient and  $y$ -intercept respectively.

$$SE = c_1 \cdot UCS + c_2 \quad (2)$$

Roxborough stated the value for  $c_1$  in Bunter sandstone was 0.25 which is in good agreement with the values found in this study of 0.36 considering it includes a range of rock types. Hence the resulting

correlation coefficients are reasonable and that they indicate statistical significance at the 95% confidence interval level.

### CONCLUSIONS

Mechanical rock cutting has become a viable means of excavation and in softer rock types is superior compared to traditional drill and blast methods. This has come about from improvements in machine design as well as better understanding of the underlying rock cutting principles.

The results presented in this paper found there was a reasonable level of correlation between strength and cutting parameters for a range of rock types associated with coal measures in Australia. The cutting parameters were determined using the Newcastle-upon-Tyne rock cuttability index text.

It is recommended further studies be undertaken to assess the effect of other rock properties on cuttability and expand the dataset for different rock types thereby increasing the confidence that can be placed in the collected results.

### ACKNOWLEDGEMENTS

The author acknowledges the assistance of Mr Kanchana Gamage, Laboratory Manager at UNSW, who assisted in sample preparation and the compression strength tests.

### REFERENCES

- Brown, E T, 1981. Suggested methods for determining the uniaxial compressive strength and deformability of rock materials, *Rock Characterisation Testing and Monitoring – ISRM Suggested Methods*. Pergamon Press.
- Hagan P, 1990. Some aspects of the application of high pressure water jets to rock cutting, PhD thesis (unpublished), University of NSW
- Hood, M C and Roxborough, F, 1992. Rock breakage: mechanical, in *SME Mining Engineering Handbook* (ed: H L Hartman), pp 680-721 (Society for Mining, Metallurgy and Exploration: Littleton, Colorado).
- Jacobs N and Hagan P, 2009. The effect of stylus hardness and some test parameters on the Cerchar Abrasivity Index, in *Proceedings 43<sup>rd</sup> US Rock Mechanics Symposium*, June, Asheville, NC, USA,
- Karakas, A R, Bilgin, N, Tumac, D, Feridunoglu, C and Akgul, M, 2005. The Performance of a roadheader in high strength rock formations in Küçüksu tunnel, paper presented to Proceedings of the International World Tunnel Congress and the 31st ITA General Assembly, Istanbul.
- McFeat-Smith, I and Fowell, R, 1977. Correlation of rock properties and the cutting performance of tunnelling machines, in *Proceedings on Rock Engineering*, University of Newcastle upon Tyne, pp581–602.
- Neil, D M, Rostami, J, Ozdemir, L and Gertsch, R, 1994. Production estimating techniques for underground mining using roadheaders, in *Proceeding of the SME Annual Meeting*, Albuquerque, New Mexico, pp1-7 (SME: New York).
- Rostami, J, 2011. Mechanical rock breaking, in *SME Mining Engineering Handbook* (ed: P Darling), pp 415-434 (Society for Mining, Metallurgy and Exploration: Littleton, Colorado).
- Roxborough, F F, 1987. The role of some basic rock properties in assessing cuttability, in *Proceedings on Seminar on Tunnels: Wholly Engineered Structures*, Sydney, Australia, (The Institute of Engineers Australia / A.F.C.C.).
- Speight, H E, 1987. The application of drag pick rock cutting machines, in *Proceedings on Equipment in the Minerals Industry: Exploration, Mining and Processing Conference*, Kalgoorlie, Western Australia, Metalliferous Mining, pp137-147 (AusIMM, Kalgoorlie).
- Tiryaki, B and Dikmen, A C, 2006. Effects of rock properties on specific cutting energy in linear cutting of sandstones by picks, *Rock Mechanics and Rock Engineering*, 39(2):89-120.

# FULL SCALE TESTS TO COMPARE THE STRENGTH OF POLYMER LINERS WITH HIGH TENSILE STEEL MESH

Ian Porter, Zhenjun Shan, Jan Nemcik and Ernest Baafi

**ABSTRACT:** Compared with welded steel mesh which is a passive support medium, Thin Spray-on Liners (TSL) have many advantages and it is believed that TSL have the potential to take the place of steel mesh support in underground coal mines. In this study, full scale tests were firstly conducted to determine the ultimate strength of a plain polymer liner and two types of plain steel mesh. In terms of load bearing capacity, it was found that the polymer liner was stronger than the mesh with thinner diameter wire and weaker than the mesh with thicker wire. The liner was much stiffer than both of the two steel mesh sizes. The polymer and steel mesh were further loaded with fractured concrete pieces. The results showed that the polymer-concrete composite not only achieved much greater maximum load but was also stiffer than the steel mesh-concrete test structure.

## INTRODUCTION

As a traditional surface support, welded steel mesh has been successfully utilised in underground coal mines as a skin confinement medium for roof and rib strata for many years. It is, however, difficult to automate the installation process, thus it is both time consuming and labour intensive. Moreover, steel mesh is a passive support and does not provide surface confinement until substantial rock displacement occurs. To meet the roadway development requirements of future longwalls the coal industry requires a significant increase in roadway development rates over those currently achieved. Thin Spray-on Liners (TSL) are an innovative rock support material which can be applied automatically so that increased roadway development rates can be achieved. In addition, they have many other merits over steel mesh, for example, they can be applied remotely to improve personnel safety and they bond to the rock surface generating resistance to rock displacement immediately after application.

Many laboratory tests have been conducted to evaluate the performance of welded steel mesh used in underground rock surface support. The effect of the size of the mesh loading area and bolt spacing on the load-displacement behaviour of welded steel wire mesh was investigated by Thompson (2001). He found that the stiffness of the mesh increases with decrease of the bolt spacing and that the size of the mesh loading area did not have much influence on the peak load resisted by the mesh, but significantly affected the mesh displacement at peak loads. A series of laboratory tests were conducted by Dolinar (2006) to evaluate the influence of bolt tension, the type of load bearing surface and the size of the bearing plate on welded steel mesh performance. The results showed that bolt tension, bearing plate size and load bearing surface influenced the yield, peak load and the stiffness of the mesh. Increasing the bearing plate size can significantly enlarge the mesh peak load and stiffness as larger plates enabled the load to be distributed to more wires.

The mechanical properties and behaviours of TSL products have also been investigated and reported in numerous publications (Lukey, *et al.*, 2008; Nemcik, *et al.*, 2009a; Nemcik, *et al.*, 2009b; Nemcik, *et al.*, 2011a; Nemcik, *et al.*, 2011b; Nemcik, *et al.*, 2013). A recent study (Shan, *et al.*, 2013) investigated behaviour of welded steel mesh and TSL in reinforcing strata with weak bedding planes and strata prone to guttering.

In order to study the feasibility of replacing steel mesh with TSL in support in underground coal mines, direct comparison between them must be conducted. In this study, the strength of the commonly used 5 mm thick steel wire mesh was measured using full scale laboratory tests. The full scale test method was designed to determine the ultimate strength of a 5 mm thick glass fibre reinforced polymer sheet 1.4 m by 1.4 m in size followed by large scale deflection tests conducted to investigate the behaviour of the polymer liner and steel mesh under simulated rock loading condition.

## FULL SCALE LABORATORY TESTS OF POLYMER LINERS AND HIGH TENSILE STEEL MESH

### Steel mesh test

The best way to study steel mesh behaviour is to conduct full scale tests that represent *in situ* conditions. Many researchers have performed tests on welded wire mesh in the laboratory, but most were of a smaller, laboratory scale tests. Tannant (2001) tested 1.5 m by 1.5 m squares of various types of mesh, but this was shown to produce different deformation characteristics when compared with larger mesh tests or with numerical modelling (Gadde, Rusnak and Honse, 2006). In order to evaluate steel mesh performance accurately, the size of the mesh sheets tested in this study were 1.5 m by 4 m and 1.35 m by 3.6 m, which are the biggest to date. This full scale test size removes the 'end effects' influence on stiffness and ultimate deflection, apparent when using smaller samples. The load was applied to the mesh by pulling a 300 mm diameter steel dome upwards to simulate rock loading.

Figure 1 shows the full scale pulling test set up. The mesh was bolted to a 'Strong Floor' with bolts spaced at 1 m intervals. In order to eliminate or at least minimise slippage of the mesh, a torque wrench was used to apply 240 Nm of torque to the bolts to provide a consistent pre-tension force, and timber spacers were also placed between the bolt holders. The dome was used to apply a centre load to the mesh. The tests were run in displacement control model with the loading rate being 24 mm/min which is slow enough to simulate static loading. During the test, the load was measured by a 100 kN load cell with an accuracy of  $\pm 0.2$  kN and the displacement was monitored by a Linear Variable Differential Transducer (LVDT) with an accuracy of  $\pm 0.6$  mm. The load and displacement were recorded by a computer during the tests.

Two types of mesh (roof and rib) were subjected to the full scale pull test. Mesh type A (roof mesh) consisted of 5.3 mm diameter longitudinal and transverse steel wires with 7 mm diameter longitudinal reinforcing wires passing below the load bearing plate, and mesh type B (rib mesh) consisted of 4 mm diameter wires without reinforcing wires. The size of mesh A was 1.35 m by 3.6 m and that of mesh B was 1.5 m by 4 m.

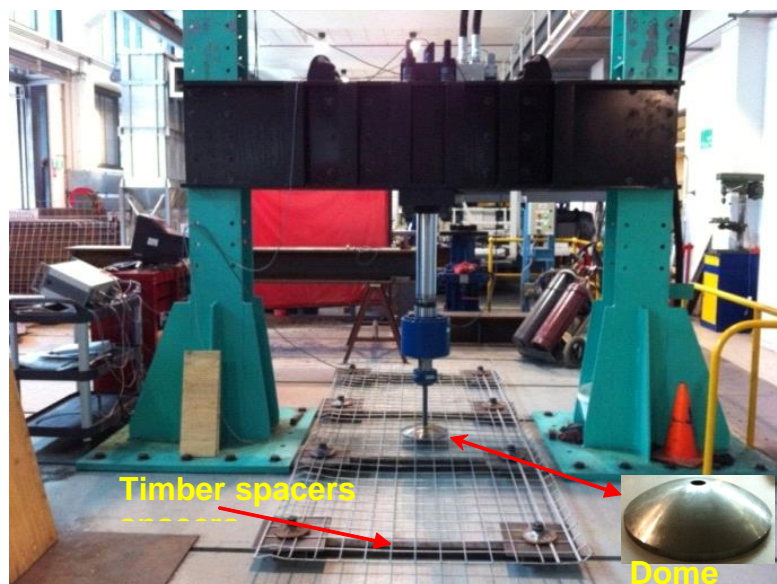
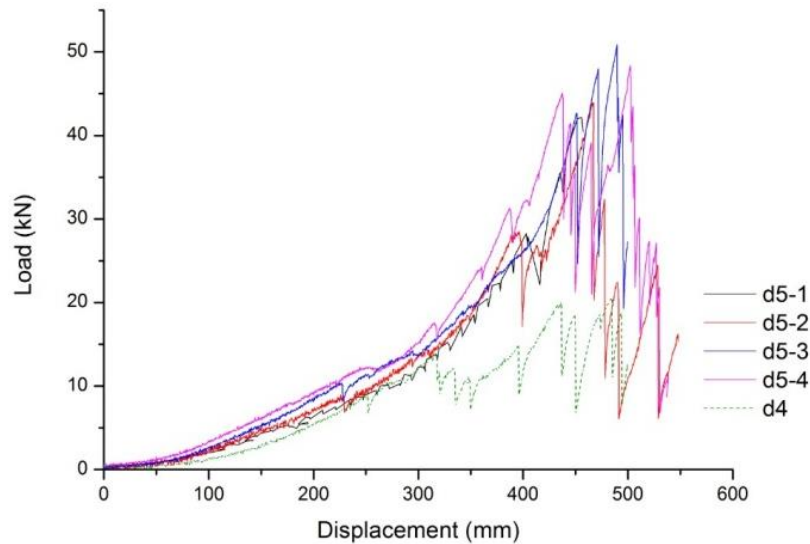


Figure 1 - Full scale pull test set up

Altogether five welded steel mesh sheets were subjected to the pull test, with four of them being mesh type A and one mesh type B. The load versus displacement curves are shown in Figure 2. The 'saw tooth' in the curves was caused by slippage of the mesh underneath the rock bolt plate, while the large drops in load generally indicate wire failure. It is obvious from the graph that the 5.3 mm mesh displays greater peak load capacity compared to the 4 mm mesh. The peak load of mesh A was approximately 48 kN, but the peak load of mesh B was only 21 kN, less than half mesh A. It is interesting to note that while the difference in peak load for the two mesh types is significant, the diversity in displacement at peak load is not so remarkable. It is also worth noting that the two different mesh types did not show much difference in stiffness before approximately 310 mm displacement. At larger displacements wire failure occurred when testing mesh B while mesh A could still bear the increasing load. Observations

during the tests revealed that almost all of the wire failure of mesh A occurred near the loading dome, however, all wire failures for mesh B occurred near the load bearing plates.



**Figure 2 - Load-displacement curves of full scale pull tests**

### Test on polymer liner

The aim of this experiment was to determine the ultimate strength of a 5 mm thick fibre reinforced polymer sheet of dimensions 1.4 m by 1.4 m.

### Sample preparation

Figure 3 shows the sample preparation procedure. The mould was firstly placed on a table and waxed seven times to guarantee that the polymer would not bond to the mould surface during curing. The mould was levelled to ensure even distribution of the polymer material. Resin was poured into the mould to cover the surface, glass-fibre mat cut to size was placed on top of the resin and rolled into the polymer with a specialised roller. This process was repeated twice with a final cover of resin rolled into the last fibre mat. It is important to note that although the fibre reinforced polymer sheet was designed to be 5 mm thick, the actual thickness was 4.5 mm.



**Figure 3 - Procedure for polymer sample preparation**

## Test procedures

The test setup is illustrated in Figure 4. The fibre reinforced polymer sheet was placed on the steel test frame and four steel channels placed on its edges were bolted to the test frame so as to restrain its translational movement. In order to replicate *in situ* conditions, four bearing plates beneath the polymer sheet were positioned in a rectangular shape with a span of 1 m and bolted to the steel channels, simulating a 1 m bolt spacing *in situ*. The polymer liner was loaded to failure by a spherical steel seat pushing downwards. Displacement loading was chosen in this experiment, with the loading rate set at 6 mm/min. Load and displacement were monitored using a load cell and a LVDT.

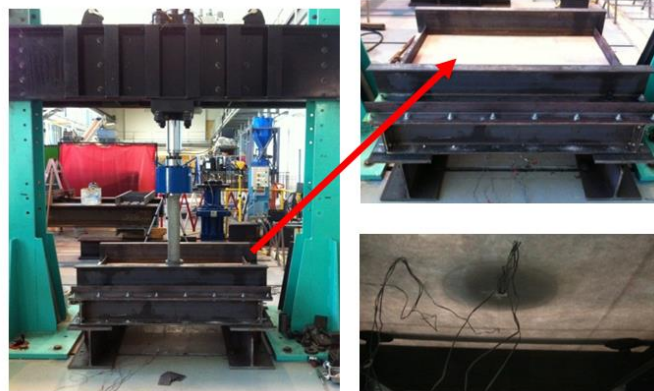


**Figure 4 - Test set up**

The load versus displacement behaviour of the polymer liner is shown in Figure 5. The maximum load achieved was 26.2 kN and the corresponding displacement was 83 mm. It is worth noting that the polymer liner can still bear a load of around 7 kN after initial failure.

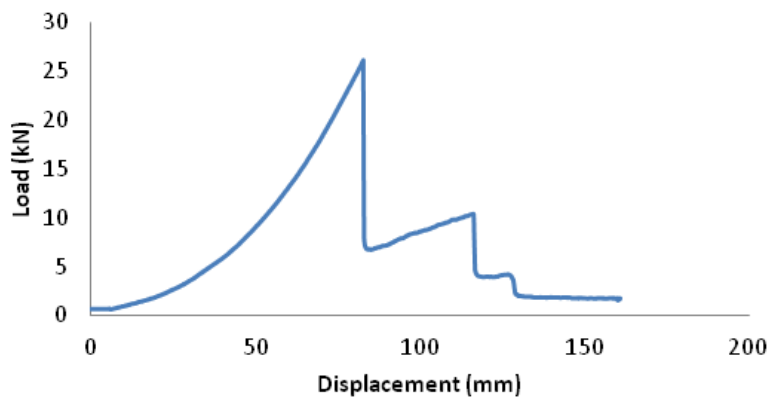


**Figure 5 - Load-displacement curve for the full scale test on a polymer sheet**

## LARGE SCALE BAGGING TESTS IN THE LABORATORY

Large scale bagging tests were conducted to enable comparison between the behaviour of plain steel mesh and a polymer liner when supporting broken strata. In particular it would allow comparison between passive support behaviour and the composite behaviour afforded by a bonded liner.

### Large scale bagging tests on steel mesh

Steel mesh cut into a rectangle of 1000 mm by 800 mm was placed in a steel frame consisting of upper and lower sections tightly clamped at the edges with 18 bolts, the bolts also stopped the mesh from slipping as they were placed on the inner edge of the outside wire. The actual loading area became 800 mm by 600 mm as 200 mm around the edge was taken up by the frame, which also helped resist slip of the mesh. A concrete slab 600 mm in width, 800 mm in length and 100 mm thick was cast using a mixture of 68.7 kg sand, 20.6 kg cement and 10.2 kg water. The concrete was then broken into sections

to simulate fractured strata in an underground coal mine roof and re-assembled on the top of the steel mesh as shown in Figure 6. To load the steel mesh evenly, a 100 mm thick layer of crushed basalt aggregate was positioned on the top of the concrete slab. A rubber mat was placed between the concrete and the aggregate to prevent the crushed basalt from falling into the cracks between the concrete pieces. Another rubber mat on the top of the aggregate protected the base of a mild steel circular loading platen which was set at the centre of the steel mesh on top of the crushed basalt. The sample was then loaded by a 5000 kN hydraulic press, the deflection of the steel mesh was measured using a wire potentiometer.



**Figure 6 - Concrete sections on the top of the steel mesh**

As shown in Figure 7, the first peak load of 80 kN occurred at a displacement of approximately 35 mm. The load began to oscillate between 60 kN and 80 kN as the displacement increased from 40 mm to 80 mm. The load oscillation was a result of steel strand necking and failing. When each steel strand failed the load dropped, but then increased again as the load was redistributed to the unbroken steel strands. The progressive failure of the steel mesh strands, however, caused a decrease in bearing capacity and subsequent structural failure of the system. The data presented in Figure 7 indicates that the mesh had structurally failed at a displacement of 80 mm. The maximum load achieved in this test was 82 kN at a displacement of 51 mm.

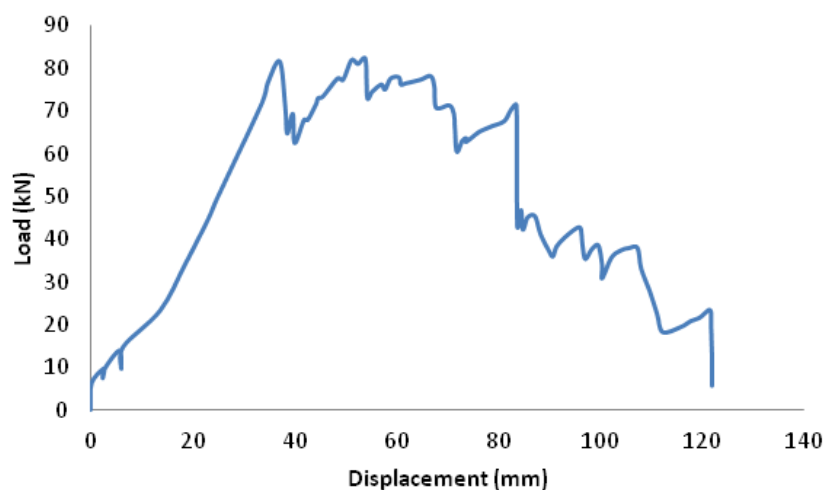


**Figure 7 - Load-displacement curve for steel mesh**

### Large scale bagging tests on polymer liner

A sheet of fibre reinforced polymer was loaded to failure and the results compared with the steel mesh tests. The polymer liner was 4.5 mm thick reinforced with 3 layers of glass fibre (Figure 8). The test set up was similar to the test on steel mesh, except that the polymer sheet was bonded to the concrete pieces to simulate the *in situ* spray application of the polymer for underground use. The sample was again loaded using the 5000 kN hydraulic press, the deflection of the polymer sheet was monitored with a laser LVDT.



**Figure 8 - Fibre reinforced polymer liner**

The test was divided into two stages: initial loading and reloading. The load versus displacement results during the two stages are shown in Figure 9. In the initial loading stage, audible sounds were noticed when the load was approximately 100 kN with a corresponding displacement of 10 mm. It was then decided to unload the sample to obtain an unloading curve before loading the polymer liner to failure. The polymer sheet was allowed to recover for 5 min after unloading. From the data it is apparent that the displacement reduced from 15.4 mm back to 7.8 mm with recovery of 7.6 mm after unloading and recovery. In the reloading stage, audible sounds were again heard at approximately 100 kN, the maximum load achieved was 128.7 kN at a corresponding displacement of 26.7 mm. It is important to note that a sudden fall in load occurred after the peak load was reached, but the sample was still able to bear a load of around 80 kN (8 t), after which the load bearing capacity gradually reduced with further deflection.

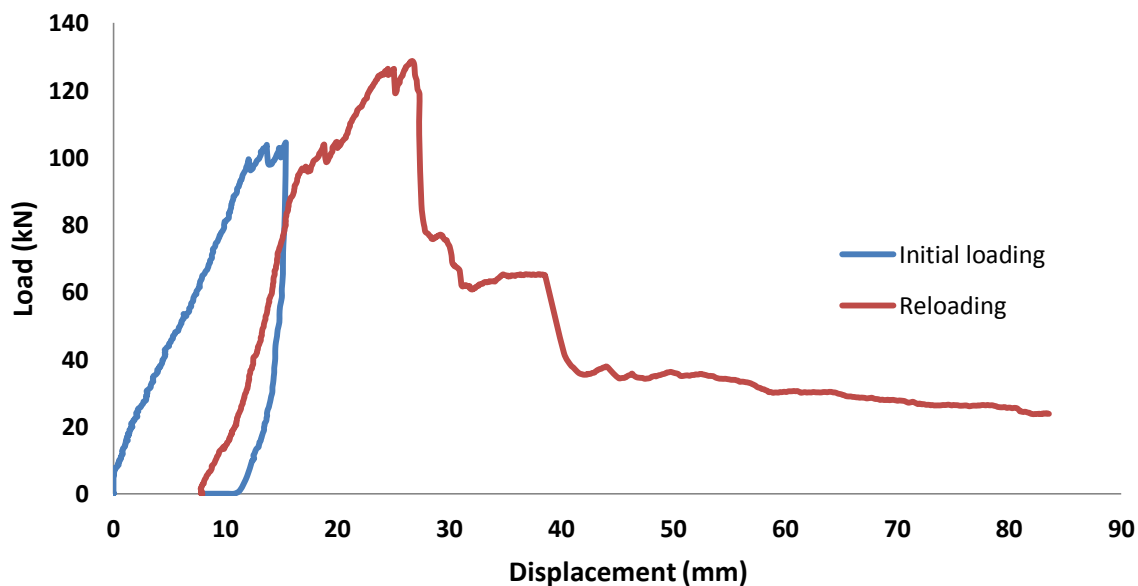


**Figure 9 - Load-displacement curve for the polymer liner**

It was observed that the polymer liner tilted to one edge of the steel frame as shown in Figure 10. The probable reason was the circular steel seat placed slightly off-centre in the steel box. The tilt of the polymer sheet contributed to the stress concentration at the place where the polymer sheet rested on the steel frame. The initial failure occurred at this edge and then spread to the other edges (Figure 11). A greater maximum load may be expected for a correctly centred steel seat. Observe the concrete sections still bonded to the polymer.

## DISCUSSION

The behaviour of two different types of steel mesh (mesh A and mesh B) and a glass fibre reinforced polymer sheet were compared by conducting *in situ* scale tests in the laboratory. The load was applied by pulling (steel mesh) or pushing (polymer liner) a 'dome like' spherical seat manufactured to simulate the *in situ* loading situation. Figure 12 shows the load-displacement curves from the tests. As expected, mesh A, with 5.3 mm diameter steel wires, had a much greater peak load and a larger load at first wire failure than the 4 mm mesh. Mesh A was slightly stiffer during the initial load-displacement stage than mesh B. The deformation characteristics of the two mesh sheets were similar, with the displacement at peak load of around 500 mm. The peak load of the fibre reinforced polymer sheet was greater than mesh B but lower than mesh A, but was much stiffer than the steel mesh, which means the polymer liner can generate greater resistance at the same rock displacement. It is worth pointing out that the dome like seat is suited for testing the steel mesh, but appeared to be acting as a point load on the stiffer polymer liner.



Figure 10 - Tilt of the polymer liner



Figure 11 - Failure along the frame edges

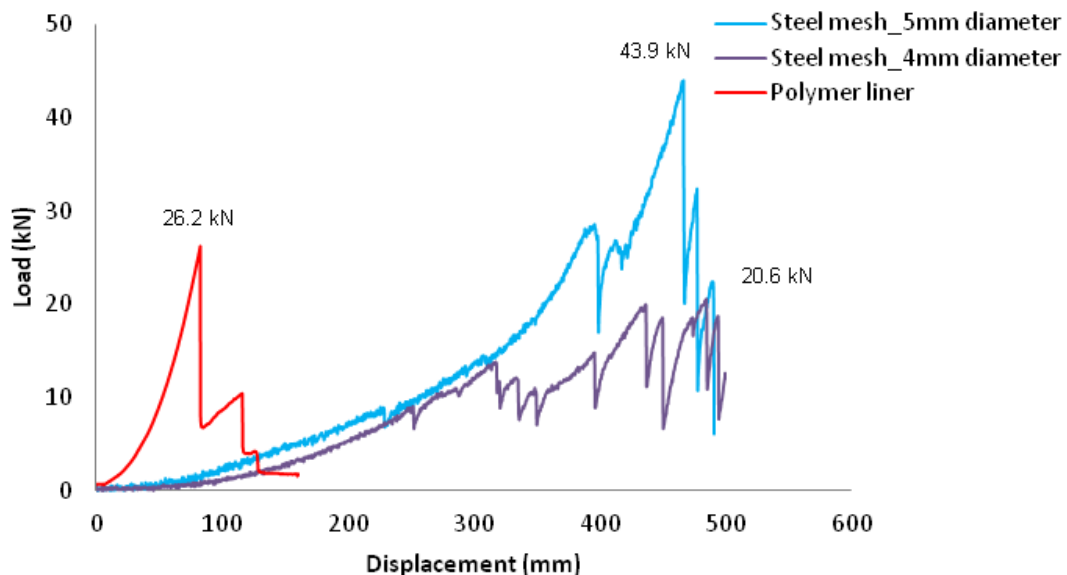


Figure 12 - Comparison of load-displacement curves for all full scale tests

When comparing the bonded polymer and the steel mesh it is evident (Figure 13) that the polymer liner provides higher support loads at lower displacements while it continues to support the strata at large displacements. The polymer liner provides greater confinement to the strata at lower displacements and when overloaded it is still able to provide significant support to the fractured strata as displacement increases.

It is not practical to prevent the formation of mining induced fractures but it is possible to enhance the excavation surface condition by applying an effective support system at an early stage of mining. The nature of rock support is to preserve the rocks self-supporting ability by the use of the rock support material rather than holding the dead weight of the rock. Even if the plain polymer sheet is weaker than steel mesh, it is able to provide better load bearing capacity when bonded to the broken concrete slab than steel mesh in a similar situation. If the performance of the bonded polymer was replicated in the full scale test, the expected peak load would be around 70 kN (7 tonnes), 50% greater than standard roof mesh.

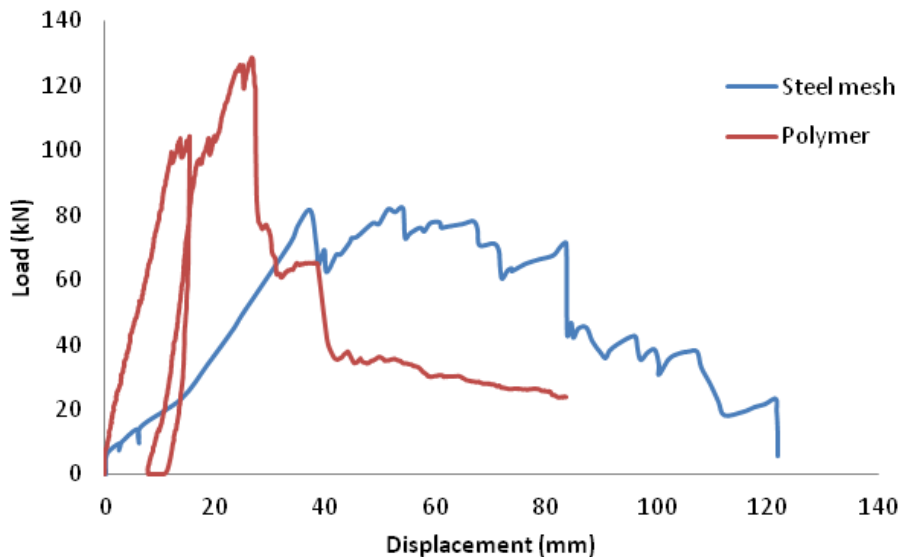


Figure 13 - Load-displacement curves for bonded polymer liner and steel mesh

## CONCLUSIONS

The objective of this study was to determine the ultimate strength of a polymer liner and steel mesh using full scale tests and to compare the results. Although the 4.5 mm thick polymer liner was not as strong as the 5.3 mm diameter steel mesh, it was much stiffer, providing confinement at an earlier stage. Shown by the large scale tests the most important property of the polymer liner is the ability to bond to the rock surface, creating a polymer-rock composite. As with all composite materials, the whole is greater than the sum of the parts. This suggests that the polymer liner shows superior potential for underground rock support.

The polymer used in the tests was not the actual thin spray-on liner being formulated at the University of Wollongong (ToughSkin), but just an off the shelf product used to validate the test procedures. ToughSkin is a fast setting thin spray-on liner with superior adhesive and mechanical properties which may replace steel mesh for rock support in underground mines. Further full scale tests will involve the spray application of the latest ToughSkin product.

## REFERENCES

- Dolinar, D R, 2006. Load capacity and stiffness characteristics of screen materials used for surface control in underground coal mines, in *Proceedings of 25th International Conference on Ground Control in Mining*, pp 152-158 (Morgantown, West Virginia).
- Gadde, M M, Rusnak, J A and Honse, J W, 2006. Behaviour of welded wire mesh used for skin control in underground coal mines, in *Proceedings of 25th International Conference on Ground Control in Mining*, pp 142-151 (Morgantown, West Virginia).
- Lukey, C, Spinks, G, Baafi, E, Porter, I and Nemcik, J, 2008. Polymer-based alternative to steel mesh for coal mine strata reinforcement, in *Proceedings of the Coal 2008 8th Underground Coal Operators' Conference* (ed: N Aziz and J Nemcik), pp 110-116 (Illawarra Branch, The Australasian Institute of Mining and Metallurgy: Wollongong). <http://ro.uow.edu.au/coal/9/>.

- Nemcik, J, Porter, I, Baafi, E and Lukey, C, 2009a. Geotechnical assessment of skin reinforcement in underground mines, in *Proceedings of 28th International Conference on Ground Control in Mining*, pp 256-260 (Morgantown, West Virginia).  
[http://icgcm.conferenceacademy.com/papers/detail.aspx?subdomain=icgcm\\_and iid=230](http://icgcm.conferenceacademy.com/papers/detail.aspx?subdomain=icgcm_and iid=230).
- Nemcik, J, Porter, I, Baafi, E, and Lukey, C, 2009b. Geotechnical assessment of polymeric materials as skin reinforcement in underground mines, in *Proceedings of the Coal 2009 9th Underground Coal Operators' Conference* (ed: N Aziz and J Nemcik), pp 70-77 (Illawarra Branch, The Australasian Institute of Mining and Metallurgy: Wollongong). <http://ro.uow.edu.au/coal/81/>.
- Nemcik, J, Porter, I, Baafi, E, and Towns, J, 2011a. Bearing capacity of a glass fibre reinforced polymer liner, in *Proceedings of the Coal 2011 11th Underground Coal Operators' Conference* (ed: N Aziz), pp 148-153 (Wollongong). <http://ro.uow.edu.au/coal/351/>.
- Nemcik, J, Porter, I, Baafi, E, and Navin, J, 2011b. Determining the ultimate strength of 'tough skin', a glass fibre reinforced polymer liner, in *Proceedings of the Coal 2011 11th Underground Coal Operators' Conference* (ed: N Aziz), pp 154-158 (Wollongong). <http://ro.uow.edu.au/coal/352/>.
- Nemcik, J, Porter, I, and Baafi, E, 2013. Tear tests of glass fibre reinforced polymer skin spray-on liner, in *Proceedings of the Coal 2013 13th Underground Coal Operators' Conference* (ed: N Aziz, B Kininmonth, J Nemcik, T Ren and J Hoelle), pp 170-175 (Wollongong).  
<http://ro.uow.edu.au/coal/452/>.
- Shan, Z, Porter, I, Nemcik, J and Baafi, E, 2013. Comparing the reinforcement capacity of welded steel mesh and a thin spray-on liner (TSL) using large scale laboratory tests, in *Proceedings of the 6th International Symposium on Green Mining* (ed: T Ren and J Xu), pp 69-73 (Wollongong).
- Thompson, A G, 2001. Rock support action of mesh quantified by testing and analysis, in *Surface Support in Mining* (ed: Y Potvin, T R Stacey and J Hadjigeorgiou), pp 391-398 (Australian centre for Geomechanics: Nedlands).
- Tannant, D. D. 2001, Load capacity and stiffness of welded wire, chain link, and expanded metal mesh, in *Surface Support in Mining* (ed: Y Potvin, T R Stacey and J Hadjigeorgiou), pp 399-402 (Australian centre for Geomechanics: Nedlands).

# EFFECTS OF SHEARING DIRECTION ON SHEAR BEHAVIOUR OF ROCK JOINTS

Ali Mirzaghobanali, Haleh Rasekh, Naj Aziz and Jan Nemcik

**ABSTRACT:** Effects of shearing direction on shear behaviour of rock joints were studied. Artificial triangular asperities with initial asperity angles of  $9.5^\circ$  (Type I) and  $18.5^\circ$  (Type II), inclined at  $0^\circ$ ,  $30^\circ$ , and  $60^\circ$  from the direction perpendicular to the shearing movement were cast using high strength gypsum plaster. Samples were tested at different initial normal stress ranging from 0.56 MPa to 2.4 MPa under constant normal stiffness of 8 kN/mm. The measured data were analysed and accompanied by a mathematical model to describe the effects of shearing direction on shear strength of rock joints. The proposed model simulated reasonably the reduction in the shear strength of rock joints with increase in the angle of shearing direction.

## INTRODUCTION

The effects of joints and discontinuities on the mechanical behaviour of rock mass and the stability of underground structures constructed in close proximity to jointed rock masses are a well understood topic. In this context, many researchers have investigated the shear behaviour of rock joints with different values of initial normal stress and initial asperity angle. Patton (1966) was among the first who studied the shear behaviour of rock joints by conducting direct shear tests on artificial triangular asperities under Constant Normal Load (CNL) conditions where the acting normal load remains unchanged during shearing. A failure criterion was also introduced by Patton (1966) to represent the sliding and breakage mechanisms captured through experiments. Barton (1973) performed direct shear tests on real joints and proposed an empirical shear strength model incorporating the concept of Joint Roughness Coefficient (JRC). Barton (1976) revised the concept of JRC and introduced the concept of mobilised Joint Roughness Coefficient ( $JRC_{mob}$ ) to replicate the hardening and softening phenomena as a function of the normalised shear displacement. Seidel and Haberfield (1995) investigated the shear behaviour of rock joints under Constant Normal Stiffness (CNS) conditions where the normal load varies due to the joint's dilation and proposed a shear strength model based on the energy balance theory. Indrarata (2000) applied the Fourier series to describe the variation of normal displacement in relation of shear displacement under CNS conditions, extending the shear strength model proposed by Seidel and Haberfield (1995). Phien-wej *et al.* (1991) investigated the shear behaviour of infilled rock joints under CNL conditions and proposed an experimental model to quantify the shear strength of infilled rock joints. Other studies on shear behaviour of infilled rock joints have been carried out by Ladanyi and Archambault (1977), Papaliangas *et al.* (1990, 1993), de Toledo and de Freitas (1993), Indraratna *et al.* (1999, 2005), and Oliveira and Indraratna (2010) under CNL and CNS conditions.

No studies have been recorded in the literature on the effects of shearing direction on shear behaviour of rock joints under CNS conditions. A systematic experimental study was carried out using artificial rock joints for various initial normal stresses, asperity angles, and angles of shearing direction under CNS conditions. The experimental data were critically investigated and a revised shear strength criterion was proposed to describe the effects of shearing direction on shear strength of rock joints.

## TEST APPARATUS, SAMPLE PREPARATION, AND EXPERIMENTAL PLAN

The large scale direct shear apparatus at the rock mechanics laboratory of University of Wollongong was used to perform the shear tests. The instrument had two main sections, a controller unit and a mechanical part as shown in Figure 1. The rate of shear displacement was set by the digital controller unit. The mechanical part consisted of two steel shearing boxes, 250 mm in length, 75 mm in width, and 150 mm and 100 mm in height of the top and bottom boxes respectively. The initial normal load was applied to the samples using a hydraulic jack located on the top of the instrument. The joint dilation was confined by a set of springs with stiffness of 8 kN/mm, simulating the effect of surrounding rock mass. A hydraulic actuator controlled by the digital controller unit, displaced the lower box laterally. The upper

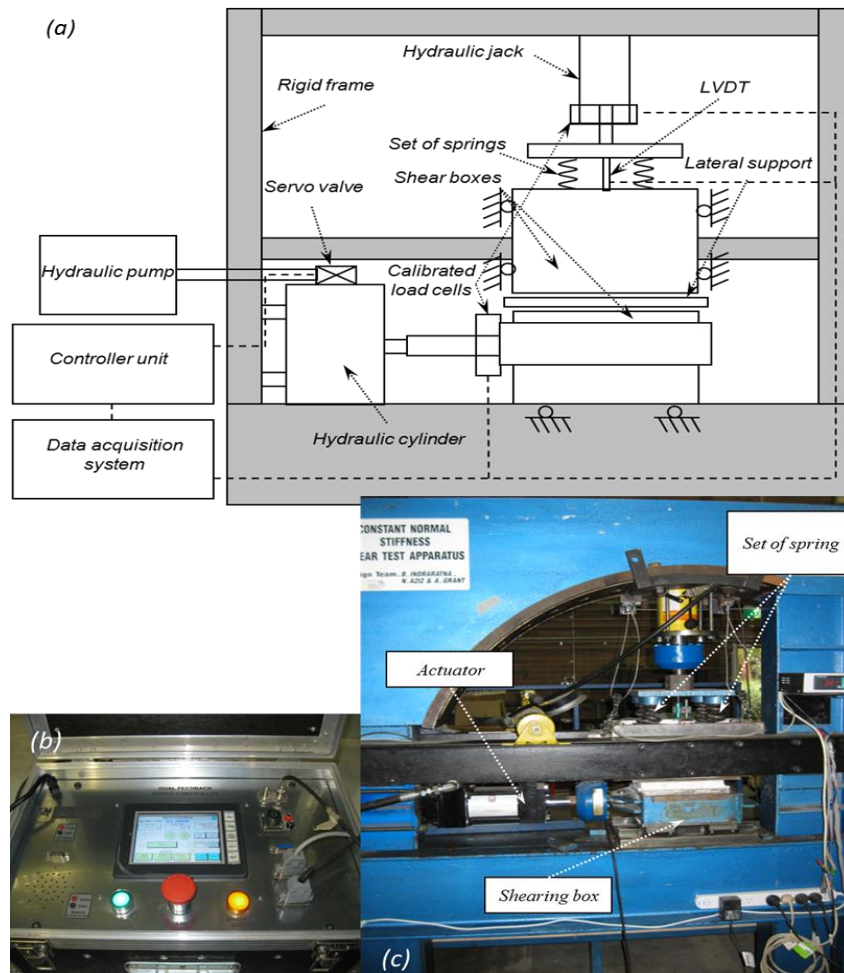


**Figure 1 - (a) Schematic diagram of the CNS cyclic direct shear apparatus, (b) Controller unit, (c) General view of the apparatus**

box moved only in a vertical direction on ball bearings such that any relative rotation of the joint surfaces was avoided. The amounts of shear and normal loads were recorded by strain meters mounted on the load cells and the normal displacement was recorded using a Linear Variable Differential Transformer (LVDT).

Two initial asperity angles  $9.5^\circ$  (Type I) and  $18.5^\circ$  (Type II) representing low and high roughness of field joints were considered to prepare moulds. For each type, tooth shaped asperities were inclined at  $0^\circ$ ,  $30^\circ$ , and  $60^\circ$  from the direction perpendicular to the shearing movement making six different asperity surfaces. High strength gypsum plaster ( $\text{CaSO}_4 \cdot \text{H}_2\text{O}$  hemihydrates) with a mixing ratio of 3.5:1 by weight of plaster to water was used to prepare the samples. The amount of plaster and water were 2100 gm and 600 gm for bottom samples respectively, while these amounts were 4900 gm and 1400 gm for top samples. During sample preparation, mild vibration was applied to the mould externally to eliminate any entrapped air within the samples. The samples were then left for two hours to satisfy the initial setting time. They were then allowed to cure in an oven for 14 days at a constant temperature of  $40^\circ\text{C}$ . Subsequently, the samples were cooled down to room temperature. A close view of the selected prepared samples is shown in Figure 2. Appropriate tests performed on samples made from high strength gypsum plaster, indicated an average basic friction angle of  $35^\circ$  and uniaxial compressive strength of 60 MPa.

More than 18 direct shear tests were conducted on the samples. The values of initial normal stress were 0.56 MPa, 1.64 MPa, and 2.4 MPa while the rate of shear displacement was set to 0.5 mm/min. A constant normal stiffness of 8 kN/mm was incorporated to restrict the dilation. The values of shear load, normal load, and normal displacement were monitored against shear displacement during the whole length of each test.

## TEST RESULTS AND ANALYSIS

The experimental results for different conditions of initial normal stress, asperity type, and angle of shearing direction are shown in Figures 3 to 5.

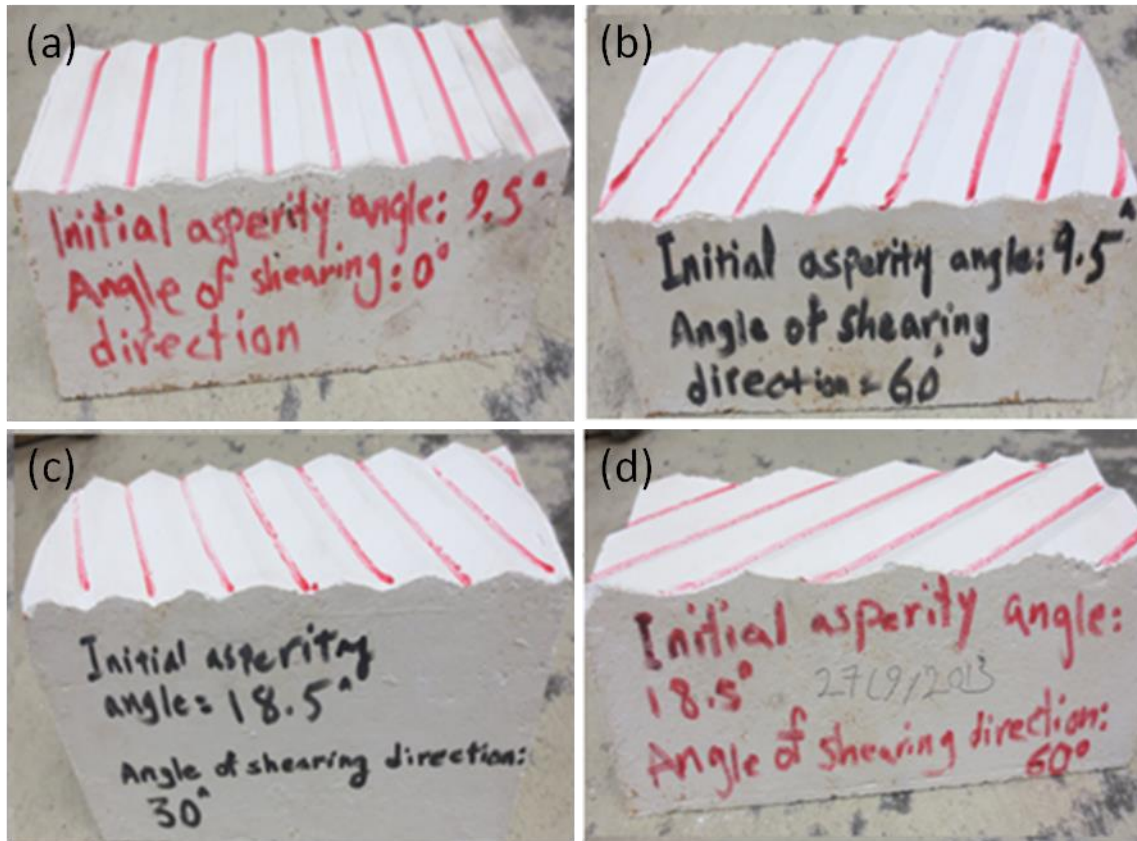


**Figure 2 - Selected prepared samples; (a) Type I and 0° angle of shearing direction, (b) Type I and 60° angle of shearing direction, (c) Type II and 30° angle of shearing direction, (d) Type II and 60° angle of shearing direction**

In general, it is observed that the shear strength decreased as the angle of shearing direction increased. For low values of initial normal stress (close to 0.56 MPa), the gap between the shear strength profiles with various angles of shearing direction, is more pronounced for the Type II asperity surface when compared to the Type I asperity surface. For the Type I asperity surface and 2.4 MPa of initial normal stress, the shear strength decreased 23 % by increasing the angle of shearing direction from 0° to 60°. This value was determined to be 29% for the Type II asperity surface.

The dilation behaviour of rock joints was decreased by increasing the angle of shearing direction. For instance, the maximum magnitude of dilation for the Type I asperity surface with 30° of shearing direction and 0.56 MPa of initial normal stress, was measured as 1.06 mm whereas this value was 0.32 mm for the 60° shearing direction. The dilation curves deviated from linearity to dome shaped with increase in the initial normal stress due to the asperity breakage mechanism.

As shearing was conducted under CNS conditions, the variations of normal stress showed similar trends with normal displacement, which affected the shear strength.

## MATHEMATICAL MODELLING

The experimental studies showed that the shear strength decreases with increase in the angle of shearing direction. This can be described by the lower asperity contact angle resists against the shearing in comparison to the initial asperity angle as shown in Figure 6.

In Figure 6,  $N$  is the normal force,  $S$  is the shear force,  $i_0$  is the initial asperity angle,  $\beta$  is the angle of shearing direction, and  $i$  is the asperity contact angle.

According to Figure 6, the relationship between the initial asperity angle and asperity contact angle is deduced as:

$$i = \tan^{-1} [\tan(i_0) \times \cos \beta] \tag{1}$$

The shear strength criterion for rock joints based on Newland and Alley (1957) is obtained as:

$$\tau = \sigma_n \tan(\phi_b + i) \tag{2}$$

where,  $\tau$  is the shear strength,  $\sigma_n$  is the normal stress, and  $\phi_b$  is the basic friction angle.

By introducing Equation (1) in Equation (2), the shear strength for rock joints oriented from the direction of shearing is extended as:

$$\tau = \sigma_n \tan(\phi_b + \tan^{-1} [\tan(i_0) \times \cos \beta]) \tag{3}$$

The comparison between the model predicted results and experimental data is depicted in Figure 7.

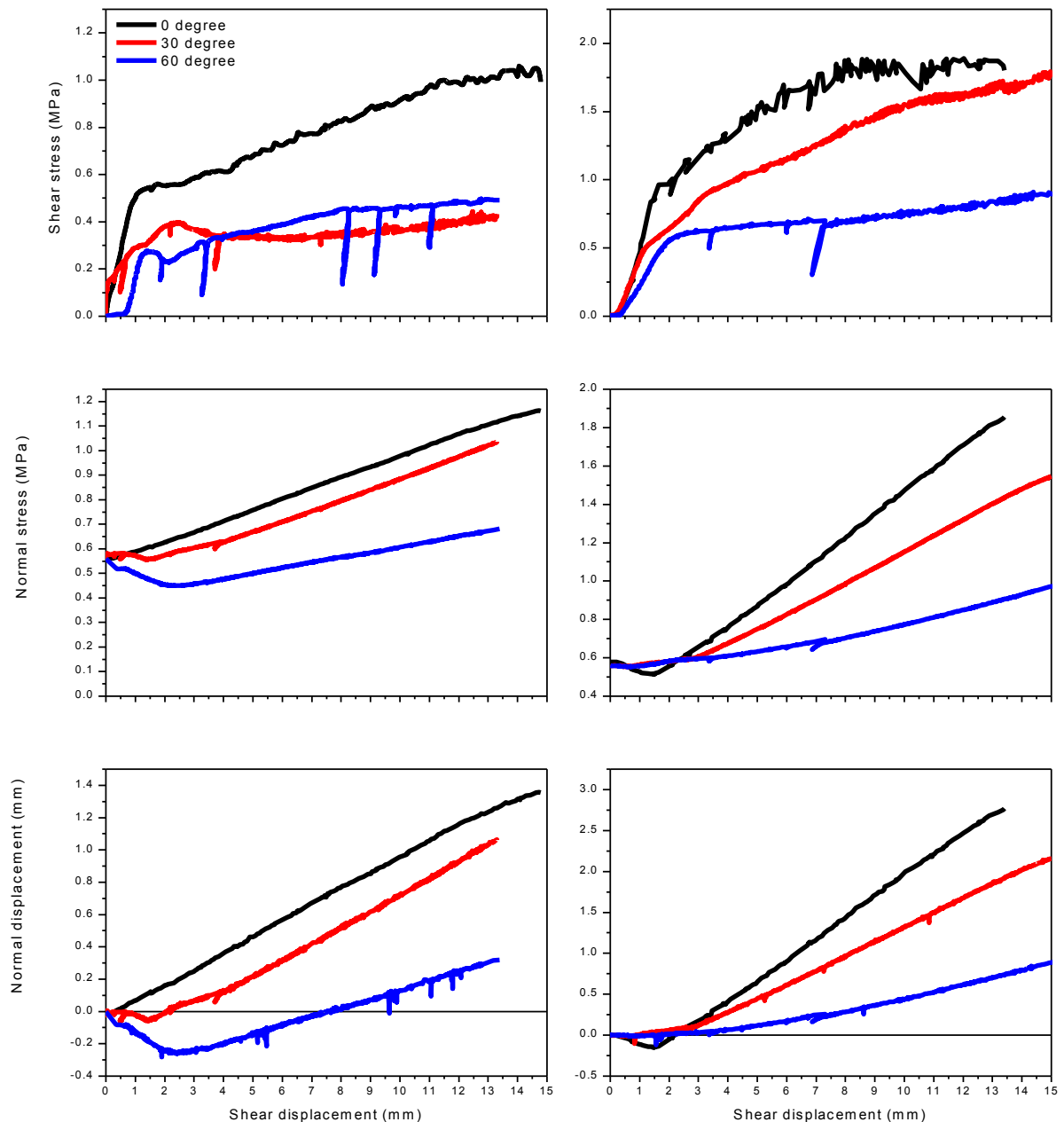


Figure 3 - Experimental results for 0.56 MPa of initial normal stress; (left) Type I asperity surface, (right) Type II asperity surface

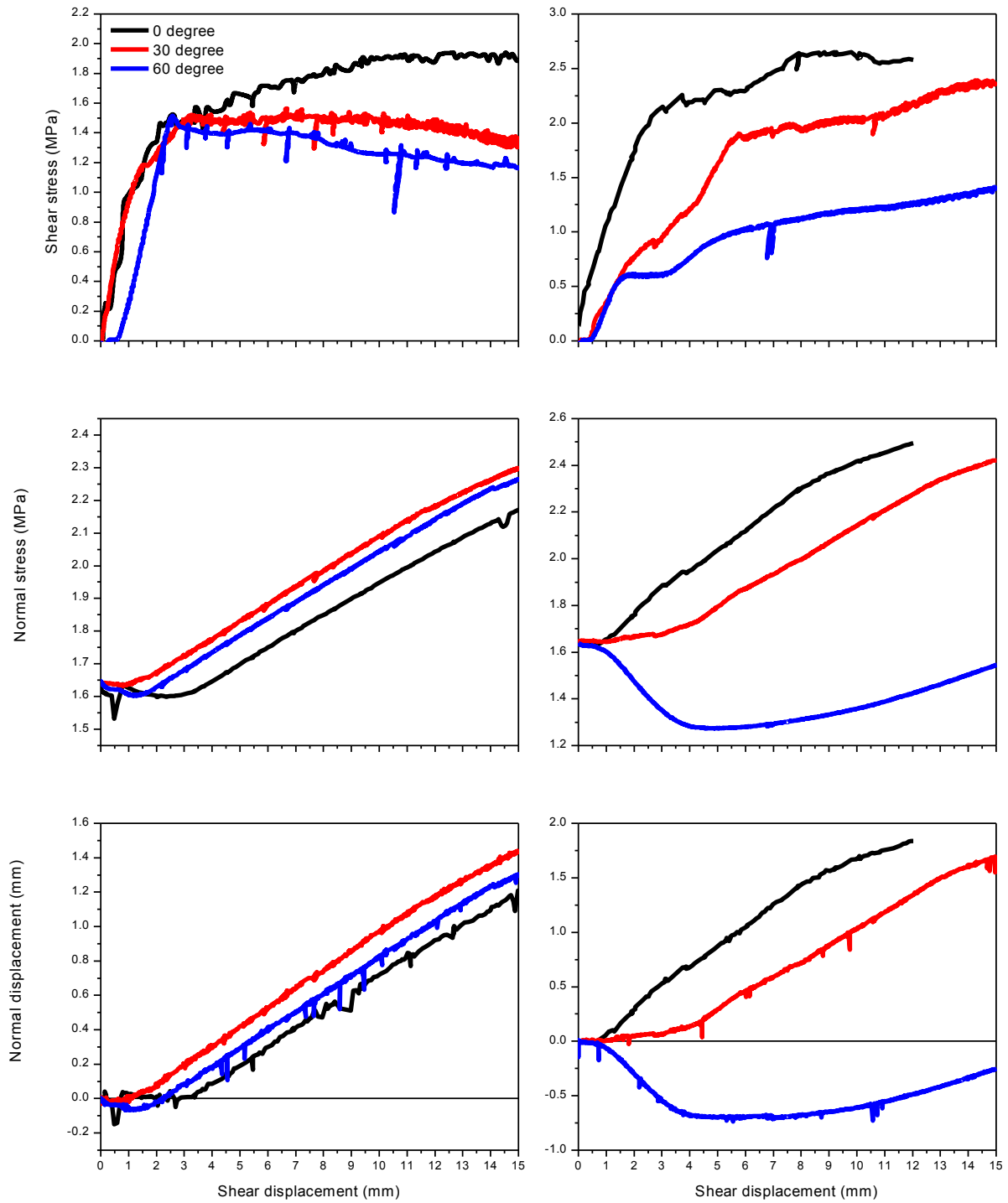


Figure 4 - Experimental results for 1.64 MPa of initial normal stress; (left) Type I asperity surface, (right) Type II asperity surface

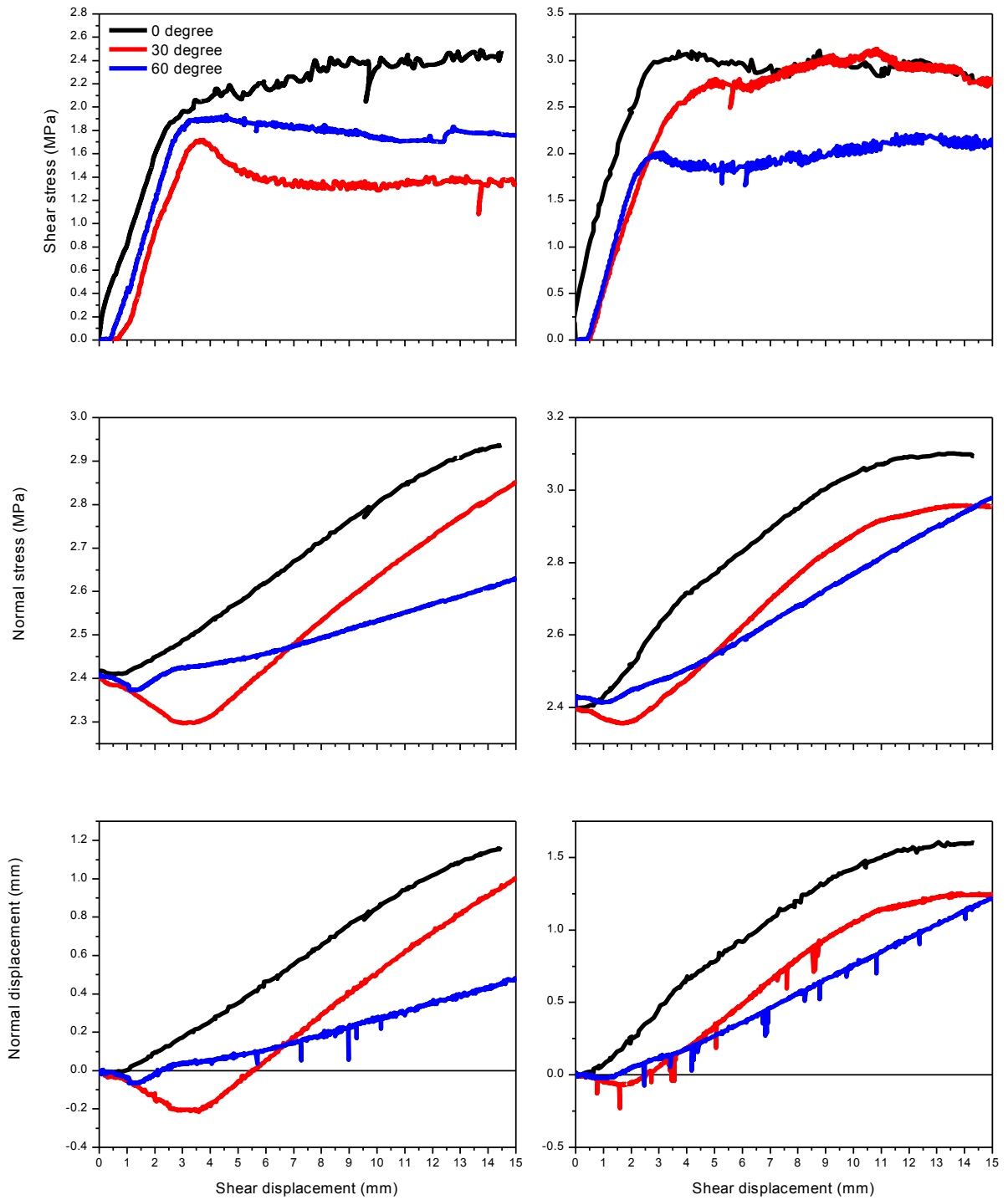


Figure 5 - Experimental results for 2.4 MPa of initial normal stress; (left) Type I asperity surface, (right) Type II asperity surface

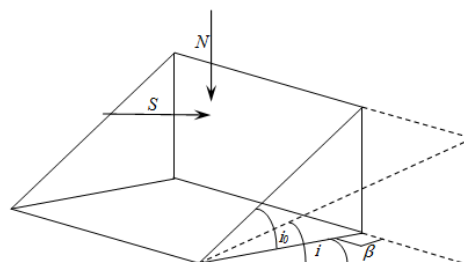
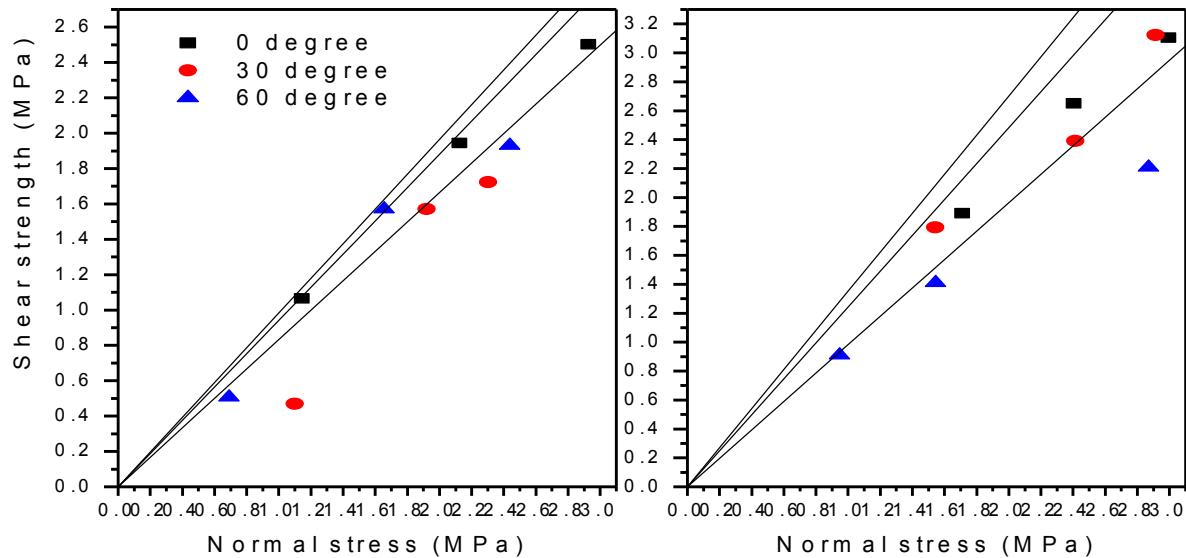


Figure 6 - Asperity shearing under shear and normal force

It is noted that the proposed model is able to replicate the reduction in the shear strength with increase in the angle of shearing direction. Generally, the results of simulation are closer to the measured data for the Type I asperity surface rather than the Type II asperity surface. Furthermore, the best agreement between the proposed model and experimental data is achieved for angle of shearing of 60° where the asperity damage is not significant. Nevertheless, discrepancies are observed between the proposed model and experimental results where the shearing mechanism is governed by the asperity breakage. This behaviour is expected for higher values of initial roughness and normal stress as the proposed model is based on the sliding mechanism.



**Figure 7 - Comparison between the proposed model and experimental data; (left) Type I asperity surface, (right) Type II asperity surface; (line) model predicted, and (symbols) experimental data**

## CONCLUSIONS

The results of the systematic experimental study conducted on the shear behaviour of rock joints oriented from shearing direction were presented in this paper. The following main conclusions were extracted based on this study:

- The shear strength of rock joints is significantly influenced by the angle of shearing direction. By changing the angle of shearing direction from 0° to 60°, the values of shear strength were observed to decrease.
- The magnitudes of dilation decreased as the angle of shearing direction increased due to a lower asperity contact angle.
- A revised shear strength criterion was proposed to describe the effects of shearing direction on shear strength of rock joints.
- The proposed model simulated the shear strength of rock joints fairly where the asperity damage was not significant. This is remarked for the tests carried out on the Type I asperity surface with 60° of shearing direction.

## REFERENCES

- Barton, N., 1973. Review of a new shear-strength criterion for rock joints. *Engineering Geology*, 7, 287-332.
- Barton, N. 1976. The shear strength of rock and rock joints. *International Journal of Rock Mechanics and Mining Sciences*, 13, 255-279.
- de Toledo, P. E. C. and de Freitas, M. H. 1993. Laboratory testing and parameters controlling the shear strength of filled rock joints., *Geotechnique*, Vol. 43, pp. 1-19.
- Indraratna, B., Haque, A. and Aziz, N. 1999. Shear behaviour of idealized infilled joints under constant normal stiffness. *Geotechnique*., Vol. 49, pp. 331-355.

- 
- Indraratna, B. A. H., A. 2000. *Shear behaviour of rock joints*, Rotterdam, Netherlands, A.A. Balkema.
- Indraratna, B., Welideniya, H. S. and Brown, E. T. 2005. A shear strength model for idealised infilled joints under constant normal stiffness. *Geotechnique.*, Vol. 55, pp. 215-226.
- Ladanyi, B. and Archambault, G. 1977. Shear strength and deformability of filled indented joints. *In: 1st International Symposium on Geotechnics of Structurally Complex Formations.*, Capri, pp. 317-326.
- Newland, P. L. and Alley, B. H. 1957. Volume changes in drained triaxial tests on granular materials. *Geotechnique.*, Vol. 7, pp. 17-34.
- Oliveira, D. A. F. and Indraratna, B. 2010. Comparison between models of rock discontinuity strength and deformation. *Journal of Geotechnical and Geoenvironmental Engineering*, 136, 864-874.
- Papaliangas, T., Lumsden, A. C., Hencher, S. R. and Manolopoulou, S. 1990. Shear strength of modelled filled rock joints. *In: Int. Conf. on Rock Joints.*, N. Barton and O. Stephansson (eds), Balkema, Rotterdam, pp. 275-282.
- Papaliangas, T., Hencher, S. R., Lumsden, A. C. and Manolopoulou, S. 1993. The effect of frictional fill thickness on the shear strength of rock discontinuities. *International Journal of Rock Mechanics and Mining Sciences.*, Vol. 30, pp. 81-91.
- Patton, F. D. 1966. Multiple modes of shear failure in rocks. *In: 1st Cong. ISRM*, 1966 Lisbon. 509-513.
- Phien-Wej, N., Shrestha, U. B. and Rantucci, G. 1991. Effect of infill thickness on shear behaviour of rock joints. *International Journal of Rock Mechanics and Mining Sciences and Geomechanics Abstracts.*, Vol. 28, A70.
- Seidel, J. P. and Haberfield, C. M. 1995. The application of energy principles to the determination of the sliding resistance of rock joints. *Rock Mechanics and Rock Engineering*, 28, 211-226.

# A STUDY ON THE SHEAR BEHAVIOUR OF INFILLED ROCK JOINTS UNDER CYCLIC LOADING AND CONSTANT NORMAL STIFFNESS CONDITIONS

Ali Mirzaghobanali, Jan Nemcik and Naj Aziz

**ABSTRACT:** Shear behaviour of infilled rock joints under cyclic loading and constant normal stiffness conditions were studied. The experiments were carried out in a cyclic loading direct shear apparatus. The laboratory studies were conducted using saw tooth shaped asperities cast in high strength gypsum plaster. Two types of triangular asperities inclined at 9.5° (Type I) and 18.5° (Type II) from the shearing direction were considered for testing. Clayey sand (75% fine sand and 25% Kaolinite) at initial moisture content of 12.5% was selected as the infill material. Profile of shear planes and strength envelopes for different conditions of infill thickness to asperity height ratio, initial normal stress, and initial asperity angle were investigated.

## INTRODUCTION

Rock masses are heterogeneous and often contain joints and discontinuities, separating them into different blocks. When a rock mass is excavated, sliding along the joints may be experienced. The magnitude and direction of these movements is controlled by the shear behaviour of joints present within the rock mass. Depending on the origin of joints and mineralogy of the rock, joints may have planar (smooth) or rough surfaces. For planar joints, the shear strength is equal to the frictional resistance only as there are no asperities. In the case of rough joints, an additional shear resistance is generated by the roughness of the joint surface. Moreover, in circumstances where the dilation is confined by the surrounding rocks, the increase in the normal stress due to overriding of asperities increases the joint shear strength. During earthquakes and blasting, cyclic loading shearing degrades the joint roughness. The asperity degradation decreases the dilation magnitude and eventually reduces the friction angle and normal stress acting on the joint surface.

By representing joint shearing as an interaction between two media, Plesha (1987) introduced a softening cyclic loading model by assuming sliding mechanism along an inclined asperity angle degraded exponentially due to a portion of the plastic shear work. The analytical model of Plesha (1987) was further verified by Hutson and Dowding (1990) under Constant Normal Load (CNL) conditions in which the normal load remains constant during shearing. The original model of Plesha (1987) was later revised to represent sinusoidal asperities and to include the second order asperity effects (Qiu and Plesha 1991; Lee, *et al.*, 2001). In another study, Jafari *et al.*, (2003) performed a series of cyclic loading shear tests on undulated joints under CNL conditions for different applied normal stresses and suggested an empirical relationship for the variation of peak shear strength against the number of loading cycles. Other studies on cyclic loading shear behaviour of rock joints under CNL conditions were carried out by Aubry *et al.*, (1990), Huang *et al.*, (1993), Souley *et al.*, (1995), Dong and Pan (1996), Fox *et al.*, (1998), Stupkiewicz and Mróz (2001), and Puntel *et al.*, (2006).

The studies mentioned above, focused on clean joints (unfilled) only. Recently, Mirzaghobanali *et al.*, (2013) investigated the effects of cyclic loading on the shear behaviour of infilled rock joints under Constant Normal Stiffness (CNS) conditions. This paper is aimed studying the strength envelopes and profile of shear planes of infilled rock joints subjected to cyclic loading for different ratios of infill thickness ( $t$ ) to asperity height ( $a$ ), initial normal stresses ( $\sigma_{n0}$ ), and initial asperity angles.

## TEST APPARATUS, SPECIMENS, AND EXPERIMENTAL PLAN

Experiments were carried out at the Rock Mechanics Laboratory, University of Wollongong, NSW, Australia, using the large scale cyclic direct shear apparatus. The instrument consisted of two main parts, controller unit and mechanical section as shown in Figure 1. The digital controller was able to assign the cyclic displacement of the sample. The mechanical part had two steel shearing boxes, 250

mm in length, 75 mm in width, and 150 mm and 100 mm in height of the top and bottom boxes respectively. A hydraulic jack located on top of the instrument was used to apply the initial normal load. A set of springs with stiffness of 8 kN/mm was incorporated to confine the joint dilation simulating the effect of surrounding rock mass. The lower box was only displaced laterally via a hydraulic actuator driven by the digital controller unit. The upper box moves only in a vertical direction on ball bearings such that any relative rotation of the joint surfaces is avoided. The shear and normal loads were measured by strain meters mounted on the load cells and the normal displacement was recorded using Linear Variable Differential Transformer (LVDT).

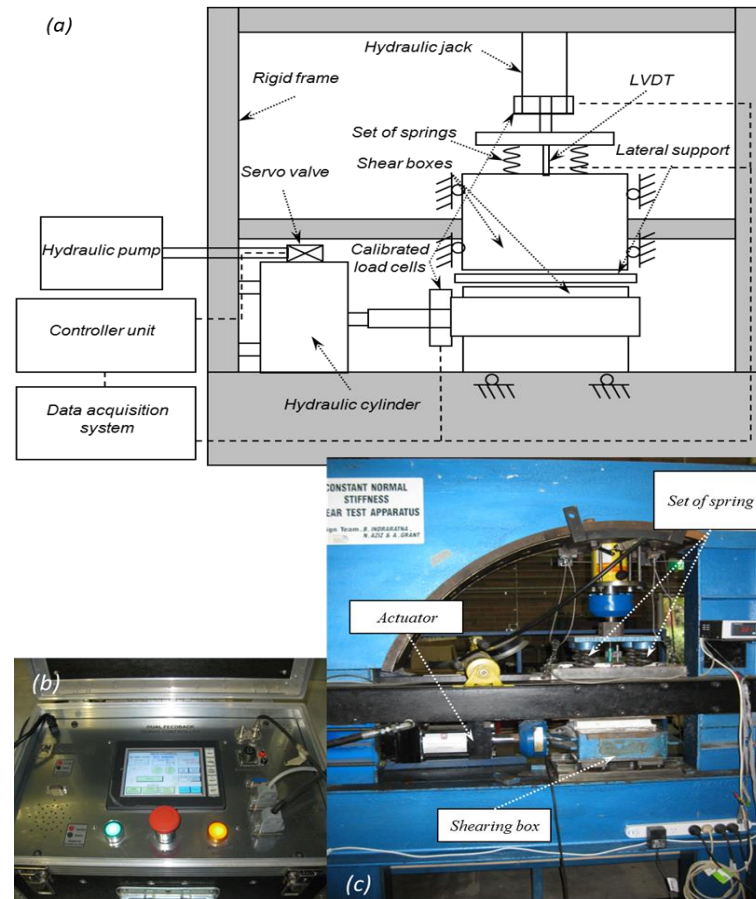


**Figure 1 - (a) Schematic diagram of the CNS cyclic direct shear apparatus (b) controller unit (c) general view of the apparatus**

Two different initial asperity angles  $9.5^\circ$  (Type I) and  $18.5^\circ$  (Type II) were selected to prepare triangular asperity moulds. The equivalent Joint Roughness Coefficient (JRC) values of 4.2 and 9 have been calculated for Types I and II asperity surfaces using the method suggested by Xie and Parisseau (1992). For each mould, a number of fully mated joints of high strength gypsum plaster ( $\text{CaSo}_4 \cdot \text{H}_2\text{O}$  hemihydrates) were cast using a mixing ratio of 3.5:1 by weight of plaster to water. The bottom block was prepared inside the bottom mould containing the required surface profile and left for two hours to cure. The matching specimen was then cast on the top of the bottom specimen to ensure the fully mated conditions and the whole assembly was left for two additional hours to satisfy the initial setting time. During sample preparation, mild vibration was applied to the mould externally to eliminate any entrapped air within the samples. The samples were then allowed to cure in an oven for 14 days at a constant temperature of  $40^\circ\text{C}$ . Prior to the cyclic shearing, the prepared samples were then acclimatised to room temperature. Clayey sand (75% fine sand and 25% Kaolinite) at initial moisture content of 12.5% was selected as infill material. After preparation of the infill material, it was kept inside a sealed container to ensure retention of the percentage of moisture. In order to prepare the infill surface, the cured bottom block was positioned inside the bottom shearing box in a way that allowed the surface profile to stay slightly above the edge of the bottom box. A closure over the specimen from the joint plane was provided by attaching an adjustable collar with the same shape as the surface profile on the top of the specimen. The collar was set to create the required infill thickness by precisely measuring the closure at four corner points. The infill material was then placed inside the collar and extended over the surface

area using a spatula. Once, the collar was filled, the infill material was trimmed and compacted with a steel plate having the same triangular shape as the asperities. The collar was then removed and the bottom part of the sample was placed in the shear apparatus. The top shear box containing the upper sample was then mounted on top of the lower sample, thus sandwiching the infill layer between the two matching plaster surfaces. The smooth lateral confinement, on both sides of the sample, made from stainless steel was assembled to prevent loss of the infill material during cyclic shearing. A close view of artificial infilled joint (Type I asperity surface) with infill thickness to asperity height ratio equals to unity is shown in Figure 2.



**Figure 2 - A close view of artificial infilled joint prepared for testing**

More than 18 cyclic loading direct shear tests were carried out on the samples. Some of the tests were repeated to ensure the accuracy and precision of the measured data. The applied initial normal stresses ( $\sigma_{no}$ ) were 0.56, 1.64, and 2.4 MPa. Three different ratios 0.3, 0.6 and 1 of infill thickness ( $t$ ) to asperity height ( $a$ ) were tested. Infill joints were subjected to predetermined initial normal stress ( $\sigma_{no}$ ) for an hour before shearing. All samples were sheared for four consecutive cycles with total accumulated displacement of 240 mm and a shear rate of 0.5 mm/min to ensure a uniform drained condition of infilled joints. A constant normal stiffness of 8 kN/mm was applied to restrict the dilation. The maximum shear displacement was set to 15 mm.

## RESULTS OF EXPERIMENTS

Figure 3 shows variations of the strength envelopes for infilled rock joints subjected to cyclic loading for different conditions of infill thickness to asperity height and initial asperity angles. At low infill thickness ( $t/a = 0.3$ ) and Type I asperity surface, there is a slight difference in strength envelopes between the first and second shear cycles (Figure 3/left a). As the infill thickness to asperity height was increased to 1, the difference between the strength envelopes of consecutive shear cycles became marginal, verifying that, at high infill thickness to asperity height ratios, the shear behaviour is dominated by the infill material (Figure 3/left c). For  $t/a = 0.3$  and Type II asperity surface, the strength envelope of the first cycle lies significantly above the later cycles (Figure 3/right a). As the number of loading cycles was increased, the strength envelopes under cyclic loading tended to become close to each other and approached that of infill material. It is deduced from strength envelopes of Type I and II asperity surfaces that the gap between the cyclic loading strength envelopes increases with increase in the asperity angle for the same infill thickness to asperity height ratio.

Figure 4 shows the profiles of shear planes for selected infilled joints at different initial normal stresses under cyclic loading. The cyclic loading shear planes were estimated from the measured normal displacement against the shear displacement data, and they are shown by dashed lines in Figure 4.

For  $t/a = 0.3$  and 0.6, the shear planes pass through both infill and asperities (Figures 4 a and b). For  $t/a$  equals to unity, the shear planes for the first cycle pass slightly below the tips of asperities (Figure 4 c). As the number of loading cycles increases, for all the cases the shear planes pass always along a lower elevation as compared to the previous cycles, indicating either the asperity damage or deformation of infill material. The portion of the asperity surface that contributes to the shear planes, increases with the number of shear cycles. The difference between the elevations of shear planes decreases during cyclic

loading. The reduction in the elevations of shear planes for the same values of infill thickness to asperity height and initial normal stress is greater for Type II asperity surfaces in comparison to Type I asperity surfaces. The gap between the shear planes of the first and last loading cycles of the joints with the same asperity type is higher for greater infill thickness to asperity height ratios and initial normal stresses.

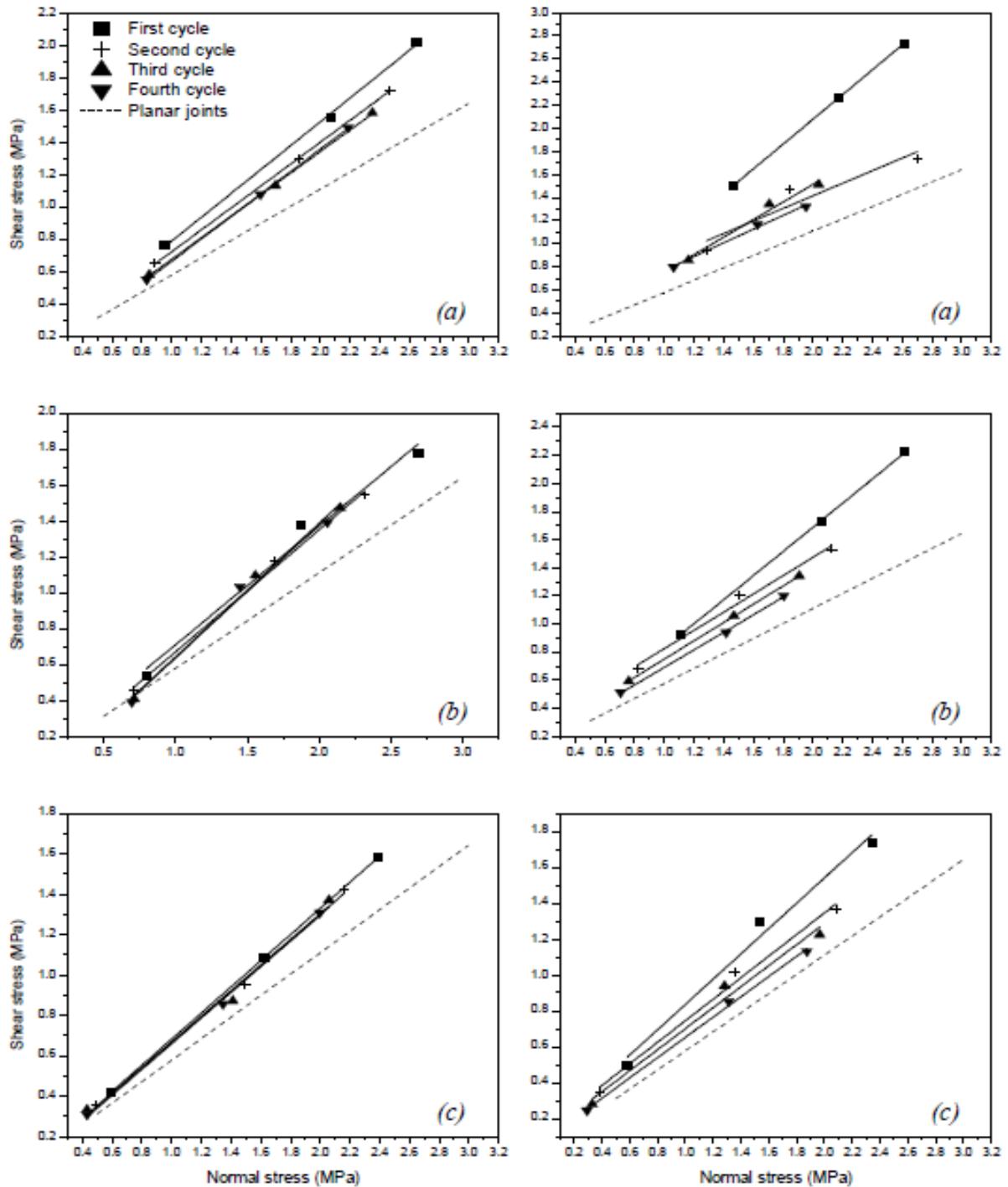


Figure 3 - Strength envelope under cyclic loading: [left] Type I asperity surface, [right] Type II asperity surface, (a)  $t/a=0.3$ , (b)  $t/a=0.6$ , (c)  $t/a=1$

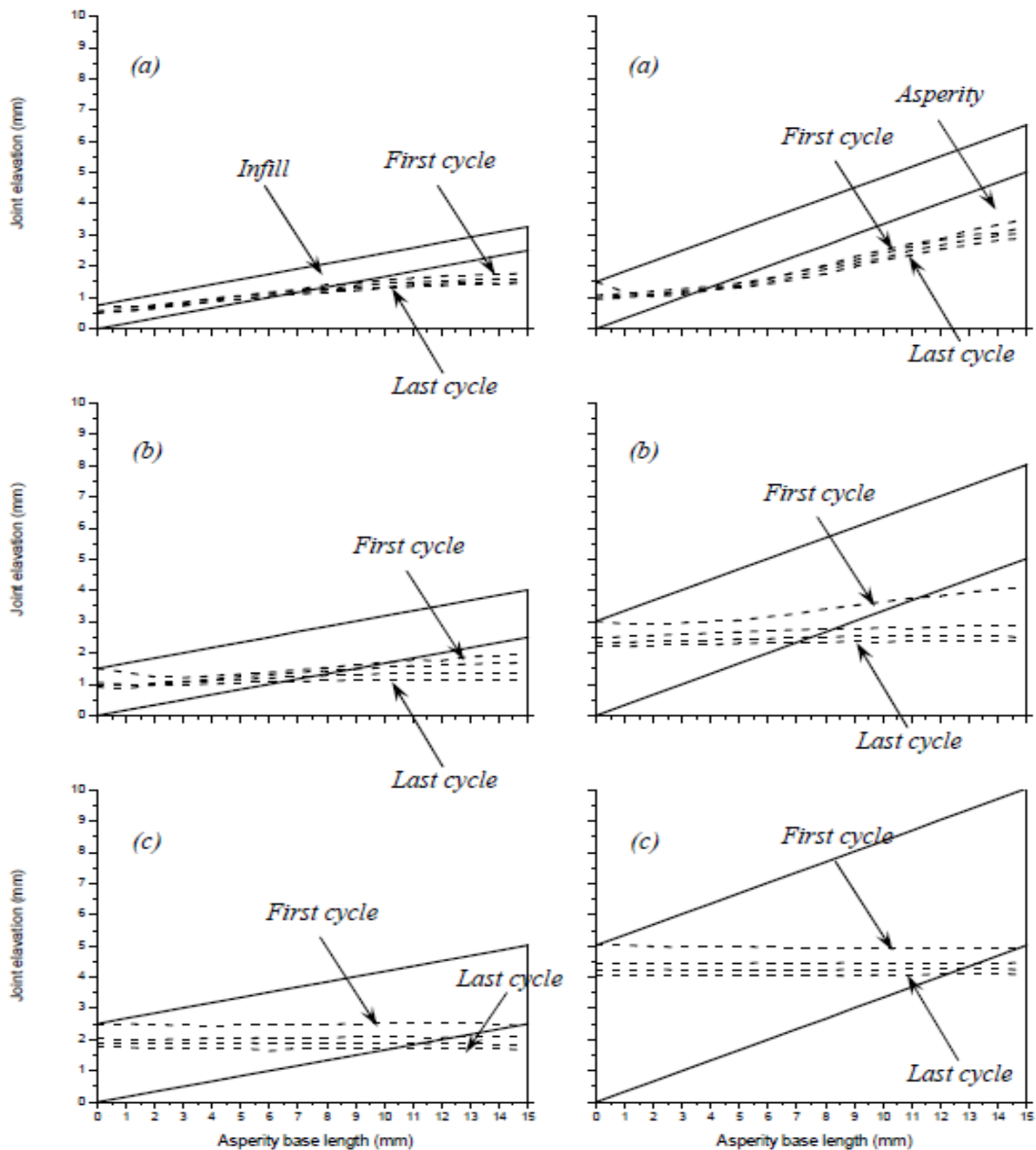


Figure 4 - Relative location of shear plane through infilled joints under cyclic loading, (dashed lines = shear planes): [left] Type I asperity surface, [right] Type II asperity surface, (a)  $t/a = 0.3$  and  $\sigma_{n0} = 0.56$  MPa, (b)  $t/a = 0.6$  and  $\sigma_{n0} = 1.64$  MPa, (c)  $t/a = 1$  and  $\sigma_{n0} = 2.4$  MPa

## CONCLUSIONS

Strength envelope and profile of shear plane of infilled rock joints subjected to cyclic loading shearing under CNS conditions were studied. The following main conclusions can be drawn based on this investigation:

- There is a slight difference in strength envelopes between the first and second shear cycles at low infill thickness ( $t/a = 0.3$ ) and Type I asperity surface.
- For  $t/a = 0.3$  and Type II asperity surface, the strength envelope of the first cycle lies considerably above the later cycles.
- The difference between the strength envelopes of consecutive shear cycles became less pronounced as the infill thickness to asperity height was increased to 1.

- The shear planes always pass along a lower elevation in comparison to the previous cycles, implying either asperity damage or deformation of infill material.
- The gap between the elevations of shear planes decreased as the number of loading cycles increased.
- A higher portion of the asperity surface is sheared with increase in the number of loading cycles.

## REFERENCES

- Aubry, D, Modaressi, A and Modaressi, H, 1990. A constitutive model for cyclic behaviour of interfaces with variable dilatancy. *Computers and Geotechnics*, 9, 47-58.
- Dong, J. J and Pan, Y. W, 1996. A hierarchical model of rough rock joints based on micromechanics. *International Journal of Rock Mechanics and Mining Sciences and Geomechanics Abstract*, 33, 111-123.
- Fox, D. J, Kana, D. D and Hsiung, S. M, 1998. Influence of interface roughness on dynamic shear behavior in jointed rock. *International Journal of Rock Mechanics and Mining Sciences*, 35, 923-940.
- Huang, X, Haimson, B. C, Plesha, M. E and QIU, X, 1993. An investigation of the mechanics of rock joints-Part I. Laboratory investigation. *International Journal of Rock Mechanics and Mining Sciences*, 30, 257-269.
- Hutson, R. W and Dowding, C. H, 1990. Joint asperity degradation during cyclic shear. *International Journal of Rock Mechanics and Mining Sciences*, 27, 109-119.
- Jafari, M. K, Amini Hosseini, K, Pellet, F, Boulon, M and Buzzi, O, 2003. Evaluation of shear strength of rock joints subjected to cyclic loading. *Soil Dynamics and Earthquake Engineering*, 23, 619-630.
- Lee, H. S, Park, Y. J, Cho, T. F and You, K. H, 2001. Influence of asperity degradation on the mechanical behavior of rough rock joints under cyclic shear loading. *International Journal of Rock Mechanics and Mining Sciences*, 38, 967-980.
- Mirzaghorbanali, A, Nemcik, J and Aziz, N, 2013. Effects of cyclic loading on the shear behaviour of infilled rock joints under constant normal stiffness conditions. *Rock Mechanics and Rock Engineering*, DOI: 10.1007/s00603-013-0452-1.
- Plesha, M. E, 1987. Constitutive models for rock discontinuities with dilatancy and surface degradation. *International Journal for Numerical and Analytical Methods in Geomechanics*, 11, 345-362.
- Puntel, E, Bolzon, G and Saouma, V. E, 2006. Fracture mechanics based model for joints under cyclic loading. *Journal of Engineering Mechanics*, 132, 1151- 1159.
- Qiu, X and Plesha, M. E, 1991. Theory for dry wear based on energy. *Journal of Tribology*, 113, 442-451.
- Souley, M, Homand, F and Amadei, B. 1995. An extension to the Saeb and Amadei constitutive model for rock joints to include cyclic loading paths. *International Journal of Rock Mechanics and Mining Sciences*, 32, 101-109.
- Stupkiewicz, S and Mroz, Z, 2001. Modelling of friction and dilatancy effects at brittle interfaces for monotonic and cyclic loading. *Journal of Theoretical and Applied Mechanics*, 3, 707-739.
- Xie, H and Pariseau, W. G, 1992. Fractal estimation of joint roughness coefficient. In: *Int. Conf. on Fractured and Jointed Rock Masses*, Myer, Tsang, Cook and Goodman (eds), Lake Tahoe, California, USA, Rotterdam, Balkema, 125-131.

---

# ALTERNATIVE EXCAVATION METHODS IN UNDERGROUND COAL MINING

C Donnelly<sup>1</sup>, G Ramage<sup>2</sup> and M Donghi<sup>3</sup>

**ABSTRACT:** With the recent turbulent nature of the global financial environment, project drivers have been challenged with the emphasis being placed on methods to gain early access to ore bodies, rapid development techniques, lower capital costs and reduced labour requirements to name a few. Recently work commenced on a project that is challenging the norm and implementing an alternative excavation method into the Australian coal mining industry by the use of a tunnel boring machine. The tunnel boring machine will mechanically excavate both the Conveyor Drift and Transport Drift at Anglo American's Grosvenor Mine in Moranbah, Queensland. This paper will review this project and provide technical and operational insight into some of the challenges faced in implementing this and other alternative excavation methods in the Australian underground coal industry.

## INTRODUCTION

In recent times, a number of underground coal mine development projects in the Bowen Basin region of Queensland Australia have been undertaken. These projects have been undertaken through varying strata conditions with differing excavation methods, support requirements and differing pieces of equipment.

With the recent turbulent nature of the global financial environment, project drivers have been challenged with an increased emphasis being placed on methods to gain early access to coal, lower capital costs and reduced labour requirements.

The development of safe and effective alternative excavation methods that comply with regulatory requirements is a challenge the industry needs to embrace. Given the current cost pressures being faced by the mining industry, some alternative excavation methods offer the potential for longer term sustainability and rapid development of resources.

Noteworthy projects that have included varying excavation methods in remote and challenging environments include:

- Carborough Downs Drift Development, Australia – Carborough Downs Coal Management Construction of 3 drift entries through drill and blast excavation.
- Kestrel Mine Extension, Australia – Kestrel Coal (Rio Tinto and Mitsui joint venture) Drift development using modified roadheaders supported by a sliding floor as Donnelly, Ramage *et al.*, (2011) explained.
- Ghaghoo Diamond Mine Sand Tunnel, Botswana – Gem Diamonds Construction of a decline through the sands of the Kalahari desert in Botswana, Buthelezi (2012).
- Ok Tedi Mine Drainage Tunnel, Papua New Guinea – Ok Tedi Mining Limited Construction of a 5.3 kilometres tunnel for the purpose of dewatering the open pit mine. The main tunnel development was driven by a 5.6m diameter tunnel boring machine (TBM).

Building on the success of these projects and lessons learnt during their execution, work has recently commenced on a project that is implementing an alternative excavation method into the Australian coal

---

<sup>1</sup> Senior Project Engineer, Redpath Australia Pty Limited, 63 Lavarack Avenue Eagle Farm Qld Australia 4009, Email: clayton.donnelly@redpathmining.com.au, P: 07 3868 5000

<sup>2</sup> General Manager – Coal, Redpath Australia Pty Limited, 63 Lavarack Avenue Eagle Farm Qld Australia 4009, Email: Gavin.Ramage@redpathmining.com.au, P: 07 3868 5000

<sup>3</sup> Operations Manager – Coal, Redpath Australia Pty Limited, 63 Lavarack Avenue Eagle Farm Qld Australia 4009, Email: Mark.Donghi@redpathmining.com.au, P: 07 3868 5000

mining industry through the use of a TBM. The TBM will mechanically excavate both the Conveyor Drift and Transport Drift at Anglo American's Grosvenor Mine in Queensland's Bowen Basin.

## GROSVENOR MINE PROJECT

### Project background

The Grosvenor Mine project (Grosvenor) owned by Anglo American Metallurgical Coal (Met Coal) includes the construction of a new underground coal mine and surface facilities on the northern boundary of the town of Moranbah in the Central Queensland Bowen Basin coal precinct. The project covers the development of an underground longwall mine and associated surface infrastructure to deliver coal to the existing Moranbah North Mine (MNM) (owned by Met Coal) which is located to the North of the Grosvenor site.

The project is the development of a single longwall operation at Grosvenor, producing up to a maximum of 7.5 Mtpa Run-of-Mine (ROM) coal with the average ROM being 6.5 Mtpa. Coal will be transported to MNM via an overland conveyor and processed through an upgraded MNM Coal Preparation Plant. Product coal will be loaded out via the Moranbah North rail facility.

The Grosvenor mine project is planning to mine the Goonyella Middle seam, which forms part of the Moranbah coal formation, by conventional longwall methods. The coal handling system will deliver coal onto a new overland conveyor belt for processing in the existing Moranbah North coal preparation plant.

The underground development scope consists of the construction of a 762 m long 1:6 gradient conveyor drift, a 993 m long 1:8 gradient transport drift, development of the pit bottom area roadways (nominally 2,520m of driveage), and the development of the first longwall tailgate (nominally 10,550 m of driveage).

The contract to undertake the underground development works was awarded in 2012 and will commence excavation of the drifts in the 4<sup>th</sup> quarter of 2013. This paper will discuss the adopted excavation method and the challenges faced in implementing a TBM into a Queensland coal mine.

### Excavation method

The original tender for the development of the underground drifts contemplated the construction using more traditional methods of excavation for coal mine drift development. It was observed in the tender drawings that the nominated ground support for the drifts (primarily rock bolts and shotcrete) was extensive and would lead to a longer construction period due to increased cycle times and slower advance rates and thus an increased cost to construct the drifts. Given these factors an alternative method to excavate the drifts using an earth pressure balance EPB TBM (refer Figure 1) was proposed in lieu of the more traditional Roadheader excavation method.

Following due diligence on the TBM excavation method by Met Coal, the parties worked together through 2012 and the beginning of 2013 to bring the concept of TBM driven drifts into reality. As a result, the two drifts at Grosvenor will be developed with a 135 m long, 8 m diameter EPB TBM commencing in the 4<sup>th</sup> quarter of 2013. The drifts will be fully lined with concrete segments on advance and waste material will be transferred to the surface via a conveyor system assembled in the drifts. The major technical specifications for the TBM are summarised in Table 1 – TBM Specifications.

The use of a TBM to develop coal mine drifts is not unique to the Grosvenor Project. Evidence of the use of TBMs to develop coal mines is referred to in 'White, (1978) and Palmer, (1985).'

### Regulations, the law and construction

For the Grosvenor project the applicable legislation is the Queensland Government's Coal Mining Safety and Health Act (CMSHA), 1999 (Act) and the Coal Mining Safety and Health Regulations (CMSHRA), 2001 (Regulations) as enacted at the time of construction activities being undertaken. As a TBM has not been used in the development of an underground coal mine in Queensland, the initial effort of the project team would be to ensure compliance of the machine to the legislative requirements.

A number of factors needed to be considered during this process including ground support, gas exposure and management, ventilation, dewatering and construction. The following outlines what was

identified by the project team and the solutions put in place to manage the identified risks and hazards to ensure compliance with the applicable laws.



Figure 1 - Assembled EPB TBM

Table 1 - TBM specifications

Bore Diameter	8.0m
Cutterhead Speed	0 - 3.2rpm, constant torque range 3.3 – 6.4rpm, constant power range
Maximum thrust	53,018 kN
Stroke	850mm
Cutters	50, 17” wedge lock, back loading
Power Supply	11kV

**Ground support**

A common practice for underground coal mine development in Queensland, is to commence the initial part of the drift construction as a cut and cover tunnel. Figure 2 and Figure 3 show the initial box cut excavation and the commencement of construction of the Armco tunnel which would subsequently be backfilled and have fibrecrete sprayed internally at the launch location.

Due to the anticipated ground conditions it was viewed that the ground support for the remaining drift lining would be a fully lined precast concrete from the box cut to the target coal seam interface. The benefits of this chosen support are numerous but it primarily added the benefit of a 50 year drift life with no necessity for remedial or rehabilitation works during the life of the mine. The precast concrete lining further provided a ground support system that would limit the possibility of gases being present in the drift both during construction and in operation.

The ground support system pre-cast concrete segments is the same type of construction used in civil tunnel construction around the world, with the ground support having a considerably extended life over traditional coal mining support mechanisms. As referred to in 'White, (1978)' the support system used in the TBM development of the West Cliff Mine in New South Wales, was rockbolts and mesh making the Grosvenor drifts the first precast concrete lined, TBM excavated drifts in Australia.

**Gas management**

The drifts at Grosvenor traverse a number of stringer (coal) seams as they head for the Goonyella Middle Seam (target seam). It has been identified that that there is potential for high levels of gas to be present in these seams and the gas if present needs to be managed effectively to minimise the risks. Given this concern the excavation of the drifts with an EPB TBM offers a significant benefit as the sealed chamber at the front of the machine will allow any gas that is encountered in the cutting area to be contained in this space.



Figure 2 - Construction of the Armco tunnel at Grosvenor



Figure 3 - Face preparation for TBM launch

Subsequent lining of the drift will ensure the gases that would usually be present in these stringer seams is contained behind the precast concrete and have no effect on the operation. With the use of an EPB TBM, the full sealing of the inherently poor ground conditions from the work environment and the improved development rates have a significant reduction on the time taken for drift development, and therefore overall project risk. The EPB chamber and screw conveyor (refer Figure 4) are pressurised during excavation.



**Figure 4 - Rear of forward shield and cutter head**

### **Ventilation**

Each drift will have exhaust ventilated through a single 1400 m diameter steel duct which will be continually installed as excavation is taking place. Each drift will be connected to a single fan equipped with gas monitoring systems to comply with legislative requirements.

The duct will have an extension tube located in the last duct at the face to allow the maximum ventilation effort to be extended to within 2 m of the face during the cutting cycle. A stuffing box is installed below the screw conveyor, which removes any gas prior to material being loaded onto the conveyor. The vent duct will be installed in-bye of the boot end and above the conveyor alignment to maximise the trafficable envelope in the drifts.

### **Dewatering**

With the design of the EPB TBM, any ground water that is encountered at the face is incorporated with the cuttings and removed along with the excavated material through the screw conveyor system. Water inflows into previous tunnelled areas will be eliminated by the grouting of the installed segment rings.

The chosen pumping system to support dewatering activities has taken into account the continuous decline of the drifts which is not normally present in civil tunnelling applications. The change is not significant but needs to take into account the additional head that is present as the depth of cover increases with the face advance.

## **KESTREL MINE EXTENSION PROJECT**

### **Project background**

The development of two drift access tunnels on the Kestrel Mine Extension (KME) Project in Emerald, Queensland, Australia was completed during the period 2009 to 2011. The works package consisted of the construction of two drifts, a conveyor drift and transport drift, followed by the in-seam development and subsequent panel development for a longwall coal mine.

The drifts at KME are exclusive of each other, designed with different grades and close in-seam interfaces at the German Creek coal seam. As a result of this, the drift portals are located a significant

distance apart on the surface. The KME drift design provided by Kestrel Coal is generally described as follows:

- Conveyor drift (Arch Profile) gradient 1 in 6, nominally 6.5 m wide x 5.2 m high x 1560 m slope distance from the start of the box cut to the in-seam phase interface; and
- Transport drift (Arch Profile) gradient 1 in 8, nominally 6.0 m wide x 4.9 m high x 1870 m slope distance from the start of the box cut to the in-seam phase interface.

A number of important factors needed to be considered during the tender period for this work given some of the constraints imposed on the works. These constraints included:

- No cross passages included in the design
- Construction through multiple coal seams
- Compliance with the Coal Mining Safety and Health Act and Regulations

It was established that to deliver the requirements of the scope of work and contract, a method that would deliver completed drift as the face advanced was what was required. The basic construction principle carried forward was to provide a completed drift cross section within 30 m of the advancing drift excavation heading. This would ensure no delays to subsequent work activities once the drifts were complete.

The final drift construction methodology proceeded with the major excavation equipment comprising of a S200MA roadheader, combined with an integrated ground support system. It was further concluded that to achieve the desired outcome systems that minimise delays to the face advance needed to be developed. The systems identified as integral to the success of the chosen method included:

- Machine capable of excavation and supporting to eliminate place changing at the face
- A continuous material handling system
- Method of extending the ventilation with minimal disruption to the works
- Pavement installation method that would work concurrent to the face advance.

### **Excavation method**

The equipment selection and design for the works required due consideration of industry regulations, codes of practice and project specific requirements and general constraints associated with the nature and environment of the work.

A significant influencing factor in the equipment selection and design was the requirements of the CMSHR. The CMSHR along with the recognised standards stipulate the controls that must be placed on equipment operating in an underground coal mine. The stipulated requirements meant that the majority of the underground equipment planned to be used to construct the drifts would require significant modifications prior to the works commencing.

To comply with the CMSHR for explosion risk zones (*State of Queensland, 2011*), it was necessary to ensure that any piece of equipment that operated in-bye of the last installed ventilation duct complied with the requirements of an Explosion Risk Zone 1 (ERZ1). Equipment operating on the out-bye side of the ventilation duct was to comply with the Negligible Explosion Risk Zone (NERZ) requirements.

A critical aspect was to achieve a construction methodology that minimised the time taken to change from one activity to another. The ability to have drift construction activities carried out concurrently provided the real advantage of the system to the project.

The Roadheader S200MA was fitted with a shotcrete boom and a roof bolting boom which satisfied the excavation and ground support design requirements. A benefit of the modified Mitsui S200MA is its capability to excavate, bolt and fibrecrete the drift heading without the introduction of supplementary equipment.

As part of the nominated support requirement, fibrecrete needed to be installed for most support types for the length of the drift. Fibrecrete was sprayed using a specifically designed spray arm assembly which was mounted onto the S200MA Roadheader. Fibrecrete was delivered to the Roadheader via a Jacon Midjet which was connected via a series of steel pipes and rubber hoses. Fibrecrete was transported underground to the Roadheader via Jacon Transit Mixers.

The last aspect of the equipment system is the ventilation duct extension and installation arrangements which are fixed to the sliding floor. The system provides for the installation of 6m long 1.8m or 1.4m diameter spiral wound steel ducts to extend the vent system as mining progresses. A telescopic vent duct section located on the inbye end of the sliding floor provides for the ventilation extension between the installed static duct and the moving / advancing duct located on the sliding floor. Additionally the vent duct system extends to within 3m of the excavated face to maintain the zone boundary between NERZ and ERZ1.

Figure 5 and Figure 6 show the bolting boom in operation and the sliding floor looking inbye to the face of the drift.



Figure 5 - Bolting boom in operation



Figure 6 - Precast floor panels and sliding floor looking inbye

---

## CONCLUSIONS

Through technology and innovation advancements, the opportunity to implement alternative excavation methods in the mining industry is becoming a reality. If a robust and well managed feasibility review is conducted of alternative excavation methods, it is possible to pursue the various opportunities of mining through poor ground conditions and subsequently deliver economical solutions for resource development that may otherwise be unviable.

When consideration is given to the matters raised in this paper, the economics of the solution must be tested and if the economic hurdles are met, a decision made as to whether the implementation of an alternative excavation method will deliver an increase in value to undertake the development of the resource.

The bringing together of knowledge from previous experiences on underground metalliferous and civil tunnelling works, has enabled the development and implementation of alternative excavation systems to construct drifts to meet differing project objectives.

## ACKNOWLEDGEMENTS

The authors wish to acknowledge the support provided by both the Anglo American Metallurgical Coal and Robbins Company.

## REFERENCES

- Buthelezi, N, 2012. Ghaghoo sand tunnel project 38% complete (online], Mining Weekly. Available from: <<http://www.miningweekly.com/article/ghaghoo-sand-tunnel-project-at-38-completion-2012-03-02>> (30 October 2013).
- Donnelly, C, Ramage, G and Donghi, M, 2013. Challenging the Norm – Alternative Excavation Methods in Mining, in Proceedings *12th AusIMM Underground Operator's Conference*, (The Australian institute of Mining and Metallurgy).
- Donnelly, C, Ramage, G and Rangi, W, 2011. Unique Coal Mine Drift Construction Method, in Proceedings *11th AusIMM Underground Operator's Conference 2011*, (The Australian institute of Mining and Metallurgy).
- Palmer, J H L, Lovat, R P and Marsh, J C, 1985. Performance of a 7.6-m diameter full-face tunnel-boring machine designed for a Canadian coal mine, in Proceedings *Tunnelling '85 The Fourth International Symposium 1985*, Paper 4 (The Institution of Mining and Metallurgy).
- State of Queensland, 1999. Coal Mining Safety and Health Act, (State of Queensland)
- State of Queensland, 2001. Coal Mining Safety and Health Regulation, (State of Queensland)
- White, SB, 1978. The Use of a Tunnel Boring Machine on a Coal Mine Decline, in *Proceedings Australian Tunnelling Conference 1987*, pp 60-70 (Institution of Engineers: Australia).

# MINIMISING MUCKING TIME BY PREDICTION OF MUCKPILE TOP SIZE IN TUNNEL BLASTING: A CASE STUDY

Mohammad Farouq Hossaini<sup>1</sup>, Mohammad Mohammadi<sup>2</sup>, Bahman Mirzapour<sup>3</sup> and Nabiollah Hajiantilaki<sup>4</sup>

**ABSTRACT:** Drilling and blasting is widely used in underground excavation projects. Timing is considered to be the most important factor in construction projects. In cyclic operations such as drilling and blasting, losing time in each cycle will cause a delay in operation for all cycles and can impose huge amounts of budget loss because of the significance of fixed costs. Therefore, this investigation tries to minimise the mucking time in drilling and blasting operations of the Alborz Tunnel in Iran via controlling the topsize of muckpile in order to eliminate the need for time consuming secondary blasting. Using the Split-Desktop system, the size distribution curve for 25 blasting rounds in Alborz Tunnel were obtained from which the topsize of the muckpile for each round was calculated. 16 datasets were used to develop a multiple linear regression model. The other nine datasets were used to validate the model. Comparing the actual and predicted values of topsizes,  $R^2$  and RMSE for the model were obtained as 0.73 and 0.14 respectively, showing that the proposed model can be used for controlling topsize of muckpile. Specific drilling and the ratio of amount of charge to the burden in contour holes are revealed to be the most important parameters in controlling the topsize of the muckpile in this particular case. The proposed model was successfully used and can be used in future excavations as long as the condition of rock mass is not changed.

## INTRODUCTION

Drilling and blasting is the most satisfactory tool for excavation of rocks because of a high progress rate and the need for low capital investment (Mandal and Singh, 2009). Since relocation of the site of a tunnel is rarely possible, engineers have to cope with the quality of encountered rock mass as it is (Ryu, *et al.*, 2006). However a standard design of practice has not been set in this area because of the complexity of the operation in which many factors contribute to the obtained results (Afeni, 2009).

The fragmentation degree (specifically the percentages of oversize and fines), displacement and looseness of muckpile can significantly affect the overall costs in mining and construction industries. Therefore, there is a strong tendency to design primary blasts in order to gain optimum muckpiles (Hagan, 1979).

The ratio of the real and theoretical pull of the round, geometry of the contour in the cross-profile, powder factor and size distribution of rock fragments along with the muckpile profile are the factors that can be used in verification of the quality of blasting operations. The fourth parameter can be used as an indicator of possibility of easiness in carrying out the created muckpile (Innaurato, *et al.*, 1998). The degree of fragmentation and the muck profile are important indicators of blast performance, particularly in open pit mining operations. However, these parameters impact the mucking operation and generally do not pose severe problems in tunnel blasting activities (Chakraborty, *et al.*, 2004). The most important factor in tunneling is time and under any circumstances, time should not be loosed (Kolymbas, 2005).

Considering the aforementioned reasons, the degree of fragmentation created in blasting operations in tunnels, will be important mainly because of muck pile top size. Creation of topsizes which can't be solved without need for secondary blasting, means losing time and a decrease in monthly advance rate. The consequence will be a significant loss of money because of huge budgets in tunneling projects. Therefore, the present paper focuses on prediction statistical methods. of the topsize of muckpile created in the Alborz Tunnel blasting operations.

<sup>1</sup>School of Mining Engineering, University College of Engineering, University of Tehran, Tehran, Iran, Email: mfarogh@ut.ac.ir

<sup>2</sup>School of Mining Engineering, University College of Engineering, University of Tehran, Tehran, Iran

<sup>3</sup>Shahran Saze Co., Tehran, Iran

<sup>4</sup>General Mechanic Co., Tehran, Iran

## CASE STUDY

Albroz Tunnel is one of the largest tunnels which is going to be excavated along the Tehran-Shomal freeway in Iran. The length of tunnel is approximately 6400 meters. The rock mass type blasted during this study was anhydrite with constant physical and mechanical characteristics for about a 70 m length. As the rock mass condition was constant, its characteristics were not considered in the prediction of topline. The parameters of blasting design used in this study, were powder factor, specific drilling, ratio of the amount of charge to burden in lifter and contour holes, drilling density (number of holes per square meter) and charge type (ratio of ANFO to Emulsion) from which a reliable equation was acquired in order to predict the topline of muckpile created after each blast.

The explosive used in the blasting operations was a combination of ANFO and Emulsion cartridges with diameter of 35mm. Compacted clay was employed as the stemming material. The area of the tunnel face was 65 m<sup>2</sup>, the diameter of drill holes 57 mm and detonation caps with half second delay were used. An example of blasting patterns used in the Albroz Tunnel is shown in Figure 1. Figure 2 shows the location of the Albroz Tunnel. The parameters used for construction of the regression model are shown in Table 1.

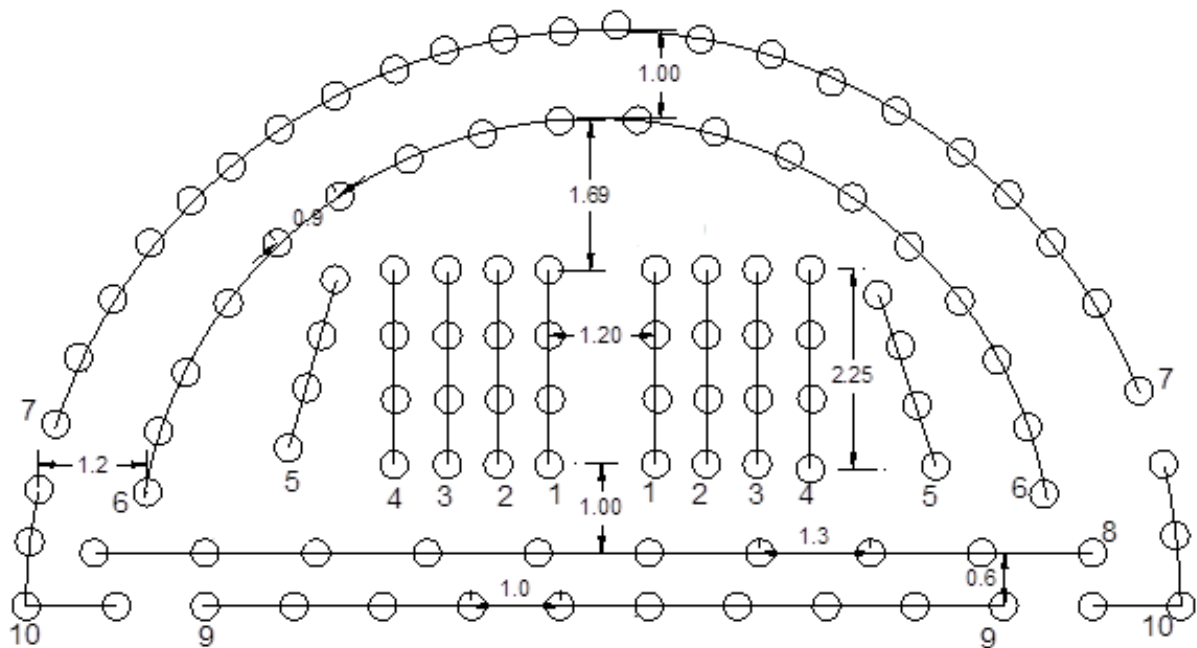


Figure 1 - An example of blasting patterns used in Albroz tunnel

## IMAGE ACQUISITION AND ANALYSIS

Size distribution of the muckpile can be assessed directly with sieving a representative sample or indirectly based on production statistics or image analysis techniques (Kanchibotla, *et al.*, 1999). Several softwares namely Split-Desktop, WipFrag, GoldSize, FragScan, TUCIPS, CIAS, PowerSieve, IPACS, KTH and WIEP. can be used in order to quantify size distribution of the muckpile. The accuracy of these systems varies from 2 to 20 percent (Siddiqui, *et al.*, 2009). In this study, the Split-Desktop system is used for computation of size distribution of the muckpile from which topline sizes were obtained.

Split-Desktop is an image-processing program designed to compute the size distribution of rock fragments with analysing digital images. Digital images can be gained manually using a digital camera, individual frame capture from video or scanned (digitised) photos.

Using the Split-Desktop system, size distribution and topline of muckpile for 25 blasting operations were obtained. An example of digital images and size distribution curve is shown in Figures 3 and 4.

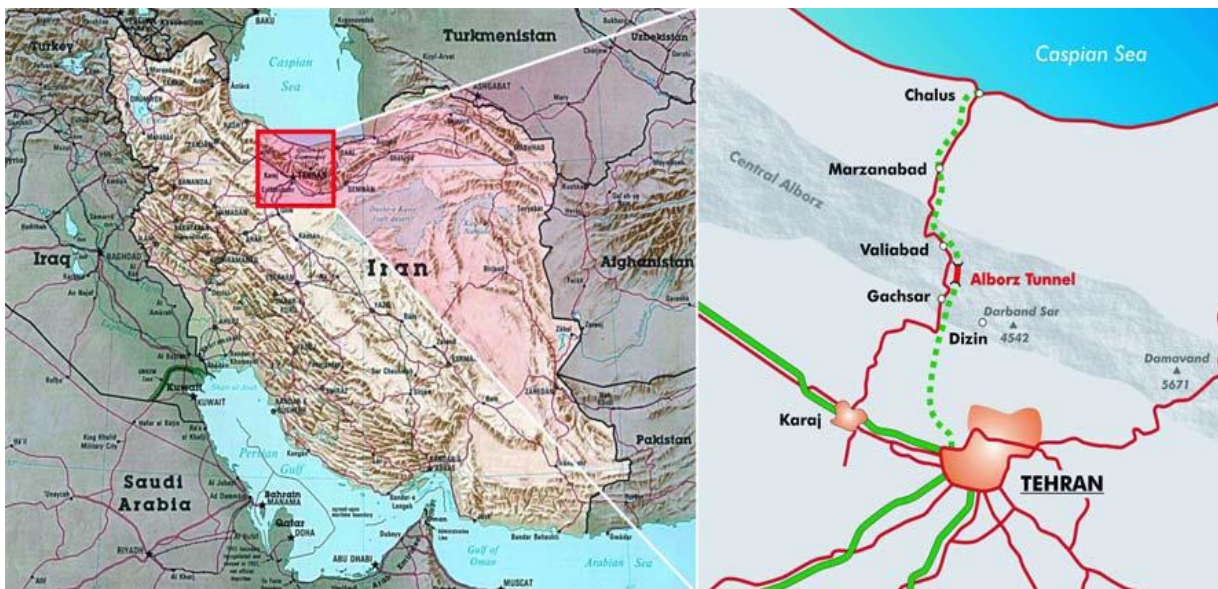


Figure 2 - Location of Alborz tunnel (Wenner and Wannemacher, 2009)

Table 1 - Description of input and output parameters used in establishing the regression model

Type of parameter	Parameter	symbol	Min.	Max.
Input	Powder factor ( $\text{kg/m}^3$ )	$P_f$	1	2.54
	Specific drilling ( $\text{m/m}^3$ )	$S_d$	1.4	1.94
	ratio of amount of charge to burden in lifter holes ( $\text{kg/m}$ )	WI	32	100
	ratio of amount of charge to burden in contour holes ( $\text{kg/m}$ )	Wc	67.6	97.6
	Drilling density or number of holes per square meter	N	1.21	1.49
	charge type (ratio of ANFO to Explosive Emulsion)	AM	1.31	2.5
output	Topsize (m)	TS	0.47	2.66



Figure 3 - An example of acquired digital image for calculating size distribution



Figure 4 - Size distribution curve obtained from Split-Desktop

### STATISTICAL ANALYSIS

In order to study or determine the relationship between different independent and dependent variables, analysing data and generating predictive models, the multiple linear regression method (MLR) can be used (Eskandari, *et al.*, 2004). This method has been used by many researchers in mining fields (Monjezi, *et al.*, 2009). The structure of the multiple linear regression model is as shown in equation 1 (Rodríguez del Águila and Benítez-Parejo, 2011).

$$Y = \beta_0 X_0 + \beta_1 X_1 + \dots + \beta_n X_n + \varepsilon \quad (1)$$

Where  $Y$  = dependent variable,  $X_0, X_1, X_2, \dots, X_n$  are independent variables,  $\beta_0, \beta_1, \beta_2, \dots, \beta_n$  are regression coefficients (constants), and  $\varepsilon$  is the error term. Parameters used for MLR have different units and their range varies widely. Therefore, using equation 2, all these parameters should be normalized (Chakraborty, *et al.*, 2004).

$$X_n = \frac{x}{x_{max} - x_{min}} \quad (2)$$

Where,  $X_n$  is the normalised value,  $x$  is the original value and  $x_{max}$  and  $x_{min}$  are the maximum and minimum values of that particular parameter.

Using 16 out of 25 datasets, the linear regression model is developed and the relationship between input and output parameters is described in Equation 3.

$$TS = 3.535 + 0.164P_f - 0.64S_d + 0.248W_l - 0.503W_c + 0.36AM - 0.11N \quad (3)$$

Where,  $P_f$  = powder factor,  $S_d$  = specific drilling,  $W_l$  = ratio of amount of charge to burden in lifter,  $W_c$  = ratio of amount of charge to burden in contour holes,  $AM$  = drilling density (number of holes per square meter) and  $N$  = charge type (ratio of ANFO to Emulsion).

Other nine datasets were used to test the accuracy of the model. The actual and predicted top sizes are compared and shown in Figure 5. Coefficient of determination and root mean square error (RMSE) are 0.73 and 0.14 respectively showing that the proposed model can be used reliably in order to prevent creation of top sizes that can cause difficulty in the mucking operation. The proposed model was used in a 70 meter length of the Alborz Tunnel to control creation of top sizes. Also, the exact condition of the rock mass is repeated in some sections of Alborz Tunnel which will be excavated in future. The

developed model can be used in these parts of the tunnel to control the topline of muckpile. Specific drilling and the ratio of the amount of charge to the burden in contour holes are revealed to be the most important parameters in controlling of topline of the muckpile. The burden of the contour holes is larger compared to other sections of the blasting patterns. This can be the reason for importance of the ratio of the amount of charge to the burden in the contour holes in creation of topline.

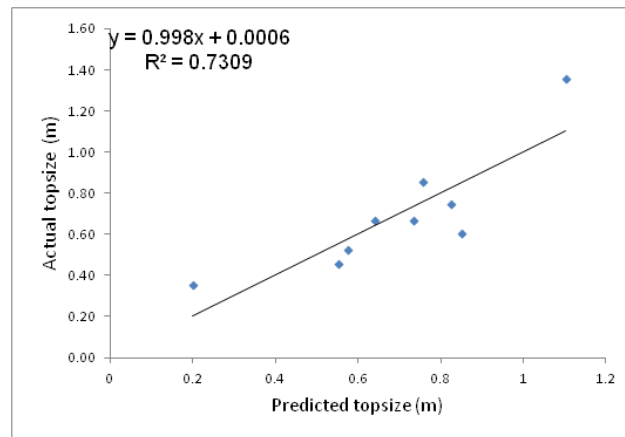


**Figure 5 - Actual topline versus predicted topline from regression model**

## CONCLUSIONS

As time is the most important factor in underground excavation projects, delay in any cycle of blasting in tunnel excavation could cause considerable loss of money. Therefore, the mucking time in the Alborz tunnel is considered to be kept to its minimum, through controlling muckpile topline with no need for secondary blasting.

In this investigation, with the above aim, the following conclusions are drawn:

- Using Split-Desktop software, the size distribution of the muckpile for 25 blasting rounds of the Alborz Tunnel were obtained from which the topline of the muckpile was found for each round.
- The actual and predicted values of topline were compared. Coefficient of correlation and root mean square error (RMSE) for the model were 0.73 and 0.14 respectively.
- The proposed model can be used reliably to control the topline of the muckpile and consequently keep the mucking time to its minimum.
- Specific drilling and the ratio of the amount of charge to the burden in contour holes were revealed to be the most important parameters in controlling the topline of the muckpile in this particular case.
- The burden of contour holes is larger compared to other sections of blasting patterns which can be the reason for the importance of the ratio of the amount of charge to the burden in the contour holes in creation of topline.
- The proposed model can be used in the remaining sections of the Alborz tunnel, to be excavated later, where the condition of the rock mass is repeated.

## REFERENCES

- Afeni, T B, 2009. Optimization of drilling and blasting operations in an open pit mine - the SOMAIR experience. *Mining Science and Technology (China)*, 19(6), 736-739.
- Chakraborty, A K, Raina, A K, Ramulu, M, Choudhury, P B, Haldar, A, Sahoo, P, and Bandopadhyay, C, 2004. Development of rational models for tunnel blast prediction based on a parametric study. *Geotechnical and Geological Engineering*, 22(4), 477-496.
- Eskandari, H, Rezaee, M R, and Mohammadnia, M, 2004. Application of multiple regression and artificial neural network techniques to predict shear wave velocity from wireline log data for a carbonate reservoir South-West Iran. *CSEG recorder*, 42, 48.

- 
- Hagan, T N, 1979. Rock breakage by explosives. *Acta Astronautica*, 6(3), 329-340.
- Innaurato, N, Mancini, R, and Cardu, M, 1998. On the influence of rock mass quality on the quality of blasting work in tunnel driving. *Tunnelling and Underground Space Technology*, 13(1), 81-89.
- Kanchibotla, S S, Valery, W, and Morrell, S, 1999. Modelling fines in blast fragmentation and its impact on crushing and grinding. In *Explo 99—A conference on rock breaking*, The Australasian Institute of Mining and Metallurgy, pp 137-144 Kalgoorlie, Australia.
- Kolymbas, D, 2005. *Tunnelling and tunnel mechanics: A rational approach to tunnelling*, (Springer: Berlin).
- Mandal, S, and Singh, M, 2009. Evaluating extent and causes of overbreak in tunnels, *Tunnelling and Underground Space Technology*, 24(1): 22-36.
- Monjezi, M, Rezaei, M, and Yazdian Varjani, A, 2009. Prediction of rock fragmentation due to blasting in Gol-E-Gohar iron mine using fuzzy logic. *International Journal of Rock Mechanics and Mining Sciences*, 46(8), 1273-1280.
- Rodríguez del Águila, M M, and Benítez-Parejo, N, 2011. Simple linear and multivariate regression models. *Allergologia et Immunopathologia*, 39(3), 159-173.
- Ryu, C H, Sunwoo, C, Lee S D, and Choi, H M, 2006. Suggestions of rock classification methods for blast design and application to tunnel blasting. *Tunnelling and Underground Space Technology*, 21(3), 401-402.
- Siddiqui, F I, Shah, S A, and Behan, M Y, 2009. Measurement of size distribution of blasted rock using digital image processing. *Engineering Sciences*, 20(2), 81-93.
- Wenner, D, and Wannemacher, H, 2009. Alborz Service Tunnel in Iran: TBM Tunnelling in Difficult Ground Conditions and its Solutions. In *1st Regional and 8th Iranian Tunneling Conference*, Tehran, Iran.

# UNDERGROUND MINE VENTILATION AIR METHANE (VAM) MONITORING – AN AUSTRALIAN JOURNEY TOWARDS ACHIEVING ACCURACY

**Bharath Belle**

**ABSTRACT:** One of the mining industry's goals is to establish a standard monitoring device that will primarily monitor gas levels and airflow side by side in real-time to assist as mine safety triggers and in Ventilation Air Methane (VAM) monitoring purposes. Unlike in most Australian mines, continuous real-time air velocity and gas monitoring has been practiced in South African coal mines for over three decades. Envisaged benefits from real-time velocity monitoring over current monthly manual ventilation monitoring are, viz., consistent and continued diagnosis of underground environment and managing catastrophic risks such as fires, explosions, and spontaneous combustion through gas make values; ability to determine real-time carbon monoxide, methane and other noxious gas make, estimation and reconciliation of specific gas emissions during panel development and longwall retreat, determining goaf capture efficiency, accurate determination of heat loads and air cooling capacity, and improving the confidence in ventilation air methane (VAM) emission data. Currently, industry is faced with the persistent and complex challenge of obtaining a 'reference true gas monitor' for 'accuracy' determination of quintessential VAM parameters, viz., CH<sub>4</sub>, CO<sub>2</sub>, air velocity, and temperature. Despite, supplier or external reviewer's claims, that one monitoring system is superior than the other in terms of its measurement 'accuracy', i.e., when compared with the "true measurement device", in almost all cases, validating these claims was not possible due to lack of data evidence. Therefore, use of measurement system/s that are deemed to provide a practically acceptable, reliable and safe system to provide transparent measurement data is important.

Underground operators are often faced with the famous and simple audit question on an important area of 'accuracy', i.e., the difference between 'true' value and measured value. There are suggestions of "slight inaccuracies" are being acceptable but currently, no such guidance or value exists. None of the studies or available guidance documents provides guidance on choice of an 'accurate' instrument for VAM monitoring. For example, it is acceptable to have an air velocity measurement error of 5 to  $\pm 20$  % that are based on research and operational practices. AS2290.3 (1990) outlines an acceptable tolerance measurement limit for instruments. For example, working limit for 1.0 % true concentration of CH<sub>4</sub> is 0.91% for real-time (electrochemical /pellistor sensor) with 5% range and 0.90% for tube bundle system with 100% range excluding span gas ranges of  $\pm 0.2$ %. Considering the above inherent instrument inaccuracies expected, a true measure of instrument performance is to obtain side-by-side results that can demonstrate the difference between the monitoring systems exposed to the same atmosphere. This paper demonstrates that over and beyond the inherent minimal instrument measurement differences, it is those operational factors that are critical to the recording of concentration of gas levels which the instruments are exposed to, viz., airflow that would affect the concentration of CH<sub>4</sub> and CO<sub>2</sub>, barometric pressure, shaft cage effect, longwall coal production levels, magnitude of gas levels, longwall production, which is the main source of the U/G VAM.

## INTRODUCTION

Adequacy and quality of controls provided for safe and healthy underground mine environment have been carried out by routine manual measurements of various hazard and control parameters. Mine ventilation is a means of such control and is monitored by manual and instrumentation means to provide assurance on regulatory requirements. In recent times, with the promulgation of Greenhouse Gases (GHGs) have resulted in the need for continuous and accurate monitoring of data. Typically, mines have established an underground Ventilation Air Methane (VAM) emission inventory using manual monthly ventilation survey and continuous monitoring (tube bundle/real-time) data in accordance with the obligations of the National Greenhouse and Energy Reporting Scheme (NGERS) Act (2007).

With the progressive and proactive approach, the practice of once-a-month ventilation survey data and use of underground tube bundle gas monitoring instruments it was identified that they may have limited

ability to record the true gas levels due to their sampling frequency. Issues related to non-emotional data, operator measurement bias and benefits of real-time air velocity versus manual vane anemometer measurement in mines have been studied by various research agencies over three decades (Belle, 2013). Therefore, simultaneous and continuous measurement of airflow, CH<sub>4</sub> and CO<sub>2</sub> levels, absolute pressure and temperature (WBT and DBT) at the same location, was seen to provide the most reliable data. This paper provides the difference between continuous and infrequent variables used in VAM calculations.

While the need for U/G VAM monitoring and reducing its emission to atmosphere, it is important to note that the elimination of methane hazards underground is the foremost requirement of mine safety and prevention of catastrophic explosions. Explosion, fires and Frictional Ignition (FI) risks in coal mines are ever present because of its inherent presence of methane gas (Figures 1 and 2) and these unfortunate events continue to call for embracing new technologies to monitor hazards and take appropriate control responses. In order to minimize the risk profiles of these catastrophic events, it is timely to accept opportunities in the following hierarchical control namely, air velocity (ventilation) monitoring:

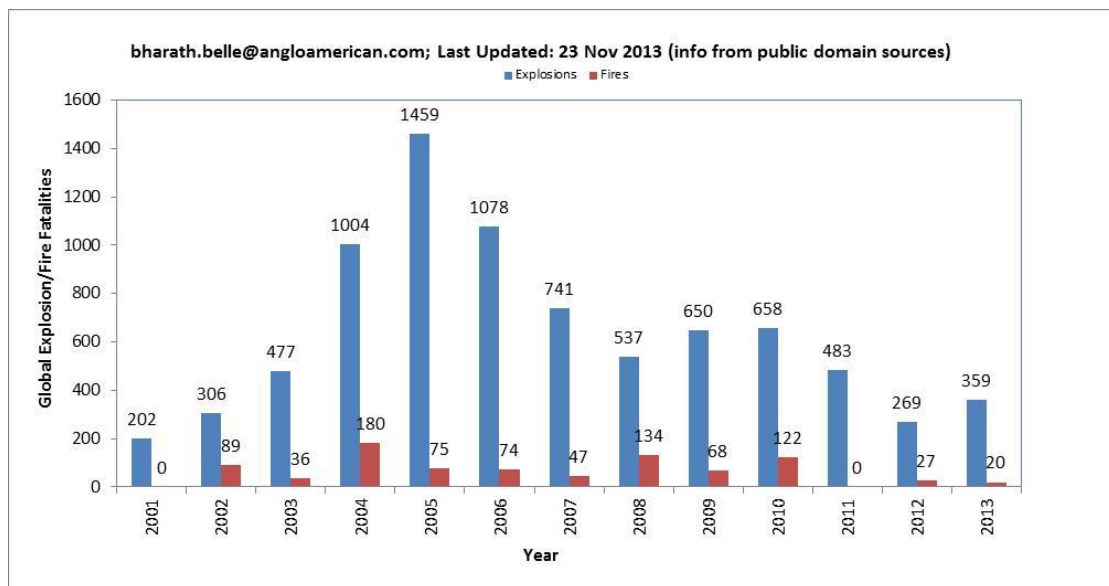


Figure 1 - Statistics on global mine explosions and fires (Belle, 2013)

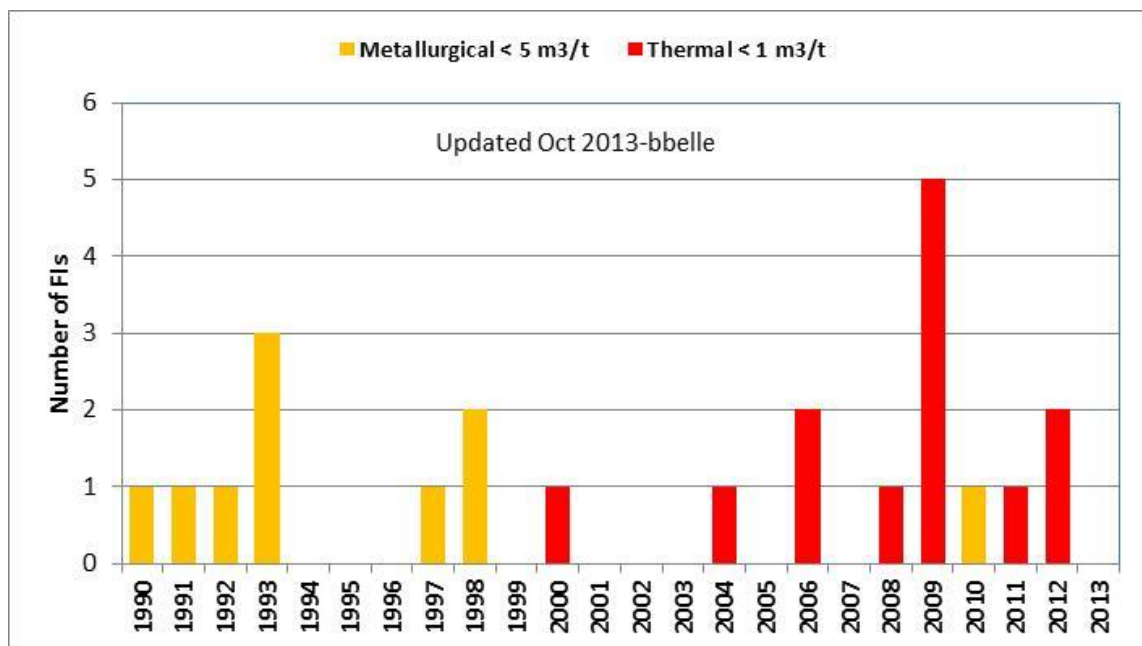


Figure 2 - Comparison of FI incidents in gassy (metallurgical) and low gassy (thermal) mines

- Accepting the practice of continuous monitoring of the environment of hazards that are continuously changing (read gases and dust)
- Accepting the need for continuous monitoring of air velocity and ventilation controls that are continuously changing (read airflow) regardless of their magnitude in a ventilation network.
- Accepting that in a complex mine ventilation network, frequent manual ventilation monitoring in main returns or intakes is a cumbersome process and has practical and time limitations.
- Accepting the availability of Intrinsically Safe (IS) real-time monitoring tools for underground use in the technologically advanced workplaces.
- Accepting that continuous air velocity monitoring devices u/g can provide leading indicators of expected conditions in the event of a failure or provide early warning of ventilation effectiveness.
- Accepting that traditional measurements aided with continuous monitoring would enhance the response time in the event of emergencies.
- Accepting that approved IS real-time velocity monitors are available in Australia and there is a need in improving the approval process for use in mines.
- Accepting that just as in other real-time monitoring tools, velocity monitors also need maintenance.
- Accepting that continuous velocity monitoring is a leading practice in other parts of the coal and metal mining world (UK, Canada, South Africa, Poland).
- Accepting that improvements in velocity monitoring would assist the mines in controlling and providing improved quality of air.
- Accepting that a real-time velocity monitor is a safety and production enabler.

### **BACKGROUND TO AUSTRALIAN GAS MONITORING JOURNEY**

The U/G VAM is significant constituent (over 70%) of past, current and future underground carbon emissions. The following section summarizes the background of current gas monitoring systems, their shortcomings if any, and the need for the use of real-time continuous monitoring for VAM assessment.

- Australia is probably the only country whereby the mines use extensive network of tube bundle gas monitoring systems that provide frequent data on gas levels for various mine safety triggers during normal and emergency scenarios. Tube bundle gas monitoring is a network of tubes running from the surface to selected underground locations and draws a small volume of air sample from the general body of air to surface and analyses the gas composition through infra-red (IR) analysers at regular intervals.
- Through the years, it has been accepted that both tube bundle and real-time monitors are effective gas monitoring systems with inherent benefits and weaknesses.
- Typically, a tube bundle system using an IR analyser, is seen to be 'superior or accurate' because of its reliability during major safety incidents or goaf sealing or as an early warning device for sponcom/fire events. Many a times, due to the number of tube monitoring stations underground, the sampling frequency would vary from every 30 minutes to 60 minutes or higher. However, it can be argued that the cost of superiority or accuracy is at the expense of misrepresenting or sacrificing the sufficient representation of the constantly changing underground gas atmosphere.
- Real-time monitors require sufficient presence of oxygen (available in almost all underground working areas except goaf) to operate which is not unlikely at shaft bottom or exhaust shafts. For the current real-time sensors, measurement range is appropriate and provides results in near real-time unlike infrequent tube bundle monitor data.
- Despite, various supplier, auditor or external reviewer's claims, that one monitoring system is superior over other in terms of its measurement accuracy, i.e., when compared with the "true measurement device", in almost all cases, validating these claims was not possible due to lack of data or evidence. As of date, there is no side-by-side comparison of tube bundle or real-time monitor or Gas Chromatography (GC) performance on measuring methane for low, medium and high gas concentration levels. For example, the acceptable air velocity measurement error of

5% to  $\pm 20$  % accuracy requirements for mine ventilation applications are based on operational practices.

- Despite the above shortcomings, real-time ventilation and gas measurement systems would provide an improved frequency of measurements, incorporate influence of any fan stoppages due to maintenance or power failures, and minimise VAM estimation errors and provide greater confidence in carbon estimates.
- Currently, there is no industry or regulator study that provides guidance or sufficient data evidence on methane measurement accuracy between IR analyser and real-time monitor (point detector) or GC for very low (<0.05%), low (0.05-0.1%), medium (0.1%-0.3%) and high (0.3-0.5%) and very high (>0.5%) concentration levels at exhaust shafts.
- The AS2290.3 outlines an acceptable tolerance measurement limit for instruments. For example, for 15% CH<sub>4</sub> true concentration, acceptable measureable concentration is 14.2%; for 1.0 % true concentration of CH<sub>4</sub> is 0.91% for real-time (electrochemical /pellistor sensor) with 5% range and 0.90% for tube bundle system with 100% range. These errors are significant in terms of carbon emission estimates.
- Similarly, for instrument calibration, variations in test gas range for calibration purposes would be in the region of  $\pm 0.2$  % for a "2.5 %" true gas. Therefore, inherent errors associated with the test gas, instrument measurement range, laboratory facility may not be superior unless sufficient data is available to validate them. There are suggestions of "slight inaccuracies" being acceptable but currently, no such guidance or value exists.
- None of the ACARP or other regulatory or research documents provides guidance on choice of an 'accurate' instrument for NGERs monitoring that would have the 'accuracy' values defined in it and comparison has been made with other available continuous monitoring devices.
- An example of SIMTARS study (Brady, 2008) on measured gas levels using gas chromatograph (GC) and tube bundle data (IR analyser) for concentration levels greater than 0.5 % methane suggested significant difference between the two analytical techniques. The SIMTARS study did not quantify the differences between the two techniques (IR and GC).
- Typically calibration gas uncertainty is 0.05% to 0.2% range over the 'true gas' concentration range of 0.94%, 2.14%, 10.4%, that demonstrates a non-linear relationship. A change in calibration gas may influence the measured values regardless of the instrument used.

### AUSTRALIAN JOURNEY OF REAL-TIME AIRFLOW MONITORING ON EXHAUST FANS

The introduction of carbon tax (July 2012) on GHG emission has necessitated the need for accurate airflow data from mine exhaust systems. The significant two variables in the VAM greenhouse gas estimates is the airflow and methane levels. Typically, most mines have established the emission inventory using the accepted manual ventilation measurement practices in accordance with the obligations of the NGERs Act (2007).

The introduction of the NGERs Act provided a significant opportunity in Australian coal mines to build robust, compliant, accurate and transparent VAM reporting through improved real-time airflow monitoring systems instead of the manual monthly ventilation surveys. Mine ventilation engineers have identified the need for a paradigm shift in VAM monitoring systems in terms of resolution and frequency of measurement of key data components even before the common findings from various auditor/reviewer's opinion on the subject through the years.

With this background, the installation of a monitoring system at exhaust shaft fan ducts to independently measure real-time exhaust airflow, CH<sub>4</sub>, CO<sub>2</sub>, wet bulb temperature (WBT), dry bulb temperature (DBT), moisture and barometric pressure to comply with NGERs Act (2007) and improve VAM measurement accuracy is becoming a reality. Typically any changes in ventilation system (such as slowing down of fans or power failures) or errors associated with the ventilation measurement are not captured in the estimated carbon emissions. For example, with 400 m<sup>3</sup>/s of airflow and 0.3% methane, a 10% change in airflow alone would relate to a difference in carbon tax of AUD\$1.4 million per annum.

The need to measure the air velocity beyond the statutory measurement location and their frequencies is increasingly becoming a practical reality. The explanations that are faced by the operators (that may be beyond their control) are:

1. Experiencing the art of velocity measurement (years of experience u/g and measurement correlation to monthly ventilation reports)
2. Location of velocity readings taken underground (high velocity turbulent regions or sharp bends)
3. Instruments used and their calibration on surface (Kestrel electronic or manual vane anemometers)
4. Underground environment conditions (humid and dusty vs. comfortable conditions)
5. Time constraints and understanding of 'value' of each velocity measurements.

With no means for measuring emissions from the mine in real-time and without compromising current mine monitoring systems dedicated for mine safety, specifically sponcom and explosion prevention, the need for dedicated real-time airflow monitoring at mine shafts is quintessential. Figure 3 shows the implementation of real-time ultrasonic air velocity monitoring system installed on main fan ducts.



**Figure 3 - Installation of real-time air velocity monitoring on main fan ducts**

As a proactive approach, most of mines are implementing the approved IS ultrasonic flow monitoring devices at the exhaust shaft fan ducts. It is also noted that a handful of coal mines are in the process of implementing these real-time monitors underground. The introduction of leading practice of real-time monitoring of airflow and low range gas measurements at fan ducts (in NSW and QLD) using real-time analysers to measure the CO<sub>2</sub>, CH<sub>4</sub>, and airflow, barometric pressure (BP), WBT, DBT has enabled mines in producing transparent emission reports.

Figures 4a to 4c shows the isovels of main fan ducts measured from four different exhaust shafts with a total of 11 different main fans. These velocity profiles provide a graphical presentation of any issues that can be identified in main fan performance or turbulence associated with the designs. What is valuable is that the velocity contours derived from velocity pressure measurements provide the status of the fan or its future long term use. The isovel plots suggest that they are definitely different to ideal velocity contours obtained in thermodynamic simulations. Furthermore, the velocity contour profiles demonstrate the complexity of recording 'true' gas levels in an u/g airway with complex airflow profile being an additional variable that may influence the measurement of gas levels.

The above contours were based on an independent underground Pressure-Quantity (PQ) survey and through mine exhaust fan flow measurements. The objective of this survey was to establish an empirical relationship between real-time ventilation flow data in exhaust fan systems and monthly underground ventilation survey data to enable the use of real-time flow data for underground VAM calculations. Based on independent measurement techniques (manometric, barometric (BP) and vane anemometer), it was established that the variation in manual ventilation flows against the real-time air flows exist. Based on the study, it was noted that the traditional monthly manual and the real-time airflow from the exhaust fan

duct tests for the same period were 511 m<sup>3</sup>/s and 464.9 m<sup>3</sup>/s respectively with a measurement error of 46.1 m<sup>3</sup>/s. Main fan airflow measurement were matching the fan performance curves.

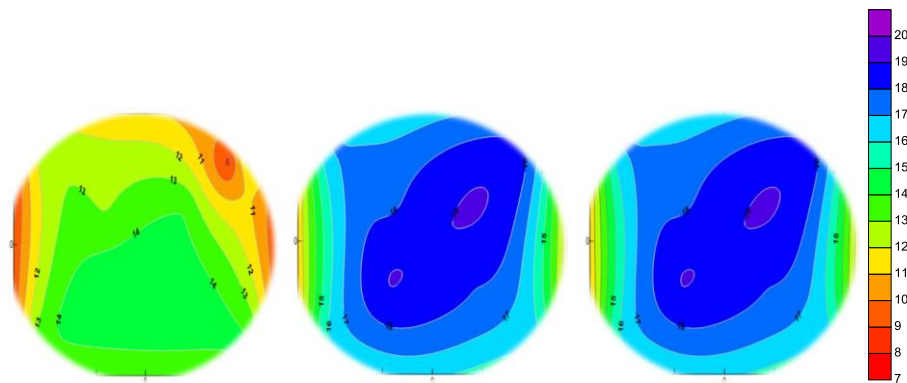


Figure 4a - Isovels measured at three different fan ducts from an exhaust shaft-A

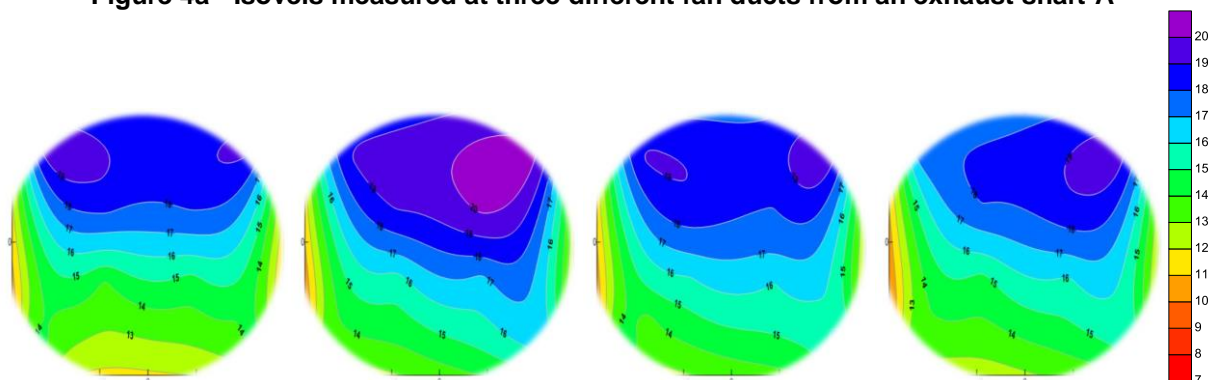


Figure 4b - Isovels measured at four different fan ducts from an exhaust shaft-B

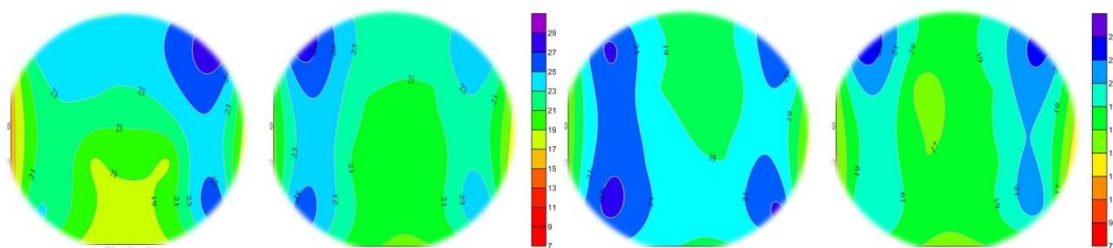


Figure 4c - Isovels for mine Exhaust Shaft 2 (Left) and Exhaust Shaft 4 (right) fan ducts

There are several studies on the use of correction factors (including factory correction factors and the given range of velocities) in the literature; its application in practice is remote. For example Thimmons and Kohler (1985) have suggested that the measurement should be always be made at a minimum distance of three roadway diameters upstream of an obstruction and 10 roadway diameters downstream of an obstruction. In reality, the presence of these ideal locations is scarce or simply they do not exist. Another parameter that is used in determining the airflow is the area of a roadway. Typically, 5% is considered to be an acceptable error during the ventilation survey. Even with this low level of acceptable error the carbon cost is significant, i.e., at 0.2% methane level for a roadway area of 20.30 m<sup>2</sup>, 5% accepted error in area would be costing around \$200, 000 per annum. Thimmons and Kohler (1985) have expressed the definitions on accuracy requirements for mine ventilation applications. They had expressed the accuracy of +- 20% is satisfactory based on the practice of the 1970s.

However, currently this issue is still persisting and the challenge even today. That is which instrument is accepted as a 'reference true velocity measurement device' to determine the accuracy of velocity measurements in mines. Measurement experiences suggest that each operation or a location underground or even the velocity contour profiles of a roadway is dynamic. This suggests that the fixed real-time monitoring systems would minimize the operator error bias against the systematic bias with a fixed velocity monitor.

## METHANE MONITORING; TUBE BUNDLE OR REAL-TIME MONITORS

Another parameter in VAM monitoring is the continuous monitoring of airflow through exhaust shafts. Currently, there are approved real-time airflow monitoring systems that are available for exhaust fan shafts. Considering the above inherent instrument inaccuracies expected, a true measure of instrument performance is to obtain the side-by-side results that can demonstrate the difference between the monitoring systems exposed to the same atmosphere. Over and beyond the inherent minimal instrument differences, it is those operational factors that are critical to the recording of concentration of gas levels which the instruments are exposed to, viz., airflow that would affect the concentration of CH<sub>4</sub> and CO<sub>2</sub>, barometric pressure, cage effect, longwall coal production levels, magnitude of gas levels, longwall production, which is the main source of the U/G VAM.

In order to demonstrate the importance of these parameters, 15 different longwall panel return side-by-side real-time and tube bundle daily data were statistically analysed. Each daily data was separated into an hourly data and collated into minimum, maximum and average CH<sub>4</sub> levels for both tube bundle and real-time monitoring systems positioned side-by-side. Figure 5 shows the real-time airflow and gas data measured in a longwall panel return, demonstrating the influence of airflow and longwall production on measured ambient gas levels. Figure 6 shows the comparison of side-by-side real-time catalytic sensor and tube bundle (IR) sensor along a longwall panel return demonstrating infrequent data affecting the average gas levels.

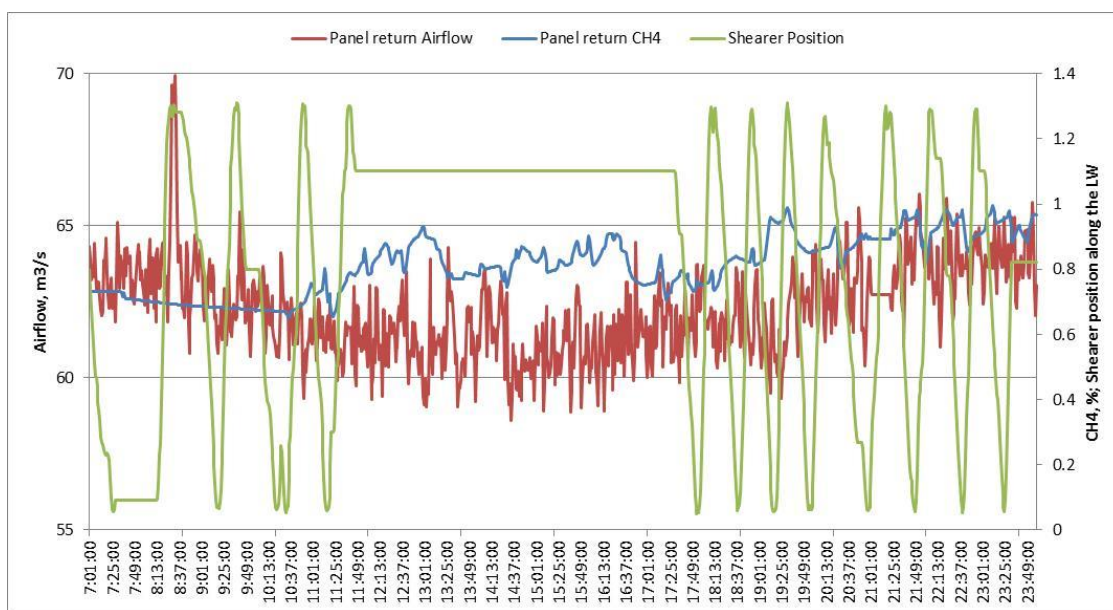


**Figure 5 - Real-time airflow and gas data in a LW panel return**

Figures 7 to 10 show the relationship between real-time and tube bundle data (daily and hourly) for various gas levels measured over different sampling periods. From the regression lines of daily data, it is noted that the tube bundle system records the methane levels 8% higher than the real-time data. Similarly, hourly minimum real-time data is 82% of the tube data suggesting the low gas levels are not recorded by the tube monitoring system. On the other hand, hourly maximum methane data from real-time monitor recorded 6% higher gas levels than the tube monitoring system as the tube monitor fails to record the peak atmosphere data due to the lower ambient sampling frequency.

## STATISTICAL ANALYSES

In order to understand the critical factors influencing the gas levels recorded by the monitoring systems, the hourly methane data recorded during daily longwall production located side by side at longwall panel return was used to perform statistical Analysis Of Variance (ANOVA) and determine significance of main factors and their interactions. The real-time monitor data are also the same value used to verify Trigger Action Response Plans (TARPs) for ventilation and gas management. Typically, methane levels were recorded every 30 sec or less, while the tube bundle data measured approximately every 50 minutes.

The hourly methane concentration data is in the form of  $C_{ijklm}$  (%). The subscripts have the following definitions:

- i.  $i$  = Statistical parameter,  $i = 0$  is minimum,  $i=1$  is maximum and  $i=2$  is average methane levels;
- ii.  $j$  = Methane concentration levels,  $j = 0$  is 0.5%,  $j = 1$  is 1 % and  $j = 2$  is 2.5%;
- iii.  $k$  = barometric pressure,  $k = 0, 1$  and  $2$  respectively indicate pressures of 98 kPa, 99 kPa and 100 kPa;
- iv.  $l$  = Daily shift period,  $l = 0, 1,$  and  $2$  are longwall production periods of 8:00 hr, 16:00 hr and 24:00 hr respectively
- v.  $m$  = longwall production,  $m = 0$  is 7000 tons,  $m = 1$  is 14,000 tons,  $n = 2$  is 21,000 tons.

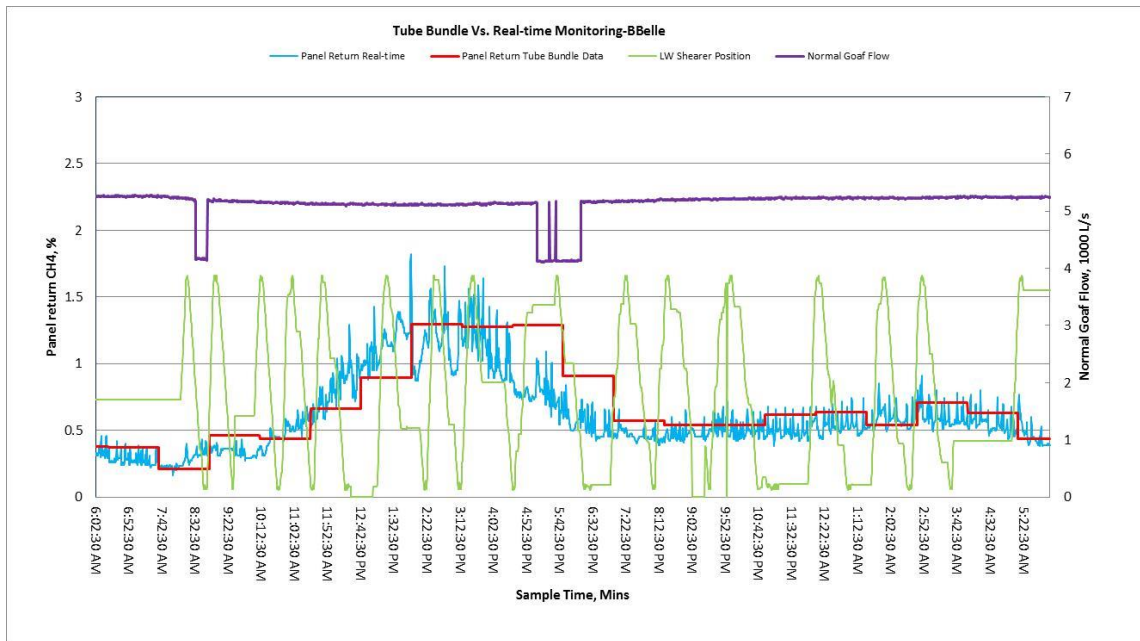


Figure 6 - Comparison of side-by-side real-time and tube bundle in a LW panel return

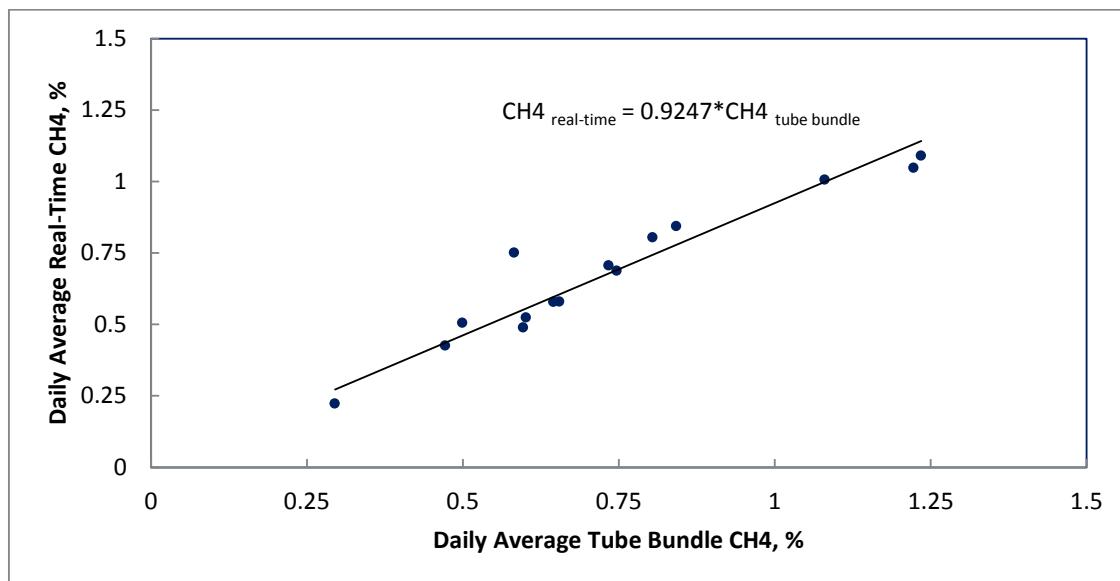


Figure 7 - Comparison of side-by-side LW panel return real-time and tube bundle monitor (Daily Avg.)

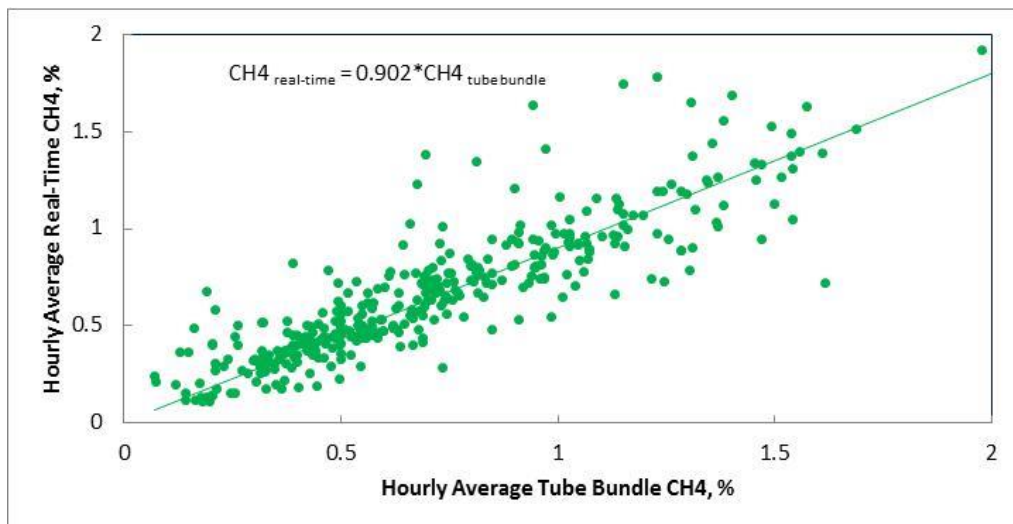


Figure 8 - Comparison of side-by-side LW panel return real-time and tube bundle monitor (Hourly Avg.)

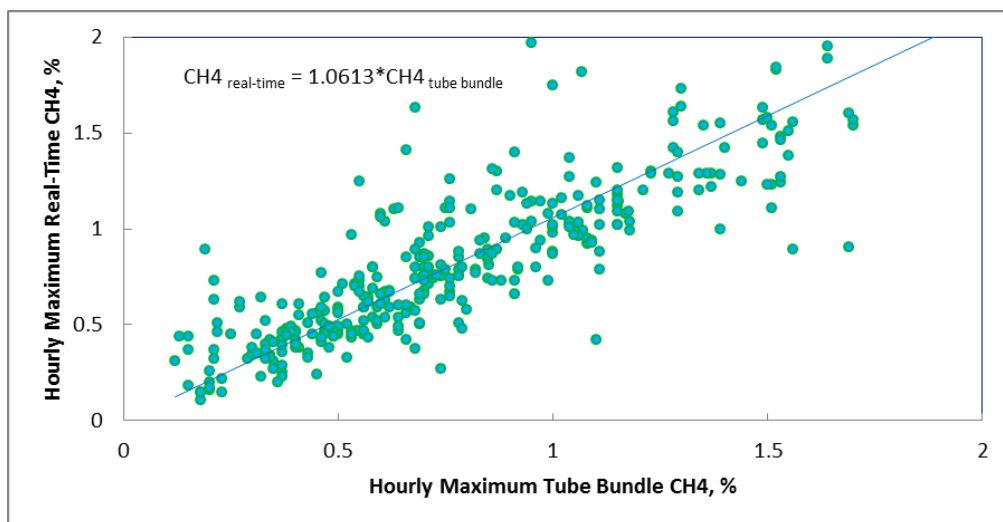


Figure 9 - Comparison of side-by-side LW Panel return real-time and tube bundle monitor (Hourly-Max)

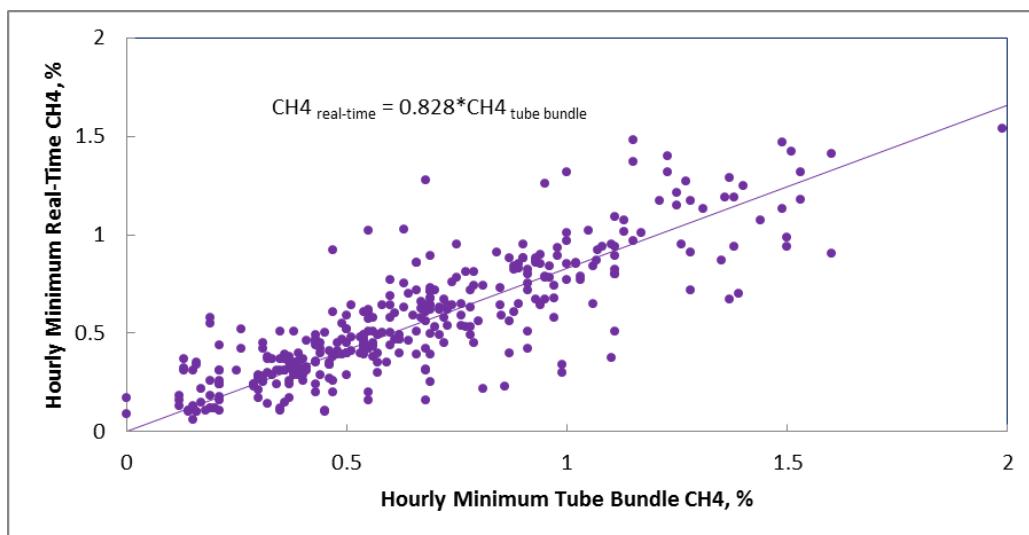


Figure 10 - Comparison of side-by-side LW panel return real-time and tube bundle monitor (Hourly-Min)

The main statistical factors in the study are barometric pressure (including cage effect), daily shift period, longwall production, and level of methane concentration measured and recorded by the real-time and tube bundle monitoring systems. P (probability) - values are often used in statistics, where one either rejects or fails to reject a hypothesis or its significance. The smaller the p-value, the smaller is the probability that one would be making a mistake by rejecting the importance of the factor effects on measured peak methane levels. In the ANOVA (Table 1), some p-values were printed as 0.000, meaning that significant evidence of factor effects influencing the recorded values.

**Table 1 - Analysis of variance (ANOVA) for CH<sub>4</sub> data**

Source	Df	Seq SS	Adj SS	Adj MS	F statistic	P value
CH4-Statistic	2	17.685	0.448	0.224	6.17	0.002
CH4 Conc. Level	2	250.613	179.459	89.729	2470.39	0.000
Barometric pressure	2	0.574	0.278	0.139	3.82	0.022
Shift period	2	1.054	1.131	0.565	15.57	0.000
Production	2	0.728	0.728	0.364	10.02	0.000
Error	2149	78.056	78.056	0.036		
Total	2159	348.710				

Considering the above results, it can be noted that the above identified factors play a crucial role in measuring the true methane levels, which would require continuous monitoring against intermittent recording by u/g shaft bottom tube bundle systems as they do not represent major factors that would significantly affect the recorded gas levels. The difference in measured concentration levels by real-time and tube bundle data are calculated and are shown in Table 2. These large differences suggest that the inherent accuracy differences associated with the gas monitors are insignificant when compared with the operational factors in measuring the gas levels.

**Table 2 - Difference between recorded side-by-side LW return real-time and tube-bundle data (hourly)**

Sample #	Min CH4 Difference, %	Max CH4 Difference, %	Avg. CH4 Difference, %
1	2.6	-6.2	-7.4
2	-33.3	-6.3	-16.7
3	-12.8	-2.5	-14.8
4	3.5	2.5	-0.1
5	0.0	2.6	-8.7
6	-12.9	15.9	-4.0
7	3.1	20.8	0.1
8	50.0	19.5	22.4
9	-72.7	16.9	-22.1
10	-20.0	7.5	-32.3
11	100.0	25.7	-10.8
12	-31.2	28.6	-12.9
13	-66.7	12.4	-13.3
14	-90.0	40.5	-11.6
15	12.5	5.4	1.1

As part of the statistical analyses, side-by-side real-time and tube bundle data were compared. A paired t-test was performed on the set of all the sample pair data to determine if there was a statistical difference in the recorded concentration levels between the monitoring pairs. A paired t-test of hypotheses was developed to compare the mean methane concentration level measured with two monitoring instruments ( $\mu_{\text{Real-Time}}$  and  $\mu_{\text{Tube Bundle}}$ ). The null and alternative hypothesis for the tested sample pairs were:  $H_0: \mu_{\text{real-time}} = \mu_{\text{Tube Bundle}}$  and  $H_1: \mu_{\text{real-time}} \neq \mu_{\text{Tube Bundle}}$ . In the paired t-test, hypothesis  $H_0$  states that the mean methane concentration levels from both monitors ( $\mu_{\text{real-time}}$  and  $\mu_{\text{Tube bundle}}$ ) are equal. On the other hand, alternative hypothesis states that the two monitors in fact measure different mean concentration levels. It is therefore necessary to use hypothesis testing to accept or reject  $H_0$ . For this work, a standard 95 % confidence level was chosen. As the hypothesis stated were  $\mu_{\text{Real-time}} = \mu_{\text{Tube Bundle}}$  and  $\mu_{\text{real-time}} \neq \mu_{\text{Tube Bundle}}$ , all analyses were two tailed to account for both conditions  $\mu_{\text{real-time}} < \mu_{\text{Tube bundle}}$  and  $\mu_{\text{real-time}} > \mu_{\text{Tube Bundle}}$ . Therefore, the critical t-values were determined by  $t_{0.025}$  rather than  $t_{0.05}$ . Results of the paired t-test statistical analyses are given in Table 3.

**Table 3 - Statistical comparison of an hourly real-time and tube bundle data**

Statistic	Paired T-test		Paired T-test		Paired T-test	
	Real-time <sub>Min</sub>	Tube <sub>Min</sub>	Real-time <sub>Max</sub>	Tube <sub>Max</sub>	Real-time <sub>Avg</sub>	Tube <sub>Avg</sub>
N	360	360	360	360	360	360
Mean	0.5639	0.6594	0.8666	0.7989	0.6839	0.7343
$\mu_{\text{Real-time}} - \mu_{\text{Tube}}$	-0.0955		0.0676		-0.0504	
Std. Dev	0.3120	0.3591	0.4856	0.4139	0.3569	0.3912
SE Mean	0.0164	0.0189	0.0256	0.0218	0.0188	0.0206
95 % CI for $\mu$	(-0.1153, -0.0757)		(0.0395, 0.0957)		(-0.0701, -0.0306)	
T-Value	-9.49		4.73		-5.02	
P-Value	0.000		0.0000		0.0000	
Hypothesis	Reject $H_0$		Reject $H_0$		Reject $H_0$	

From Table 3, it is observed that, for maximum methane levels,  $t$ -statistic  $C_{\text{real-time}} - C_{\text{Tube bundle}}$  was 4.73. This indicates that recorded maximum methane level from the real-time monitor was generally greater than the maximum methane level from the tube bundle system and the null hypothesis is rejected ( $p$ -value of 0.000). A paired  $t$ -test was also performed on daily methane data (15 days) to determine if there was a statistical difference in the results obtained between two monitoring systems for different statistical parameter. The result of the paired  $t$ -test was a test statistic with 14 degrees of freedom,  $p = 0.197$  (Table 4) indicating no difference between the two monitoring devices for minimum gas levels but significant difference on measured levels for maximum and daily average methane levels.

**Table 4 - Statistical comparison of daily real-time and tube bundle data**

Statistic	Paired T-test		Paired T-test		Paired T-test	
	Real-time <sub>Min</sub>	Tube <sub>Min</sub>	Real-time <sub>Max</sub>	Tube <sub>Max</sub>	Real-time <sub>Avg</sub>	Tube <sub>Avg</sub>
N	15	15	15	15	15	15
Mean	0.3113	0.3447	1.673	1.424	0.6839	0.7342
$\mu_{\text{Real-time}} - \mu_{\text{Tube}}$	-0.0333		0.2487		-0.0503	
Std. Dev	0.1998	0.2303	0.645	0.481	0.2452	0.2695
SE Mean	0.0516	0.0595	0.166	0.124	0.0633	0.0696
95 % CI for $\mu$	(-0.0861, -0.0194)		(0.0811, 0.4162)		(-0.0940, -0.0065)	
T-Value	-1.35		3.18		-2.47	
P-Value	0.197		0.007		0.027	
Hypothesis	Accept $H_0$		Reject $H_0$		Reject $H_0$	

Although the two commonly used monitors differ according to their design, operation, cost, maintenance, frequency of sampling, and ease of use, the hypothesis tests results of the methane data have demonstrated that significant difference in the relative mean methane levels are recorded in the longwall panel return between two monitoring systems. However, for maximum methane values,  $\text{CH}_4$  levels from the real-time monitor were generally higher than the  $\text{CH}_4$  level measured by the tube bundle system. This does not hold true for the minimum and average data, where the concentration value obtained by the real-time monitor was less than by the tube bundle system.

Furthermore, Relative Standard Deviation (RSD) values between real-time and tube bundle systems were calculated. The measured overall variability includes all the variability associated with location of the monitoring systems in a sampling environment, as well as spatial and temporal variability that occurs underground during various production scenarios. The overall variability for each monitoring system accounts for all variability introduced by real-field effects and is based on valid statistical methods. This measured variability includes the inherent instrument sampling error, measurement error (fixed sample), and daily or hourly variability of methane concentration, and represents the best estimate of the long-term variability to quantify the measured concentration levels. The smaller of the overall variability is a more appropriate parameter to use when selecting the monitoring system for assessment. The RSD values for real-time and tube bundle using daily average methane data were 0.358 % and 0.367% of methane respectively. This further demonstrates that for VAM calculation purposes, a monitoring system with the minimal variation and that records continuous and frequent detection is a preferred choice.

## CONCLUSIONS

Air velocity and area of a roadway, WBT, DBT, CH<sub>4</sub>, CO<sub>2</sub>, BP are the key parameters that will assist in understanding the key hazards (gas, dust, sponcom, thermal), associated risks and the effectiveness of controls provided at workplace. Therefore, it is important that these parameters are accurately measured by those who are responsible for them.

The monitoring of air velocity at strategic positions assist in U/G VAM monitoring purposes instead of the monthly single surveys, which fail to record reduced air flow conditions or stoppage of fans for maintenance and thus fail to record the 'true' airflow and GHG estimations. Also, they will indicate the status of the air distribution in the mine on a continuous basis. The velocity monitors will give early warning of a weakening in airflow or a ventilation failure and timely action can therefore be taken before a gas accumulation develops. Benefits of real-time velocity monitors will provide the ventilation engineers additional information on whether the increase in gas levels is due to increase in gas release rate or reduced ventilation.

In an underground environment or exhaust shaft, the ideal 'true monitor' would measure the atmosphere that represents the mine methane levels accurately. In this study, it is noted that 'accuracy' of a specific monitoring system was not possible in the absence of an approved 'true reference monitor' or acceptance criteria currently available in the mining or gas measurement industry. Since the real-time monitor measures the gas levels in near real-time, its use as a 'true reference monitor' is justified as it records the changes in gas levels that are affected by various mining related parameters which are not monitored by the current intermittent tube-bundle monitoring system at underground locations such as shaft bottom or exhaust shaft.

The maintenance of an environmental monitoring system is of vital importance as the confidence in the system will be lost if the system is not maintained. All existing real-time and tube bundle systems require adequate maintenance as per the Australian Standard 2290.3 (1990). Failure to address will lead to misinterpretation of conditions underground and should be addressed without delay by relevant responsible person for the installation and maintenance of the monitoring systems. As in the case of existing gas monitoring systems, the inspection should include cleaning of monitors, testing of response of monitors, replacing malfunctioning monitors, a documentation system to include installation, cleaning, testing and date of replacement.

Based on the compelling evidence of data as demonstrated using the side-by side data analyses of two monitoring systems at LW panel return location, viz., real-time and tube bundle, it is noted that the tube bundle system records significantly higher daily average gas levels than the real-time monitors by approximately eight per cent. This difference in values can be attributed to the tube bundle system not sampling of atmosphere on a continuous basis.

For the statistical parameters of interest for U/G VAM calculations, minimum, maximum and daily/hourly average methane data, the per cent difference between the two monitoring systems is over and beyond the 'accuracy' differenced inherent between the two systems, i.e., tube bundle and real-time catalytic sensors. Finally, for VAM determination purposes, based on the overall variability calculations (RSD values), a monitoring system with the minimal variation and that records continuous and frequent detection such as real-time monitor is a preferred choice.

## WAY FORWARD

Mines should be safe places in which to work and any drivers that will endanger the safety and lives of underground worker to minimize the GHG emission through surface gas drainage networks need to be avoided. An opportunity to improve the underground ventilation and gas monitoring system (robust, complaint, accurate and transparent) by using continuous real-time air flow and gas measurement devices has been identified, viz.,

1. Based on the independent fan test evaluations, and the data analyses carried out in this study, it is recommended that mines implement real-time airflow, IR continuous gas (CH<sub>4</sub> and CO<sub>2</sub>) analyser, BP and temperature monitors at exhaust shaft fan ducts for underground ventilation air methane (VAM) estimations.
2. Currently, industry is faced with the persistent and complex challenge of obtaining a 'reference true monitor' for accuracy determination on quintessential U/G VAM parameters, viz., CH<sub>4</sub>, CO<sub>2</sub>,

air velocity, and temperatures. Also, evidence of supplier claims of 'accuracy' between the various monitoring systems is not readily available despite views of external auditors and reviewers. Therefore, operations are using the system/s that is deemed to provide practically acceptable, reliable and safe system to provide transparent UG VAM data.

### ACKNOWLEDGEMENTS

Author is indebted to various sources of knowledge that were developed in the past that have resulted in a better understanding of U/G VAM measurement and reporting in mines.

### REFERENCES

- Australian Standard 2290.3, 1990, Electrical Equipment for Coal Mines-Maintenance and Overhaul Part 3-Maintenance of gas detecting and monitoring equipment.
- Belle, B., 2013, Real-time air velocity monitoring in mines – a quintessential design parameter for managing major mine health and safety hazards, U/G Operators Conference, Wollongong, Feb 2013, pp 184-198. <http://ro.uow.edu.au/coal/454/>.
- Belle, B., 2013, AA Internal FI and Global Methane and Coal Dust Explosion Database, Australia.
- Brady, D., the influence Analytical techniques and Uncertainties in Measurement Have on the Assessment of Underground Coal Mine Atmospheres, SIMTARS.
- Thimmons, E.D., and Kohler, J.L., 1985, Measurement of Air Velocity in Mines, BOM RI 8971, USA.
- National Greenhouse and Energy Reporting Scheme (NGERS) Act, 2007.

---

# LEVERAGING GAS RESERVOIR DATA

Ray Williams

**ABSTRACT:** At a time when budgets are tight, it is increasingly important to maximise the use of gas reservoir information. This paper presents methods for leveraging gas content and permeability data and quantifying uncertainty. The objective is to adequately define the gas reservoir in terms relevant to how the data will be applied - for the least expenditure and risk. In the case of gas content, reduction in data noise reveals underlying trends that can then be mapped across a deposit. Essentially defining gas domains, with equations and uncertainty, it permits more targeted drilling and rationalisation of exploration plans. Permeability data are invariably sparse and yet critical in reservoir assessments. Two methods are presented to extend the range of direct well test data – the first maps inherent fracture development based on residuals of the Initial Desorption Rate (IDR30)/gas content relationship. The second provides a process for utilising observed relationships between permeability, depth and gas saturation to map permeability distribution with quantified uncertainty. The quantified relationships and uncertainty can then be used as inputs to probability modelling for gas emission, gas drainage and life of mine gas production.

## INTRODUCTION

Acquisition of gas reservoir data is costly. Data quality is paramount – the higher the quality, the greater is the likelihood of quantifying underlying trends, potentially resulting in reduction of both data quantity and expenditure for the same level of risk. This paper addresses two key reservoir parameters – gas content and permeability, with a view to maximising the usefulness of the information obtained. Models that identify and describe trends are fundamental to leveraging data. The uncertainty inherent in such models determines the extent of their usefulness.

## GAS CONTENT AND COMPOSITION

Gas content is the most basic and important gas reservoir property. There are standards (AS 3980-1999, ASTM D7569-10) which aid in governing their determination but none are sufficiently prescriptive to result in acceptable inter-laboratory reproducibility. This is especially so between fast and slow desorption testing in mixed CH<sub>4</sub> and CO<sub>2</sub> environments and between laboratories for fast desorption testing. The first requirement therefore is to know what influences the gas content result and how to undertake such testing in a manner that truly does reflect the gas adsorbed in the core sample being tested.

Every gas content test must report the following three parameters:

- Gas content expressed as the volume of gas desorbed per unit mass (m<sup>3</sup>/t)
- The gas composition of the component gases, primarily CO<sub>2</sub> and CH<sub>4</sub>
- The corresponding material properties of the coal - proximate analysis, Relative Density (RD)

The extent to which each is accurately measured dictates the overall accuracy of the result. A highly accurate gas content and component determination can be rendered useless if the associated coal properties are not similarly well defined. Probably the worst problem arises in conflicting use of the core – coal quality washability testing and gas content testing. For washability testing, the core sample requires a minimum of disturbance and small, discrete sections are selected for Q<sub>3</sub> residual gas determination. The resulting lack of sub sample representation can be overcome by undertaking proximate analysis on the remaining core, but frequently this core is recombined into coal plies prior to analysis resulting in poor characterisation of the coal core properties.

Both depth and mineral matter have a profound effect on gas content and in assessing underlying trends for gas domain analysis, the effect of mineral matter needs to be removed. A good gas content dataset

over a narrow depth range (e.g. < 30 m), should always correlate well with mineral matter unless the coal properties have been changed by devolatilisation from igneous activity. Often, zero gas content does not occur at 100% Ash+Inherent Moisture (IM) due to carbonates in the coal (example Figure 1). Here, zero gas content equates to 88% Ash+IM. Corrections are commonly done in the coal bed methane industry to a dry ash free (daf) basis. These corrections assume zero gas content at 100% Ash+IM and result in increasingly large errors with increasing mineral matter. Corrections to a daf basis are unnecessary and only serve to increase error and mask underlying trends.

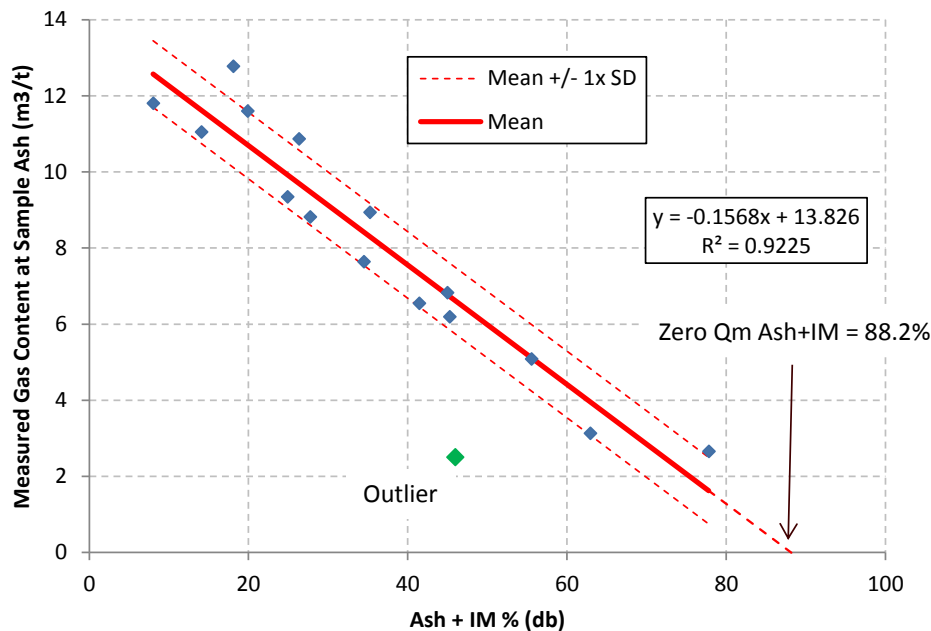


**Figure 1 - Example of relationship between gas content and mineral matter**

An anomalous value such as the outlier in Figure 1 could be the result of an error in gas volume determination or an error in assignment of coal properties. An outlier on its own should never be discounted unless there is corroborating evidence to that effect. A range of tests can be applied to rule on such outliers, such as relationship to initial desorption rate (Williams, *et al.*, 2002) and mismatches between calculated core density and measured RD.

Once the gas content data are validated and corrected to a common ash, underlying trends against depth can be discerned (Figure 2). Data may be affected by lesser quality results, ultimately expressed in the standard deviation about the mean (e.g. 1.46 m<sup>3</sup>/t in Figure 2). Good data sets normally have standard deviations less than 1 m<sup>3</sup>/t.

Resolution of these groupings (where data overlap) is made on the basis of spatial mapping of the gas domains as described in Williams *et al.* (2002, example Figure 2).

While probably the majority of gas domains can be defined by mappable depth/gas content relationships, many are more complex as indicated for Mount Arthur North/Saddlers Creek and Goonyella Riverside in Esterle *et al.*, (2006).

The gas domain boundaries are often quite sharp, although frequently difficult to relate to geological features. On a mine scale, they give direction for further drilling in defining boundaries, and enable rationalisation of drilling within boundaries.

## PERMEABILITY

### Factors affecting

Permeability is a measure of the ease with which a fluid can pass through a material. Coal itself (i.e. the coal matrix), is essentially impermeable and it is the cleat system that primarily determines the

permeability of a coal seam. How well it is developed is a reflection of the coals burial and tectonic history but it is also sensitive to material properties.

Bright coal contrasts with dull coal in containing a higher frequency of cleats and the reduced permeability of dull coal is well documented. Cleat development is also affected by mineral matter and is retarded as mineral matter content increases. The cleat system can be in-filled by secondary mineralisation such as calcite, significantly reducing the permeability of a well cleated coal.

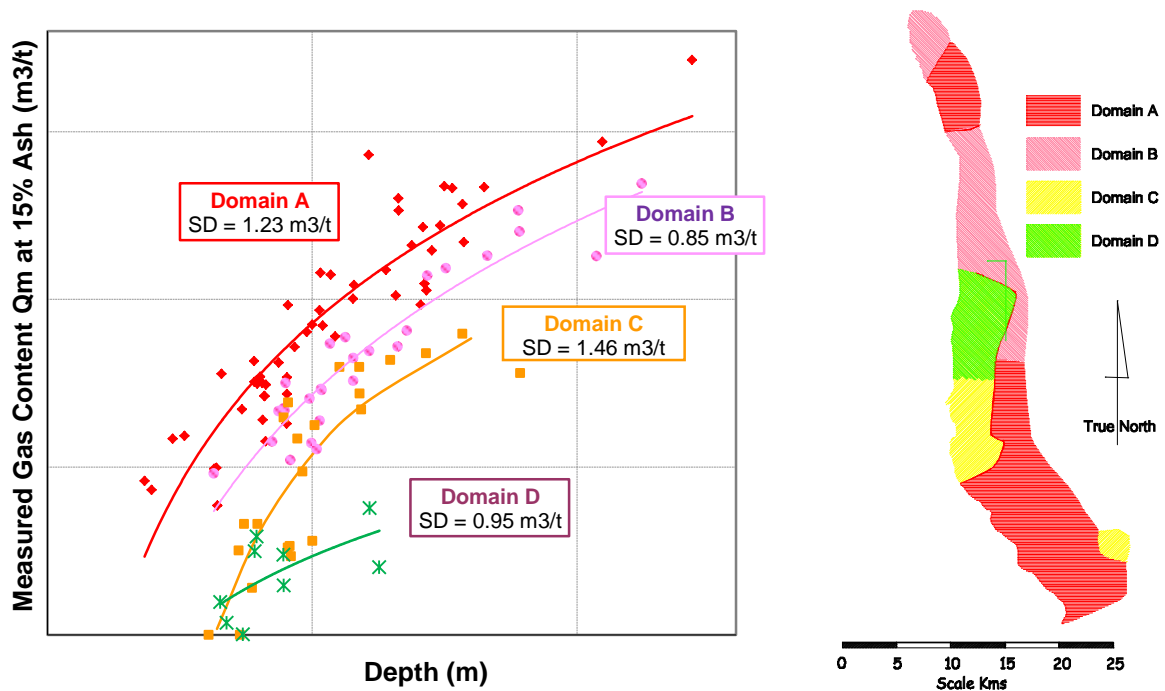


Figure 2 - Gas domain defined by gas content depth gradients

Coal has a low Young's Modulus and is especially sensitive to stress. Increased stress squeezes the cleat system, usually resulting in a marked reduction of permeability with depth of cover. For example, the Goonyella Middle seam of the Moranbah Coal Measures is particularly stress sensitive exhibiting a 12 fold decrease in permeability for every MPa increase in stress. Because of the sensitivity of permeability to stress, permeability values should always be accompanied by at least depth measurements but also pore pressure.

Simply plotted against depth, variations can be large, reflecting the combined effects of cleat development (burial/tectonic history, coal properties of mineral matter and coal type, mineral in-filling) and stress (depth of cover and local perturbations). In Figure 3 the response of decreasing permeability with depth is clearly seen in Seam C. Even so, the scatter is quite large (around two orders of magnitude) presumably reflecting smaller scale changes in coal properties, stress and cleat development. Seam A and to a large extent, Seam B show the effect of lower cleat development, which happens to be due to relatively high ash coal.

The higher ash coal with its higher Young's Modulus attracts more stress. For Seam A, this results in lower permeability, but this reduction is also influenced by a lack of cleating in the high ash coal (right side diagram, Figure 3).

### A proxy for cleat development

Gas content determinations using the direct method initially involve the field measurement of gas desorption rate for calculation of gas lost between taking the core and sealing in a canister (as described in AS3980-1999). From these initial desorption measurements, the calculation of the IDR30 desorption rate is reported as the quantity of gas desorbed in the first 30 minutes after time  $t_0$  per unit mass (IDR30 =  $v/m$  m<sup>3</sup>/t where  $v$  = l volume in ml,  $m$  is coal mass in g, Figure 4).

IDR30 is strongly related to:

- Gas content
- Gas composition
- Core diameter, and less clearly related to
- Degree of fracturing of the intact core – drilling induced and geological

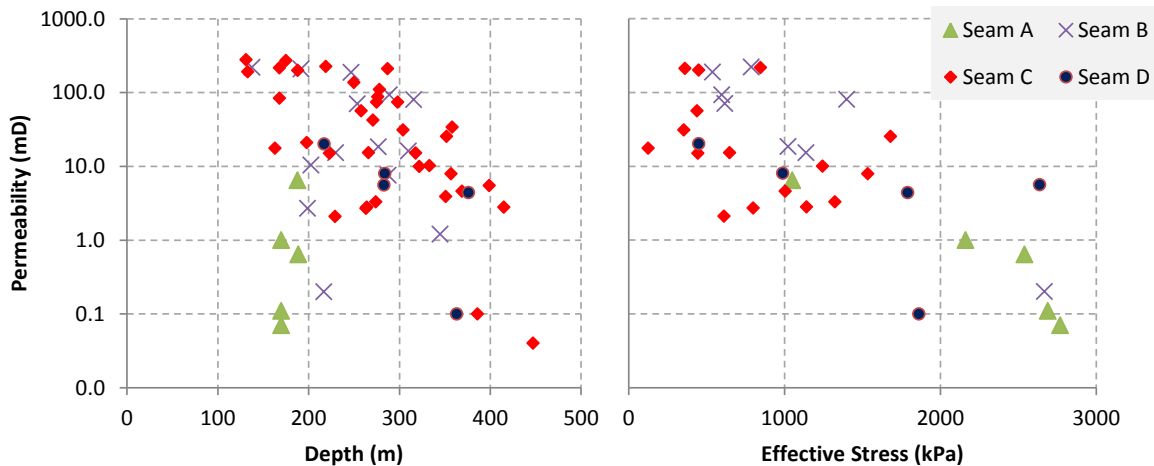


Figure 3 - Variation in permeability with depth and effective stress

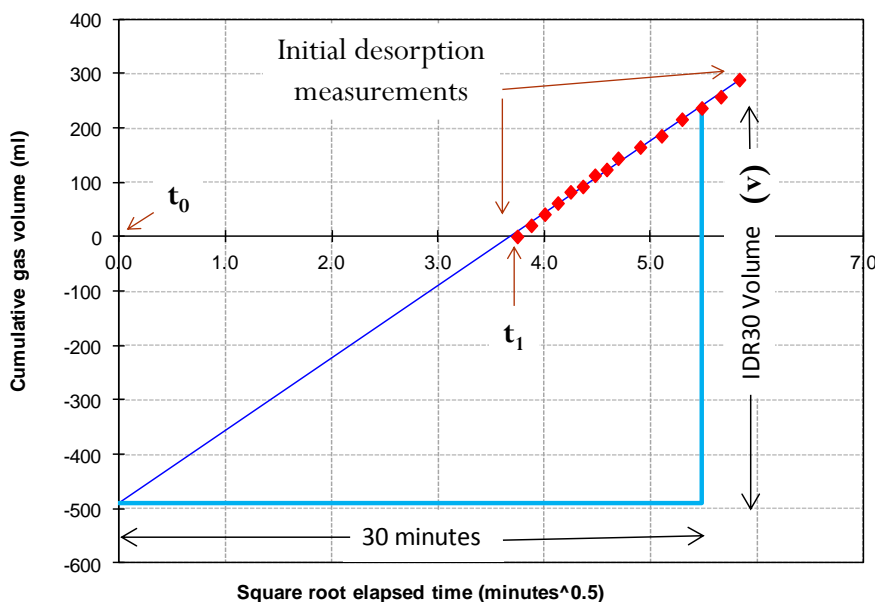


Figure 4 - Derivation of IDR30

Gas content increases with IDR30, but the relationship always shows a degree of scatter about the mean (Figure 5). For a relatively constant gas composition and consistent core size, the scatter is arguably related to variable fracturing in the core itself. In the great majority of cases the fractures are geological in nature (cleats).

The implication is that where the IDR30 is high for a given gas content, the core is more fractured and vice versa (Figure 5). Residuals about the mean can be calculated and mapped (Figure 6).

A major advantage of the method is the universality of IDR30 data, calculable from any laboratories Q1 gas content test data. But extraneous effects can affect the outcome:

- Gas content data must be validated. A high IDR30 can also be an indication of canister leakage

- The gas content/IDR30 relationship must be robustly defined and be devoid of bias from too few end data (e.g. excluded data, Figure 5)
- Where more than one laboratory has done the gas content testing, reproducibility needs to be good.
- In mixed gas ( $\text{CO}_2$ ,  $\text{CH}_4$ ) environments, it should only be applied for specific ranges of gas composition where a low sensitivity to gas composition can be demonstrated.

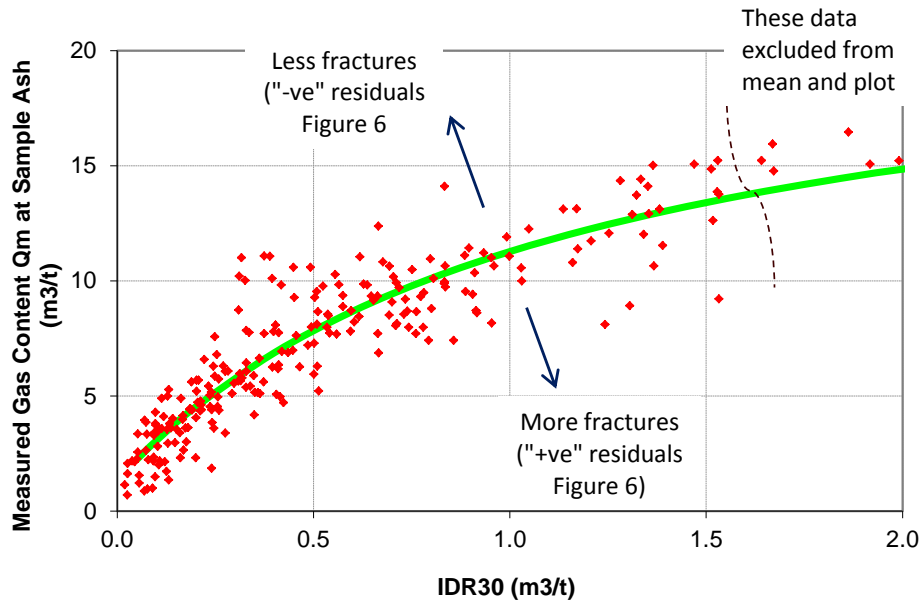


Figure 5 - Relationship between IDR30 and measured gas content

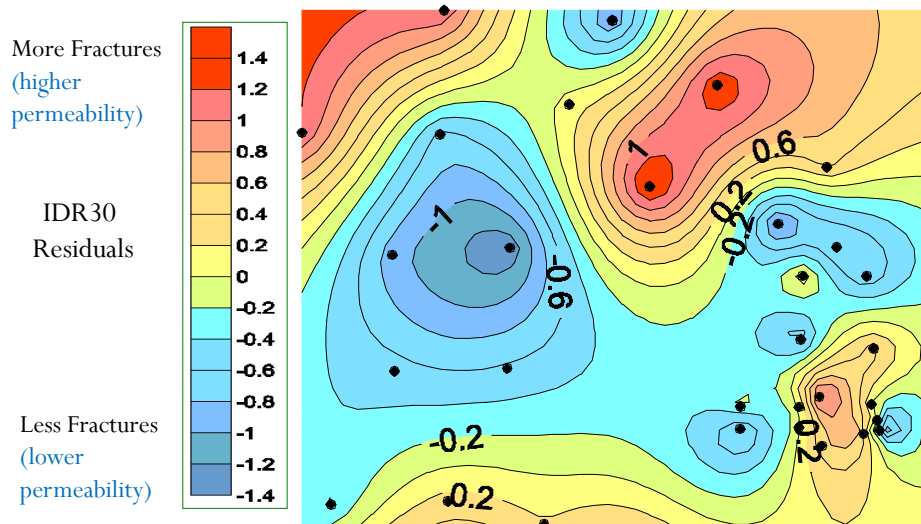


Figure 6 - Mapping implied fracture variations

This method is an adjunct, not a replacement for well test determinations of permeability. While it ignores stress effects, there are a number of potential applications:

- Combined with well test results it can improve understanding of variations in measured permeability data where those variations are due to changes in cleat frequency
- Areas of variable drainage behaviour may be better understood and predicted. Difficult to drain areas due to low cleat frequency may be identified
- More informed selection of locations for pilot well drilling and interpretation of gas production outcomes

**A permeability model**

The most common permeability model is simply one of plotting the trend (or lack of it) of permeability against depth. Such a model can be quite difficult to apply with a range of uncertainty usually greater than two orders of magnitude.

For Australian coal mines it is common to see highly saturated coals with low permeability and under-saturated coals with high permeability. The inference is that the lower saturation is caused by migration of water in the geological past removing adsorbed CH<sub>4</sub> (this reasoning is not necessarily as applicable to CO<sub>2</sub>).

Large areas of the Moranbah Coal Measures from North Goonyella Mine south to Saraji characteristically show decreasing gas saturation with depth of cover below a horizon that becomes increasingly shallow to the south. In the north (Grosvenor to Goonyella), gas content and saturation increase with depth to around the Goonyella Middle seam. Below this seam the gas saturation and gas content decreases primarily affecting the Goonyella Lower seam. South of Grosvenor, the zone of under-saturation/low gas content moves up the stratigraphy, ultimately affecting all seams in the sequence.

A good, but by no means atypical example for a borehole just south east of Grosvenor shows reducing gas content and saturation below the Goonyella Middle seam, where a gas content of 9 m<sup>3</sup>/t at 500 m reduces to a gas content of ~3 m<sup>3</sup>/t at 640 m depth (Figure 7). Corresponding to this change is an increase in permeability from 1 mD at 340 m to 13 mD at 637 m. The increase in permeability and decrease in gas content with depth is quite unusual and more than coincidental. It is argued the gas content is low at depth because the permeability is high, gas having been removed by migrating water. That the permeability actually increases in spite of the sensitivity to stress of these coals is quite remarkable.

For coals nearer to the subcrop, variable saturation is more easily explained from gas leakage to sub crop and removal from shallow fluids. But the relationship of increasing permeability with decreasing saturation at equivalent depths has been demonstrated. How wide spread or universal such a relationship is remains to be seen, but the cause and effect mechanism is plausible.

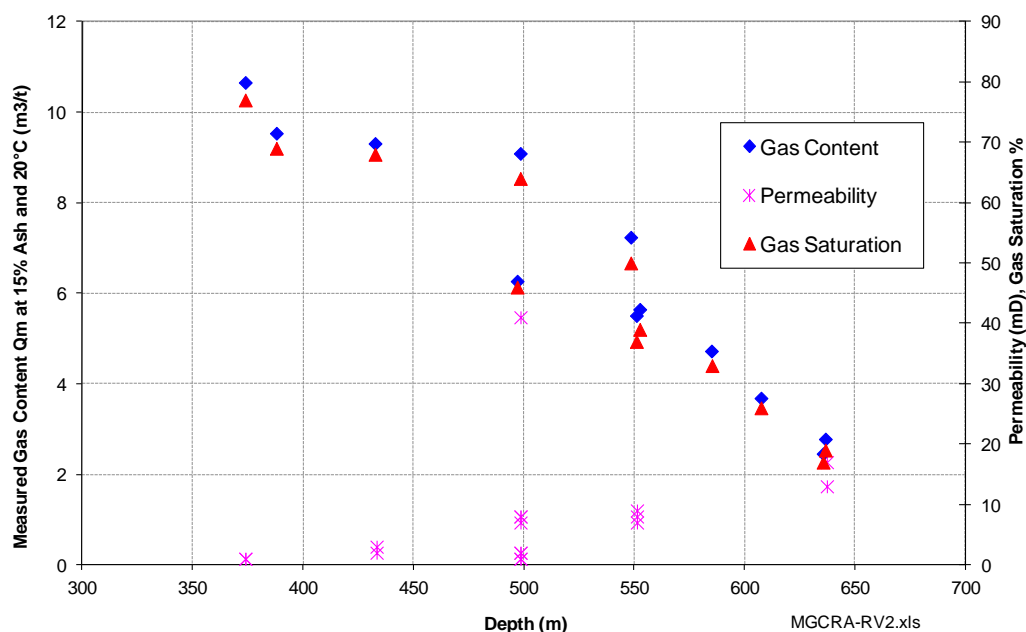


**Figure 7 - Reducing gas saturation and increasing permeability with depth – River Paddock No.2 well**

On this basis, permeability can be related to depth of cover (stress) and gas content (saturation) according to the equation:

$$\ln \text{ Permeability (mD)} = A * \text{ Depth (m)} + B * \text{ Qm} + C$$

Where coefficients A, B and C are determined from a multivariate analysis of depth and gas content against permeability (example Figure 8).

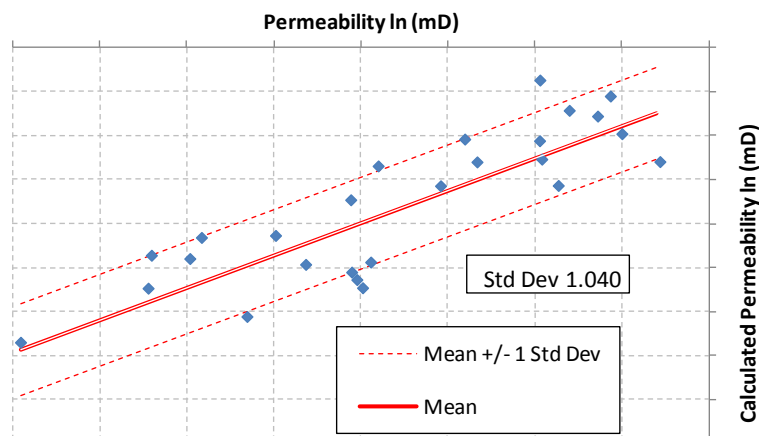


**Figure 8 - Basis for indirect assignment of permeability as a function of gas content and depth**

The assignment is tested and the error (uncertainty) quantified by comparing measured results against ones calculated from depth and gas content for those boreholes with well test data (Figure 9).

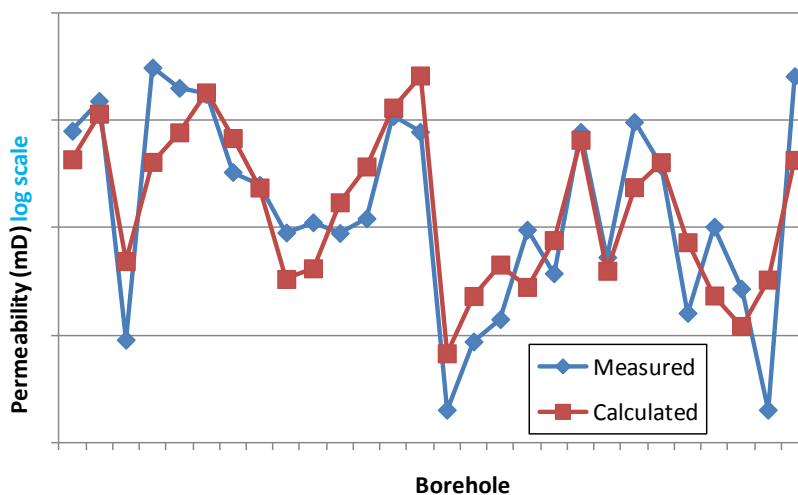


**Figure 9 - Test of calculated against measured permeability**

Assignment is now possible from comparatively few boreholes where permeability has been measured, to a far greater number of wells that contain depth and gas content data for the seam in question. The uncertainty in the assignment is quantified and the permeability distribution mapped (Figure 10).

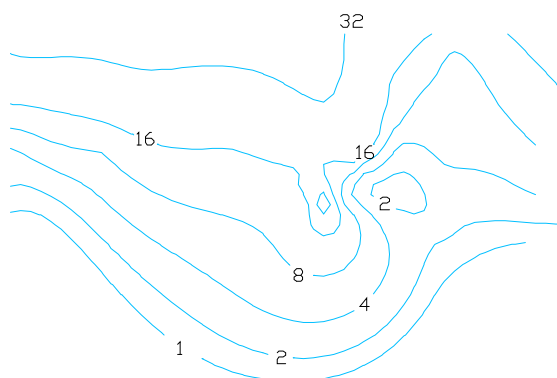


**Figure 10 - Spatial distribution of permeability**

Mapped variations in gas content and permeability can be applied in defining “Reservoir Regions” across a mine (Figure 11). These regions are a means of discretising for gas reservoir modelling purposes, what is a continuum of changing properties over a mining area. Quantification of uncertainty in the leveraged gas content and permeability data, together with uncertainty in gas desorption pressure enables gas drainage, emission and gas production outcomes in terms of probability distributions.

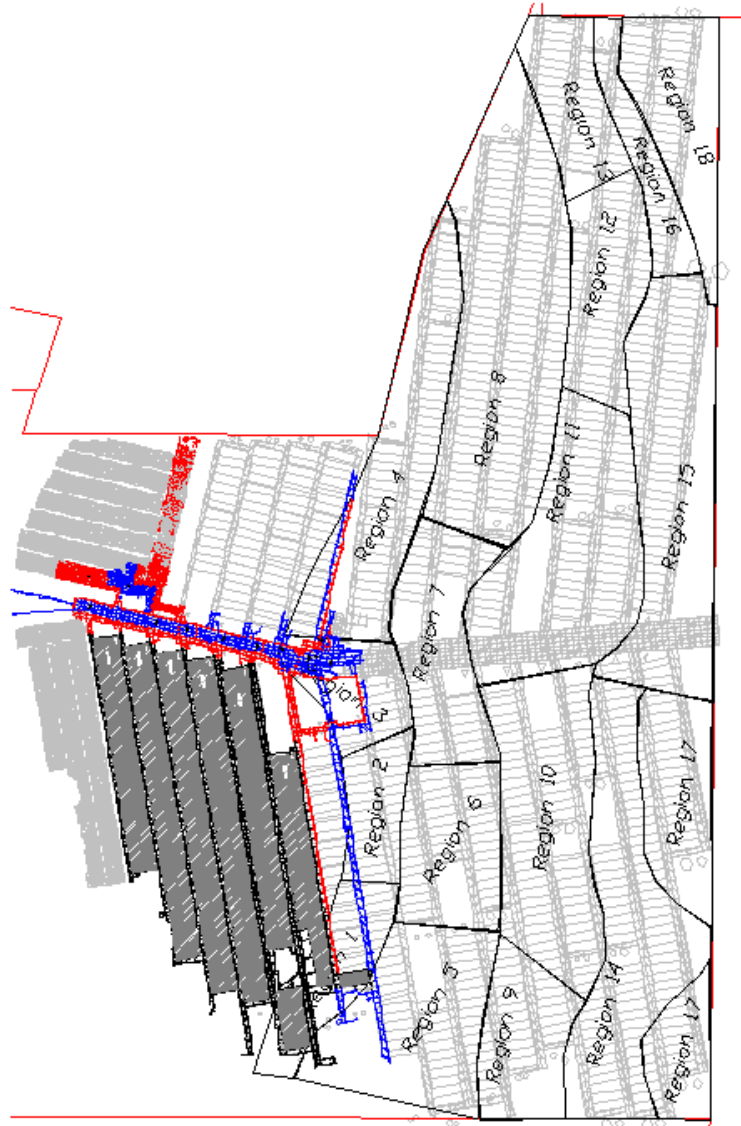


Figure 11 - Example of reservoir regions, Moranbah North Mine (Luckhurst-Smith and Williams, 2007)

## CONCLUSIONS

Australian coal seam gas reservoirs display a wide range of conditions from zero gas content to as high as 20+ m<sup>3</sup>/t, gas saturation 0% to 100%, undrainable coal (<0.1 mD) to highly permeable (>1000 mD) and gas composition ranges from 100% CH<sub>4</sub> to 100% CO<sub>2</sub>. Every deposit will have its own peculiarities and a “one method approach fits all” is unlikely to work.

That said, almost always, logical relationships will be found that will enable leveraging of gas reservoir data. This paper has given examples of models for leveraging gas content and permeability that should have broad application. In any event, such approaches can be tested and progressed if warranted.

The key drivers are to define the gas reservoir for the least cost and risk and provide inputs that facilitate subsequent modelling of gas drainage, emission and gas production with quantifiable uncertainty.

**REFERENCES**

- AS3980-1999. Guide to the determination of gas content of coal-direct desorption method. Standards Australia ISBN 0 7337 2906 1.
- ASTM D7569-10. Standard practice for determination of gas content of coal-direct desorption method. ASTM International.
- Esterle, J, Williams, R, Sliwa, R and Malone, M, 2006. Variability in gas reservoir parameters that impact on emissions estimations for Australian black coals, *ACARP project C13071*.
- Luckhurst-Smith, H and Williams, R, 2007. Moranbah North coal seam gas development – technical and statutory, *ACARP gas and outburst workshop, Mackay*.
- Williams, R.J., Casey, D.A. and Yurakov, E. 2000. Gas reservoir properties for mine gas emission assessment. *Bowen Basin Symposium 2000, Rockhampton Queensland*.

# CHANGES IN GAS COMPOSITION DURING COAL SEAM DRAINAGE AND LABORATORY TESTING

Dennis John Black<sup>1</sup> and Naj Aziz<sup>2</sup>

**ABSTRACT:** Analysis of gas emissions from underground-to-inseam (UIS) gas drainage boreholes located in the Bulli seam found methane gas liberated from the coal in preference to carbon dioxide gas, particularly in mixed gas (CH<sub>4</sub> and CO<sub>2</sub>) conditions. The rate of emission of the methane gas component from the *in situ* coal seam was also found to be greater than the rates observed during laboratory gas desorption testing on coal cores recovered during the drilling of the UIS gas drainage boreholes. The nature of changes in the composition of the gas mixture liberated from coal, and the relative differences in gas composition determined by fast and slow desorption testing, and UIS gas production, may have a potentially significant impact on outburst risk assessment and coal seam gas reservoir assessment. Results of gas composition measurement from the three sources are presented and discussed.

## INTRODUCTION

A comprehensive investigation was conducted in an underground coal mine, operating in the Bulli seam in the southern Sydney basin, which focussed on gas emissions and the factors that impact gas emissions from coal. Part of the investigation analysed coal core samples and included a comparative analysis of the content and composition of gases desorbed from coal samples during fast desorption (FD) and slow desorption (SD) testing in accordance with AS3980:1999 (SAA, 1999). The investigation also measured flow rate and composition of gas produced from underground-to-inseam (UIS) gas drainage boreholes. The term "gas composition" used in this paper refers to the mixture of methane (CH<sub>4</sub>) and carbon dioxide (CO<sub>2</sub>) gas contained in the coal.

Gas liberated from the core samples and UIS boreholes was analysed using a Hewlett Packard quad micro gas chromatograph to determine the relative concentrations of the gases, CH<sub>4</sub>, CO<sub>2</sub>, N<sub>2</sub>, O<sub>2</sub>, C<sub>2</sub>H<sub>6</sub>, CO and C<sub>2</sub>H<sub>4</sub>. In addition to the individual component gases, air dilution and the gas composition [CH<sub>4</sub>/(CH<sub>4</sub>+CO<sub>2</sub>)] was calculated. The flow rate of gas produced from UIS boreholes was measured using orifice plate measuring sets and the volume of gas desorbed from core samples was measured in the laboratory using a calibrated gas volume measurement apparatus. Both the gas chromatograph and the volume measurement apparatus, shown in Figure 1, are located in the University of Wollongong Gas Research Laboratory.

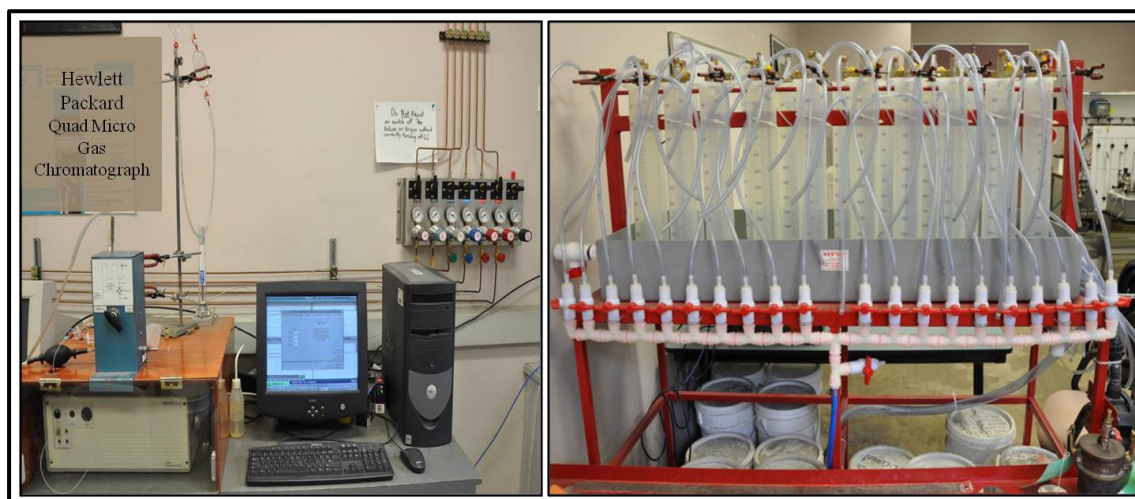


Figure 1 - Testing equipment located in the gas and outburst research laboratory, University of Wollongong

<sup>1</sup> Pacific Mining and Gas Management Consultants, Australia. [www.pacificmgm.com.au](http://www.pacificmgm.com.au). Tel: 0401999542

<sup>2</sup> Department of Civil, Mining and Environmental Engineering, University of Wollongong, Australia. [naj@uow.edu.au](mailto:naj@uow.edu.au)

Analysis of gas composition data from the three sources, (a) FD (quick crush) testing, (b) SD testing, and (c) UIS gas drainage boreholes, indicated differences in the rate of emission of CH<sub>4</sub> and CO<sub>2</sub> from coal core samples and *in situ* coal. This paper discusses the results of gas content and gas composition measurements from core samples and the UIS boreholes from which the core samples were collected. Following recovery from the borehole and completion of initial Q<sub>2-field</sub> gas emission testing, each core sample was divided, with half used for FD testing and half used for SD testing.

Details of the coal core samples and the corresponding UIS gas drainage borehole from which they were collected are listed in Table 1, and the location of the core samples along each UIS borehole are shown in Figure 2.

**Table 1 - Reference numbers of coal core samples collected during drilling of UIS boreholes**

UIS BOREHOLES	COAL CORE SAMPLES
519-18/9	WE1183; WE1189
519-21/8	WE1205; WE1208
519-33A/2	WE1191; WE1199
519-33A-4	WE1201; WE1202; WE1203; WE1209; WE1210
519-33A/6	WE1308; WE1309

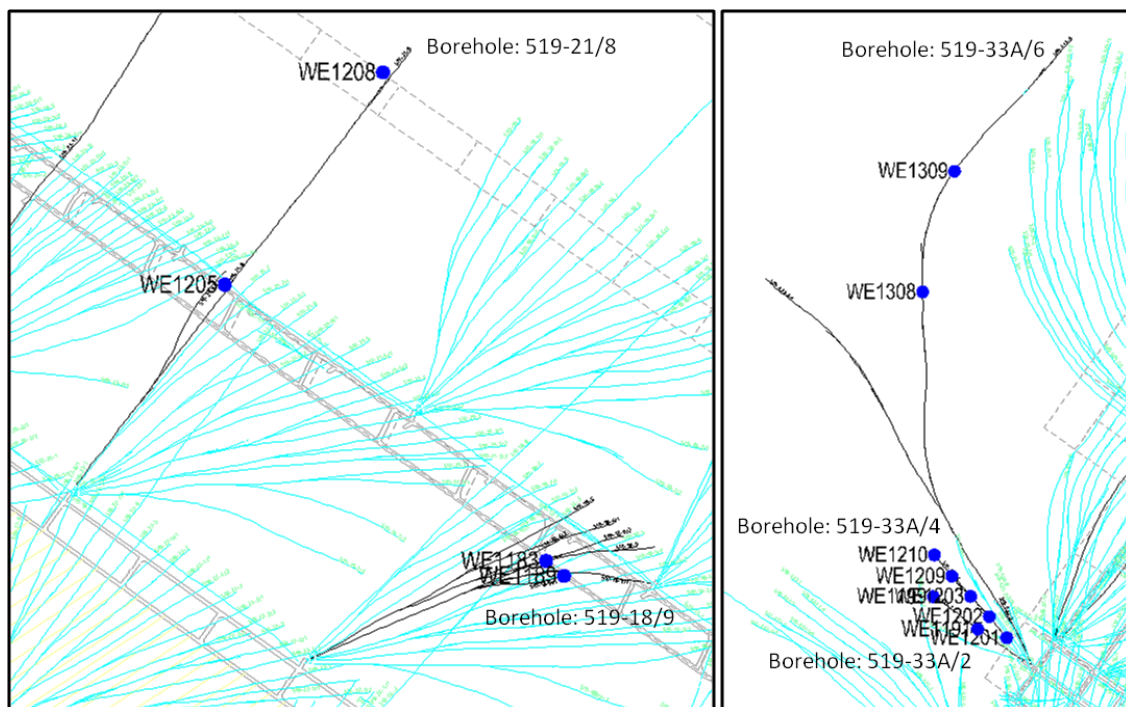


**Figure 2 - Location of coal core samples along UIS gas drainage boreholes**

### ANALYSIS OF GAS MIXTURE COMPOSITION FROM UIS BOREHOLES AND COAL CORE SAMPLES

Figure 3 shows the location of core samples along UIS boreholes 519-18/9 and 519-21/8 relative to (a) gas content contours and (b) gas composition contours generated using data collected from gas analysis of coal samples collected from the Bulli seam during surface-based exploration drilling. The proximity of the exploration boreholes, S1399, S1437, S1462, S1488, S1488, S1791, are shown relative to the UIS boreholes.

Figure 4 shows the location of core samples along UIS boreholes 519-33A/2, 519-33A/4, and 519-33A/6 relative to (a) gas content contours and (b) gas composition contours generated using data collected from gas analysis on coal samples collected from the Bulli seam during surface-based exploration

drilling. The proximity of the exploration boreholes, S1126, S1454, S1716, and S1840, are shown relative to the UIS boreholes.

It can be seen that the gas content values determined from FD testing on UIS core samples varies relative to the contoured gas content values generated using gas content data from adjacent exploration boreholes. The FD gas content values are shown to be lower than individual exploration contours in the areas of borehole 519-18/9 and 519-21/8 while being substantially higher in the area of borehole 519-33A. Three potential reasons for the differences include (a) inaccurate estimation of the Q1 gas content component desorbed from the core samples during drilling and extraction of the samples from the coal seam, (b) gas content contours generated from exploration data may not be truly representative of the distribution of gas content within these areas of the Bulli seam, and (c) the vertical coal seam section collected by exploration drilling may contain plies that have variable gas content that was not present in the seam section sampled by UIS drilling.

Details of the gas content value determined from FD testing of the core samples collected from UIS boreholes 519-18/9 and 519-21/8, and the estimated gas content value at each core location, based on contoured exploration data, are listed in Table 2 and Table 3 respectively.

Details of the gas content values determined from FD testing of the core samples collected from UIS boreholes 519-33A/2, 519-33A/4, and 519-33A/6, and the estimated gas content value at each core location, based on contoured exploration data, are listed in Table 4, Table 5 and Table 6 respectively.

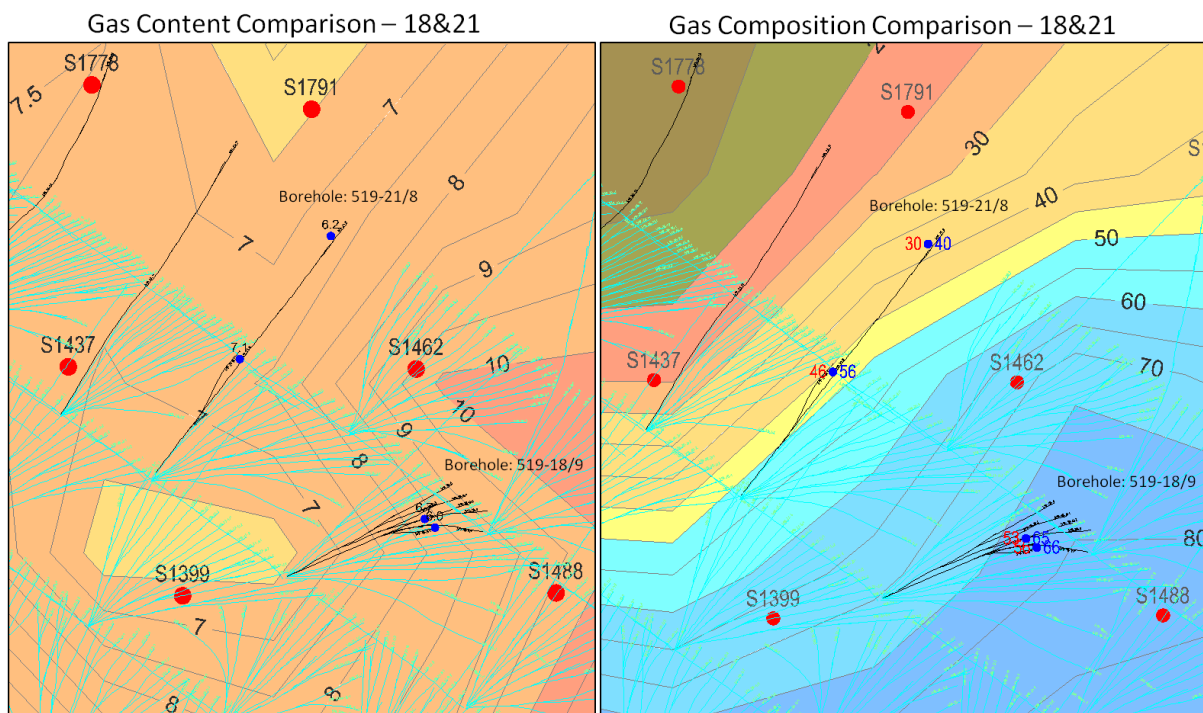


**Figure 3 - UIS boreholes (519-18/9 and 519-21/8) and gas data relative to exploration gas content and composition (CH<sub>4</sub>:CO<sub>2</sub> ratio) contours**

#### Gas data recorded along UIS borehole 519-18/9

The total length of UIS borehole 519-18/9 was 676m and based on gas composition contours generated from exploration boreholes, located less than 300m from this borehole, the CH<sub>4</sub> component [CH<sub>4</sub>/(CH<sub>4</sub>+CO<sub>2</sub>)] of the seam gas along the length of the borehole varied between 70% to 80%, as shown in Figure 3.

Two core samples, WE1183 and WE1189, were collected during the drilling of this borehole. The CH<sub>4</sub> component of the gas released from the core samples determined by FD testing was 53% and 56% respectively. The average CH<sub>4</sub> component of the gas desorbed from the core samples WE1183 and WE1189 recorded during SD testing over a period of 151 days and 341 days was 65% and 66%

respectively. The CH<sub>4</sub> component of the gas released from the two core samples during SD testing varied between 53% and 69% (WE1183) and 58% and 69% (WE1189), as shown in Figure 5.

One gas composition measurement was taken during gas production from UIS boreholes 519-18/9 on day 24 and the CH<sub>4</sub> component at that time was 57%, as indicated in Figure 5. Additional gas composition monitoring was conducted on adjacent UIS boreholes 519-18/6 and 519-18/7 that recorded CH<sub>4</sub> component values ranging between 56% and 62% from 519-18/6 (59% average) between day 120 and 155, and 63% and 75% from 519-18/7 (68% average) between day 31 and 157. The results of periodic gas composition measurement from these two boreholes are shown in Figure 6.

Table 2 provides a summary of the gas composition values recorded from FD testing, and the average gas composition values recorded during SD testing, on the core samples collected from UIS borehole 519-18/9 along with the estimated gas composition values based on contoured exploration data and the average composition of the gas produced from the UIS borehole.

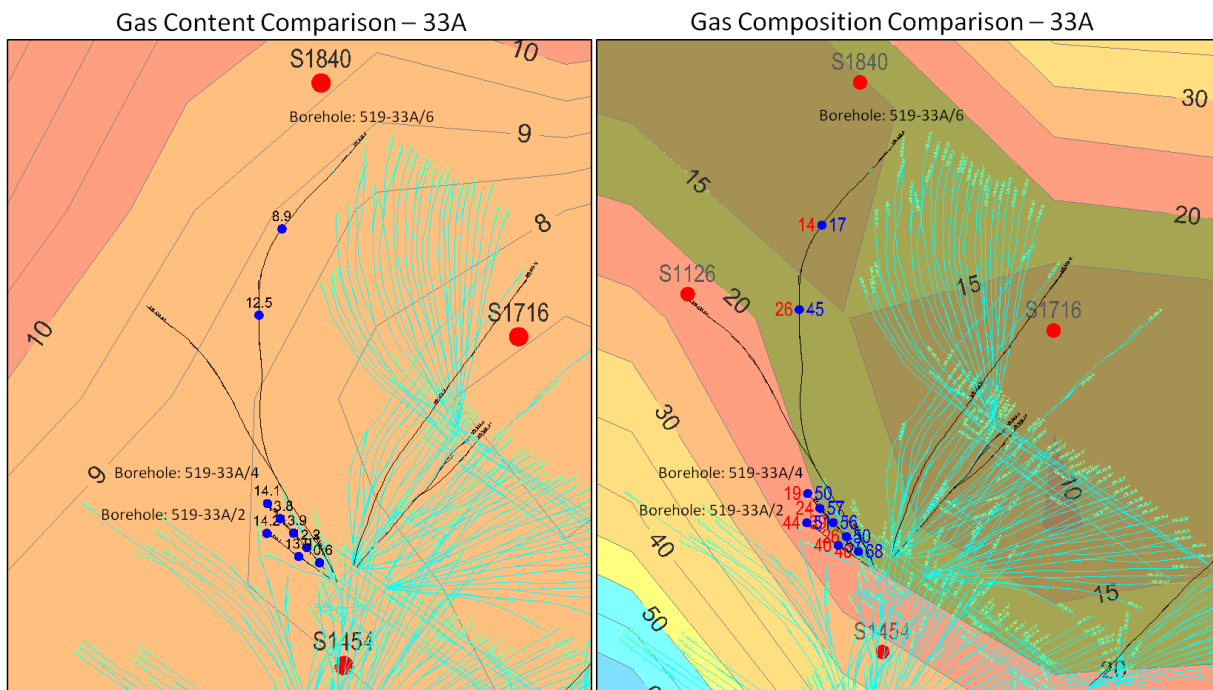


Figure 4 - UIS boreholes (519-33A/2, 519-33A/4 and 519-33A/6) and gas data relative to exploration gas content and composition [CH<sub>4</sub>÷(CH<sub>4</sub>+CO<sub>2</sub>) %] contours

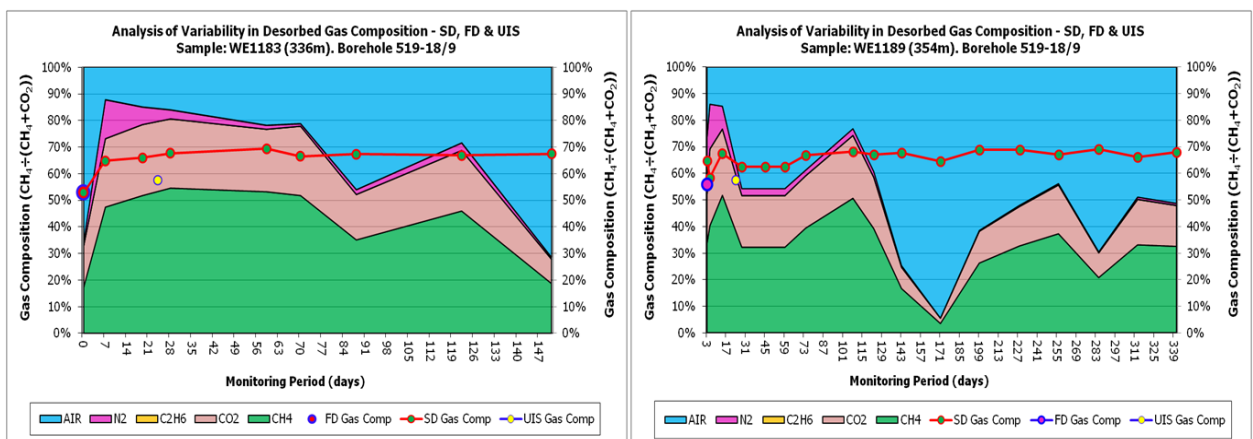


Figure 5 - Recorded gas composition during SD testing of WE1183 and WE1189 including FD and UIS gas composition values

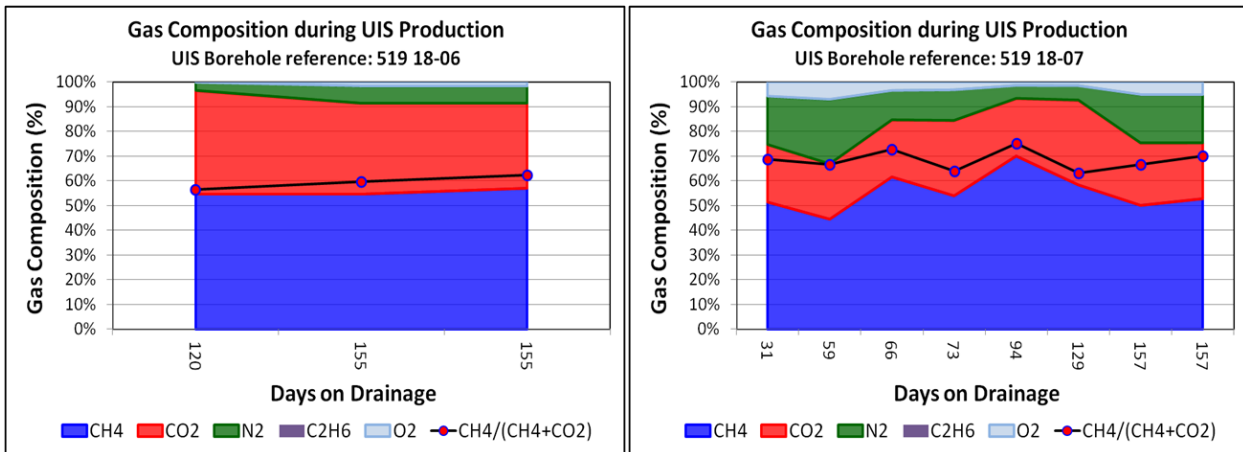


Figure 6 - Recorded gas composition during gas production from UIS boreholes 519-18/6 and 519-18/7

Table 2 - Summary gas content and gas composition data at core sample locations in UIS borehole 519-18/9

Reference Borehole: 519-18/9

UIS Core Samples	Gas Content (m <sup>3</sup> /t)		Gas Composition (CH <sub>4</sub> +{CH <sub>4</sub> +CO <sub>2</sub> })(%)			
	Exploration contours (est.)	UIS Gas Content	Exploration contours (est.)	Fast Desorption	Slow Desorption (average)	UIS Gas Production (average)
WE1183	8.3	6.7	77	53	65	57
WE1189	8.3	6.0	78	56	66	57
Note: Average gas composition from adjacent boreholes:					519-18/6	59
					519-18/7	68

The CH<sub>4</sub> component of gas desorbed from WE1183 and WE1189 during SD testing was 12% and 10% greater than the composition measured during the FD test. The increased CH<sub>4</sub> detected during SD suggest CH<sub>4</sub> desorbs from coal samples at a faster rate than CO<sub>2</sub>, with CO<sub>2</sub> being retained within the sample and potentially not being released until late stage desorption or until the coal sample is crushed (e.g. Q3 gas content measurement during FD testing).

The increased CH<sub>4</sub> component indicated by the contoured exploration gas data may be the result of sections of the coal seam (coal plies) containing elevated levels of CH<sub>4</sub> being present in the exploration core sample. Details of gas composition testing on vertical section of the Bulli seam were not available therefore the potential variability in gas composition within vertical section of the Bulli seam cannot be confirmed.

**Gas data recorded along UIS borehole 519-21/8**

The total length of UIS borehole 519-21/8 was 865m and based on gas composition contours generated from exploration boreholes located less than 350m from this borehole, the CH<sub>4</sub> component along the length of the borehole ranges from 37% to 52%, as shown in Figure 3.

Two core samples, WE1205 and WE1208, were collected during the drilling of this borehole. The CH<sub>4</sub> component of the gas released from the core samples determined by FD testing was 46% and 30% respectively. The average CH<sub>4</sub> component of the gas desorbed from core samples WE1205 and WE1208 during SD testing over a period of 140 days and 110 days was 56% and 40% respectively. The CH<sub>4</sub> component of the gas released from the two core samples during SD testing varied between 49% and 64% (WE1205) and 29% and 46% (WE1208), as shown in Figure 7.

Three gas composition measurements were taken during gas production from UIS borehole 519-21/8, on day 1, day 71 and day 99, and the recorded CH<sub>4</sub> component progressively increased from 67% (day 1) to 82% (day 99), as indicated in Figure 7. Additional gas composition monitoring was conducted on adjacent UIS boreholes 519-21/5 and 519-21/7 that recorded CH<sub>4</sub> component values ranging between 50% and 71% from 519-21/5 (59% average) between day 8 and day 127, and 44% and 55% from

519-21/7 (48% average) between day 36 and day 120. The results of periodic gas composition measurements from these two boreholes are shown in Figure 8. The recorded CH<sub>4</sub> component of the gas produced from the three UIS boreholes was consistently greater than the values recorded from core sample testing. In this area, the UIS boreholes may have been drilled through sections of the coal seam containing elevated CH<sub>4</sub> levels. Should this be the case, it is reasonable to assume that CH<sub>4</sub> would be preferentially desorbed from the coal, particularly in the comparatively high CH<sub>4</sub> zones, and the total component volume of CH<sub>4</sub> would exceed the volume of the CO<sub>2</sub> desorbed from the less CH<sub>4</sub> rich sections of the borehole. Details of incremental gas composition measurements along the length of the UIS boreholes were not available therefore the potential variability in gas composition and increased emission rate from possible CH<sub>4</sub> rich zones cannot be confirmed.

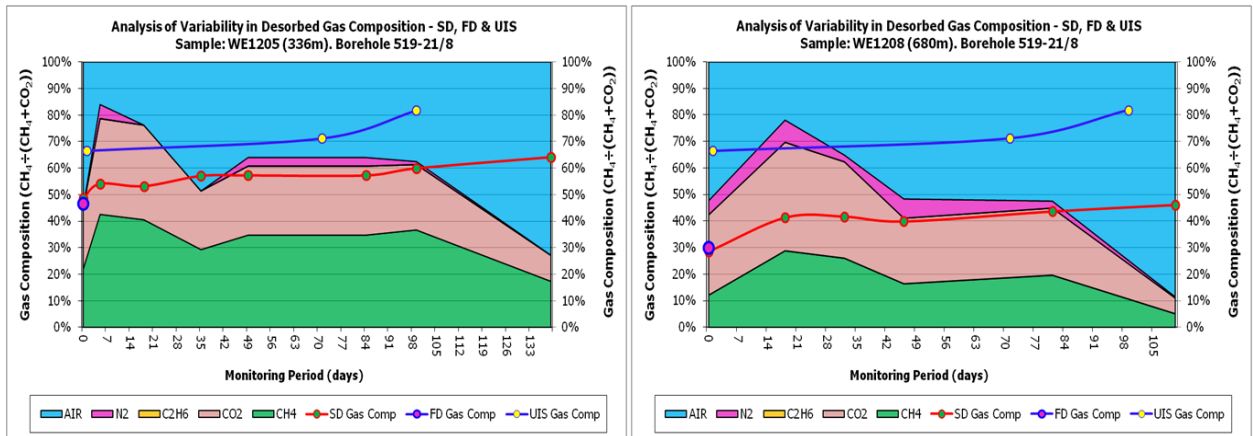


Figure 7 - Recorded gas composition during SD testing of WE1205 and WE1208 including FD and UIS gas composition values

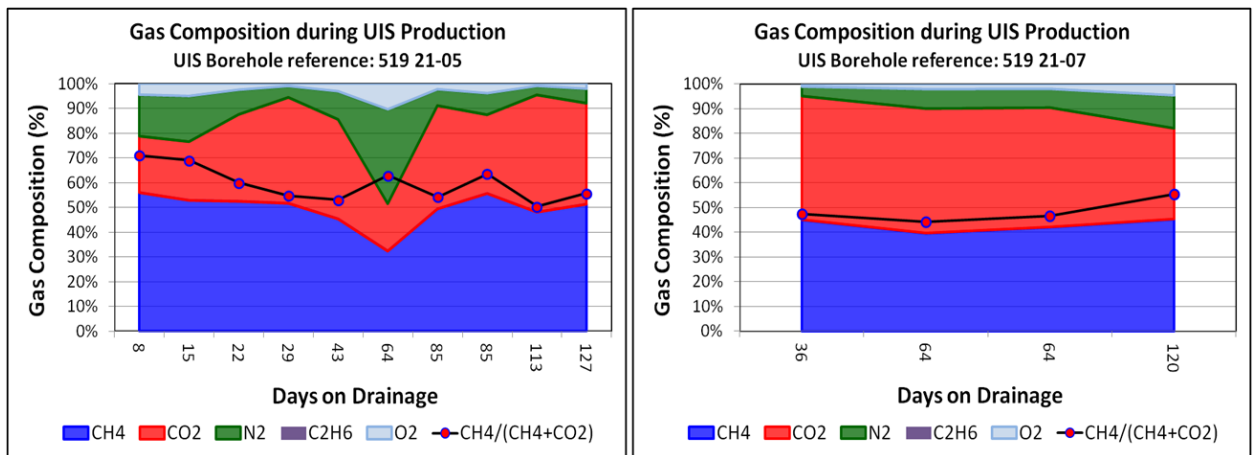


Figure 8 - Recorded gas composition during gas production from UIS boreholes 519-21/5 and 519-21/7

Table 3 provides a summary of the gas composition values recorded from FD testing, and the average gas composition values recorded during SD testing, on the core samples collected from UIS borehole 519-21/8 along with the estimated gas composition values based on contoured exploration data and the average composition of the gas produced from the UIS borehole.

The CH<sub>4</sub> component of gas desorbed from WE1205 and WE1208 during SD testing was 10% greater than the composition measured during the FD test. The increased CH<sub>4</sub> detected during SD suggest CH<sub>4</sub> desorbs from coal samples at a faster rate than CO<sub>2</sub>, with CO<sub>2</sub> being retained within the sample and potentially not being released until late stage desorption or until the coal sample is crushed (e.g. Q3 gas content measurement during FD testing).

In this area of the Bulli seam the CH<sub>4</sub> composition indicated by the contoured exploration gas data is similar to the values determined during FD testing.

**Table 3 - Summary gas content and gas composition data at core sample locations in UIS borehole 519-21/8**

Reference Borehole: 519-21/8						
UIS Core Samples	Gas Content (m <sup>3</sup> /t)		Gas Composition (CH <sub>4</sub> +[CH <sub>4</sub> +CO <sub>2</sub> ])(%)			
	Exploration contours (est.)	UIS Gas Content	Exploration contours (est.)	Fast Desorption	Slow Desorption (average)	UIS Gas Production (average)
WE1205	7.3	7.1	46	46	56	73
WE1208	7.3	6.2	37	30	40	73
Note: Average gas composition from adjacent boreholes:					519-21/5	59
					519-21/7	48

**Gas composition data recorded along UIS borehole 519-33A/2**

The total length of UIS borehole 519-33A/2 was 162m and based on gas composition contours generated from exploration boreholes located less than 700m from this borehole, the CH<sub>4</sub> component along the length of the borehole ranges from 20% to 25%, as shown in Figure 4.

Two core samples, WE1191 and WE1199, were collected during the drilling of this borehole. The CH<sub>4</sub> component of the gas released from the core samples during FD testing was 40% and 44% respectively. The average CH<sub>4</sub> component of the gas desorbed from core samples WE1191 and WE1199 during SD testing over a period of 383 days and 264 days was 57% and 51% respectively. The CH<sub>4</sub> component of the gas released from the two core samples during SD testing varied between 50% and 60% (WE1191) and 39% and 58% (WE1199), as shown in Figure 9.

Ten gas composition measurements were taken during gas production from UIS borehole 519-33A/2, commencing day 1 of gas production, with periodic measurement to day 140. The average CH<sub>4</sub> component of the seam gas progressively increased from 66% (day 0) to 73% (day 49) and then progressively decreased to 67% (day 126) prior to the final measurement on day 140 that recorded 76%. The results of gas composition measurement from borehole 519-33A/2 are presented in Figure 10 and shown relative to the SD results from the two core samples in Figure 9.

The recorded CH<sub>4</sub> component of the gas produced from the UIS borehole was consistently greater than the values recorded from core sample testing. In this area, the UIS borehole may have been drilled through sections of the coal seam containing elevated CH<sub>4</sub> levels. Should this be the case, it is reasonable to assume that CH<sub>4</sub> would be preferentially desorbed from the coal, particularly in the comparatively high CH<sub>4</sub> zones, and the total component volume of CH<sub>4</sub> would exceed the volume of the CO<sub>2</sub> desorbed from the less CH<sub>4</sub> rich sections of the borehole. Details of incremental gas composition measurement along the length of the UIS boreholes were not available therefore the potential variability in gas composition and increased emission rate from possible CH<sub>4</sub> rich zones cannot be confirmed.

Table 4 provides a summary of the gas composition values recorded from FD testing, and the average gas composition values recorded during SD testing, on the core samples collected from UIS borehole 519-33A/2 along with the estimated gas composition values based on contoured exploration data and the average composition of the gas produced from the UIS borehole.

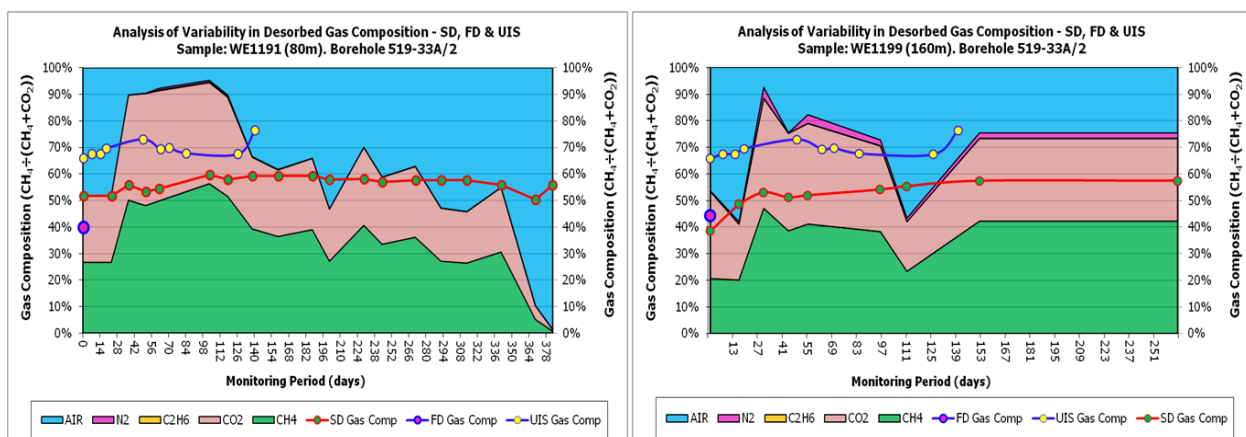


**Figure 9 - Recorded gas composition during SD testing of WE1191 and WE1199 including FD and UIS gas composition values**

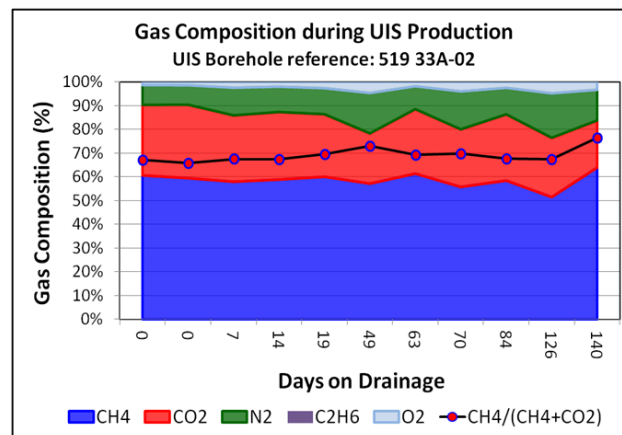


Figure 10 - Recorded gas composition during gas production from UIS boreholes 519-33A/2

Table 4 - Summary gas content and gas composition data at core sample locations in UIS borehole 519-33A/2

Reference Borehole: 519-33A/2

UIS Core Samples	Gas Content ( $\text{m}^3/\text{t}$ )		Gas Composition ( $\text{CH}_4 + \{\text{CH}_4 + \text{CO}_2\}$ )(%)			
	Exploration contours (est.)	UIS Gas Content	Exploration contours (est.)	Fast Desorption	Slow Desorption (average)	UIS Gas Production (average)
WE1191	8.3	13.9	20	40	57	69
WE1199	8.5	14.2	23	44	51	69

The  $\text{CH}_4$  component of gas desorbed from WE1191 and WE1199 during SD testing was 17% and 7% greater than the composition measured during the FD test. The increased  $\text{CH}_4$  detected during SD suggest  $\text{CH}_4$  desorbs from coal samples at a faster rate than  $\text{CO}_2$ , with  $\text{CO}_2$  being retained within the sample and potentially not being released until late stage desorption or until the coal sample is crushed (e.g. Q3 gas content measurement during FD testing).

In this area of the Bulli seam the  $\text{CH}_4$  component indicated by the contoured exploration gas data is approximately 20% lower than the values determined during FD testing. The results suggest this borehole is located in an isolated zone where the seam gas contains increased concentrations of  $\text{CH}_4$ .

#### Gas data recorded along UIS borehole 519-33A/4

The total length of UIS borehole 519-33A/4 was 204m and based on gas composition contours generated from exploration boreholes located less than 700m from this borehole, the  $\text{CH}_4$  component of the seam gas along the length of the borehole ranges from 19% to 21%, as shown in Figure 4.

Five core samples, WE1201, WE1202, WE1203, WE1209, and WE1210, were collected during the drilling of this borehole. The  $\text{CH}_4$  component of the gas released from the core samples during FD testing was 70%, 26%, 39%, 24%, and 19% respectively. The average  $\text{CH}_4$  component of the gas desorbed from the five core samples during SD testing was 68% (WE1201, 647 days), 50% (WE1202, 145 days), 66% (WE1203, 627 days), 57% (WE1209, 112 days), and 50% (WE1210, 613 days), as shown in Figure 11. The  $\text{CH}_4$  component of the gas released from the core samples during SD testing varied between 64% and 80% (WE1201), 43% and 57% (WE1202), 47% and 63% (WE1203), 52% and 62% (WE1209), and 47% and 62% (WE1210).

Six gas composition measurements were taken during gas production from UIS borehole 519-33A/4, commencing day 1 of gas production, with periodic measurement to day 72. The average  $\text{CH}_4$  component of the seam gas was 66% and varied between 60% and 69% during the monitoring period. The results of gas composition measurement from borehole 519-33A/4 are presented in Figure 12 and shown relative to the SD results from the two core samples in Figure 11.

The recorded  $\text{CH}_4$  component of the seam gas produced from the UIS borehole varied relative to the values determined from testing on the five core samples collected along the length of the borehole. The average  $\text{CH}_4$  component recorded during SD testing from core WE1201 was 2% greater than the

average value recorded from the UIS borehole, while the average CH<sub>4</sub> component recorded from the other four core samples was between 9% and 16% less than the borehole average. This result suggests a large portion of the total gas produced from borehole 519-33A-04 is likely to have originated from the coal seam adjacent to core sample WE1201 and/or from sections along the length of the UIS borehole containing comparatively high CH<sub>4</sub> levels.

Table 5 provides a summary of the gas composition values recorded from FD testing, and the average gas composition values recorded during SD testing, on the core samples collected from UIS borehole 519-33A/4 along with the estimated gas composition values based on contoured exploration data and the average gas composition of the gas produced from the UIS borehole.

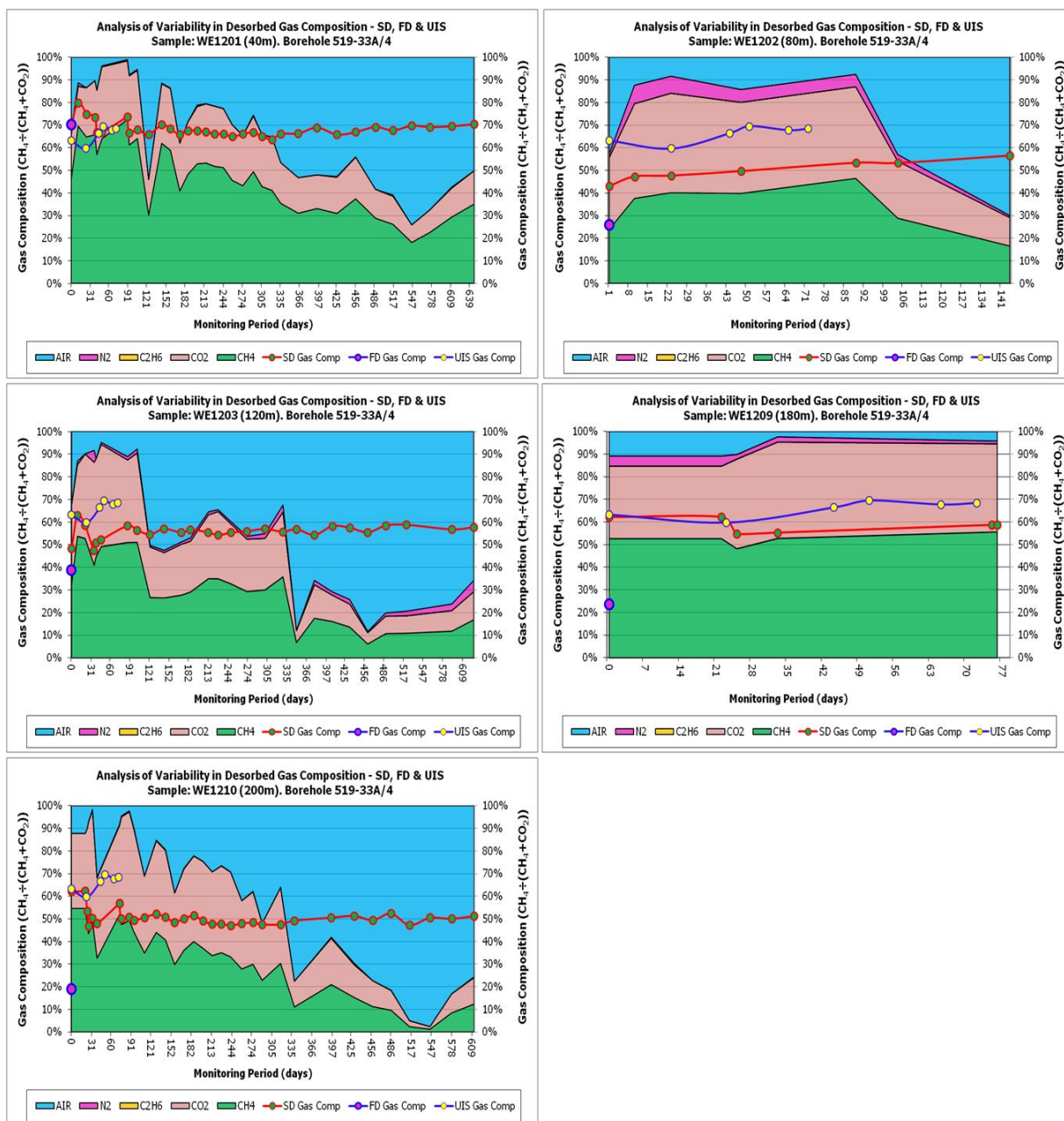


Figure 11 - Recorded gas composition during SD testing of WE1201, WE1202, WE1203, WE1209 and WE1210 including FD and UIS gas composition values

The CH<sub>4</sub> component of gas desorbed from the five core samples during SD testing was between 17% and 31% greater than the composition measured during the FD test. The increased CH<sub>4</sub> detected during SD suggest CH<sub>4</sub> desorbs from coal samples at a faster rate than CO<sub>2</sub>, with CO<sub>2</sub> being retained within the sample and potentially not being released until late stage desorption, or until the coal sample is crushed (e.g. Q3 gas content measurement during FD testing).

In this area of the Bulli seam the CH<sub>4</sub> composition indicated by the contoured exploration gas data varies from being approximately 1% higher to approximately 20% lower than the values determined during FD testing. The results suggest the outbye section of this borehole is located in an isolated zone where the seam gas contains increased concentrations of CH<sub>4</sub>.

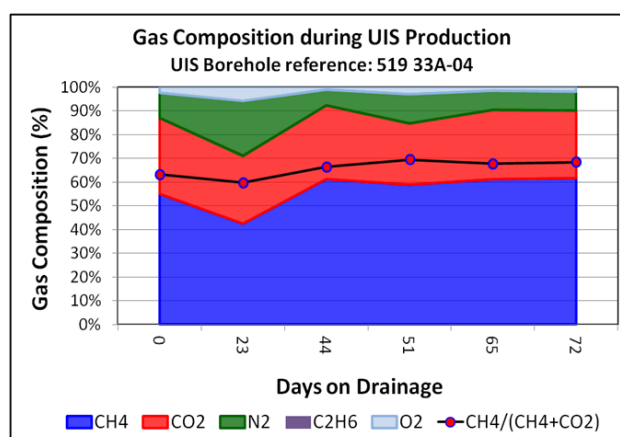


Figure 12 - Recorded gas composition during gas production from UIS boreholes 519-33A/4

Table 5 - Summary gas content and gas composition data at core sample locations in UIS borehole 519-33A/4

UIS Core Samples	Gas Content (m <sup>3</sup> /t)		Gas Composition (CH <sub>4</sub> +{CH <sub>4</sub> +CO <sub>2</sub> })(%)			
	Exploration contours (est.)	UIS Gas Content	Exploration contours (est.)	Fast Desorption	Slow Desorption (average)	UIS Gas Production (average)
WE1201	8.3	10.6	20	70	68	66
WE1202	8.3	12.2	19	26	50	66
WE1203	8.4	13.9	20	39	56	66
WE1209	8.4	13.8	20	24	57	66
WE1210	8.5	14.1	20	19	50	66

#### Gas data recorded along UIS borehole 519-33A/6

The total length of UIS borehole 519-33A/6 was 1500m and based on gas composition contours generated from exploration boreholes located less than 750m from this borehole, the CH<sub>4</sub> component of the gas present in the coal seam along the length of the borehole varied between 14% to 23%, as shown in Figure 4.

Two core samples, WE1308 and WE1309, were collected during the drilling of this borehole. The CH<sub>4</sub> component of the gas released from the core samples during FD testing was 26% and 14% respectively. The average CH<sub>4</sub> component of the gas desorbed from core samples WE1308 and WE1309 during SD testing over a period of 196 days and 391 days was 45% and 17% respectively. The CH<sub>4</sub> component of the gas released from the two core samples during SD testing varied between 36% and 53% (WE1308) and 15% and 21% (WE1309), as shown in Figure 13.

One gas composition measurement was taken during gas production from UIS boreholes 519-33A/6 on day 18 and the CH<sub>4</sub> component at that time was 62%, as indicated in Figure 13. Additional gas composition monitoring was conducted on adjacent UIS borehole 519-33A/5 that recorded CH<sub>4</sub> component values ranging between 57% and 69% (65% average) between day 42 and day 182 of gas production from that borehole.

The recorded CH<sub>4</sub> component of the gas produced from 519-33A/6, and adjacent UIS boreholes, was consistently greater than the values recorded from core sample testing. In this area, it appears likely that 519-33A/6 was drilled through sections of the coal seam containing highly variable CH<sub>4</sub> levels, with high CH<sub>4</sub> levels present in the outbye end of the borehole and low CH<sub>4</sub> levels present at the inbye end of the borehole. Should this be the case, it is reasonable to assume that CH<sub>4</sub> would be preferentially desorbed from the coal, particularly in the comparatively high CH<sub>4</sub> zones, and the total component volume of CH<sub>4</sub>

would exceed the volume of the CO<sub>2</sub> desorbed from the less CH<sub>4</sub> rich sections of the borehole. Details of incremental gas composition measurement along the length of the UIS boreholes were not available however the results of FD and SD gas content testing from core samples collected from the 519-33A boreholes, presented in Figure 14, show a decreasing CH<sub>4</sub> component from the outbye most samples (WE1201) to the inbye most sample (WE1309).

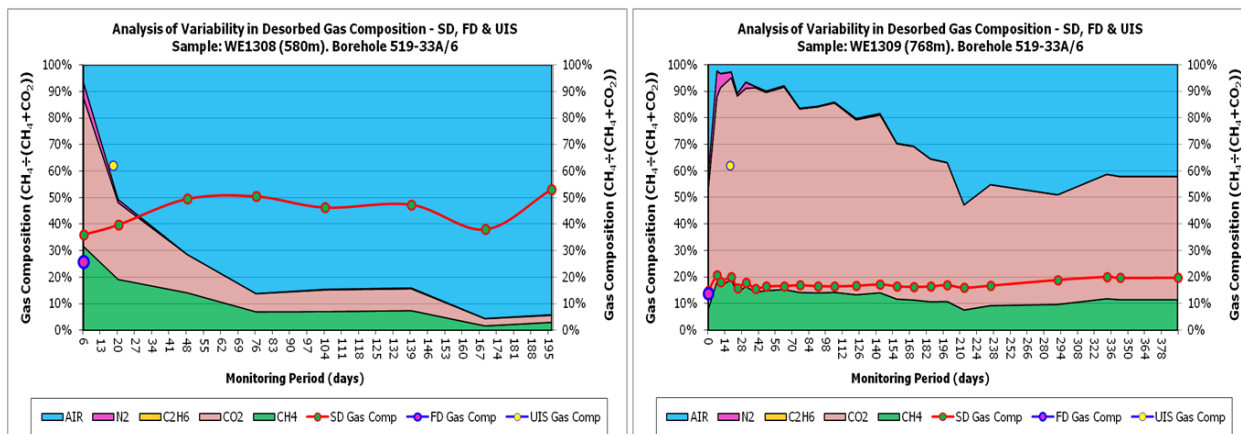


Figure 13 - Recorded gas composition during SD testing of WE1308 and WE1309 including FD and UIS gas composition values

Table 6 provides a summary of the gas composition values recorded from FD testing, and the average gas composition values recorded during SD testing, on the core samples collected from UIS borehole 519-33A/6 along with the estimated gas composition values based on contoured exploration data and the average gas composition of the gas produced from the UIS borehole.

Table 6 - Summary gas content and gas composition data at core sample locations in UIS borehole 519-33A/6

Reference Borehole: 519-33A/6

UIS Core Samples	Gas Content (m <sup>3</sup> /t)		Gas Composition (CH <sub>4</sub> +{CH <sub>4</sub> +CO <sub>2</sub> })(%)			
	Exploration contours (est.)	UIS Gas Content	Exploration contours (est.)	Fast Desorption	Slow Desorption (average)	UIS Gas Production (average)
WE1308	8.8	12.5	14	26	45	62
WE1309	8.9	8.9	17	14	17	62

The CH<sub>4</sub> component of gas desorbed from the two core samples during SD testing was between 3% and 19% greater than the composition measured during the FD test. The increased CH<sub>4</sub> detected during SD suggest CH<sub>4</sub> desorbs from coal samples at a faster rate than CO<sub>2</sub>, with CO<sub>2</sub> being retained within the sample and potentially not being released until late stage desorption or until the coal sample is crushed (e.g. Q3 gas content measurement during FD testing).

In this area of the Bulli seam the CH<sub>4</sub> component of the seam gas indicated by the contoured exploration gas data varies from being approximately 3% higher to approximately 12% lower than the values determined during FD testing. The results suggest the outbye section of this borehole is located in an isolated zone where the seam gas contains increased concentrations of CH<sub>4</sub>.

**SUMMARY**

Analysis of gas composition data collected during FD and SD testing on coal core samples collected from the Bulli seam while drilling UIS gas drainage boreholes has clearly shown that in the 13 core samples used for duplicate testing that the CH<sub>4</sub> component of the gas desorbed from the core during SD testing was an average of 20% greater with the difference ranging between 3% and 33%.

Figure 15 shows gas content and CH<sub>4</sub> component determined by FD and SD testing on 18 coal core samples collected from the Bulli seam. The results show similar gas content values were obtained using

the two methods while the CH<sub>4</sub> component determined from FD testing was consistently lower than the values recorded during SD testing.

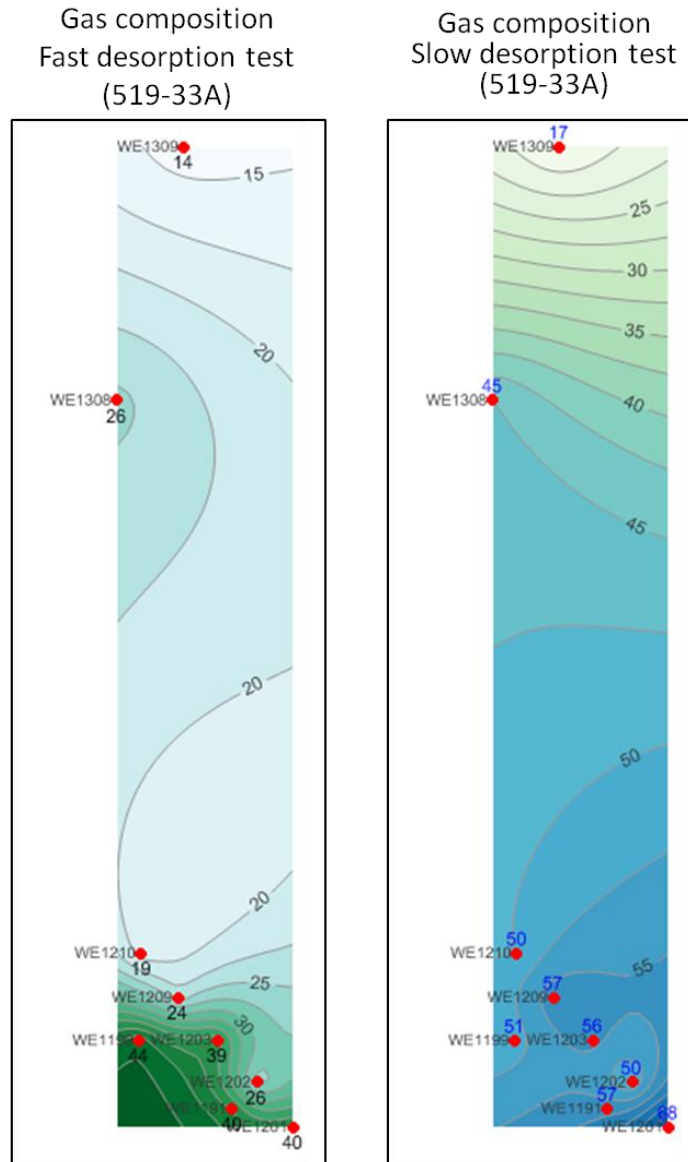


**Figure 14 - CH<sub>4</sub>/(CH<sub>4</sub>+CO<sub>2</sub>) (%) values from FD and SD testing on core samples from 519-33A boreholes**

The increased CH<sub>4</sub> component of the gas released from the core during the SD test suggests the preferential release of CH<sub>4</sub> from the intact core sample with a preference for the CO<sub>2</sub> component to be retained within the coal matrix. At the completion of the SD test analysis of the composition of gas released during Q3 testing was not performed therefore the predicted decreased CH<sub>4</sub> component cannot be confirmed. This observation is consistent with previous work conducted by Crosdale (1998) who reported reduced CH<sub>4</sub> concentration of gas liberated from coal during residual gas content testing following the completion of SD testing.

Composition analysis of the seam gas produced from the UIS gas drainage boreholes from which the 13 core samples were collected also showed that in all but one case the CH<sub>4</sub> component was greater than the average values recorded during SD testing. The CH<sub>4</sub> component of the seam gas produced from the five UIS boreholes was on average 16% greater than the average value determined from SD testing on the core samples, with the difference ranging from being 2% lower (WE1201) to 45% higher (WE1309).

Figure 16 shows median CH<sub>4</sub> component values determined from composition analysis on gas produced from UIS boreholes drilled into the Bulli seam from 20 drill stubs located along gateroads within the

mine. The CH<sub>4</sub> components of the gas from individual core samples collected from those boreholes, tested using the FD method, are shown. The CH<sub>4</sub> component values obtained from FD and SD testing on duplicate coal core test samples that were collected from nine of the boreholes is also shown. The results clearly show that in all 20 cases the CH<sub>4</sub> concentration of the gas produced from UIS boreholes is greater than CH<sub>4</sub> concentration recorded from core samples collected from those boreholes. The difference is particularly significant in mixed gas zones where the naturally occurring levels of CO<sub>2</sub> in the coal seam exceed 20-30%.

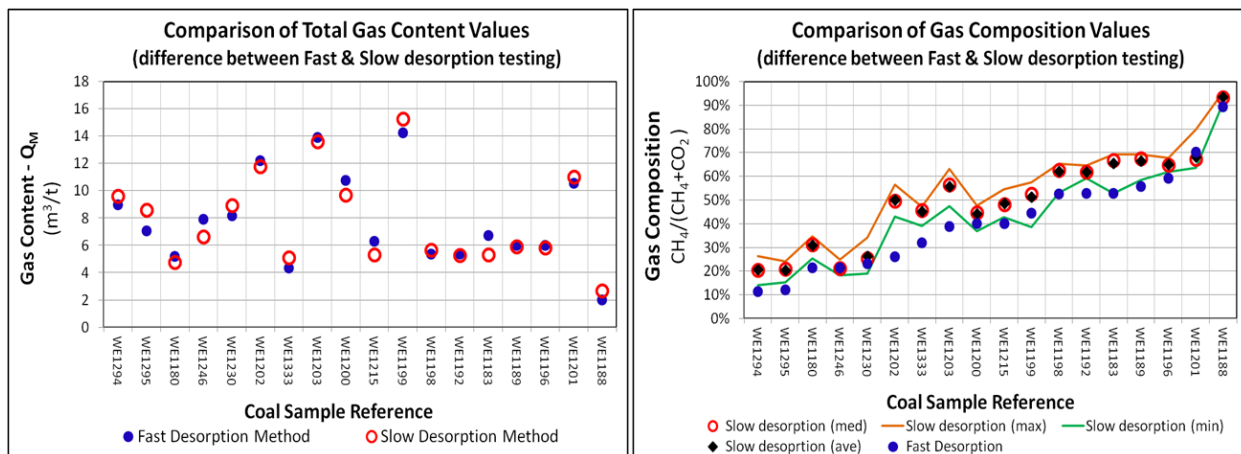


Figure 15 - Results of FD and SD gas content and composition testing on duplicate Bulli seam coal core samples

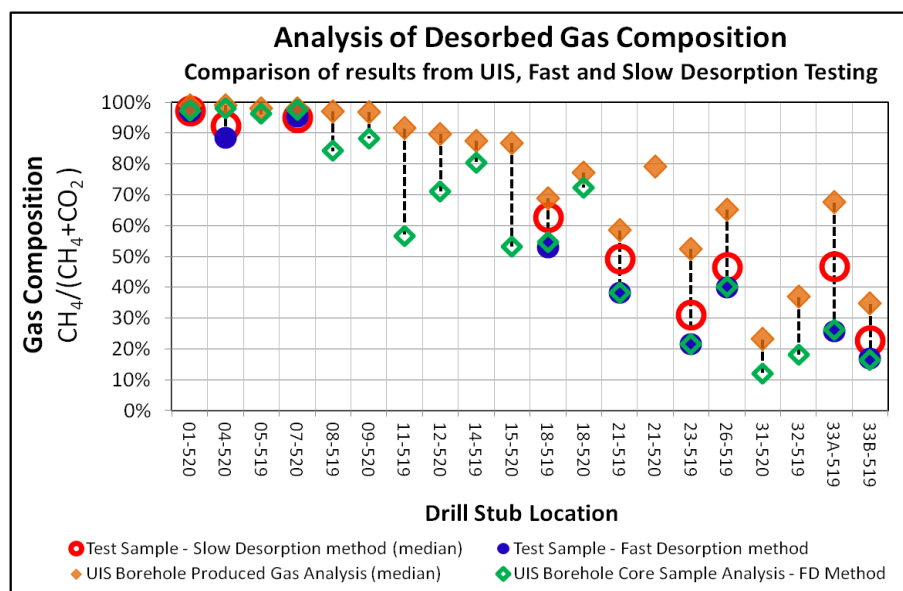


Figure 16 - CH<sub>4</sub>:(CH<sub>4</sub>+CO<sub>2</sub>) ratio values from duplicate FD and SD testing with values from FD testing and UIS gas production from boreholes drilled into the Bulli seam from gateroad drill stubs

Gas desorption measurements during mixed gas isotherm studies conducted by Mavor *et al.* (1992), Harpalani and Pariti (1993) and Greaves *et al.* (1993), cited in Crosdale (1998), suggest coal's affinity for CO<sub>2</sub> results in preferential liberation of CH<sub>4</sub> in response to reducing pressure, with coal retaining CO<sub>2</sub> until the pressure was less than 0.7 MPa. Mavor *et al.* (1992) suggest the significance of this behaviour is that boreholes producing predominantly CH<sub>4</sub> during the early periods of operation may produce an increased concentration of CO<sub>2</sub> as the reservoir becomes depleted.

The composition of the seam gas produced from the five UIS boreholes included in this study, whilst variable, did not show any clear sign of CO<sub>2</sub> enrichment during late stage desorption, as proposed by Mavor *et al.* (1992). The monitoring period was however relatively short, less than 150 days, therefore it

is possible that during the monitoring period the reservoir pressure remained above the 0.7 MPa threshold level proposed by Mavor.

It is also quite probable that during the initial gas production phase from the UIS boreholes that gas is preferentially released from zones of comparatively higher CH<sub>4</sub> composition, in addition to the preferential liberation of CH<sub>4</sub> from the coal seam containing a mix of CH<sub>4</sub> and CO<sub>2</sub>.

## CONCLUSIONS

This study has clearly shown that in this area of the Bulli seam, where the seam gas contains a variable mix of CH<sub>4</sub> and CO<sub>2</sub>, that the CH<sub>4</sub> component of the gas produced from UIS boreholes is greater than the CH<sub>4</sub> component of the gas liberated from cores samples collected from the UIS boreholes and tested using the SD method. The CH<sub>4</sub> component of the gas produced during SD testing was also found to be greater than the CH<sub>4</sub> component of the gas released from the core samples during FD testing.

The results of this study have highlighted a number of potentially significant factors that should be considered by mine planners when assessing the potential impact of coal seam gas on mine operations. The potential impacts, particularly in areas where seam gas is a mix of CH<sub>4</sub> and CO<sub>2</sub>, include:

- Potential inaccurate estimation of gas content and composition when contouring between measured data points obtained by surface-based exploration. This study has shown that in eight of the nine locations considered, the gas content, determined by FD testing of core samples collected during UIS drilling, was at least 2.0 m<sup>3</sup>/t greater than the values indicated by contour values generated using values measured by testing core samples collected during surface exploration drilling. The contours of the CH<sub>4</sub> component of the seam gas, generated using data obtained from surface exploration drilling and testing was also, in the majority of cases, less than the values measured during testing on core samples collected during UIS drilling. The results highlight the non-uniform distribution of gas content and composition of seam gas within coal seams and the potentially significant difference that may exist between actual conditions and the conditions that are indicated by contouring surface exploration data.
- FD testing on coal core samples will potentially understate the level of CH<sub>4</sub> present in the produced gas, particularly in mixed gas conditions. This study has shown that the CH<sub>4</sub> component of gas measured during FD testing was less than (a) the CH<sub>4</sub> component measured during SD testing, and (b) less than the CH<sub>4</sub> component of the gas produced from the UIS boreholes from which the core samples were collected. In such areas, where FD testing understates the actual CH<sub>4</sub> levels released during mining, there is a risk that CH<sub>4</sub> emissions will exceed expected levels.
- Preferential release of CH<sub>4</sub> from the coal seam may result in increased levels of CO<sub>2</sub> being naturally retained within the coal seam. If CO<sub>2</sub> is preferentially retained within the coal seam, what potential impact does such a condition have on outburst risk and the determination of appropriate outburst threshold limit? Further investigation is therefore warranted to closely monitor variations in gas composition during SD testing of coal samples containing a mix of CH<sub>4</sub> and CO<sub>2</sub> and to assess the significance of any potential reduction in CH<sub>4</sub> component of the gas remaining in the core samples determined during Q3 testing.

## REFERENCES

- Crosdale, P J, 1998. Degassing of methane and carbon dioxide: prediction of gas composition, Australian Coal Association Research Program, Project Report C5037.
- Harpalani, S and Pariti, U M, 1993: Study of coal sorption using a multi-component gas mixture; Paper 9356; International Coalbed Methane Symposium, May 17-21, Tuscaloosa, Alabama, USA
- Standards Association of Australia (SAA), 1999. Guide to the determination of gas content of coal – direct desorption method, Australian Standard, AS3980:1999.
- Mavor, M J, Close, J C and Pratt, T J, 1992. Review of recent US coalbed natural gas reservoir research, in Proceedings of the Symposium on Coalbed Methane Research and Development in Australia, Coalseam Gas Research Institute – James Cook University, Townsville, November 19-21, Volume 2, pp 109-152.

# GAS WETTABILITY OF COAL AND IMPLICATIONS FOR GAS DESORPTION AND DRAINAGE

Abouna Saghafi<sup>1</sup>, Kaydy Pinetown<sup>2</sup> and Hoda Javanmard<sup>1</sup>

**ABSTRACT:** A key parameter affecting the flow of gas in coal is the wetting potential of gas, in comparison to water, to spread over the wall of coal micropores and microfissures. Wettability is quantified in terms of the contact angle of the fluid interface with the solid surface. A fluid with a small angle of contact would spread over the pore walls and eventually displace the non-wetting fluid. Depending on the nature of the coal, gas type and environmental conditions in coal reservoirs, either water or the gas phase could wet coal more strongly. Furthermore, in mixed gas conditions, one gas may be more strongly attached to coal than the other gases. In water-saturated coal, gas desorption in small pores -where most adsorbed gas is stored - can be totally inhibited by water if it is a strong wetting phase. Reducing the hydraulic head (drawdown to achieve the gas desorption pressure) should allow desorption of gas in larger fractures, whereas in small pores, gas desorption could be inhibited by capillary pressure due to the effect of interfacial tension and gas-wetting properties of coal. In this study, we built a new system to quantify the wettability of coal by gas. The contact angle of the water-gas interface with the coal surface inside the gas phase was measured using a captive gas bubble technique. The contact angles of CH<sub>4</sub> and CO<sub>2</sub> bubbles in water with a coal from the Sydney Basin were measured at different gas-water pressures of up to 15 MPa for CH<sub>4</sub> and 6.1 MPa for CO<sub>2</sub>. The results show that as gas bubbles dissolve in water, the contact angle of the bubble with the coal surface reduces. The contact angle values were smaller for CO<sub>2</sub> gas than CH<sub>4</sub>, and in general, the contact angle value decreases as gas–water pressure increases.

## INTRODUCTION

In coal-bearing sedimentary sequences, the fluid phases consist of gas and water. For effective coal seam gas drainage in deep coal mines or gas recovery, removal of formation water eases the desorption of gas from the coal matrix and its flow into the larger cleat and crack system. The resistance to gas desorption by the medium could be partly due to coal being preferentially wet by water rather than by gas. The release of gas from coal can be inhibited by a water-wet coal, which does not allow the diffusion of gas to the surface of the cracks and desorption from coal matrix. This is experienced in gas adsorption experiments using moist coals or gas recovery operations, which require discharging sufficient volumes of water from the borehole before gas flow is established. In a water-wet coal, water is generally in contact with the surface of pores, and gas movement and desorption from the coal matrix is resisted by molecules of water on the pore wall. In a gas-wet coal, gas molecules – not water molecules – are in contact with the pore wall, and gas molecules readily spread over the surface of the pore walls. Hence, the movement of gas in and out of the coal matrix and along the connecting microfissures into macrofissures and large cracks is largely facilitated. Since wettability plays such an important role in the migration and drainage of gas from coal, its quantification and relative ranking with respect to gas and coal types are vital to optimise gas recovery and drainage from coal seams.

Quantification of coal wettability by water and other liquids has been an area of significant interest in the coal cleaning and flotation industry. Numerous studies have aimed to evaluate coal floatability (see for example Keller, 1987; Arnold and Aplan, 1989; Drelich, *et al.*, 2000; Drelich, 2001; Gosiewska, *et al.*, 2002). These authors studied the effect of mineral matter on the water wettability of coal.

To date, limited research has been undertaken to study the relative wettability of coal by gas and water (Siemons, *et al.*, 2006; Sakurovs and Lavrencic, 2011; Shojai Kaveh, *et al.*, 2011). All of these studies have been in the context of CO<sub>2</sub> sequestration in coal seams and dealt with CO<sub>2</sub> wettability of coal. As far as is known no work has been published in the context of CH<sub>4</sub> drainage and flow in coal seams, and our study is the first on CH<sub>4</sub> wettability of coal. The data can be used to evaluate the effect of wettability properties on gas drainage efficiency in water-saturated coals.

<sup>1</sup> CSIRO Energy Technology, P.O. Box 52, North Ryde, NSW 1670, Australia, abouna.saghafi@csiro.au; Tel: 02 9490 8670

<sup>2</sup> CSIRO Earth Science and Resource Engineering, P.O. Box 137, North Ryde, NSW 1670, Australia

After presenting some background to surface interaction phenomena, this paper discusses the results of recent experimental research on gas wetting of a coal collected from a Sydney Basin coal mine.

## WETTABILITY

Wettability is measured in terms of the contact angle of the interface between the two immiscible phases (gas and water) against the surface of the solid phase (pore walls in coal capillaries). In this work, contact angle is measured in the phase for which the wettability is to be estimated (gas phase). Using this convention, a contact angle of less than  $90^\circ$  indicates that the targeted phase (gas) is the wetting phase, and a contact angle larger than  $90^\circ$  indicates that the other phase (water) is the wetting phase. Figure 1 shows a pore in coal that contains water and gas. In this example, water is the wetting phase, because the contact angle of gas phase with solid surface ( $\theta$ ) is larger than  $90^\circ$ . This means that water is attached more strongly to the pore walls and has low mobility, and that the interfacial forces draw water into small pores and inhibit the non-wetting phase (gas) from penetrating or escaping from these pores

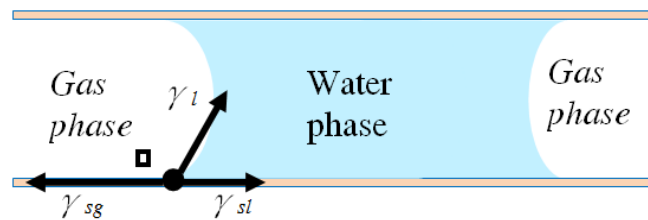


**Figure 1 - Gas and water in a pore: the gas wettability of the solid (coal) is measured in terms of the contact angle of the gas–water interface with the solid surface inside the gas phase ( $\theta$ )**

The magnitude of the contact angle is a function of the interfacial tension, which is the energy required to separate a unit area of the interface between two phases; it is expressed in terms of energy per unit area or force per unit length ( $\text{J/m}^2$  or  $\text{N/m}$ ). An equilibrium of the cohesive and adhesive forces at the line of contact between the three phases (solid, liquid and gas) is reached when the interface between the liquid and gas forms a certain angle  $\theta$  (contact angle) with the solid. Assuming equilibrium of forces on the line of the intersection of the three phases (gas–water interface and solid in Figure 1) it can be shown that the magnitude of the contact angle between the gas–water interface and the solid should follow the Young (1850) and Laplace (1806) equation:

$$\gamma_{lg} \cos \theta = \gamma_{sl} - \gamma_{sg} \quad (1)$$

where the subscripts *s*, *l* and *g* denote solid, liquid and gas. For example,  $\gamma_{sg}$  is the interfacial tension between the solid and gas phases.

Since the interfacial tensions are properties of materials, the contact angle is also considered as a material property of the fluid and solid system independent of any particular configuration. Note that if  $\gamma_{sg} > \gamma_{sl}$ , then  $\theta > 90^\circ$  and water is the wetting phase (Figure 1). The magnitude of the interfacial tension is a function of the difference between the cohesive and adhesive forces acting on the interface of the two phases. Strong adhesive forces produce contact angles of less than  $90^\circ$ , which is a characteristic of the wetting phase. Similarly, strong cohesive forces produce contact angles larger than  $90^\circ$  (non-wetting phase).

The curvature of interface between the two fluid phases (gas and water) produces a discontinuity in fluid pressure across the interface. For the non-wetting phase (gas in Figure 1) to desorb and move through the capillary, the free gas pressure needs to be more than this pressure difference. The pressure difference across the interface of gas and water can be estimated using the geometrical form of the Young–Laplace Equation. If the effect of gravity is neglected, the difference in fluid pressure across the interface is (see for example Bear, 1988; Butt, *et al.*, 2006):

$$\delta p = p_{nw} - p_w = \gamma \left( \frac{1}{R_1} + \frac{1}{R_2} \right) = \gamma C \quad (2)$$

where  $p_{nw}$  and  $p_w$  are fluid pressures in the non-wetting and wetting phases,  $\gamma$  is the interfacial tension between the two fluid phases, and  $R_1$  and  $R_2$  are the two principal radii of curvature on the fluids'

interface. The principal radii are determined in two orthogonal directions at the point of interest on the surface. The quantity  $C = 1/R_1 + 1/R_2$  is called the mean curvature. It is a geometrical property that determines the shape of the interface and does not depend on the orientation.

### Measurement of wettability

Evaluation of the wettability of a solid by a fluid has been the subject of research and applications in various disciplines, and various methods have been developed and used (see for example Neumann and Good, 1979). The two main methods for directly measuring a contact angle from the profile of a fluid drop or bubble on a flat solid surface are the sessile drop and captive gas bubble techniques.

In the sessile drop method, the solid sample is ground to form two horizontal surfaces and then mounted on a horizontal stage. A drop of liquid for which the contact angle against the solid surface is required is placed on the solid surface using a device (such as a pipette with small tip) to form the drop. The solid sample and fluid drop may be placed in a water-filled cell. The profile of the fluid drop on the solid surface and the contact angle are evaluated using a telescope and a protractor. A camera may also be used to take frequent pictures of the drop profile. The image data are logged and stored digitally. Image analysis software is then used to calculate the drop geometry and contact angle.

In the captive gas bubble technique, the solid sample is placed at the top of a water cell with the sample facing down. A gas bubble is introduced from the bottom of the water cell. The gas bubble rises and comes into contact with the solid surface. As in the sessile drop technique, measurement of contact angle is undertaken from the profile of the bubble adhered to the surface. Similarly, a camera is used to record images of the profile and calculate the contact angle from the bubble profile using an image processing method.

## GAS FLOW IN COAL AND WETTABILITY

Coal seam reservoirs are generally water saturated, which largely restricts the flow of gas. The retaining effect of water is significantly larger in small pores, where most adsorbed gas is stored. A main indicator of the resistance to gas movement is the relative wettability of coal by water and gas. Hence, quantifying the wettability of coal in terms of the contact angle of the gas–water interface with the coal surface will improve understanding of gas flow and drainage in coal seams.

The  $\delta p$  in Eq (2) can be seen as a pressure barrier for the movement of the non-wetting fluid through the medium. In larger cracks and fractures, the mean curvature ( $C$  in Eq 2) is small and hence  $\delta p$  remains small. However, in smaller micropores, the curvature of the fluid interface can be significant, and very large  $\delta p$  can develop across the interface, preventing the movement of gas through the coal. If the pores are modelled as tubular capillaries, it can be shown that the curvature of the fluid interface in the tubular pore is:

$$C = \frac{-4 \cos \theta}{d} \quad (3)$$

where  $d$  is the diameter of the tubular pore. Substituting  $C$  from Eq (3) in Eq (1) yields:

$$\delta p = \frac{-4\gamma \cos \theta}{d} \quad (4)$$

Therefore, if gas is the non-wetting phase in coal, then to allow gas desorption from pore walls, it is not enough to reduce water hydrostatic pressure to below the gas desorption pressure by pumping water out of gas drainage boreholes. Instead, the total water pressure, including the capillary pressure ( $\delta p$ ), should be reduced. In other words, to allow desorption and flow of gas bubbles from micropores into larger cracks and cleats, the desorption pressure must be larger than the sum of the hydrostatic and capillary pressure:

$$p_g > p_w + \delta p \quad (5)$$

where  $p_g$  is gas desorption pressure and  $p_w$  is the hydrostatic pressure (hydraulic head). Note that when  $d$  is large enough (e.g. in fractures and larger-aperture cleats)  $\delta p$  becomes quite small relative to the hydrostatic pressure, and gas desorbs from coal as soon as the hydrostatic pressure falls below the gas

desorption pressure. Therefore, for larger fractures, reducing hydraulic head alone can allow gas desorption. This is usually achieved by pumping out a certain volume of water from gas drainage boreholes.

### Numeric example of the effect of wettability on gas desorption and drainage

To illustrate the effect of wettability (in terms of contact angle), a parametric example is presented.

Assume a water-saturated coal seam at depth of 500 m, and assume that gas content is  $10 \text{ m}^3/\text{t}$  and gas adsorption capacity of coal in terms of Langmuir parameters is  $V_L = 27 \text{ m}^3/\text{t}$  and  $P_L = 3.1 \text{ MPa}$ . Based on these data, the hydrostatic pressure at this depth would be about 4.9 MPa, whereas the gas desorption pressure is about 1.8 MPa. Therefore, to allow the onset of gas desorption, water (hydrostatic) pressure should be reduced from 4.9 MPa to 1.8 MPa (3.1 MPa of water drawdown). This reduction in water pressure would allow gas desorption to take place in larger fractures and cleats (e.g. millimetre-aperture cracks). For small pores (micrometre-sized and smaller), where most adsorbed gas is stored, the effect of capillary pressure should be taken into account, because it can prevent gas desorption and migration toward drainage pathways. For example, for pores of  $1 \mu\text{m}$  diameter, assuming a contact angle of  $170^\circ$ , the capillary pressure is 275 kPa. However, for pores of  $0.1 \mu\text{m}$ , the capillary pressure will be much larger at 2.8 MPa. For very small pores (nanometer-sized) the capillary pressure might become a full barrier to desorption and movement of gas in pore voids. For a pore of  $1 \text{ nm}$  diameter, capillary pressure is 27.6 MPa (contact angle of  $170^\circ$ ).

Figure 2 plots the capillary pressure developed in tubular pores of  $1.0$ ,  $0.1$  and  $0.01 \mu\text{m}$  diameter as a function of contact angle of the gas–water interface with pore walls.

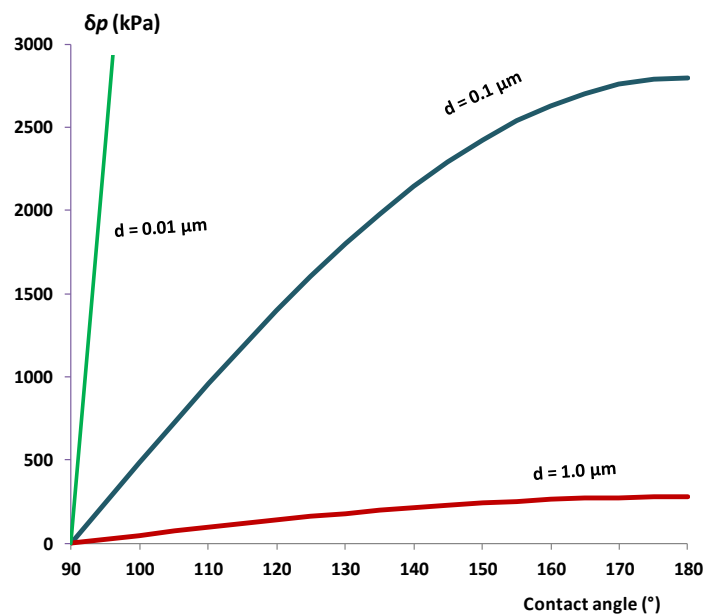


**Figure 2 - Capillary pressure ( $\delta p$ ) developed in tubular pores of coal, the magnitude of this pressure depends on pore diameter and the contact angle of the gas–water interface with pore walls (water is the wetting phase)**

### MEASUREMENT METHOD USED IN THIS STUDY

The CSIRO system for measurement of gas wettability of coal is a variant of the captive gas bubble technique. In this system, a coal disc is prepared from a lump or core coal sample. The disc is then fixed to the end of a sample holder in the form of a rod, which is introduced into a high-pressure water-filled cell with the coal surface facing down. Pressurised gas is slowly released from a nozzle below the coal sample to form a gas bubble, which rises and comes into contact with the coal surface. The formation of bubbles at very high pressures and fixation of bubbles on the coal surface is a delicate operation, and requires the presence of an experienced operator and sufficient time (hours) to obtain suitable results. The gas pressure is set using an ISCO-260D syringe pump, while water is pressurised using a

Shimadzu LC-9A water pump. Distilled water (pH 5 to 6) is used to fill and pressurise the cell. The water pressure is set slightly below the gas pressure so that gas bubbles can form.

A camera is used to capture images at a pre-determined rate. These settings are adjusted in the software prior to the start of measurement. The image data are then processed using an image analysis code to deliver the right and left contact angle values as a function of time. Figure 3 shows a photograph of a gas bubble in contact with the coal surface where the contact angle is larger than  $90^\circ$ .

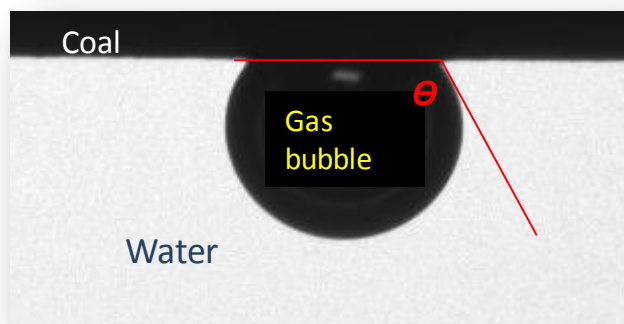


**Figure 3 - Image of a gas bubble in contact with a solid coal surface. The coal and gas bubble are immersed in pressurised water; in this instance, gas is the non-wetting phase ( $\theta > 90^\circ$ )**

#### Experimental parameters

The image processing software reports the contact angle of the bubble ( $\Theta$ ) with the solid surface on the right and the left side of the image frame. The software matches the boundary of bubble against the solution of the Young–Laplace equation to yield the best fit. The values of the right and left contact angles are then calculated based on the best fit. Other values reported by the software include the length of contact ( $L$ ), which is the diameter of the circle the bubble makes where it intersects the surface of the coal sample (the line of contact between the three phases), and height ( $H$ ) of the bubble. The software also calculates the bubble's volume and total surface area from the fitted curve.

### RESULTS OF MEASUREMENT OF GAS–WATER CONTACT ANGLE WITH COAL

Coal lump samples were obtained from a coal mine in the Sydney Basin. The studied coal was of medium volatile rank with a vitrinite reflectance of  $\sim 1.3\%$  and a dry-ash-free volatile matter content of  $\sim 24\%$ . Suitable samples were prepared by drilling to prepare discs with a diameter of 16 mm and a thickness of 10 mm.

Two sets of measurements of contact angles were undertaken using pure  $\text{CH}_4$  and pure  $\text{CO}_2$  gases. All measurements were conducted at a constant temperature of  $22^\circ\text{C}$ .

#### Contact angle of $\text{CH}_4$ with coal

For  $\text{CH}_4$  gas, measurements were undertaken at gas–water pressures of 1.8, 5.0, 7.7, 9.6, 12.9 and 15.2 MPa.

The contact angle and the length and height of the bubble were monitored for 1–2 h following the formation of the bubble and its fixation on the coal surface. Figure 4 shows the evolution of the contact angle of  $\text{CH}_4$  bubbles with the coal surface at various gas–water pressures. The contact evolution follows a similar pattern for all pressures; at the start of the experiment, the contact angle is larger, and then reduces to reach a relatively constant value.

Further analysis shows that the evolution of the contact angle is influenced by the size of the gas bubbles. As the experiment progresses, the gas bubble slowly dissolves in water. The reduction in bubble size is, however, constrained by resistance from the three-phase contact line to shrink and gas–coal contact area to reduce. Hence, the reduction of gas bubble volume is manifested by a larger reduction in the height compared with the area of contact of gas bubble with coal, leading to smaller contact angle. As the bubble size reduces, the contact angle also reduces, to reach a minimal value after which it stays relatively constant. The pattern of evolution of the contact angle suggests that the

contact angle curve can be characterised by a maximum value ( $\theta_{max}$ ) at the start of the experiment and a minimum value ( $\theta_{min}$ ) at the plateau section of the curve.

Overall,  $\theta_{max}$  varied between 130° to 140° and  $\theta_{min}$  between 78° and 96°. The contact angle values were in general smaller under higher pressures.

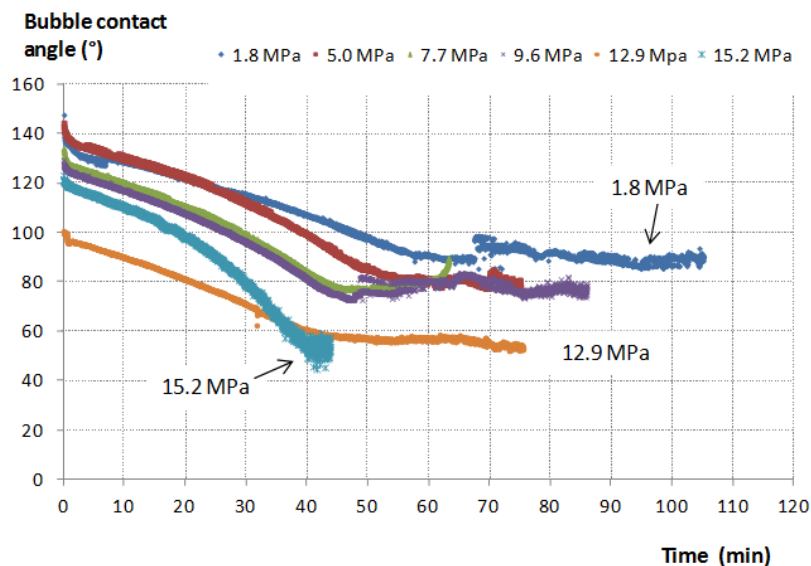


Figure 4 - Evolution of contact angle of CH<sub>4</sub> gas bubbles with coal at various gas–water pressures

Contact angle of CO<sub>2</sub> with coal

For CO<sub>2</sub> gas, contact angle measurements were undertaken at gas–water pressures of 1.8, 5.2 and 6.1 MPa. To maintain the sub-critical conditions for CO<sub>2</sub> gas, larger pressures were not applied.

CO<sub>2</sub> gas bubbles were rapidly dissolved in water, and hence measurements could be conducted only for a few minutes as the bubbles' volume quickly reached the system's limit of detection for image analysis (less than 0.2 μL). Figure 5 plots the evolution of the contact angle. A similar pattern to that seen with CH<sub>4</sub> occurs for CO<sub>2</sub>. The contact angle with coal reduces as the CO<sub>2</sub> bubbles dissolve in water and the size of a bubble reduces.

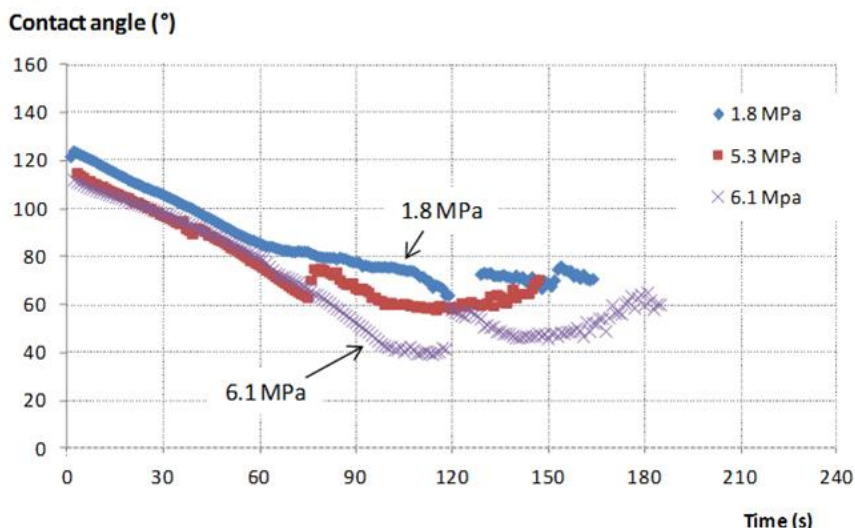


Figure5 - Evolution of contact angle of CO<sub>2</sub> bubble with coal surface at various gas–water pressures

For the three CO<sub>2</sub> experiments,  $\theta_{max}$  varied between 112° to 122° and  $\theta_{min}$  between 40° and 68°. The contact angle values were smaller for the higher pressures.

## CONCLUSIONS

We have developed a new system for the quantification of gas wettability of coal in terms of the contact angle of gas with the coal surface in the presence of water. The contact angles of CH<sub>4</sub> and CO<sub>2</sub> gas bubbles with a coal from the Sydney Basin were measured at various gas–water pressures and a constant temperature of 22°C.

The data from this study show that contact angle evolution follows a specific pattern; the angle reduces from a maximum value at the start of the experiment to reach a relatively minimum value at the plateau section of the curve. Hence, the contact angle pattern can be characterised by a maximum value ( $\theta_{max}$ ) at the start of the experiment and a minimum ( $\theta_{min}$ ) at the plateau section of the curve.

The reduction in bubble size affects the height of the bubble more strongly than it affects the area of contact between the bubble and the coal surface. This results in an apparent reduction in contact angle as the size of the bubble reduces. However, after a certain period of time, the height of gas bubbles and the contact surface reduce simultaneously, resulting in a relatively constant value of the contact angle (in the plateau section of the curve).

For both gases, the contact angle reduces as the applied gas–water pressure is increased. Moreover, the contact angle is generally higher for CH<sub>4</sub> than for CO<sub>2</sub>, indicating that coal is more CO<sub>2</sub>-wet than CH<sub>4</sub>-wet.

Contact angle data can assist in evaluating the effect of gas wettability of a particular coal on gas desorption and drainage in various pore sizes of that coal. For calculation of capillary pressures, it is recommended to use  $\theta_{max}$  values to ensure that these pressures are not underestimated. However, note that the data generated in this study is specific to the coal sample measured and should not be used for other coals. We did not investigate the effect of coal rank, coal composition, ash yield or nature of minerals on gas wettability. To characterise a given coal, specific experiments for that coal should be undertaken.

## ACKNOWLEDGEMENT

The author wishes to thank CSIRO for providing the necessary funds to allow this work to be undertaken. Assistance from the coal mine is acknowledged and the staff who provided required coal samples are sincerely thanked. Our thanks also go to CSIRO colleagues, including Ian Campbell and Paul Marvig, for their assistance in setting up the system and preparing coal samples.

## REFERENCES

- Arnold, B. J. and Aplan, F. F., 1989. The Hydrophobicity of Coal Macerals, *Fuel*, Vol. 68, pp. 651–658.
- Bear, J., 1988. *Dynamics of fluids in porous media*, Dover Publications, New York.
- Butt, H.J., Graf K. and Kappl, M., 2006. *Physics and chemistry of interfaces*, Wiley VCH Verlag GmbH and Co. KGaA, Weinheim, 386 pp.
- Drelich, J., Beach, E., Gosiewska, A. and Miller, J.D., 2000. Limitation of the Young-Dupré equation in the analysis of adhesion forces involving surfactant solutions, *The Journal of Adhesion*, Vol 74 (1-4), pp. 361–372.
- Drelich, J., 2001. Contact angles measured at mineral surfaces covered with adsorbed collector layers, *Minerals and Metallurgical Processing*, Vol 18(1), pp. 31–37.
- Gosiewska, A., Drelich, J., Laskowski, J. S. and Pawlik, M., 2002. Mineral matter distribution on coal surface and its effect on coal wettability, *Journal of Colloid and Interface Science*, Vol 247, pp. 107-116.
- Keller, D. V. Jr., 1987. The contact angle of water on coal, *Journal of Colloids and Surfaces*, Vol 22, p. 21.
- Laplace, P. S., 1806. *Traité de mécanique céleste*, supplement à Livre 10. France.
- Neumann, A. W. and Good, R. J., 1979. Technique of measuring contact angles, R. J. Good and R. R. Stromberg (Ed), Plenum Press: New York, *Journal of Surface and Colloid Science*, Vol. 11, pp. 31-91.

- Sakurovs, R. and Lavrencic, S., 2011. Contact angles in CO<sub>2</sub>-water-coal systems at elevated pressures, *International Journal of Coal Geology*, Vol. 87, pp. 26–32.
- Shojai Kaveh, N., Rudolph, E.S.J., Wolf, K.-H.A.A. and Ashrafizadeh, S.N., 2011. Wettability determination by contact angle measurements: hvBb coal–water system with injection of synthetic flue gas and CO<sub>2</sub>, *Journal of Colloid and Interface Science*, Vol 364, pp. 237–247.
- Siemens, N, Bruining, H., Castelijn, H. and Wolf, K., 2006. Pressure Dependence of the Contact Angle in a CO<sub>2</sub>-H<sub>2</sub>O-Coal System, *Journal of Colloid and Interface Science*, Vol. 297, pp. 755–761.
- Young, T., 1805. An Essay on the Cohesion of Fluids, the *Philosophical Transactions of the Royal Society (Phil. Trans.)*, the Royal Society of London, Vol. 95, pp. 65–87.

# CONCURRENT *IN SITU* METHODS FOR MEASURING PERMEABILITY, GAS CONTENT AND SATURATION

Quentin Morgan<sup>1</sup>, John Pope<sup>2</sup> and Peter Ramsay<sup>3</sup>

**ABSTRACT:** A new core-less testing capability has been developed to provide concurrent measurements of coal seam flow capacity and gas content at *in situ* conditions. The fluid-based measurement principles are intended to overcome time constraints, accuracy limitations, and cost implications of discrete measurements attributed to traditional *off site* measurements on core samples. Field trials were conducted with this new service for both coal mine operators and CSG operators. This paper will detail pre-job planning, well site execution, and data analysis for one of these trials, which involved testing several seams across two wells, and will illustrate comparison with data acquired using conventional testing techniques from offset wells. This paper will also highlight key learnings and overall performance, and explain how the lessons can be applied to improve testing efficacy and data quality.

## INTRODUCTION

Existing ex-situ techniques for measuring the gas content and permeability of coals require collection and laboratory analysis of core samples. In some cases, those samples do not reflect the complex, distributed characteristics of the coal seam being evaluated. In other cases, the analyses are complicated by changes to the samples that may occur during collection.

### Gas content measurements

Gas content of coals is typically measured using the Direct Method Analysis (DMA) on freshly cut cores. The problem with the DMA technique is that overall results can be greatly influenced by artefacts of the test apparatus and procedures used by core sample type, sample collection methodology, and analysis conditions. Even if all these factors are precisely controlled, the accuracy of *in situ* gas content values obtained using the DMA technique can still be greatly compromised through large errors in Q1 values, which can only be predicted, not measured. Compounding this inherent error of the technique is the fact that core desorption is a destructive testing method that cannot be completed twice on the same sample. This means it is not possible to assign error bars on core desorption data, or on the major safety implications of decisions made by using them.

### Permeability measurements

It is possible to quantify permeability from tests on whole cores under precisely controlled laboratory conditions. The accuracy of such tests, however, can be impacted by a number of factors including: the method used to capture the cores; the extent of filtrate invasion; damage to cores during retrieval; poor core preservation at the surface; improper re-stressing of cores in the laboratory; re-stress hysteresis of cores; and, scaling effects (core diameter relative to primary, secondary, and tertiary fracture network spacing).

### Combined *in situ* measurements

A new capability has been developed for simultaneously determining both parameters *in situ*. This new combined method provides some advantages; it can be performed more quickly and at a greater density than typical *off site* methods. Its *in situ* methodology is, furthermore, well-suited to challenging downhole environments such as those containing friable coals, and mixed carbon dioxide and methane gases. Additionally, it can be performed in remote locations without local laboratory support. This new capability has involved the integration of two very different technology platforms that, nevertheless, use reservoir fluid as a key component of their measurement modes. Drill Stem Testing (DST) technology is used to determine flow capacity based on monitoring of fluid behaviour as it is drawn from the coal cleat system.

<sup>1</sup> WellDog Pty Ltd, Brisbane QLD 4000, Email: qmorgan@welldog.com, O: 07 3834 9100

<sup>2</sup> WellDog Pty Ltd, Brisbane QLD 4000, Email: jpope@welldog.com, O: 07 3834 9100

<sup>3</sup> WellDog Pty Ltd, Brisbane QLD 4000, Email: pramsay@welldog.com, O: 3834 9100

Reservoir Raman Spectroscopy (RRS) logging technology is used to derive gas content based on measurement of various properties of the extracted fluid.

A description of both enabling technologies, operating principles, and the innovative surface system developed to facilitate concurrent operation of both has been documented in a recent publication by Pope and Morgan (2013). In it, the authors show that of the many DST technology platforms, both tubing deployed and wireline deployed, only one - involving the use of tubing pressure to set packers and vertical movement of the work string to manipulate a tester valve - is suited for facilitating simultaneous production and logging of formation fluids. A wireless surface readout formation pressure monitoring system is incorporated between the straddle packers, which uses a low- frequency Electromagnetic (EM) signal to propagate formation pressures through the surrounding overburden to the surface. To facilitate concurrent wireline operations and manipulation of the DST system tester valve, a unique load-bearing Wireline Entry Guide (WEG) system was developed, along with a load- bearing quick-union connection system.

Pope and Morgan (2013) also detail a generic test program to showcase the ability to examine produced fluids located in either the wellbore or displaced to the surface under pressure, while simultaneously monitoring the behaviour of fluids still residing in the cleat system. The publication also provides insight into data validation techniques that have been developed to prove self-consistency. Not disclosed, however, are the methods developed to enable the appropriate generation of the adsorption isotherms that are required to accurately calculate gas content from the measured fluid properties. This will be addressed in this paper as part of the case studies review.

This case studies review will also reveal mitigation measures and procedures developed to address the challenges of the new technique. These include the need to manage fluids wisely to ensure representative data and minimise test duration, and the need to use a pragmatic approach in identifying a coal sorptivity that represents a well's drainage area (versus a single core sample) for each coal intersected.

## FIELD TRIAL TERMS OF REFERENCE

A major coal mine operator with an active ongoing exploration program funded testing of their coal seams during a pre- commercialisation beta field trial. Their interest in facilitating this crucial test was driven by the recognition that, if successful, they would then have access to a new technical service yielding immediately actionable data. This availability would, in turn, allow the operator to optimise their future exploration activities, and well spacing and location, and alleviate bottlenecks through existing service channels

### Objectives

DST technology has been used extensively by both the coal mining and CSG industries to obtain *in situ* estimates of bulk permeability to avoid the challenges associated with *off site* analysis of permeability on coal core samples. RRS technology has separately amassed an extensive track record of determining the gas content of coal seams following its commercialisation in 2005. Consequently, the principle objectives established for the field trial were as follows:

1. To confirm the ability to effectively and safely integrate operations of a wireline-deployed RRS logging system with the actuation of a tubing-deployed DST system.
2. To evaluate the robustness of fluid management guidelines, set thresholds, establish decision criteria, and optimise underlying workflow processes.
3. To assess the operational efficiencies achieved in a multi- seam open hole environment.

A further aim of the field trial was to benchmark analyses of acquired data with results obtained from traditional core laboratory studies and permeability tests using alternative DST technology and testing techniques.

### Field trial deliverables

The wireline-deployed RRS and tubing-deployed DST systems incorporate a variety of different sensor types to continuously monitor *in situ* fluid properties and behaviour during the testing of each coal seam.

Additional sensors are included to aid diagnosis of the mechanical and seal integrity of the hardware testing platforms, and to monitor system health. A variety of reports could, therefore, be generated, encompassing various treatments of measured data, data validation results, pressure transient analyses, and RRS analyses.

The key deliverables specified for the field trial were derivation of permeability, skin damage, critical desorption pressure, gas saturation, required pressure drawdown and gas content.

### **Field trial scope**

To fully evaluate the capabilities of this new service, it was decided to test multiple seams in multiple wells exhibiting a wide range of permeability and gas contents. Candidate well selection was based on following criteria:

1. Boreholes needed to be newly drilled to limit borehole instability risk and minimise uptake of wellbore fluids by the coal seams.
2. Boreholes needed to be PQ (122.6 mm) size or larger to accommodate the downhole equipment footprint.
3. Close proximity to other boreholes that had been previously cored and tested for gas content and permeability was undesirable.

### **Field trial evaluation criteria**

To assess the merits of the newly integrated service, the success of the field trial was to be judged based on evaluation criteria, which are:

1. accuracy of acquired data;
2. veracity of data analyses;
3. test expediency;
4. extent of operational support requirements; and,
5. comparison of testing and operational costs with alternative techniques.

## **FIELD TRIAL EXECUTION**

Test execution forms part of an Operation Process Management System (OPMS) to provide a common global system for the planning and execution of installations and tests across the various business units and product lines. This is achieved through strict adherence to prescriptive guidelines that are formalised under the OPMS in the form of process maps. These maps constitute the topmost level of a multi-tiered structure that drills down to more extensive written procedures and controls governing each step. These in turn link to very detailed work instructions and supporting documentation. Through adherence to OPMS the tests were completed without incident, with the time breakdown for the tests conducted on the three zones in the second well, presented in Figure 1.

## **FIELD TRIAL SUMMARY**

Two wells were selected for testing, with three seams targeted in each; however, due to geomechanical instability problems, only one seam was ultimately tested in the first borehole. No such problems were encountered in the second borehole, with tests conducted on all three target seams. Depictions of the two boreholes, along with estimates of gas and reservoir parameters derived for each seam are shown in Figures 2 and 3. Gas data from the second borehole has been withheld to respect client confidentiality, with scaling applied to other data revealed for this borehole.

Key deliverables were met on all four seams tested across the two boreholes. Furthermore, computed gas contents were found to closely match those derived from fast desorption tests on cores, with comparison results for Borehole 2 shown in Figure 4. Permeability data was found to be self-consistent, but differed with values obtained through earlier DSTs in neighbouring boreholes. Several possible

reasons have been attributed to account for the difference. One reason identified from the AAR process is the potential impact of surging while running in hole.

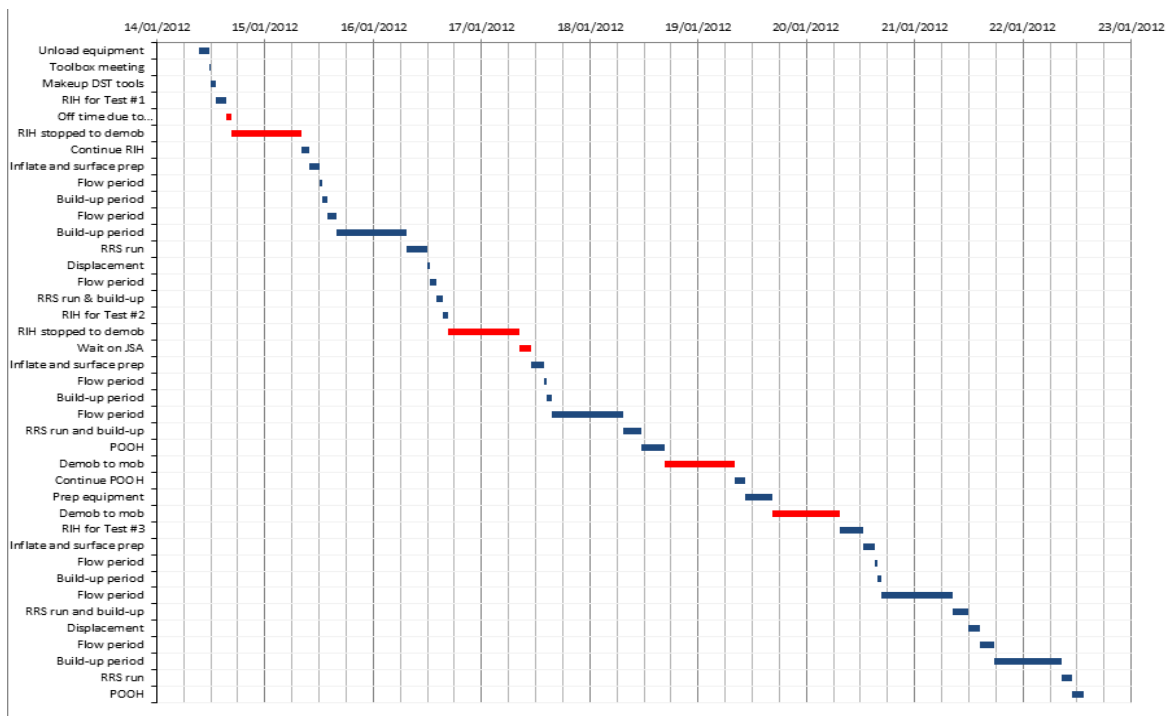


Figure 1 - Time breakdown Gantt chart for borehole 2

DST No.	Interval Name	Interval (m BS)	Flow Capacity (mD-ft)	Skin	Pressure (psia)	CDP (psia)	Std. Dev. (%) Spectra (No.)	V <sub>i</sub> (m <sup>3</sup> /ton) L <sub>p</sub> (psia)	G <sub>c</sub> (m <sup>3</sup> /ton)	G <sub>i</sub> (m <sup>3</sup> /ton)	G <sub>i</sub> /G <sub>c</sub> (%)	Drainage dP (psi)	P <sub>abandon</sub> (psia)	Recovery (m <sup>3</sup> /ton)	R.F. (%)
1	Seam 1	114.6-118.2	950	3.8	90	20	12.5 / 25	23.11 / 289.0	1.5	5.49	27	70	10	0.72	48

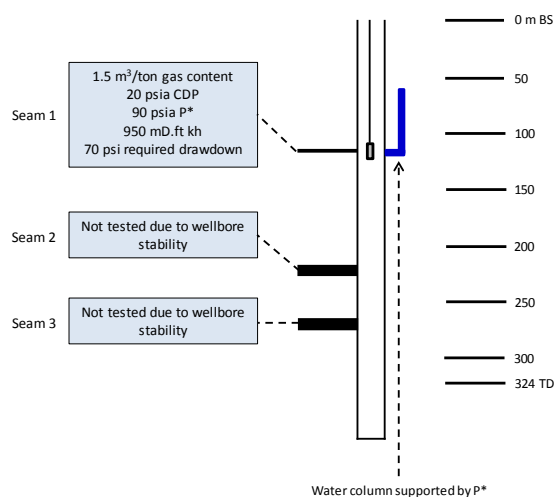


Figure 2 - Borehole 1

DISCUSSION

Synthesis of bulk sorption isotherms

RRS technology measures the concentration of solubilised gases in the water drawn from the cleat system. This is equated to a partial pressure for each gas, including methane, using an appropriate solubility law such as Henry's law. The partial pressure of methane in the cleats is the same as the partial pressure of methane occupying the micropores and coal matrix itself. It is also the same as the Critical Desorption Pressure (CDP) of methane adsorbed to the coal structure. While, however, partial pressure of solubilised methane in the water and CDP of methane adsorbed to the coal are the same,

concentrations (as determined by Henry's law and an adsorption isotherm, respectively) are different. It is thus necessary to reference a suitable sorption isotherm for the coal to compute a gas content.

DST No.	Interval Name	Interval (m BS)	Flow Capacity (mD-ft)	Skin	Pressure (psia)	CDP (psia)	Std. Dev. (%) Spectra (No.)	V <sub>L</sub> (m3/ton) L <sub>p</sub> (psia)	G <sub>c</sub> (m3/ton)	G <sub>s</sub> (m3/ton)	G <sub>c</sub> /G <sub>s</sub> (%)	Drainage dP (psi)	P <sub>abandon</sub> (psia)	Recovery (m3/ton)	R.F. (%)
1	Seam 1	xxx.x – xxx.x	474	3.8	147	xxx	11.1 / 135	23.53 / 364	x.xx	xx.xx	33	xxx	10	xx.xx	82
2	Seam 2	xxx.x – xxx.x	39	2.0	158	xxx	5.4 / 64	24.28 / 387	x.xx	xx.xx	47	xxx	10	xx.xx	88
3	Seam 3	xxx.x – xxx.x	823	25.3	224	xxx	6.5 / 77	24.20 / 410	x.xx	xx.xx	47	xxx	10	xx.xx	90

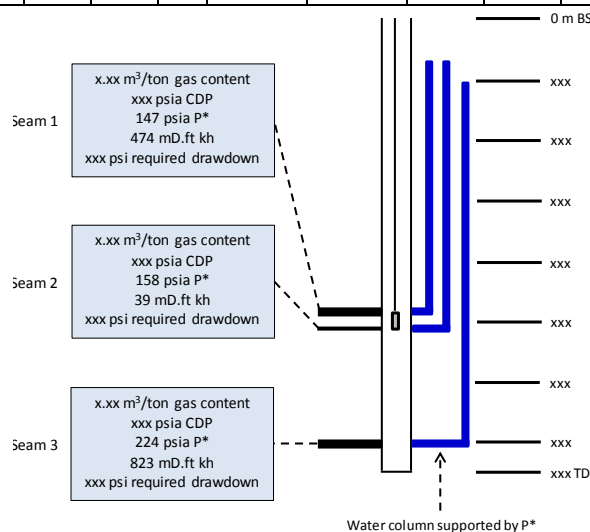


Figure 3 - Borehole 2

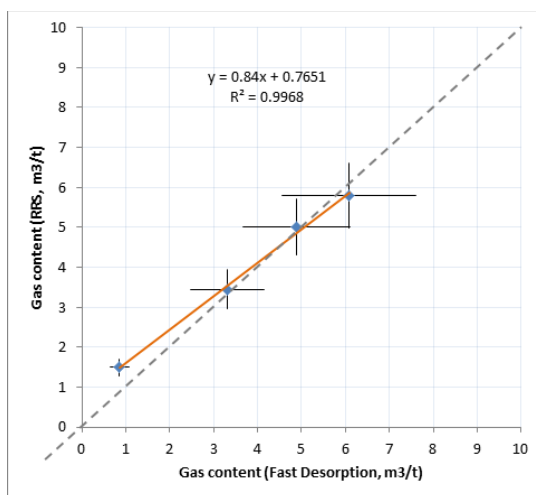


Figure 4 - RRS versus fast desorption gas content comparison

The advantage of the RRS measurement technique is that the measured partial pressure, and consequently CDP, is not impacted by geological heterogeneity. Its validity, therefore, extends some distance away from the wellbore. Furthermore, with the spacing of the DST straddle packers chosen to induce flow from the cleat system spanning the entire thickness of the target seam, the technique effectively yields a bulk averaged value of methane partial pressure that is applicable to the entire region of constant CDP, and which can then be used to calculate a gas content that likewise is applicable to the entire coal. In an optimised dewatering or pre-drainage strategy, this region would represent the accessible drainage volume for each well.

With the spectrometer exhibiting little sampling or measurement error, the uncertainty in computed gas content values is thus dominated by the errors accumulated in synthesising a suitable bulk sorption isotherm. This isotherm must be representative of the coal sorptivity in the drainage area of the well. At a minimum, its construct is also corrected for differences between average near wellbore ash content and ash content in the individual samples used to determine Langmuir pressure and volume. If appropriate, the synthesised sorption isotherm can also be corrected for differences between coal seam temperature and bath temperature used to quantify coal sorptivity. The same approach can be applied to correct for

differences between average seam moisture content, if known, and moisture content of the coal sample used to determine the sorption isotherm.

A statistical approach is used to analyse dry-ash free Langmuir volumes and ash contents to separate variations in sorptivity from variations in ash content. The process developed to perform this analysis involves the following seven steps:

1. Evaluate available isotherm data of coal samples similar to the target seam being tested (such as similar depth and temperature) for variation in underlying sorptivity (reflecting variations in coalification or chemical/maceral content).
2. Investigate any outliers individually, and identify a representative Langmuir pressure with a statistical measure of deviation.
3. Derive dry ash-free adsorption isotherm values (i.e., correct Langmuir volume to ash-free basis), and check the consistency of similar coals.
4. Establish the density to ash correlation.
5. Determine the average density of the target seam from an evaluation of the density log using appropriate cut-off values.
6. Customise Langmuir volume for the target coal seam based on average ash content.
7. Identify and correct for temperature effects to derive new Langmuir pressure and Langmuir volume.

If the mean moisture content for the target seam is known then steps 2-6 can be conducted on a Dry, Ash-Free (DAF) basis. In addition, the results of these analyses can be rigorously evaluated for statistical variation, providing an indication of how representative they are for the coal in question. An example of pre- and post-processed Langmuir volumes from the first two steps is shown in Figure 5, with an established ash correlation as a function of coal density from step 3 shown in Figure 6. The synthesised value for the Langmuir volume derived for the target coal seam from steps 4–6 is shown in Table 1.

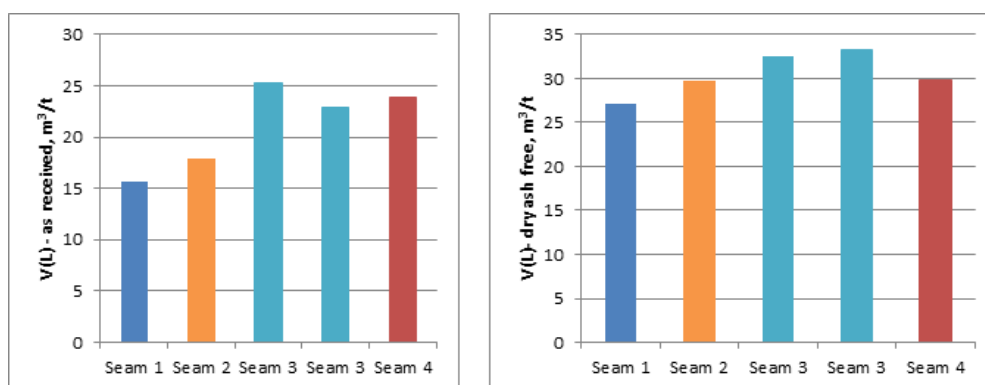


Figure 5 - Example pre- and post-processed Langmuir volumes

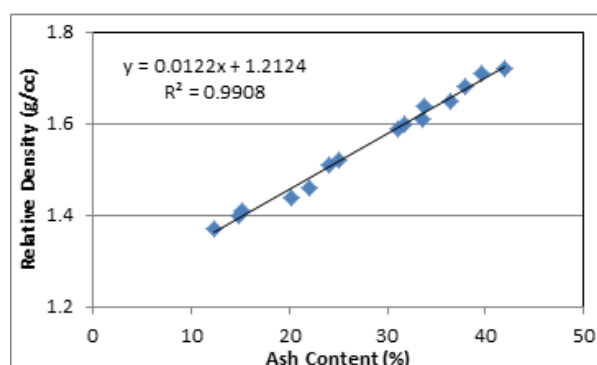


Figure 6 - Example density-ash correlation

**Table 1 - Example synthesised Langmuir volumes for the target coal seam**

Seam Number	Average Density (g/cc)	Average Ash (%)	V(L) – DAF (psi)	Synthetic V(L) – AR (psi)
Seam 1	1.57	29	27.06	19.21
Seam 2	1.63	34	29.74	19.65
Seam 3	1.50	23	32.87	25.17
Seam 4	1.62	33	29.84	19.93

### Fluid management

Determining CSG content using the RRS logging technique involves drawing water from the cleat system until under-saturated conditions are observed on the RRS logs. These conditions need to extend for more than a certain minimum fluid column height in the work string to ensure self-consistency. Depending on the extent, if any, of drilling fluid invasion prior to testing the seam, the hydrostatic head of the overall fluid height attained could approach reservoir pressure; however, this would violate the criteria established for the maximum permissible fluid height that can be tolerated.

This threshold is set to ensure that a sufficiently large pressure transient is induced during the subsequent build-up period to accurately compute coal seam permeability. Under this circumstance the well would be shut-in once the fluid height in the work string reaches this threshold. At the end of the build-up period, the work string contents are reversed out, with the coal seam then allowed to produce additional fluid into the work string. RRS logging operations are then repeated, and possibly alternated with inflow of additional fluid from the coal seam, until the specified acceptance criteria are achieved.

This is just one of a number of scenarios impacting fluid management. The following is a list of all six scenarios that need to be accommodated through development and implementation of a suitable fluid management decision tree and associated contingencies:

1. Permeability and gas content are required. Extensive fluid invasion has occurred.
2. Permeability and gas content are required. Minimal fluid invasion has occurred.
3. Only gas content is required. Extensive fluid invasion has occurred.
4. Only gas content is required. Minimal fluid invasion has occurred.
5. Coal seam permeability is very low.
6. Coal seam pressure is very low.

An examination of the fifth scenario will illustrate the robustness of the processes and procedures developed to manage fluid ingress and displacement. Coals with low permeability would be referred to the decision tree shown in Figure 7. This uses a prediction for work string fill time as an evaluation criterion, with results of an example study shown embedded in Figure 7.

### DST PRESSURE GAUGE DATA

Data acquired by the various pressure sensors is validated by comparing pre- and post-test atmospheric readings, and through comparison with each other. Results of such a comparison from the second test in the second borehole are shown in Figure 8. This reveals that all three gauges accurately measured the atmospheric pressure prior to being installed in the DST string and that the difference in coal seam pressures recorded by the two gauges placed between the two packers was very small. Most importantly, the plot shows that the pressure difference was constant during the build-up periods. Collectively, these observations provide conclusive proof that all three gauges functioned correctly, and that the data from all three is, therefore, valid.

### RRS LOGGING DATA

The pressure and temperature data acquired by the RRS logging string is compared with the data acquired by the DST pressure gauges. The conductivity sensor readings are compared with measurements obtained by using a precise, handheld instrument on samples of produced fluids after

reverse circulation to the surface. The accuracy of solubilised gas concentrations obtained with the spectrometer is verified through post-test calibration verification. RRS log data for the second test in the second borehole is presented in Figure 9. Note that the measured bubble point of gas in the fluid column is not equivalent to that of the coal seam due to differences in physical conditions between the coal seam and the fluid column measurement point, and due to the super-saturation of gas in the fluid column. Measurement of gas under sub-saturated conditions, therefore, is required for accurate results.

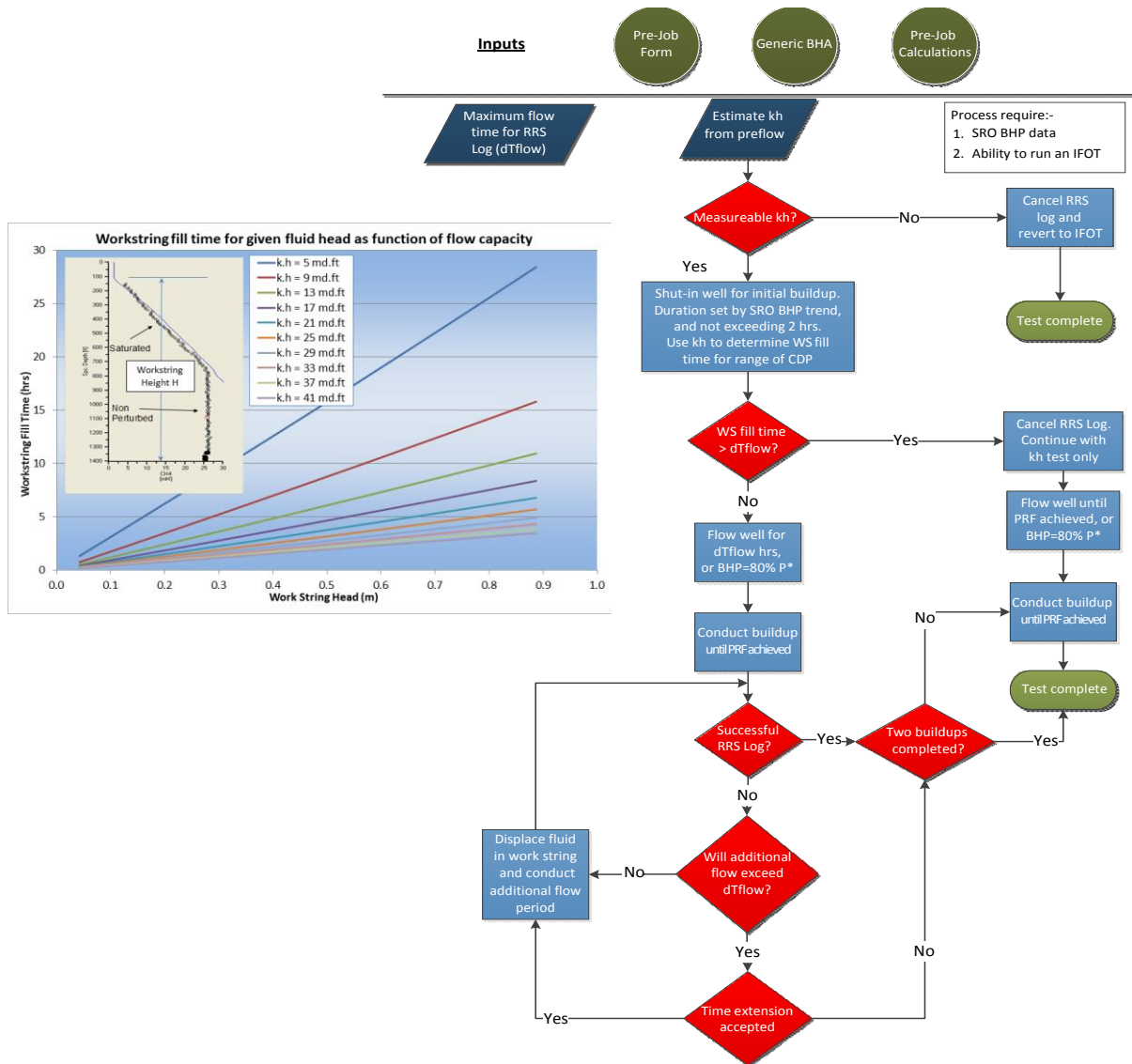


Figure 7 - Low permeability fluid management decision tree

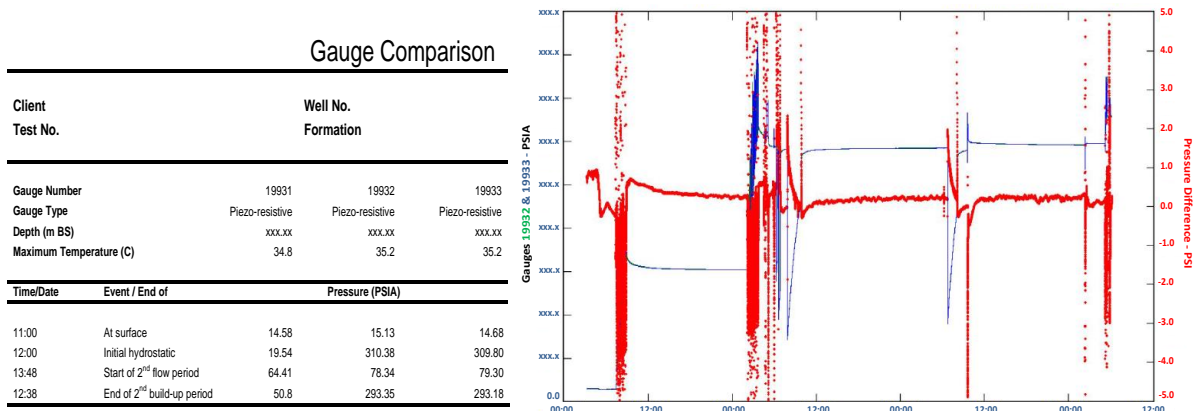


Figure 8 - Borehole 2, Zone 2 gauge comparison and gauge difference data

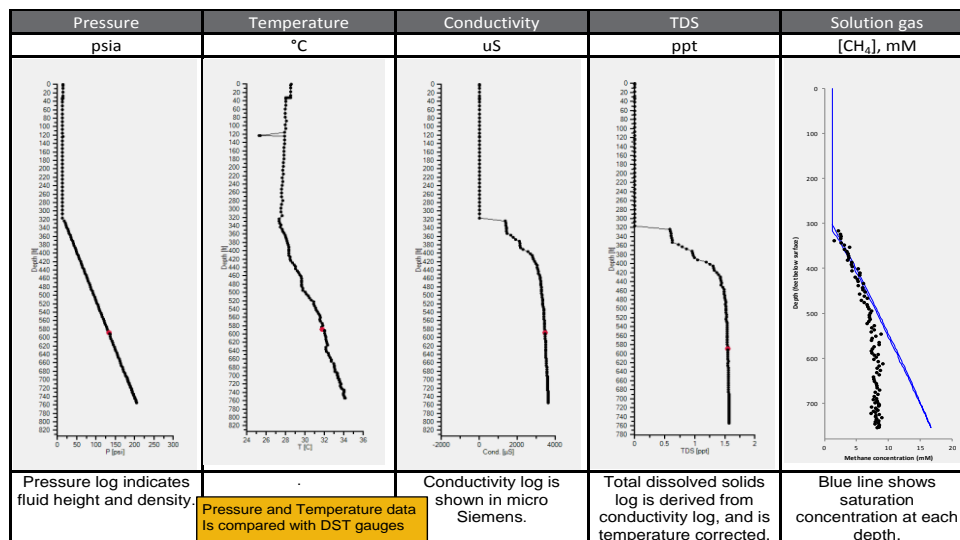


Figure 9 - Borehole 2, Zone 1 RRS log

**PRESSURE TRANSIENT ANALYSIS DATA**

As with any modelling study, it is imperative that model inputs are validated to avoid the rubbish-in-rubbish-out trap. Succeeding in this best practice involves close collaboration with the lease holder engineers, applying extensive due diligence and independent peer-review. For Pressure Transient Analysis (PTA) analyses, flow-rate computation errors are one of the most common sources of discrepancy. To ensure consistency, two flow-rate data sets are generated using data from two different DST pressure gauges. Both sets are then cross-referenced with an independent, single point estimate of flow rate. To limit flow-rate uncertainties, rolling averaging techniques are used. To validate the permeability values derived from PTA, the values are cross-referenced with results from proprietary quasi-pseudo steady state analyses, as shown in Figure 10 for the first zone in the second borehole.

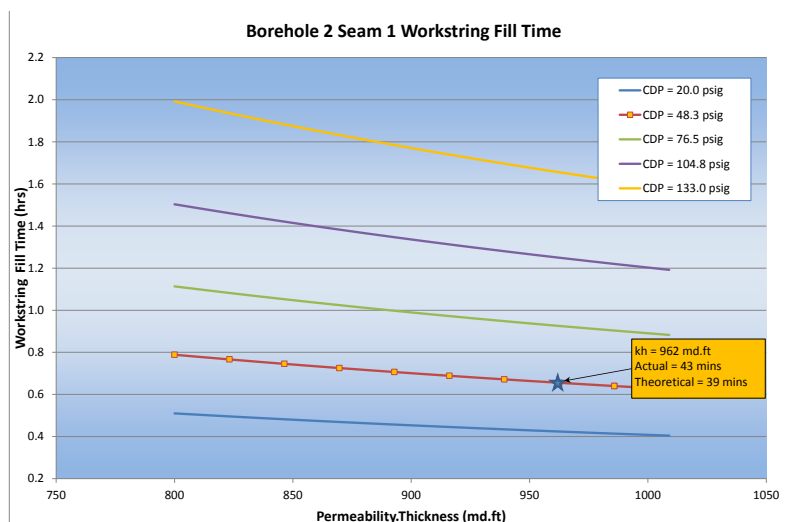


Figure 10 - Borehole 2, Zone 1 permeability verification

**AFTER ACTION REVIEW WORKSHOP**

The aim of this review process is to analyse what happened, why it happened, and how it can be done better by the participants and those responsible for the project. An After Action Review (AAR) workshop was conducted with the field crew following the completion of the second well field trial. Findings from the review of each step were captured and rigorously analysed. One such finding was that surging while running in hole could affect (increase) permeability of the coals. This led to a formal Opportunity For Improvement (OFI) being implemented, involving a change to SOP that limits tripping speed during deployment of the DST string.

The AAR also resulted in a number of system refinements and improvements being identified, some of which were incorporated prior to official product launch, such as the integration of a wireless real-time surface readout monitoring system. Other suggestions were placed with the sustaining engineering function to help ensure that the integrated service is matured. Ideas requiring development of new subsystems were referred to the Stage-Gate ideation management process. This includes the top-drive WEG system referred to in the publication by Pope and Morgan (2013).

### KEY FINDINGS

Following the AAR, a separate review was conducted with the lease holder to assess the performance of the new *in situ* permeability and gas content measurement service. The evaluation criteria listed previously were used to assign key performance indicators, with key findings as follows:

1. Standard well design and completion techniques do not conflict with RRS and DST testing methods.
2. It is possible to quickly retrieve reservoir fluids from coal seams isolated in open holes, with all seams tested to date having flow capacities ranging from 39–1,646 mD.ft.
3. The RRS logging technique can readily distinguish between reservoir and non-reservoir fluids.
4. The design of the surface pressure and flow control system can safely manage methane-laden fluids at the rig floor.
5. The RRS system has a wide dynamic range, with all seams tested to date having gas contents ranging from 1.5-13.3 m<sup>3</sup>/t. The limit of detection (LOD) of existing generation RRS logging systems equates to around 0.8 m<sup>3</sup>/t, with a new high-sensitivity instrument presently being developed by research and development to lower LOD to around  $\pm 0.1$  m<sup>3</sup>/t.
6. The DST and RRS systems both provide early indications of hole instability.
7. It is possible to obtain data needed to quantify gas content and permeability for a target coal seam in less than 24 hours.
8. The field trial proved the DST system's ability to facilitate multiple individual tests in separate seams in a single trip, saving test time.
9. The inflatable straddle packer system can successfully pack- off coal seams without inducing hole instability in wells that have been left unsupported for two or more months.
10. Testing time can be compressed significantly by certain equipment refinements, which have been verified on sub-sequent wells.

### CONCLUSIONS

1. A new core-less testing capability has been developed to provide concurrent measurements of coal seam permeability and gas content at *in situ* conditions.
2. The testing capability involves the integration of DST technology and a proprietary Raman spectroscopy logging system, both using reservoir fluid as a key component of their measurement modes.
3. The testing methodology involves the extraction and examination of fluids from the coal clear structure, with sufficient pressure budget kept in reserve for pressure build-up surveys. Effective fluid management is, therefore, crucial to achieving accurate representative results.
4. The analyses of fluid behaviour and properties yield bulk averaged values of permeability and gas content applicable to the accessible drainage volume of the seam being tested.
5. Operation of this integrated service has been successfully demonstrated in a field trial involving tests on multiple coal seams in two multi-zone wells.
6. All key deliverables established for the field trial were met, with computed gas contents found to be closely matching those derived from fast desorption tests on cores

---

**REFERENCES**

- Koval, E and Pope J, 2006. Seeing a reservoir's character from solution gas, *World Oil*, November, pp 144-146.
- Lamarre, R A and Pope J, 2007. Critical gas content technology provides coalbed-methane-reservoir data, SPE 103539, *Journal of Petroleum Technology*, 59(11):108-113.
- Pope, J, Buttry, D, Lamarre, R, Noecker, B, MacDonald, S, LaReau, B, Malone, P, Van Lieu, N, Perosli, D, Accurso, M, Harak, D, Kutz, R, Luker, S and Martin, R, 2005. Downhole geochemical analysis of gas content and critical desorption pressure for carbonaceous reservoirs, in Proceedings West Texas Geological Society Fall Symposium 2005, 26-28 October 2005.
- Pope, J M, 2006. Get accurate, CBM reservoir data, *E and P*, September
- Pope, J M, 2009. CBM Challenges, *World Coal*, December, pp 51-54.
- Pope, J M, 2009. Best Practices for multi-zone coalbed methane completions, 0933, International Coalbed and Shale Gas Symposium 2009, 18-22 May 2009.
- Pope, J M, 2009. Retaining coalbed methane water discharge permits, 0934, International Coalbed and Shale Gas Symposium 2009, 18-22 May 2009.
- Renouf, P and Pope J, 2011. Measuring gas content without cores, *CBM Review*, September.
- Pope, J and Morgan, Q, 2013,. A new in-situ method for measuring simultaneously coal seam gas content and permeability, In *Proceedings of 13th Underground Coal operators Conference*, Wollongong, February 12-14, ISBN 0 8 6418 7785 (Eds. N Aziz, B Kininmonth), pp 284-290. <http://ro.uow.edu.au/coal/465/>.

# CLASSIFICATION OF COAL SEAMS FOR COAL AND GAS OUTBURST PRONENESS IN THE ZONGULDAK COAL BASIN, TURKEY

**Olgun Esen, Samet Can Ozer and Abdullah Fisne**

**ABSTRACT:** Coal and gas outbursts can be defined as a sudden release of coal and rock accompanied by large quantities of gas into the working face or other mine workings. It has been a major geological hazard to underground coal mining for over 150 years, and continues to cause serious problems all over the world. The outburst events have appeared rarely in metal mines and have generally occurred in salt and coal mines especially bituminous coal mines. Coal outbursts have occurred in at least 18 nations including Turkey. The most important factors that influence the occurrence of outbursts are gassiness of the coal seam and the desorption rate of the gas in the seam and or part of the coal seam. It is necessary to investigate these factors separately to predict the outburst prone zones. The aim of this study is to determine the outburst prone zones in the Zonguldak Coal Basin. In order to determine the outburst proneness of the coal seams, coal samples were taken from Kozlu and Karadon Collieries. 19 coal samples were taken from underground working areas, from 7 different coal seams, at different depths and with variable borehole lengths. Gas content of the coal seams was measured with US Bureau of Mines (USBM) Direct Method. Desorption rate of the gas in coal was investigated and a threshold limit determined for the study area. According to the experimental results, the coal seams have been classified with regard to outburst prone zones.

## INTRODUCTION

Instantaneous coal and gas outbursts in underground coal mines are violent and spontaneous ejections of coal and gas from the working coalface. In the process, a large amount of coal and gas (CH<sub>4</sub> gas, CO<sub>2</sub> gas, or both) is expelled violently, and coal is pulverized. These violent outbursts are major disasters in coal mines (Guan, *et al.*, 2009). There are known cases of gas and coal outbursts resulting from the disintegration of the immediate roof or floor rock of the worked coal seam. One of the causes of difficulties connected with the definition of an outburst is the lack of distinction between the quasi-static and the dynamic phenomena induced by mining (Lama and Bodziony, 1998). Gases associated with coal seams are formed as a result of the coalification process. Coal seams contain a mixture of gases in which methane makes up 80 – 90 % (Creedy, 1991) and varies from 0 to > 25 m<sup>3</sup>/ton (Noack, 1998). Outbursts of gas, coal and rock is a worldwide phenomenon. Perhaps over 30,000 outbursts have occurred in the world coal mining industry. Most of the outbursts, almost one third of the total, have occurred in China followed by CIS countries leading the world in the frequency of occurrence of outbursts. The most important factors that influence the occurrence of outbursts are: 1) Gassiness of the coal seam, 2) tectonics, 3) properties of the coal and rock and 4) vertical and lateral stresses occurring in the seam and/or rock or part of the coal seam (Lama and Bodziony, 1998). The techniques of prediction may be applied to control and prevent underground coal-mine outbursts. For example measurements of gas content and pressure from drill holes on the surface and subsurface permits determination of threshold conditions for outburst occurrence (Zhang, 1995). These measurements provide information on the irregular distribution of gas and changes in gas trends allowing the emplacement of methods to control and prevent coal-mine outbursts (Flores, 1998).

In Turkey, the first recorded instantaneous outburst of coal and gas was at Kozlu Colliery in the Zonguldak Coal Basin in 1962. Unfortunately, not enough official data was collected for this event. The second outburst was also occurred at Kozlu colliery in 1969. There have been 90 gas and coal outbursts in Zonguldak Coal Basin between the years of 1969 and 2013 resulting in 374 fatalities. The disastrous outburst resulted to 263 deaths in Kozlu Colliery at depths of between -560 and -485 longwall panel in 1992.

The objective of this study is to investigate the relationship between the outbursts events and gas content of the coal seams and the desorption rate of gas in coal. In addition the risk indices were used

for determining the outburst prone zones in the Zonguldak Coal Basin. These risk indices were used to classify the coal seams about their proneness to outbursts.

### Description of the Zonguldak Coal Basin

Zonguldak Coal Basin, located on the Black Sea coast is the only bituminous coal basin of Turkey (Figure 1). Mining activities in the basin started in 1848 and have been carried out in the region for over 160 years. Several national and international companies operated various coal mines in the basin. In 1938, the basin was acquired by Ereğli Coal Enterprise (EKİ) which operated these mines until 1983, when the Turkish Hardcoal Enterprise (TTK) was founded (Okten, *et al.*, 1995; Cakir and Baris, 2009). Since then the mines in the basin have been operated by TTK. This State owned agency occupies an area of 6885 km<sup>2</sup>.

Zonguldak Coal Basin is the main part of the Upper Carboniferous bituminous coal basin of Turkey. Much of the bituminous coal mining has thus been concentrated in the Zonguldak Basin (Karayigit, 2001). The coal seams are located in a Carboniferous deltaic sequence of Westphalian-A age. The coal field has been disturbed by tectonic activity, first by Hercynian and later by Alpine orogenesis resulting in folding and faulting of strata (Okten, *et al.*, 1995). The Carboniferous coal-bearing sequence of the Zonguldak basin contains the Namurien Alacaağzı Formation, Westphalian-A Kozlu Formation and Westphalian B-D Karadon Formation (Gurdal and Yalcin, 2000).

The estimated coal reserve, down to 1,200 m under sea level, is about  $1.32 \times 10^9$  tons of coal in this basin (Karayigit, *et al.*, 1998). The coal has been produced by five collieries, namely, Armutçuk, Kozlu, Uzulmez, Karadon and Amasra from west to east. The saleable production in 2011 is about 1.6 mt using a labor force of workers of 10 709 of which 8 629 were underground.

The average gas content of the coals in the Zonguldak Basin is about 12 m<sup>3</sup>/ton according to the laboratory measurements on coal samples contained in canisters, while the measurements in coal mines have shown that the gas contents of the coals in the basin are between 1 and 14 m<sup>3</sup>/ton (Karacan and Okandan, 2000).

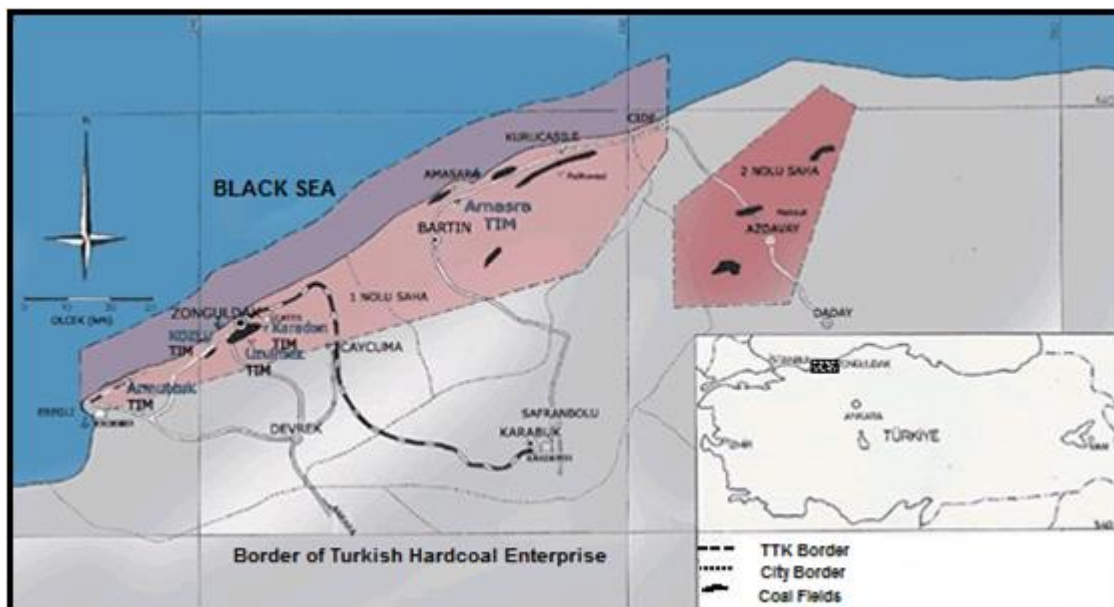


Figure 1 - Location of the Zonguldak Coal Basin

### Experimental study

In this study, the coal seams were classified for outburst proneness using gas content and gas desorption rate properties. This classification is aimed to determine outburst prone areas in Kozlu and Karadon Collieries and to protect the working areas of the coal seams.

Coal and gas outbursts are the most important events in underground coal mining operations. Factors influencing the gas and coal outbursts are; structure properties of the coal (the friability of the coal and

the coalification process), the gas desorption rate, gas content of the coal seam and the rock pressure. These are the most important factors to predict the outburst prone zones. In this study, the outburst prone zones in Kozlu and Karadon Collieries will be determined and classified with risk indices.

### **Investigation of gassiness of the coal seams**

The most commonly used gas content determination methods subdivide the total gas content of a coal sample into three parts: lost, desorbed and residual gas. The *lost gas* is that portion of the total gas that escapes from the sample during its collection and retrieval prior to being sealed into an airtight desorption canister. Some portion of this free gas will escape during sample retrieval and will not be accounted for by lost gas estimation methodologies based on diffusion of desorbed gas. Once a coal sample is sealed in the desorption canister, the desorbing gas accumulates and can be measured directly, commonly by some variation of the water displacement method. The volume of gas desorbing from a coal sample gradually declines with time. Desorption measurements for the extended desorption techniques are terminated at some point when an arbitrary low desorption rate is reached. This rate may be reached in a matter of days for very friable samples or can take months for some blocky coals. Generally, when the desorption rate reaches an established termination point, some volume of gas remains in the sample. Traditionally, this *residual gas* has been thought of as gas that is 'trapped' within the coal structure due to slow diffusion rates (Diamond and Schatzel, 1998). 19 coal samples were taken from seven different coal seams from different borehole lengths as both Karadon and Kozlu Collieries are at different depths.

The desorbed gas ( $Q_d$ ) was measured by the experimental apparatus that is shown in Figure 2, which was designed according to USBM Direct Method. The samples were sealed into the canisters then taken to TTK (Türkiye Taskomürü Kurumu, Turkish Hard Coal Enterprises) Gas and Dust Laboratory at the Research and Development Department. The measurements were recorded every 15 minutes in the first day. The measurements have taken 4 – 8 days. Furthermore the dimension of canisters is 10 cm wide and 40 cm high and has 3140 cm<sup>3</sup> inner volume.



**Figure 2 - The canisters and the USBM direct method design**

The lost gas ( $Q_l$ ) was calculated from the graph that are generated by the desorption values. The graph consists of the desorption values which are plotted against to the square root of desorption time as is shown in Figure 3. The most important thing when measuring the lost gas, the coal samples have to be sealed as quickly as possible into the canisters.

A sealed crusher mill was used to measure the residual gas ( $Q_r$ ). The crusher mill's inner volume is 3685 cm<sup>3</sup> and there were 12 balls to grind the coal samples. At the point when the periodic measurement of desorbed gas is discontinued; the residual gas, which were trapped in coal sample's micro and macro cracks, is measured by crushing the sample to a powder (- 200 mesh). The recommended procedure for determining the residual gas requires the transfer of all or a portion of the desorbed coal sample to a desorption ball mill canister for crushing on a roller mill (Diamond and Levine, 1981) to measure the gas. The volume of gas released was measured in the same way as that shown in Figure 2 with a water displacement apparatus. The Figure 4 shows the mill and the experimental design.

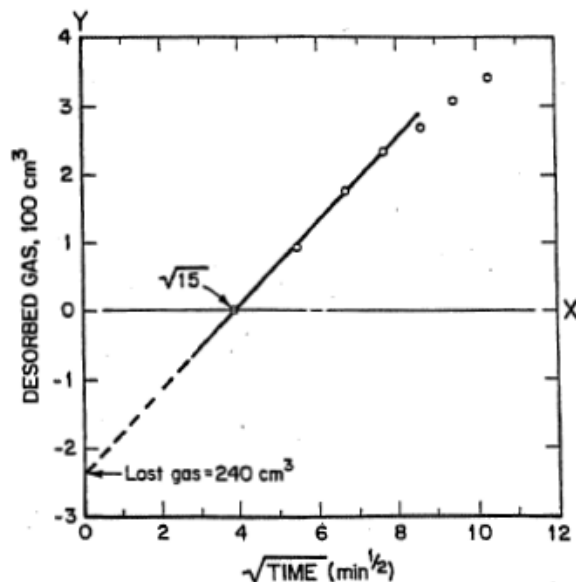


Figure 3 - Measurement of lost gas from the plotted graph



Figure 4 - The mill and the experimental design

Finally all direct gas measurements were continued with the calculation of total gas contents of coal samples. The total gas is calculated with the equation 1 given below (Diamond and Schatzel 1998);

$$Q_t = \frac{(Q_t + Q_d)}{M_t} + \frac{Q_r}{M_c} \tag{1}$$

Where  $M_t$  is the total air-dried mass (weight) of the sample and  $M_c$  the air-dried mass (weight) of the sample crushed to a powder in the ball mill. The value  $Q_t$  called *total gas*, is calculated in  $\text{cm}^3/\text{g}$ , but is commonly converted to  $\text{ft}^3/\text{short t}$  ( $= \text{cm}^3/\text{g} \times 32$ ) in the United States for ease in making gas resource calculations.

**Investigation of desorption rate of gas in coal seams**

For the occurrence of gas and coal outburst events, it is necessary for the coal and the rock material have to desorb with high velocity into the working area after the sorption / desorption stability is disrupted. Due to this reason, investigation of desorption rate of gas in coal is being important while researching the proneness of coal seams to gas and coal outburst events. In this study, desorption rates are basically measured according to decrease of the pressure at a certain time owing to adsorption of high pressured gas. Desorption rate measurement experimental apparatus is shown in Figure 5.

For determining the  $\Delta P_{\text{express}}$  index a coal sample of about 70 g in the range of 0.25–0.5 mm for bituminous (2–3 mm for anthracite) is enclosed in a chamber. The sample is evacuated for 2 min and then methane is allowed to enter into it to raise the gas pressure to 0.2 MPa as quickly as possible. The

gas flow into the chamber is closed. The chamber is immediately connected to a manometer and the change in pressure after 1 min is read, which gives the  $\Delta P_{\text{express}}$  index (Paul, 1977; Lama and Bodziony, 1998). However nitrous gas ( $\text{N}_2\text{O}$ ) was used in this study because of safety measures.

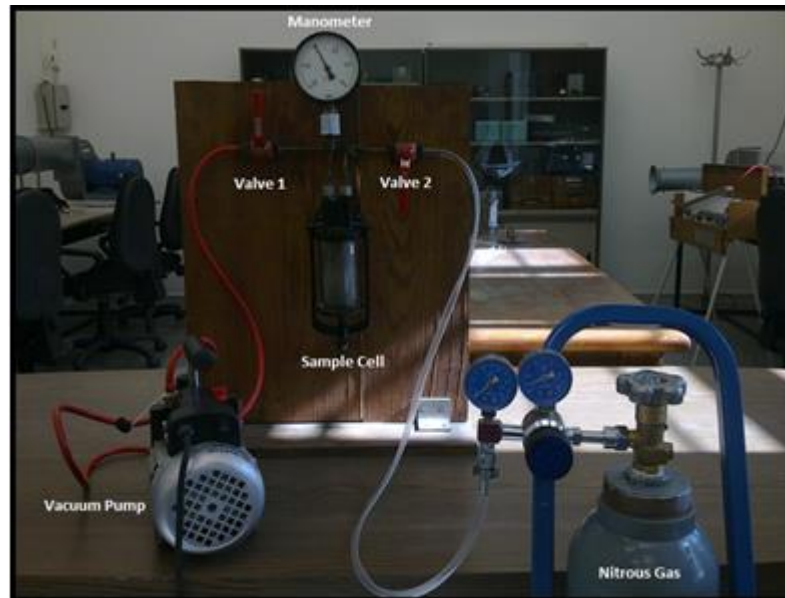


Figure 5 - Desorption experiment measurement design

## Results and discussions

In underground coal mining, coal and gas outburst events have an important role which result in such dangerous risks for both workers and working areas. Due to this fact the prediction of outburst prone zones in an underground coal mine is more important. For this reason, many methods have been developed and investigated concerning factors influencing coal and gas outbursts.

19 coal samples were taken from both TTK Kozlu and Karadon Collieries where the most coal and gas outbursts events have been occurred in Turkey. The borehole lengths are varied between 4 m and 18 m and the diameters are constant at 42 mm. Coal samples were taken from these boreholes as drill cuttings, at different depths and from seven different coal seams. 12 coal samples out of 19 are from Kozlu Colliery and the other seven coal samples are from Karadon Colliery.

### Gas content measurements of coal seams

The amount of gas content of the coal seams has an important role in the occurrence of coal and gas outbursts. As is shown in Table 1; 12 coal samples which were taken from Kozlu Colliery, have gas content values varying between 3.8 – 16.9  $\text{m}^3/\text{t}$  and 7 coal samples that were taken from Karadon Colliery, have gas content values varying between 3.0 – 15.5  $\text{m}^3/\text{t}$ .

Investigations in many countries have shown that the coal and gas outbursts occurred in coal seams which have 9  $\text{m}^3/\text{t}$  gas content or higher. These coal seams are described that outburst prone areas (Paul, 1977; Okten, 1983). In this study, as a gas content threshold value 9  $\text{m}^3/\text{t}$  gas content or higher was used to classify the outburst proneness of the coal seams in both Kozlu and Karadon Collieries of the Zonguldak Coal Basin.

The comparisons of the gas content values of coal seams with the threshold limit value of 9  $\text{m}^3/\text{t}$  are shown in Figure 6.

### $\Delta P_{\text{express}}$ Index measurements of coal seams

Measuring the  $\Delta P_{\text{express}}$  Index values there are 3 experiments for each 70 g. coal sample. The results were calculated as an average value, were determined  $\Delta P_{\text{express}}$  Index value as bar. The results are shown in Table 2 which were taken from Kozlu and Karadon Collieries at different depths and 7 different coal seams.

As it is shown in Table 2; 12 coal samples which were taken from Kozlu Colliery, have gas content values that varied between 0.40 and 0.72 bar and 7 coal samples that were taken from Karadon Colliery, have gas content values that varied between 0.34 and 0.68 bar.

From this point, it's required to compare the results as proneness. Due to the fact that, the threshold limit was determined for the coal basin and 3 coal samples were taken from areas where outbursts occurred on different years in Zonguldak Coal Basin. Measurement results for determining the threshold limit are shown in Table 3.

As it is seen on Table 3;  $\Delta P_{\text{express}}$  values of coal samples which were taken from areas where outburst occurred are lower than 0.43 bar. Depending on this result, in the Zonguldak Coal Basin, for the Karadon and Kozlu Collieries; the coal seams are described as outburst prone areas which are closer to 0.43 bar or lower than this value, was determined as threshold value (Esen, 2013).

The comparisons of  $\Delta P_{\text{express}}$  Index values of coal seams with the threshold limit value of 0.43 m<sup>3</sup>/t are shown in Figure 7.

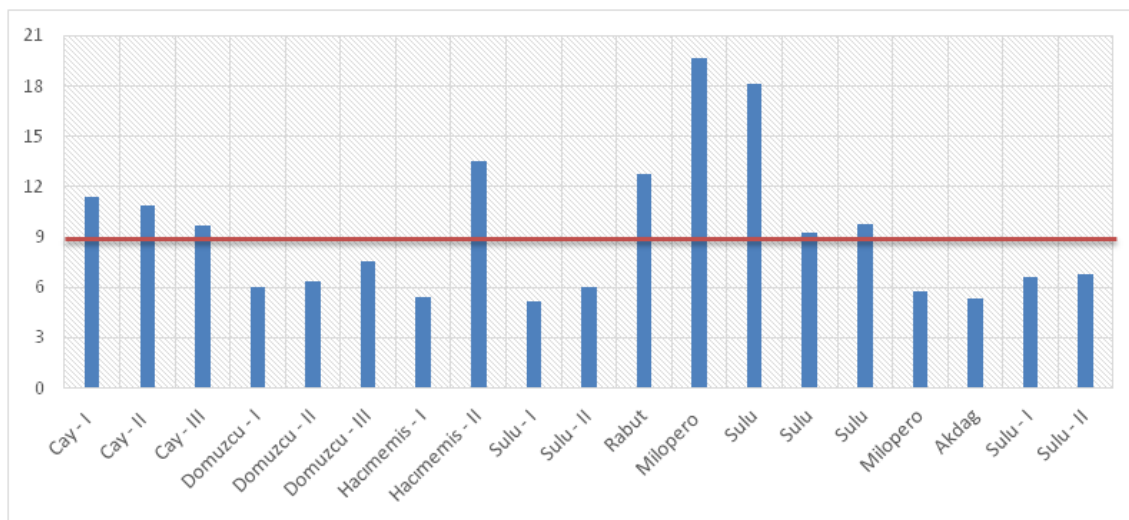


Figure 6 - Gas content values compared with threshold limit

Table 1 - Results of gas content measurements of the coal seams

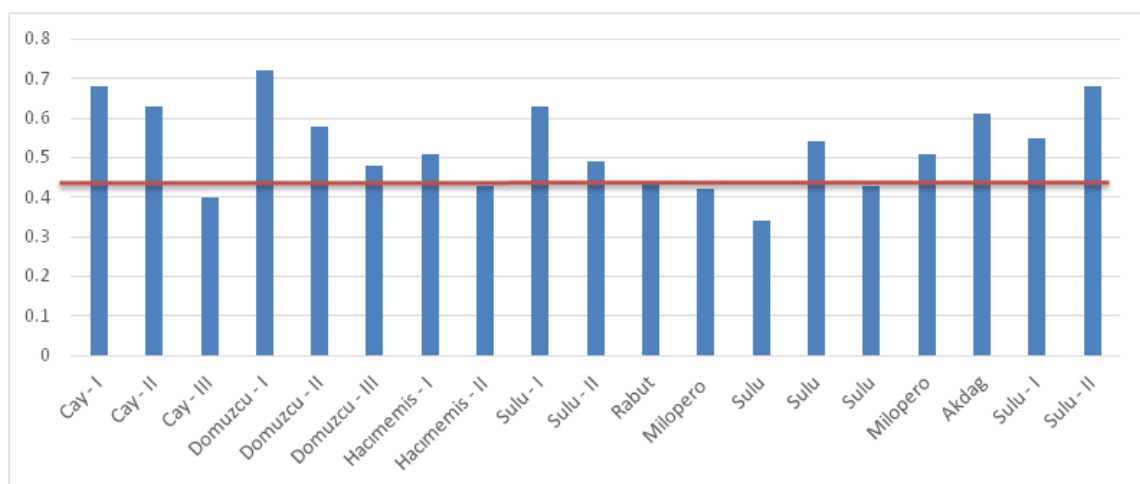
Sample No.	Colliery	Name of Seam	Working Area	Depth (m)	Lost Gas (m <sup>3</sup> /t)	Desorbed Gas (m <sup>3</sup> /t)	Residual Gas (m <sup>3</sup> /t)	Total Gas Content (m <sup>3</sup> /t) (ar)
1	Kozlu	Cay - I	Gateway	-582	2.31	4.07	0.53	6.9
2	Kozlu	Cay - II	Gateway	-579	2.09	4.80	0.78	7.7
3	Kozlu	Cay - III	Gateway	-510	1.72	5.86	0.67	8.3
4	Kozlu	Domuzcu - I	Gateway	-437	1.94	2.34	0.20	4.5
5	Kozlu	Domuzcu - II	Gateway	-437	2.54	3.08	0.29	5.9
6	Kozlu	Domuzcu - III	Gateway	-437	3.28	3.40	0.18	6.9
7	Kozlu	Hacimemis - I	Gateway	-547	0.88	4.01	0.17	5.1
8	Kozlu	Hacimemis - II	Gateway	-547	1.82	6.52	0.27	8.6
9	Kozlu	Sulu - I	Gateway	-560	0.98	2.67	0.16	3.8
10	Kozlu	Sulu - II	Gateway	-560	1.71	3.49	0.22	5.4
11	Kozlu	Rabut	Gateway	-485	2.28	8.76	0.66	11.7
12	Kozlu	Milopero	Raise	-547	1.36	14.49	1.06	16.9
13	Gelik	Sulu	Gateway	-260	2.71	12.04	0.78	15.5
14	Gelik	Sulu	Gateway	-360	1.64	2.48	0.18	4.3
15	Gelik	Sulu	Raise	-360	2.09	6.25	0.71	9.1
16	Gelik	Milopero	Gateway	-360	0.89	2.17	0.23	3.3
17	Kilimli	Akdag	Raise	-460	0.95	1.71	0.32	3.0
18	Kilimli	Sulu - I	Gateway	-360	1.58	3.74	0.40	5.7
19	Kilimli	Sulu - II	Gateway	-360	1.53	3.27	0.30	5.1

**Table 2- Results of  $\Delta P_{\text{express}}$  Index values of the coal seams**

Sample No.	Colliery	Name of Seam	Working Area	Depth (m)	Measurements			$\Delta P_{\text{exp}}$ Index (bar)	Standard Deviation
					1	2	3		
1	Kozlu	Cay - I	Gateway	-582	0.68	0.680	-	0.68	0.002
2	Kozlu	Cay - II	Gateway	-579	0.62	0.630	0.643	0.63	0.01
3	Kozlu	Cay - III	Gateway	-510	0.4	0.397	-	0.4	0.002
4	Kozlu	Domuzcu - I	Gateway	-437	0.72	0.720	-	0.72	0.002
5	Kozlu	Domuzcu - II	Gateway	-437	0.583	-	-	0.58	-
6	Kozlu	Domuzcu - III	Gateway	-437	0.483	-	-	0.48	-
7	Kozlu	Hacimemis - I	Gateway	-547	0.480	0.523	0.523	0.51	0.02
8	Kozlu	Hacimemis - II	Gateway	-547	0.467	0.433	0.403	0.43	0.026
9	Kozlu	Sulu - I	Gateway	-560	0.635	0.573	0.670	0.63	0.04
10	Kozlu	Sulu - II	Gateway	-560	0.503	0.480	0.487	0.49	0.01
11	Kozlu	Rabut	Gateway	-485	0.300	0.520	0.500	0.44	0.122
12	Kozlu	Milopero	Raise	-547	0.417	0.41	0.423	0.42	0.005
13	Gelik	Sulu	Gateway	-260	0.332	0.364	0.335	0.34	0.014
14	Gelik	Sulu	Gateway	-360	0.533	0.55	-	0.54	0.008
15	Gelik	Sulu	Raise	-360	0.390	0.45	0.45	0.43	0.035
16	Gelik	Milopero	Gateway	-360	0.487	0.52	0.533	0.51	0.02
17	Kilimli	Akdag	Raise	-460	0.620	0.607	0.61	0.61	0.006
18	Kilimli	Sulu - I	Gateway	-360	0.570	0.527	0.557	0.55	0.01
19	Kilimli	Sulu - II	Gateway	-360	0.673	0.697	0.683	0.68	0.018

**Table 3 - Results of  $\Delta P_{\text{exp}}$  index values of the areas where outbursts occurred**

Sample No.	Outburst Event Date	Place of Coal and Gas Outburst Event	Depth (m)	No. of Samples	Measurements		
					Avg (bar)	St.Dev.	Range
1	17.05.2010	-540/51506 Karadon New Shaft - Drift	-540	3	0.40	0.009	0.39-0.41
2	31.03.2011	-360/41406 Gelik Acilik Seam - Gateway	-360	3	0.43	0.013	0.41-0.44
3	11.04.2012	-460/42504 Karadon Acilik Seam - Gateway	-460	3	0.41	0.019	0.39-0.43

**Figure 7 -  $\Delta P_{\text{express}}$  values compared with threshold limit**

## CONCLUSIONS

According to the results, the coal seams were classified for coal and gas outbursts to give information about the Zonguldak Coal Basin. Coal seam gas contents in Kozlu Colliery varied between  $3.8 \text{ m}^3/\text{t}$  and  $16.9 \text{ m}^3/\text{t}$  for 12 coal samples and in Karadon Colliery it varied between  $3.0 \text{ m}^3/\text{t}$  and  $15.5 \text{ m}^3/\text{t}$  for 7 coal

samples. These gas content value results are on original coal basis. The  $9 \text{ m}^3/\text{t}$  threshold limit value was considered to compare the gas content values to classify the coal seams for their outburst proneness on the received (original coal) basis. According to the results in Kozlu Colliery -480 Rabut Seam (Sample 11), -560 Milopero Seam (Sample 12); in Karadon Colliery -260 Sulu Seam (Sample 13), -360 Sulu Seam (Sample 15) it can be said that these coal seams are explained as outburst prone zones. In addition it can be also described as outburst prone zones which are closer to the threshold limit, -560 Hacimemis Seam (Sample 8) and -485 Cay Seam (Sample 3), with respectively  $8.6 \text{ m}^3/\text{t}$  and  $8.3 \text{ m}^3/\text{t}$ .

The desorption rate of the coal seams, in other words the  $\Delta P_{\text{express}}$  Index values in Kozlu Colliery changes between 0.40 and 0.72 bar for 12 coal samples and in Karadon Colliery changes between 0.34 and 0.68 bar. In past studies on the Zonguldak coal basin, no threshold value was determined. Due to this, a new threshold value for Kozlu and Karadon Collieries' formations was determined in terms of  $\Delta P_{\text{express}}$  Index research. For determining the threshold value, coal samples were taken from outbursts area, which occurred which were experienced in the years between 2010 and 2012.

Then by comparing these study values and the samples which were taken from outburst experienced areas, it can be said for -485 Cay Seam (Sample 3), -560 Hacimemis Seam (Sample 8), -480 Rabut Seam (Sample 11), -560 Milopero Seam (Sample 12), -260 Sulu Seam (Sample 13) and -360 Sulu seam (Sample 15), these coal seams are described as outburst prone seams.

## REFERENCES

- Cakir, A and Baris, K, 2009. Assessment of an underground Coal mine fire: A case study from Zonguldak, Turkey, in Aziz, N (ed), Coal 2009: Coal Operators' Conference, University of Wollongong and the Australasian Institute of Mining and Metallurgy, 259-270.  
<http://ro.uow.edu.au/coal/108/>.
- Creedy, D P, 1991. An introduction to geological aspects of methane occurrence and control in British deep coal mines. *Q J Eng Geol* 24, pp.209-220.
- Diamond, W P and Levine, J R, 1981. Direct method determination of the gas content of coal: procedures and results, *US Bur. Mines, Rep. Invest.* 8515, pp.36.
- Diamond, W P and Schatzel, S J, 1998. Measuring the gas content of coal: A review, *Int J Coal Geol* 35, pp.311-331.
- Esen, O, 2013. Assessment of gas and coal outbursts in Turkish Hard Coal Enterprise collieries and investigation of factors influencing the outbursts, M.Sc. thesis, Faculty of Mines, Mining Engineering Department, Istanbul Technical University, Istanbul, Turkey (in Turkish).
- Flores, R M, 1998. Coalbed methane: From hazard to resource, *Int J Coal Geol* 35, pp.3-26.
- Guan, P, Wang, H and Zhang, Y, 2009. Mechanism of instantaneous coal outbursts, *Geology*, 37, pp.915-918.
- Gurdal, G and Yalcin, M N, 2000. Gas adsorption capacity of carboniferous coals in Zonguldak basin (NW Turkey) and its controlling factors, *Fuel*, V. 79, pp. 1913-1924.
- Karayigit, A I, Gayer, R A and Demirel, I H, 1998. Coal rank and petrography of upper carboniferous seams in the Amasra coalfield, Turkey, *Int J Coal Geol* 36, pp.277-294.
- Karayigit, A I, 2001. Mineralogy and trace element contents of the Akalin seam, Gelik mine, Zonguldak-Turkey, *Energy Sources*, V. 23, pp. 699-709.
- Lama, R D and Bodziony, J, 1998. Management of outburst in underground coal mines, *Int J Coal Geol* 35, pp.83-115.
- Noack, K, 1998. Control of gas emissions in underground coal mines, *Int J Coal Geol*, 35, pp.57-82.
- Okten, G, 1983. Assessment of coal and gas outbursts in Zonguldak coal basin and investigation for determining outburst prone zones, PhD thesis, Istanbul Technical University, Faculty of Mines, Mining Engineering Department, Istanbul, Turkey (in Turkish).
- Okten, G, Biron, C, Saltoglu, S and Ozturk, M, 1995. Gas and coal outburst of Zonguldak coalfield of Turkey and preventive measures, *International Symp.-Cum-Workshop on Management and Control of High Gas Emissions and Outbursts in Underground Coal Mines*, Wollongong, Australia, 20-24 March, pp. 451-458.
- Paul, K, 1977. Early detection and prevention of outbursts, *Glückauf*, Vol. 113, No. 13, Sf. 656-62.
- Zhang, G, 1995. Area prediction of danger of coal and gas outbursts: Example of application in Jiaozuo mining area in China. In: Lama, R.D. Ed., *Int. Symp. cum Workshop on Management and Control of High Gas Emission and Outbursts in Underground Coal Mines*, Wollongong, Australia, 20-24 March, pp. 195-199.

# POLY-CRYSTALLINE DIAMOND DRILL BIT DEVELOPMENT

Frank Hungerford<sup>1,2</sup> and Ting Ren<sup>1</sup>

**ABSTRACT:** The development of directional drilling in the coal industry has been enhanced by access to Poly-Crystalline Diamond (PCD) bit technology. This technology has been developed in the oil industry with ongoing improvements driven by the need for improved drilling rates, more robustness for longer life and ability to penetrate a wider range of strata types. Although the underground drilling applications require smaller bit diameters, the technology has been applied with modifications to create suitable smaller bits. This paper describes PCD and bit design technology and identifies a range of drill bits now available and their applications in the underground in-seam directional drilling industry.

## INTRODUCTION

As in-seam drilling of gas drainage boreholes became an established aspect of gas management, the technology in drill bit design and construction has also evolved. The early bits used for in-seam drilling in the coal were fitted with tungsten carbide cutters. These bits were usually “home-made” or produced by bit manufacturers for the surface drilling industry rather than being specifically designed for in-seam drilling applications (Hungerford, 1995).

Most drill bit technology has been driven and financed by the oil and gas industry with the flow on effect benefiting other drilling industries with that technology being adapted to suit differing needs. Improvements in the technology have benefitted the underground drilling industry with improved drilling performance in an increasing array of drilling applications.

## INTRODUCTION OF THE PCD BIT

A key development in bit technology in Australia was the access to poly-crystalline diamond (PCD) bits through an experimental bit acquired by ACIRL from the USA in 1982. This “Terratek” 80 mm Stratapax bit (Figure 1) (Allen, 1982) was an early version of the PCD bits developed for the oil and gas drilling industry in the mid-1970's with PCD cutters mounted on tungsten carbide pillars secured into the face of a steel body. The PCD cutters penetrated both coal and stone without requiring the constant sharpening associated with tungsten carbide faced bits.



Figure 1 - “Terratek” 80 mm Stratapax PCD bit (Allen, 1982)

<sup>1</sup> School of Civil, Mining & Environmental Engineering, University of Wollongong, Wollongong, NSW 2522, Australia

<sup>2</sup> Global Technical Services Manager, Drilling Division, Valley Longwall International Pty Ltd, FHungerford@vli.com.au, Tel: +61 2 4964 2300

## CUTTING ACTION

The comparative cutting action of the PCD cutter with other bits is demonstrated in Figure 2 (Triefus, 1982). The roller cone bit fractures rock with a crushing action, the natural diamond bit ploughs and grinds while the PCD cutter shears rock much like a lathe action.

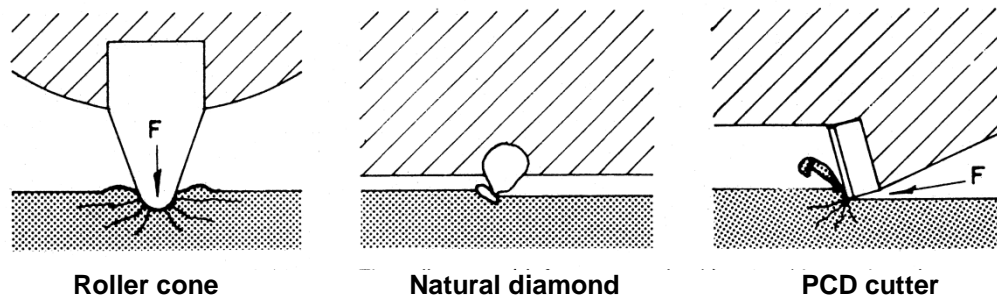


Figure 2 - Cutting mechanics of various bit types (Triefus, 1982)

## POLY-CRYSTALLINE DIAMOND TECHNOLOGY

The PCD cutter (Figure 3) (Brown, 2007) (usually referred to in the surface drilling industry as a PDC – Polycrystalline Diamond Compact) consists of a tungsten carbide blank (Substrate) which has a thin layer of synthetic diamond matrix (Diamond Table) bonded to it through a sintering process under high pressure and temperature in a synthesis press (Figure 4) (Brown, 2007). The matrix is formed from a mix of synthetic diamonds and a cobalt bonding agent with the diamond size, portions, temperature and pressure being regulated to produce improved diamond table.

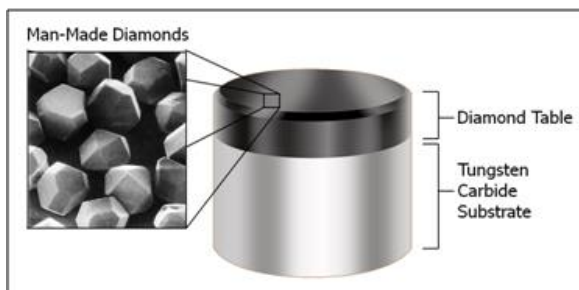


Figure 3 - PCD cutter (PDC - Polycrystalline Diamond Compact)

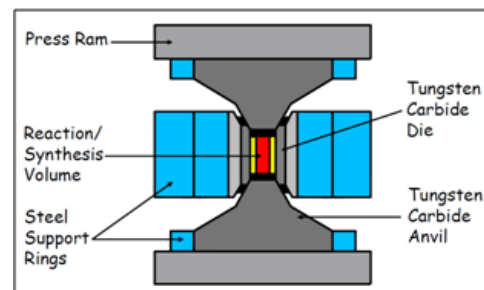


Figure 4 - Synthesis press for creating PCD cutters (Baker Hughes, 2007)

Continual evolution in the PCD technology has improved the matrix to be more robust to manage the abrasive and shock loading it is subjected to. Early PCD matrix was prone to flaking fracture failure (Figure 5) and occasional total failure of the bond with the tungsten carbide substrate. The PCD cutters are also sensitive to temperatures over 800°C and can be adversely affected during the process of silver soldering into the bit face.

Modern technology allows finite element analysis of load transfer and stress distribution (Figure 6) (Baker Hughes, 2007) from the cutting point of contact through to the mount in the bit face aimed at reducing the damaging stresses. The PCD / tungsten carbide interface is now modelled and analysed (Figure 7) (Mensa-Wilmot, *et al.*, 2003) with various substrate profiles (Figure 8) to reduce stresses in the PCD cutter and improve the bond strength. This improves resistance to chipping and/or fracturing. The modelling also considers various table thicknesses, interface shape and grade of tungsten carbide in the substrate to provide PCD cutters suitable for specific load applications. Further developments have included a chamfered edge and polished face on the PCD table to enhance the cutting action and removal of cuttings.

PCD cutters are available with diamond table thicknesses up to 3.5 mm and diameters up to 30 mm. The PCDs used in underground directional applications are usually 13 mm diameter with a diamond table thickness of 1.0-1.5 mm. PCDs are also available in 8 mm diameter (Figure 9). The general rule is that small cutters and high cutter count are chosen for hard and abrasive rock formations, whereas large cutters and a reduced cutter count are preferred for soft to medium formations.



Figure 5 - Fractured PCD table with eroded tungsten carbide substrate

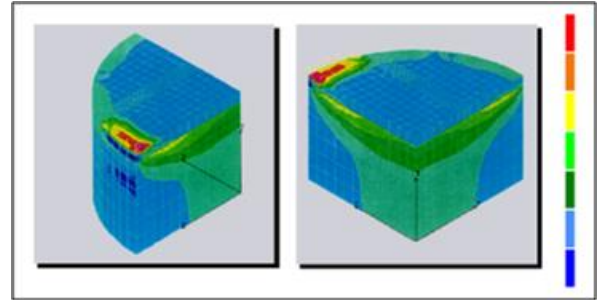


Figure 6 - Finite element analysis of stress distribution in a PCD cutter from contact point loading

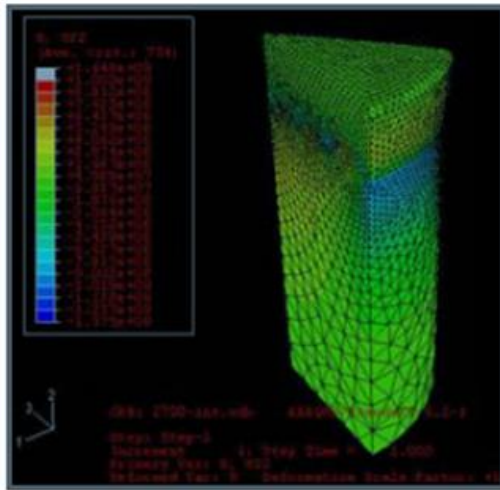


Figure 7 - Finite element analysis of tungsten carbide substrate and diamond table interface (Mensa-Wilmot, et al., 2003)

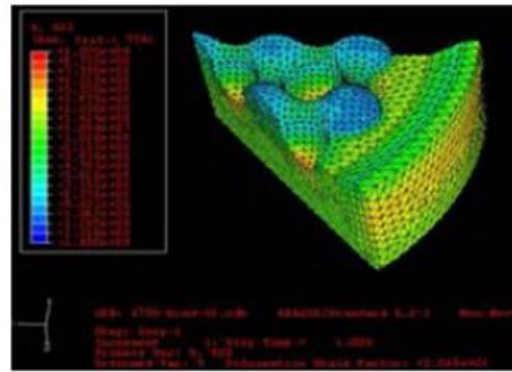


Figure 8 - Substrata profile - radial symmetry, axial symmetry and ripple (Baker Hughes, 2007)

The diamond Table is much harder but relatively brittle compared to the tungsten carbide Substrate. Progressive wear removes the tungsten carbide behind the diamond Table to present a leading cutting edge of PCD matrix (Figure 10). When the diamond Table fractures, the tungsten carbide Substrate is rapidly eroded to re-expose a cutting edge of PCD matrix (Figure 5).

### BIT STRUCTURE

PCD bits are classified as either post (tungsten carbide posts mounted in a steel body) or cast matrix face (Figure 11) (Brown, 2007). With the latter, a mix of tungsten carbide and cobalt binding agent are cast and bonded at high temperature and pressure to a steel body. The face is designed with mounting recesses which position each cutter in a precise location at a prescribed angle. The cast matrix offers

more resistance to erosion than that of a steel bodies bit. With improved technology, the matrix has become more robust with improved resistance to erosion and shock loading from vibration. In high erosion areas, tungsten carbide blocks or strips can be inserted in the cast to enhance erosion resistance.



Figure 9 - Flat faced bit with spiral layout of 8 mm PCD cutters



Figure 10 - Progressive wear of a PCD cutter

With relatively small diameter bits (96 mm) in use, there is insufficient space to design the usual blade face layout of larger diameter PCD bits (Figure 12) (Brown, 2007). The smaller bits are designed as flat or relatively flat faced (Figures 9 and 13) with the cutters arranged in a spiral from the centre outwards. The spiral layout assists in reducing torque vibration and promotes removal of cuttings towards the periphery of the bit. The coverage of the cutters is overlapped (Figure 13) to provide total coverage of the cutting face with the placement designed to generate balanced torque loading on the face. Outer cutters provide both axial and gauge cutting with tungsten carbide inserts providing passive gauge protection along the outside of the bit. Exposure of the outer cutters and a flat face are preferred elements to starting and propagating a lip for branching with directional drilling.

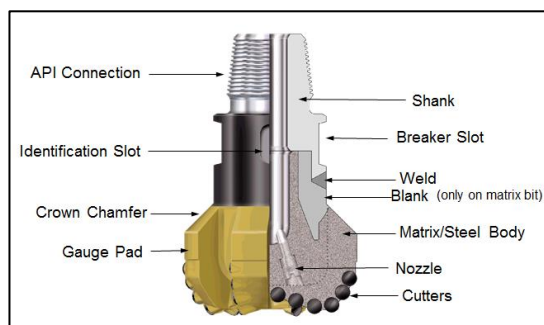


Figure 11 - PCD bit structure

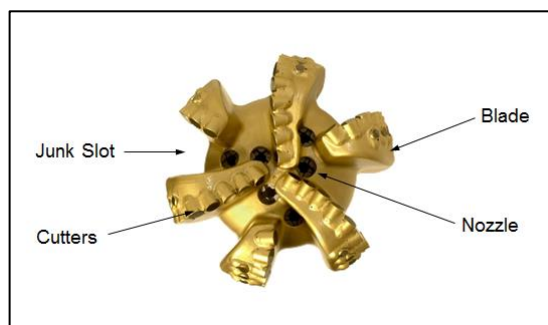


Figure 12 - PCD blade face layout

### RAKE ANGLES

The PDC cutter characteristics, back rake angle, cutter layout, cutter count and cutter size are the main parameters that control the drillability of the bit. The PCD cutters are mounted at an angle relative to the axial direction of drilling/penetration. This is referred to as the back rake angle (Figure 14) (Triefus, 1982). This angle is required to present the cutting edge of the cutter in contact with the strata. It controls how aggressively cutters engage the rock formation. Generally, as the back rake is decreased, the cutting efficiency increases but the cutter becomes more vulnerable to impact breakage. A large back rake angle will result in lower rate of penetration but will give a longer PCD bit life. The general trend is for the inner cutter to have a back rake angle of 20-25° with the angle reducing to 10° for the outer cutters.

The side rake angle (Figure 14) aligns the cutter so that the back of the cutter is within the cutting circumference of that cutter (Figure 15) (Baker Hughes, 2007). It also enhances the shearing action of the cutter and helps to direct the cuttings toward the periphery of the bit.

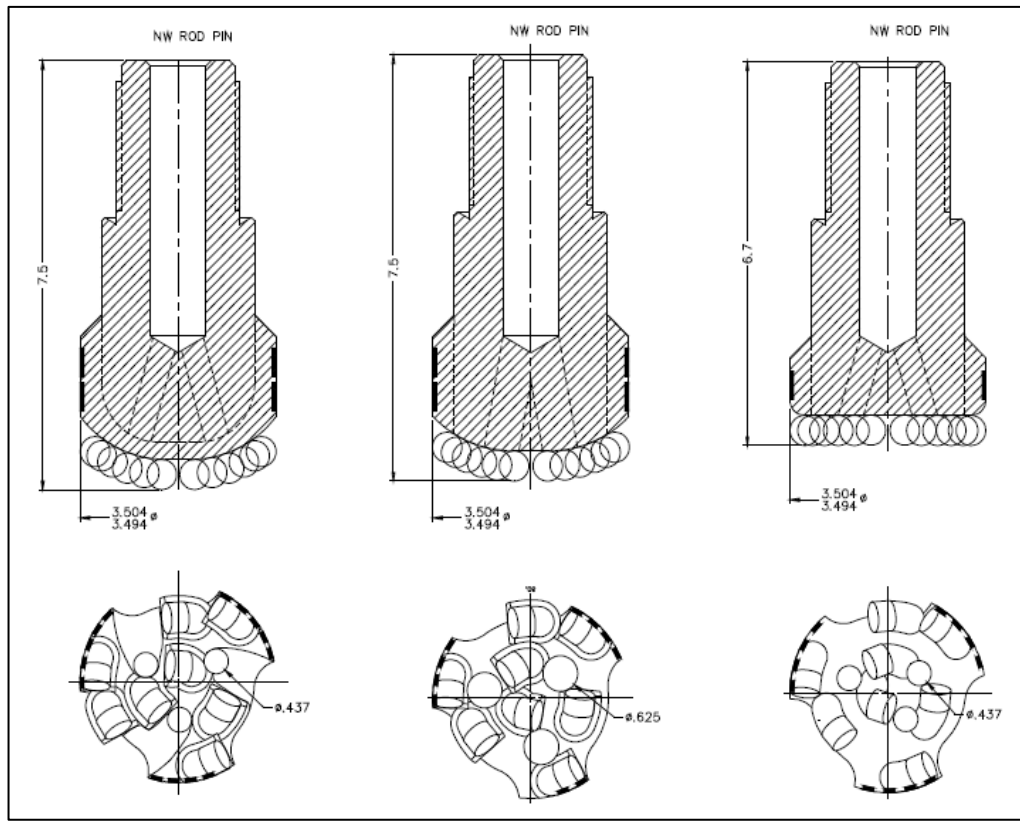


Figure 13 - PCD cutter layout and coverage

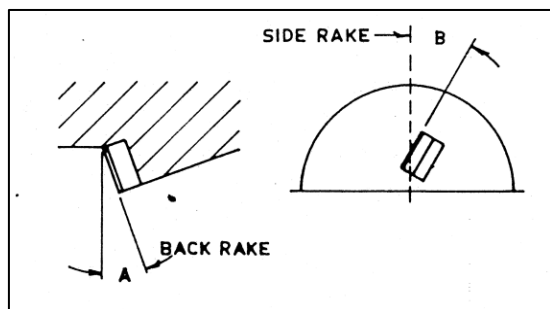


Figure 14 - Back and side rake angles of mounted PCD cutters (Triefus, 1982)

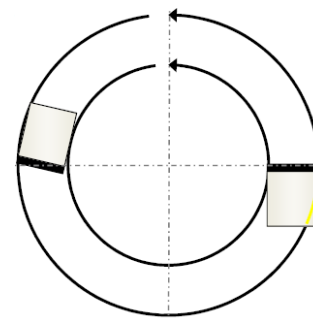


Figure 15 - Clearance provided by side rake angle (Baker Hughes, 2007)

### DEVELOPMENT OF PCD BITS

Steel bodied PCD bits of similar design to the Terratek bit (Figure 1) were available for Down Hole Motor (DHM) drilling. As these were regarded as relatively expensive and with long delivery times from the USA, emphasis was directed towards developing a locally available product Longyear's had advertised cast matrix technology for drill bit construction so they were approached to design and manufacture a PCD bit with a cast matrix face. Tungsten carbide (T/C) inserts can be incorporated into the matrix at the casting stage to reinforce high erosion zones.

Longyear produced an 80 mm PCD rotary bit and an 89 mm flat faced PCD bit with exposed side cutting action for DHM drilling. The 80 mm design was used successfully for in-seam rotary drilling for exploration. The initial design of 89 mm bit was found to have design flaws, which had adverse

influences on drilling performance and bit life (Hungerford, *et al.*, 1988). The problems were with the security of the outer cutters and uniform water flushing:

- The steep angle of the back of the cutter mounts (Figure 16) led to several break-out failures of the outer cutter mounts.
- Erosion under the outer mounts led to failure of the mount (Figure 16).
- The angled choke directly under the inner-most cutter mount in the central flushing port (from full round profile in the body of the bit to the half round profile as it exited the face adjacent to the inner-most cutter mount) was directing high water flow at an angle to the alignment of the DHM. This caused severe vibration of the DHM when operating.

Modifications proved successful and were adopted by Longyear (Figure 17). They were also incorporated into their rotary designed bits with semi-parallel sided gauge protection. Directional drilling eventually adopted rotary drill bits when the side cutting feature was regarded as not being essential for branching.

Asahi Pty Ltd Australia produced similar in their Claw bit series (Figure 18) with semi-parallel side gauge protection. These bits are reasonably aggressive and used extensively in underground gas drainage drilling. They are available with a non-return valve incorporated inside the threaded section.

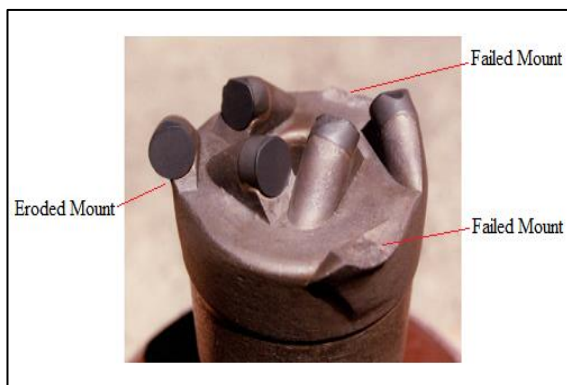


**Figure 16 - Worn and damaged Longyear 89 mm bit**



**Figure 17 - Modified Longyear 89 mm DHM PCD bit**

Several PCD bits are now more readily available from the USA. Their differing design and cutter configurations provide cutting characteristics suited to differing drilling environments and conditions. Smaller cutters (Figure 9) and recessed cutters (Figure 19) produce smaller cuttings and slower penetration rates more suited for longer boreholes or drilling in boggy conditions. The convex bit (Figure 20) with fully exposed 13 mm cutters is a very aggressive bit with very good penetration rates but is not conducive to branching.

To enhance the ability to drill back out of boggy conditions, back-cutting facilities have recently been added to bits in the form of tungsten carbide pieces (Figure 21) or PCD cutters with back-flushing port (Figure 22) and proved successful.

## CONCLUSIONS

The development of PCD technology has been driven and financed by the oil and gas drilling industry. The technology has allowed improved drilling performance in an expanding number of drilling applications.

The key design aspects required for directional drilling bits are:

- Flat faced design with slightly exposed outer cutters to enhance the ability to branch,
- Complete coverage and balanced torque loading of PCD cutters on the face,
- Back rake angles determined to suit relative loading and frictional exposure,

- Axially balanced water flushing ports in the face to avoid vibration during rotation,
- Some form of back-cutting facility to assist recovery from boggy environments.

Drill bit design has also provided smaller diameter bits for use in underground directional drilling applications although most bits used are as provided by the manufacturers. Studying the performance of these bits can provide information to improve the design for specific applications.



Figure 18 - Asahi 96 mm PCD bit



Figure 19 - DPI flat-faced PCD bit with 50% recessed 13 mm cutters



Figure 20 - DPI convex-faced PCD bit with fully exposed 13 mm cutters



Figure 21 - Asahi PCD bit with tungsten carbide back-cutters



Figure 22 - DPI bit with PCD back-cutters and flushing ports

---

**REFERENCES**

- Allen J, 1982. Private communication.
- Baker Hughes, 2007, unpublished presentation.
- Brown A, 2007. Product roadmap 2007, Company presentation, Baker Hughes Incorporated, Abu Dhabi, Nov, 2007.
- Hungerford F, 1995. Status of underground drilling technology, keynote address, International Symposium cum Workshop on Management and Control of High Gas Emission and Outbursts, Wollongong 20-24 March, pp 397404 (Ed: R D Lama.) ISBN 0 646 22810 2. <http://eis.uow.edu.au/outburst/pdfs/C3079%20Final%20Report.pdf>.
- Hungerford F, Saghafi A and Williams R J, 1988. In-seam and cross measure methane pre-drainage by long-hole drilling. *End of grant report NERDDP project No. 874*.
- Mensa-Wilmot G and Penrose B, 2003. Advanced cutting structure improves PDC bit performance in hard and abrasive drilling environments, prepared for presentation at the SPE Latin American and Caribbean Petroleum Engineering Conference held at Port-of-Spain, Trinidad, West Indies, 27-30 April, 2003.
- Triefus Pty Ltd, 1982 – Triefus product data sheet, Clore Drill Bits - Ref, No. BITS-REAMERS-4.

---

# FLUID PRESSURE MONITORING IN DEEP CEMENT GROUTED BOREHOLES

**Bruce Neels and Ian Gray**

**ABSTRACT:** The installation of pressure transducers in deep boreholes is a key feature of determining the effectiveness of gas drainage and the effect of mining on the groundwater regime. This paper covers the work undertaken to ensure reliability of data obtained from deep formation monitoring boreholes for both coal seam gas and groundwater. Cementing technology has enabled strings of transducers to be installed at greater depths with reliable zonal isolation between close sensing points. However the behaviour of grout at depth can be problematic with the effect of filtration, consolidation, skin and dehydration of the grout rendering the installation only partially effective. A review of cementing grouts and additives was undertaken and mix designs developed, to suit the requirements of deep borehole monitoring. Techniques were developed to mitigate the vicissitudes of grout and ensure both zonal isolation and connectivity of the transducer to the formation. The paper also reviews the automated data acquisition systems used for monitoring installations.

## INTRODUCTION

It is extremely important for many purposes to be able to monitor the fluid pressure existing in the ground. These range from the effect that fluid has on effective stress and hence failure of a soil or rock mass, the movement of groundwater, and the production or drainage of hydrocarbon fluids.

In the coal mining context all of these aspects are important. Failure of coals, and in particular outbursts and the energy release associated with them, are a direct function of the sorption pressure of the gas contained within the coal. The effectiveness of the drainage of water, methane and carbon dioxide is best determined by the use of long term pressure monitoring. The use of such pressure monitoring has the advantage over spot gas content measurement in that it provides a potentially continuous source of information on the drainage process rather than a single measurement. It is very cost effective as it does not require a hole to be re-drilled to obtain a coal sample for gas content measurement. Indeed, pressure measurement may be considered to be a more useful measurement for all these purposes than gas content alone, provided that the relationships between reservoir pressure, sorption pressure and gas content are understood.

The installation of pressure monitoring transducers for this purpose however needs to be undertaken carefully, with techniques to ensure that the correct values of fluid pressure are being measured, and with an adequate rate of response to pressure changes. This is particularly important where any transient testing is being used to determine reservoir properties.

## HISTORY OF INSTALLATION PRACTICES

### Transducers

The history of ground fluid pressure monitoring goes back to the measurement of the water level in hand dug wells. It was followed by the use of open stand pipe piezometers. Initially these were in connection with the entire formation through which they passed, and therefore they provided unreliable estimates where multiple heads existed. Later permeable tips were fitted to the open impervious tube. These were usually placed in a gravel or sand pack sealed above by bentonite, and grouted in place. In all cases these open tube devices could be monitored by hand dipping or later by the use of bubbler systems, where the pressure of the compressed air causing bubbles to be emitted from a tube was measured.

Point pressure monitoring without standpipes was developed for use in fill dams and embankments. Here installation was achieved between layers of compacted fill. Because electronic pressure transducers were not reliable enough in the long term, the transducers developed used compressed air to open an elastomeric valve to return air flow when the pressure reached that of the groundwater.

These required a twin tube system and accurate gauges on the surface. These were inherently very accurate systems, some of which are still in use after many decades.

Because of the drift characteristics of early strain gauge based Wheatstone bridge type transducers, and more importantly the lack of stable electronics to get the signal from the bridge up a cable to the surface, an alternative was developed. This alternative was the vibrating wire pressure transducer. It has a diaphragm which is in contact with the fluid which is to have its pressure measured. Attached to the diaphragm is a steel wire which is stretched between it and a fixed end. Changing pressure alters the tension in the steel wire. To produce a measurement, the wire is vibrated by the use of a swept frequency series of electrical pulses through coils which are wrapped around a magnet and cause the wire to vibrate. This vibration settles down to become the natural harmonic of the wire under the load induced by wire pre-tension and fluid pressure. The same coils that were used to excite the wire pick up the signal and enable it to be transmitted up the connecting wire. Such transducers may be made to be essentially drift proof. The digital nature of the signal (a frequency) means that the signal does not degrade until it becomes so faint that electronics can no longer isolate it from background noise. The reduction in signal comes with time after the swept frequency excitation, and with increased cable length and deterioration of its properties. Signal deterioration comes with extended length of cable and is caused by capacitance and resistance. It may also come from cable deterioration leading to current leakage between cables.

In the last two decades electronics have improved dramatically to reduce drift, and bridge type transducers can now be used to monitor fluid pressures. The limitation is how the signal is transmitted from the borehole. The measurement of voltage directly from a bridge or even from an amplified bridge is subject to the behaviour of the cable. This also applies to current loop transducers where leakage between the conductors will lead to an incorrect reading. The only reliable way in which to get data from such transducers is to digitise it and send the digital signal to the surface. Digital signals can take many forms such as a frequency or pulse width output. More usually it involves a standard form of data transmission such as an RS485 signal.

In recent times the most precise forms of transducer are considered to be the resonant quartz devices. These are incorporated into an electronic circuit and change their natural frequency of vibration as a function of the pressure applied to them. They are however expensive and the additional accuracy they afford is often not warranted.

All modern pressure transducers have diaphragms that move very little over their pressure range. This has important consequences for installations in low permeability grouts or rocks as very little fluid volume is required to actuate them. This is in contrast to an open standpipe which has a high volumetric requirement to fill the pipe.

### **Borehole installations**

The use of the standpipe type piezometer has obvious limitations not least of which is that it is unsuitable for formations in which the fluid is a gas, as this would escape unless sealed in by a packer. It is also difficult to install multiple standpipes in a single hole due to space restrictions. This applies particularly where each standpipe tip or pressure transducer has to have placed around it a porous sand or gravel pack which is then isolated by bentonite and grout.

Early work by Penman (1961) demonstrated that the development of gauges utilising low vibrating wire technology enabled direct placement in clay soils or in bentonite plugs within a well. Penman demonstrated, in accordance with sound soil mechanics theory, that clay will respond to a change in stress by an equivalent change in pore pressure. This work was further developed by Vaughan (1969) and McKenna (1995), in quantifying the relationship and requirements between the borehole backfill using bentonite grouts and the surrounding ground, and in doing so established the suitability of the new sensor technology for ground water monitoring.

Mikkelsen and Green (2003) demonstrated the use of Portland cement to stabilise bentonite grouts and improve placement. They also demonstrated the effectiveness of grout for zonal isolation, and quantified permeability and transducer response times for various grout mixes. This work was for shallow wells used for monitoring soil. It should be noted that the early work by McKenna (1995) used cement to stabilise bentonite slurries, and later bentonite was used as a viscosifier to stabilise cement slurries. The practice of cementing multiple pressure gauges in a cement grouted borehole grew, and was taken up by the oil and gas industries, with transducers attached to the outside of casing which

would be cemented into a well (borehole). In the coal seam gas industry a number of transducer installations have been made in specific monitoring wells. Unfortunately this rush to install single or multiple transducers in cement grouted boreholes has not been without its failures. As suppliers of equipment (transducers and data acquisition systems) Sigra Pty Ltd has been in a good position to gain feedback on installation successes and failures. This information has assisted in development of systems for reliable installation.

The problems observed by Sigra in transducer installation include:

- 1) Improper location of transducers. This particularly applies to the cases where transducers are connected to polyethylene pipes which are dimensionally unstable and tend to float in water, and do so to a greater degree when cement grout is pumped into the borehole.
- 2) Damage to the transducer string or failure to reach the correct depth due to collapse within the borehole.
- 3) Gas movement to surface within the cable sheath.
- 4) The use of high water content cement grouts, without correct admixtures, which then exhibit excessive separation within the borehole (bleed). These are usually used as they are easy to pump.
- 5) The use of bentonite, which raises the cement grout viscosity, causing pumping difficulties at suitable mixtures.
- 6) Excessive heat generation on cement grout hydration causing failure of the transducer or cable.
- 7) Channelling of the cement grout caused by gas bleed or water movement, leading to interconnection of zones.
- 8) Loss of water from cement grout into the formation causing dense, ultra-low permeability zones within it, thus impeding the transducer's hydraulic connection to the zone where pressure is to be monitored.
- 9) The occurrence of hydrofracturing of the formation caused by the pressure of the cement grout within the borehole exceeding the minimum stress of the rock. This is primarily a function of the density of the grout and the depth of the hole.
- 10) Excessive cement grout pressure causing a shift in transducer calibration.

Some of these problems were observed closely, some were discovered by experience, and others were obtained anecdotally. The exact number of failures in installation is not known but it is estimated that most installations conducted in the coal seam gas and mining industry are less than ideal and therefore unreliable. For these reasons special installation and grouting systems for transducer installation have been developed.

### **Cement grout behaviour**

Cement grouts are a mixture of water and Portland cement with various admixtures so that they develop the correct properties. The process of setting involves the hydration of the cement and the development of bonds between the hydrated particles. In a cement water paste with just enough water for hydration the void volume left after setting will be approximately 18% (Neville and Brooks, 1987). Excess water will lead to the filling of this space with water. As additional water is added the void space will increase. However additional dilution leads to a dispersed mixture of particles, and in water which will ultimately settle in the borehole, either before or late in the hydration process. If the latter occurs the cement will be weak. In both cases the density of cement grout will be greater in the lower levels of the hole as will its strength, while its permeability will be lower at the base of the hole.

In an endeavour to suspend the cement particles in the water and prevent this effect it is necessary to increase the viscosity of the mixture. Increasing its viscosity however causes problems as the pressure losses associated with pumping the cement grout down a pipe into the hole may increase significantly. There is thus a need for a shear thinning cement grout so that it is pumpable.

Cement grout columns in boreholes during the fluid state suffer from sedimentation (consolidation) of the cement where the coarser grains settle more quickly. This effect may be improved by reducing the cement particle size by high energy mixing. However this is offset in part by particle agglomeration after

mixing and pumping. The grout also undergoes a change of state in its transition from a fluid, which provides hydrostatic pressure to the borehole, to a solid which has inherent structural strength. During this transition the grout becomes unstable and is susceptible to gas ingress into the internal capillary pores of the cement paste formed by the chemical hydration of the cement. This is exacerbated by the effects of consolidation and its resulting pockets of fluid. Bleed pathways can be linked together by the seam gas to form channels which will migrate naturally to these void spaces. This can affect the isolation of monitoring zones or in the worst cases even create pathways to the surface. Prevention of consolidation, with its resulting fluid pockets, is critical where a seal is required. The addition of colloidal (very fine) additives to the mix is designed to mitigate this phenomenon by maintaining the mix in a colloidal state to offset the segregation of cement grains. Gas channelling is thus resisted by the interlocking grains of cement in its fluid state until initial set occurs. Cement grouts are also susceptible to pressure filtration. A cement grout will exhibit filtration behaviour when it is being forced through any orifice be it a constriction in the pump line or a cleat in coal. This means that the thicker material remains behind and a more watery mix is passed.

In extreme cases, this will result in the formation of a skin of cement around the periphery of the borehole. This leaves behind a grout with insufficient fluid for full hydration. The process is then reversed as formation pore water is drawn back into the dehydrated zone to reach a chemical equilibrium and hydrate the remaining cement. In extreme cases this reversal can take several months or years to stabilise. If this has occurred at a transducer location the result is a zone of very low permeability around the sensor with the transducer exhibiting long stabilisation and slow response times. This effect is shown in Figure 1. The long term pressures of the aquifer being monitored show complete stabilisation, however this took three months.

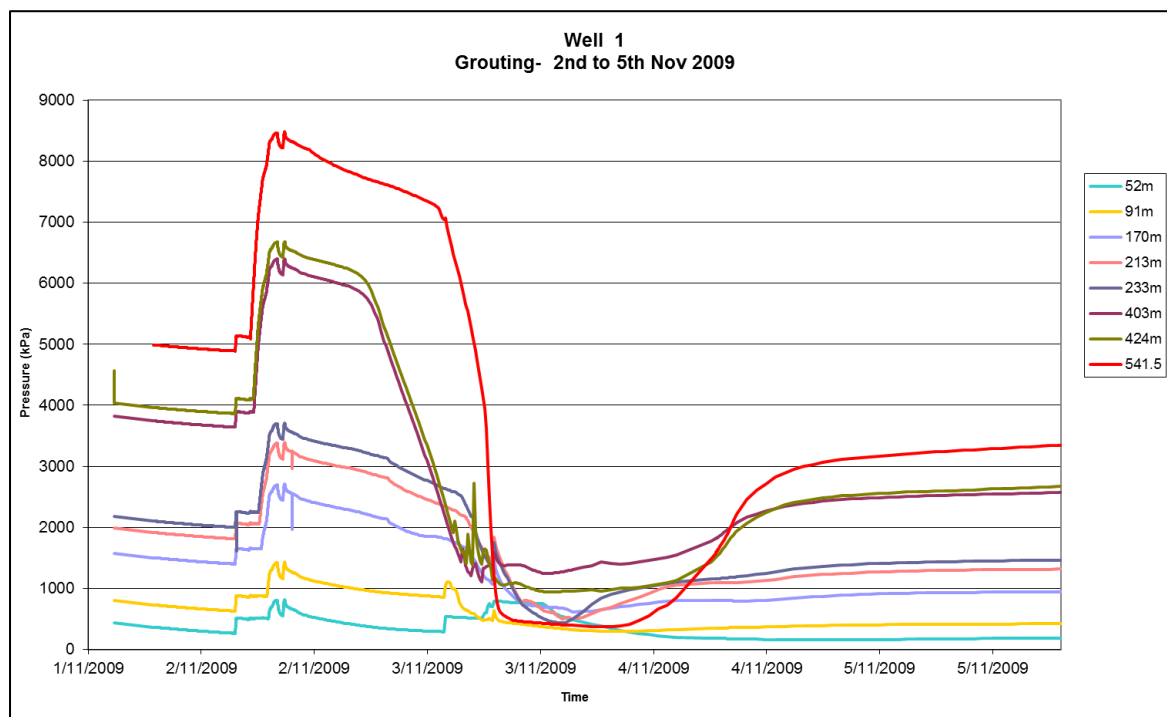


**Figure 1 - Piezometric head plots showing hydrostatic head, grout head and post grouting change of state of grout, dehydration with slow recovery on deeper transducers**

To minimise filtration, the cement grout needs to exhibit cohesion. Cohesion is essentially the shear stress of the cement grout at a very low shear rate.

The fluid grout is also susceptible to washout from aquifers. The grout is therefore also required to exhibit filtration to plug the washout zone. This characteristic is contrary to that required to minimise filtration behaviour.

It can be seen that grout for transducer monitoring wells, requires a complex set of engineering properties in both the fluid and set phase of the mix. It must have the correct rheology to be pump-able without segregation, remain in a suspension in its fluid state, be dense to displace drilling fluids and

isolate zones, remain porous for permeability when set, resist filtration to prevent dehydration, resist consolidation and formation of bleed pockets, remain cohesive to prevent gas migration, able to plug up washout zones and have a predictable set control for the given *in situ* conditions.

After extensive grout testing a suitable thixotropic (shear thinning) mix with set control which controlled most of these requirements was developed. However grout dehydration was the one aspect that could not be eliminated due to the unpredictability of the interaction of the grout with the formation. This was determined to be critical to the relevance of the data and focus shifted to eliminate this uncertainty from the transducer installation.

### NEW INSTALLATION TECHNIQUES

When making a new installation the following matters should be considered:

- 1) Improper location of transducers. The use of steel tubing enables the transducer string to be located precisely. Where coal seams exist that may need to be mined in the future, the steel is substituted by fibreglass tube.
- 2) Damage to the transducer string or failure to reach the correct depth due to borehole collapse may be prevented by installing the tubing and transducer string through an HRQ drill string and then withdrawing the drill string over the top of the transducers.
- 3) Gas movement to surface within the cable sheath. This may be readily prevented by the use of gel filled cable. Alternatives are the use of geophysical cable or Tubing Encapsulated Cable (TEC). The cost of the latter option is seldom justified.
- 4) A correct cement grout mixture requires an adequately low density, good pumping characteristics, and will remain in suspension in the borehole until it sets. This cement has a low heat of hydration to avoid overheating the transducers.
- 5) Channelling of the cement grout, caused by gas bleed or water movement and leading to interconnection of zones, is prevented by preventing segregation from the mix, maintaining a colloid in the borehole.
- 6) Loss of water from cement grout, and mitigating dehydration and filtration effects into the formation causing dense, ultra-low permeability zones within it. This problem is overcome by the use of a positive means to connect the transducer to the formation that involves water injection into the partially set cement grout around the transducer. The cement grout then sets and the connection between the transducer may be tested by injecting further water into the zone and observing the decay of pressure. The system for undertaking this is shown in Figure 2 and the results of its operation are shown in Figure 3.
- 7) The occurrence of hydrofracturing of the formation. This is caused by the pressure of the cement grout within the borehole exceeding the minimum stress of the rock and excessive cement grout pressure causing a shift in transducer calibration. These problems must be overcome by ensuring that the hydrostatic pressure of the cement grout mixture remains within adequately low limits. This gets to be more problematic with deeper holes. The solutions are to keep the density of the cement grout as low as possible, and the adoption of staged cement grouting operations. The cement grout's density can only be modified to a certain degree by the use of non-filling additives, and beyond this the use of lightweight filling additives such as hollow glass beads (cenospheres) needs to be adopted. Stage grouting involves cement grouting a lower portion of the hole, waiting for that to gain some strength and then cement grouting above this level. Figure 2 shows the inclusion of a stage cementing valve in a cementing pipe.

Figure 2 shows the fluid line to the transducer location. This is used to pressurise the grout after its initial set. This achieves a pathway from the filter tip of the transducer to the formation by fracturing the weak grout. This pathway is permanent and can be checked by re-pressurisation if required. The response of the transducer will not be affected by any filtration or dehydration of the grout. The cement displacement technique was trialled and the results are shown in Figure 3. Pressurisation of the fluid lines was carried out the morning following grouting. The fracture pressure spike and fall off is clearly seen.

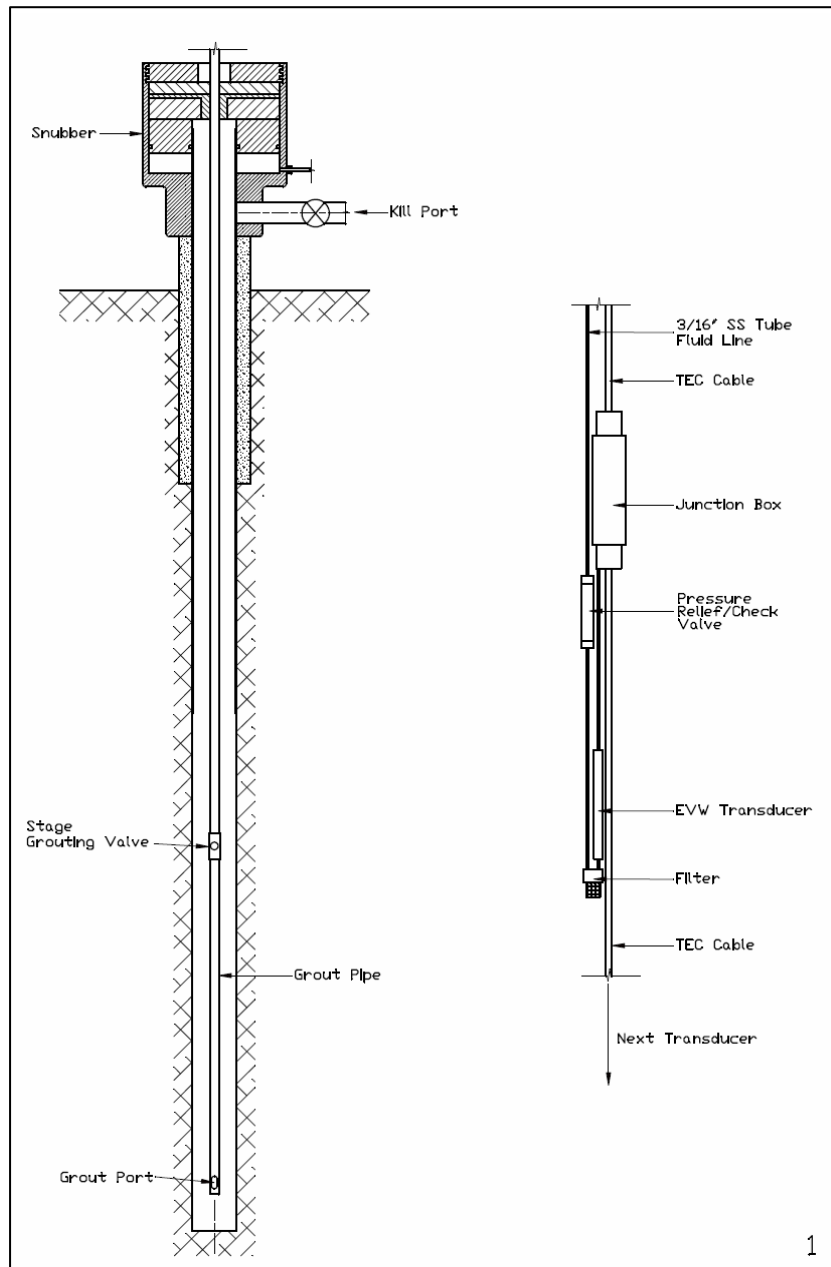


**Figure 2 - Stage grouted cemented transducer installation with details of transducer system for cement displacement on right**

### THE MONITORING SYSTEM

Monitoring pressure transducers, generally of the vibrating wire type, are connected to a data logger. The frequency of monitoring needs to be tailored to suit its intended purpose and the predicted speed at which changes may occur. The frequency may vary, from recording daily for monitoring a stable aquifer, to seconds for transient testing. To reduce the amount of data recorded it is desirable to set the data acquisition system to measure frequently but record on change with a minimum recording rate (say once per day) to ensure that the system itself can be monitored and to confirm it is working.

### DATA ACQUISITION

Sigra provides its own data acquisition equipment. This is based on a building block which will read multiple kinds of sensor and communicate with other devices through a variety of systems including cable, radio and the cell phone network. These devices have the ability to record on change, send messages when instructed or turn devices such as pumps, on and off.

These units can communicate with each other in a mesh or array. This array is frequently connected to a master unit that communicates with the cell phone network. This automated delivery of data can be further enhanced with access via a secure web based server, with data in its raw form and/or managed with graphics interface. The system can also be used with manual download of data by cable or radio. The installed units are inherently weatherproof in instrumentation cabinets with solar cells, modems and rechargeable batteries contained in the one box for security. Atypical installation is shown in Figure 4.

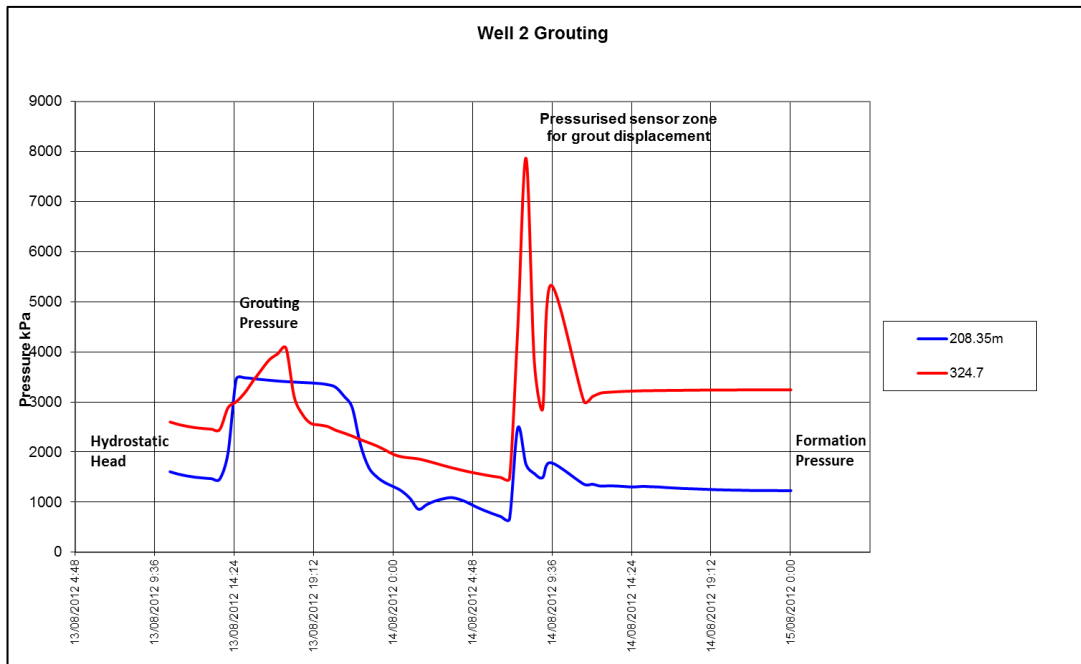


Figure 3 - Plot of post grouting displacement of cement to achieve connectivity to the formation



Figure 4 - Data acquisition system with logger box and modem

## CONCLUSIONS

A review of pressure sensing hardware and the engineering practice for installation and cementing of transducers in relatively shallow ground water monitoring wells was carried out. This revealed the suitability of both vibrating wire transducer technology and the use of cement grouts for monitoring soil formations. However, it was found that this success did not readily transfer across to deeper wells or for monitoring coal seams. Poor installation and cementing techniques resulted in suspect or no data.

Research into installation methodologies was undertaken and extended to understand both the chemistry and rheology of cement grout. A grout was developed and tested to address the criteria for cementing transducers, namely pumpability, grout consolidation, and prevention of gas migration and channelling from coal seams. This technology had been applied to coal seam gas monitoring wells with some success, although evidence was found that grout dehydration could occur, resulting in long recovery times for transducer response.

The mechanism within grout columns such as consolidation, filtration, dehydration and gas channelling, which would result in poor transducer response, was revealed through the review of the chemistry of hydration of Portland cement in boreholes. It was found by close examination of current transducer data that the critical problem of grout dehydration needed to be addressed.

Laboratory testing was carried out on a range of mix designs and additives. A thixotropic grout mix design performed best to address most of the engineering requirements, but transducer response remained at the mercy of the fickle formation / grout interaction. A method for providing a direct connection to the seam at the transducer location was developed and tested in the field. This method effectively solves the problem of grout dehydration affecting the transducer response. For deeper or highly gaseous wells, staged cement grouting techniques are required to prevent hydraulic fracturing of the formation.

Technological developments in electronic data logging can now provide real time data acquisition from remote sites using either mobile dial up or radio telemetry. This ensures the user is only an iPhone, iPad or web-link away from the current data download and its integrated graphics interface. Some of the installation techniques described in this paper are the subject of patent applications.

## REFERENCES

- McKenna G.T. 1995. Grouted-in installations of piezometers in boreholes. *Canadian Geotechnical Journal* 32, pp. 355-363.
- Mikkelsen, P.E. and Green, G.E. 2003. Piezometers in fully grouted boreholes. *Symposium on Field Measurement in Geomechanics, FMGM 2003, Oslo, Norway*.
- Neville A.M. and Brooks J.J. 1987. *Concrete Technology*, pp. 101-108, Essex, Longman Scientific and Technical.
- Penman, A.D.M. 1961. A study of the response time of various types of piezometers. In *Pore Pressure and Suction in Soils*. British Geotechnical Society: 53-58. London: Butterworths.
- Vaughan, P.R. 1969. A note on sealing piezometers in boreholes. *Geotechnique*, Vol.19, No. 3 pp. 405-413.

# ASSESSMENT OF AN ENVIRONMENTAL SUSTAINABILITY INDEX FOR THE UNDERGROUND COAL GASIFICATION PROCESS BY USING NUMERICAL ANALYSIS

Vidal Navarro Torres<sup>1</sup>, Anthony Steven Atkins<sup>2</sup> and Raghu Nath Singh<sup>3</sup>

**ABSTRACT:** In this study, an innovative numerical model is developed to quantify the environmental sustainability situation of an in-situ underground coal gasification (UCG) process which is expressed in terms of an Environmental Sustainability Index (ESI). This approach is based on four environmental indicators, namely: (i) rock and soil subsidence, (ii) groundwater quality, (iii) surface water quality and (iv) atmospheric quality, respectively. Based on the ESI values, this paper proposes a methodology for classifying the environmental sustainability state of the underground coal gasification (UCG) process and also proposes the corresponding Threshold Limit Value. Finally, a mathematical model is developed which is applied to El Tremedal Spanish trial.

## INTRODUCTION

The Underground Coal Gasification (UCG) technique is an environmentally friendly process of extracting thermal energy compared to conventional underground and surface coal mining operations. The UCG process produces gas suitable for high-efficiency power generation by providing high-pressure product gas which can be easily treated to eliminate solid waste discharge and also has fewer particulates such as NO<sub>x</sub> and SO<sub>x</sub>. The UCG cavity is a potential for CO<sub>2</sub> sequestration locations and a source of low-carbon hydrogen for transport and other applications. In spite of these potential benefits, the process still creates environmental risks.

The UCG process, involves air or oxygen pumped into an underground coal seam through an injection well. The introduction of an oxidizing gas produces heat, which partially combusts the coal in-situ and creates the synthesis gas (syngas) product Friedman(2009), primarily composed of hydrogen, carbon monoxide, and smaller amounts of carbon dioxide and methane Friedman (2009), Stephen *et al.* (1985). The syngas is extracted from the UCG burn cavity by a production well, which brings the gas product to the surface for energy or power station utilization.

A review of the world's historical UCG sites in the former Soviet Union, Europe, United States, New Zealand, Australia and China between 1974 and 2002 revealed a limited number of pilot projects and full-scale operations, suggesting two main environmental risks associated with UCG processes.

Firstly there is a risk of groundwater contamination and organic contaminants such as Polycyclic Aromatic Hydrocarbons (PAHs) may be generated during combustion of coal, and trace metals in the coal may be released through geochemical reactions induced by the UCG process. Contaminants may also be released from adjacent geological formations and these organic and metal contaminants could migrate and contaminate groundwater aquifers. Secondly, because the *in situ* burning of coal creates cavities in the subsurface, there is a risk of ground subsidence, whereby the overlying rock layers partially collapse into the newly created void space. Subsidence creates a hazard for any surface infrastructure that might be present above the UCG zone, and may create detrimental changes in surface or groundwater hydrology above the cavity (Sury, *et al.*, 2004, Walter, 2007).

Another potential environmental impact risk in UCG constitutes the atmosphere air pollution following gas utilization and surface water pollution. These UCG environmental situations need to be managed on the basis of sustainability. In this context, the research focuses on the Environmental Sustainability Index and will be an important contribution to sustainable UCG. Currently there are no standard references for the assessment of sustainability levels and this paper makes an attempt to quantitatively

<sup>1</sup> Department of Mining Engineering, Technical University of Lisbon, A.V. Rovisco Pais 1049-011, Portugal

<sup>2</sup> Professor, Faculty of Computing, Engineering and Sciences, Staffordshire University, Stafford ST18 0AD, U.K

<sup>3</sup> Professor, Centre for Geo-mechanical Research, Department of Civil Engineering, University of Nottingham, University Park, Nottingham NG7 2RD, U.K.

assess by developing and Environmental Sustainability Index (ESI) for UCG (Navarro Torres, Singh and Pathan, 2008), based on four main environmental indicators: atmosphere quality, surface water quality, rock and soil subsidence, and groundwater quality.

The quantitative model to calculate the environmental sustainability condition developed by the first author (Navarro Torres) was first applied to underground mines in 2006 having been introduced to model three environmental indicators: geotechnical, groundwater and underground atmosphere (Navarro and Dinis, 2006). Based on these encouraging results, in 2008 this was applied to mine water environmental assessment considering three environmental indicators: physic-chemical properties, toxic components and other components (Navarro, *et al.*, 2008).

In both cases the results were excellent, so it was decided to apply this concept and develop the numerical model of the environmental sustainability in UCG process based on the Environmental Sustainability Index (ESI).

## POTENTIAL OF ENVIRONMENTAL IMPACT IN UCG

### Environmental interactions in the UCG process

In the UCG process the physic-chemical interactions changes the natural stress state in the surrounding rock mass, influencing in contaminants formations in the UCG reactor and through the surrounding ground, as well as inducing potential subsidence and pollutions of the groundwater, surface water and atmospheric Quality (Figure 1).

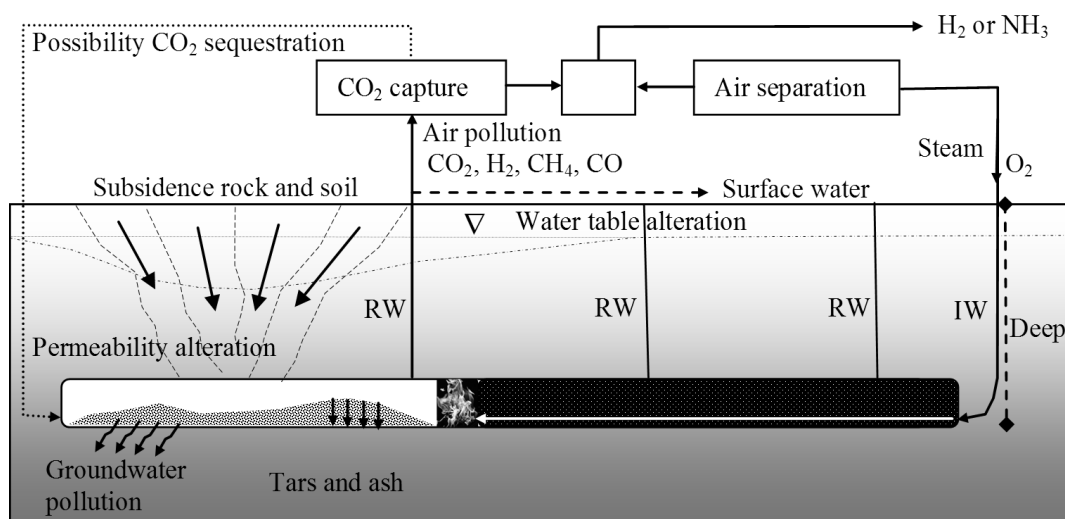


Figure 1 - Summary of UCG vs. environment interactions

Drilling and gasification actions would cause important alteration in the rock mass and in the virgin water table. These alterations would adversely influence the effects of subsidence. The gasification cavities of the coal seams are sources of gaseous and liquid pollutants and they constitute some environmental risks to groundwater in the adjacent strata, depending on whether the contaminants can migrate beyond the immediate UCG reactor zone.

### Characterisation of the environmental indicators in the UCG process

#### Subsidence

In the UCG process, the potential of subsidence will be quite small compared to underground mining, as exemplified in Centralia and Chinchilla where negligible subsidence was experienced (Friedman and Upadhye, 2004). However, subsidence risk is present, as demonstrated by numerical modelling results (Ren, *et al.*, 2003), while observed important displacements occurred around UCG cavities. In the UCG process an underground cavity is opened from coal seam burning into a stressed rock mass and the stresses in the vicinity of the new opening are re-distributed.

Before the cavity is opened, *in situ* stresses are uniformly distributed in the area of rock under consideration. After removal of the coal seam from within the cavity, the stresses in the immediate vicinity of the cavity are changed and new stresses are induced. The stresses values are varied depending of depth, the structural and geotechnical properties of the rock mass surrounding UCG cavity. As the induced stresses overcome the tensile or compressive rock mass strength this will cause failure and a potential horizontal or vertical extension of the cavity and may ultimately lead to a subsidence above cavity (Hoek, 2000, Navarro, *et al.*, 2011).

### Ground water contamination

The main pollutants of groundwater quality in UCG are results of the coal burning processes; these could include benzene, toluene, ethyl-benzene, and xylenes (BTEX), phenols, coal ash and tars, aromatic hydrocarbons and sulphides, NO<sub>x</sub>, NH<sub>3</sub>, boron, cyanide, CO and H<sub>2</sub>S (Creedy, *et al.*, 2001) (Table 1). Phenol leachate is regarded as the most significant environmental hazard due to its high water solubility and high affinity to gasification (Shuquin and Jun-hua, 2002).

Uncontrolled migration and leakage of the syngas itself could result in contamination of overlying aquifers. In addition, bye-products, such as organic contaminants (PAHs, phenols, and benzene), as well as inorganics (sulphate, boron, and metals and metalloids such as mercury, arsenic, and selenium), may be inadvertently generated from the coal during the UCG process (Sury, *et al.*, 2004; Liu, *et al.*, 2006). Mercury, arsenic, and selenium are volatile, and they can also be released as gases during the UCG process. Their liberation could possibly negatively affect the underground water and air qualities.

**Table 1 - Main groundwater pollutants found in Texas UCG pilot sites (Creedy, *et al.*, 2001)**

Chemical constituent		Before burn (mg/l)	After burn (mg/l)	Increase	
Name	Symbol			(mg/l)	%
Hydrogen sulphide	H <sub>2</sub> S	4	1150	1146	28650
Ammonia	NH <sub>3</sub>	1	100	99	9900
Phenols	C <sub>6</sub> H <sub>5</sub> OH	0.1	20	19.9	19900
Acidity	pH	-	7.6	-	-

Rock masses, the mineralogy and trace impurities, immediately adjacent to the targeted coal seam will also likely be influenced by UCG operations, and thus, oxidation and other geochemical processes in the surrounding rock could also result in the release of contaminants (Stratus Consulting Inc. 2010).

### Surface water contaminations

The potential pollution of surface water in UCG is extremely low, and the common pollutants are phenols, ammonia, chemical oxygen demand (COD), pH, conductivity and sulphides (Sury, *et al.*, 2004). The surface water can be affected by groundwater pumping and drilling operations and in a Spanish trial, the water pumped to the surface was polluted with phenol (500 ppm) (Green, 1999).

### Atmosphere contamination

The major constituents of the product gas from UCG are CO<sub>2</sub>, H<sub>2</sub>, CH<sub>4</sub>, and CO. An example for UCG trial process for bituminous coal with sulphur, chlorine and nitrogen contents of 2.0%, 0.8% and 0.2% in weight respectively give a product gases emission which was 22.7% of H<sub>2</sub>O, 46.1% of CO<sub>2</sub>, 19.2% of CO, 9.4% of CH<sub>4</sub>, 1.6% of H<sub>2</sub> and 1.0% of others (H<sub>2</sub>S, HCl, N<sub>2</sub>).

For air quality, however, the unused gases are not put into the atmosphere, but this process end by gas clean-up and then combustion. It seems therefore, that the environmental impact should be assessed on the amount of contamination that is emitted after utilization, and since these are controlled by emissions legislation for SO<sub>x</sub>, NO<sub>x</sub>, etc, the abated plant will always meet the current standards. For control action the CO<sub>2</sub> emissions are penalised by payment of the carbon tax (Green, 1999).

**MATHEMATICAL MODEL TO ASSESS AN ENVIRONMENTAL SUSTAINABILITY INDEX FOR UCG**

**Structure of Environmental Sustainability Index of UCG**

The key for sustainable development of UCG will comprise of three "basic pillars": economic, social and environmental. In the present paper a quantitative model is developed to assess the environmental component of UCG process, which is called the Environmental Sustainability Index ( $ESI_{UCG}$ ) (Figure 2).

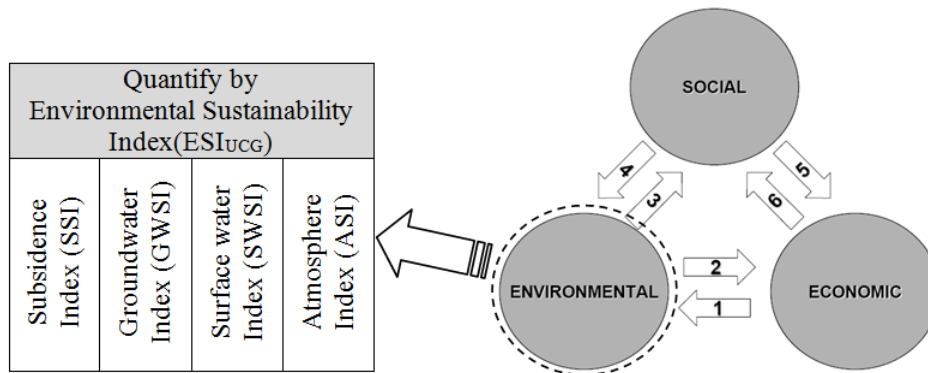


**Figure 2 - Pillars of UCG sustainable development and quantification of the environmental components by environmental sustainability index**

The global quantitative expression of sustainable development (SD) in UCG is a complex task since it involves a large numbers of parameters (6 shown in Figure 2) and data involved throughout the life cycle of the UCG process. In the proposed model the expression of the SD by Sustainability Index that is an innovative and important method, because it allows a quantification of SD and enables efficient management of SD, compared with admissible sustainability values previously defined.

The proposed  $ESI_{UCG}$ , is a composite of a four dimensional structure as shown in Figure 3, that is formed by indicators which have many sub-indicators depending on the type, dimension, location and other characteristics of the UCG operations.

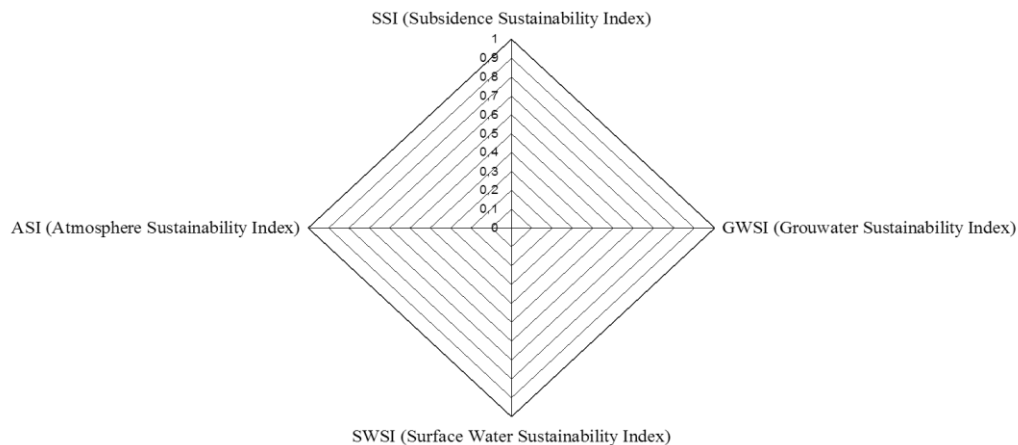


**Figure 3 - Structure of Environmental Sustainability Index for UCG**

The relationship between the four SD indicators of the potential environmental impact and the Environmental Sustainability Index of the UCG ( $ESI_{UCG}$ ) is given by equation (1), which is a function of a Subsidence Sustainability Index (SSI), Groundwater Sustainability Index (GWSI), Surface Water Sustainability Index (SWSI) and Atmosphere Sustainability Index (ASI).

$$ESI_{UCG} = \frac{1}{4}(SSI + GWSI + SWSI + ASI) \tag{1}$$

Equation (1) expresses the Environmental Sustainability Index of the UCG process based on the criterion of equal weighting of the four environmental indicators. Section 2.2 i of this paper shows that in the UCG process, where contamination of groundwater and subsidence are major environmental hazards and the pollution of surface and atmosphere have only a few incidences there is still a potential risk. This difference in size or occurrence of each of the four environmental indicators are considered in their specific mathematical models and presented as follow.

To calculate the sustainability index (SI) of each component, the condition of sustainability of each pollutant is based on environmental standards given for the norms. Three criteria are taken considering the local environmental condition with variable  $x_i$ :

- 1) When the sustainability is  $x_i \leq X$ , when X is maximum standard
- 2) When the sustainability is  $x_i \geq Y$ , when Y is minimum standard
- 3) When the sustainability is  $Y \leq x_i \leq X$ , when Y and X are minimum and maximum standards.

Considering the conditions of criterion 1, the SI can be calculated using the equation (2), based on condition  $x_i \leq X$ . In this criterion when  $x_i$  values are less the sustainability is high. In this case X is a maximum standard (Figure 5).

$$SI = 1 - \left| \frac{x_i}{X} \right| \quad (2)$$

Incorporating the following two conditions:

- 1) If  $x_i = X$  or  $x_i > X \rightarrow SI = 0$
- 2) If  $x_i = 0 \rightarrow SI = 1$

In the conditions of criterion 2, the SI can be calculated using the equation (3), based on condition  $x_i \geq Y$  where high values of  $x_i$  generate high values of sustainability. In this case X corresponds to a minimum standard (Figure 6).

$$SI = \left| \frac{x_i}{Y} \right| \quad (3)$$

Incorporating the following two conditions:

- 1) If  $x_i = Y$  or  $x_i > Y \rightarrow SI = 1$
- 2) If  $x_i = 0 \rightarrow SI = 0$

Considering the criterion 3 for minimum and maximum admissible standards values, the SI can be calculated using equation (4) when  $x_i \geq X$  and when  $x_i = X_1$  is unsustainable and, also considering the criterion 3, the SI can be calculated by equation (5) when  $x_i \leq Y$  and  $x_i = Y_1$  is unsustainable.

If

$$x_i \geq X \rightarrow SI = 1 - \frac{x_i - X}{X_1 - X} \quad (4)$$

Incorporating the following two conditions:

- 1) If  $Y < x_i < X$  or  $x_i = X \rightarrow SI = 1$
- 2) If  $x_i = X_1 \rightarrow SI = 0$

$$\text{If } x_i < Y \rightarrow SI = 1 - \frac{Y - xi}{Y - Y_1} \tag{5}$$

Incorporating the following two conditions:

- 1) If  $Y < x_i < X$  or  $x_i = Y \rightarrow SI = 1$
- 2) If  $x_i = Y_1 \rightarrow SI = 0$

**Subsidence Sustainability Index (SSI)**

Reactor cavities formed during UCG process may affects the surface and subsurface structures (such as landscapes, surface water, water table, etc.), but their presence also alters ground movement around these cavities. The terms defining the geometry and settlement and the coordinate system which will be adopted throughout this paper are defined in Figure 4.

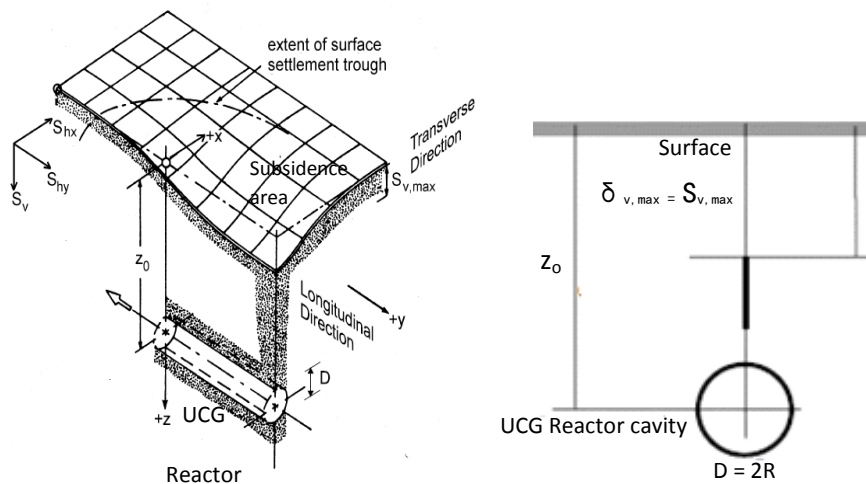


**Figure 4 - Subsidence model of UCG process and parameters influencing ESI<sub>UCG</sub>**

Building risk damage from subsidence classification is based in horizontal tensile strain in five categories:

- categories 0 to 2 ( $\epsilon_h = 0 - 0.15\%$ ) correspond to aesthetical damage,
- serviceability damage occurs in categories 3 and 4 ( $\epsilon_h = 0.15 - 0.3\%$ )
- stability of the structure is affected by damage of category 5 ( $\epsilon_h > 0.3\%$ ) (17).

Horizontal tensile strain develops as a change in length over the corresponding length.

The mathematical model for obtaining SSI is based on the limiting horizontal tensile strain as given in Table 2, where  $\epsilon_h > 0.15$ . Using the limiting values of the potential damage to the modern infrastructures (buildings) in equation (2), the subsidence sustainability index (SSI) can be calculated by using equation (6) as follows:

$$SSI = 1 - \frac{\epsilon_h}{\epsilon_{h(L)}} = 1 - 6.67\epsilon_h \tag{6}$$

where,

- $\epsilon_h$ , horizontal soil displacement (%) as calculated by equation (7), and
- $\epsilon_{h(L)}$  is the admissible horizontal soil displacement (0.15%).

Note :  $\epsilon_{h(L)}$ : Limiting Tensile strain

$$\epsilon_h = \frac{\delta_{v,max}}{z_o} \left( \frac{x^2}{i_x^2} - 1 \right) \tag{7}$$

In Equation (3)  $\delta_{v,max}$  is the maximum vertical settlement above the reactor cavity axis and can be calculated by equation (8),  $z_o$  is the depth of the cavity axis below the surface,  $x$  that denotes the distance from the tunnel centre line in the transverse direction and  $i_x$  is the distance of cavity axis to the point of inflection in Gauss curve as shown in Figure 4.

**Table 2 - Subsidence standard based in the limiting tensile strain (Burland, 1995)**

Category of Damage	Normal Degree of Severity	Limit Value- $\epsilon_{h(L)}$ (%)
0	Negligible	0-0.05
1	Very slight	0.05-0.075
2	Slight	0.075-0.15
3	Moderate	0.15-0.3
4 to 5	Severe to Very severe	>0.3

$$\delta_{v,max} = \sqrt{\frac{\pi}{2}} \frac{V_L D^2}{4i_x} e^{\frac{x^2}{i_x^2}} \tag{8}$$

where  $V_L$  is the volume loss calculated by equation (9) based on Borms and Bennemark proposals(9) and  $D$  is the reactor cavity diameter (Figure 5).

$$V_L = 1.33 \left( \frac{P_t - P_s}{\sigma_t} \right) - 1.4 \tag{9}$$

where,

$P_t$  is the total overburden pressure at tunnel axis level (including any surcharges);

$P_s$  is the cavity pressure (if present), and

$\sigma_t$  is the un-drained shear strength of rock or soil.

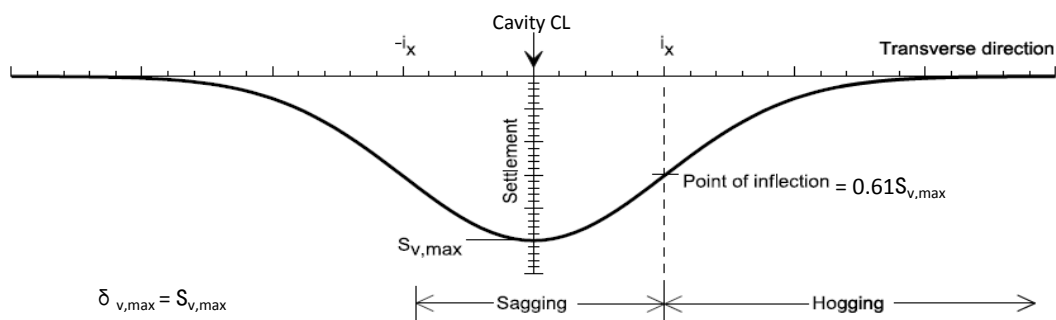


**Figure 5 - Gauss curve of displacements in transverse direction**

### Groundwater Sustainability Index (GWSI)

The groundwater sustainability index (GWSI) can be calculated by using equation (10).

$$GWSI = \frac{1}{n} \left( n - \frac{\sum_{i=1}^{l_1} GW_{1(i)}}{l_1.LV_1} - \frac{\sum_{i=1}^{l_2} GW_{2(i)}}{l_2.LV_2} - \frac{\sum_{i=1}^{l_3} GW_{3(i)}}{l_3.LV_3} - \dots - \frac{\sum_{i=1}^{l_n} GW_{n(i)}}{l_n.LV_n} \right) \tag{10}$$

where,

$n$  is the number of groundwater pollutants,

$l_1, l_2, l_3, \dots, l_n$  are local quantities,

$GW_1, GW_2, GW_3, \dots, GW_n$  are groundwater pollutants and

$LV_1, LV_2, LV_3, \dots, LV_n$  are limit values of the groundwater quality standard.

For six environmental indicators number ( $n=6$ ), when pollutants are Hydrogen sulphide ( $H_2S$ ), Ammonia ( $NH_3$ ), Phenols ( $C_6H_5OH$ ), pH, conductivity ( $C$ ) and Benzene ( $C_6H_6$ ), using the average Groundwater Quality Standards (Table 3) and applying equation (2), the groundwater sustainability index (GWSI) can be calculated for the following two conditions:

- For the pH values  $<6$  and unsustainable  $pH=0$ , applying equation (4) results in equation (11);
- For  $pH>9$  and unsustainable  $pH=14$ , applying equation (5) results in equation (12).

Thus, for  $pH<6$  and unsustainable  $pH=0$ :

$$GWSI = 0.8 - 2.86H_2S - 8NH_3 - 0.0033C_6H_5OH - 0.04C_6H_6 - 0.0002C + 0.03pH \quad (11)$$

For  $pH>9$  and unsustainable  $pH=14$ :

$$GWSI = 1.3 - 2.86H_2S - 8NH_3 - 0.0033C_6H_5OH - 0.04C_6H_6 - 0.0002C - 0.04pH \quad (12)$$

**Table 3 - Groundwater quality standards (Wisconsin Natural Resource Board, 2008; State Water control Board, 2004)**

Pollutant	Limit Value	Institution	Application
$H_2S$	0.07 mg/kg	US – EPA, 2004	Human health
$NH_3$ ( $N_2$ )	0.025 mg/l	Virginia State, US, 2004	Public health or welfare
$C_6H_5OH$	6 mg/l	Wisconsin State, US, 2008	Public Health
pH	6 – 9	Virginia State - US , 2004	Public health or welfare
$C_6H_6$	5 $\mu$ g/l	Pennsylvania State, US, 2001	Public health
Conductivity	1000 $\mu$ S/cm	European quality at 20 °C	Public health

It is well known that the pH scale ranges from 0 to 14 and it measures the acidity for values less than 7; with a pH value of 7 is neutral and a pH greater than 7 is basic. The  $pH=0$  and  $pH=14$  are unsustainable values, because they represent the extreme acidic and basic conditions.

### Surface Water Sustainability Index (SWSI)

The surface water sustainability index (SWSI) can be calculated by using equation (13) as follows:

$$SWSI = \frac{1}{m} \left( m - \frac{\sum_{i=1}^{l_1} SW_{1(i)}}{l_1 \cdot VL_1} - \frac{\sum_{i=1}^{l_2} SW_{2(i)}}{l_2 \cdot VL_2} - \frac{\sum_{i=1}^{l_3} SW_{3(i)}}{l_3 \cdot VL_3} - \dots - \frac{\sum_{i=1}^{l_m} SW_{m(i)}}{l_m \cdot VL_m} \right) \quad (13)$$

where,

$m$  is the surface water pollutants quantity;

$l_1, l_2, l_3, \dots, l_m$  are local quantity;

$SW_1, SW_2, SW_3, \dots, SW_m$  are surface water pollutants and

$LV_1, LV_2, LV_3, \dots, LV_m$  are limit values of surface water quality standard.

For the following four environmental indicator ( $m=4$ ): Phenols ( $C_6H_5OH$ ), Ammonia ( $NH_3$ ), pH and Conductivity using the Surface Water Quality Standards (Table 4) and applying equation (2) for pH values between 6 to 9, the surface water sustainability index (SWSI) can be calculated for the following two conditions:

- Applying equation (4) when  $pH<6$  and unsustainable when  $pH=0$ , and results in equation (14) as follows.

$$SWSI = 1 - 250C_6H_5OH - 10NH_3 - 0.00025Conduct + 0.042pH \quad (14)$$

- For  $pH>9$  and unsustainable  $pH=14$ : results are given by equation (15)

$$SWSI = 1.45 - 250C_6H_5OH - 10NH_3 - 0.00025Conduct - 0.05pH \quad (15)$$

**Table 4 - European surface water quality standards**

Pollutant	Limit Value	Application
C <sub>6</sub> H <sub>5</sub> OH	0.001 mg/l	Human
NH <sub>3</sub> (N <sub>2</sub> )	0.025 mg/l	Fish
pH	5.5 – 9.0	Human
Conductivity	1000 to μS/cm at 20 °C	Human

**Atmosphere Sustainability Index (ASI)**

The Atmosphere Sustainability Index (ASI) in UCG process will be calculated by equation (16) where  $s$  is the number of atmosphere pollutants;  $l$  is the local quantity around the emission points.

$$ASI = \frac{1}{p} \left( p - \frac{\sum_{i=1}^{l_1} A_{1(i)}}{l_1 \cdot VL_1} - \frac{\sum_{i=1}^{l_2} A_{2(i)}}{l_2 \cdot VL_2} - \frac{\sum_{i=1}^{l_3} A_{3(i)}}{l_3 \cdot VL_3} - \dots - \frac{\sum_{i=1}^{l_p} A_{p(i)}}{l_p \cdot VL_p} \right) \quad (16)$$

where,

$p$  is the atmosphere pollutants quantity;

$l_1, l_2, l_3, \dots, l_p$  are local quantity and ASI;

$A_1, A_2, A_3, \dots, A_n$  are groundwater pollutants and

$LV_1, LV_2, LV_3, \dots, LV_p$  are limiting values of air quality standard.

For four environmental indicators ( $r=4$ ), using average values of Atmospheric Quality Standards (Table 5) and applying equation (16) for CO<sub>2</sub> and equation (2) for CO, and equations (4) and (5) for H<sub>2</sub> and CH<sub>4</sub> gases respectively, results in equations (17) and (18). The H<sub>2</sub> standard varies from 4% to 74.2% and CH<sub>4</sub> from 5% to 14%.

(a) For H<sub>2</sub><4% and CH<sub>4</sub><5% and unsustainable H<sub>2</sub>=0 and CH<sub>4</sub>=0: equation (17) gives:

$$ASI = 0.5 - 0.00005CO_2 + 0.063H_2 + 0.05CH_4 - 0.005CO \quad (17)$$

(b) For H<sub>2</sub>>74.2% and CH<sub>4</sub>>14% and unsustainable H<sub>2</sub>=100 and CH<sub>4</sub>=100: equation (18) represents:

$$ASI = 1.76 - 0.00005CO_2 - 0.0097H_2 - 0.0029CH_4 - 0.005CO \quad (18)$$

**Table 5 - Atmosphere quality standard (Navarro, 2006)**

Pollutant	Limit Value	Institution
CO <sub>2</sub>	5000 ppm	Mine Safety and Health Administration - USA
H <sub>2</sub>	4% - 74.2%	Bureau of Mines Diagram - USA
CH <sub>4</sub>	5% - 14%	Bureau of Mines Diagram - USA
CO	50 ppm	Mine Safety and Health Administration - USA

The environmental pollutant quantities ( $n, m, s$ ) depend upon geological, hydro-geological, physicochemical, operational conditions, etc. of UCG process.

**PROPOSED PERMISSIBLE MINIMUM LEVEL OF ESI<sub>UCG</sub>****Proposed ESI<sub>UCG</sub> levels and sustainability criteria**

The proposals of ESI<sub>UCG</sub> for standardizing the permissible minimum level of SD in UCG are expressed by coefficients varying between 0 and 1, Table 6.

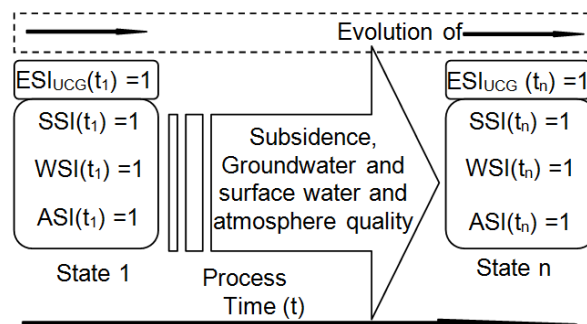
**Table 6 - Proposals of  $ESI_{UCG}$  for permissible minimum level assessment**

$ESI_{UCG}$	$ESI_{UCG}$	$ESI_{UCG}$	$ESI_{UCG}$	$ESI_{UCG}$
$0.0 \leq 0.25$	$0.25 \leq 0.50$	$0.50 \leq 0.75$	$0.70 \leq 1.00$	1.00
Very Low	Low	Moderate	Good	Very Good

The UCG sustainability will vary when subsidence, groundwater, surface water, and atmosphere quality vary with time. The permissible sustainability is obtained when  $ESI_{UCG}$  is 1 (Figure 6).

### Environmental quality standards

The UCG subsidence assessment can be used to evaluate the type of damage to landscape, or buildings, etc. In this paper, a typical example of possible building damage is based on the tensile strain (Wisconsin Natural Resource Board Rules, 2008 ) (Table 2).

**Figure 6 - Permissible level of Environmental Sustainability Index of UCG**

Normally each region or countries have the groundwater quality standards for substances of public health or environmental goal (Navarro, 2006; El Tremedal, Final Summary Report, 1999) (Tables 3).

Based on the main potential pollutants for surface water as phenols, ammonia, chemical oxygen demand (COD), pH and conductivity, as an example are shown in the Table 4, the European surface water quality standard. As discussed earlier, the major and main potential pollutant gases emitted in the UCG process are  $CO_2$ ,  $H_2$ ,  $CH_4$ , and  $CO$ . The atmospheric air quality standard is presented in Table 5.

## NUMERICAL MODEL APPLICATION TO THE EL TREMEDAL SPANISH CASE-HISTORY

### Technical data of El Tremedal Spanish trial

The mathematical model developed above was applied to the El Tremedal trial of UCG in the Province of Teruel, Spain, with the following site characteristics:

- two dipping coal seams separated by 7 to 14 metres of limestone,
- depth of 500-700 metres and
- a seam thickness varies between 1.9 and 7.0 metres with
- a thin layer of carbonaceous clay lays under both coal seams and
- an area of continuous coal seam is at least 200 metres from any significant faults (Figure 7).

The following conditions are assumed for the measured environmental indicators in the El Tremedal trial:

- measured pollutants concentrations would be similar with hypothetical production at commercial level; measured pollutants values used any after remedial action.

- In a hypothetical production at commercial level applied to the CO<sub>2</sub> capture and underground sequestration technique; in local atmospheric air velocity the CO gas dilution even 50 meters surrounding emission point at average 40 ppm.

**9Main environmental results**

In El Tremedal UCG Spanish trials there is no report on the soil or rock subsidence because the site condition is not favourable for potential subsidence.

For the El Tremedal trial, excess water is produced during gasification and the main pollutants show in Table 7. The product gas composition in the 1<sup>st</sup> and 2<sup>nd</sup> gasification period was 14% of CO<sub>2</sub>, 12.8% of CO, 24.8% of H<sub>2</sub>, 13.2% of CH<sub>4</sub> and 8.3% of H<sub>2</sub>S (Table 8 and Figure 8) (El Tremedal, Final Report 1999).

In the El Tremedal UCS trial project the environmental impact observed on the surface facilities and the plant operations including surface water are shown in Tables 7 and 8 ( Skousan, *et al.*, 2000).

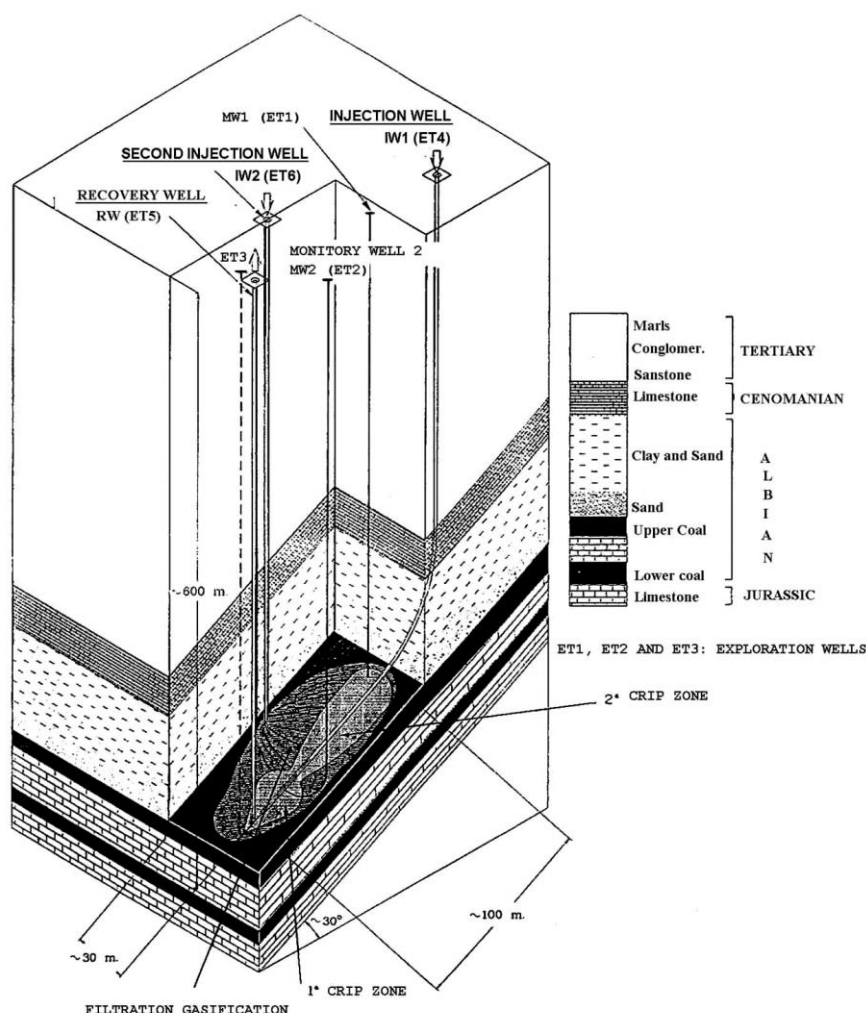


**Figure 7 - Geological and well layout of El Tremedal UCG trial (Skousen, *et al.*, 2000)**

**Table 7 - El Tremedal wastewater record concentrations (Sury, *et al.*, 2004)**

Pollutants	Record Concentrations	Pollutants	Record Concentrations
Phenols	2.6 - 575 ppm (0.26 – 57.5 mg/l)	Conductivity	1410 – 5640 μ S/cm
Ammonia	5.9 - 1080 ppm (0.59 – 108 mg/l)	COD	102 – 5880 ppm
Sulphurs	0.94 - 148 ppm (0.095 – 14.8 mg/l)	pH	8.4 – 7.6

**Table 8 - Product Gas Composition in El Tremedal Trial (El Tremedal Final Report, 1999)**

Product Gas	Gasification Period		Total	
	1 <sup>st</sup>	2 <sup>nd</sup>	%	ppm
CO <sub>2</sub>	43.4%	39.4%	41.0	410000
CO	8.7%	15.6%	12.8	128000
H <sub>2</sub>	24.9%	24.7%	24.8	248000
CH <sub>4</sub>	14.3%	12.4%	13.2	132000
H <sub>2</sub> S	8.8%	7.9%	8.3	83000

**Environmental Sustainability of El Tremedal UCS trial**

**Calculation of SSI**

The subsidence sustainability index (SSI) is calculated by using equation 6, taking the horizontal soil displacement  $\epsilon_{h(L)}$  as 0 that is negligible according to the standard quality adopted, and

$$SSI = 1 - \epsilon_h / \epsilon_{h(L)} = 1 - 6.67 \times 0 + 1$$

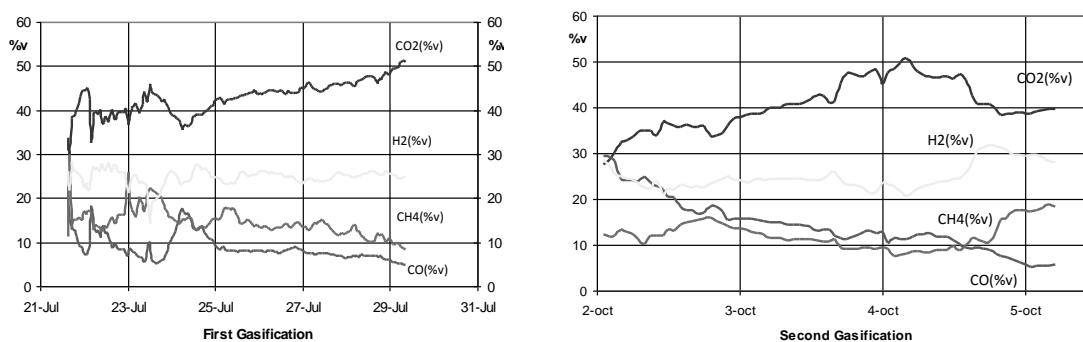


**Figure 8 - Gas Composition on Dry N<sub>2</sub> Free – 1<sup>st</sup> Gasification and 2<sup>nd</sup> gasification period (Skousan, et al., 2000)**

**Calculation of GWSI**

For calculating the Ground Water Sustainability Index (GWSI), it is necessary to analyse pH as a measured pollutant that varies between the permissive limits of Groundwater Quality Standard between 7.6 and 8.4, therefore the sustainability index of this pollutant is 1. Based on this result, with groundwater standards presented in Table 3 (H<sub>2</sub>S=0.07 mg/kg, NH<sub>3</sub>=0.025 mg/l, C<sub>6</sub>H<sub>5</sub>OH=6 mg/l, Conductivity=1000  $\mu$ s/cm-1) are applied to equations (2), (4) and (5) resulting in equation (10) as follows:

$$GWSI = \frac{1}{5} \left( 1 - \frac{H_2S}{0.07} + 1 - \frac{NH_3}{0.025} + 1 - \frac{C_6H_5OH}{6} + 1 - \frac{C}{1000} + 1 \right)$$

However, the four environmental groundwater indicators measured in El Tremedal as shown in Table 8 are greater than groundwater quality standards (Table 4) except pH. For these situations applying four pollutants values (H<sub>2</sub>S, NH<sub>3</sub>, C<sub>6</sub>H<sub>5</sub>OH and Conductivity) to equation (10) and equation (2), the ground water sustainability Index is calculated, using

$x_i = X$  or  $x_i > X \rightarrow SI = 0$ , as follows:

$$GWSI = \frac{1}{5} (0 + 0 + 0 + 0 + 1) = 0.25$$

Applying equation (13) to the condition of equation (2) for SWSI calculation, with  $SI_{pH} = 1$  for Surface Water Quality Standard, the general equation for the main pollutants result in the following equation:

$$SWSI = \frac{1}{4} \left( 1 - \frac{C_6H_5OH}{0.001} + 1 - \frac{NH_3}{0.025} + 1 - \frac{C}{1000} + 1 \right)$$

In El Tremedal UCG trial no report of surface water pollution was obtained. Therefore, the pollutant value is taken as zero and the SWSI result is as follows:

$$SWSI = \frac{1}{4}(1+1+1+1) = 1$$

### Calculation of ASI

Finally, in order to calculate atmospheric Sustainability Index (ASI) air pollutants CO<sub>2</sub>, H<sub>2</sub>, CH<sub>4</sub> and CO are measured in El Tremedal trial. Concentrations of pollutants H<sub>2</sub> and CH<sub>4</sub> are 24.8% and 13.2%, respectively, applying to Equations 16 and equation (2) and CH<sub>4</sub> which is applying the equation (16) and equation (2) results in the following equation:

$$ASI = \frac{1}{4} \left( 1 - \frac{CO_2}{5000} + 1 + 1 + 1 - \frac{CO}{50} \right)$$

The gases obtained from the El Tremedal trial production well (CO<sub>2</sub>=410000 ppm and CO=128000 ppm), are processed for utilization and after which there are air pollution potential risk, so that, for purposes of developed model application, assumes a CO<sub>2</sub> and CO of 5000 ppm and 40 ppm, respectively, to about 50 meters from the emission source for atmospheric local air velocity condition. For this assumed condition the Atmospheric Sustainability Index results in the following equation:

$$ASI = \frac{1}{4} \left( 1 - \frac{5000}{5000} + 1 + 1 + 1 - \frac{40}{50} \right) = 0.60$$

If it is assumed that all CO<sub>2</sub> gas is captured and sequestered in underground cavern, the sustainability for CO<sub>2</sub> gas result 1. The CO gas assumed 40 ppm concentration above 50 meters for certain atmospheric local air velocity condition, the ASI of El Tremedal UCG trial result:

$$ASI = \frac{1}{4} \left( 1 + 1 + 1 + 1 - \frac{40}{50} \right) = 0.80$$

The result of application the quantitative ESI model with measured and assumed environmental indicator in El Tremedal Spanish UCG trial assessment by proposal sustainability levels for UCG process (Table 6) shows the sustainability due subsidence and surface water is very good, due to atmosphere pollution is good and due groundwater is extremely low.

Applying equation (1) the ESI results in 0.74 and globally environmental sustainability of El Tremedal UCG trial as shown in Figure 9 is good.

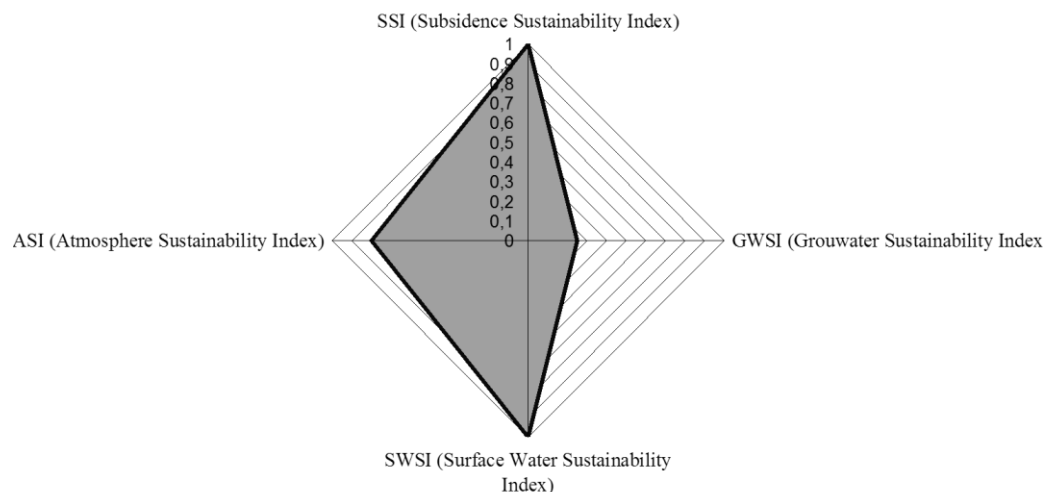


**Figure 9 - Environmental Sustainability Index of El Tremedal UCG trial**

The ESI determination process and the results demonstrate that the implementation of remediation action is needed for reducing ground water pollutants (H<sub>2</sub>S, NH<sub>3</sub>, C<sub>6</sub>H<sub>5</sub>OH and Conductivity) to

permissible levels. The ESI is very useful index for indicating remediation actions and applications of the Management of Sustainable UCG Practices.

### DISCUSSION OF RESULTS

In the quantitative assessment of the Environmental Sustainability Index of the UCG process, for most of the environmental pollution components (H<sub>2</sub>S, NH<sub>3</sub>, C<sub>6</sub>H<sub>5</sub>OH, pH, C<sub>6</sub>H<sub>6</sub>, CO, CO<sub>2</sub>, SO<sub>x</sub>, NO<sub>x</sub>, phenols, conductivity, etc.) are applied to the mathematical model and conditions of sustainability criterion 1 (equation 2) based on their minimum standards.

For only subsidence then the mathematical model and conditions of sustainability criterion 2 based on the maximum standards (admissible horizontal tensile), and for pH, CH<sub>4</sub> and H<sub>2</sub> applies the mathematical models and conditions of sustainability criterion 3 (equations 4 and 5) based on a permissible range from a low to a high standard.

Table 9 shows the calculated Environmental Sustainability Index for El Tremedal Underground Coal Gasification trial, as compared to those for underground tungsten mining in Portugal (6) and surface water And groundwater sustainability index in underground mining showing close resemblance of results with reference to GWSI and other Environmental Indicators.

**Table 9 - Environmental Sustainability Index (ESI) of El Tremedal UCG trial compared with underground mining and mine water**

Sustainability Index	El Tremedal UCG trial	Panasqueira Portuguese mine(5, 6]	
		Underground mining	Mine water
SSI	1		
GWSI	0.25	0.27	0.35
SWSI	1		
ASI	0.70		
GSI		0.98	
UASI		0.54	
ESI	0.74(high)	0.45(Low)	0.35(low)
SSI: Subsidence Sustainability Index; GWSI: Groundwater Sustainability Index; SWSI: Surface Water Sustainability Index; ASI: Exterior Atmosphere Sustainability Index; GSI: Geotechnical Sustainability Index; UASI: Underground Atmosphere Sustainability Index			

Table 9 also indicates that the ESI result 0.74, equivalent to *good* level according to (Table 6); Compared with ESI=0.45 for underground tungsten mining (d] and equivalent to *low* level and ESI=0.35 for mine water (Stephan et. al. 1985), also equivalent to *low* level.

During assessment of the environmental sustainability of El Tremedal UCG trial, low sustainability of groundwater (GWSI = 0.25) greatly reduces the global Environmental sustainability Index (ASI), this behavior is also observed in the case of mining underground (GWSI = 0.27) and even for mine water (GWSI = 0.35).

### CONCLUSIONS

Underground coal gasification, in the future, will be an important activity for human development, but the future projects must be implemented based on acceptable environmental sustainability.

The environmental sustainability of underground coal gasification can be quantified by calculating the Environmental Sustainability Index through the developed mathematical model.

The numerical model presented in this paper opens a way for analysis, assessment, remediation and contribution to effective Sustainable management of the underground coal gasification process.

The Environmental Sustainability Index, calculated by the developed model, is a quantitative indicator of the environmental sustainability of an UCG project. In the future, this index will be able to standardize the minimum level of sustainability of UCG process.

---

**ACKNOWLEDGEMENT**

This project was funded by the Portuguese Science and Technology Foundation (Fundação para a Ciência e a Tecnologia – FCT). Thanks are also due to Professor C. Dinnis da Gama for his contribution to this project.

**REFERENCES**

- Burland J B, 1995. Assessment of risk of damage to buildings due to tunnelling and excavation. Invited Special Lecture. In: 1st Int. Conf. on Earthquake Geotech. Engineering, IS Tokyo '95.
- Burton E, Firedmann J and Upadhye H, 2004. Best Practices in Underground Coal Gasification. Livermore National Laboratory. Livermore CA, US, pp. 119.
- Creedy D P, Garner K, Holloway S, Jones N and Ren T X, 2001. Review of underground coal gasification technological advancements. Report No. Coal r211 DTI/Pub URN 01/1041, UK, pp. 64.
- Friedmann J, 2009. Accelerating development of underground coal gasification: Priorities and challenges for U.S. research and development. Chapter 1 in Coal Without Carbon: An Investment Plan for Federal Action. Expert Reports on Research, Development, and Demonstration for Affordable Carbon Capture and Sequestration. Clean Air Task Force, Boston, MA. September. pp. 1–16.
- Final Summary Report, 1999. El Tremedal Underground Coal Gasification (UCG) Spanish trial.
- Green M B, 1999. Underground Coal Gasification – a joint European Field Trial in Spain. ETSU Report No. COAL R169. DTI/Pub URN99/1093.
- Hoek E, 2000. Rock engineering. Course notes by Evert Hoek Consulting Engineer Inc. Vancouver, Canada, p. 324 Web site. [http://www.rockscience.com/education/hoeks\\_corner](http://www.rockscience.com/education/hoeks_corner).
- Liu S, Wang Y, Yua YL and Oakey J, 2006. Volatilization of mercury, arsenic and selenium during underground coal gasification. Fuel 85:10-11(July August), p. 1550 - 1558.
- Navarro Torres V F, Singh RN, Pathan AG, 2008. Mine water sustainability and Management of sustainable mining practices with special reference to tungsten mining. Archives of Mining Science. Volume 53, Issue 1, pp. 75-85.
- Navarro Torres V F and Dinis da Gama C., 2006. Quantifying the Environmental Sustainability in Underground Mining. V International Symposium on Mine Planning and Equipment Selection (MPES 2006) Torino – Italy, Vol.2, p. 872 – 878.
- Navarro Torres, V F, Dinis da Gama C, Costa e Silva M, Neves PF., Qiang X., 2011. Comparative stability analyses of traditional and selective room-and-pillar. International Journal of Minerals, Metallurgy and Materials. v.18, p.1 - 8.
- Navarro Torres V F, 2006. Sustainability indicators in underground works. III Portuguese-Brazilian Geotechnical Congress, Florianópolis, Brazil, pp.7
- Niklas F J, 2003. Behaviour of buildings due to tunnel induced subsidence. PhD Thesis, Imperial College of Science, UK, pp. 358.
- Ren T X, Whittles D and Reddish DJ, 2003. Coupled geotechnical and thermal modelling for the prediction of UCG cavity growth. International Workshop on UCG, London, October 1-2, 2003.
- Stephens D R, Hill RW and Borg IY, 1985. Status of Underground Coal Gasification. UCRL-92068. Mineral Processing and Extractive Metallurgy Review: An International Journal, Volume 1, Issue 3-4, p. 265 – 296.
- Sury M, White M, Kirton J, Carr P and Woodbridge R, 2004. Report No. COAL R272 DTI/Pub URN 04/1880, 2004. Review of Environmental Issues of Underground Coal Gasification. University of Liège Belgium: 126.
- Shu-qin, L and Jun-hua Y, 2002. Environmental Benefits of underground coal gasification. Journal of Environmental Sciences, vol. 12, no. 2, pp.284-288.
- Skousen J G, Sexstone A and Ziemkiewicz P F, 2000. Acid mine drainage control and treatment. Chapter 6 in Reclamation of Drastically Disturbed Lands. American Society of Agronomy and American Society for Surface Mining and Reclamation. Agronomy No. 41.
- Stratus Consulting Inc., 2010. Potential Environmental Impacts of the Proposed CIRI Underground Coal Gasification Project, Western Cook Inlet, Alaska. Washington, US, p. 39.
- State Water Control Board, 2004. 9 VAC 25-280-10 et seq Groundwater Standards Statutory Authority: § 62.1-44.15(3a) of the Code of Virginia, US. Effective February 12.
- Walter K, 2007. Fire in the hole: Underground coal gasification may provide a secure energy supply and reduce greenhouse gas emissions. Lawrence Livermore National Laboratory, Science and Technology Review, p. 12-18.

# COMMISSIONING ADIABATIC OVEN TESTING – AN INTER-LABORATORY COMPARISON

B Beamish<sup>1,2</sup>, J Theiler<sup>3</sup>, J Saurat<sup>4</sup> and T Levi<sup>4</sup>

**ABSTRACT:** Adiabatic oven testing for spontaneous combustion assessment has been a primary method used by the Australian and New Zealand coal industries for input to the development of Principal Hazard Management Plans for mining operations. Consistency of results is important to ensure that the ratings obtained are accurate and reliable for maintaining the integrity of the database used to compare between mines and for obtaining site specific relationships. This paper presents the results from commissioning tests of four new adiabatic ovens at two different laboratories, which show the high level of reproducibility and repeatability needed for confidence in planning of future mining operations. The results cover a range of coal self-heating rates to show the validity of the testing and the reliability of the adiabatic ovens.

## INTRODUCTION

Adiabatic oven testing has been used routinely by Australian and New Zealand coal mine operations since the early 1980's to rate the propensity of coal to spontaneously combust (Humphreys, Rowlands and Cudmore, 1981). The parameter obtained from these tests is known as the  $R_{70}$  initial self-heating rate and is simply a measure of the temperature rise rate of the coal as it reacts with oxygen under adiabatic conditions from a start temperature of 40 °C until it reaches 70 °C. The higher the  $R_{70}$  value the higher the intrinsic reactivity of the coal and therefore the more prone it is to spontaneous combustion.  $R_{70}$  values are strongly rank dependent (Beamish and Arisoy, 2008a,2008b; Beamish and Beamish, 2012), with low rank coals having high  $R_{70}$  values (up to 99 °C/h for lignite) and high rank coals having low  $R_{70}$  values (less than 0.5 °C/h for medium and low volatile bituminous coals). Other coal properties such as mineral matter and coal type (dull or bright) can also affect the  $R_{70}$  value (Beamish and Blazak, 2005; Beamish and Clarkson, 2006; Beamish and Sainsbury, 2008). To gain a proper perspective of the overall propensity of a particular coal for spontaneous combustion it is therefore important to obtain a reliable result for  $R_{70}$  as an input to management planning.

Unlike other coal quality tests, there are no established repeatability and reproducibility limits for  $R_{70}$  testing. This is partly due to the fact that the test is very specialised and only a limited number of laboratories are available to do the test and partly due to the fact that this would be a costly exercise in terms of time and resources. To date there has been no published inter-laboratory comparison of  $R_{70}$  results. This paper provides an insight into the reliability of the  $R_{70}$  test by presenting the results of inter-laboratory comparisons during the commissioning of four adiabatic ovens at two new laboratories. Results from a decommissioned third laboratory are used for comparison to validate a seamless transition for the coal industry into the future.

## ADIABATIC OVEN TESTING

### Laboratories and coal samples

Two new laboratories have recently been established in Australia (LAB A) and New Zealand (LAB B) to provide testing capabilities for spontaneous combustion assessment. At each laboratory, two adiabatic ovens have been commissioned and comparison of the test results from each laboratory has been performed to establish repeatability for the ovens and reproducibility between the laboratories. In addition, a comparison has also been possible with previous results from a decommissioned third laboratory (LAB C) using a stored (frozen) block of coal from one particular mine. Other comparisons with previous mine results are on-going as new testing is performed for compliance at existing mines.

<sup>1</sup> B3 Mining Services Pty Ltd, PO Box 1565, Toowong BC QLD 4066, basil@b3miningservices.com, M: +61 488 708 949

<sup>2</sup> School of Mechanical and Mining Engineering, The University of Queensland, Brisbane QLD 4072

<sup>3</sup> CB3 Mine Services Pty Ltd, PO Box 1089, Mt Ommaney QLD 4074

<sup>4</sup> CRL Energy Ltd, PO Box 31-244, Lower Hutt, New Zealand

The samples used in this inter-laboratory comparison cover a range of reactive high volatile bituminous and sub-bituminous coals from several mining regions.

### R<sub>70</sub> self-heating test procedure

The R<sub>70</sub> testing procedure essentially involves drying a 150 g sample of <212 μm crushed coal at 110 °C under nitrogen for approximately 16 hours (Beamish, 2005). Whilst still under nitrogen, the coal is cooled to 40 °C before being transferred to an adiabatic oven. Once the coal temperature has equilibrated at 40 °C under a nitrogen flow in the adiabatic oven, oxygen is passed through the sample at 50 mL/min. A data logger records the temperature rise due to the self-heating of the coal. The time taken for the coal temperature to reach 70 °C is used to calculate the initial self-heating rate for the rise in temperature due to adiabatic oxidation. This is known as the R<sub>70</sub> index, which is in units of °C/h and is a good indicator of the intrinsic coal reactivity towards oxygen.

## ADIABATIC TESTING RESULTS AND DISCUSSION

### Oven repeatability and reproducibility tests at LAB A

The R<sub>70</sub> self-heating curves for a Newcastle high volatile bituminous coal are shown in Figure 1. These tests were conducted over consecutive days in the same oven. This comparison shows that Oven 1 at LAB A obtained R<sub>70</sub> values of 4.73 °C/h and 4.90 °C/h, indicating excellent repeatability that is well within the limits of ±5% reported by Beamish, Barakat and St George (2000). The same sequence of repeat testing was applied to an Australian and US sub-bituminous coal and the results are shown in Figures 2 and 3, which confirm the same excellent repeatability for the adiabatic oven testing of a higher reactivity coal. In addition, the R<sub>70</sub> value obtained by Oven 2 at LAB A for the US sub-bituminous coal (Figure 3) shows good reproducibility between the two different ovens.

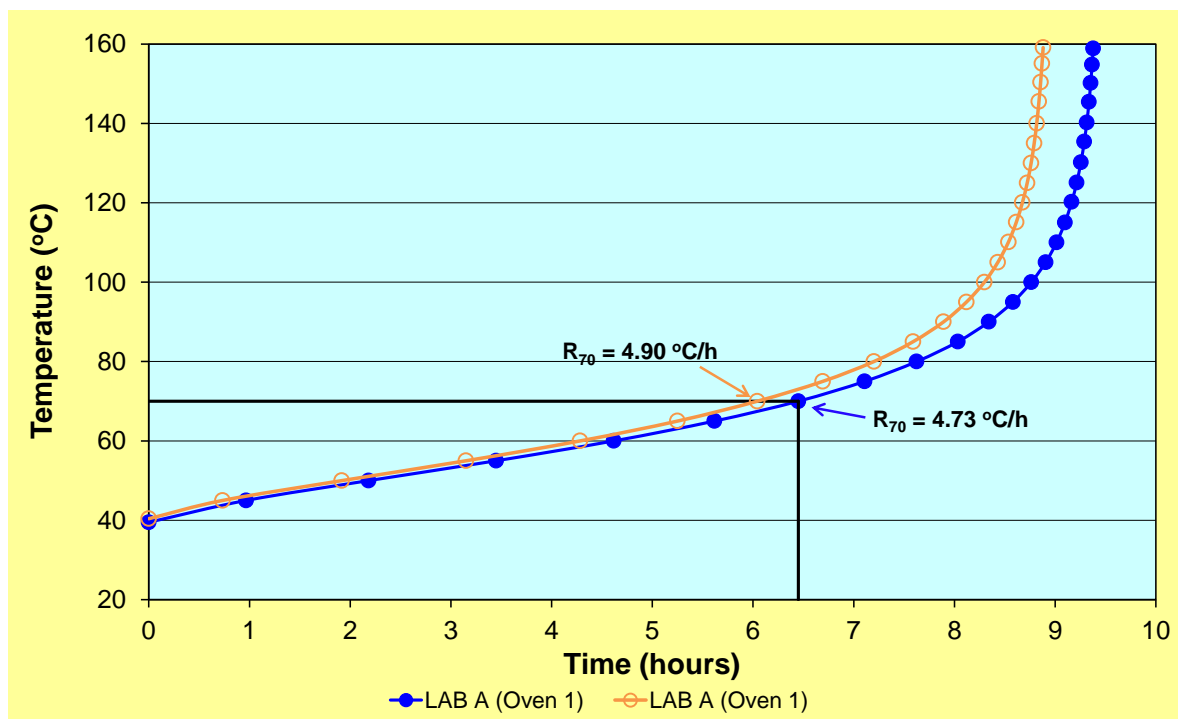


Figure 1 - Adiabatic self-heating curves for a Newcastle high volatile bituminous coal showing consistency of results between tests performed on consecutive days in oven 1 at LAB A

### Oven repeatability and reproducibility tests at LAB B

The R<sub>70</sub> self-heating curves for a New Zealand sub-bituminous coal are shown in Figure 4. The repeatability for Oven 1 and the repeatability for Oven 2 are almost identical for this highly reactive coal and both are within the limits of ±5% reported by Beamish, Barakat and St George (2000). The reproducibility between the two ovens is also very high as the average R<sub>70</sub> value for Oven 1 is

18.45 °C/h and for Oven 2 it is 17.98 °C/h. The  $R_{70}$  self-heating curves for a New Zealand high volatile bituminous coal are shown in Figure 5 for tests conducted in Oven 1 and Oven 2 at LAB B. Again there is good reproducibility between the two ovens.

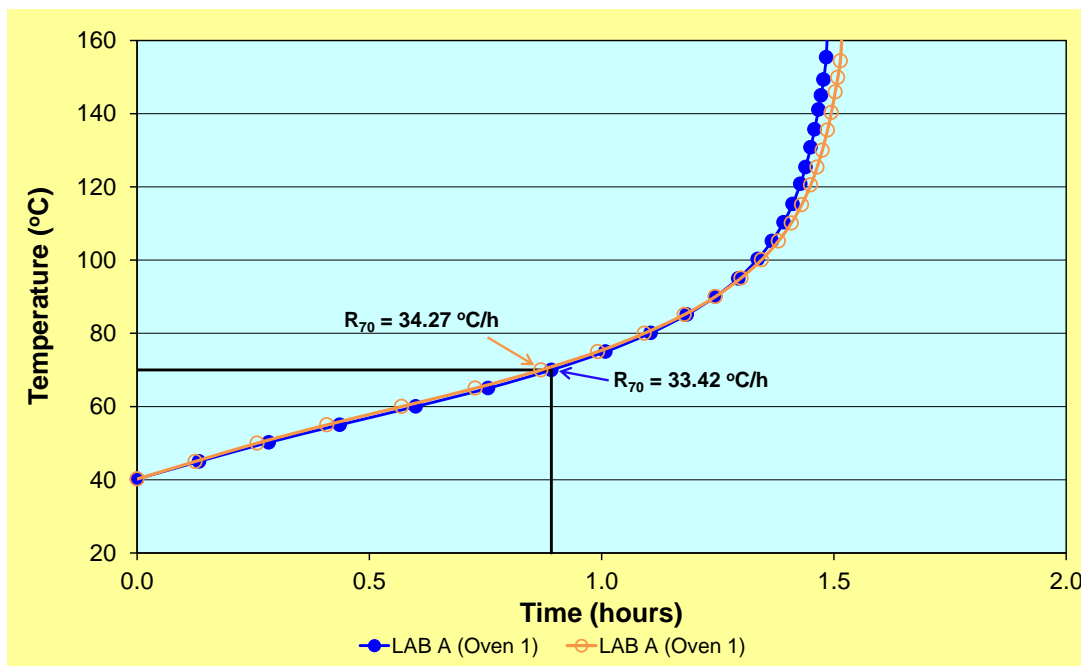


Figure 2 - Adiabatic self-heating curves for an Australian sub-bituminous coal showing consistency of results between tests performed in oven 1 at LAB A

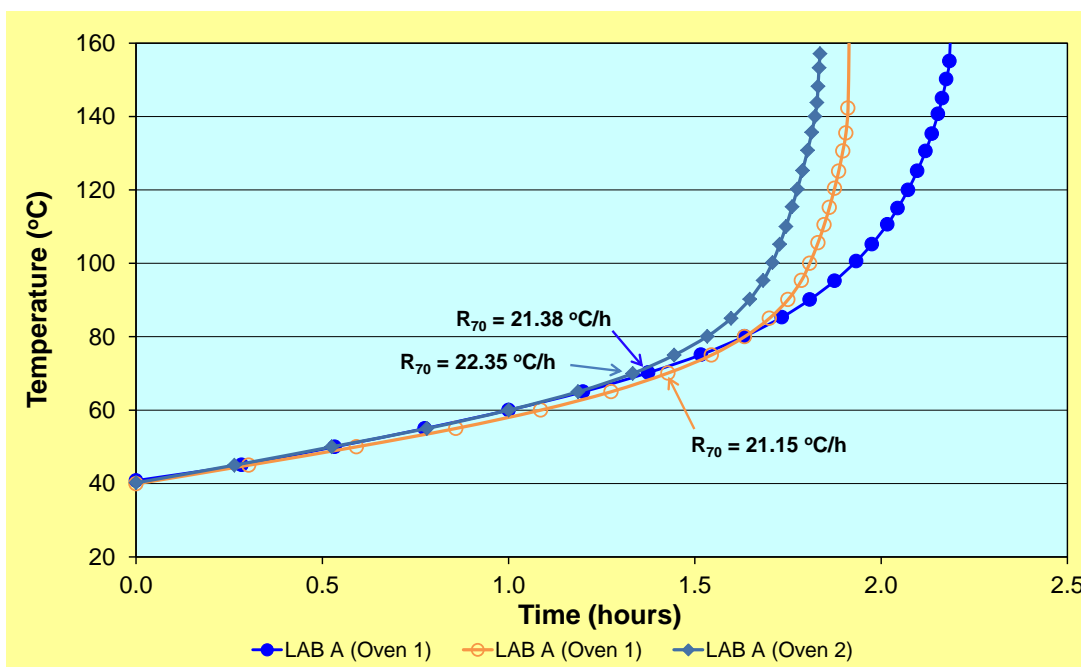


Figure 3 - Adiabatic self-heating curves for a US sub-bituminous coal showing consistency of results between tests performed on consecutive days in oven 1 at LAB A and a test in oven 2 at LAB A on the same coal

**Reproducibility between LAB A and LAB B**

$R_{70}$  test results for US sub-bituminous coal sample tested at both LAB A and LAB B are shown in Figure 6. There is excellent reproducibility between the  $R_{70}$  values obtained, which indicates that the sample preparation procedures as well as the oven performance at each laboratory are working very effectively.

Consequently, there is a considerable degree of confidence in comparing results between these two laboratories.

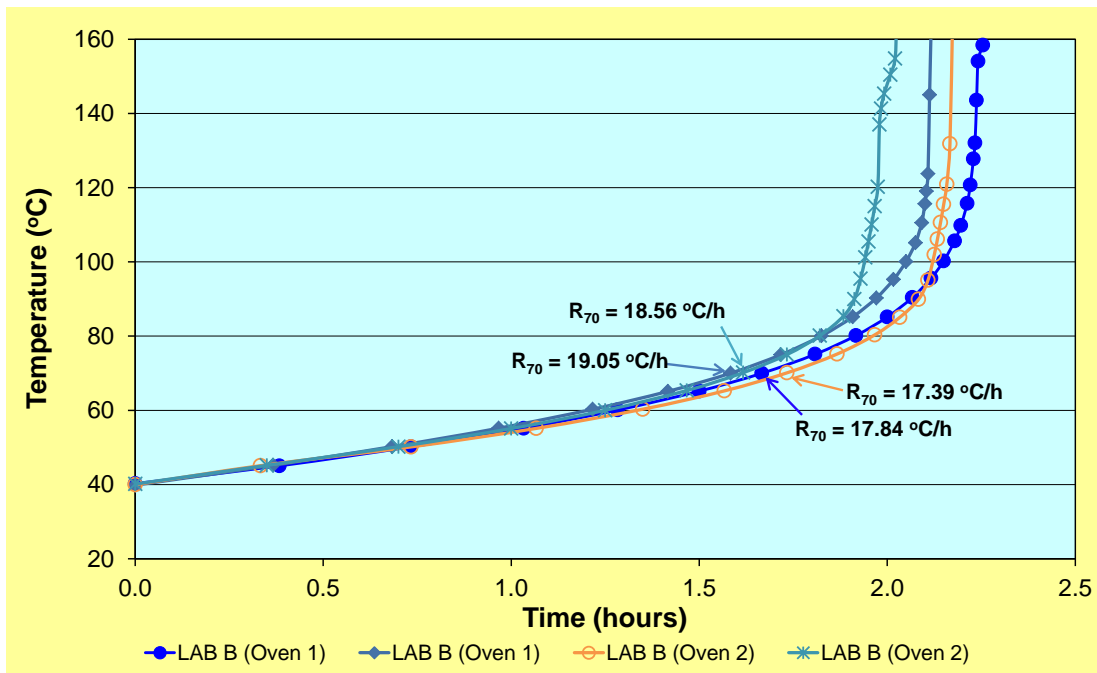


Figure 4 - Adiabatic self-heating curves for a New Zealand sub-bituminous coal showing consistency of results between ovens

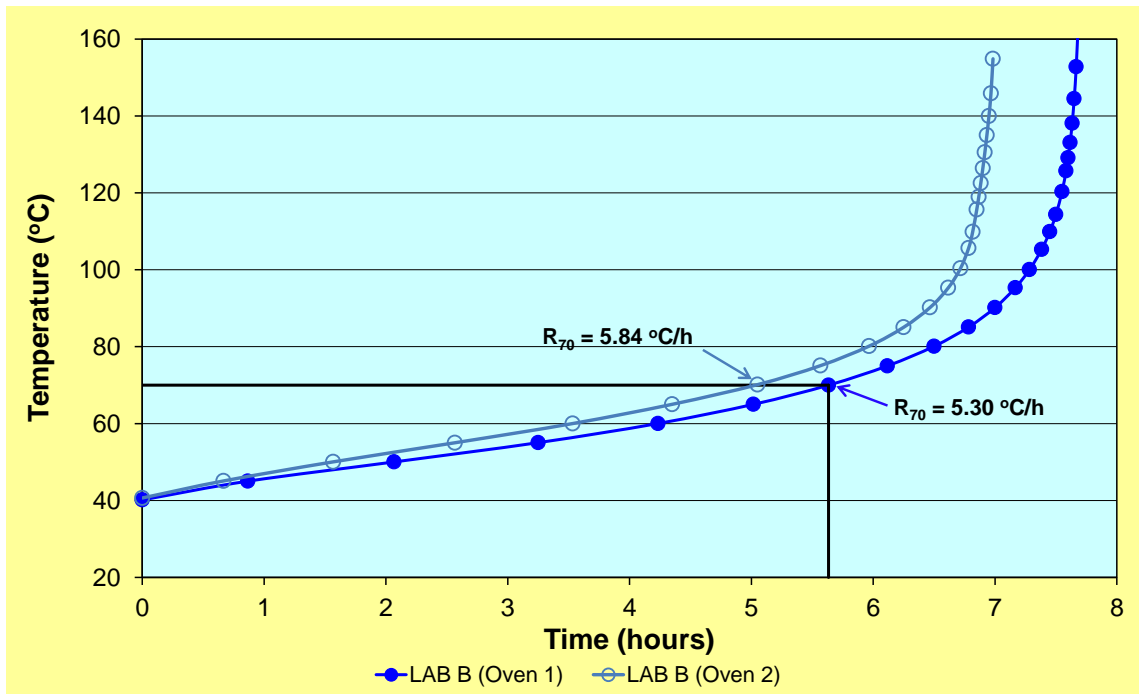


Figure 5 - Adiabatic self-heating curves for a New Zealand high volatile bituminous coal showing consistency of results between ovens

**Comparison between results from LAB A and previous results from LAB C**

The block of Newcastle high volatile bituminous coal tested at LAB A in 2013 was also tested at LAB C in 2007. Figure 7 shows that the self-heating test results overlap, indicating excellent reproducibility between these two laboratories. These results provide on-going confidence in the continuity of spontaneous combustion assessment at the mine extracting this particular coal. Test results from other

mines previously tested at LAB C are also showing good overlap with results from LAB A, thus maintaining the integrity of the large database across a range of mining operations around the world.

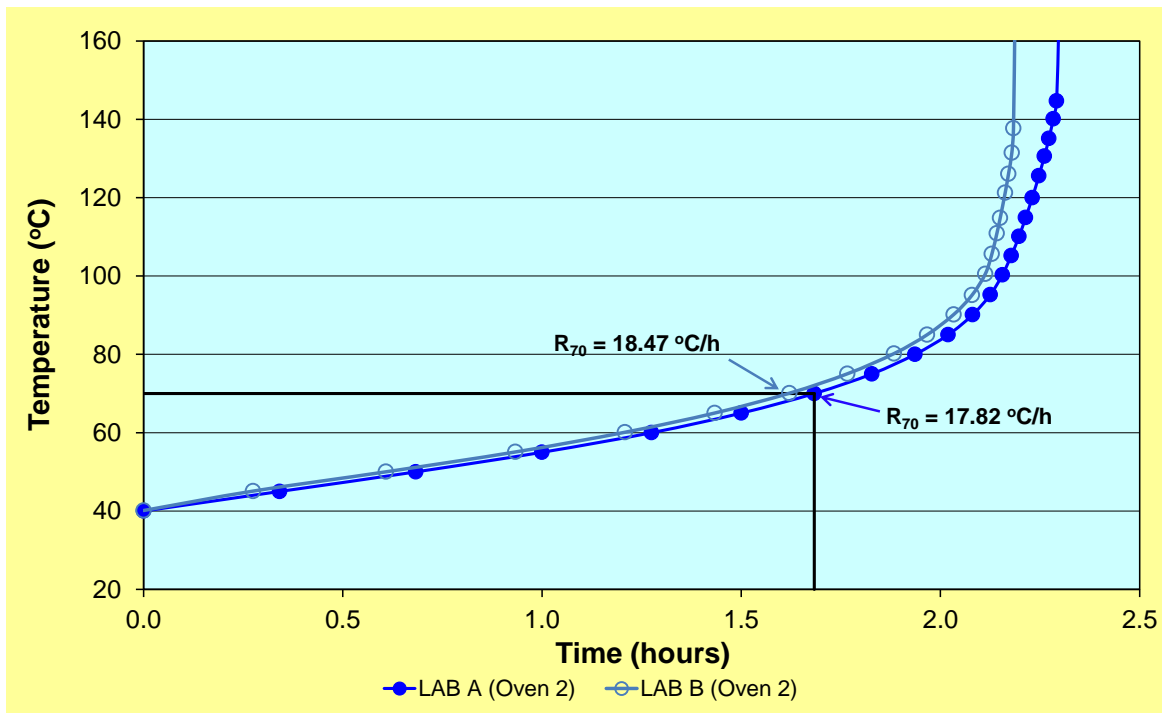


Figure 6 - Adiabatic self-heating curves for a US sub-bituminous coal showing reproducibility between LAB A and LAB B

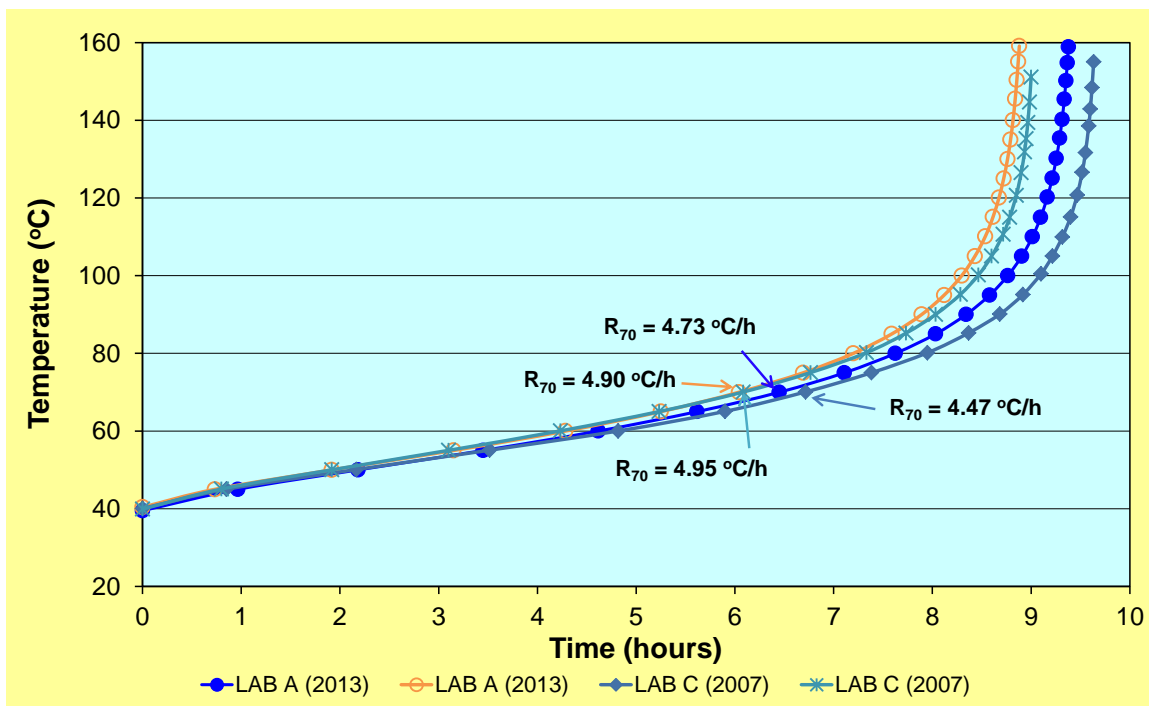


Figure 7 - Adiabatic self-heating curves for a Newcastle high volatile bituminous coal showing continuity of results over a long period of time

### CONCLUSIONS

The coal mining industry expects reliable and accurate results to be available for spontaneous combustion assessment as an input to the development of an appropriate Principal Hazard

Management Plan. No published data exists to establish the reproducibility of  $R_{70}$  self-heating rates between laboratories. As part of the due diligence process in establishing two new laboratories an inter-laboratory comparison has been performed that shows the high degree of repeatability and reproducibility that can be obtained for this parameter. The results obtained provide the industry with confidence when comparing results across mining operations and also in terms of establishing site specific relationships that can be used for developing a hazard map model. Comparison of results with a laboratory that is no longer in operation shows a good degree of consistency that provides continuity for future mining operations.

### ACKNOWLEDGEMENTS

The authors would like to thank the Coal Industry for their continued support of spontaneous combustion benchmarking, along with The University of Queensland for allowing the comparison with LAB C.

### REFERENCES

- Beamish, B B, 2005. Comparison of the  $R_{70}$  self-heating rate of New Zealand and Australian coals to Suggate rank parameter, *International Journal of Coal Geology*, 64(1-2):139-144.
- Beamish, B B and Arisoy, A, 2008a. Effect of intrinsic coal properties on self-heating rates, in *Proceedings 12<sup>th</sup> US/North American Mine Ventilation Symposium* (ed: K G Wallace Jr), pp 149-153 (The Society of Mining, Metallurgy and Exploration Inc., Littleton, USA).
- Beamish, B B and Arisoy, A, 2008b. Effect of mineral matter on coal self-heating rate, *Fuel*, 87:125-130.
- Beamish, B and Beamish, R, 2012. Testing and sampling requirements for input to spontaneous combustion risk assessment, in *Proceedings of the Australian Mine Ventilation Conference* (eds: B Beamish and D Chalmers), pp 15-21 (The Australasian Institute of Mining and Metallurgy: Melbourne).
- Beamish, B B and Blazak, D G, 2005. Relationship between ash content and  $R_{70}$  self-heating rate of Callide coal, *International Journal of Coal Geology*, 64(1-2):126-132.
- Beamish, B and Clarkson, F, 2006. Self-heating rates of Sydney Basin coals – The emerging picture, in *Proceedings of the 36<sup>th</sup> Sydney Basin Symposium*, pp 1-8 (University of Wollongong).
- Beamish, B B and Sainsbury, W, 2008. Development of a site specific self-heating rate prediction equation for a high volatile bituminous coal, in *Proceedings 8<sup>th</sup> Coal Operator's Conference* (ed: N Aziz), pp 161-165, (University of Wollongong and The Australasian Institute of Mining and Metallurgy). <http://ro.uow.edu.au/coal/16/>.
- Beamish, B B, Barakat, M A and St George, J D, 2000. Adiabatic testing procedures for determining the self-heating propensity of coal and sample ageing effects, *Thermochimica Acta*, 362 (1-2):79-87.
- Humphreys, D, Rowlands, D and Cudmore, J F, 1981. Spontaneous combustion of some Queensland coals, in *Proceedings of Ignitions, Explosions and Fires in Coal Mines Symposium*, pp 5-1 - 5-19 (The AusIMM Illawarra Branch).

# DEVELOPMENTS IN THE MANAGEMENT OF SPONTANEOUS COMBUSTION IN AUSTRALIAN UNDERGROUND COAL MINES

David Cliff<sup>1</sup>, Darren Brady<sup>2</sup> and Martin Watkinson<sup>3</sup>

**ABSTRACT:** In 1996 the book *Spontaneous Combustion in Australian Underground Coal Mines* was first released (Cliff, *et al.*, 1996). Since that time it has been reprinted several times and minor updates have been made. A major overhaul of the book was commissioned by ACARP and this paper reports on some of the changes to spontaneous combustion management that have occurred over the past eighteen years. Our knowledge of the fundamental chemical processes that control spontaneous combustion has improved materially in that time. In addition preventive control measures such as good ventilation and proactive inertisation coupled with computer modelling of goaf behaviour have emerged, as well as improved reactive control measures including the use of foams and gels to control airflow into active goafs. Mine environment monitoring techniques and technology have also undergone major development with sophisticated automated continuous gas monitoring systems being the norm in our mines and ultrafast ultra sensitive gas chromatographs being widely used. Pressure and air flow measurements are also used routinely to monitor and predict airflows not only in roadways but across seals and through goafs.

## INTRODUCTION

The last incident in Australia where lives were lost due to spontaneous combustion was the Moura No. 2 mine disaster in August 1994. Since that time no lives have been lost however, significant incidents have still occurred in underground mines requiring the evacuation of the mine and protracted remote treatment of the incident. The most recent major incident was at Carborough Downs mine in 2012. Spontaneous combustion continues to be a problem in some open cut mines as well, especially where they are mining through old underground workings, in stockpiles and waste heaps which have carbonaceous or pyritic waste material. It is thus still relevant to ensure that spontaneous combustion is given sufficient importance when considering potential hazards at our mines.

Over the years ACARP has expended many millions of dollars on research aimed at improving our knowledge and ability to manage spontaneous combustion and other types of mine fires. The fact that no lives have been lost since Moura must be in large part due to the outcomes of this research, which has pioneered such things as computerised fluid dynamic modelling of goafs and proactive inert gas injection. Other initiatives funded by ACARP included the use of gels and polymers to control air ingress into coal, laboratory studies to better understand the science of coal oxidation and the development of camera based borehole investigation systems to investigate goafs. At the same time major effort has gone into understanding spontaneous combustion in coal stockpiles and waste heaps, in part due to concerns over greenhouse emissions.

Over the years there have been a number of reviews of spontaneous combustion, (e.g. Cliff and Bofinger, 1998; Nalbandian, 2010). In addition the then New South Wales Department of Industry and Investment have released an updated Mine Design Guideline MDG-1006 Spontaneous Combustion Management Guideline supported by a comprehensive technical reference guide (NSW DII, 2011a and 2011b).

## DEVELOPMENTS IN THE UNDERSTANDING OF THE OXIDATION PROCESS

Whilst it is reasonable to say that many of the factors that affect the ability of coal to exothermically oxidise and reach spontaneous combustion have been well known for many years (see for example Table 1 extracted from Cliff and Bofinger 1998), it is also reasonable to say that it is only in recent years that the significance of a number of these factors has been recognised and quantified.

<sup>1</sup> Minerals Industry Safety and health Centre, Sustainable Minerals institute, Univesriosty of Queensland, d.cliff@mishc.uq.edu.au; Tel: +61 7 3346 4086

<sup>2</sup> Mine Safety Institute of Australia Pty Ltd, darren@minesafetyinstitute.com.au; Tel: 0417496 550

<sup>3</sup> Executive Mining Engineer, SIMTARS, Brisbane, Qld, 4000, martin.watkinson@simtars.com.au; Tel: +61 4 3764 8886

**Table 1 - Factors affecting the oxidation of coal (extracted references cited in Cliff and Bofinger, 1998)**

Intrinsic Factors	Extrinsic Factors
Low rank of coal	Faults
Low ash	Folds
High friability	Dykes
Weak caking properties	Weak and disturbed strata conditions
High reactivity	Seam thickness
High heat capacity	Steepness of seam
Low thermal conductivity	Shallow cover
High coefficient of oxygen absorption	Multi seams in close proximity
High proportion of oxygen functional groups	Porous petrographic structure
High volatile matter	Mining parameters that increase the amount of broken coal exposed to air for significant periods of time
Pyrites	Mine ambient temperature
Moisture content	
Particle size and surface area of coal	

Laboratory testing at both the small and medium scale has added significantly to our understanding of the processes both chemical and physical that influence the ability of coal oxidation to become spontaneous combustion. The complex role of moisture has been demonstrated. Adsorption of moisture has been shown to increase the temperature of coal which causes the acceleration of the oxidation rate. Conversely coal with significant inherent moisture is appreciably inhibited as the coal has to dry out before oxidation can develop (Wang, *et al.*, 2003; Beamish and Beamish, 2012). Finally it has also been shown that there needs to be some moisture present for low temperature oxidation to occur (Wang, *et al.*, 2003). Other studies have quantified parameters that have been demonstrated to enhance oxidation, e.g. pyrites, (Miron, *et al.*, 1992) or inhibit it, e.g. mineral matter (Beamish and Blazak, 2005)). These studies have also identified the key components of the odour generated during spontaneous combustion as well as confirming one significant non oxidation related source of hydrogen gas (H<sub>2</sub>) (the reaction of acidified water on mild steel) (Hitchcock, *et al.*, 2011). The odour associated with coal oxidation is typically due to the presence of aldehydes and other unsaturated oxygenated species, principally acetaldehyde and acrolein (Clarkson and Usher, 2008, Hitchcock, *et al.*, 2011). Increasing ash content reduces the reactivity of the coal (Beamish and Arisoy, 2008). Laboratory tests have also confirmed the impact of weathering on deactivating coal to the oxidation process (Beamish, *et al.*, 2000), through removing active reaction sites without retaining the heat of oxidation.

It is also worth stressing that laboratory testing is only one part of the process required to develop adequate control systems to manage spontaneous combustion. A number of recent incidents have occurred in coals that based upon laboratory testing would not be regarded as prone to spontaneous combustion. In those cases the propensity for spontaneous combustion was enhanced due to exposure of coal to air for much longer than normal due to mining difficulties and/or the coal temperature being lifted appreciably above ambient temperature. The ambient temperature has been shown to be a significant influence in determining whether or not spontaneous combustion will occur (Beamish and Beamish, 2012). An increase in coal temperature of less than 10 °C may be sufficient to change the balance between heat loss and heat generated from the oxidation process to promote spontaneous combustion.

Recently medium scale and large scale laboratory testing has been able to link the small scale testing to the reality of what may occur in coal mines (Hitchcock, 2013). Large scale testing can take many months and thus is not really a viable routine proactive testing process (Cliff, *et al.*, 2000b). Medium scale (70 kg) testing offers a viable way of including many of the conditions found in underground mines such as the particle size distribution, moisture content, and ash content and then exploring mechanisms for control. Large scale testing has confirmed that it is possible for a small mass of coal to reach flame temperature insulated by a much larger mass of cooler coal (Cliff, *et al.*, 2000a) (Figure 1). This underlines the difficulties in detecting spontaneous combustion at an early stage, and why some events have developed to an advanced stage before they were detected.

PROACTIVE CONTROLS

Probably the most important area of improvement in the control of spontaneous combustion in underground coal mines is the prevention of spontaneous combustion through appropriate design of mining operations. Computational fluid dynamic modelling, coupled with control over pressure differentials around goafs and proactive application of inertisation, has reduced the potential for oxidation to occur in sealed areas (Ren and Balusu, 2005; Balusu, *et al.*, 2010). Figure 2 demonstrates the application of CFD modelling to goaf gas flows.

Dartbrook 4 9:00 pm Day 149

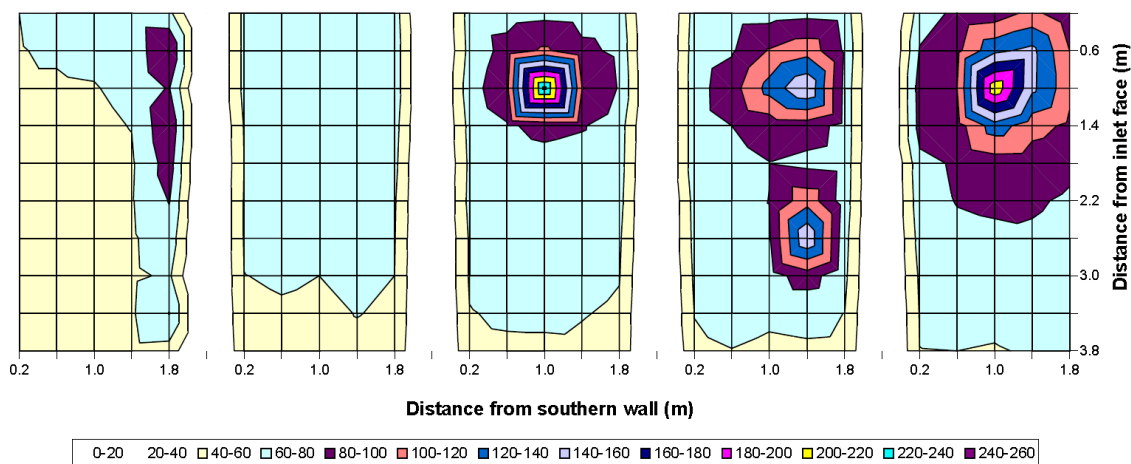


Figure 1 - Hot spot development in 16 tonne reactor (Cliff, *et al.*, 2000a)

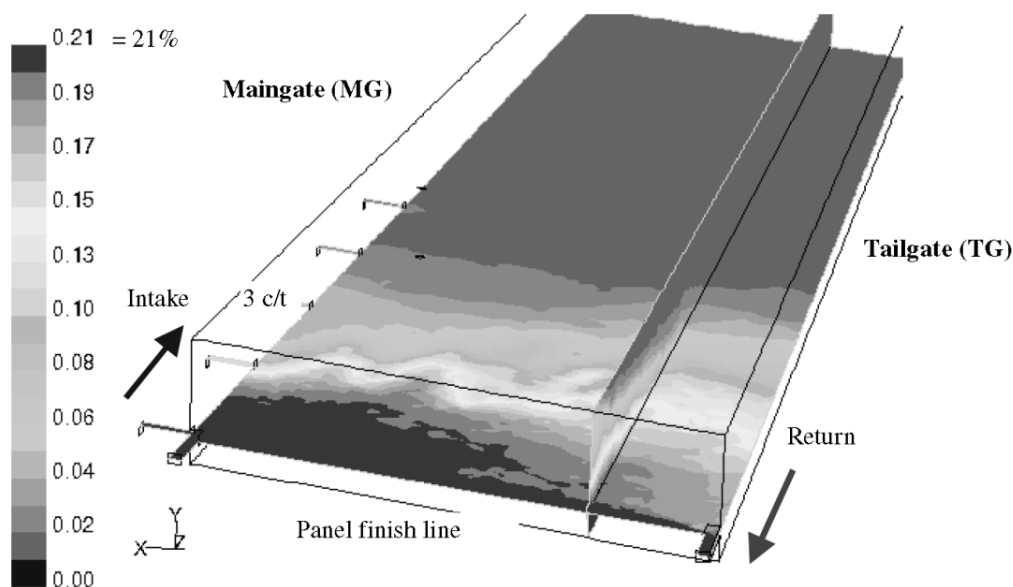


Figure 2 - Oxygen gas distribution in the longwall goaf near the finish line – with 50 m<sup>3</sup>/s airflow (Balusu, *et al.*, 2002)

These techniques are assuming increasing importance as longwall panels become wider and longer and thicker seams are mined.

Modelling has also enabled the potential impacts of goaf gas drainage on the distribution of gases in the goaf to be evaluated, as well as scouring of the goaf due to high face ventilation quantities and pressure differences (Ren, *et al.*, 2005; Balusu, *et al.*, 2010).

Ventilation models are able to evaluate the pressure changes around mining panels under various configurations, including two or three gate roads and bleeder roadways. The modelling has been validated using tracer gas studies (Luxbacher and Jong, 2013).

A number of mines now minimise air ingress into active longwall goafs by constructing pressure balancing chambers in gate-road seals. These chambers can be linked to remove any pressure differential between seals, or they can be pressurised with inert gas to prevent air ingress (Brady, *et al.*, 2008).

## REACTIVE CONTROLS

Gas monitoring has also developed enormously over the past seventeen years. Much more comprehensive monitoring is undertaken with continuous monitoring systems being installed routinely. Monitoring also extends to bag sampling through seals. Detection systems have also increased their sensitivity and the range of gases that can be monitored. Four gas systems are the norm- methane (CH<sub>4</sub>), oxygen (O<sub>2</sub>), carbon monoxide (CO) and carbon dioxide (CO<sub>2</sub>). Gas chromatographs have made the biggest improvements. The time taken to analyse a sample has shrunk from over thirty minutes to under one minute and the sensitivity for key gases such as CO and H<sub>2</sub> have improved from 10 ppm for CO to less than 1 ppm and from 50 ppm to 1 ppm for H<sub>2</sub> (Brady, 2008a).

This monitoring is supported by much better computer based data collection and analysis systems. Indeed now it is often difficult to identify which indicators are best suited to monitor for spontaneous combustion (Toth, 2005). The limitations of the various detection systems and associated analysis techniques are also much better understood (Brady, 2008b; and Cliff, 2005), including detection limits and the impact of inert gas on gas concentration based ratios. It is clear that detection should not rely on just one system or one indicator rather a range of indicators that give independent evaluation of the mine atmosphere (Cliff, 2005).

One of the more novel techniques that have been trialled in Australia is the use of radon detection on the surface above heating events; this technique is widely used in China (Xue and Cui, 2004).

Inertisation and ventilation controls are also applied to control advanced oxidation, particularly high volume techniques such as the GAG jet engine and the MINESHIELD liquid nitrogen vaporisation system. Gillies and Wu (2008) have provided an excellent comparison of the various inertisation techniques available as well as applying mine ventilation software to identify the optimum location to apply the inert gas to control an active mine fire under various scenarios.

The use of fillers and sealants to exclude oxygen from a heating has also been extensively studied (Humphreys, 2013). Guar gum based gels were found to exhibit the most suitable properties to minimise air ingress into goafs as well as offer quenching of any hot spots. Formulations were found to last up to twelve months (Miron, 1995). Others have demonstrated the value of applying water based fogs to mitigate the potential for spontaneous combustion, these fogs may contain additives to retard any combustion or improve their retention properties (Tripathi, 2008). High pressure foam plugs, generated using air, nitrogen or carbon dioxide have successfully been used to control spontaneous combustion (Ray and Singh, 2007).

## HAZARD MANAGEMENT PLANS

A consequence of the Moura No.2 mine disaster was the reform of the coal mining safety and health legislation in NSW and Queensland to include the requirement for principal/major hazard management plans to control the risk due to spontaneous combustion. This facilitated a more systematic control approach whereby risk management principles were applied and mines had to demonstrate that they had assessed the potential for spontaneous combustion, identified the controls required. These plans must then outline the details of how the controls would be implemented and how their effectiveness would be monitored. Consistent with AS4804:2001, Occupational Health and Safety Management Systems – General Guidelines on principles, systems and supporting techniques, the plans must then identify key responsibilities, resourcing requirements and training needs.

To provide guidance in developing these plans the then NSW Department of Industry and Innovation, issued a revised Mine Design Guideline MDG1006 with an accompanying technical reference guide (TRG) (NSW DII, 2011a and b). The TRG is an excellent and detailed technical reference document,

and includes details of 23 incidents that have occurred since 1970. The table of contents for MDG1006 provides a skeleton for the development of Spontaneous Combustion Management Plans:

1. Introduction – including overview, scope and policy
2. Consultation
3. Risk identification
4. Risk analysis and evaluation
5. Risk management controls
6. Monitoring - including inspections, gas monitoring and Trigger Action Response Plans (TARPS)
7. Information – documents that support the plan
8. Training
9. Roles and responsibilities
10. Supervisors
11. Audit
12. Review
13. References
14. Appendices

TARP's are key elements of the plan that provide triggers for mine personnel to react to abnormal conditions. They should provide a graded response depending upon the severity of the situation. At the lower levels it is intended that change from normal is recognised in sufficient time to apply corrective actions before people are placed at risk. At the highest level the trigger is to allow people to evacuate from the mine or workplace before there is significant risk to life. TARP's should be set particular to individual areas in the mine, eg sealed goaf, active goaf and development headings. In addition they should be reviewed regularly and updated if conditions change or information becomes available that modifies any of the underlying parameters. TARP's should not just relate to gas concentrations or derived indicators but also to deviations from normal mining conditions or other operating parameters such as ventilation change or seal damage (Cliff, 2009).

### **TRAINING**

Another major initiative that has occurred over the past twenty years is the development of industry-wide competency standards regarding spontaneous combustion management for statutory positions. In addition the position of ventilation officer has been recognised as being important and is supported by formal competency requirements. Training to achieve these competencies must be undertaken by suitably qualified personnel from registered training organisations. In addition awareness training in spontaneous combustion has been included in induction training for workers.

### **OPEN CUT MINING**

Spontaneous combustion is also an issue for open cut mining. Research in recent years has highlighted the processes that promote spontaneous combustion in stockpiles and waste heaps. This has allowed improved controls to be implemented to reduce the risks.

Day (2008) published a comprehensive handbook of spontaneous combustion in open cut coal mines. This summarises the essential information from earlier research (Carras, *et al.*, (1994), Carras *et al.* (1998), Carras *et al.* (1999) Carras (2005) and Haneman and Roberts (1998), not only in terms of the causes of and major factors affecting spontaneous combustion in open cut coal mines, but also the potential contribution to greenhouse gas emissions and other forms of pollution. It also describes the management practices for avoiding and controlling spontaneous combustion. The problems associated with the emissions from spontaneous combustion can pose a significant issue not only to workers attempting to control a heating but also to the wider community. Of particular concern are the large

quantities of carbonaceous waste that can be produced at open cut coal mines, rejects from the coal processing plants and overburden containing coal seams that are not economic to mine.

The focus of the handbook is on stockpiles and spoil-piles rather than *in situ* heatings. Figure 3 summarises the key factors the handbook identified as contributing to self-heating. It discusses the effects of the usual parameters in terms of the environment of the open cut. The report discusses modelling stockpiles and spoil piles and identifies the difficulties in undertaking such modelling, due to the necessary complexity of the models and the need to make assumptions and simplifications to make the problem manageable. Day suggested that the value of modelling is in making comparisons between various spoil pile configurations (Day 2008).

A number of researchers have undertaken computer modelling of stockpiles. Akgun and Essenhigh (2001) modelled the impacts of a number of factors such as pile height, slope angle, particle diameter of the coal and coal moisture. Their research indicated that there was a critical pile height above which spontaneous combustion becomes likely given sufficient time.

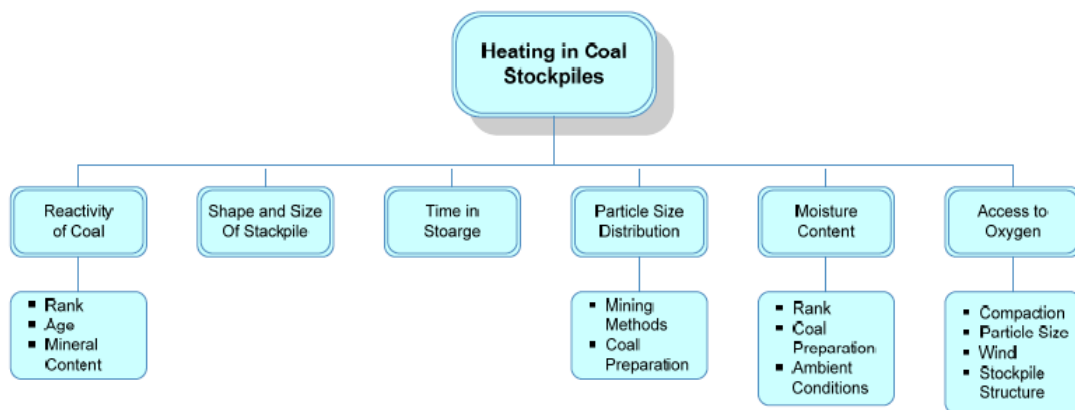


Figure 3 - Contributing factors to coal stockpile heatings (Day, 2008)

Carras *et al.* (1994) as described in Day (2008) depicts a typical spoil pile as reproduced in Figure 4. Not surprisingly the carbon content of the spoil pile is directly related to the likelihood of spontaneous combustion. Heatings tend to be quite localised and can be buried quite deep into the pile if there are cracks or fissures that allow air to travel into the pile.

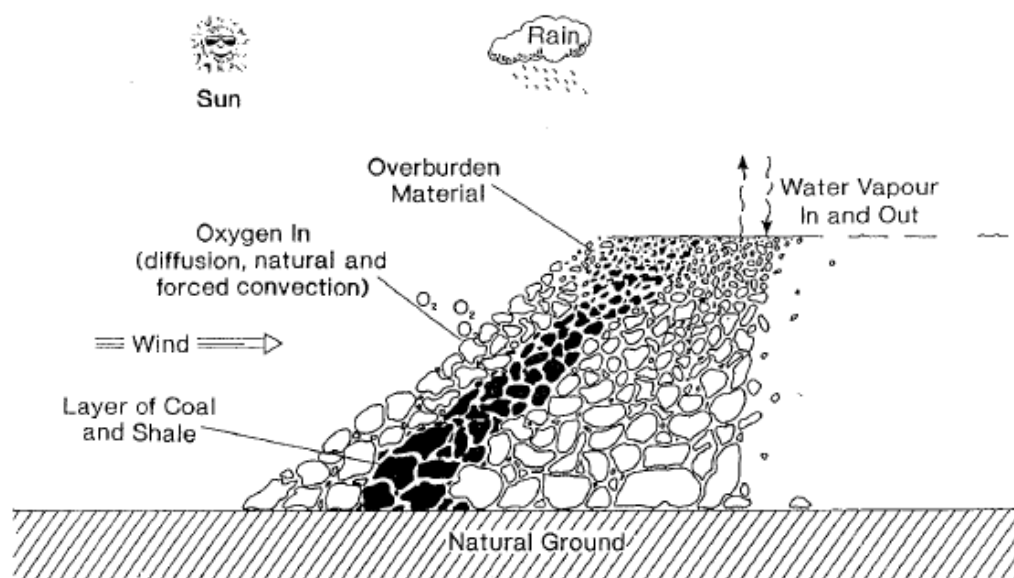


Figure 4 - Schematic representation of a spoil pile (from Carras, *et al.*, 1994) as reported in Day (2008)

Control is usually best achieved by prevention of air ingress using the techniques for coal stockpiles. Spoil piles can be covered more thickly than stockpiles as they are not required for transport elsewhere and it does not matter if the cover material mixes with the pile material. The covering material should be appropriately moist as this greatly reduces the voids in the cover and hence reduces the potential for air inflows. Clay rich materials with high water retention capacity can form effective barriers when 1-2 m thick. Sandstones which have lower water retention capacity have been found to need to be much thicker (5-10 m). The covering material must also be resistant to erosion and geotechnical instability.

Eroglu (2005) described the difficulties in open cut mining of old underground coal mines in South Africa. During surface mining air enters through cracks into the old underground workings causing spontaneous combustion. Where the old mines are close to the surface it is also possible for collapse of ground above the old bords, mainly at intersections, allowing air into the old workings. Eroglu discusses the effectiveness of a range of control measures including:

- cooling agents. High pressure water is used to cool hot spots. It can be difficult to get the water to the hot spot which may be buried deep within a pile or maze of underground workings.
- sealing agents. These combine an inhibitor of spontaneous combustion, such as calcium chloride with a binding agent and a filler such as bentonite. Often the inhibitors have poor stability and widespread application over exposed faces can be very expensive.
- dozing over. Here sand is dumped directly over the highwall to close off the old workings as soon as possible after they have been exposed to the atmosphere. The sand has to be pushed into the old openings and compacted to minimise air ingress. Venting can still occur, and so this technique can have limited impact.
- buffer blasting. This is the process of blasting material *in situ* to form a barrier to air ingress by collapsing the old roadways and forcing material into them in advance of extraction. This has been found to be the most effective method in South Africa. This technique has the added advantage of improving highwall stability and reducing the risk of subsidence.
- cladding. This is the process of placing weathered overburden on top of a buffered highwall. This reduces the air flow and heat through the buffer, which helps reduce the chimney effect inside the highwall.

## CONCLUSIONS

The developments in research over the past twenty years have contributed significantly to the reduction in risk posed by spontaneous combustion to Australian Coal Mines. Incidents still occur which suggest that there is an ongoing need to remain vigilant to this hazard. ACARP has made significant investment in spontaneous combustion research and this has facilitated this improvement in safety performance. It is important always consider the potential for spontaneous combustion when designing mines and the advent of new technology, and bigger, longer, wider longwalls will pose their own issues that require management.

## REFERENCES

- Akgun F and Essenhigh R H, 2001. Self-ignition characteristics of coal stockpiles: theoretical prediction from a two dimensional unsteady-state model, *Fuel*, 80, pp 409 – 415.
- A4804-2001. AS4804:2001, Occupational Health and Safety Management Systems – General Guidelines on principles, systems and supporting techniques, Standards Australia
- Balusu R, Ren T, Schiefelbein K, O'Grady P and Harvey T 2010. Proactive Strategies to Prevent Fires and Explosions in Longwall Mines – in *A Century of Mining Research*, SME Littleton, USA, pp 408-417.
- Balusu R, Humphries P, Harrington P, Wendt M and Xue S, 2002. Optimum inertisation strategies, in *Proceedings of Queensland Mining Industry Safety and Health Conference*, Townsville, pp 133-144.
- Beamish B B, and Arisoy A, 2008. Effect of intrinsic coal properties on self-heating rates, *12th North American Mine Ventilation Symposium*, pp 149 -153.
- Beamish B B, Barakat M A and St George, J D, 2000. Adiabatic testing procedure for determining the self-heating propensity of coal and sample ageing effects, *Thermochimica Acta*, 362, pp 79 -87.

- Beamish B and Beamish R, 2012. Benchmarking moist coal adiabatic oven testing, 14th United States/North American Mine Ventilation Symposium – Calizaya and Nelson, University of Utah, Department of Mining Engineering, USA, pp 423 – 427.
- Beamish B B and Blazak D G, 2005. Relationship between ash content and R70 self-heating rate of Callide Coal, *International Journal of Coal Geology*, 64, pp126-132.
- Brady D M, 2008a. The role of gas monitoring in the prevention and treatment of mine fires. In *Proceedings of 12th US/North American Mine Ventilation Symposium*, pp 569-574.
- Brady D, 2008b. Problems with determining oxygen deficiencies for use in ratios used in assessing spontaneous combustion activity. In *Proceedings of 12th US/North American Mine Ventilation Symposium*, pp 165 -170.
- Brady J P, Burra S, and Calderwood B, 2008. The Positive Pressure Chamber, In *Proceedings 12th U.S./North American Mine Ventilation Symposium 2008*, pp 171 -177.
- Carras J N, Bainbridge N W, Saghafi A, Szemes F, Roberts O C and Haneman D, 1994. The self-heating of spoil piles from open cut mines; Volume 1 – characterisation , field measurements and modelling. NERDDC 1609.
- Carras J N, Maitra A, Roberts O C, Saghafi A and Szemes F, 1998. The Self heating of spoil piles: A field Trial of Fly-ash grouting and an assessment of cover materials. ACARP Project C3055 Final Report Volume 1, Australian Coal Association, Brisbane.
- Carras J N, Bus J, Roberts O C and Szemes F, 1999. Monitoring of temperatures and oxygen profiles in self-heating spoil piles. ACARP Project C 6003 Final Report, Australian Coal Association, Brisbane.
- Carras J N, Day S, Saghafi A, Roberts O C, 2005. Spontaneous Combustion in Open Cut Coal Mines – Recent Australian Research, in *Proceedings of Coal 2005 Conference*, Brisbane, pp 195 – 200.
- Clarkson F, Usher D, 2008. Low temperature volatile organic profile of Australian coals, in *Proceedings of Queensland Mining Industry Safety and Health Conference*, Townsville.
- Cliff D, 2005. The Ability of Current Gas Monitoring Techniques to Adequately Detect Spontaneous Combustion. In *Proceedings of Coal 2005 Conference*, Brisbane, Queensland, Australia. pp 219 – 223.
- Cliff D, 2009. Trigger Action Response Plans (TARPs) in Underground Coal Mines - Tips, Tricks and Pitfalls. in *Proceedings of the Queensland Mining Industry Health and Safety Conference 2009*, 23 – 26 August, Townsville, Queensland, Australia.
- Cliff D, and Bofinger C, 1998. Spontaneous Combustion A Review 1998. A report submitted as part of ACARP project c6001 final report, SIMTARS, Ipswich, Queensland.
- Cliff D, Clarkson F, Davis R, Bennett A, and Smalley M, 2000a. C5031 Final Report, Better Indicators of Spontaneous Combustion, Australian Coal Association Research Program, Brisbane, Qld.
- Cliff D, Clarkson F, Davis R and Bennett T, 2000b. The implications of large scale tests for the detection and monitoring of spontaneous combustion in underground coal, *Proceedings of the Queensland Mining Industry Safety and Health Conference 2000*, A New Era in Mine Health and Safety Management, pp 421 – 428.
- Cliff D, Rowlands D and Sleeman J, 1996. Spontaneous combustion in Australian Underground Coal Mines, edited by C Bofinger, SIMTARS, Queensland, ISBN 0646290193.
- Day S, 2008. Spontaneous Combustion in Open Cut Coal Mines, Australian Coal Association Research Program Project C17006 final report.
- Eroglu N, 2005. Controlling Spontaneous Combustion in surface coal mines, *Proceedings of the 31st International Conference of Safety in Mines Research Institutes*, Brisbane, pp36 – 38.
- Gillies A D S, and Wu H W, 2008. Challenges in undertaking inertisation of fires in underground mines, 12th US/North American Mine Ventilation Symposium, pp 539 – 546.
- Haneman D K and Roberts O C 1998. Guide to the recognition, management and prevention of spoil pile self-heating. ACARP Project C3055 Final Report Volume 2, Australian Coal Association.
- Hitchcock W K, 2013, The relationship of gas evolution and odour to the stages of coal self-heating, A thesis submitted for the degree of Doctor of Philosophy at The University of Queensland in 2013
- Hitchcock W K, Cliff D and Beamish, B B 2011. Medium scale laboratory testing of coals for propensity to spontaneous combustion – Sources of hydrogen and smell. In *Proceedings of Coal 2011 Conference*, Wollongong NSW.
- Humphreys D, 2013. Scoping Study: Application of new forms of fire suppression and hydrocarbon absorption materials to underground coal mines, ACARP Final Report C21015.
- Luxbacher K and Jong E, 2013. Development of a passive tracer gas source for mine ventilation applications, 24th Annual General Meeting of the Society of Mining Professors, 26-99 June, Milos Island, Greece.
- Miron Y, 1995. RI 9585 Gel Sealants for the Mitigation of Spontaneous Heatings in Coal Mines, Report of Investigations, United States Bureau of Mines, United States Department of the Interior.
- Miron Y, Lazzara C P, and Smith A. C. 1992. RI 9415 Cause of Floor Self-Heatings in an Underground Coal Mine, Report of Investigation, United States Department of Interior, Bureau of Mines.

- 
- Nalbandian H, 2010. Propensity of coal to self-heat. Clean Coal Centre report 172, International Energy Agency. ISBN 978-9-9029-492-4.
- NSW Department of Industry and Investment, 2011a. MDG 1006 Spontaneous Combustion Management Guideline, NSW Department of Industry and Innovation, Mine Safety Operations Branch.
- NSW Department of Industry and Investment, 2011b. MDG 1006 -Technical reference, Technical Reference for Spontaneous Combustion Management Guideline, NSW Department of Industry and Innovation, Mine Safety Operations Branch.
- Ray S K, Singh R P, 2007. Recent developments and practices to control fire in underground coal mines, *Fire Technology*, 43, pp 285 – 300.
- Ren TX, Balusu R and Humphries P, 2005. Development of Innovative Goaf Inertisation Practices to Improve Coal Safety, in *Proceedings of Coal 2005*, Brisbane, Queensland, Australia, pp 315 – 322.
- Toth I, 2005. Monitoring the evolution of spontaneous combustions based on fire indices at coal mines. In *Proceedings of 31st International Conference of Safety in Mines Research Institutes*, Brisbane, Queensland, Australia pp 81 -83.
- Tripathi D D , 2008. New Approaches for Increasing the Incubation Period of Spontaneous Combustion of Coal in an Underground Mine Panel, *Fire Technology*, 44,pp 185-198.
- Wang H, Dlugogorski B Z, and Kennedy E M, 2003. Coal oxidation at low temperatures; oxygen consumption, oxidation products, reaction mechanisms and kinetic modelling, *Progress in Energy and Combustion Science*, 29, pp 487 -513.
- Xue S and Cui H, 2004. Innovative techniques for detection and control of spontaneous combustion of coal, in *Proceedings of the Coal Operators Conference*, AUSIMM Illawarra Branch. <http://ro.uow.edu.au/coal/140/>.

# MEASUREMENT OF CRITICAL SELF-IGNITION TEMPERATURES OF LOW RANK COAL PILES

Yongjun Wang<sup>1</sup>, Kyuro Sasaki<sup>2</sup>, Yuichi Sugai<sup>2</sup>, Xiaoming Zhang<sup>3</sup>

**ABSTRACT:** Considerable research exists on self-heating or spontaneous combustion of coal stockpiles from various aspects. The equation for critical temperature of self-ignition was derived from the Frank-Kamenetskii model expressing heat balance between heat generation rate in the centre of a coal pile and heat transfer from the outer surface of the pile. However, critical ignition-temperatures of low-rank coals have not been established for safety criteria in storing and transporting these coal. In this study, experimental apparatus and measurement procedures of thermal diffusivity and internal temperature in the coal pile have been presented to evaluate the critical self-ignition temperature of coal samples. The coal samples tested were low-rank lignite and sub-bituminous. Their critical ignition-temperatures were evaluated based on laboratory temperature measurements of coal piles in cube mesh-boxes of three different sizes (25, 50 and 100 mm side length) placed in hot ambient-air at temperatures ranging from 50 to 140 °C under standard atmospheric pressure. Analysis of the results has enabled the critical ignition-temperature of the coal sample to be presented as a function of stockpile volume.

## INTRODUCTION

Coal is a major energy resource for the world, and its production and consumption will increase with increasing demand for electricity in developing countries. Low rank coal, such as sub-bituminous coal and lignite often referred to as brown coal, is expected to be the predominant thermal coals in the future, because their reserves are abundant and constitute over 50% of total global reserves of coal in the world. Consequently, spontaneous combustion issues will increase with increasing usage of low rank coals, due to their high propensity to spontaneously combust. In particular, thermal drying of these coals to increase the calorific value poses an additional risk as the removal of moisture may enhance the potential for spontaneous ignition and combustion. Other factors on self-heating characteristics of coal stockpiles are wind flow or natural convection flow in the stockpile (Moghtaderi, *et al.*, 2000), chemical reactions and the equivalent oxidation exposure time, that was reviewed by Sasaki and Sugai (2011), to understand the temperature behaviour of spontaneous combustion of a coal stockpile.

Spontaneous combustion or self-heating of coal is a naturally-occurring process caused by many chemical reactions and oxidation of the coal matrix (Nordon, 1979). Gray and Lee (1967) measured the pre-ignition-temperatures of coal samples at different positions in a cylindrical reaction vessel. They used the heat balance model presented by Frank-Kamenetskii (1959) in considering a size of the stockpile, such as radius of the equivalent sphere. Bowes (1984) also presented simplified self-heating models based on the Frank-Kamenetskii model. However, previous studies did not show the methodologies to determine accurate Critical Self-Ignition Temperature (CSIT) and to expand CSIT for larger volume of coal stockpiles.

This paper presents the results of a study using experimental results to estimate CSIT of an actual coal stockpile from theoretical equations for scaling. In the experiments, temperature profiles at the centre of the coal pile set in a cube mesh-box was measured for different ambient air temperatures and three pile volumes of 15, 120 and 960 cm<sup>3</sup>. Two lignite samples (one raw and one thermally dried) and one sub-bituminous coal sample were used in the experiments.

## EQUATION FOR CRITICAL TEMPERATURE

Based on the Frank-Kamenetskii's model, CSIT can be formulated from heat balance at the temperature between heat generation and heat loss rates of the coal pile. Suppose the heat generation rate is

<sup>1</sup> Kyushu University, School of Engineering, Nishiku, Fukuoka 819-0385, yongjunwang2012@mine.kyushu-u.ac.jp: +81 92 802 3329

<sup>2</sup> Kyushu University, Faculty of Engineering, Nishiku, Fukuoka 819-0385

<sup>3</sup> Institute of Engineering and Environment Liaoning Technical University, Huludao 125000, China

expressed by the Arrhenius equation consisting of parameters for activation energy,  $E$ , frequency factor,  $A$ , and critical radius of the coal pile,  $r_c$ ,

$$\ln\left(\frac{\delta T_c^2}{r_c^2}\right) = \beta - \frac{E}{R}(T_c)^{-1} ; \quad \beta = \ln\left(\frac{EQA\rho}{R\lambda}\right) \quad (1)$$

By plotting  $\ln(\delta T_c^2/r_c^2)$  against  $(T_c)^{-1}$ ,  $\beta$  and activation energy,  $E$ , can be obtained from the intercept and slope of the linear equation, respectively. Finally, heat generating rate,  $Q$ , and CSIT or  $T_c$  as shown in Equation (1) can be obtained as a function of  $r_c$  to predict CSIT for larger volume coal piles.

### COAL SAMPLES AND EXPERIMENTAL APPARATUS

The characteristics of two lignite coals (sample #1, thermally dried lignite and sample #2, raw lignite) and one sub-bituminous coal sample (sample #3) are listed in Table 1. Their density, specific heat capacity and results of proximate analyses are quite different from each other.

**Table 1 - Density, heat capacity and proximate analyses of coal samples**

Sample No. and Coal Rank	Density $\rho$ (g/m <sup>3</sup> )	Heat Capacity $C_p$ (kJ/kg/°C)	Fixed Carbon (%)	Ash (%)	Volatile Matter (%)	Moisture (%)
#1 Lignite	0.740	1.270	30.7	10.5	55.8	3.0
#2 Lignite	1.028	3.825	16.3	0.62	24.1	59.0
#3 Sub-bituminous	1.290	2.181	54.0	6.98	33.62	5.5

The coal samples were crushed into the size range of 0.25 to 0.75 mm. The coal piles were formed by filling them in the three different sized cube boxes (25, 50 and 100 mm) composed of one open top and five screened (270 mesh) faces so that air can permeate into the coal pile. Their net stock volumes were 15, 120 and 960 cm<sup>3</sup>, respectively.

As shown in Figure 1, the cube mesh-boxes were set in the constant temperature chamber where ambient air temperature was controlled to be a constant temperature ranging from 50 to 150 °C. Temperature sensors (thermocouple) were used to detect internal temperatures at 2 to 5 positions including the centre of the coal pile. They were installed from the open top into the coal pile.

The coal was loaded into the constant temperature chamber at room temperature (around 23°C). Each of the coal heating experiments using the cube mesh-box was done with separate constant temperature conditions to establish the self-heating characteristics of coal samples to ignition if it occurred.

### MEASUREMENT RESULTS AND DISCUSSIONS

Prior to measurements of CSIT, apparent density and thermal conductivity of the coal pile,  $\lambda$ , was evaluated. The samples have significantly different densities and heat capacities as shown in Table 1.

Figure 2 shows the difference in temperature profiles between the three samples after sitting in the hot ambient-air of 140°C. During the first 20 minutes from the start of the test, two samples #1 and #3 indicated similar temperature profiles, while sample #2 showed a smaller temperature rise rate than the others. The reason for this difference can be attributed to sample #2 having the highest moisture content and heat capacity of the three coal samples. After this initial stage of the heat conduction process, sample #2 showed a gradual temperature rise to reach a maximum temperature of 150 °C after 300 min, before decreasing to the set ambient air temperature. In contrast, samples #1 and #2 showed self-heating curves reaching ignition. Thus, it is clear that the CSIT value of samples #1 and #3 is lower than 140 °C, while that of sample #2 is over 140 °C.

Sample #1 had the shortest time to reach ignition. As such it is used to show the process of obtaining the CSIT value for the coal and the subsequent kinetic analysis derived from this value. Figure 3 shows test results for Sample #1 at different ambient air temperatures, to find the critical point of self-ignition. In this case the value is determined to be 123 °C (396 °K).

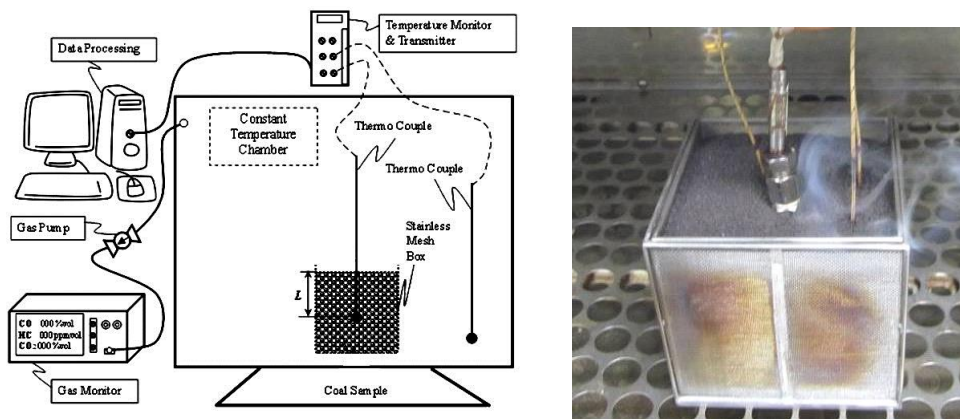


Figure 1 - Schematic figure and a photo of experimental apparatus

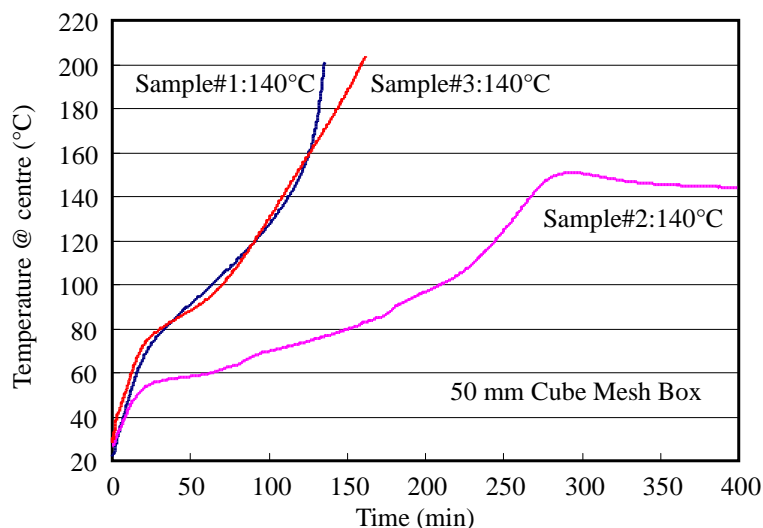


Figure 2 - Examples of temperature profiles at centre of 50 mm cube mesh-box for 140°C ambient air)

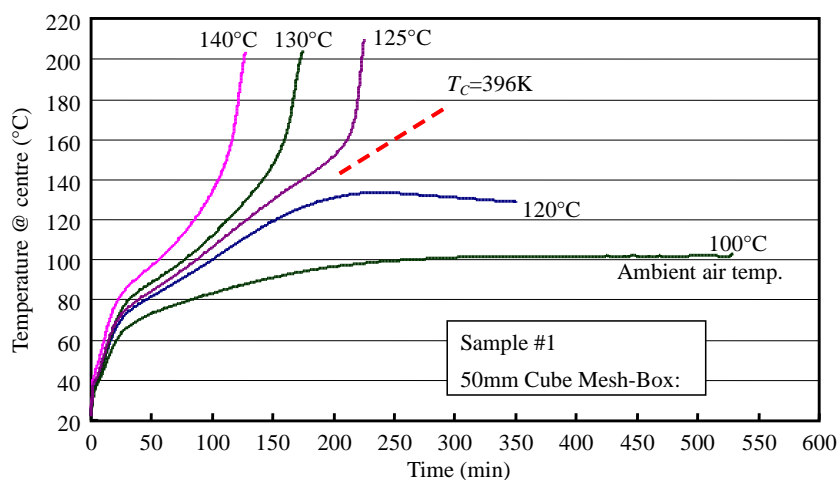


Figure 3 - Examples of temperature profiles for sample #1 at different ambient air temperatures at centre of 50mm cube mesh-box)

The data for the different mesh-box sizes are shown in Figure 4. Sample #1 shows a distinct linear relationship exists between CSIT and mesh-box size. The measured CSIT was lower for the large coal pile size and higher for the small coal pile size. This data can therefore be used to examine CSIT values for larger stockpile volumes.

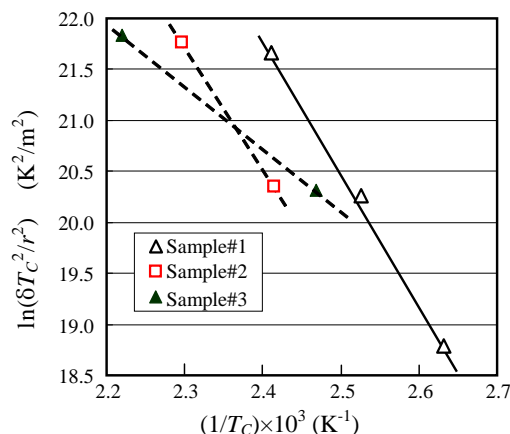


Figure 4 - Plotting  $\ln(\delta T_c^2/r^2)$  against  $(T_c)^{-1}$  based on critical self-ignition temperature (CSIT), showing results for different mesh-box sizes

### EVALUATION OF CRITICAL SELF IGNITION-TEMPERATURE FOR STOCKPILE VOLUMES

By using actual data from the experimental heating test results direct knowledge of the individual values of molar heat of reaction, apparent activation energy, frequency factor, thermal conductivity or specific heat of the coal samples is not needed, so far as the calculation of CSIT is concerned. By analysing the coal inside temperature and application of Fourier equation boundary conditions the self-heating data of the coal sample can be calculated. For example, the data for sample #1 in Figure 4 produces the linear relationship shown in Equation (2) and the slope of the line is equivalent to  $-E/R$ , which yields the activation energy for the coal as shown in Equation (3).

$$\ln\left(\frac{\delta T_c^2}{r_c^2}\right) = 52.8 - 1.29 \times 10^4 \frac{1}{T_c} \tag{2}$$

$$E = 107.4 \text{ kJ/mol} \tag{3}$$

The relation of  $(T_c - 273 = -7.0 \cdot \ln(V) + 65]$ , between CSIT ( $=T_c - 273$ ) ( $^{\circ}\text{C}$ ) and stockpile volume  $V$  has been obtained from Equations (2) and (3) for stockpile volumes extrapolated over  $0.1 \text{ m}^3$ . Figure 5 shows this relationship. The CSIT decreases with stockpile volume, while the elapsed time to get to CSIT increases with stockpile volume. Thus, preserving a large volume of coal stock without upsetting inside and outside has a large possibility inducing spontaneous combustion but takes longer elapsed time to get it.

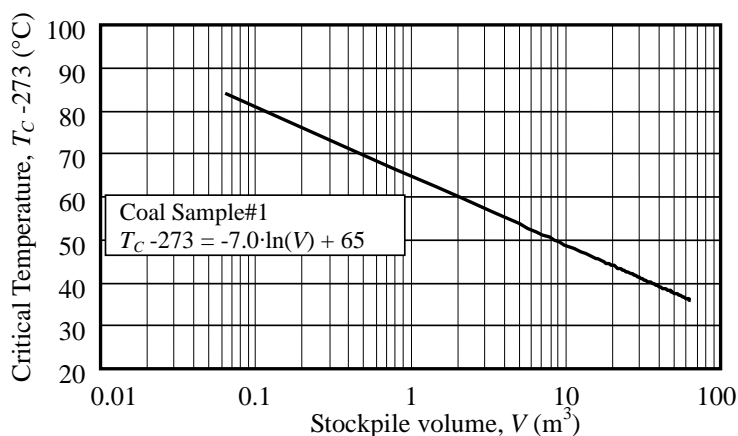


Figure 5 - A typical estimation of critical self-ignition temperature (CSIT) vs. corresponding to stockpile volume (Sample #1)

---

## CONCLUSIONS

The Critical Self-Ignition Temperature (CSIT) of coal is important to evaluate the possibility of spontaneous combustion of coal stockpiles. In this study, the profiles of temperature at the centre of a coal pile were measured for different ambient air temperatures from 50 to 140 °C, to calculate CSIT values for coal piles in cube mesh-boxes 25, 50, and 100 mm in length. Based on the Frank-Kamenetskii model, CSIT as function of pile size or volume was determined. Finally, the function of critical temperature has been applied to predict CSIT of larger stockpile volumes less than 50 m<sup>3</sup>.

## REFERENCES

- Bowes, P. C, 1984. Self-heating: Evaluating and Controlling the Hazards, pp 17-70 (HMSO: London).
- Frank-Kamenetskii D A, 1959. Wärme- und Stoffübertragung in der chemischen Kinetik (in German), (Springer Verlag: Berlin).
- Gray P and Lee P R, 1967. Thermal explosion theory, in Oxidation and Combustion Reviews (ed: CFH Tipper), vol. 2 (Elsevier: Amsterdam).
- Moghtaderi, B, Dlugogorski, B Z and Kennedy, E M, 2000. Effects of wind flow on self-heating characteristics of coal stockpiles, *Trans IChemE*, 78(6): 445-453.
- Nordon, P, 1979 Model for the self-heating reaction of coal and char, *Fuel*, 58(6): 456-464.
- Sasaki, K and Sugai, Y, 2011. Equivalent oxidation exposure - time for low temperature spontaneous combustion of coal, in *Heat Analysis and Thermodynamic Effects* (ed: A Ahsan), pp 235-254 (InTech).

# NUMERICAL MODELLING OF LOW RANK COAL FOR SPONTANEOUS COMBUSTION

Kyuro Sasaki<sup>1</sup>, Yongjun Wang<sup>2</sup>, Yuichi Sugai<sup>1</sup>, Xiaoming Zhang<sup>3</sup>

**ABSTRACT:** Transporting and stockpiling low-rank coals are puts them under risk of spontaneous combustion, because they are very easy to get self heating ignition after drying or removing moisture due to high moisture and oxygen contents. In this study, the modified concept of Equivalent Oxidation Exposure-time (EOE-Moisture time) has been presented for low-rank coals. The equations for the EOE-Moisture time have been formulated by considering moisture content and oxidation capacity in low temperature range to predict the heat generating rate as functions of coal moisture saturation and oxygen concentration in the pile. Numerical simulations were carried out by applying the EOE-Moisture time on self-heating of low rank coal by changing the coal stockpile size. It has been shown based on the numerical simulations that the temperature rising rate of the pile is increased with lower initial moisture saturation of low rank coal. It has been shown that coal including a large percent of moisture is easy to increase temperature and has a smaller critical diameter of coal stockpile size compared with coals with low moisture.

## INTRODUCTION

Demand for low rank coals, such as brown coal and lignite, has been increasing, because they have better characteristics for coal gasification and Coal Water Mixture (COM). However, they include high contents of water and oxygen and during transport are under risk of spontaneous combustion, because they are prone to self-ignition after drying or removing moisture that ranges around 30 to 50 % of their weight. Thus, some schemes to transport the low rank coals have been required.

As shown in Figure 1, the schematic process of spontaneous combustion was presented by Sasaki and Sugai (2011). Oxidation heat generated in the coal starts from the outside surface of the stockpile, because oxygen is supplied from the atmosphere. Some heat is lost to the atmosphere, but some also diffuses to inward to the centre of the stockpile. The outer part of the stockpile returns to the atmospheric temperature,  $\theta^0$ , after enough time. However, the oxygen concentration in the pile is kept at a relatively low concentration, because oxygen does not diffuse to the inner zone via the oxidation zone. When coal at the centre of the pile is preheated slowly without oxygen, a high temperature spot at the centre is generated. The oxidation and heat generation zone gradually moves from the pile surface to the centre while shrinking and rising in temperature. Finally a hot spot is formed at the centre.

In this study, the modified model on high moisture and reactive coal (hereinafter EOE-Moisture) has been presented based on the Equivalent Oxidation-Exposure time (EOE-time) that was presented by Sasaki and Sugai (2011) for bituminous coal piles in a low temperature range. The models of heat generation rate or  $O_2$  consumption rate and the EOE-Moisture time have been derived by multiplying a function of moisture saturation in micro pores characterizing low-rank coal matrix to the EOE-time model for a bituminous coal-pile. The model of EOE-Moisture time has been applied to simulate changes of temperature, oxygen concentration and moisture saturation in the coal pile.

## EOE-MOISTURE TIME AND HEAT GENERATION RATE OF LOW RANK COAL

### Heat generation rate from coal

In the present model, coal oxidation reaction includes physical adsorption and chemical adsorption via oxygen reaction at low temperatures. Measurement of the heat generation rate at the early stages of the process show that an exponential decrease has been reported by many experiments, such as that by Kaji *et al.*, (1987), as shown in Figure 2. Based on their measurement results, the heat generation rate

<sup>1</sup> Kyushu University, Faculty of Engineering, Nishiku, Fukuoka 819-0385, krsasaki@mine.kyushu-u.ac.jp: +81 92 802 3326

<sup>2</sup> Kyushu University, School of Engineering, Nishiku, Fukuoka 819-0385

<sup>3</sup> Institute of Engineering and Environment Liaoning Technical University, Huludao 125000, China

per unit mass of coal at temperature  $\theta(^{\circ}\text{C})$ ,  $q$  (W/g), can be expressed with a function of elapsed time after being first exposed to air,  $\tau$ (s):

$$q = C \cdot A \exp(-\gamma\tau) \quad (1)$$

where,  $A$  (kW/kg) is heat generating constant,  $C$  is molar fraction of oxygen, and  $\gamma(\text{s}^{-1})$  is the decay power constant. The initial order of heat generating rate of coal for exposing air is  $q(0) \approx 0.01$  to  $0.001$  kW/kg.

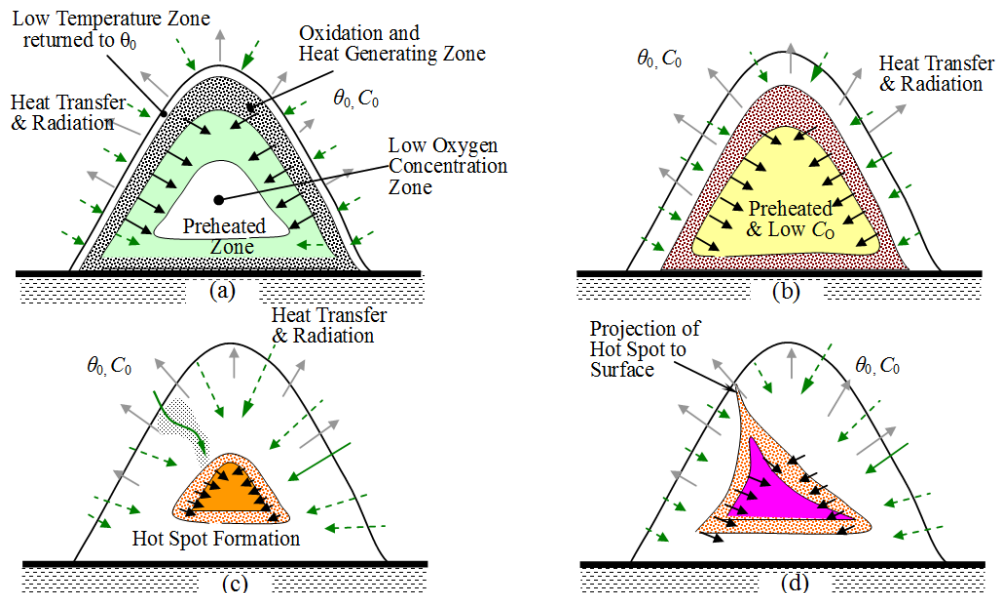


Figure 1 - Schematic figure showing self-ignition process of coal stockpile (Sasaki and Sugai, 2011)

### Arrhenius equation by oxidation

Kaji *et al.* (1987) measured rates of oxygen consumption due to coal oxidation in the temperature range 20 to 170  $^{\circ}\text{C}$  using coals ranging from sub-bituminous to anthracite. They reported that heat generated per unit mole of oxygen at steady state is  $h = 314$  to  $377$  (kJ/mole), and their results of the Arrhenius plots, the oxygen consumption rate versus inverse of absolute temperature  $T^{-1}$  ( $\text{K}^{-1}$ ), shows the model of Arrhenius equation. Thus, the higher the coal temperature; the faster the oxidation or adsorption rate. When the heat generation rate is proportional to oxygen consumption rate, the heat generated,  $A$ , can be estimated using the following equation,

$$A = A_0 \cdot \exp\left(-\frac{E}{RT}\right) \quad (2)$$

where,  $A_0$  (kW/kg) is the pre-exponential factor,  $E$  (J/mole) is the activation energy,  $R$  is the gas constant (J/mol/K), and  $T (=273+\theta)$  (K) is the absolute temperature. Kaji *et al.* (1987) has reported that the coals have almost the same activation energy of around  $E=50$  kJ/mole for the temperature range of 20 to 170  $^{\circ}\text{C}$ . On the other hand, the activation energy of fresh coal is expected to be much lower than that of exposed coal in air, because fresh coal adsorbs oxygen physically at an initial stage of self-heating. Average activation energy and decay power constant. For Japanese bituminous coals (see Tables 1 and 2), were used for the present numerical simulations.

### Equivalent oxidation exposure time (EOE-time)

The heat generating rate,  $q$ , is expressed as a function of  $\theta$ ,  $C$ , and  $\tau$ . Equations (1) and (2) can be used to calculate  $q$  for a constant temperature. However, they are not applicable for the calculation of the normal coal temperature change versus elapsed time. Its concept is partly similar to Elovich equation (see Nordon, 1979), but it provides a scheme to estimate  $q$  follows change of temperature of coal and

EOE-time (see Figure 3). For an example, assume a coal lump is placed in an environment in which  $C = 0.1$  and  $\theta = 45^\circ\text{C}$ , for elapsed time;  $\tau = 1$  h, and then it is stored in one of  $C = 0.2$  and  $\theta = 70^\circ\text{C}$  for another 1 h period. It is not possible to reconstruct this situation by adding the former and later times with different oxidation rates. In the numerical simulations, suppose the coal pile surface is exposed to air of oxygen concentration,  $C_0$ , air temperature,  $\theta_0$ , thermal diffusion and  $\text{O}_2$  gas diffusions are numerically calculated (see Figure 1).

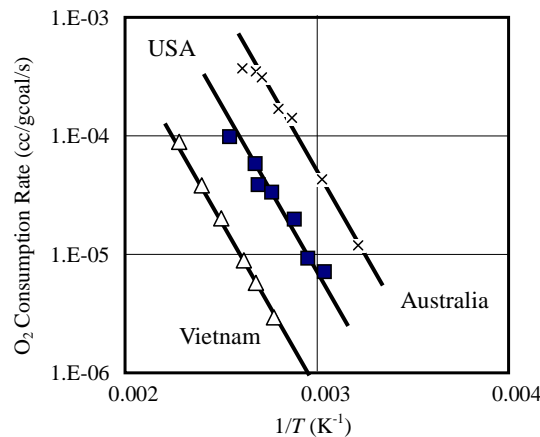


Figure 2 -  $\text{O}_2$  consumption rate of coals vs. inverse of absolute temperature measured by Kaji et al. (1987) (Coal samples were mined in USA, Australia and Vietnam)

Table 1 - Physical properties of coal used for numerical simulations (Sasaki and Sugai, 2011)

Coal Density	Moisture Content	Specific Heat of Coal	Thermal Diffusivity of Coal	Diffusion Coefficient
$\rho_{\text{coal}}$	$w_0$	$C_p$	$A$	$D$
1291 kg/m <sup>3</sup>	Bituminous c. : 5g/g Low rank c.: 30g/g	1.21 kJ/kg/°C	$6.8 \times 10^{-8} \text{ m}^2/\text{s}$	$7.1 \times 10^{-6} \text{ m}^2/\text{s}$

Table 2 - Heat generating properties of coal used for numerical simulations (Sasaki and Sugai, 2011)

Decay Power Constant	Pre-exponential Factor	Activation Energy
$\Gamma$	$A_0$	$E$
$3.0 \times 10^{-4} \text{ s}^{-1}$	Bituminous coal: 29 kW/kg Low rank coal: 88 kW/kg	20 kJ/mol

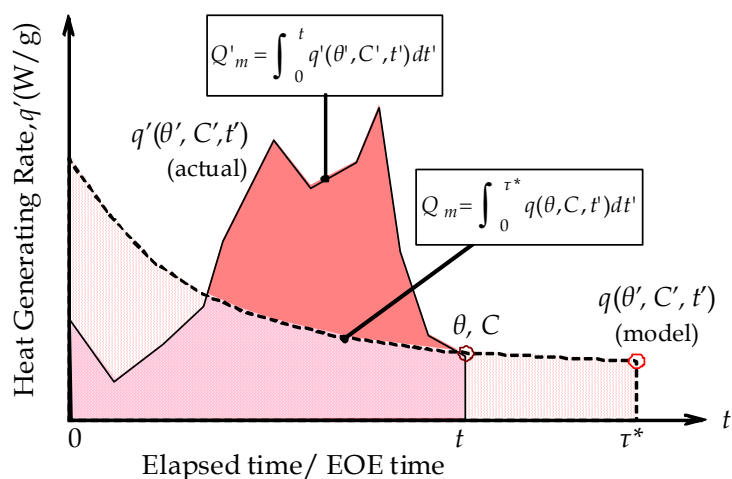


Figure 3 - Schematic definition of EOE-time of bituminous dry-coal to estimate heat generating rate by matching total heat generations (Sasaki and Sugai, 2011)

A new model of the elapsed time that considers the aging degree of the coal is required to overcome this difficulty. The cumulative generated heat of the coal,  $Q'_m$  (J/g) from elapsed time 0 to  $t$ , is defined as,

$$Q'_m = \int_0^t q'(\theta', C', t') dt' \tag{3}$$

where, the actual heat generation rate,  $q'(\theta', C', t')$ ,  $\theta'$  and  $C'$  are changing with the elapsed time,  $t'$ . However, the cumulative heat,  $Q'_m$ , for constant  $\theta$  and  $C$ , can be derived using Equations (1) and (2) from time 0 to  $\tau^*$ :

$$Q'_m = \int_0^{\tau^*} q(\theta, C, t') dt' = Q_m \tag{4}$$

If the amounts of accumulated heat,  $Q'_m$  and  $Q_m$ , defined in Equations (3) and (4), are equal,  $\tau^*$  in Eq. (4) expresses the aging time of the coal for constant temperature;  $\theta = \theta'(t)$  and constant concentration;  $C = C'(t)$ , for the actual elapsed time ( $t = t'$ ). In this paper,  $\tau^*$  is defined as the EOE-time (see Figure 3). It is calculated based on a summation of generated heat  $q'(\theta', C', t') \cdot \Delta t'$  over a numerical calculated interval time,  $\Delta t'$ .

**Characterisation of low-rank content of low-rank coals**

Low-rank coals are characterised by high porosity and internal surface area with low-rank content. As shown in Figures 4 and 5, internal surface area porosity were characterised against saturated moisture value based on measurement results of Illinois coals (Thomas and Damberger, 1976) in order to build up a modified numerical-model on oxidation and self-heat generation for low-rank coal.

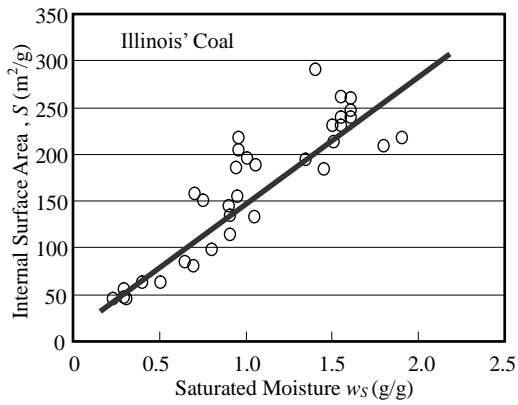


**Figure 4 - Model of the relationship between saturated moisture and internal surface area of low rank coal (see Thomas and Damberger, 1976)**

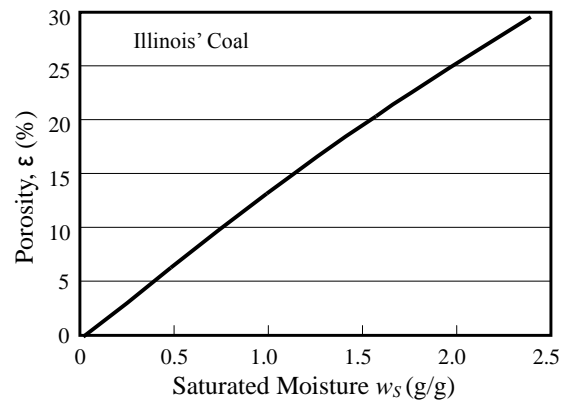


**Figure 5 - Model of the relationship between saturated moisture and porosity of low rank coal (see Thomas and Damberger, 1976)**

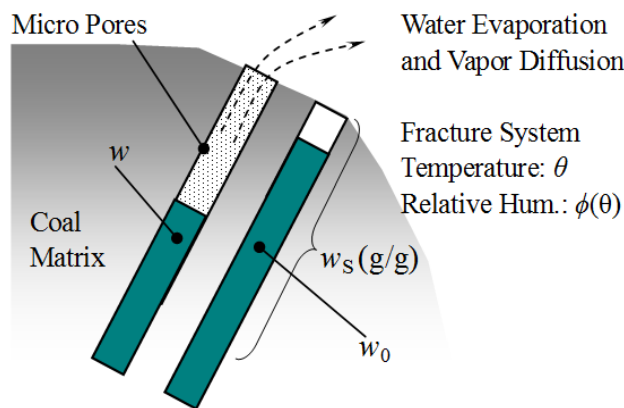


**Figure 6 - Model of moisture saturation in micro-pores of low-rank coal matrix**

### Formulation of EOE- Moisture model

Figure 6 shows a physical model of moisture saturation in micro-pores of coal matrix. The water evaporation rate (g/s),  $\partial w/\partial t$ , from micro pores to fracture channels in coal matrix is assumed to be proportional to the difference between moisture saturation and relative humidity as given by

$$\frac{\partial w}{\partial t} = \beta \left( \frac{w}{w_s} - \phi(\theta) \right) \quad (5)$$

where  $\beta$  (g/s) is mass transfer rate,  $\phi(\theta)$  is relative humidity at coal temperature  $\theta$ , and  $w_s$ (g/g) and  $w$ (g/g) are saturated moisture and moisture at a elapsed time in the micro pores of unit mass of coal matrix, respectively. The numerical modified models of frequency factor,  $A$ (kW/kg), and EOE-Moisture time,  $\tau^*$ , for low-rank coal are given by following equations (6) and (7) using moisture saturation as the analytical variable, because the internal surface area in the coal matrix can be assumed to be proportional to  $(1-w/w_s)$ .

$$A(\theta, w) = A_0 \cdot \exp\left(-\frac{E/R}{273+\theta}\right) \cdot \left(1 - \frac{w}{w_s}\right) \quad (6)$$

$$Q_m(\theta, w, \tau^*) = \int_0^{\tau^*} q(\theta, w, C, t) dt \quad (7)$$

For examples, when moisture is saturated ( $w=w_s$ ), the frequency factor becomes  $A=0$ , while  $A=A_0$  for bituminous dry coal ( $w=0$ ). Thus, the presented model has a function to promote self-heating after drying of coal matrix often observed in low-rank coals.

In the present numerical simulations, molecular diffusions of  $O_2$  and water vapor (moisture) in the coal pile as a porous media are considered by solving both partial differential equations for their concentrations with  $O_2$  consumption and water vapor evaporation rates. The block temperatures in the coal pile are also calculated numerically at each time step based on heat generation, EOE-Moisture time defined by Equation (7) and latent heat for water evaporation from micro pores. The drying process of coal matrix in the pile starts from initial moisture saturation,  $w_0$ (g/g), and relative humidity,  $\phi(\theta_0)$ , in atmospheric air.

## NUMERICAL SIMULATION RESULTS AND DISCUSSION

### Case of bituminous coal pile

Figure 7 shows the numerical simulation results of centre temperature,  $\theta_c$ (°C), of a bituminous dry-coal pile with sphere shape (diameter range:  $d_0=0.3$  to 10 m) versus elapsed time. The temperature at the centre of the pile is increased with elapsed time, but the cases of  $d_0 \leq 2$  m show the temperature returns to atmospheric and initial temperature  $\theta_0=25$  °C. This is because that the EOE-time increased by heat transfer to surrounding air makes reducing heat generation rate of coal lump even if its location is at the centre. However, the case of  $d_0 \geq 4$  m, coal at the sphere centre receiving enough heat in low oxygen concentration before oxygen diffuses into the centre, and lower EOE-time induces higher heat generation than that of  $d_0 \leq 2$ m before ignition and combustion of coal. The critical diameter getting self-ignition is roughly evaluated as  $d_0=3$ m for the initial temperature of  $\theta_0=25$  °C. The critical diameter depends on the activation energy,  $E$  and the decay power constant,  $\gamma$ , of the heating of coal pile.

### Case of low-rank coal pile

Numerical simulations on self-heating were carried out by applying the EOE-Moisture model for low-rank coal by setting various initial moisture saturation and relative humidity levels for atmospheric air. Figure 8 shows comparisons of temperature-time curves at the centre of a pile 10m in diameter to compare bituminous and low-rank coals. The results show that temperature rising of low-rank coal with  $w_0=0.3$  and  $\phi=0.7$  is higher than that with  $w_0=0.8$  and  $\phi=0.7$  after 400 days. The reason that low-rank coal of  $w_0=0.8$  showed low temperature rise is due to large latent heat of the drying process.

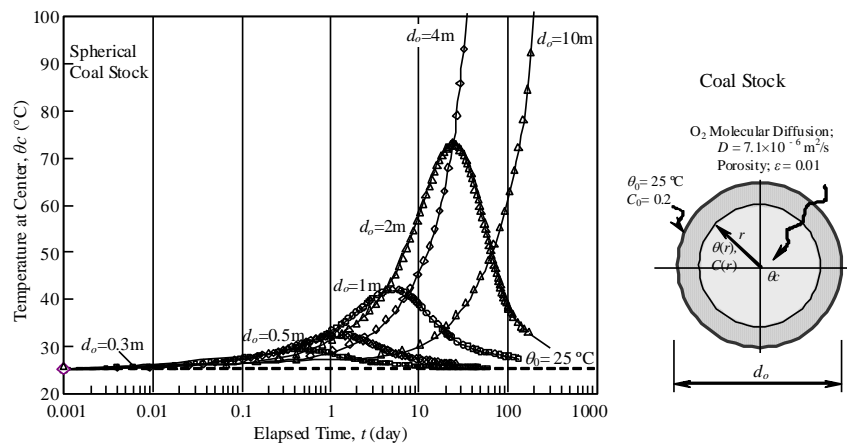


Figure 7 - Numerical simulation results on centre temperature of spherical coal stockpile of bituminous dry-coal with different diameter,  $d_0$  (m) (Tables 1 and 2)

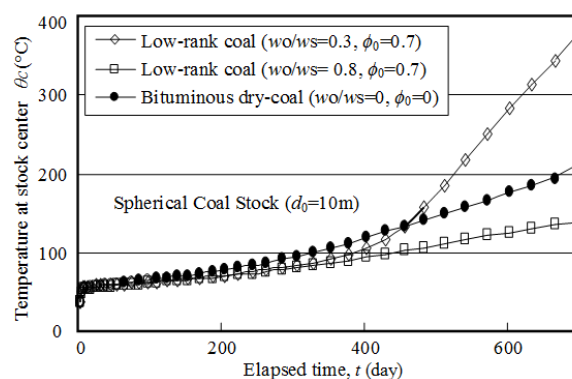


Figure 8 - Temperature-time curves at the centre in pile of bituminous and low-rank coals

## CONCLUSIONS

In this study, the modified concept of EOE-Moisture time has been presented for low-rank coals. The equations for the EOE-Moisture time have been formulated by considering moisture content and oxidation capacity in a low temperature range to predict heat generating rate as functions of coal moisture saturation and oxygen concentration in the pile. Numerical simulations were carried out successfully by applying the EOE-Moisture time on self-heating of low rank coal by changing the coal pile size. It has been simulated that temperature rising rate of the pile is increased with lower initial moisture saturation of low rank coal.

## ACKNOWLEDGMENTS

This work was supported by JSPS KAKENHI Grant Number 25303030, and thanks Dr. Arif Widiatomojo for his kind discussion.

## REFERENCES

- Kaji, R, Hishinuma, Y and Nakamura, Y, 1987. Low Temperature Oxidation of Coals-A Calorimetric Study, *FUEL*, 66-2, 154-157.
- Norder, P, 1979. A model for The Self-heating Reaction of Coal and Char, *FUEL*, 58(6): 456-464.
- Sasaki, K and Sugai, Y, 2011. Equivalent Oxidation Exposure - Time for Low Temperature Spontaneous Combustion of Coal, in *Heat Analysis and Thermodynamic Effects* (ed: A Ahsan), pp 235-254 (InTech).
- Thomas, J J and Damberger, H H, 1976. Internal surface area, moisture content, and porosity of Illinois coals: variations with coal rank, *Illinois State Geological Survey Circular*, 493, 1-38.

# ACTIVE BARRIER PERFORMANCE PREVENTING METHANE EXPLOSION PROPAGATION

Johannes Jacobus Labuschagne du Plessis<sup>1</sup> and Helmut Späth<sup>2</sup>

**ABSTRACT:** Over the past century, the coal mining industry experienced a large number of explosions leading to a considerable loss of life. Research was directed at preventing the accumulation of methane through good ventilation practice, eliminating frictional sparking by the use of water, minimising dust generation and dispersal, and using stone dust to inert coal dust to prevent it from participating in mine explosions. The final line of defence, though, is the use of barriers to prevent a coal dust explosion from propagating. However, the design of passive explosion barrier systems has remained unchanged for many years. The traditional stone dust and water barriers were originally designed and developed as much as 50 years ago. In the 1990s the CSIR of South Africa developed a new type of stone dust explosion barrier, which has been implemented in South Africa and Australia. This barrier is considered to be better suited to modern-day mining practice. It is based on an array of specially manufactured bags holding stone dust and suspended from the mine roof.

Preventing the propagation of methane or coal dust explosions through the use of active explosion-suppression systems remains one of the most underutilised explosion controls in underground coal mines. As part of the effort to develop better technologies to safeguard mines, the use of active barrier systems was investigated at Kloppersbos in South Africa. The system is designed to meet the requirements of the European Standard (EN 14591-4:2007) (European Standard, 2007), as well as the Mine Safety Standardisation in the Ministry of Coal Industry, Coal Industrial Standard (MT 694-1997) of the People's Republic of China.

From the tests conducted, it can be concluded that the HS Suppression System was successful in stopping flame propagation for a methane explosion, as well preventing methane explosions from progressing into methane and coal dust hybrid explosions when ammonium phosphate powder was used as the suppression material. The use of this barrier can provide coal mine management with an additional explosion control close to the point of ignition and may find application within longwall faces, further protecting mines against the risk of an explosion propagating.

## INTRODUCTION

Since the 1930s, increased use of mechanised mining machinery exacerbated the risk of frictional ignitions in working headings in which the interaction of cutting tools with quartz bands can result in incendive sparking capable of igniting methane. In recent times the introduction of powerful coal winning machines has further increased the number of frictional ignitions. For example, the mine disaster at Glace Bay, Nova Scotia, in 1979 claimed 12 lives. This explosion was attributed to a frictional ignition and the 1993 explosion at Middelbult Colliery in South Africa was also found to be the result of friction at a continuous miner pick. Many safety measures were researched and developed during the last century. Of these, the following have been instrumental in reducing the frequency and severity of explosions:

- The mixing of inert material with coal dust deposits
- Explosion barriers, both active and passive
- Knowledge and understanding of explosions and their prevention
- Development of permitted explosives
- Flameproofing of electrical apparatus and the use of intrinsically safe electrical circuits
- Improved ventilation practices
- Improved devices for the detection of flammable gases.

<sup>1</sup> Associate Professor, Department of Mining Engineering, University of Pretoria, Email: bagbarrier@gmail.com, Tel: +27 83 448 3737

<sup>2</sup> HS Design and Engineering, Email: hsd@icon.com, Tel: +27 827750910

Research conducted by Philips (1995) concluded that in South African mines an explosion starts at the working face where methane accumulations may occur during the coal-cutting activities. Although intense research attention has been paid to the development of preventive and protection measures against coal mine explosions, disasters still occur.

*“Of all the risks inherent in coal mining, the one most feared by coal miners is an explosion. Explosions are not the biggest cause of loss of life. On a statistical basis, explosions may be amongst the less frequent events in mining causing loss of life but, apart from fires and flooding, there is no other cause capable of wiping out the entire workforce below ground at the time.”* These words, written by Joseph Dickson, an Inspector of Mines in the Lancashire coalfield, United Kingdom, in 1850 remain equally valid today.

In this paper a summary of the development and evaluation work done utilising the ExploSpot active suppression system against methane gas explosions developing into coal dust explosions will be described.

## BACKGROUND

According to Du Plessis and Späth (2002), the aim of using active suppression systems is to contain the methane flame in the immediate vicinity of the ignition. This will prevent a methane explosion from developing which, in turn, could be the ignition source of a coal dust explosion. Active suppression systems have the following main components:

- Detecting sensor/s
- Electronic control and self-checking system
- Dust containers
- Flow nozzles.

These individual components are combined into systems, which are mounted on continuous heading machines. When an ignition occurs, its presence is detected by means of the sensor/s. These sensors are normally sensitive to the ultraviolet light range. An electronic signal from the sensor triggers the suppression system, creating a barrier of flame-suppressing material and containing the flame in the immediate vicinity of initiation. The flame-suppressing material most frequently used is ammonium phosphate powder, but gases such as NAF SIII chemical fire extinguishing agent may also be considered.

There are two testing facilities for the evaluation of these systems, namely the tunnel at BVS-Derne in Bochum, Germany, and the 20 m tunnel at Kloppersbos, South Africa. A number of systems have been developed by the Deutsche Montan Technologie (DMT) (Faber, 1990) for roadheaders. These have been in underground use since 1989 and are well proven and trusted. A test facility capable of testing such systems against a set protocol (Du Plessis, 1998) was built and completed during 1995 at the CSIR's Kloppersbos Research Facility. The facility simulates the various mining configurations encountered in bord-and-pillar mines. To date, three systems have undergone successful evaluations. The first system was developed for low-seam continuous miners (Du Plessis, 2001) and the second for a Dosco 1300H auger-type roadheader (Du Plessis, *et al.*, 1999) capable of excavating a seam height of up to 4.5 m. The third system was the ExploSpot system (Du Plessis and Späth, 2001) for medium seam conditions and some of the results will be discussed in the paper.

The second system is used in mining conditions where the roof slopes at an angle of 12 degrees and a double-pass mining method is employed. For this specific evaluation, the maximum height of the roof was 4.5 m. The system was deployed at the HBCM mine in the south of France (Du Plessis and Van Dijk, 2001).

### Description of system and components

ExploSpot is an intrinsically safe, high-speed flammable gas-ignition detection and suppression system capable of creating an extinguishant barrier within 100 milliseconds.

The ExploSpot system consists of three main components, namely the control electronics, the dual-spectrum sensor units and the discharge assemblies. The control electronics are connected to the peripheral sensor units and discharge assemblies, constantly monitoring the connections so that the system will always be functional when required. The sensor units are placed to monitor the entire tunnel area for any methane ignition or coal dust flame. These units are specially designed to react only to certain light wavelengths specific to burning methane and coal dust, thus reducing the risk of a false ignition. The discharge assemblies are configured for the particular conditions found within a specific mine, the cross-sectional area of the tunnel and the method of coal extraction being applied. They are also configured to ensure the correct powder distribution and concentration for the successful extinguishing of any explosion or ignition.

The system is designed to meet the requirements of the European Standard (EN 14591-4:2007), as well as the Mine Safety Standardisation in the Ministry of Coal Industry, Coal Industrial I Standard of the People's Republic of China (MT 694-1997). It is also designed to comply with the International Standards (IEC) to meet the intrinsically safe and flameproof standards: IEC 60079-11:1999 and IEC 60079-0:2005 for intrinsically safe equipment, and IEC 60079-0:2004 and IEC 60079-1:2004 for flameproof equipment.

The severity of an explosion is directly related to the rate of flame propagation (Cashdollar and Hertzberg, 1989). Figure 1 shows a typical methane gas flame propagation speed and distance plot.

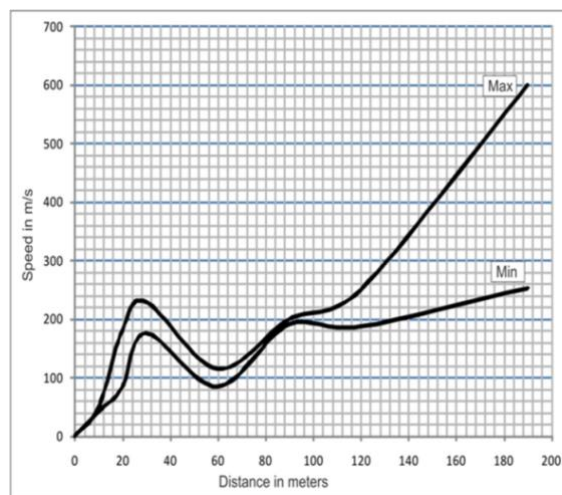


Figure 1 - Typical plot of gas explosion speed versus distance

As such the design of any active barrier system requires rapid and accurate response and distribution of flame suppressant material.

## TYPES OF SYSTEM

### Machine-mounted systems

The objective of suppressing methane ignitions within the face area where frictional ignition caused by the mining of coal occurs can be achieved by using machine-mounted systems. These systems detect the ignition of methane caused by the continuous miner or roadheader picks. They will also detect any other ignition sources (e.g. electrical) and will prevent the methane ignition from propagating within the face area. Modern continuous miners utilise a combination of systems to prevent a methane gas ignition from occurring: the use of flameproof equipment, ventilation of methane gas from the face and around the continuous miner (CM), a wet cutter head and active suppression barriers. Figure 2 shows the components of a CM ExploSpot system.

### Roadway systems

The use of an active barrier system for inbye protection, close to the face area, has the additional advantage that it is capable of protecting outbye areas by preventing methane explosions from developing into coal dust explosions. Furthermore, it does not require any dynamic pressure build-up for

activation as activation is dependent on flame detection. Figure 3 shows a graphical representation of all the system components. This includes the complete unpacked system of detectors, controllers, high-pressure bottles and spray bar and nozzles.

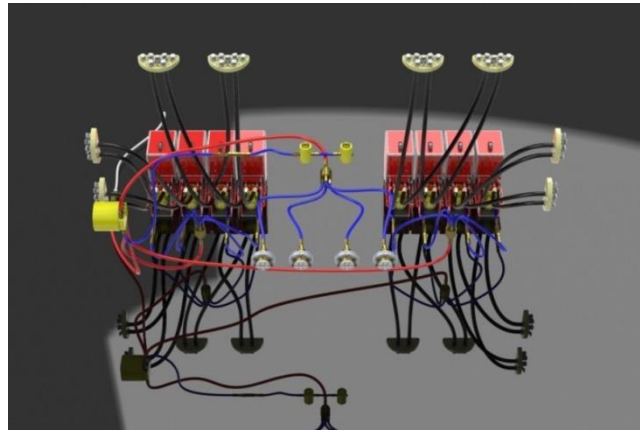


Figure 2 - Typical continuous miner layout for the ExploSpot system



Figure 3 - Graphical representation of the active barrier system components Testing facilities and Evaluations

### 10 m test tunnel results

The objective of the test work was to investigate the operational effectiveness of the triggered barrier system in stopping the methane/coal-related explosions that can occur during typical auger mining operations and to demonstrate its effectiveness to Auger mining of South Africa AMSA, DME and the coal mining industry (Moolman, *et al.*, 2006). Tests were conducted in the 10 m explosion test tunnel to determine the effectiveness of the triggered barrier system in stopping propagating methane explosions, simulating flame exiting from the opening of a production hole. Employees of HS Design Engineering undertook the set-up of the suppression system 1.5 m outside the 10 m tunnel, while CSIR employees prepared the tunnel for testing. Only ammonium phosphate powder was used as the suppression agent.

The evaluation simulated a typical auger operation set-up as far as practically possible. In order to test the system under the most severe conditions, no auger flights were placed in the 10 m tunnel. In the auger mining application, the active suppression system can only be mounted on the auger outside the production hole, thus far away from the cutter head. As the cutter head is most likely to be the only ignition source and the auger hole the only roadway for the ignition to propagate in, it can be expected that the explosion would exit the auger hole in due course. This is, however, dependent on the amount of fuel and oxygen available and on the amount of confinement achieved by the number of auger flights trailing the cutter head.

The 10 m test tunnel had previously been erected at the CSIR's Kloppersbos Research Facility for the purpose of testing machine-mounted active suppression systems. This tunnel was used to simulate the dimensions of an auger hole, and a full-scale model of the triggered barrier system was constructed 1.5 m in front of the tunnel opening for test purposes. The Kloppersbos explosion tunnel is 10 m long, with a diameter of 2 m. It is raised 700 mm above a cement floor with one side is sealed off by a steel plate. During a suppressed explosion, the steel plate acts as an emergency pressure-release mechanism in the event of very high pressures building up in the tunnel (see Figure 4 which shows the 10 m test tunnel with an explosion-stopping wall built over it). During normal tests, the pressure wave and the flame exit the mouth of the tunnel unhindered.



**Figure 4 - 10 m test tunnel at Kloppersbos**

In one test a fuse cap was used to ignite the methane/air mixture. In all the other tests a shielded detonator was used to ignite the flammable gas mixture. The fuse cap was initially chosen for use as it produced a flame that would not be seen or recognised by the triggering mechanism of the suppression system. The detonator was shielded from the triggering system; the reason for using it was to create a more violent methane explosion. The chamber containing 23 m<sup>3</sup> of methane/air mixture was obtained by placing a plastic membrane 7 m from the closed end of the tunnel. This amount of methane/air mixture will produce enough wind pressure to lift the coal dust into the air, supply sufficient heat to the coal dust particles for flame propagation to take place and be sufficient to ensure flame growth up to 5 m beyond the tunnel mouth.

For most of the active suppression system tests conducted in the 10 m test tunnel, an explosion mixture of 9% methane/air per volume was used. This was done to test the triggered barrier system under simulated worst-case scenarios. A small amount of coal dust was placed on racks at the open end of the 10 m tunnel. The main reason for adding this dust was to change the colour of the methane flame to assist in the visual evaluation of the system's success or failure. The amount of coal dust used did not change the characteristics of the explosion.

The measure of success was defined to indicate whether the flame propagation was stopped inside the tunnel opening (referred to as "stopped inside"). The results of the methane explosion tests are shown in Table 1:

In every test the flame was stopped at the tunnel opening, with no flame visible from the front and perpendicular to the tunnel. Each explosion was further captured on camera, and a record of the photos and the video material was used to evaluate the success of the flame suppression.

The ExploSpot system registered a methane ignition and opened the extinguishing cylinders within 20 ms. The suppressing agent sealed off the tunnel opening completely within 30 ms, preventing the flame from penetrating the suppressant material. During these tests the suppressing agent was initially dispersed at high pressure (stored at 60 MPa in the cylinder) and velocity into the propagating flame front. From the tests conducted, it was concluded that the machine-mounted ExploSpot system was successful in stopping a methane flame in the tunnel opening.

**Table 1 - Results of the performance of the ExploSpot system**

Test No.	Methane concentration	Initiator used	Visible flame	Comments
1	7.5%	Detonator	None	One cylinder failed, flame stopped successfully
2	9%	Detonator	None	Flame stopped successfully
3	9%	Detonator	None	Flame stopped successfully
4	9%	Fuse cap	None	Flame stopped successfully
5	12%	Detonator	None	Flame stopped successfully
6	9%	Detonator	None	Flame stopped successfully. Small flame could be seen at the back of the tunnel.

### 20 m test tunnel: Facility for testing machine-mounted systems

A 20-m test tunnel was erected at the Kloppersbos Research Facility to suit the double-pass mining method associated with the use of a continuous miner. The protocol for testing the ExploSpot system was developed by a forum including representatives from industry, government and labour organisations. The tests were carried out in accordance with a protocol developed by the CSIR for such testing (Du Plessis, 2001). This protocol drew on experience with a similar protocol which had been accepted by the South African Safety in Mines Research Advisory Committee (Du Plessis, *et al.*, 1999) for previous tests, as well as a protocol accepted by INERIS of France (Du Plessis, 1998).

The protocol defines acceptance criteria in accordance with which the results of the tests would be either accepted or rejected, and the tests themselves either passed or failed (Du Plessis, 2001). The protocol stipulates the following acceptance criteria:

- The flame should not propagate along the tunnel in line with the operator's position – so that the operator is not exposed to any direct flame.
- The temperature increase at the operator's position should not exceed human tolerance levels (in this case 100 °C for less than half a second).
- Both the dynamic and static pressures measured should be within human tolerance limits.
- There must be no false triggering of the system due to other equipment being used underground.
- The system should be up and running again within eight hours of a detonation.

This tunnel was modified to simulate the dimensions of mine workings of medium seam height, and a full-scale model of the Joy 12HM9 continuous miner was used for test purposes. The test tunnel is 20 m long and 7 m wide, with a variable height of 2 to 6 m. It has a cement floor and springs along both sides, on the outside, supporting and guiding it. For the case of an un-suppressed explosion, the tunnel is able to lift up to 140 mm off its base to provide an alternative escape route for the expanding gases. For the full-face conditions, the cross-sectional area was approximately 21 m<sup>2</sup>. Later, after the full-face tests had been completed, a shoulder was built into the left front of the test tunnel to simulate the out-shoulder conditions. A 4 m-long shoulder was built into the right-hand front corner of the tunnel to simulate the two-cut scenario where the machine was mining next to the shoulder.

In accordance with the protocol (Du Plessis, 1998), the test sequence was carried out in order of ascending difficulty. Three main placements of the machine inside the tunnel were tested, as well as sub-conditions for the placements of the boom (and thus ignition) for these machine positions, and, of course, the various methane concentrations. The testing began with the 9% methane/air explosion for full-face conditions (see Table 2). This was successful, with no flame being detected along the right-hand wall of the tunnel (the operator's cab position is on the right-hand side of the machine). Some flame was, however, detected at the roof and along the left-hand wall of the tunnel.

The pressure rises caused by the explosion were so small that they were almost zero. For these tests, the highest temperature rise at the operator's position was approximately 93 °C. The operator and the rest of the crew working at the face would be safe under the worst possible conditions.

Once the full-face tests were complete, a 4-m shoulder was put in place against the front right-hand wall of the tunnel, simulating the second cut. The machine was moved in adjacent to this wall for the in-shoulder tests. The results of these tests are shown in Table 3.

**Table 2 - Full-face active suppression test results**

Test	CH <sub>4</sub> /air (%)	Flame length (m)	Temp. increase (°C)
77	9.0	6	80
78	9.0	6	NR*
79	9.0	6	93
80	9.0	6	70
81	9.0	6	NR*
82	12.0	5	58

\* NR = no temperature rise

**Table 3 - In-shoulder active suppression test results**

Test	CH <sub>4</sub> /air (%)	Flame length (m)	Temp. increase (°C)
92	9.0	6	33
93	9.0	3	33
94	9.0	4	33
95	9.0	5	33
96	12.0	5	33
97	9.0	5	33

For the in-shoulder testing, all tests complied with the protocol, with the system successfully suppressing all the explosions for the different ignition (and machine-boom) positions. For this series of tests, the highest temperature rise measured at the operator's cab was approximately 33 °C, and once again the pressure sensors detected almost no pressure variations due to the explosion. In none of the cases was any flame detected at the operator's cab position.

For the final series of tests, the machine was pulled out from next to the shoulder, and the boom moved to simulate cutting the shoulder. The results of these tests are shown in Table 4.

**Table 4 - Out-shoulder active suppression test results**

Test	CH <sub>4</sub> /air (%)	Flame length (m)	Temp. increase (°C)
85	9.0	8	100
86	9.0	7	96
87	9.0	8	100
88	12.0	8	81
89	9.0	8	98
90	12.0	8	32
91	7.5	6	32

The tests were completed uneventfully for all the given positions and different concentrations for the out-shoulder machine conditions. The maximum length of the flame extension was 8 m (the operator's position was now at 9 m for the out-shoulder tests). Once again, the pressure sensors detected almost no pressure changes.

The system proved itself to be effective in detecting and suppressing explosions when configured and mounted on a Joy 12HM9 model for a cross-section with an area of approximately 21 m<sup>2</sup>. To test the system for South African medium-seam mining conditions, a second mining cut was simulated, resulting in a potential increase in the explosive volume of methane. The ExploSpot system complied effectively with all the requirements of the test protocol.

### 200 m test tunnel: Facility for testing roadway barriers

The 200-m test tunnel was used to conduct various tests. A comprehensive description of the tunnel was given by Cook (1993). The test tunnel was instrumented with flame sensors and a data acquisition

system for the evaluation. The tests were conducted with and without coal dust present. The different baseline explosions were:

- Baseline 1:  $75 \pm 1 \text{ m}^3$  methane/air mixture without coal dust
- Baseline 2:  $75 \pm 1 \text{ m}^3$  methane/air mixture with coal dust

For the ExploSpot system evaluation in the 200 m test tunnel both explosions were used to evaluate the performance of the system. For the Baseline 2 explosion, coal dust is distributed on the floor and shelves of the tunnel (for 60 m after the membrane position). This results in a methane-initiated coal dust explosion. The test sequence included the placement of the HS Design Suppression System at the following positions within the 200-m test tunnel:

- some 5 m from the closed end, i.e. within the methane chamber
- some 7 m from the closed end, i.e. within the methane chamber
- some 12 m from the closed end, i.e. within the methane chamber

The purpose of the tests was to attempt to simulate explosion scenarios and to relate the results obtained in the test tunnel to those likely to be obtained in a mine. The Measure of success was defined to indicate whether the flame propagation was:

- stopped inside the barrier (referred to as "stopped inside" in tables)
- stopped at the barrier (referred to as "stopped on the spot")
- "stopped".

An explosion is considered to have been "stopped on the spot" if the flame does not exceed a distance of 30 m beyond the end position of the barrier. Furthermore, the barrier is considered to have "stopped" an explosion if the flame propagation (i.e. flame distance) is less than what it would have been without a barrier installed.

Test 2 was the baseline test in which no suppression system was placed in the tunnel. In this test the methane explosion propagated beyond the 71-m sensor position with an average calculated flame speed of 216 m/s at the 41-m sensor position, reaching a maximum calculated flame speed of 249 m/s. Figure 5 shows the flame speeds for the baseline methane explosion and for the tests with the active system in place for the installation positions at 5, 7 and 12 m.

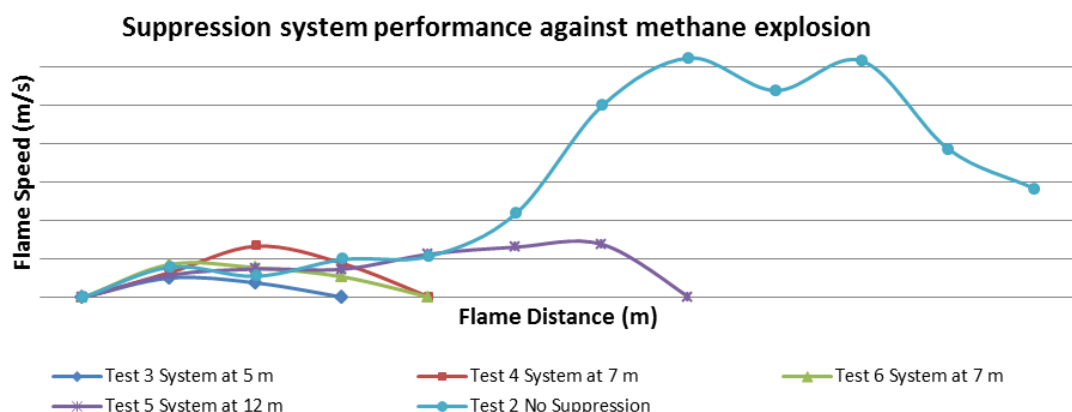


**Figure 5 - Test 2 (baseline) flame and performance of the active barrier**

The active barrier successfully suppressed the propagating methane flames approaching the barrier at flame speeds varying from 13.4 m/s during test 3 to 53.2 m/s during test 4. In test 5 the flame stop position was at 21 m and only in this test did the flame progress beyond the barrier position, although the flame is still considered to have been "stopped on the spot".

Tests 1 and 7 were baseline explosion tests with coal dust placed outbye of the methane chamber. In these tests no suppression system was placed in the tunnel; they were done to determine flame propagation speeds and maximum flame travel. In these tests the coal dust explosion flames propagated beyond the final sensor positions at 81 m and reached maximum speeds of between 306.8 and 366.3 m/s at the 41 m sensor position.

In the tests with a single suppression system installed at 5 and 7 m and a double system at 7 and 12 m respectively, it was clear that the methane ignition was inhibited to such an extent that no coal dust participated outbye of the barrier position.

The average flame speed for the baseline and for the flame inhibition by the active barrier system when installed at 5 m, 7 m and at 7 and 12 m is shown in Figure 6.

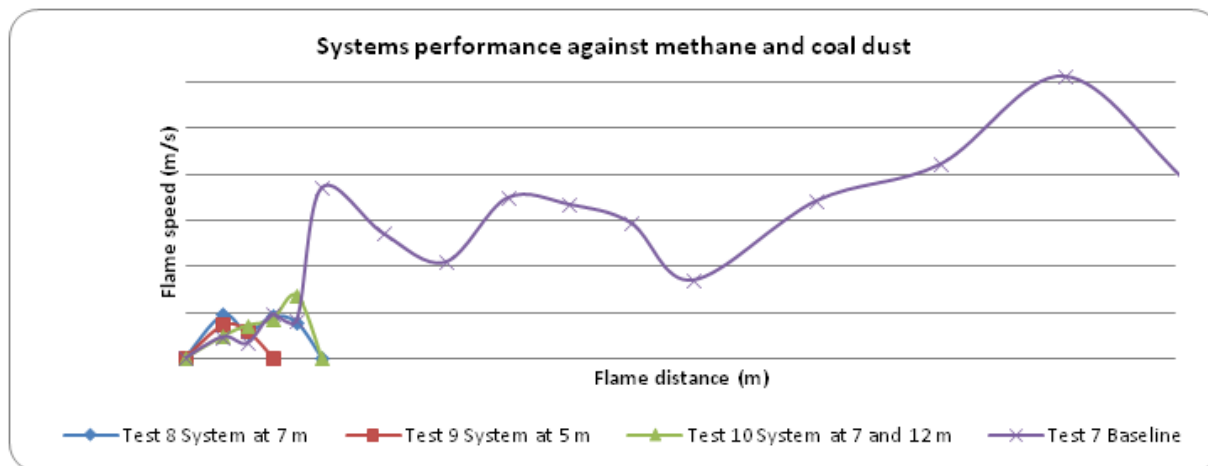


**Figure 6 - Tests 8, 9, 10 and 7 average (baseline) flame speed and active barrier performance**

In all the tests the system was successful in suppressing flame propagation. In each case the performance of the system can be classified as “stopped on the spot”, i.e. the flame was stopped at the position at which the system was placed. The active barrier successfully suppressed propagating coal dust flames approaching the barrier at flame speeds varying from 24.4 to 62.2 m/s.

In the unsuppressed explosion, the flame front reaches a distance of 180 m within 750 milliseconds, while the flame front, with the system installed at 30 m from the end of the tunnel, does not reach 50 m.

The test results in the 200-m Kloppersbos tunnel were extrapolated to design the active suppression protection system for longwall mining. The 200-m tunnel provides a means of conducting large-scale evaluations and assessments of barrier performance and other requirements that cannot be done economically by other means.

## DEPLOYMENT OF SYSTEMS

A total of 17 machine-mounted systems have been deployed in South Africa at Sasol mines and Anglo Thermal Coal operations. The system has successfully suppressed methane gas ignitions on five separate occasions.

In China more than 400 systems have been deployed. The system is utilised within longwall operations to protect against ignitions associated with shearer frictional events. It is also deployed as a roadway barrier within 30 m of the tailgate position. Recent legislative changes in China have resulted in it being made mandatory to install ExploSpot systems on roadheaders and to install roadway barriers in all returns in Shanxi Province and Liaoning Province.

## CONCLUSIONS

In protecting a mine against methane and/or coal dust explosions many different controls are implemented. However, many of these controls remain under the control of man. In this context the use

of active barrier systems can assist mine management in the prevention and control of the risk associated with mine explosions.

The results obtained in the 10 m, 20-m and 200-m test tunnels at Kloppersbos still need to be considered in terms of the constraints of the different tunnels and different evaluation protocols. Nevertheless, from the tests conducted it can be concluded that the ExploSpot system was successful in stopping methane explosions and the associated flame propagation when ammonium phosphate powder was used as the suppression material.

In all the tests conducted, both methane explosions and methane and coal dust hybrid explosions, the ExploSpot system stopped the flame spread, thus successfully preventing coal dust from participating in the methane ignition.

## REFERENCES

- Cashdollar KL and Hertzberg M. 1989. Laboratory study of rock dust inerting requirements: Effect of coal volatility, particle size and methane addition. In *Proceedings of the 23rd International Conference of Safety in Mines Research Institutes*, Washington DC, USA.
- People's Republic of China, Coal Industrial Standard I of the, MT 694-1997.
- Cook P. 1993. The inhibition of coal-dust explosions with stone dust in a large-scale explosion gallery. Report ENER 93-001, CSIR Division of Energy Technology, South Africa.
- Du Plessis J.J.L. 1998. Roadheader active suppression protocol. Internal Report, CSIR Division of Mining Technology, South Africa.
- Du Plessis J.J.L. 2001. Evaluation protocol for active machine-mounted explosion suppression systems for continuous miners. EC 01-0149, CSIR Division of Energy Technology, South Africa.
- Du Plessis J.J.L, Oberholzer J.W and Bryden D.J. 1999. Testing of active ignition on-board suppression systems for use in South African collieries. *Proceedings of the 6<sup>th</sup> International Mine Ventilation Congress*, Paper 19.
- Du Plessis J.J.L and Späth H. 2001. Development and testing of an on-board active suppression system for continuous miners in medium-seam mining conditions. Paper presented at the Occupational Health and Safety Congress, Terrigal, NSW, Australia.
- Du Plessis J.J.L and Späth H. 2002. Triggered barrier system performance in a 200-m test gallery at Kloppersbos. Paper presented at the 9<sup>th</sup> North American Ventilation Congress, Kingston, Ontario, Canada, June.
- Du Plessis J.J.L and Van Dijk R. 2001. Testing of an on-board active suppression system for French mining conditions. *Journal of the SAIMM*, July.
- European Standard EN 14591-4. 2007. *Explosion Prevention and Protection in Underground Mines Protective Systems Part 4: Automatic Extinguishing Systems for Road Headers*.
- Faber M. 1990. Development of automatic extinguishing systems for roadway drivage with cutter head subcut machines. DMT Research Report 323/408/84, Bochum, Germany.
- International Standard, IEC 60079-11, 1999: *Intrinsic Safety*, IEC 60079-0, 2005: *General Requirements*, IEC 60079-0, 2004: *Hazardous Locations* and IEC 60079-1, 2004: *Flameproof enclosures 'd'*.
- Moolman C.J, du Plessis J.J.L and Späth H. 2006. Explosion-suppression system for surface augers. Mining achievements, records and benchmarks. SAIMM Conference, Johannesburg, South Africa.
- Philips H.R. 1995. Coal mine explosions – The South African experience. *Proceedings of the 26th International Conference of Safety in Mines Research Institutes*, Katowice, Poland, Vol. 2, pp 89-102.

# IS CARBON MONOXIDE SENSING AN EFFECTIVE EARLY FIRE DETECTION OPTION FOR UNDERGROUND COAL MINES?

Frank Mendham<sup>1</sup>, David Cliff<sup>2</sup> and Tim Horberry<sup>3</sup>

**ABSTRACT:** The ability of carbon monoxide (CO) sensing to detect early stage smouldering of fixed plant fires in underground coal mines was recently assessed as part of an ongoing fire detection research project. Experiments were carried out to record the level of CO concurrent at the time of alarm activation of a Video Based Fire Detection (VBFD) system. The tests were carried out under simulated mine conditions within the SIMTARS facility at Redbank, Queensland. The experimental setup initially located the CO sensors in the positions at where they would typically be installed underground. On testing the experimental setup, it was found that the amount of CO produced from simulated overheating conveyor belt bearing housings did not display a reading on the CO sensors. The VBFD system however detected smoke and alarmed on each of the trial tests. To enable the experiments to proceed and a comparison to be made, the CO sensors were moved considerably closer to the weak pyrolysis fire source. The question of CO sensor capability in typical operational mine positions was highlighted as a result of this experiment. Computational Fluid Dynamics (CFD) modelling was used to estimate the fire size required to activate CO sensors under typical mining conditions. This modelling reinforced the limitations in using CO detectors on fixed plant. As such, the study presented here indicates that CO sensing may not be the most effective early fire detection option available, and that further research and development work with VBFD should be undertaken.

## INTRODUCTION

A recently completed stage of an ongoing fire detection experimental research project recorded the levels of carbon monoxide (CO) from a series of comparable small fires (Mendham, *et al.*, 2013) concurrent with the time of smoke recognition by a Video Based Fire Detection (VBFD) system. Whilst the project is part of an investigation into the potential to improve fire life safety and asset loss control in underground coalmines (Mendham, *et al.*, 2012) using VBFD, it revealed some interesting conclusions in relation to the limitations of CO detection.

The initial challenge in developing VBFD was perceived to be the underground mining environment itself, which has poor light levels, variable ventilation rates and the possible presence of water mist, dust and other pollutants, potentially obscuring the target video image from the VBFD. This situation seems not to provide a very suitable environment for quality video capture (Damjanovski, 2005), so the primary purpose of the experiments was to simulate such conditions to test the capability of the VBFD whilst comparing its performance with CO detection.

To obtain consistent and repeatable results, a controlled and closely monitored simulated underground mining environment was sought. Additionally, an aim of the experiments was to acquire a base line for possible modifications that may be required to develop VBFD to operate effectively underground. SIMTARS (Mendham, *et al.*, 2013) at Redbank in Queensland, Australia, was able provide a suitable testing environment.

Although the proposed reference fire was considered 'small' in fire engineering terms (ABCB, 2005), it was appropriate for its intended purpose. The aim was to simulate the overheated housing of a conveyor belt bearing undergoing seizure whilst being layered with combustible coal debris and grease. The resultant designed fire produced a non-flaming pyrolysis plume with the heating source being a propane gas heated 250 mm diameter circular surface. The fire source was estimated to have a Heat Release Rate (HRR) of 0.99 kW (Mendham, *et al.*, 2013). This heat release rate is analogous to the heat release rate of a typical single bar household electric strip heater.

<sup>1</sup> PhD Candidate, Minerals Industry Safety and Health Centre, Sustainable Minerals Institute, University of Queensland, M: 04 2 140 7633 E: f.mendham@uq.edu.au

<sup>2</sup> Professor of Occupational Health and Safety in Mining, and Director, Minerals Industry Safety and Health Centre, Sustainable Minerals Institute, University of Queensland, M: 04 0199 3760; E: d.cliff@mishc.uq.edu.au

<sup>3</sup> Associate Professor of Human Factors, Minerals Industry Safety and Health Centre, Sustainable Minerals Institute, University of Queensland

Figure 1 shows the experimental test rig with the propane burner obscured from the remote video detectors using a metal shield to prevent false activation caused by the burner flames. A thermocouple in the centre of the coal covered heated metal surface can also be seen. The CO sensors are not shown in this image, however they were suspended from the ceiling using taut metal wire in predefined proximity to the test rig.

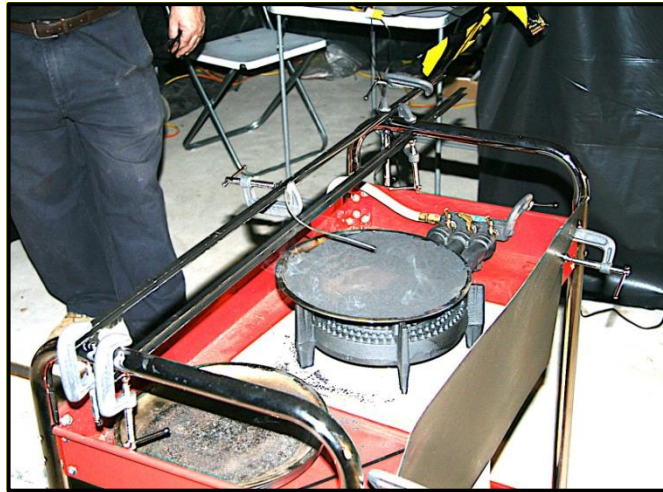


**Figure 1 - Experimental test rig used to simulate an overheated bearing housing**

The experimental plan initially located the three CO sensors, with respect to the position of the fire source and as viewed from the VBFD end of the room, in the following positions:

- 10 m outbye the fire source (i.e. 10m outwards towards the mine portal)
- 1.2 m above the fire source
- 9.5 m inbye the fire source (i.e. 9.5m inwards into the mine with respect to the fire source)

The experimental setup located two independent VBFD cameras adjacent to each other with both focussed on the fire source on the outbye end of the room. The purpose of this was to compare the VBFD response time between cameras. When the first VBFD camera detected smoke, CO readings from the three strategically located CO sensors (Mendham, *et al.*, 2013) were recorded, as were the VBFD alarm times.

It was found during the initial setup experiments that display readings greater than the default value of "0.00 ppm" of CO would not display on the CO sensors in any of the planned experimental setup positions even though the VBFD system detected smoke on each test at an early fire growth stage. The CO sensors were subsequently rechecked for operability and calibration by the SIMTARS technicians and found to be correctly functioning (Mendham, *et al.*, 2013).

The CO sensors were progressively moved closer to the fire source after each unsuccessful setup test until the correct readings were eventually displayed. This action was essential, as the planned VBFD experiments could not proceed without comparative CO levels at the time of VBFD activation.

The final positions of the three suspended CO sensors are shown in Figure 2. These were the CO sensor positions that allowed the final VBFD experiments to proceed. Note that Figure 2 shows a light haze of visible smoke at the ceiling level concurrent with the time that the CO sensors commenced to display values of CO.

In summary, the final positions of the CO sensors used in the experiments were:

- 1.0 m outbye the fire source
- 0.1m adjacent the fire source
- 0.8 m inbye the fire source

This paper addresses the following research question:

“What is the approximate Heat Release Rate (HRR) of a belt fire that can generate CO at a concentration recognised under legislative requirements so as to activate CO sensors in locations where they would typically be installed in an operational underground coal mine”



**Figure 2 - Positions of CO sensors during the experimental setup showing low-level readings**

## METHOD

Following the SIMTARS experiments, a Computational Fluid Dynamics (CFD) model (McGrattan, *et al.*, 2007) was developed to simulate the subject small pyrolysis plume formed from the combustion of coal fines and grease (Mendham, *et al.*, 2013) on the surface of an overheated conveyor belt bearing housing. CO production was one of several outputs modelled and it was found that the numerically estimated CO levels were consistent with the recorded levels of CO produced in the experiments. Based on this verification, it followed that by increasing the design fire size in the CFD model, a virtual increase in CO would result. This CO modelling capability provided the means to test the hypothesis that VBFD sensing is a more effective means than CO sensing for detecting fixed plant fires in the very early stage of development in underground coalmines.

As the Fire Dynamics Simulator (McGrattan, *et al.*, 2007) CFD model could be used to simulate larger fires involving increased products of combustion, including CO, the development of the numerical assessment method necessarily incorporated the following steps:

1. Determine the target fire alarm concentration of CO required under legislation

The target concentration of CO typically indicative of a fire alarm event in an underground mine in ppm was sourced to be used as a reference value in describing the effectiveness of CO sensors compared with VBFD. Supplementary information was also sought from a Queensland coalmine Senior Ventilation Officer and an Underground Mine Manager.

2. Define additional CO sensor locations to simulate an actual mine setup

Additional CO sensors were required to be incorporated in a new CFD model. The final SIMTARS experiments located the CO sensors in positions much closer to the fire source than they were intended (Mendham, *et al.*, 2013). The two (2) other scenarios relating to additional CO sensor positions involved the positioning of the sensors at increased distances from the fire source.

- a. One scenario involved the CO sensors being positioned according to the initial experimental plan.
- b. The other scenario involved the location of further CO sensors where they would typically be installed in an operational underground coalmine (Qld Dept. Mines and Energy, 2005).

3. Develop the CFD model/s to simulate a larger model space for the experimental design fire and a further model using the same model space simulating a larger design fire capable of producing significantly greater levels of CO.

A CFD model was originally developed to simulate the pyrolysis plume formed from the combustion of 40g of coal fines and 40g of grease (Mendham, *et al.*, 2013) being typical of deposits on the surface of an overheated conveyor belt bearing housing in a 35 m model space. The updated numerical modelling achieved:

- a. The existing input parameters and assumptions of the actual experiments into two redefined CFD models. One model maintained the original small pyrolysis design fire, but in an increased model space length of 135 m. Some of the experimental parameters included air velocity, temperature, coal and grease characteristics. The second model incorporated a larger design fire (1 m<sup>2</sup> of coal surface) in order to achieve a much greater CO production to activate remote CO sensors and to demonstrate more onerous escape conditions for mine workers under simulated conditions in the 135 m model space.
  - b. The incorporation of six in total additional CO sensors including the three sensors associated with the original planned experimental locations, which were found to be unsuccessful in the experimental setup tests and a further three sensors located at 25 m, 50 m and 100 m inbye the fire. Each detector was located at a height of 2m above floor level, except for the detector, which was 0.1 m adjacent to the fire source, as it was located 1.3 m above floor level, which was the height of the fire source itself above floor level.
4. Compare the CFD results showing CO levels between the two different fires and a comparison of heat release rates between the fires. Develop graphs from the FDS (McGrattan, *et al.*, 2007) output that:
    - a. Compare the growth in fire size in HRR in kW with the amount of CO produced in ppm over time.
    - b. Compare the response times for the CO sensors at each location to reach legislated alarm levels in ppm. indicative of a fixed plant fire underground.

## RESULTS

Methods headings Parts 1 to 4 above correspond respectively with Results headings Parts 1 to 4, as follows: -

- 1 The target fire alarm concentration of CO required under legislation

Both New South Wales statute (Coal Mine Health and Safety Regulation (NSW), 2006) and Queensland coal mining legislation (Coal Mining Safety and Health Regulation (Qld), 2001) are risk based, so do not prescribe the concentration levels of CO indicative of an event that would require a fire alarm alarm to be activated.

For example, the legislative requirement for Queensland (Coal Mining Safety and Health Regulation (Qld), 2001) is: "when the products (of combustion) are detected, the automatic activation of an alarm located on the surface in a position that is generally under observation to warn persons of the products' presence" is required. To understand how this risk is managed, information received from a Queensland coalmine Senior Ventilation Officer stationed at an anonymous mine, but indicative of many Australian coalmines indicated that:

"The monitors that are setup for the purpose of monitoring for fire in the belt roads alarm at 2 ppm and 5 ppm and the returns from the panels are 5 ppm and 10 ppm." (Anonymous, 2013, pers. comm., 15 May) and;

"There is only one monitor installed along the length of the belt, at the down wind end, and one in the return of each panel." (Anonymous, 2013, pers. comm., 15 May) and

"No we don't have CO monitor points at transfers, as there is a monitor mounted at the down wind end of the belt." (Anonymous, 2013, pers. comm., 15 May)

Further information was sought from an experienced Underground Mine Manager relating generally to underground coalmines. "The setting for underground CO monitors varies but generally is in the range of 4 to 10 ppm. They are set after determining background levels, which are normally determined by diesel equipment exhaust concentrations. They are also set differently for different mining panels e.g. a mains panel sees the total exhaust concentrations from vehicles travelling into the mine whereas a longwall panel will only see concentrations from the machinery operating in that panel during long wall moves where there is a large number of operating equipment, the levels again will be different. Another place where levels will need to be set higher is on the return side of a diesel service bay where diesel equipment is tested." (Hart, 2013, pers. comm., 1 July)

For the purposes of the CFD modelling developed for this research, the CO sensor threshold point was set at 10 ppm being an average level recorded experimentally.

## 2 Additional CO sensor locations

The CO sensor locations used in the experiments and included in the original CFD model were: -

- 1.0 m outbye the fire source at 2 m above floor level
- 0.1 m adjacent the fire source at 1.3 m above floor level
- 0.8 m inbye the fire source

The additional CO sensor locations defined in the original experimental plan, but found to be unsuccessful during the experimental setup and now included in the additional CFD model, are as follows:

- 10 m outbye the fire source at 2 m above floor level
- 0.8 m above the fire source at 2 m above floor level
- 9.5 m inbye the fire source at 2 m above floor level

The additional CO sensor locations based on the expert independent advice provided by a) the experienced Underground Manager (Hart, J 2013, pers. comm., 1 July) and b) the Ventilation Officer In Charge (Anonymous, 2013, pers. Comm., 15 May), indicated that the CO monitor could be located a significant distance from the source of the fire in practice. These further CO sensors were located: -

- 25m inbye the fire source at 2m above floor level
- 50m inbye the fire source at 2m above floor level
- 100m inbye the fire source at 2m above floor level

The fire source was located between 30 m and 30 m from the opening of the model space, so effectively 30m inbye the simulated mine portal.

In the CFD model, CO sensors are numerically ordered from 'CO#1' to 'CO#9'. Table 3 summarises the CO sensor locations and CO sensor reference numbers, as well as the fire source location.

## 3 Redefine and develop the CFD model

### *CFD model results*

'CFD Model 1' (CFD1) simulated the experimental pyrolysis fire representing the overheating of the surface of a conveyor belt bearing housing undergoing failure due to seizure, whereas 'CFD Model 2' (CFD2) simulated a larger coal fire where the coal surface was 1m<sup>2</sup>, therefore representing fire spread beyond the point of origin. Figure 4 compares the fire plume development for both CFD1 and CFD2 at the same time (750 seconds). Note that a considerably larger smoke yield in CFD2 compared with CFD1 indicating the larger fire size of the CFD2 model.

4 Compare the CFD results showing CO levels between the two (2) different fires and a comparison of heat release rates between the fires.

*CO Production*

Figure 5 graphically compares the CFD1 simulation with the CFD2 simulation showing considerably greater CO development in the latter compared with the former. The tenability for escaping mine workers in the scenario represented by CFD1 simulation is less onerous compared with the scenario represented by the CFD2 simulation, based on CO production (Qld Dept. Mines and Energy, 2005 – 2012) and on visible smoke.

Note that even with a large fire producing up to ten (10) times more CO than the smaller fire, only CO#2 and CO#5 exceeded 10 ppm. CO.

**Table 3 - Summary of CO sensor and fire source locations**

Point	Location (All set at 2m above floor level except CO#2, which was set at 1.3m.)	Comment
Fire Source	Between 30m and 30.2m from the simulated mine portal (CFD1)	The fire associated with CFD2, the larger fire, is between 29.6m and 30.6m from the simulated mine portal.
CO#1	0.7m outbye the fire source	CO#1 – 3 represents the CO sensor locations that were the result of their relocation closer to the fire source until a CO reading occurred on at least one (1) sensor. These sensor locations were those used in the experiments
CO#2	0.1m adjacent the fire source	
CO#3	0.8m inbye the fire source	
CO#4	10m outbye the fire source	CO#4 – 6 are the additional sensor locations included in the CFD models representing the CO sensor locations that were planned to be used, but unsuccessful as the CO sensors could not detect CO.
CO#5	0.8m above the fire source	
CO#6	9.5m inbye the fire source	
CO#7	25m inbye the fire source	CO#7 – 9 are the additional sensors based on typical mine sensor locations informed by expert independent advice.
CO#8	50m inbye the fire source	
CO#9	100m inbye the fire source	



CFD1



CFD2

**Figure 4 - Comparison of simulated smoke plume development CFD1 and CFD 2 at 750 seconds**

*Heat release rate*

CFD1 is based on a weak pyrolysis plume resulting from the overheating of a coal fines covered bearing housing associated with an underground conveyor belt. CFD2 is based on a 1m<sup>2</sup> coal fire representing the growth of the fire beyond CFD1 to a much larger section of belt. The heat released from the fire estimated in CFD2 is significantly greater (nearly 30 times greater) than that of CFD1. This demonstrates that if a fire is left undetected it may fully develop (ABCB, 2005) and be more difficult for mine workers to traverse the section of roadway where the larger fire exists compared with the smaller fire typical of CFD1.

The estimated maximum HRR of CFD1 is approximately 11 kW, whereas should the fire grow to a 1m<sup>2</sup> surface area in the same time period, the estimated HRR for CFD2 is almost 340 kW.

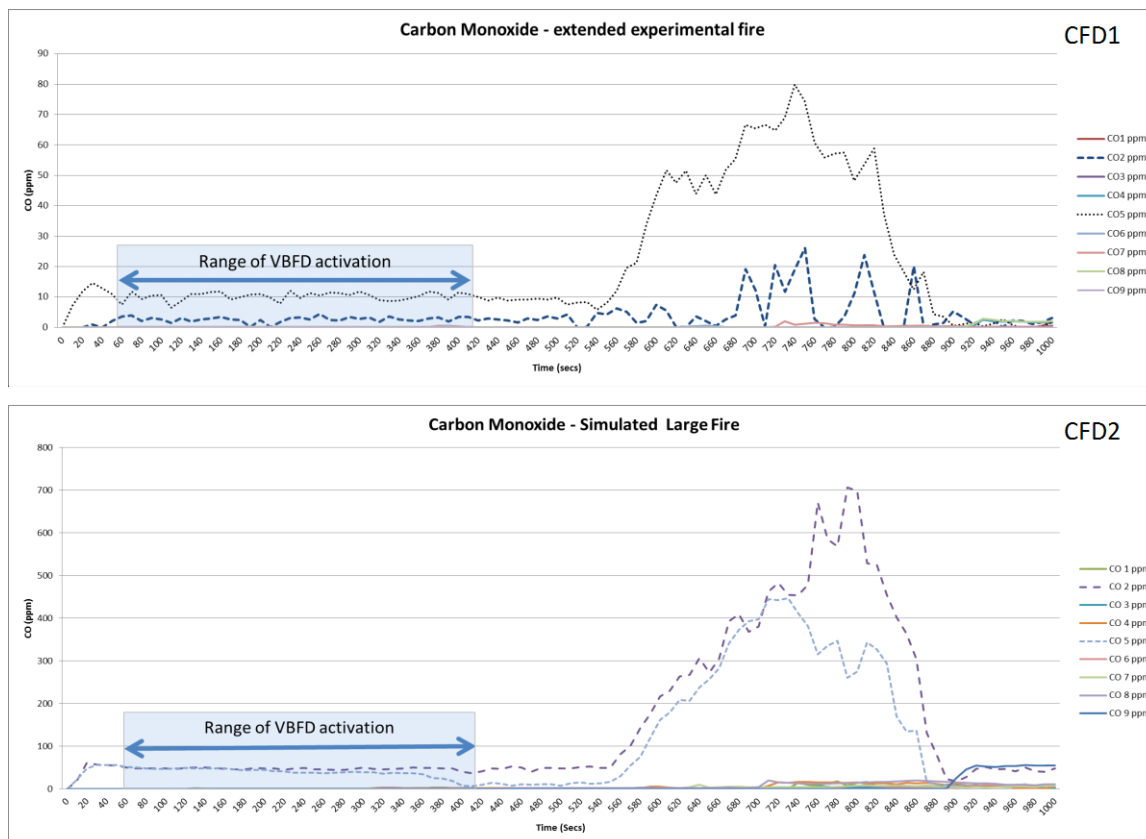


**Figure 5 - Comparison of CFD simulations of a small fire validated against the SIMTARS experimental fire (CFD1) with a larger fire (CFD2) both referenced to the experimental VBFD activation range**

The Available Safe Evacuation Time (ASET) (ABCB, 2005) under such larger fire conditions is typically less than that for fires detected in their early stage of development, so a significant increase in the fire life safety risk as a result of increased radiant heat flux on mine workers attempting to pass the larger fire source is likely to exist, as well as the increase in products of combustion.

Figure 6 compares the Heat Release Rate (HRR) of the two fire scenarios modelled in CFD1 and CFD2.

## DISCUSSION AND CONCLUSIONS

Three significant conclusions were derived from the comparative CFD modelling validated by the testing at SIMTARS:

1. A significant fixed plant fire can be developing that CO detectors, as currently employed by underground coalmines, would not detect but VBFD would.

Figure 5 clearly shows that for either fast growing larger fires (340 kW in 750 seconds) or slow weak smouldering fires (11 kW in 750 secs) VBFD can detect smoke reliably at an early stage of growth (40 to 400 seconds). CO detectors located where they would typically be located in an operational mine however did not receive adequate levels of CO from the either the small or large fires to exceed the notional alarm levels required to initiate an evacuation as a result of CO concentration. Only the CO detectors located very close to the fire source in both simulations received a significant level of CO in the order of 10 to 50 ppm.

2. CO as a detection means is complicated by the other sources of CO in a mine.

Opinion from expert mining officials indicates that varying ambient CO levels result from mine development activities. Under such circumstances, background CO levels could easily mask levels of CO commensurate with an early stage fixed plant fire. This might result in delayed fire detection, therefore delayed evacuation and significantly greater asset loss.

3. If a fire reaches the size where CO detectors would alarm, there already exists a significant risk to life and assets.

The results of the subject experiments and numerical simulations indicate that CO levels from fixed plant fires are slow to migrate throughout a mine to a level required to register a CO detector reading commensurate with the need to evacuate an underground mine. The results show that if typically located CO detectors cause a fire alarm level to be achieved, then the fire is likely to be quite significant. Ominously, CO detection is considered under most legislative regimes to be an effective form of early detection of fires in underground coalmines, but its actual and simulated performance has been shown to be less effective than VBFD in experimental and simulated environments. For this reason, VBFD should be subject to further testing in an operational underground coal mine to validate and check its robustness.

In practice, if mine workers are warned of a potentially growing fire, avoidance action can be taken to escape the fire in its early stages to a place of safety before the fire grows. The activation of an alarm to initiate the evacuation is essential either by means of properly located CO gas level monitoring points or, as proposed in the experimental research, by VBFD. In this research, it was shown that the very early detection of fixed plant fires using VBFD outperformed CO sensing in both the experimental and numerically simulated environment and is likely do so in an operational environment. More robust testing of VBFD in operational mines is required to confirm the reliability of VBFD.

At this time it is recommended that fire detection systems able to detect early products of combustion, such as VBFD, be used in conjunction with CO detection, as considerable detection delay is encountered for small fires where only low levels of CO are released in the early pre-growth stage.

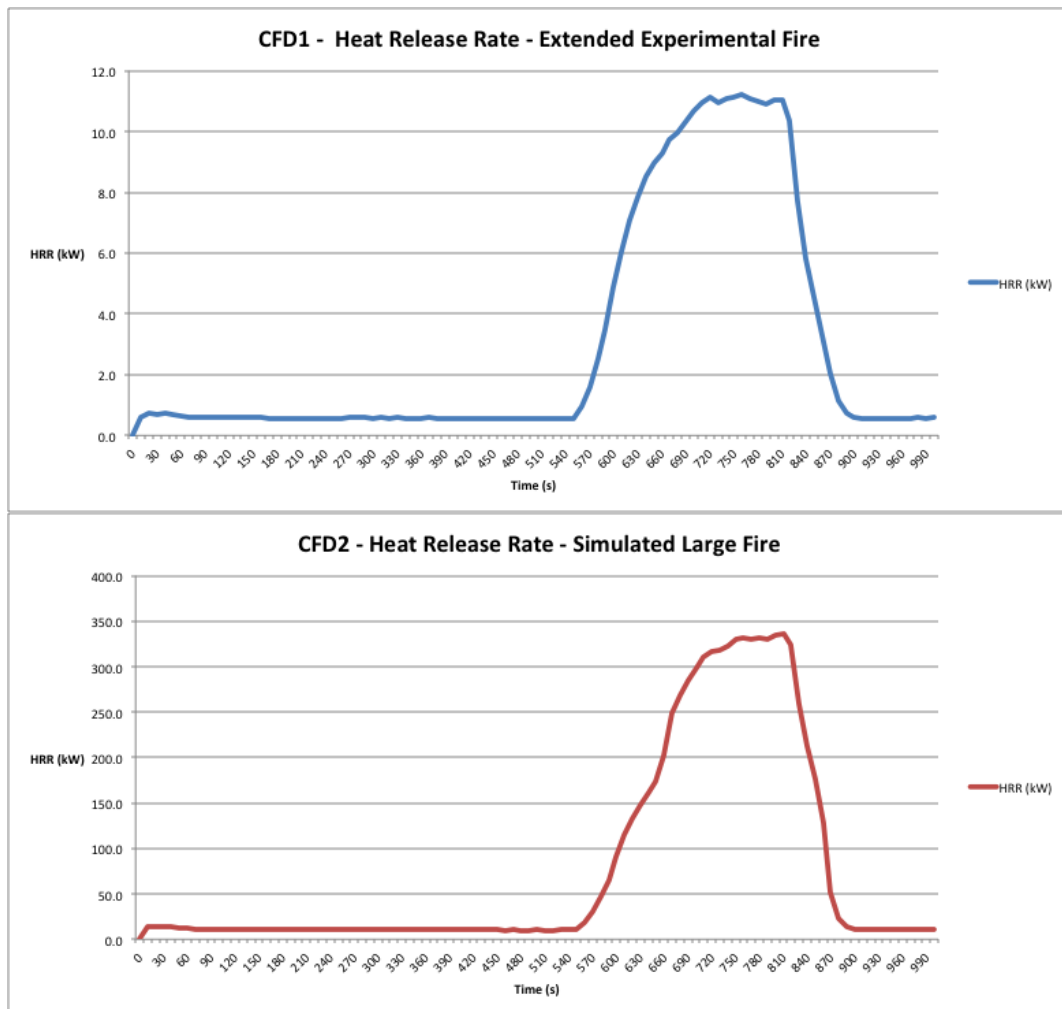


Figure 6 - Comparison of CFD1 and CFD2 - heat release rates

---

**REFERENCES**

- Australian Building Codes Board, 2005. *International Fire Engineering Guidelines Edition 2005*, 2005 edn, Australian Building Codes Board, Canberra, ACT.
- Coal Mining Safety and Health Regulation, 2001* (Qld).
- Coal Mine Health and Safety Regulation, 2006* (NSW).
- Damjanovski, V, 2005. *CCTV Networking and Digital Technology, 2<sup>nd</sup> edn*, Elsevier Butterworth Heinemann, Burlington, MA, USA.
- McGrattan, K., Klein, B., Hostikka, S., Floyd, J, 2007 *NIST Special Publication 1018-5 - Fire Dynamics Simulator (Version 5) - Technical Reference Guide*, Baltimore, Maryland, USA.
- Mendham, F, Cliff, D, Horberry, T and De Kocke, A, 2013. *Early fire detection in underground coal mines*, in proceedings of Coal 2013, pp 259 - 265. (AusIMM and University of Wollongong: Wollongong). <http://ro.uow.edu.au/coal/462/>.
- Mendham, F, Cliff, D and Horberry, T, 2012. *A quantitative approach to engineering fire life safety in modern underground coal mines*, in proceedings of Coal 2012, pp 326 - 334. (AusIMM and University of Wollongong: Wollongong). <http://ro.uow.edu.au/coal/422/>.
- Queensland Department of Mines and Energy, 2005 – 2012, *Level 1 Evacuation Reports (various)*.

# DEVELOPMENT AND UTILISATION OF FIBRE OPTIC-BASED MONITORING SYSTEMS FOR UNDERGROUND COAL MINES

Saied Mostafa Aminossadati<sup>1</sup>, Mohammad Amanzadeh<sup>1</sup>, Mehmet Siddik Kizil<sup>1</sup> and Tongyu Liu<sup>2</sup>

**ABSTRACT:** The continuous economic growth and depleting shallow reserves have increased the number of deeper mining operations worldwide which has made safety and productivity more challenging due to the higher stresses, heat and increased gas contents. Any major improvements in safety and productivity require a reliable and real-time monitoring system that provides more comprehensive information about various processes. The current monitoring systems suffer from lack of reliability, accuracy and high capital and operating costs. Recent advancements in fibre-optic based sensing technology have introduced unique solutions for various underground coal mine applications such as health and safety, geotechnical, ventilation, borehole, mine environment and condition monitoring. This paper presents recent research, development and utilisation of this technology by a group of researchers at the University of Queensland (UQ) and CRCMining in Australia and Shandong Academy of Science in China.

## INTRODUCTION

The capacity of optical fibres to transmit large quantities of information has revolutionised the world of telecommunications. The advancement of research and development of fibre-optic sensing technology has resulted in the production of various fibre-optic sensors such as temperature, strain, displacement, rotation, pressure, gas, liquid level, radiation and vibration sensors. The advantages of these sensors have extended their applications in various engineering and medical fields. Fibre-optic sensors are chemically inert, non-electrical and intrinsically safe. They offer high sensitivity, real-time measurements and immunity to radio frequency and electromagnetic interference. The capacity to transmit light over many kilometres makes fibre-optic sensors a natural candidate for remote sensing in mining applications; however, there has been limited strategic planning for identification and adoption of potential fibre-optic sensing technology in mining applications. The mining industry needs to realise the importance of this technology in improving safety and productivity in various mining operations. The main challenge for the mining industry is to distinguish between the fibre-optic sensing systems that bring immediate value exhibiting a small technology implementation gap and those that need further fundamental research and development.

## FUNDAMENTALS

A fibre-optic cable normally consists of a number of optical fibres. An optical fibre mainly consists of three components: the core, the cladding and the coating. The typical structure of an optical fibre is presented in Figure 1. Light propagates mainly along the core of the fibre that is generally made of glass or plastic. The cladding layer is also made of glass or plastic but with a smaller index of refraction compared to that of the core. The role of the cladding is to keep the light within the core and prevent any loss of light from the core into the surrounding. The cladding also increases the strength of the fibre and protects it from the environmental effects. Extra protection of the fibre is provided by the coating that is a layer of plastic on the cladding.

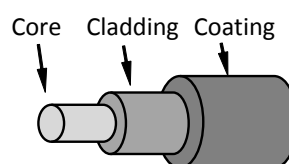


Figure 1 - Main components of an optical fibre

<sup>1</sup> The University of Queensland, CRCMining, Australia, Email: uqsamino@uq.edu.au, Tel: 07 3365 3676

<sup>2</sup> Shandong Academy of Science, China

## Fibre-optic sensing

The main parts of a fibre-optic sensing system are an optical fibre cable, an optical source, a transducer, and an optical detector (Figure 2). Depending on the application of the sensing system, the optical source can be lasers, diodes, and/or LEDs. The transducer is either an external sensing head or the optical fibre. In recently developed sensors, new types of optical fibres such as Fibre Bragg Gratings (FBGs) are used as the sensing head (transducer). In a fibre-optic sensor, the variation in the optical signal through the transducer that is caused by the physical perturbation is detected by the optical detector. This variation corresponds to the absorption, transmission, reflection, and/or scattering of the optical light that travels through the core of the fibre. For example; in micro-bending-based sensors, if the fibre is bent due to any physical perturbation, the amount of light that is lost through the cladding due to bending of the fibre is related to the amount of physical perturbation.

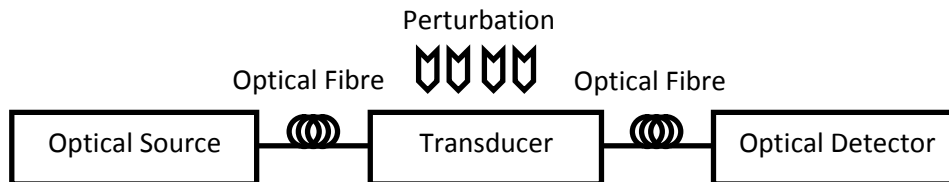


Figure 2 - Main parts of a fibre-optic sensing system

## Types of fibre-optic sensors

Fibre-optic sensors are generally divided into two types based on their functionality: intrinsic and extrinsic sensors. Intrinsic fibre-optic sensors utilise an optical fibre as the sensor head as well as the transmitter of the optical light (Figure 3). In these sensors, the light does not leave the fibre until it reaches the end that is connected to the optical detector. Some examples of these sensors that use interferometry configurations are Tapered Fibre, Drilled-hole Hollow-core Fibre, FBG, LPFG and other special fibres such as Doped Fibre.

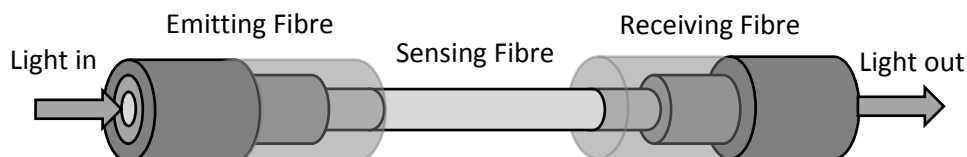


Figure 3 - Schematic diagram of an intrinsic fibre-optic sensor

Extrinsic fibre-optic sensors utilise an optical fibre to guide the light to and from a location at which an external optical sensor head (transducer) is located (Figure 4). The sensor head is basically designed to modulate the properties of light in response to changes in the environment with respect to physical perturbations of interest.

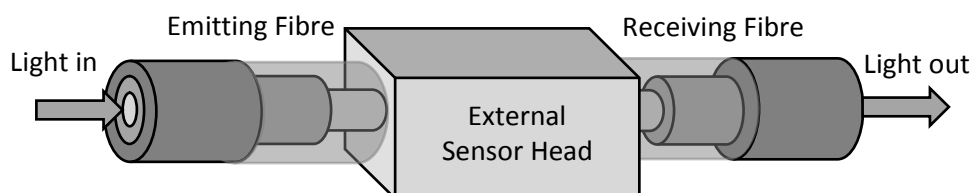


Figure 4 - Schematic diagram of an extrinsic fibre-optic sensor

## MINING APPLICATIONS OF FIBRE-OPTIC SENSORS

A number of studies have been reported in the literature that include the research and development of innovative fibre-optic sensors and the application of these sensors in various industries. For example, fibre-optic sensing has been used to measure electrical current (Werthen, *et al.*, 1996), to monitor buildings and structures (Jackson, 1995), to detect the fluid leakage (Vogel, *et al.*, 2001), to perform fluid logging in shallow bore holes (Hurtig, *et al.*, 1994), in different biomedical applications (Passia, *et al.*,

2002) and in buildings and structures (Hurtig and Grobwig, 1998). The optical fibre technology has also been introduced in the mining industry for sensing strain (Naruse, *et al.*, 2007), detecting mine gases such as methane (Li, *et al.*, 2005 and 2006) and underground environment monitoring (Sen and Datta, 1991).

The potential applications of fibre-optic sensing technology in mining can be classified into five main categories (Figure 5). Some of these applications have commercially available solutions while other need extensive fundamental research and technology development. It is recommended that a more detailed review in conjunction with technical experts is carried out in order to determine the technology requirements for the development of fibre-optic sensors. The research and development of fibre-optic sensing technology should account for identification of advantages and disadvantages of this technology in various mining applications.

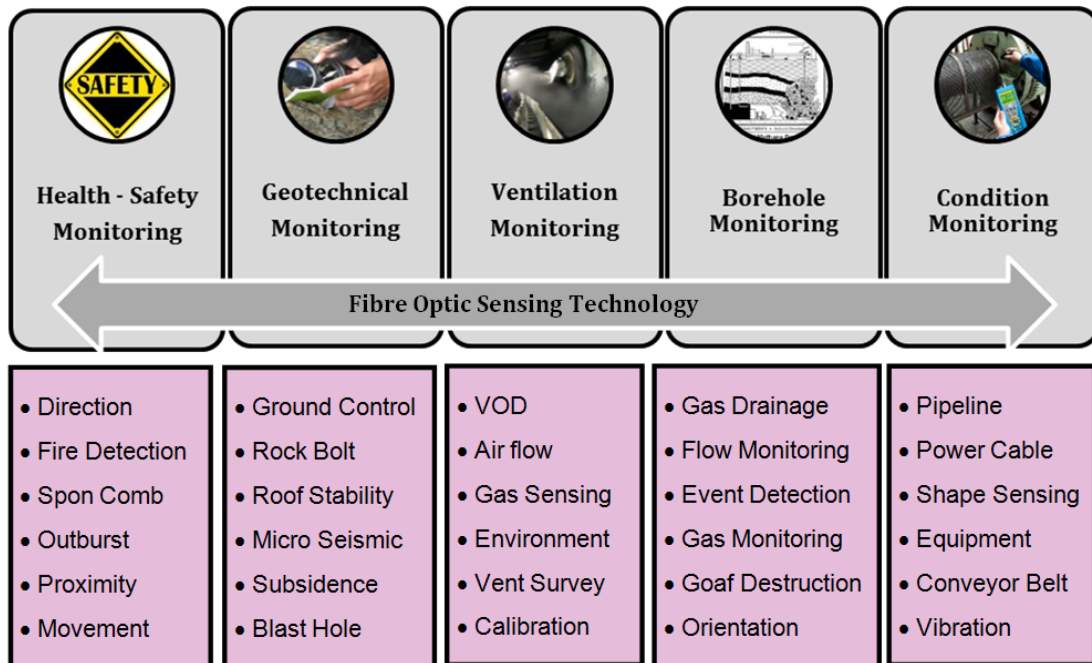


Figure 5 - Main potential applications of fibre-optic sensing technology in mining

### FIBRE-OPTIC SENSING RESEARCH AT UQ

#### Research group formation

A research group in collaborations with the Mining Engineering Division and Quantum Optics Laboratory at The University of Queensland (UQ) and CRCMining was established in 2010 to develop fibre-optic based sensors for mining applications. The research has so far received financial support from UQ, Australian Coal Association Research Program (ACARP) and CRCMining. The scope of research includes the investigation of potential mining applications of existing fibre-optic sensing technology in various mining areas such as ventilation, borehole monitoring, health and safety, geotechnical and condition monitoring. Research has also been conducted on the development of new fibre-optic sensors especially in the area of gas sensing. In the following, a summary of the projects that have been conducted by the research team is presented.

#### Underground mine environmental monitoring

The research project aimed to experimentally investigate the suitability of a fibre-optic based Distributed Temperature Sensing (DTS) system in monitoring underground mine environments. This study was prompted by earlier studies that examined the application of the DTS system in underground mines for detecting underground fire (Dubaniewicz, *et al.*, 1993; Zhang, *et al.*, 2002), monitoring trailing cables (Dubaniewicz, *et al.*, 1998), and developing automatic underground alarm systems (Zhang, *et al.*, 2000 and 2001).

DTS systems measure temperature by using fibre-optic cables as a continuous linear sensor. The principle of temperature measurement by DTS systems is generally based on the thermal effects inducing lattice oscillations within the core of the optical fibre that is made of silicon dioxide with amorphous solid structure. The light photons interact with the oscillated molecules of optical fibre as it travels through the fibre. As a result of this interaction, the light is scattered (Raman scattering) back which contains Stokes and anti-Stokes line components. The temperature of the optical fibre at any location is determined from the ratio of anti-Stokes and Stokes light intensities. There are basically two basic principles of measurement for distributed temperature sensing, Optical Time Domain Reflectometry (OTDR) and Optical Frequency Domain Reflectometry (OFDR). In OTDR, the location of the temperature event can be determined based on the generation of a narrow laser pulse and the travel time of the backscattered light to return to the detection unit.

DTS systems consist mainly of a mainframe and a fibre-optic cable. The mainframe includes a laser source, a pulse generator, an optical module, a photo detector and a micro-processor unit. The fibre-optic cable may consist of a number of quartz-glass optical fibres that can each be considered a linear temperature sensor. Commercially available DTS systems with normal specifications can measure temperature along more than 30 km of the fibre-optic cable with a spatial resolution of 1 m, accuracy of  $\pm 1^\circ\text{C}$  and a resolution of  $0.01^\circ\text{C}$  (Figure 6).

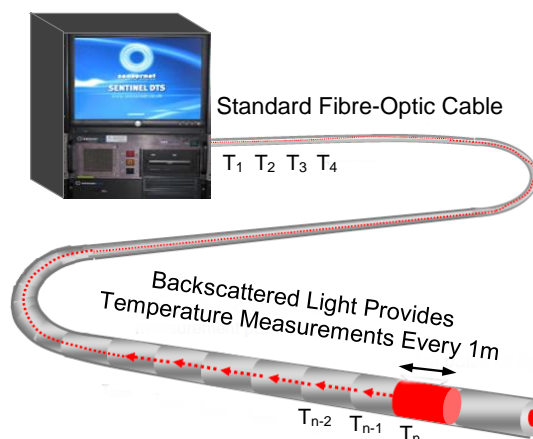


Figure 6 - Schematic diagram of distributed temperature sensing system (after Mendez, 2009)

Approximately, one km of the fibre-optic cable was installed in the University of Queensland Experimental Mine for these experiments (Figure 7). The experimental setup consisted of a *Sensornet* system that included the sentinel DTS unit for control and data acquisition, a display monitor, a multiplexer, a power supply and a fibre-optic cable both as a distributed temperature sensor and a transmission medium. The fibre-optic cable consisted of graded-index multimode optical fibres with a core diameter of  $50\ \mu\text{m}$  and a clad diameter of  $125\ \mu\text{m}$  sheathed with a low density polyethylene. Sentinel DTS-R system had a temperature sensing range of 10 km with a spatial resolution of 1 m. For a distance of one km, the system had temperature resolutions of  $0.01^\circ\text{C}$  and  $0.1^\circ\text{C}$  for the measurement times of 60 mins and 10 s, respectively.

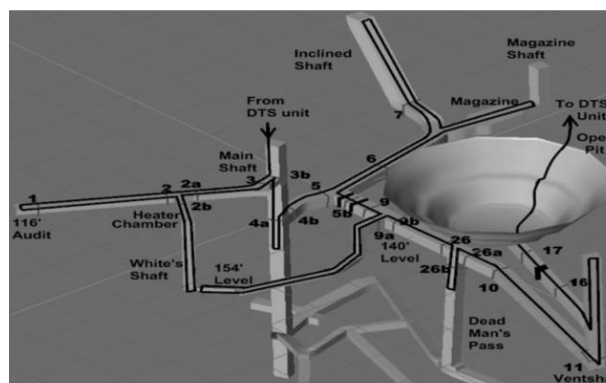


Figure 7 - Fibre optic cable installation in UQEM (Aminossadati, et al., 2010)

The fibre-optic cable was installed in the mine covering all the accessible roadways. The experimental conditions were varied by opening and closing the ventilation doors located on level 140 at station 9a. Various experiments were conducted to measure the air temperature throughout the mine and during the heating and cooling processes at different air flow and heat generation rates. With a distance resolution of within 1 m and temperature accuracy within 1°C, the DTS system could scan the entire underground mine and locate any high temperature spots. An example of the results is presented in Figure 8. The DTS system proved to be a reasonably accurate temperature measuring device as an underground mine environment monitoring system. The DTS system deploys a standard telecommunication fibre and does not need any special sensor to take the temperature measurements. Thus, this system is a very cost effective solution when a large number of measurement points are required. This system provides many of the features and benefits required by underground mine ventilation designers and operators.

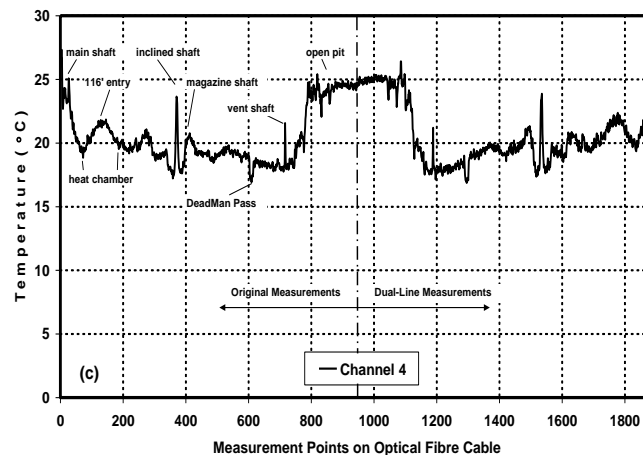


Figure 8 - UQ experimental mine temperature profile obtained by DTS (Aminossadati, *et al.*, 2010)

### Multipoint fibre-optic based methane gas sensing

Many research studies have attempted to develop and test fibre-optic based methane gas sensing systems in underground coal mines using single open-path gas cell sensor heads (Zhang and Zhang, 1992; Ni, *et al.*, 2008; Tong, *et al.*, 2010; Shemshad, *et al.*, 2012a and 2012b). The aim of this project was to experimentally investigate the performance of a sequential multipoint fibre-optic sensing system using open-path gas cells for the measurements of methane gas concentration. The potential advantages of utilising a multipoint fibre-optic sensing system is that measurements can be taken from different locations using a single laser and a single fibre-optic line. The system has potential applications in underground mines. For instance; a network of open-path gas cells could be installed around a mine exhaust shaft to accurately measure the average concentration of methane entering the atmosphere. In this research project, open-path gas cells containing certified concentrations of methane were purchased from Wavelength References Inc. and used in the experiments. These gas cells consisted of sealed chambers containing a known methane concentration (0.1% – 10%) in nitrogen. The gas cells had a fibre-optic input and output so that light could be passed through the gas in the cell and then focused back into a fibre and detected at a photo detector. Thus, each individual cell simulated a situation where methane diffused from the environment into the cell for detection. However, for these initial tests the cell remained sealed (Figure 9).



Figure 9- A pre-filled methane gas cell from Wavelength References Inc. (Shemshad, 2012)

The experimental set-up is shown in Figure 10. Light from a Distributed Feedback (DFB) laser was split so that 90% passed through the open path gas cell and then reached a photo detector. The other 10% went straight to a detector so that the absorption intensity could be normalized to variations in the laser output intensity. Both direct absorption and wavelength modulation spectroscopy were used. For the direct absorption spectroscopy, absorption at a particular wavelength was determined by subtracting the intensity of light transmitted through the gas cell from the intensity in the absence of methane. The open path gas cells could be switched so that the methane concentration could be varied. When wavelength modulation spectroscopy was employed, the experimental set-up remained the same, except the wavelength was modulated using a function generator and the output was monitored with a lock-in amplifier.

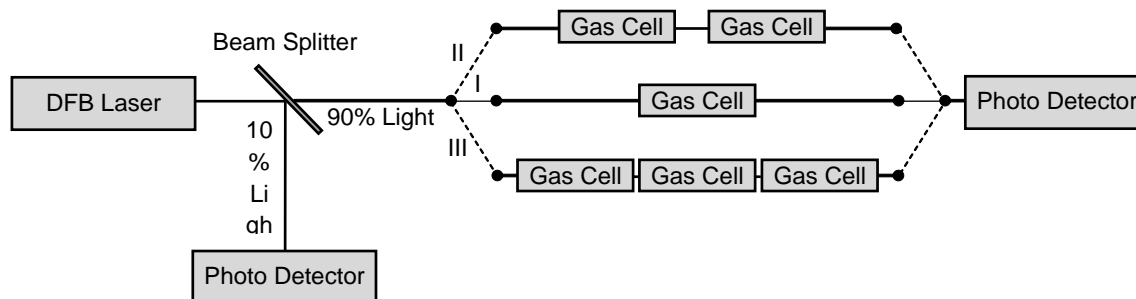


Figure 10 - Schematic diagram of experimental set-up for methane sensing in open-path gas cells

Having experimentally determined the appropriate conditions for sensing methane in a single open-path gas cell (I), the method was adapted to perform sensing of multiple open-path gas cells (II: two gas cells - III: three gas cells) connected to a single laser and fibre optic line. Light from the DFB laser is passed through multiple gas cells containing varying methane concentrations, and the second harmonic response signal is linear with respect to the average methane concentration of the cells (Shemshad, 2012). So, for instance, Figure 11a shows that the response increases as the average methane concentration of two cells, connected in series, increases, and Figure 11b shows that the same trend occurs when three cells are used instead of two. The important point is that the response is proportional to the average methane concentration in all of the cells. The results also showed that the response was independent of the order in which the gas cells are connected. This was the first time that an experimental study was conducted to investigate the feasibility of second harmonic measurements using multiplexed open-path gas cells.

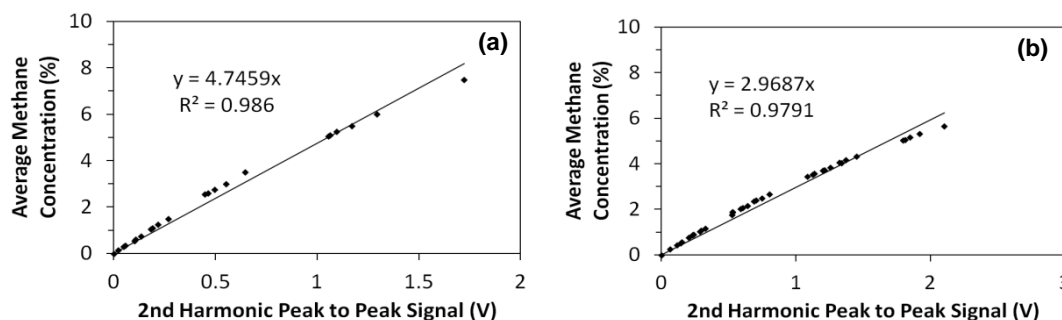


Figure 11 - Calibration curve for second harmonic peak to peak signal from light passed through (a) two, and (b) three open path gas cells to determine the average methane concentration in those cells. Methane peak was at 1,665.9 nm at different concentrations. Wavelength modulation depth was  $0.10\text{cm}^{-1}$ .

$$T = 296 \text{ K}, P = 101.325 \text{ kPa}, l = 16.5 \text{ cm. (Shemshad, 2012)}$$

#### Development of all-fibre methane gas sensor

The aim of this research project was to develop three all-fibre methane gas sensor heads (1- Tapered fibre, 2- Drilled single mode fibre and 3- Drilled hollow core fibre) and experimentally evaluate their methane gas detection capabilities for underground coal mines (Figure 12). Details of development of the sensor heads can be found in the research paper published by Sheridan *et al.* (2012). All-fibre

methane gas sensor heads are expected to have several advantages over conventional open-path gas cell sensor heads. These advantages include relatively faster response, easier and cheaper installation, more flexibility and manageable size and minimal temperature effects on the physical characteristics of the sensing head.

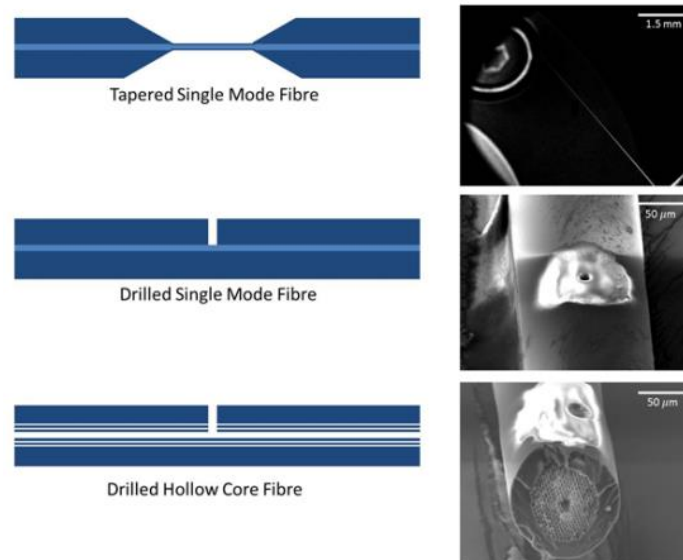


Figure 12 - Fibre optic sensor heads (Aminossadati, *et al.*, 2013)

An experimental setup was developed to accommodate and test the three all-fibre sensor heads at various known methane concentrations. The details of experimental setup can be found in the research paper published by Amanzadeh *et al.* (2012). The methane concentration setup consisted of a chamber, two gas cylinders and two flow meters (Figure 13). All the parts are connected through stainless steel pipes and flexible hoses. Flexible hoses are used to connect an IR detector to monitor methane concentration inside the chamber.

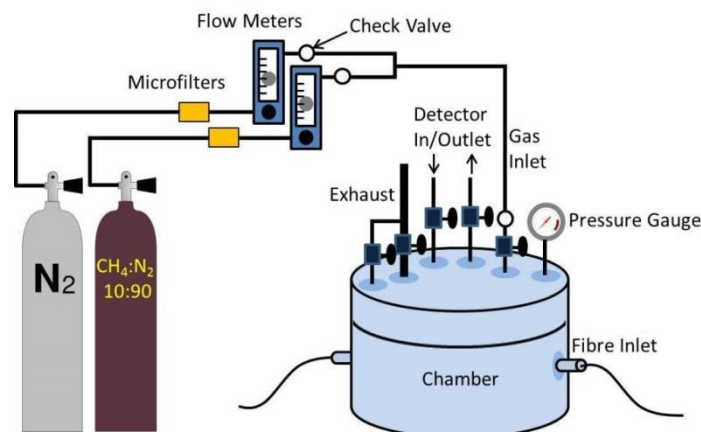


Figure 13 - Schematic diagram of all-fibre methane sensing setup (Amanzadeh, 2014)

Tapered fibre sensor heads had a relatively simpler configuration than open path gas cells (no lenses/alignment), but at the cost of a much smaller interaction volume compared to an open path gas cell and this resulted in these sensor heads being unable to detect methane. Drilled single mode fibres were simpler than open path gas cells and more robust than tapered fibres, but the light interaction volume was even smaller meaning methane could not be detected with these sensor heads. Drilled hollow core fibres offered the simplicity of an all-fibre set-up and the advantage of a large light interaction volume, but are more expensive than single mode fibre. Drilled hollow core fibres had good sensitivity but unacceptable accuracy when direct absorption was used. When wavelength modulation spectroscopy was used, the accuracy levels improved significantly. The response time for drilled hollow core fibres was slower than open path gas cells due to the time required for methane to diffuse into the hollow core fibre. This response time was a function of the fibre sensor length, and an inverse function of

the number of holes in the fibre (Aminossadati, *et al.*, 2012). The advantage of drilled hollow core fibres are their compactness, flexibility, high light interaction volume, low gas sample volume requirement and the prospective development of a distributed gas sensing system.

### Development of conveyor monitoring system

This research project aimed to develop a real-time fibre-optic based temperature monitoring system that predicts the costly failure of conveyor idlers. The project involved a DTS system and fibre-optic cables as temperature sensors. Various fibre-optic installation strategies were investigated to identify the most effective technique. The laboratory tests on conduction and convection proved that the conduction-based system was only able to detect the temperature rise due the heat emitted from the hot source. This means that the fibre-optic cable should be installed on the frame and as close as possible to the rollers to detect the temperature rise as a result of heat build-up in the faulty idler (Aminossadati and Yang, 2013). A number of laboratory and site tests were conducted using different installation configurations of the fibre-optic cable at UQ Fibre-optic Sensing Laboratory and Queensland Bulk Handling (QBH) site (Figure 14).

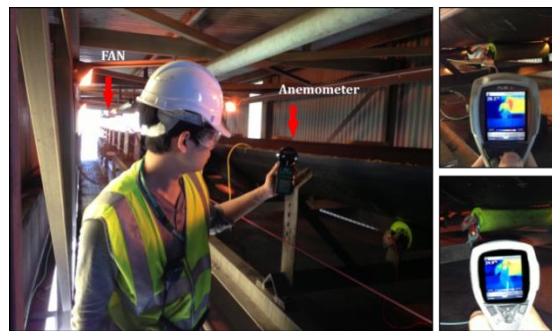


**Figure 14- Fibre-optic based conveyor belt monitoring tests at Queensland bulk handling site**

The results of this study suggested that four fibre-optic cables must be installed along the frame of the conveyor belt at each end of the rollers. A schematic diagram of the proposed system is presented in Figure 15. The fibre-optic cables accurately measure the temperatures of the frames in the vicinity of the end of the rollers. This temperature was indicative of the intensity of heat generation by the roller. If this temperature was greater than the ambient temperature, this could indicate that the roller starts to get hot.

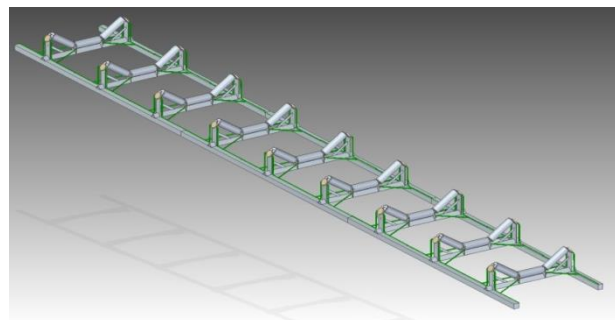


**Figure 15 - Schematic diagram of fibre-optic based conveyor belt monitoring system**

## FIBRE-OPTIC SENSING RESEARCH AT SHANDONG ACADEMY OF SCIENCE

### Research team scope

Shandong key laboratory of fibre-optic sensors at Shandong Academy of Science is located in high-tech development zone of Jinan City of Shandong Province in China. The scope of activities in this laboratory is research, development and production of various novel types of industrial fibre-optic sensors, intelligent instruments and integrated monitoring systems. In the field of coal mining, the projects include fibre-optic based sensors for methane detection, goaf spontaneous combustion alarm system, seismic monitoring, rock stress and roof pressure monitoring and electric equipment safety. Field test data of

these new sensors demonstrated that the fibre-optic sensors offer a number of advantages compared to conventional electrical sensors on sensitivity, accuracy and reliability. As a result, there is a great potential for coal mine safety monitoring and hazard detection. A summary of the two recent projects developed by the research team follows

### Mining machinery fault diagnosis system

The mining machinery fault diagnosis system includes fibre-optic vibration acceleration sensors, fibre-optic temperature sensors, fibre ring, light source, optical demodulator, data analyser and computer display. The fibre-optic vibration and temperature sensors are fixed on the shell surface of the machinery. Through the transmission cable, the sensor connects the first output terminal of the fibre ring. The fibre ring is connected to the output of the broadband light source and the second output terminal of the fibre ring is connected to the optical demodulator. The optical demodulator transforms optical signals into electrical signals and converted electrical signals are transmitted to the data analyser by the TCP/IP protocol. The temperature and vibration signals are finally processed and displayed by the data analyser (Figure 16).

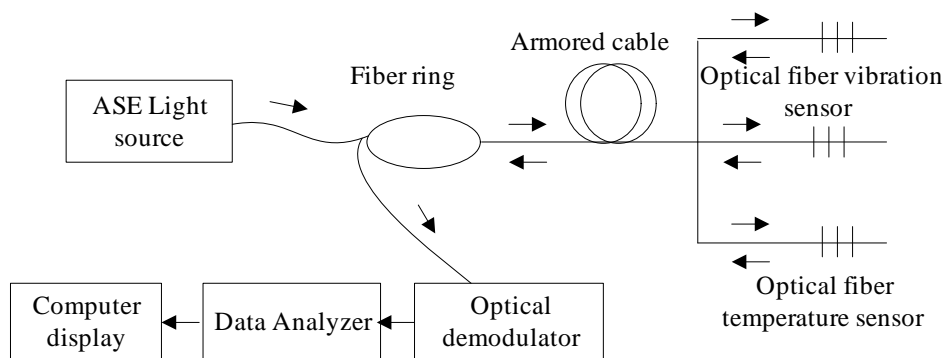


**Figure 16 - Schematic diagram of the fibre-optic machinery fault diagnosis system**

This system has been tested in Xinglong Zhuang coal mine of Yanzhou Mining Group in China. In this system, the vibration acceleration sensor was installed at different locations on a motor as shown in Figure 17.



**Figure 17 - Installation of machinery fault diagnosis system**

A sample of the results (Figure 18) shows the temperature and vibration velocity profiles for one of the motors. The results showed that the motor power instantaneous shock and vibration was relatively large when the motor was started. The temperature gradually rose and the vibration fluctuation range became relatively stable within a certain range.

### Micro-seismic monitoring

Fibre-optic based micro-seismic monitoring sensing system consists of fibre micro-seismic sensors (Figure 19a) demodulator and data processor (Figure 19b) and fibre transmission cable. It is an

intrinsically safe sensing system that requires no additional power supply and can achieve long distance transmission. The system is also an all-fibre design that is able to work in a strong magnetic field and high-risk environments. The measurement accuracy is independent of ambient temperature, light fluctuations and optical fibre bending loss. The system includes the demodulating unit that is placed in a ground dispatch room with high-speed synchronous data acquisition that detects the abnormal activities in the surrounding rock area.

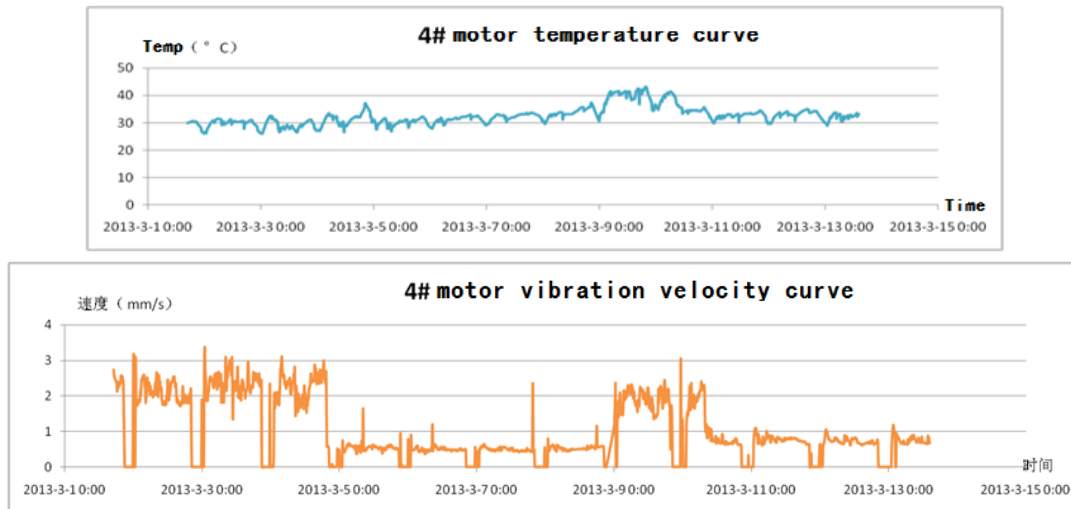


Figure 18 - The temperature and vibration history curve



Figure 19 - (a) Micro-seismic acceleration sensor (b) Micro-seismic demodulator and data processor

## CONCLUSIONS

Fibre-optic sensing technology has the potential to revolutionise the way mines are monitored, planned and controlled. The remote and real-time sensing capabilities of passive fibre-optic sensors indicate that fibre-optic sensing has obvious application in the mining industry where hazardous area compliance limit technology uptake. Recent research, development and production of fibre-optic sensors as well as the field trails of these sensors by the fibre-optic sensing research teams at the University of Queensland and Shandong Academy of Science demonstrate that fibre-optic sensors offer a number of advantages compared to conventional electrical sensors on sensitivity, accuracy and reliability. Future collaboration between the teams from Australia and China will enhance the research capabilities in the area of fibre-optic sensing technology for mining applications. This can be achieved by extending the understanding of the present states of monitoring systems used in the mining industry in Australia and China and actual conditions of quality assurance. The focus of future work should be towards accumulating and organising knowledge about potential and innovative monitoring systems that would contribute to the improvement of mining safety and economics. The research teams need to identify and implement plans for potential areas of research, development and utilisation of fibre-optic sensors in the mining industry and develop international exchange programs.

## REFERENCES

- Amanzadeh, M, 2014. Investigation of All-fibre Methane Sensors for Underground Coal Mines, MPhil Thesis, The University of Queensland.
- Amanzadeh, M, Aminossadati, S M, Kizil, M S, Sheridan, E and Bowen, W P, 2012. A microfabricated fibre optic sensor for methane gas measurement in underground coal mines, in Proceedings 2012 photonic Global Conference, 13-16 Dec 2012, Singapore, C120382, P3-06.
- Aminossadati, S M, Bowen, W, Sheridan, E, Amanzadeh, M and Kizil, M, 2013. An Innovative Fibre Optic Based Methane Sensor, ACARP (Australian Coal Association Research Program), C20014, Feb 2013.
- Aminossadati, S M, Mohammed, N M and Shemshad, J, 2010. Distributed temperature measurements using optical fibre technology in an underground mine environment, *Tunnelling and Underground Space Technology*, 25(3): 220-229.
- Aminossadati, S M and Yang, B, 2013. A Scoping Study on Fibre-Optic Based Temperature Monitoring of Underground Coal Conveyor Belts, in Proceedings The Australian Mine Ventilation Conference, July 2013, Adelaide, South Australia, pp 35-41.
- Dubaniewicz, T H, Chilton, J E and Dobroski, H, 1993. Fibre optic for atmospheric mine monitoring, *IEEE Transactions on Industry Applications*, 29 (4): 749-754.
- Dubaniewicz, T H, Kovalchik, P G, Scott, L W and Fuller, M A, 1998. Distributed measurement of conductor temperatures in mine trailing cables using fibre-optic technology, *IEEE Transactions on Industry Applications*, 34(2): 395-398.
- Hurtig, E, Großwig, S, Jobmann, M and Kuhn, K, 1994. Fibre-optic temperature measurements in shallow boreholes: experimental application for fluid logging. *Geothermics* 23 (4): 355-364.
- Hurtig, E and Grosswig, S, 1998. Distributed fiber optics for temperature sensing in buildings and other structures, in Proceedings IECON Industrial Electronics Conference, 3, pp 1829-1834.
- Jackson, D A, 1995. Potential of fibre optic point and distributed fibre optic sensors for structural monitoring, *IEE Colloquium-Digest*, 87: 4/1-4/5.
- Li, S, Wei, Z, Yin, Z, Cui and H L, 2005. Optical fiber gas sensor for remote detection of CH<sub>4</sub> gases in underground mine, in Proceedings SPIE, The International Society for Optical Engineering, 5770(25), pp 205-212.
- Li, S, Zhang, Y, Koscica, T and Cui, H L, 2006. Near-infrared fiber optics gas sensor for remote sensing of CH<sub>4</sub> gas in coal mines, in Proceeding SPIE, The International Society for Optical Engineering, 6299, pp 1-8.
- Mendez, A, 2009. Overview of trends in optical fibre sensors, in Proceedings the 14<sup>th</sup> OptoElectronics and Communications Conference, Hong Kong Convention and Exhibition Centre, July 2009, Hong Kong.
- Naruse, H, Uehara, H, Deguchi, T, Fujihashi, K, Onishi, M, Espinoza, R, Guzman, C, Pardo, C, Ortega, C and Pinto, M, 2007. Application of a distributed fibre optic strain sensing system to monitoring changes in the state of an underground mine, *Measurement Science and Technology*, 18(10): 3202-3210.
- Ni, J, Chang, J, Liu, T, Li, Y, Zhao, Y and Wang, Q, 2008. Fiber methane gas sensor and its application in methane outburst prediction in coal mine, in *Proceedings 1<sup>st</sup> Asia-Pacific Optical Fiber Sensors Conference*, APOS 2008: 5226294.
- Passia, H, Szade, A, Motyka, Z and Bochenek, W, 2002. Technical solution and experience in laser anemometry for underground mining, other industrial and biomedical applications, in Proceedings SPIE, The International Society for Optical Engineering, 4827, pp 458-465.
- Sen, S K and Datta, A K, 1991. Microprocessor based fibre optic environmental monitoring system for underground mine, *IEEE Xplore*, 0-7803-0453-5191: 1270-1274.
- Shemshad, J, 2012. Development of a Sequential Multipoint Fibre Optic Methane Measurement System for Coal Mines, PhD Thesis, The University of Queensland.
- Shemshad, J, Aminossadati, S M and Kizil, M S, 2012a. A review of developments in near infrared methane detection based on tunable diode laser, *Sensors and Actuators: B. Chemical*, 171-172: 77-92.
- Shemshad, J, Aminossadati, S M, Bowen, W and Kizil, M S, 2012b. Effects of pressure and temperature fluctuations on near-infrared measurements of methane in underground coal mines, *Applied Physics B: Laser and Optics* 106 (4): 979-986.
- Sheridan, E, Amanzadeh, M, Aminossadati, S M, Kizil, M S and Bowen, W P, 2012. Fibre Microfabrication and Characterization for Gas Sensing, in Proceedings OSA Imaging and applied Optics, Monterey, California, USA, June 2012.
- Tong, M, Niu, J, Hao, J and Jia, C, 2010. Study on a fiber optic sensor for CH<sub>4</sub> in mine, in *Proceedings 2010 Symposium on Photonics and Optoelectronic*, SOPO 2010: 5504404.

- Vogel, B, Cassens, C, Graupner, A and Trostel, A, 2001. Leakage detection system by using distributed fiber optical temperature measurement, in Proceedings SPIE, The International Society for Optical Engineering, 4328, pp 23-34.
- Werthen, J G, Andersson, A G, Weiss, S T and Bjorklund, H O, 1996. Current measurements using optical power, in Proceedings IEEE Power Engineering Society Transmission and Distribution Conference, IEEE Transactions on Power Delivery 3522-8/96, pp 213-218.
- Zhang, Z W and Zhang, J L, 2011. Optical fiber network sensor system for monitoring methane concentration, in Proceedings SPIE, The International Society for Optical Engineering 8191, 81910R.
- Zhang, Z, Kim, I S and Wan, J, 2001. 10 km distributed optical fire sensors system and application, in Proceedings SPIE, The International Society for Optical Engineering, 4540, pp 386-390.
- Zhang, Z, Kim, I S and Wang, J, 2002. 10 km distributed optical fire sensors and measuring network, in Proceedings 2<sup>nd</sup> International Symposium on Instrumentation Science and technology, 3: 3/302-3/307.
- Zhang, Z, Wang, K, Kim, I S, Wang, J, Feng, H, Guo, N, Yu, X, Zhou, B, Wu, X and Yohee, K, 2000. Distributed optical fiber temperature sensor (DOFTS) system applied to temperature automatically alarm of coal-mine and tunnel, in Proceedings SPIE, The International Society for Optical Engineering, 4077, pp 128-132.

---

# BELT ROAD SEGREGATION AND ESCAPEWAYS - COMPLIANCE OR RISK MANAGEMENT?

**Martin Olsen**

**ABSTRACT:** Segregation of conveyor roadways is a ventilation practice that is being increasingly applied in Australia. It is largely driven by the legislated requirements in Queensland pertaining to separation of escape ways from the mine. This legal requirement was based on a recommendation from the Moura No. 2 Wardens Inquiry into the mine disaster that claimed 11 lives. The report recommended "the introduction of a requirement for all underground mines to have one intake airway that is completely segregated from other parallel intake airways so as to provide two separate means of egress from the mine via an intake airway". This recommendation seeks to assist mineworkers to escape from a mine after a fire by providing them with an airway that is free from smoke or contaminants. The concept of an airway being "completely segregated" is an ideal that is challenging to implement in practice when considering the effect of leakage. The practice of belt segregation is concerned with the potential for fires in the belt roadway although there are numerous other potential fire sources in underground coal mines. A review of segregation practices has been conducted applying ventilation engineering principles. Four different scenarios have been analysed with regard to the effectiveness of the segregation stoppings in preventing potential fire contaminants migrating to other parts of the mine. The results show that in some cases the benefits of segregation to a person evacuating a mine in the event of a fire range from beneficial to detrimental. This is influenced by many factors including the location of that individual in that particular mine. There is room for improvement in the design and implementation of escape ways in underground coal mines. Escape ways need to be planned and designated with regard to the potential sources of fire, pressure differentials between escape ways and the operational practicalities of maintaining the pressure differential between them.

## INTRODUCTION

The term "segregation" is used widely in the Australian underground coal industry today but this term cannot be found in any legislation relating to underground coal mining. The intent of this paper is to identify the origins, reason and purpose for segregation and also to assess its practical effectiveness. It is worth noting that this paper is focused on the modelling of contaminants from fires on main conveyors and that there are other types of mine fires or "reasonably foreseeable events" that can cause the intakes of a mine to become contaminated. The reason for this is in response to the industry practice of belt road segregation as means of mitigating the risks to underground personnel in the event of a belt fire.

Maintaining separated intake escapeways is a legal requirement in Queensland and one that is often complied with by segregation of the main belt road from the main travel road. Mines inspectors ensure compliance with the legislation by enforcing the segregation of the belt road at individual sites by issuing directives to bring the segregation into compliance. For the mining operation the segregation of the belt road is often a nuisance as it limits access to the belt road. It can be a headache for the ventilation officer to control and maintain as there is often operational requirements to breach the segregation stoppings for access purposes.

Mining operation invest considerable amounts of time and money in the installation and maintenance of these ventilation control devices. It is important that they are serving a purpose and reducing the risk to underground personnel. If they are not, then they are a waste of time and money and are providing a false sense of security to underground personnel and management at the mine.

## HISTORY IN AUSTRALIA

The legal requirement for belt segregation started in the Queensland coal mining legislation in the 1970s. The Queensland Coal Mining Act 1925-1981 General Rules for Underground Coal Mines (Queensland Government 1981) rr. 4.2 stated:

---

*Olsen Consulting Group, Wollongong. Email : martinolsen@ocg.net.au, M: 0409 010976*

“(1) In an underground coal mine other than a mine existing at 1st July, 1978, provisioning shall be made for an intake airway other than a roadway containing a belt conveyor. This requirement shall apply to any part of such mine other than a panel or sub-panel where the method of working limits the number of roadways to less than three: Provided that in the initial development of a new mine the belt conveyor roadway may serve as the only intake airway for such time as is reasonably required to provide a second intake roadway.

(2) All belt conveyor roadways shall be segregated from other intake airways and from return airways”.

This rule was very specific about what was required and when it was required.

The current legislation in Queensland does not call for belt segregation. Section 296 of the Coal Mining Safety and Health Regulation 2001 (Queensland Government, 2001) calls for two intake escapeways to be established that are separated in a way to prevent any reasonably foreseeable event happening in one of the escapeways affecting the ability of persons to escape through the other escapeway. In Schedule 4 - Ventilation control devices and design criteria, the stoppings used for establishing separation are specified as being of substantial construction with no overpressure rating. This section of the regulations came about in response to a recommendation on p67 of the Wardens Inquiry Report for the Moura No. 2 Mine Explosion, which called for: “the introduction of a requirement for all underground mines to have one intake airway that is completely segregated from other parallel intake airways so as to provide two separate means of egress from the mine via an intake airway”.

Despite the change in legal requirement the practice of belt segregation is often used to achieve the requirement for two intake escapeways.

It is also worth noting that s296 of the CMS and HR 2001 is part of Division 4 of Part 9 which deals with mine design and that it is an obligation of the Site Senior Executive and not the Ventilation Officer to ensure that this is in place. The Ventilation Officer is however usually tasked with the responsibility of ensuring this is compliant. This responsibility is often begrudgingly accepted, as it is a constraint that is in some cases a hindrance to the ventilation of the mine. It is not surprising then that the separation of escapeways is not planned and modeled to the same extent as the ventilation of production panels.

The Queensland Mines Inspectorate issued a Safety Bulletin titled, “Lessons of mine segregation must be applied” (Taylor, 2008). This Safety Bulletin explains the legislated requirements and the origin of these requirements. It also warns operations that non-compliance with this requirement will result in a directive to suspend operations being issued under section 167 of the Coal Mining Safety and Health Act 1999 (Queensland Government, 1999).

In NSW there is no requirement for two escapeways in intake air. Some mines have implemented a separate escapeway in intake air to part of the mine. The legal requirement for escapeways or means of egress is in cl 45 of the NSW Coal Mine Health and Safety Regulation 2006 (NSW Government, 2006)

*(b) (iv) at least 2 means of egress from each production area or other part of the mine to the surface part of the mine so that, in the event of any roadway becoming impassable, another is always available,*

## INTERNATIONAL PRACTICE

### USA

The United States has very prescriptive requirements on segregation of conveyor roadways. The principle that is applied is that no air from a conveyor roadway is allowed to ventilate a working face. Leakage through ventilation control devices is included in this requirement and results in the practice of ensuring the pressure in the conveyor roadway is always less than the pressure in the travel road. This is achieved in practice by the routine placement of regulators in the conveyor roadway and overcasts where necessary to dump conveyor roadway air to the return airway.

These requirements come from § 75.350 of the Title 30 Code of Federal Regulations (30 CFR) (Federal Government of USA, 2008), which include the following:

(a) The belt air course must not be used as a return air course; and except as provided in paragraph (b) of this section, the belt air course must not be used to provide air to working sections or to areas where mechanized mining equipment is being installed or removed.

(1) The belt air course must be separated with permanent ventilation controls from return air courses and from other intake air courses except as provided in paragraph (c) of this section.

The double fatality at the Aracoma Alma No. 1 Mine in 2006 after a conveyor fire filled the primary escapeway of a working section with thick smoke increased the focus placed on this section of the 30 CFR by MSHA.

### **South Africa**

In South Africa the Regulations under section 98 of the Mine Health and Safety Act, 1996 (Act No. 29 of 1996) call for two means of egress from the mine (Government of South Africa, 1996). There is no requirement for the provision of two separate intake airways or for the segregation of belt roadways from intake air. The safety systems for dealing with mine fires rely on:

- Emergency lifelines
- Establishing refuge chambers with borehole to the surface and small fan for fresh air supply
- Capacity to ream out refuge chamber boreholes for evacuation of personnel

### **United Kingdom**

The UK contains similar legislative requirements to those required under the Queensland legislation but contains some more clarity on when the requirements are applicable. The Mines (Safety of Exit) Regulations 1988 Regulation 9 (Government of the United Kingdom, 1998) states the following:

Intake airways

9. The manager shall ensure that, apart from those persons who are going to or leaving their place of work at the beginning or end of a shift, not more than 50 persons are employed below ground in any part of the mine unless;

(a) there are two separate intake airways into that part of the mine which are connected only in such a way that in the event of a fire, transmission of the products of combustion from one airway to the other is prevented so far as is reasonably practicable; or

(b) there is one intake airway which is constructed of suitable fire resistant materials and is free, so far as is reasonably practicable, from the risk of fire.

In addition to this regulation there is a requirement for at least two means of egress to the surface, ie. an intake and a return.

## **DIFFERENT SCHOOLS OF THOUGHT**

From looking at the different segregation practices used locally and around the world several different concepts emerge. These may not be immediately clear so they are listed below:

1. No segregation of intake roadways
2. Segregation of the belt to prevent belt fire contaminants entering intake roadways
3. Segregation of the belt to prevent belt fire contaminants entering working faces
4. Provision of a separated intake airway for use as an escapeway

These four different approaches all have advantages and disadvantages and different levels of complexity with regard to implementation.

It is important to understand what is trying to be achieved before an appropriate arrangement can be adopted. Too often, it seems, segregation stoppings are installed purely from a compliance standpoint with little understanding or interest in the purpose or effectiveness.

## MINE SCENARIOS

For the purpose of analysis of belt segregation four different mine layouts were used to model the effectiveness of the segregation. The first scenario, called Case 0 is a conceptual model and does not represent the workings of an actual mine. This was used so that any ventilation layouts and analysis results could be published without concern for confidentiality. The other three scenarios, called Case 1, Case 2 and Case 3 are based on the ventilation models from actual longwall coal mines in Queensland, Australia. For the purposes of confidentiality only the analysis results are published.

### Methodology

#### Pressures

Pressure gradient plots were generated for each scenario. These display the relative static pressure in the mine roadway from the surface intake to the longwall and along the return back to the main fans. The belt road pressure gradient was also plotted. The pressure gradients of any additional separated intake roadways were also plotted.

#### Contaminant test

A 100 ppm contamination was placed into the model inside the belt portal and then modeled to see where the contaminant would migrate throughout the mine. This test was applied to each of the scenarios and the results recorded. The models were then modified with all the segregation stoppings in the mine removed and the same 100 ppm contamination test reapplied. This allowed the two results for the same mine to be compared. One set of results with segregation stoppings in place and one with the segregation stopping removed. This was used so the effectiveness of the segregation stoppings of the scenario could be measured. It is important to note that the numerical value of the contamination concentration in the results table is only relevant with respect to the 100 ppm contaminant that was used for the test. It is primarily for comparison between models and between segregation and no segregation. For example, a 20 ppm contamination in a primary escapeway may appear to be acceptable until you consider that if the contamination at the belt portal was 1000 ppm then the concentration in the escapeway would be 200 ppm. Table 1 displays the model results for each scenario with the segregation stoppings in place and also with the segregation stoppings removed.

**Table 1 - Contamination test - Modelled segregation stopping effectiveness**

	Modeled Number of Segregation Stoppings	Modeled Contaminant Concentration (ppm)					
		Belt Portal	LW face	Mains	Dev 1	Dev 2	Primary Escapeway Maximum
Case 0	157	100	14	76	16	14	18 or 4*
	0	100	31	28	30	27	33 or 27*
Case 1	203	100	7	30	25	0	31
	0	100	17	22	21	1	22
Case 2	106	100	53	15	1	1	6
	0	100	53	1	7	0	31
Case 3	64	100	21	44	29	44	26
	0	100	22	26	24	25	29

\* Depending on which heading is classified the Primary Escapeway

The purpose of this test is to measure the effectiveness of segregation stoppings to reduce the spread of contaminants to other parts of the mine. No consideration has been given to the dynamic nature of a fire, the buoyancy and pressure differentials that are possible from an active fire.

#### Case 0

The ventilation layout for Case 0 is shown in Figure 1. This fictitious mine consists of seven heading mains, 3 headings with flanking returns and a segregated belt road in the middle heading. As the mine does not exist there is not a designated primary escapeway. There are two results for the contaminant test for the primary escapeway shown in Table 1 depending on which set of intake roadways is adopted

as the primary escapeway. The results show that with the 157 segregation stoppings in place the contaminant is directed predominantly into the mains development area with a concentration of 76 ppm. The other three panels (including LW) modeled a contamination around 15 ppm. The greatest benefit modelled with this arrangement of segregation was the contaminant concentration of 4 ppm adjacent to the 76 ppm in the mains. The 4 ppm result came from the single intake airway to the left of the middle heading belt road in Figure 1.

The reason for the relatively low level of contamination can be seen in the pressure gradient plot for Case 0 in Figure 2. The heading that returned the result of 4 ppm is referred to in Figure 2 as "Primary". This heading for the most part sat at a higher static pressure than the surrounding roads particularly the belt road where the contaminant was concentrated. This resulted in leakage paths flowing away from this "Primary" heading. The instances where the static pressure in this roadway drops below the belt road is due to the placement of segregated belt underpasses that were put into the model to allow for transport movements (operational requirement) and balancing of the intake airway pressures. It is this balancing that has caused the drop in static pressure to below that of the belt road in some instances. This could be mitigated in practice by the installation of machine doors at the segregated underpasses. The results in Table 1 also show that by removing all segregation from the model all inbye areas of the mine received similar contaminant concentrations of around 30 ppm. This includes all working faces and escapeways.

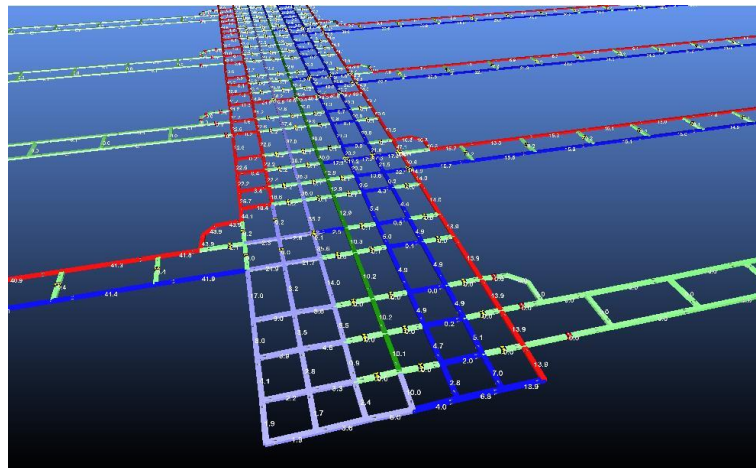


Figure 1 - Case 0 – ventilation layout

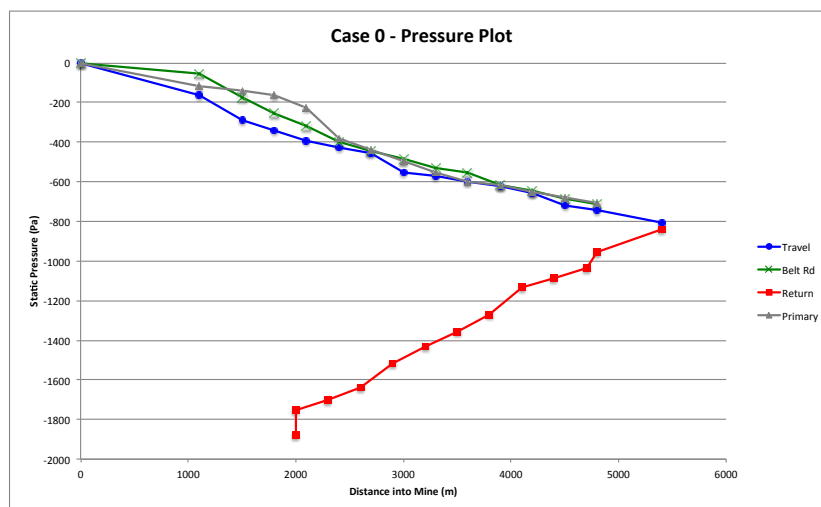


Figure 2 - Case 0 – pressure plot

### Case 1

Case 1 is based on a longwall mine in the Bowen Basin in Queensland, Australia. The trunk conveyor of the mine is segregated on both sides from the surrounding intakes with 203 segregation stoppings. The

primary escapeway of the mine is the main travel road. The contaminant test in Table 1 shows some very interesting and unexpected results. The highest contaminant results with the segregation stoppings in place were 31 ppm in the primary escapeway, 30 ppm in the mains development panel and 25 ppm in one of the gateroads. Without the segregation stoppings in place the most significant result was the reduction of contaminant in the primary escapeway by 30% down to 22 ppm. The longwall result increased from 7 ppm to 17 ppm without the segregation stoppings in place and the mains development and one of the gateroads both had reductions in the level of contaminant. As expected, the contaminant was more spread out and diluted without the segregation stoppings and more concentrated in particular areas.

The pressure gradient plot for Case 1 in Figure 3 shows the belt road at a higher pressure than the primary escapeway most of the time. The first 1000 m the primary escapeway and the belt are in separate drifts so the leakage would be almost non-existent. The time where the primary escapeway sits above the belt road in static pressure around the 2000 m mark is due to a significant reduction in the number of main headings which causes the static pressure of primary escapeway to peak in this area. It is possible to see that the general pressure gradient trend of the segregated belt road is flatter than that of the primary escapeway causing the belt road to be at a higher static pressure than the primary escapeway. This results in the leakage of contaminant into the primary escapeway in the event of a belt fire. This scenario had 17 vehicle doors positioned along the trunk belt system. This highlights the need for vehicle and personnel access to the belt road and subsequent issues with quality of stoppings and leakage.

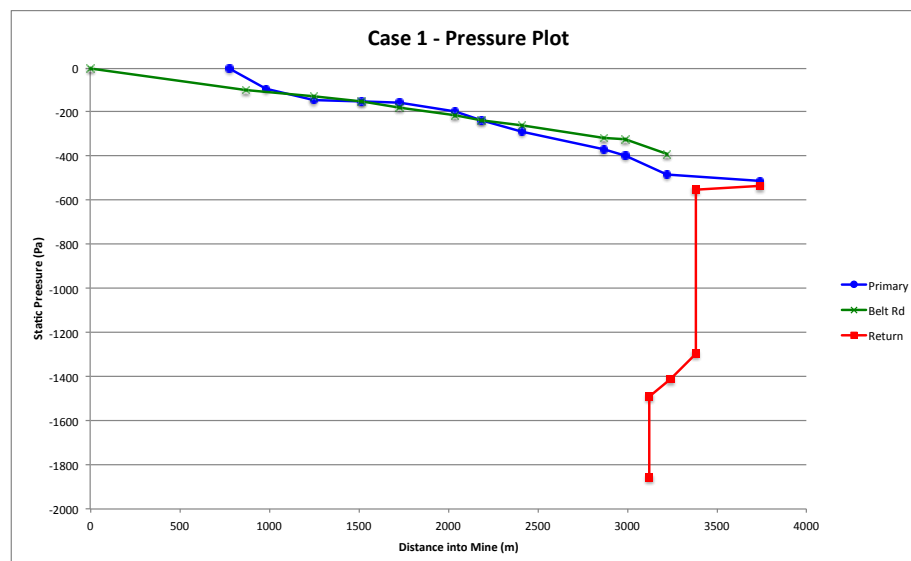


Figure 3 - Case 1 – pressure plot

## Case 2

Case 2 is based on a longwall mine in the Bowen Basin in Queensland, Australia. The trunk conveyor of the mine is generally segregated on both sides from the surrounding intakes with 106 segregation stoppings. The primary escapeway of the mine is the main travel road. This scenario involved the most elaborate layout for segregation of the belt road of all the scenarios analysed. Table 1 shows that the contaminant result for the longwall face is 53 ppm regardless of whether the segregation stoppings are in place or not. The mains development panel showed a reduction of 15 ppm to 1 ppm with the removal of the segregation stoppings and another development panel showed a rise from 1 ppm to 7 ppm. The primary escapeway however showed a significant increase from 6 ppm to 31 ppm with the removal of the segregation stoppings. The pressure gradient plot for Case 2 shown in Figure 4 shows the extent that this particular operation has gone to get the pressure in the belt road to below the pressure in the primary escapeway (travel road).

The step in the pressure gradient for the belt road at the 2000 m mark is due to the placement of a regulator and an air dump in the belt road. This does a good job to reduce the pressure of the belt road and largely prevents leakage of the contaminant into the primary escapeway. The infrequent instances when the belt road has a higher static pressure than the adjacent primary escapeway results in the low

result of 6 ppm. The air dump directs air out of the belt road into adjacent intake roadways. It is this air that is directed to the longwall and this is the reason for the 53 ppm result for the longwall face.

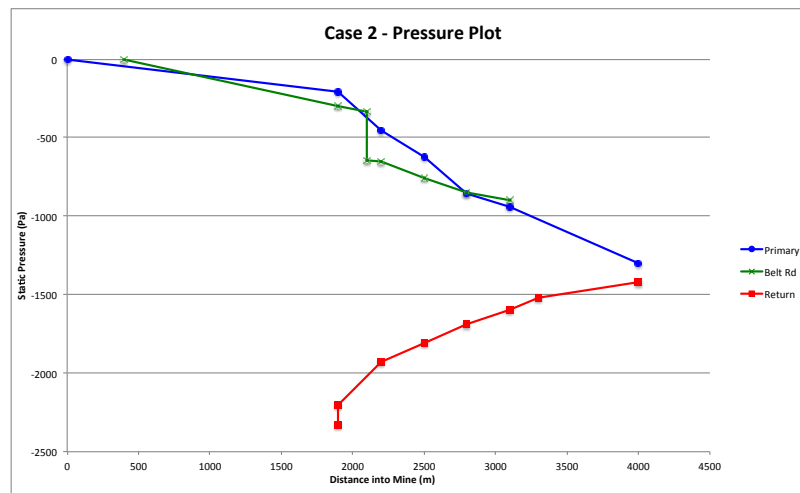


Figure 4 - Case 2 – pressure plot

### Case 3

Case 3 is based on a longwall mine in the Bowen Basin in Queensland, Australia. The trunk conveyor of the mine is generally segregated on both sides from the surrounding intakes with 64 segregation stoppings. The primary escapeway of the mine is a roadway separate from the main travel road and on the other side of the trunk conveyor. This scenario initially showed the most promise for having a simple design and maintaining a primary escapeway at a pressure above the adjacent belt road. The pressure gradient plot in Figure 5 shows that this is not the case. The belt road is generally at a greater static pressure than the adjacent primary escapeway. This is reflected in the results in Table 1 with arguable better results achieved with the segregation stoppings removed from the model. The primary escapeway showed an increase in contaminant concentration from 26 ppm to 29 ppm with the segregation stoppings removed.

There are two ways this scenario could be dramatically improved. The primary escapeway loses significant pressure early in the mains due to a segregated belt underpass. This allows air to travel from the primary escapeway to the travel road. This could be easily corrected with the installation of a vehicle door. Additionally there is a 200 Pa pressure drop in the belt road around the 2500 m mark. This is due to a high resistance Ventilation Control Device (VCD) located in the belt road. This VCD would have very likely been installed to achieve compliance with belt segregation. The result is an increase in the static pressure of the belt road and the increased level of contamination of the primary escapeway in the event of a belt fire. In fact the primary escapeway suffers less contamination if this VCD is removed from the model. This is a good example of where compliance does not necessarily result in lower risk.

## CONCLUSIONS

A line of stoppings will not prevent contaminants from a belt fire entering a primary escapeway if the belt road is at a higher static pressure than the primary escapeway. For the examples analysed, segregation of the belt road from all other roadways usually resulted in the belt road being at a higher pressure than surrounding intake airways.

Consideration needs to be given to the static pressure differential between separated escapeways. The only way to ensure that a contaminant does not enter the primary escapeway is to ventilate the mine such that the primary escapeway is generally at a higher pressure than the surround roadways. Ideally the primary escapeway should have the highest static pressure of any adjacent roadways.

Consideration should be given to establishing primary escapeways that are not the main travel road in the mine. This will allow for the following:

- Provide a primary escapeway for the full length of the main headings free from contaminants in the event of a fire in the belt road or travel road
- To better meet the requirements of s298 of the Qld CMS and H Reg 2001 for primary escapeways. Specifically "As far as practicable, free from the risk of fire"
- Ease of access to the belt road and less issues with damaged stoppings or leaking vehicle doors
- Improve early detection of heatings and small fires(ie. via smell)

Consideration should be given to putting more focus on reducing the level of risk to personnel than just being compliant. There are several examples from the modelling conducted where compliance is achieved but a more hazardous result is also achieved.

Based on the modelling work conducted the following observations have been made:

- In the event of a belt fire, segregation of the conveyor roadway will result in the smoke generated by the fire being concentrated in particular areas of the mine. This will usually be the mains but may be elsewhere, eg. Case 2 where the contaminant showed up greatest at the longwall face

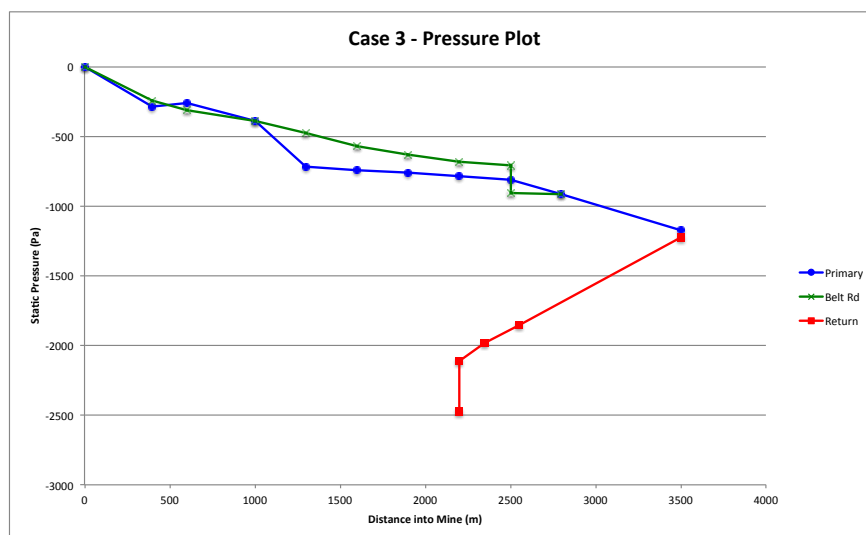


Figure 5 - Case 3 – pressure plot

## REFERENCES

- Federal Government of the United States, 2008. Title 30 Code of Federal Regulations Part 75 - Mandatory Safety Standards Underground Coal Mines, USA.
- Government of South Africa, 1996. Mine Health and Safety Act, 1996 (Act No. 29 of 1996), Republic of South Africa.
- Government of the United Kingdom, 1988. The Mines (Safety of Exit) Regulations 1988, United Kingdom.
- New South Wales Government, 2006. Coal Mine Health and Safety Regulation 2006, New South Wales.
- Queensland Government, 1981. Coal Mining Act 1925-1981 General Rules for Underground Coal Mines, Queensland.
- Queensland Government, 1999. Coal Mining Safety and Health Act 1999, Queensland.
- Queensland Government, 2001. Coal Mining Safety and Health Regulation 2001, Reprint 4A, Queensland.
- Taylor, G, 2008. Safety Bulletin 81 - Lessons of mine segregation must be applied, Department of Mines and Energy, Queensland.
- Windridge, F, 1996 Report on an Accident at Moura No 2 Underground Mine on Sunday, 7 August, 1994 Wardens Inquiry, Department of Mines and Energy, Queensland.

# RISKGATE AND AUSTRALIAN COAL OPERATIONS

Philipp Kirsch<sup>1</sup>, Jill Harris<sup>2</sup>, Darren Sprott<sup>1</sup> and David Cliff<sup>1</sup>

**ABSTRACT:** The major Australian Coal Association Research Program (ACARP) project, RISKGATE has now completed three years of knowledge capture and system development. The body of knowledge for risk management of tyres, collisions, fires, isolation, strata underground, ground control open cut, explosions, explosives underground, explosives open cut, manual tasks and slips/trips/falls was launched in December 2012. Recently, the project added knowledge about outbursts, coal bumps and bursts, human-machine interface, tailings dams, occupational hygiene and inrush to the original 11 topics. In 2014, the project plans (pending ACARP funding approval) to focus on issues around Fitness for Work. RISKGATE provides an environment for knowledge capture and knowledge exchange to drive innovation and cross industry sharing of current practice in the identification, assessment and management of risk. By capturing operational knowledge from industry experts, RISKGATE provides a cumulative corporate memory at a time of high personnel turnover in the coal industry. RISKGATE is the largest single ACARP Occupational Health and Safety (OHS) initiative to date. This paper presents an overview of the first seventeen topics, topic structures, and contrasts and inter-relationships between topics. The second part of the paper discusses some early steps that companies are taking to integrate RISKGATE into their operations; and conclude with some thoughts on where RISKGATE can go in the future.

## INTRODUCTION

RISKGATE is a web-based tool (RISKGATE, 2013) providing clear, up-to-date and practical checklists for controlling risks across 17 specific high priority unwanted events in Australian coal mining. Based on interactive Bow-Tie Analysis (BTA) to assist in the implementation of safer operations, each RISKGATE topic and each bow-tie is centred on a specific unwanted or initiating event. The funneling of causal factors and consequences through this initiating event keeps the information concise, intuitive and targeted. Users can generate checklists that will deliver on-site managers and engineers quick and relevant access to broad industry-based current practice controls for consideration at their own site. These checklists are designed as prompts regarding current practice that could assist with risk assessment, auditing, accident investigation, and training. User guides and other materials that assist in implementation of this body of knowledge in coal mining operations can be obtained from the author, or online (RISKGATE, 2013).

RISKGATE is funded by the Australian Coal Association Research Program (ACARP); managed and implemented by the University of Queensland; and each of the thousands of specific controls loaded into the RISKGATE system have been instigated and assessed by industry experts from Australia's leading mining companies. RISKGATE is built on a foundation of industry expert knowledge gathered through topic specific action research workshops (Kirsch, *et al.*, 2012, 2013ab; Worden, *et al.*, 2013). Topics which have been completed to date include: fires (Harris *et al.*, 2012), underground strata control (Kirsch, *et al.*, 2013c), open cut ground control, collisions, tyres, isolation, explosions (Kirsch, *et al.*, 2013c), explosives (Harris, *et al.*, 2013), manual tasks, and slips trips and falls (Lynas, *et al.*, 2014, in press). The intent of RISKGATE is not to specifically assess risk for any unique site, but instead provide a decision support tool, resources and outputs, such as tailored checklists, that can assist users in their site-specific risk assessment and risk management.

## RISKGATE 2011-2013

In response to a request from ACARP, in 2010 the University of Queensland's Minerals Industry Safety and Health Centre (MISHC) developed a RISKGATE scope in consultation with selected coal industry representatives (Kirsch, *et al.*, 2012). Importantly, this identified key coal mining hazards (referred to as topics in RISKGATE) that RISKGATE would address. Over the last three years, this scope has expanded at the request of the industry from the original 12 topics to the current set of 17 topics

<sup>1</sup> Minerals Industry Safety and Health Centre, Sustainable Minerals Institute, University of Queensland, Sir James Foots Building, Brisbane, Queensland Australia 4072, Email: p.kirsch@uq.edu.au, Tel: 0433998255

<sup>2</sup> Design Solutions Pty. Ltd., 4 Mankina Court, PO Box 1199, Buddina, Queensland, Australia 4575

described herein (Figure 1). Every RISKGATE topic is focused on coal industry activities (mining, processing, transport and storage) in both open cut and underground mine environments. The scope includes mine sites, lease areas, and mine infrastructure (e.g. mobile, fixed plant, field equipment, buildings and transport, including road and rail); and all aspects of the mine life cycle from design through to decommissioning. The topics recognise that 'loss of control' can result in personnel injury and/or fatality, equipment damage, production loss, reputation loss and environmental damage. However, the priority focus throughout RISKGATE is personnel safety.

2011	 COLLISIONS	 FIRES	 ISOLATION	 GROUND CONTROL	 STRATA CONTROL	 TYRES
2012	 EXPLOSIONS	 EXPLOSIVES OPENCUT	 EXPLOSIVES UNDERGROUND	 MANUAL TASKS	 SLIPS TRIPS & FALLS	
2013	 COAL BURSTS & BUMPS	 INRUSH	 INTERFACE	 OCCUPATIONAL HYGIENE	 OUTBURST	 TAILINGS DAM
2014	Fitness for Work					

Figure 1 - RISKGATE topics and development schedule 2011-2014

### RISKGATE topic summaries

The RISKGATE system applies a standard structure across the body of knowledge. Each topic is defined in terms of what is considered, and also in terms of areas that have been excluded. Within each topic, a further definition has been developed to provide terms of reference for the individual initiating events. The intention is that any users can quickly understand the way knowledge is structured, and zero in on the areas that are most relevant to their task. For example, a RISKGATE user conducting an incident investigation might start with the information about the consequences of an unwanted event (i.e. information on the right-hand side of the bow-tie), while a user conducting a risk assessment scoping exercise might initially focus their attention on the various causes and preventive controls of the event (i.e. information on the left-hand side of the bow-tie). Individual topic definitions are summarised as follows:

- **FIRES** relates to the unwanted or unexpected combination of a fuel source and an ignition source that results in fire. It provides controls to address four mining-related contexts: fires in mobile plant and field equipment, on fixed plant and infrastructure, on stockpiles and spoil heaps, and in the natural environment. Fuel sources are any flammable material including flammable liquids (i.e. motor fuel, lubricant, transformer fluid, hydraulic fluid and coolant), pressurised gases (LPG, natural gas, acetylene) coal, other solids (e.g. rags, timber, etc.) and other flammable fluids (e.g. cleaning fluids). Ignition results from sources of energy that include electrical, friction, hot work, lightning induction, hot surfaces and other miscellaneous sources (e.g. contraband). FIRES does not address explosions or spontaneous combustion which are addressed in RISKGATE EXPLOSIONS.
- **TYRES** provides information about management and prevention of incidents and accidents associated with the use of off-the-road (earthmover), industrial and other types of tyres, rims and wheels in open cut and underground coal mining. Here, the use of tyres includes all aspects of the tyre and rim management lifecycle - including selection, procurement, transport, fitting (installation and removal), maintenance, operation, storage and disposal. The scope includes the management of tyres, rims and wheels on the mine site and lease.
- **ISOLATION** provides information about management and prevention of incidents and accidents due to failure of the isolation process in open cut and underground mining. Relevant energies include electrical, hydraulic, pneumatic, gravity, mechanical, kinetic, chemical, thermal, and radiating (radioactive/microwave/other). Specifically, this topic addresses the control of energies and establishment of barriers to separate energies and prevent interaction with people. Each element of the isolation process (i.e. identification of an energy point/source, operation of the

- physical isolation device, verification, and lock-out) is considered across the full life cycle of the isolation device/s.
- STRATA CONTROL provides information on the management and prevention of failures due to loss of strata control in the underground mine environment. Eight core initiating events have been identified as priority areas where heightened awareness of preventive and mitigating controls could dramatically reduce the likelihood and/or severity of consequences. The initiating events are:
    - Loss of strata control at/in: longwall face, outbye roadways, development roadway and face, shafts, goaf edge in pillar extraction, and stress relief mining systems
    - Pillar system instability, and control of caving
  - GROUND CONTROL provides information on the management and prevention of incidents and accidents due to ground instability in open cut coal mining. Ground instability refers to the failure of mining slopes that is outside expectation of the ground/strata control management system (e.g. collapse or displacement). Controls are provided to manage potential unwanted events (i.e. initiating events) associated with activities conducted at the following locations: box cuts, highwall, end wall, low wall, truck dump, stockpiles, and truck and shovel benches (also known as pre-strip benches). Outcomes range from small individual rock falls to large-scale rock mass failures (e.g. wedge and slab failures).
  - COLLISIONS relates to the unwanted or unexpected interaction between people, mobile and field equipment, or fixed plant; including uncontrolled movements of mobile plant (where no other vehicle or pedestrian is involved), resulting in skidding, sliding, roll-over and falling over edges or down voids. Mobile and field equipment (vehicles) are defined as self-propelled machines or machines that are transportable around the mine in order to perform core functions (e.g. heavy and light vehicles, including dump trucks, industrial lift trucks (forklift), mobile cranes, earthmoving equipment, drag-lines, skid mounted equipment, lighting towers, continuous miners, shuttle cars, 4WD, utes). Fixed plant refers to non-transportable infrastructure or equipment (e.g. buildings, park up areas, installations, dams, tank farms, stockpiles, power lines, and transport networks). It addresses unwanted vehicle-vehicle, vehicle-people (including rollover), and vehicle-infrastructure interactions that may result in a single or multiple incidents.
  - EXPLOSIONS is defined as the unwanted or unexpected combination of a fuel and an ignition source that results in a fire or explosion. This topic focuses on coal mining and processing in open cut and underground mining. It addresses the potential for a fire or ignition to propagate into a larger fire or explosion with the consequent potential for multiple fatalities and widespread damage. Fuel sources are coal or flammable gases such as methane, ethane, carbon monoxide and hydrogen. Ignition results from sources of energy that include electrical, friction, hot work, lightning induction, hot surfaces, spontaneous combustion and other miscellaneous sources (e.g. contraband). They also include fires already existing on mobile plant, infrastructure, the natural environment, stockpiles and spoil heaps. Control of flammable gas atmospheres is to be achieved through adequate ventilation practice, including gas drainage. Here, mine workings include all areas of the mine where coal is being produced, areas that are being prepared for coal extraction and those areas which have had coal extracted from them.
  - EXPLOSIVES OPEN CUT relates to the unplanned release of energy from explosives. This topic is focused on overburden removal and coal extraction in open cut mine operations. It also relates to post blast events both within and beyond established exclusion and management zones for machinery and people. The topic covers the manufacturing, transport, storage and use, as well as disposal of explosive products on a mine lease. This material may be applicable to other (non-coal) open cut blasting operations (e.g. metal mining, quarrying, civil engineering).
  - EXPLOSIVES UNDERGROUND relates to the unplanned release of energy from explosives and unplanned fire or explosion consequent to explosives activity, with a focus on the use of explosives in underground coal mine operations. It also relates to post blast events both within and beyond established exclusion and management zones for machinery and people. The topic covers the transport, storage and use, as well as disposal of explosive products on a mine lease. Aspects of this material may be applicable to other underground operations (e.g. metal mining, tunnelling).
  - MANUAL TASKS is focussed on hazardous manual tasks which lead to musculoskeletal disorders. Musculoskeletal disorders caused by hazardous manual tasks include sprains, strains, or tears of connective tissues (muscle, ligament, tendon, intervertebral discs); stress

fractures; tendonitis; and vascular or neural disorders. This topic considers hazardous manual tasks performed by people during exploration and the surface and underground extraction of coal; as well as the transport of coal to, and processing in, coal handling and preparation plants.

- SLIPS, TRIPS and FALLS provides information to manage hazards associated with people slipping or tripping at ground level or on stairs, ladders, or platforms including temporary structures (e.g. scaffolding), and the hazard of falling. The topic covers mobile equipment (especially access and egress) and fixed plant (including coal preparation plants), and includes consideration of construction, operation and maintenance tasks, as well as pedestrian movement around sites. The topic includes loss of balance or falls of people on the same level, and falls from one level to another. Potential consequences include minor or serious injury (e.g. sprained/twisted ankles/knees, bruising, broken bones, skull fracture), fatalities, loss of control of loads or being carried or equipment being operated (e.g. power tools). The scope of this topic extends across all life of mine stages from exploration through to decommissioning (including the transport of coal to, and processing in, coal handling and preparation plants).
  - Controls address both short term and long term situations. For example, different measures may be needed for long term existing infrastructure that does not conform to current standards.
- COAL BUMPS AND BURSTS provides information on the management and prevention of strata failures due to bump or burst in underground coal mining. The terms bump and burst are often used interchangeably, and bump is used throughout this topic. The term bump describes a violent, brittle, dynamic failure of strata (pillar, rib, face, roof, floor) in or adjacent to the working section due to stress with a sudden release of energy. There may also be a liberation or ejection of coal or rock as a result of the energy release. This is more commonly described as a burst. The occurrence of bump and burst is directly related to stress, and will potentially increase with depth. (In the hard rock mining environment, bump or burst phenomena are called strainburst or rockburst.)
- INRUSH is the sudden and unplanned or uncontrolled inflow of liquid, gas or other material into coal mine workings which may result in unacceptable risk to health and safety. The risks are considered under two initiating events: inrush into surface workings and inrush into underground workings. To characterise the hazard associated with inrush requires a comprehensive three-dimensional spatial understanding to enable development and implementation of effective controls. Given the nature of risk associated with inrush, it is important to continuously verify that ongoing changes in the environment do not impact the validity of the original risk assessment (e.g. change in circumstances in neighbouring mines, different surface infrastructure). Inrush is a broad subject that interacts with a range of other management systems, including ground control (surface and underground), ventilation, water, engineering maintenance plan, survey control, inspections, defect management, and emergency response plan.
- HUMAN-MACHINE INTERFACE relates to interfaces (e.g. controls and displays) which are the means by which people:
  - operate and maintain plant or equipment, whether fixed, portable or mobile
  - gain and maintain situation awareness about the current and potential future state of plant within the mine and/or relevant aspects of the mine environment (e.g., the presence and location of other equipment or people; presence of methane; slope stability)
  - gain and maintain situation awareness about the current and potential future states of the mine and relevant environment (e.g. ventilation; manning, vehicle and machinery movements; production, development and maintenance activities; water management; security; and weather forecasts)
- Operator interfaces include levers, push buttons, dials, pedals, wheels, switches, touch screens, joy sticks, valves, keyboards, remote controls and communication devices. Display interfaces include sources of visual information (eg. windows, mirrors, computer screens, gauges, video monitors, cap lamps, mimic boards, tag boards, labels, signage, visual indicators, lights, pictograms, and white boards) as well as auditory displays (e.g. audio alarms, buzzers, communication devices) and haptic feedback devices (e.g. vibrating joystick). The detection and perception of information provided by displays allows situation awareness to be gained and maintained. This situational awareness is typically discussed in terms of individual awareness but may also include more complex automated systems and multiple operators. Errors in the use of controls, or suboptimal operation of controls, may result in unintended, delayed or sub-optimal movement or action of the plant or equipment being operated, leading to unwanted

- consequences including injury, fatality, equipment damage/increased maintenance and/or poor performance).
- o The loss of awareness of the state of the mine, or plant, may result in making incorrect, delayed or sub-optimal decisions which lead to unwanted consequences including fatality, injury or poor performance.
  - OCCUPATIONAL HYGIENE addresses chemical, physical and biological stressors. It focuses on coal mining and processing in open cut and underground environments across the lifespan of the mine (exploration, operations, closure). It addresses the key hazards of coal dust, silica dust, Diesel Particulate Matter (DPM), noise, and the thermal environment (e.g. heat stress, and cold). Other hazards include other air-borne contaminants (e.g. fumes, fibres, gases, vapors, combustion products; including the effect of confined spaces), waterborne contaminants (e.g. Legionella, E. coli (UG sanitation)), chemicals (e.g. PUR, solvents, glues, cleaning compounds), ionizing and non-ionising radiation (e.g. welding flash), vibration, and not fit for purpose lighting. Less than adequate control of these stressors in the working environment may result in harm to workers. Adverse health outcomes might be felt immediately, short-term or many years after exposure (e.g. acute, cumulative or chronic effects, long latency period).
  - OUTBURST relates to the sudden release of gas and material under pressure from the working place that has the potential to affect health and safety in coal mining. Outbursts occur when there is gas of sufficient volume and pressure to exceed the confining strength of the material within the seam being mined, or within seams above and below the active seam. Outbursts generally occur at the working face (development, driveage or longwall). Historically, outbursts have mostly occurred at the development face, though a lesser number have occurred at the longwall face.
  - TAILINGS DAMS addresses a key risk of catastrophic dam failure due to geotechnical instability of the dam itself or of its foundation, overtopping and erosion of the dam wall and piping failure of the dam itself or of its foundation. Coal mine tailings dams are also prone to seepage to the foundation and through the wall, particularly during operation when large volumes of water are discharged with the tailings. The most significant risk associated with this is the spillage and seepage of potentially contaminated water. Contamination can take the form of elevated salinity, acidity and dissolved metals, and sulphate. Run-off from coal mine tailings storages can cause erosion and can also potentially contain contaminants. Both the tailings and the water could be benign or potentially contaminating. Tailings can potentially be released by failure of the dam. Such failure could be by geotechnical slope instability, piping, or erosion due to overtopping. Water can potentially be released by failure of the dam, or by overtopping of surface run-off, or by seepage to the foundation and/or through the wall.

The RISKGATE team assembled individual topic panels (teams of industry experts) to discuss and develop the expert content (industry knowledge) for each specific topic. Optimal system content and wording was captured from discussion and debate within the group via a semi-structured action research workshop cycle described in more detail in Kirsch *et al.* (2012, 2013a,b) and Worden *et al.* (2013). As a result, each of the thousands of specific causes, controls and consequences within RISKGATE was identified, created, assessed and confirmed by industry experts from Australia's leading mining companies prior to upload into the system.

### **RISKGATE RESEARCH PROGRAMME AND PARTICIPANTS, 2011-2013**

Workshop activity can be summarised as follows:

- 2011: 86 workshop days, 422 individual days of mining industry expert time
- 2012: 39 workshop days, 164 individual days of mining industry expert time
- 2013: 34 workshop days, 149 individual days of mining industry expert time

These experts, bringing broad ranging experience and training in underground, open cut, coal and hard rock environments, have contributed a collective equivalent of 735 individual days to the RISKGATE programme, with the mean years of experience in the industry for specific topics ranging from 10.5 years (Slips, Trips, Falls) to 31.4 years (Outburst) (Table 1).

**Table 1 - Industry expert participation in RISKGATE workshops**

Topic	Number of workshop days	Workshop attendance (personnel days of Mining and Industry Experts)	Mean workshop participant experience (yrs)
Collisions	11	51	24.8 (1-39)
Fires	15	81	26.5 (9-48)
Isolation	15	83	19.3 (14-39)
Ground Control	14	45	21.3 (5-37)
Strata Control	16	75	19.4 (5-37)
Tyres	15	142	22.0 (1-42)
Explosions	11	47	26.9 (15-38)
Explosives Opencut	11	62	22.9 (9-40)
Explosives Underground	3	14	20.0 (5-41)
Manual Tasks	8	58	17.7 (4-38)
Slips, Trips and Falls	9	39	10.5 (1-22)
Coal Bursts and Bumps	3	14	24.0 (7-40)
Inrush	8	42	30.5 (15-39)
Interface	4	20	15.5 (1-23)
Occupational Hygiene	10	49	17.8 (3-24)
Outburst	4	20	31.4 (16-40)
Tailings Dam	4	15	20.7 (10-27)
	161	857	

Workshop participants represented a broad array of industry knowledge and professional expertise acquired across a spectrum of ten mining companies, fourteen OEM or suppliers, two universities, and two regulatory agencies (NSW, QLD) (Table 2). Collaborative industry efforts provided the foundation upon which RISKGATE was built, with outcomes a reflection of how leading practitioners share and negotiate current practice. Integration of cross-sectorial industry knowledge, further supported by a substantive and diverse array of industry, academic and technological resources, means RISKGATE can offer a continuum for knowledge transfer and redefining best practice in risk identification, assessment and management in the coal industry.

**Table 2 - Workshop participants 2011-2013**

Anglo American BMA/BHP Bandana Centennial Coal Downer EDI Gujarat Peabody Energy Rio Tinto Glencore Adani Caledon	Bridgestone Good Year Marathon Michelin Titan	Aystar Dyno Nobel Golder Ergo Enterprises Job Fits System Orica Mining Services Otraco Klinge Group Pulford	The University of Queensland  University of New South Wales  University of Wollongong	Qld Department of Employment, Economic Development and Innovation (DEEDI)  Qld Department of Natural Resources and Mines (DNRM)  New South Wales Trade and Industry Workplace Health and Safety
---	---	--	---	---

### Knowledge distribution across the RISKGATE Bow-Tie

RISKGATE's body of knowledge is built using BTA, a risk management method that helps users consider the entire context of an unwanted event associated with a particular hazard: its causes, consequences and most importantly the controls used to prevent the unwanted event or to mitigate or reduce the consequences of it should it occur. A key advantage of this method is its focus on control effectiveness.. Detailed explanation of BTA application within the RISKGATE program can be found in Kirsch *et al.* (2012, 2013a,b) and Worden *et al.* (2013). A brief summary is presented here for the any new users.

### Bow-Tie elements

There are typically between four and nine bow-ties within each RISKGATE topic with each bow-tie centred on a specific *initiating event* (or unwanted event). The initiating event, or 'knot', of the bow-tie represents the point at which energy control is lost; with the primary causes and the unwanted consequences of the initiating event tabulated on either side of the knot. A *cause* is any occurrence or reason that could lead to an event via the release of the hazard(s). Correspondingly, a *consequence* is any negative outcome that arises from an initiating event. In RISKGATE consequences primarily are associated with injury or illness of people, but also include damage to equipment and/or the environment, though there may be other important negative consequences.

*Controls* include any process, policy, device, practice, or other action that is intended to reduce the likelihood of an unwanted event occurring or that reduces the magnitude of the consequences of an unwanted event. Causes are prevented from triggering the event through specific preventive controls. Should these preventive controls fail, the severity of the consequences of the unwanted event are minimised through mitigating controls designed and implemented before the event occurs.

The RISKGATE BTA tool has sufficient flexibility to accommodate a growing depth of knowledge beyond forecast user requirements, as has been experienced during this project. The actual number of data elements collected to date for each initiating event per topic is summarised in Table 3. Note, these estimates are conservative as many of the controls are further broken into multiple options or 'sub-control' data points. Totals for Inrush, Tailings Dams and Occupational Hygiene are not included in Table 3, as this topic content is still going through final review at the time of preparation of this conference manuscript.

**Table 3 - Summary of RISKGATE bow-tie element data (one initiating event per topic)**

Topic	Number of Initiating Events	Causes	Preventive Controls	Consequences	Mitigating Controls
Tyres	4	28	146	9	29
Collisions	2	45	133	4	11
Strata Control	8	114	383	21	4
Ground Control	7	86	204	23	35
Fires	4	46	165	9	54
Isolation	5	301	792	11	65
Explosives O/C	5	55	127	18	39
Explosives U/G	4	35	84	10	24
Explosions	7	50	240	7	43
Manual Tasks	3	39	114	3	6
Slips Trips and Falls	3	26	57	3	11
Coal Bumps and Bursts	3	3	20	9	20
Outburst	1	7	31	1	6
Interface	3	52	216	3	31

### RISKGATE: Knowledge models per topic

During the workshops the industry experts found BTA to be more effective when structured within a recognised industry model to assist in system design and user implementation. The expert panels within each topic area chose a different model or industry framework to structure knowledge acquisition and presentation in the online system. These tended to match the unique approaches that the different mining experts used '*in situ*' to manage their particular hazard. For example, both the Fires and Explosions topics were structured around fuel or ignition sources, with fuel sources for the Fires topic divided into flammable liquids; coal; other solids; pressurised gases; and other flammable fluids. The Strata (underground) and Ground (open cut) topics were divided according to unwanted events at different mine locations, and controls for each of these were categorised according to whether they addressed design or operational issues. The information in the tyres topic was developed around the tyre life cycle from procurement to disposal. The explosives open cut topics also took this format, focussing on the lifecycle of the various classes of explosives on the mine site, from manufacturing to disposal. The Isolation topic was possibly the most complex structure with a 5x4 matrix between the 'Life

of the Asset' (design/procurement; installation/commissioning); operation/maintenance; modification; and decommissioning) and the 'Isolation Steps' (identification; operation; verification; and securing). These models or frameworks were used throughout the action research workshops to ensure that different hazards were addressed in a systematic and comprehensive way.

### **RISKGATE: Integration in company operations**

The first 11 RISKGATE topics were launched in December 2012, with an additional six topics coming online by the end of December 2013. Therefore, technology transfer and system implementation is still in an early phase within the Australian coal industry. However, the following case studies provide examples of how RISKGATE is currently being used within different coal mining companies:

#### ***Use of RISKGATE as a reference / body of knowledge***

The first entry point for new RISKGATE users is to familiarise themselves with the structure of the site, and then download information in the form of customised checklists that can be used to inform corporate or site-level risk assessments, incident investigations, audits and for the development of management systems. For example, Peabody Energy Australia is using the RISKGATE Strata Underground and Ground information as reference material for audits of their geological/geotechnical principal hazard management plans at specific operations.

#### ***Consideration for RISKGATE content in development of corporate practice***

Once familiar with the system, and this detailed body of knowledge, companies are starting to use the RISKGATE information as a comparative data base for gap analysis of corporate standards and to inform the development of new standards or recommended practice. Anglo American has used RISKGATE to benchmark their global isolation standard; and their new recommended practice for collision avoidance systems was built using the RISKGATE Collisions knowledge as a primary source.

#### ***Integration of RISKGATE content into operating systems***

Some coal companies are actively integrating RISKGATE into their risk management processes. In the vanguard of these is Centennial Coal, which has fully embraced the use of RISKGATE and developed a software interface that enables seamless integration of the RISKGATE knowledge base into their internal risk management software system, Stature. Centennial staff can log into the RISKGATE site, customise information checklists for their specific application, save these checklists into a Stature format on their home computer; and then log into Stature on their home computer and upload the RISKGATE file so that it is displayed within the Stature page. When this is completed, the risk manager is able to return to the standard and routine procedures established for management of hazards, but equipped with the Australian coal industry's body of knowledge for that hazard. It is simply like bringing the whole industry into the room at one time. This process has particularly proven beneficial in the scoping of risk assessments, where users are able to compile a collection of their own current controls with those of RISKGATE about a particular unwanted event or hazard, and then bring this information to the wider group to conduct the risk assessment task.

### **RISKGATE: Next steps and future opportunities**

In 2014, RISKGATE will focus on the remaining topic Fitness for Work, pending continuing ACARP funding. It is proposed that the topic will be divided into five key areas to address drugs (legal and illegal), alcohol, fatigue, physical wellbeing and psychological wellbeing. In August 2013, the RISKGATE team surveyed 106 mining industry representatives in Australia to help the team develop a fitness for work project scope and obtain further input for the proposed action research workshops. The survey results showed very strong support for the five topic categories and respondents provided suggestions on what could be included within these categories. These included:

- Caffeine, synthetics and the impact of families – drugs
- Understanding what 'normal' consumption might be – alcohol
- Commuting, personal duty of care, self-management, performance impact, personal health, and alcohol and sleep – fatigue

- Pain management, sleep disorders, personal duty of care, physical fitness requirements for emergency egress, musculoskeletal conditions – physical wellbeing
- Cognition, medication impacts, assessment techniques, family support – psychological wellbeing.

The RISKGATE team is seeking industry experts who can contribute their knowledge to the 2014 Fitness for Work action research workshops. Workshop participation presents opportunities for networking, reflection and sharing of lessons learned, keeping abreast of current and emerging control technologies, instigating a shift in existing safety culture, and elevating the accepted levels of current practice.

However, this body of knowledge has application beyond the coal industry. Many hazards in the coal industry, such as collisions, hazardous energy (for example electricity or hydraulic pressure), fires, explosions and slips, trips and falls are common to other mining domains and beyond in other industries. Coal mining is recognised globally as a hazardous activity and, as a result, operates under high levels of regulatory and public scrutiny. Other high-risk industries, often associated with the coal supply or energy chains – including power generation and transmission, construction, rail transport, road transport and shipping – and other mining industries all need to manage workforces operating in similar high-risk environments. From a broad industry perspective, the RISKGATE platform provides an environment for knowledge capture and knowledge exchange regarding current practice, and facilitates the establishment of a cumulative corporate memory. Practitioners from other high-risk industries are encouraged to engage with the RISKGATE process to help improve their risk management outcomes.

#### ACKNOWLEDGEMENTS

We thank RISKGATE administration, design and communications support (Barbara Whittaker, Sandy Worden) and topic leaders (Bruce Hebblewhite, Guldidar V. Kizil, Tilman Rashe, Alastair Torrance, Duncan Chalmers, David Williams, Robin Burgess-Limerick, Mark Spinks, Jim Galvin, Peter Bergin). This project is funded through ACARP grant no. C20003. We especially thank each of the Australian coal industry professionals who gave generously of their time and knowledge on individual RISKGATE topic panels, and express thanks to each of the companies for their support and provision of both experts and technical resources. Finally, we acknowledge the contributions of anonymous reviewers towards tightening up this manuscript.

#### REFERENCES

- Harris, J, Kirsch, P, Sprott, D, Spinks, M, Goater, S and Cliff, D, 2012. RISKGATE - a case study in application to fires on mobile plant. *Proceedings of the Eighth AUSIMM Open Pit Operators Conference*, Perth, 18-19 September 2012, Perth, Australia. The Australasian Institute of Mining and Metallurgy (The AusIMM)
- Harris, J, Sprott, D, Torrance, A, Shi, M, Ranjan, A, Sharma, S, Biswas, T, Sharma, S. and Kirsch, P A, 2013. Sharing industry knowledge to improve management of risks and safety in the use of explosives in surface mining. *Proceedings of the World Mining Congress*, Montreal, Canada, August 11-15, 2013.
- Kirsch, P, Goater, S, Harris, J, Sprott, D, and Joy, J, 2012. RISKGATE: Promoting and redefining best practice for risk management in the Australian coal industry. *Proceedings of the 12th Coal Operators' Conference*, University of Wollongong and The Australasian Institute of Mining and Metallurgy, 2012, 315-325. <http://ro.uow.edu.au/coal/421/>.
- Kirsch, P, Harris, J, and Sprott, D, 2013a. Vertical integration of risk management in the Hunter Valley Coal Chain – application of the coal industry's RISKGATE platform. *The AUSIMM Bulletin* February 2013, 45-49.
- Kirsch, P A, Harris, J, Cliff, D and Sprott, D, 2013b. Industry scale knowledge management – RISKGATE and Australian coal operations. *Proceedings of the World Mining Congress*, Montreal, Canada, August 11-15, 2013.
- Kirsch, P A, Harris, J, Cliff, D, Hebblewhite, B, Sprott, D, Shi, M, Ranjan, A, Sharma, S, Biswas, T, and Sharma, S, 2013c. Industry scale knowledge management – introducing the RISKGATE Underground Strata and Explosions Body of Knowledge. *Proceedings of the World Mining Congress*, Montreal, Canada, August 11-15, 2013.

- Kirsch, P, Harris, J, Sprott, D, and Cliff, D, 2014. RISKGATE and Australian coal operations. *Proceedings of the 14th Coal Operators' Conference*, University of Wollongong and The Australasian Institute of Mining and Metallurgy, 2014 (this volume).
- Lynas, D, Burgess-Limerick, R, and Kirsch, P A, 2014 (in press). RISKGATE analysis of Slips, Trips and Falls at NSW surface and underground coal mines. *Journal of Health and Safety Research and Practice*
- RISKGATE, 2013. [www.riskgate.org](http://www.riskgate.org).
- Worden, S, Sprott, D, and Whittaker, B, 2013. Risk management competence in Australia gets a boost from new software. *Mining Engineering* 65 (July): 22-33.

# COMPARATIVE ANALYSIS OF COAL FATALITIES IN AUSTRALIA, SOUTH AFRICA, INDIA, CHINA AND USA, 2006-2010

Jill Harris<sup>1</sup>, Philipp Kirsch<sup>1</sup>, Meng Shi<sup>1</sup>, Jirui Li<sup>1</sup>, Ankita Gagrani<sup>2</sup>, Anand Krishna ES<sup>3</sup>, Ahmad Tabish<sup>4</sup>, Deepanshu Arora<sup>5</sup>, Kishore Kothandaraman<sup>6</sup> and David Cliff<sup>1</sup>

**ABSTRACT:** Coal mining (especially underground) is considered one of the most hazardous industries, and as a result considerable focus is applied to eliminating or mitigating hazards through careful mine planning, equipment selection and certification, and development of management systems and procedures. Regulatory agencies have developed in-house methods for reporting, classification and tracking of fatalities and other incidents according to the type of event, often including consideration of different hazard types. Unfortunately, direct comparison of mining safety statistics between countries is confounded by considerable differences in the way that individual countries classify specific fatalities or incidents.

This paper presents a comparative analysis of coal mining fatality data in Australia, South Africa, India, China and the United States from 2006 to 2010. Individual classification definitions are compared between the five countries, and methods presented to normalise each country's hazard definitions and reporting regimes around the RISKGATE framework of seventeen different priority unwanted events (or topics). Fatality data from individual countries is then re-classified according to the different RISKGATE topics, thereby enabling a comparative analysis between all five countries.

This paper demonstrates the utility and value of a standard classification approach, and submits the RISKGATE framework as a model for classification that could be applied globally in coal mining. RISKGATE is the largest health and safety project ever funded by the Australian coal industry (<http://www.riskgate.org>) to build an industry body of knowledge to assist in managing common industry hazards. A comprehensive knowledge base has been captured for risk management of tyres, collisions, fires, isolation, strata underground, ground control open cut, explosions, explosives, manual tasks and slips/trips/falls. This has been extended to outburst, coal burst and bumps, interface displays and controls, tailings dams and inrush.

## INTRODUCTION

Globally, coal continues to be vitally important to energy production as well as manufacturing and construction. In 2012 it provided about 30% of the world's energy needs and was used in the production of about 70% of the world's steel (World Coal Association, 2013). It has driven the development of advanced countries and is now a leading contributor to the rapid economic growth of emerging countries such as China and India. Its pioneering role in the development of nations, has meant that coal mining is often embedded in the psyche of a country, its activities both influencing and being influenced by the peculiar historical, cultural, political, economic, labour, environmental and social factors of the location in which it operates. It was a key driver of the industrial revolution in Britain (Allan, 2006). Lahiri-Dutt (2014 in press) argues that coal is considered a symbolic icon of national pride in India, and is protected as a national asset. How this industry has and continues to manage worker safety is therefore no doubt influenced by broader and often hidden societal factors.

<sup>1</sup> Minerals Industry Safety and Health Centre, Sustainable Minerals Institute, University of Queensland, Sir James Foots Building, Brisbane, Queensland Australia 4072. Corresponding author: [p.kirsch@uq.edu.au](mailto:p.kirsch@uq.edu.au), Tel: 0433998255

<sup>2</sup> Department of Metallurgical and Materials Engineering, Indian Institute of Technology Roorkee, Roorkee, Uttarakhand, India, 247667

<sup>3</sup> Department of Mining Engineering, National Institute of Technology Karnataka Surathkal, Mangalore, India, 575025

<sup>4</sup> Zakir Husain College of Engineering and Technology, Aligarh Muslim University, Aligarh, India, 202002

<sup>5</sup> Department of Chemical Engineering and Technology, Aligarh Muslim University, Aligarh, India, 202002

<sup>6</sup> Department of Mechanical Engineering, Indian Institute of Technology Madras, Chennai, India, 600036

Coal mining is inherently dangerous due to its combustible nature, the extraction process and the high level of mechanisation involved. Underground compared to open cut mining, is generally considered to be more hazardous due to the risk of explosions and strata failure. The enclosed nature of underground mining forces personnel to work in close proximity to risks and this compounds worker's potential for harm. For example, miners work near to the face and mechanical equipment and under a strata-roof and should there be a failure, they have restricted exit points. Also, the underground environment has low visibility and is often noisy. Open-cut mining hazards such as fall of ground and loss of control of explosives similarly have the potential for severe consequences.

While the risk associated with mining hazards, can now be managed to a tolerable or acceptable level, significant numbers of miners continue to die. In 2010, explosions in the Pike River Mine in New Zealand and the Upper Big Branch mine in West Virginia both killed 29 men and in 2007 underground strata failure caused the death of six miners (and three rescuers) in the Crandall Canyon Mine in Utah. Unfortunately, the number of fatalities in coal mines in developing countries is generally much higher. For example, between 2001 and 2008 strata failure and explosions caused over 14,000 workers' deaths in China (strata: 6,173 deaths from 4,653 accidents; explosions: 8,013 deaths from 1,027 accidents, Wang, *et al.*, 2011). Wang *et al.* (2011) also reported that there were seven underground mine explosions in China between 2008 and 2011 and that each resulted in more than 100 deaths. Due to the underreporting of coal mine deaths in China, it is likely that many more miners lost their lives during this period (Jianjun, 2007).

Most research in the area of prevalence of mining fatalities has been limited to understanding direct causal factors at the operational site without reflection on the broad organisational, societal, economic, legislative or environmental conditions in which production takes place. It is proposed here that a comparative analysis of coal mining fatalities across different countries could provide a foundation of information for a more informed debate on safety management priorities for coal mining in both developed, and less developed countries that currently experience high rates of mining fatalities.

This paper describes preliminary research undertaken at the Minerals Industry Safety and Health Centre to develop a global framework for researching coal mining fatalities. It focuses on fatalities caused by underground explosions and strata fall and open cut ground fall and use of explosives in five major coal mining countries: Australia, China, India, South Africa and the United States. An important first stage has been to access different countries' fatality databases. Most coal mining countries have legislation requiring mining companies to report their accident, fatality and/or injury statistics, and sometimes their near misses or mishaps. This is because in high risk industries, a reporting culture is critical to identify prevalence and causation of incidents and sharing of lessons learnt (Reason, 1997, 2000). It engenders a safety culture at an individual organisational level and at a broader industry and regulatory level. At an organisational level an accident/incident database can trigger continuous improvement in site standards and controls, and training in accident prevention.

Benefits of industry-wide safety databases include continual improvement of standards and regulations, a more comprehensive understanding of safety risks – particularly infrequently occurring risks, better engagement of stakeholders, and design advances (Barach and Small, 2000). Regulatory bodies disseminate the information collected in these databases in various forms. Some provide detailed narratives of all fatalities (e.g. United States Mine Safety and Health Administration, MSHA) while others only disseminate higher-level analysis of statistics, such as annual fatality and injury frequency rates and/or safety alerts and bulletins. Safety bulletins typically alert the mining community to the circumstances of a fatality or dangerous event or report increased incidences of a particular risk or hazard, to encourage vigilance and provide information on better management of these unwanted events. Annual incident rates are generally categorised according to key mining hazards or risks, equipment type, environment (e.g. open cut, underground), and mining lifecycle (e.g. exploration, operations). The various categorisation methods used by regulatory bodies in different countries make it difficult to compare the causes of incidents at a broader global level.

It is vital to take into account the various contextual factors that influence coal mining activities and might drive variances in worker safety across countries. Table 1 provides general information about production and use of coal by the five countries that are the focus of this article. While this information provides some insight into potential explanations for between country disparities in safety performance, it does not tell the full story. It does however indicate why fatality rates need to be standardised across differences in workforce numbers and coal production rates. Also it may hint at differences in mechanisation, for example while Australia and India produce a relatively similar amount of coal, their numbers of workforces differ considerably, with India's workforce being ten times more than that of

Australia. This suggests a higher level of mechanisation in Australian mines and therefore it could be expected that this variance drive a between countries difference in the causes of fatalities. The numbers of underground and surface coal mines across countries may help to inform differences in the types of hazards that are more likely to be prevalent, although this must be tempered by information about the rates of production and numbers of employees across surface and underground contexts. For example, even though India has more underground mines, surface mines produced more coal (over 80%).

**Table 1 - A comparison of coal production and consumption information for Australia, China, India, South Africa and the USA for 2011**

Country	Number of coal mines			Coal production (per million tonnes)			Workforce (x1,000)	Coal exports (per million tonnes)			Coal imports (per million tonnes)			Coal consumption (per million tonnes)
	Total	Surface	Underground	Total	Surface	Underground		Steam	Coking	Total	Steam	Coking	Total	
Australia	135	75%	25%	415.5	80%	20%	100	144	140	284			^	130.1
China	18,557	5%	95%	3,520			5,000			*	218	71	289	3471.7
India	572	36%	64%	588.5	84%	16%	1,000				123	37	160	654.5
South Africa		53%	47%	255.1	40%	60%	55	72	0	72			^	182.7
USA	1,325	62%	38%	993.7	68%	32%	91.6	34	63	97			^	972.3

Notes to Table 1: \*China and India have negligible coal exports, with nearly all coal used domestically; ^Australia, South Africa and USA have negligible coal imports, as most coal is supplied domestically; Australian information sourced from Australian Bureau of Agricultural and Resource Economics and Sciences website, Australian Bureau of Statistics, Bureau of Resources and Energy Economics; Chinese information sourced from the World Coal Association website; Indian information sourced from Directorate General of Mines Safety and Indian Bureau of Mines websites; South African information sourced from South African Chamber of Mines website; US information sourced from the Mine Safety and Health Administration and US Energy Information Administration websites; General information taken from International Energy Agency: Coal Information 2012.

Australian Fatality Injury Frequency Rates (FIFR) 10 year averages indicate that open cut mines have a rate less than 50 % of the USA and underground coal mines less than 16 %, yet the mining methods are the same (Minerals Council of Australia, 2007/2008). It appears that Australia's safety record outperforms that of the US, despite there being gross similarities between Australia and the US, including culture, language, education, Gross Domestic Product (GDP), and value of life. In regards to coal mining operations, both countries are highly invested in safety, have similar mining methods and levels of technology and mechanisation. Some of the more 'hidden' factors that may drive this difference in safety performance across countries are mine size, production rates, unionisation of workforce and key differences in the legislative environment and enforcement processes. For example, it has been shown that in Australia between 1991 and 2010 85 men lost their lives working in coal mines (Kirsch, *et al.*, 2013b). Across this period there was a dramatic reduction in deaths, with 65 recorded fatalities between 1991 and 2000 and only 20 in the following decade (2001 to 2010). Such a reduction is even more significant when one considers it occurred during a period of rapid expansion in Australian resources (Connolly and Orsmond, 2011). Also, the relative proportion of deaths caused by non-principal hazards (i.e. incidents that are less likely to cause multiple deaths) compared to those from principal hazards has changed across decades. Whereas most deaths between 1991 and 2000 were caused by principal hazards (~52%), in the last decade, most deaths were actually caused by non-principal hazards (~68%). Therefore it could be said that workers in Australian coal mines are now no longer dying as a result of significant disasters that take the lives of many people, rather fatalities are occurring one-by-one, as a result of more innocuous hazards, such as collisions, slipping or falling from heights, loss of control of tyres, or uncontrolled release of hydraulic energy.

A potential explanation for this difference is the legislative change that occurred in the late 1990's and early 2000's regulating health and safety legislation for coal mines in Queensland and New South Wales. Part of a global shift in health and safety practice (Foster, *et al.*, 1998), this change represented a move from a compliance-based to a risk management approach to safety (Cliff, 2012a, 2012b). Incorporated into this legislation was the concept of 'duty of care' that makes individuals legally responsible to take reasonable care so that others are unharmed. Another key element of these new legislations was the implementation of risk assessment based Mine Safety Management Plans for principal or major hazards. In response to these changes, it is perhaps significant that all major mining incidents in Australia since 1996 have been in metalliferous mines (at North Parkes, 1999; Bronzewing, 2000; and Beaconsfield, 2006).

As can be seen, coal mining safety performance is influenced not only by the immediate geographical or geotechnical environment in which mining activities take place, but also by broader political and social trends. The aim of this project was to develop and test a standardised incident classification framework that could be used to categorise fatalities according to key coal mining hazards across different

countries. Different countries' fatality narratives (as available) would be categorised according to this incident classification framework. In this way we can begin to describe within and between country shifts in rates and distribution of fatalities by hazard. This would include the reporting of timelines of fatalities (by hazard) for countries, to identify shifts resulting in improving or declining safety performance. Ultimately this method will be used to attribute higher-level hidden factors to shifts in rates and distribution of fatalities by hazard within and between countries.

In this report, the preliminary stages of this project are described, including the gathering of narrative information of coal mining fatalities in Australia, China, India, South Africa and the United States and classification outcomes for four coal mining hazards.

## Introduction to RISKGATE

RISKGATE is a web-based tool ([www.riskgate.org](http://www.riskgate.org)) providing clear, up-to-date and practical checklists for controlling risks across 17 specific high priority unwanted events (hazards, called topics in the RISKGATE system) in Australian coal mining. A brief definition of each of these 17 RISKGATE topics is provided by Kirsch *et al.* (2014, this volume). Based on interactive Bow-Tie Analysis (BTA) to assist in the implementation of safer operations, each RISKGATE topic and each bow-tie is centred on a specific unwanted or initiating event. The funnelling of causal factors and consequences through this initiating event keeps the information concise, intuitive and targeted. Users can generate checklists that will deliver on-site managers and engineers quick and relevant access to broad industry-based current practice controls for consideration at their own site. These checklists are designed as prompts regarding current practice that could assist with risk assessment, auditing, accident investigation, and training.

RISKGATE is funded by the Australian Coal Association Research Program (ACARP); managed and implemented by the University of Queensland; and each of the thousands of specific controls loaded into the RISKGATE system have been instigated and assessed by industry experts from Australia's leading mining companies. RISKGATE is built on a foundation of industry expert knowledge gathered through topic specific action research workshops (Kirsch, *et al.*, 2012, 2013a, 2013 b, Worden, *et al.*, 2013). Topics which have been completed to date include: fires (Harris, *et al.*, 2012), underground strata control (Kirsch, *et al.*, 2013c), open cut ground control, collisions, tyres, isolation, explosions (Kirsch, *et al.*, 2013c), explosives (Harris, *et al.*, 2013), manual tasks, and slips trips and falls (Lynas, *et al.*, 2014, in press). The intent of RISKGATE is not to specifically assess risk for any unique site, but instead provide a decision support tool, resources and outputs, such as tailored checklists, that can assist users in their site-specific risk assessment and risk management.

## METHOD

The narratives of coal mining fatalities occurring between 2006 and 2010 were obtained for five countries (Australia, India, South Africa and the United States). Data from the United States was accessed via the Mining Safety and Health Administration website (MSHA; <http://msha.gov>). Indian and South African data was sourced with permission from private communication with personnel in those country's coal mining regulatory bodies. We accessed Australian fatality data from a University of Queensland, Minerals Industry Safety and Health Centre (MISHC) database. Each country's narratives differed in detail as shown in the fall of Strata examples below<sup>1</sup>:

- While drilling into roof to do the brushing, a slab of rock, the size of the intersection came off the roof and fell on the workers drilling.
- At approximately time on date, age-year-old name and age-year-old name, mobile roof support (MRS) machine operators, were fatally injured when a portion of the mine roof collapsed, pinning both individuals. They had x years and x years of mining experience respectively. They were repositioning MRS machines after the completion of the third lift in the #3 entry while performing retreat mining on the North Section. The slicken-sided portion of the mine roof that collapsed measured approximately 8 feet in width by 9 feet in length and was up to 18 inches thick.
- Crushed when roof collapsed while inspecting conditions in pillar extraction area.
- Fall of roof

<sup>1</sup> Note, Personal details have been removed from these narratives; while these narratives only refer to underground fall of strata all narratives for all of the different accident causes were collected.

Data from China was most difficult to obtain as their mining regulatory bodies do not provide public access to coal mining fatality databases. As a result, data was obtained from the United States Mine Rescue Association (USMRA, <http://www.usmra.com/chinatable.htm>) website. The moderators of this website collate media reports of accidents and resulting fatalities in mines in China. Therefore, only major incidents with multiple fatalities are reported - single fatalities are not reported. Also, the reports only give the number of deaths at the time of reporting, they do not give the final number of fatalities; including those who later died as a result of their injuries. Therefore, the number of Chinese fatalities reported in our study are conservative, and do not represent all coal mining deaths in China. The reliability of the information also rests on the accuracy of the media reports. However, the reports are quite detailed which enabled it to be classified for each incident according to the hazard taxonomy. An example of an incident report is:

- Location, Date - Nine workers were killed and 11 others injured after a tunnel collapsed on Thursday afternoon in a coal mine in China's Location Province. The incident happened at time p.m. when a 80-meter section of a tunnel suddenly collapsed in the Name Coal Mine, which belongs to Name in Location, said a spokesman of the group on Friday. The injured were hospitalised. An investigation into the cause of the incident has begun.

Once data was obtained, each incident for each year and country was then categorised according to 11 key coal mining hazards; see Kirsch *et al.* (2014) for brief hazard definitions). While the RISKGATE system now covers and provides definition for 17 coal mining hazards, this classification study was initiated when only the first 11 hazards were completed (Kirsch, *et al.*, 2012). The RISKGATE categories of mining hazards were identified as priority unwanted events in coal mining by ACARP members and comprehensively defined through the action research workshop process, thereby providing a framework for standardised and accurate re-classification of the five country's fatality narratives.

An example of a RISKGATE hazard (termed Topic in RISKGATE) definition is displayed in Box 1, which highlights the depth of information that was used to guide our incident classification (detailed definitions can also be accessed at [www.riskgate.org](http://www.riskgate.org)). Further, RISKGATE provides more specific second level definitions for each hazards' 'initiating events' (or points at which control is lost according to bow-tie analysis; Detailed explanation of the application of bow-tie analysis within the RISKGATE program can be found in Kirsch *et al.* (2012; 2013a, 2013b) and Worden *et al.*, 2013). So for the Explosives open cut topic, there was not only the general topic definition (Box 1) but also definitions for each of the five initiating events listed in this definition. Shown in Table 2 are examples of definitions that regulatory bodies use to categorise fatality narratives as being caused by explosives. These are included here to highlight their brevity in comparison to the RISKGATE definition.

## Procedure

Individual student researchers, all studying engineering (and mostly mining engineering) worked on classifying fatality narratives for each country. Prior to commencing this process, each was thoroughly trained on using the RISKGATE topics to classify fatality narratives. Any narratives that researchers found difficult to classify were identified, and then discussed and finally classified during regular team meetings. Outside expertise was sought to classify narratives that the group was unable to categorise. Narratives that did not fit any of the 11 RISKGATE categories were classified 'Other'<sup>1</sup>.

## RESULTS

In this article only preliminary fatality statistics for four hazards: explosions, fall of strata – underground, fall of ground – open cut, and explosives – open cut are presented. Table 2 reveals that nearly half of the fatalities in coal mines in the United States are caused by explosions and strata failure. Further, these hazards cause two out of three fatalities in China and nearly four out of ten fatalities in India. Strata failure alone results in about 20 to 25 % of all coal fatalities in India and South Africa. Explosions are quite infrequent in South Africa, with only three recorded deaths (or 3.5% of the total), probably due to the low gas content in coal in that region. This table also shows that the two underground hazards are much more dangerous (in terms of fatalities) than the two open cut hazards. It appears that for these countries, the likelihood of fatalities due to explosives and surface ground fall is low compared to that of the underground hazards of explosions and strata fall.

<sup>1</sup> Note, since the time of this study RISKGATE has now added more hazards to its body of knowledge including outbursts, coal bumps and bursts, interface, inrush, tailings dams, occupational hygiene

There are a number of possible explanations as to why explosives cause fewer incidents in surface coal mines. One is that drilling and blasting is now a relatively automated process. For example, computers are used to drill and monitor blast holes and assist in the delivery of explosives (e.g., ANFO, heavy ANFO and pumped emulsion blends) to blast holes. Automation improves the reliability and accuracy of these tasks as well as reduces the number of personnel required for potentially hazardous jobs. It is now not uncommon for loading of blast holes to be completed by one person, sitting in an explosive loading vehicle with an additional shot firer ensuring the collar length is achieved on the bench. Further, the development of remote firing systems allows operators to fire the blast from safe distances. Mine-site personnel who do supervise blasting operations are required to hold shot firing licenses and associated mandatory competencies. These risk treatments are common to blasting operations around the world, including developing countries. In Australia the handling and use of explosives must also be done in accordance with national standards that further drive safe practice.

### Box 1 - Example of a RISKGATE hazard definition (Explosives Open Cut topic)

#### Explosives Opencut

This RISKGATE topic area relates to the unplanned release of energy from explosives. This topic is focused on overburden removal and coal extraction in open cut mine operations. It also relates to post blast events both within and beyond established exclusion and management zones for machinery and people. This material may be applicable to other (non-coal) open cut blasting operations (e.g. metal mining, quarrying, civil engineering)

The result of such events may lead to personnel injury, fatality and/or equipment damage, closing of mine operations during the resolution of an event, or regulatory non-compliance.

The EXPLOSIVES topic covers the manufacturing, transport, storage and use, as well as disposal of explosive products on a mine lease. Different streams are considered:

- High explosives (initiation systems) including detonators, detonating cord and primers. These are generally Explosives of Class 1.1B or 1.1D.
- Explosive precursors such as ammonium nitrate, emulsion phase. These are generally Dangerous Goods Class 5.1.
- Manufactured explosives for use in open cut blasting. Generally Explosives of Class 1.1D.
- Permitted explosives used in secondary blasting in confined spaces (e.g. hoppers, coal bins, crusher)

Five key INITIATING EVENTS are covered:

- IE1: Loss of control of explosives and associated chemicals in storage on site
- IE2: Loss of control of explosives and associated chemicals during transport
- IE3: Loss of control of explosives and associated chemicals during manufacture
- IE4: Loss of control of explosives and associated chemicals during handling and blast operations
- IE5: Loss of control of explosives and associated chemicals during disposal

The information in this RISKGATE topic does not address:

- Use of explosives in underground mine environments
- Transport of explosives and explosive precursors to site
- Off-site explosive manufacture
- Off-site use of explosives
- Manufacture of explosives precursors either on the mine lease or off site. (The process of manufacturing emulsions in specific fixed plant is highly specialised and the responsibility of the manufacturer, not the mine management team)
- Prevention of Tyre Fires – see RISKGATE Tyres Topic
- Prevention of vehicle collisions – see RISKGATE Collisions Topic
- Combustible atmospheres

**Table 2 - Examples of national hazard definitions (Explosives)**

Country	Definition
India	Accident in the course of using explosives
South Africa	Any un-authorised or accidental ignition or detonation of explosives
United States	Accidents involving the detonation of manufactured explosives, Airdox, or Cardox, that can cause flying debris, concussive forces, or fumes

Notes to Table 2: Indian definition taken from Mandel and Sengupta, 1999; RSA Department of Mineral Resources, 2012; US definition taken from MSHA website

**Table 3 - Coal mining fatalities caused by explosions, fall of strata, open cut explosives, fall of ground and all fatalities (including other causes) in Australia, China, India, South Africa and the United States between 2006 and 2010**

Country	underground hazards			open cut hazards			All coal mining fatalities
	Explosions	Strata fall	Explosions and Strata	Explosives	Ground fall	Explosives and Ground	
Australia	0	0	0	0	0	0	8
China	2145 (60.7%)	188 (5.3%)	2333 (66.1%)	17 (.5%)	35 (1%)	52 (1.5%)	3532
India	74 (14.3%)	114 (22%)	188 (36.2%)	0	5 (1%)	5 (1%)	519
South Africa	3 (3.5%)	21 (24.7%)	24 (28.2%)	0	0	0	85
USA	49 (27.7%)	26 (14.7%)	75 (42.4%)	0	4 (2.3%)	4 (2.3%)	177

Note: percentages represent the number of fatalities caused by that hazard relative to the total number of fatalities in that country

Within China, it was found that the top five hazards, accounting for 94% of reported coal mining deaths, were all associated with underground mining. These were explosions (60.7% of all fatalities for China), inrush (16%), fire (primarily all underground, 6.5%), explosives underground (5.5%) and fall of strata (5.3%). These outcomes are as expected considering 95% of coal mines in China are underground, also coal seams have a relatively high gas content.

## DISCUSSION

In this article we have the importance of considering how higher-level hidden factors might impact shifts in rates and distribution of coal mining fatalities by hazard within and between countries has been described. Also a hazard taxonomy that has now been used to successfully categorise fatality narratives was presented across Australia, China, India, South Africa and the United States. This is an important first step in having a standardised method of categorising fatality narratives across different countries. This study describes this taxonomy and the method we used to gather fatality databases and then carefully categorise these. The next steps involve beginning to describe within and between country shifts in rates and distribution of fatalities by hazard for these countries. It is the aim to then evaluate these trends in terms of broader organisational, societal, economic, legislative and environmental conditions in which production takes place. It is believed that this will provide for a more informed debate on global safety management priorities for coal mining.

Future work will extend the study to include the fatality data from other mining countries (e.g. Colombia, and Mozambique) as well as investigate methods to better normalise results across countries so that safety indicators account for variations in number of mining employees, hours worked and production of coal.

Finally, this project has proven utility in engaging high level undergraduate engineering and/or science students in direct research activity. Over two cohorts of students, a research program (structure and process) that is successfully building towards a comprehensive global database of coal mining fatality and injury outcomes normalised using RISKGATE definitions has been developed. Students gain first hand knowledge of risks and human costs in coal mining, and the opportunity to manage these risks through application of the RISKGATE body of knowledge. Over time, and with adequate resources, this exercise will be expanded to include as many coal mining countries as possible, and then further expanded with the addition of metalliferous mining outcomes.

## ACKNOWLEDGEMENTS

The authors gratefully acknowledge the funding support from ACARP and Australia's coal mining companies, the dedicated participation and wealth of knowledge generously provided by more than 100 industry experts, and the support of MISHC and the Sustainable Minerals Institute of the University of Queensland for time and resources necessary to complete and present this paper. This project also

thanks personal contacts in India and South Africa for providing non-published national mining narrative injury and fatality data for use in our classification program. Special appreciation to Ms. Barbara Whittaker for research support and RISKGATE administration.

## REFERENCES

- Allan, R C, 2006. The British Industrial Revolution in Global Perspective: How Commerce Created The Industrial Revolution and Modern Economic Growth. Retrieved from <http://www.nuff.ox.ac.uk/users/allen/unpublished/econinvent-3.pdf>.
- Australian Bureau of Resources and Energy Economics, 2001. Resources and Energy Statistics: Annual 2013. Retrieved from: [http://www.bree.gov.au/documents/publications/res/Annual\\_RES\\_2013.pdf](http://www.bree.gov.au/documents/publications/res/Annual_RES_2013.pdf).
- Barach, P and Small, S D, 2000. Reporting and preventing medical mishaps: lessons from non-medical near miss reporting systems. *British Medical Journal*, 18: 759-763.
- Cliff, D, 2012a. The management of occupational health and safety in the Australian mining industry. Crawley, Western Australia: International Mining for Development Centre. Retrieved from: [http://im4dc.org/wp-content/uploads/2012/01/UWA\\_1698\\_Paper-03.pdf](http://im4dc.org/wp-content/uploads/2012/01/UWA_1698_Paper-03.pdf).
- Cliff, D, 2012b. Managing a risky business. *Issues* (June 2012) 99: 29-31.
- Connolly, E, and Orsmond, D, 2011. The mining industry: from bust to boom, pp. 111-156, in Gerard, H. and Kearns, J. eds., *The Australian Economy in the 2000s*. Proceedings of a conference held in Sydney on 15-16 August 2011. Reserve Bank of Australia, Sydney, Australia.
- Foster, P J, Rose, H J M and Talbot, C F, 1998. Risk assessment - an opportunity to change health and safety performance. *Journal South African Institute of Mining and Metallurgy*, 98, 333-338.
- Harris, J, Kirsch, P, Sprott, D, Spinks, M, Goater, S and Cliff, D, 2012. RISKGATE - a case study in application to fires on mobile plant. *Proceedings of the Eighth AUSIMM Open Pit Operators Conference*, Perth, 18-19 September 2012, Perth, Australia. The Australasian Institute of Mining and Metallurgy (The AusIMM)
- Harris, J, Sprott, D, Torrance, A, Shi, M, Ranjan, A, Sharma, S, Biswas, T, Sharma, S. and Kirsch, P A, 2013. Sharing industry knowledge to improve management of risks and safety in the use of explosives in surface mining. *Proceedings of the World Mining Congress*, Montreal, Canada, August 11-15, 2013.
- Indian Bureau of Mines. Retrieved: December 2013, <http://ibm.nic.in>.
- Indian Directorate General of Mines Safety. Retrieved: December 2013, <http://www.dgms.net>.
- Jianjun, T. 2007. Coal mining safety: China's Achilles' heel. *China Security* 3: 36-53.
- Kirsch, P, Goater, S, Harris, J, Sprott, D, and Joy, J, 2012. RISKGATE: Promoting and redefining best practice for risk management in the Australian coal industry. *Proceedings of the 12th Coal Operators' Conference*, University of Wollongong and The Australasian Institute of Mining and Metallurgy, 2012, 315-325. <http://ro.uow.edu.au/coal/421/>.
- Kirsch, P, Harris, J, and Sprott, D, 2013a. Vertical integration of risk management in the Hunter Valley Coal Chain – application of the coal industry's RISKGATE platform. *The AUSIMM Bulletin* February 2013, 45-49.
- Kirsch, P A, Harris, J, Cliff, D and Sprott, D, 2013b. Industry scale knowledge management – RISKGATE and Australian coal operations. *Proceedings of the World Mining Congress*, Montreal, Canada, August 11-15, 2013.
- Kirsch, P A, Harris, J, Cliff, D, Hebblewhite, B, Sprott, D, Shi, M, Ranjan, A, Sharma, S, Biswas, T, and Sharma, S, 2013c. Industry scale knowledge management – introducing the RISKGATE Underground Strata and Explosions Body of Knowledge. *Proceedings of the World Mining Congress*, Montreal, Canada, August 11-15, 2013.
- Kirsch, P, Harris, J, Sprott, D, and Cliff, D, 2014. RISKGATE and Australian coal operations. *Proceedings of the 14th Coal Operators' Conference*, University of Wollongong and The Australasian Institute of Mining and Metallurgy, 2014 (this volume).
- Lahiri-Dutt, K. 2014 (in press). *The Coal Nation: Histories, Ecologies and Politics of Coal in India*. Aldershot: Ashgate.
- Lynas, D, Burgess-Limerick, R, and Kirsch, P A, 2014 (in press). RISKGATE analysis of Slips, Trips and Falls at NSW surface and underground coal mines. *Journal of Health and Safety Research and Practice*
- Mandal, A., and Sengupta, D. (1999). Fatal accidents in Indian coal mines. Technical Report No. ASD/99/33, Applied Statistics Unit, ISI, Calcutta 700 035.
- Minerals Council of Australia, 2007/2008. Safety Performance Report of the Australian Minerals Industry. Retrieved from [http://www.minerals.org.au/file\\_upload/files/resources/safety\\_health/performance\\_reporting/annual\\_safety\\_reports/2007\\_2008\\_Safety\\_Performance\\_Report.pdf](http://www.minerals.org.au/file_upload/files/resources/safety_health/performance_reporting/annual_safety_reports/2007_2008_Safety_Performance_Report.pdf).

- Reason, J, 1997. *Managing the Risks of Organizational Accidents*. Aldershop: Ashgate.
- Reason, J, 2000. Human error: models and management. *British Medical Journal* 18: 768-770.
- South African Department of Mineral Resources. Retrieved: December 2013, <http://www.dmr.gov.za>.
- United States Mining Safety and Health Administration. Retrieved: December 2013, <http://msha.gov>.
- Wang, M-X, Zhang, T, Xie, M R, Zhang B, and Jia, M-Q, 2011. Analysis of national coal mining accident data in China, 2001-2008. *Public Health Matters* 126: 270-275.
- Worden, S, Sprott, D, and Whittaker, B, 2013. Risk management competence in Australia gets a boost from new software. *Mining Engineering* 65 (July): 22-33.
- World Coal Association, 2013. Retrieved from: <http://www.worldcoal.org/resources/coal-statistics/>.

---

# OPEN RISK - AN UPDATE ON THE USE OF A PIT HIGHWALL RISK RATING SYSTEM

**John Hoelle**

**ABSTRACT:** Open Risk is a semi-quantitative risk rating system that takes into account the relative differences in the importance of hazards as experienced at each mine site as a result of different combinations of geotechnical factors and mining conditions. Open Risk provides an unbiased, standard quantified assessment of risks (as input parameters are quantifiable); that rates the likelihood of failure and stability and the consequences/severity of failure. The program is used by technical personnel as a pit inspection tool at several Anglo American coal mines in Australia to assist in evaluating hazards around high walls and to assist in rectifying or avoiding these hazards. The results of the system (severity and likelihood) are approximately analogous with the Anglo American 5 by 5 Risk Rating matrix (consequences and likelihood). The results from these pit inspections indicate a consistency across different personnel and different pits.

## INTRODUCTION

Anglo American's Metallurgical Coal business unit operates five open cut operations located in Central Queensland and New South Wales, NSW, Australia. In order to accomplish the vision of zero harm, Anglo American has implemented pro-active ground control management strategies for a safe and effective production of open cut and underground reserves (Hoelle, 2010). In order to prevent these unexpected failures, Anglo American has initiated a project to evaluate and implement a risk rating system, called Open Risk, that was developed by Canbulat *et al.*, 2004 for Anglo American's Thermal Coal in South Africa. The background and development of the program has been presented in several previous papers (Canbulat, *et al.*, 2004; Hoelle and Canbulat, 2012; Canbulat, *et al.*, 2013). The input parameters and the controls used in the program have been modified for local conditions in order to ensure that the results are representative of the environment in which the open cuts operate in Australia. The ultimate aim of this implementation is to minimise the risk to personnel and machinery by identifying the risks and by recommending a set of generic controls.

## DESCRIPTION OF PROGRAM AND USE

Prior to the introduction of Open Risk at the mine sites, a number of check sheets have been used. The one that was used most recently is the check sheet shown in Figure 1. While the check sheets were valuable in evaluating an individual pit at a specific time period, the evaluations were somewhat subjective and relied on the experience of the evaluator. While the check sheet is objective, there was not an easy method to create a comparison between different sites and to compare changes over time in the same pit.

The Open Risk program and method has been used by a number of personnel at the five Anglo American mines. The personnel were trained in the system, which consisted of the background as to why the program was initiated, an explanation of each of the components and a field trial. The field trial for the groups indicated that the results obtained from the several personnel are close but not identical. Once personnel became familiar with the process, approximately 10 minutes are required to fill out the sheet for a section of high wall in a pit. Another 10 minutes are required to input the data in the program. The input sheets are shown in Figures 2 and 3. It should be emphasised that the evaluation using Open Risk is based on surface observations of a pit wall and does not necessarily include structures and features that are back in the pit wall.

Anglo Coal Australia Highwall Inspection Sheet				Inspection Ref No.:
Location:		Date:		
WORK ASSESSMENT CHECK LIST	RISK RATING			CONTROL & COMMENTS
	LOW	MEDIUM	HIGH	
Local movement detected by laser (over 8 hour period)	Yes	No	No	
Highwall Geometry				
Overall batter angle (degrees)	< 15	> 15	> 20	
Highwall Integrity				
Free wall batter	Classy surface	Partly rocky	Rocky surface	
Crack development	None	Minor or Long narrow cracks	Development and/or spacing or width	
Spill (inclined or horizontal frequency)	< 1 per 50m	1-2 per 50m	> 2 per 50m	
Blind & flying debris (stones/rocks)	None	Yes	No	
Potential margin sets identified in 24 hr	None	Yes - 50m	Yes - 100m	
Loose rocks	None	Present in lower 100m	Present in upper 100m	
Weak falls/fabric (water/ice)	None	< 50m	> 50m	
Highwall Crest				
Undermining	Present in lower 100m	Present but not in upper 100m	Not present	
Open face (over 24 hours)	< 20m	> 20m	> 50m	
High Wall				
Top face	None		Yes	
Undermining (vertical)				
OW average from rock	None	< 200m off face	> 200m off face	
OW average from coal seam	None or 50m	< 200m off face	> 200m off face	
Face in process 24 hours	None	Minor	Significant	
Highwall Stability				
Current/Recent mining activity likely to impact OW integrity	None	Yes		
Current/Recent mining activity likely to impact HW integrity	None	Yes		
History				
Relevant work done fully in process at site	None	Yes	No	
Failure last 24hr	None	Yes	No	
Failure in previous 24hr	None	Yes	No	
Modification to design during inspection	None	Minor design modification	Major design modification	
TOTAL RISK	LOW	MEDIUM	HIGH	
Number in each of medium or high risk ratings since last inspection	0	0	0	

Figure 1 - Check sheet used prior to introduction of Open Risk

**ACTUAL USE AND RESULTS**

The Open Risk program is currently being used by geotechnical engineers, geotechnical technicians and geologists at the Anglo American Australian coal mines. The program is used whenever a high wall is inspected. It is being monitored or will be monitored and as part of the production of hazard plans produced at all of the mines. The normal method is to take a hard copy of the components in the field and check off the appropriate box, as shown in Figures 2 and 3. The data is then transferred to the computer program to obtain the output of the categories (Figures 4, 5 and 6). The chart, shown in Figure 7, is used to show trends so that observations obtained over time can be plotted, possibly indicating deterioration of the high wall.

For this study, a random sample of results from the different mines has been plotted. The output of the program consists of three parts: the geotechnical rating, the mining rating and the rating of the combination of the two categories. The results of the geotechnical ratings are shown in Figure 8 and the results of the mining ratings are shown in Figure 9. In the Geotechnical rating there are seven high walls in the high risk category and nine in the medium risk category. The risk rating for the same high walls in the mining rating show three high walls in the high risk and two high walls in the low risk categories. This indicates that the physical conditions of some of the pits are adverse and that these adverse conditions are being managed by good mining practices. The overall ratings shown in Figure 10 also indicate that the adverse conditions are being managed. The two high walls in the high ratings in the geotechnical and mining consequences were evaluated. The “highest” rated high wall is the same in both categories. The “second” highest rated system in the geotechnical category is not the same high wall as the “second” highest rated high wall in the mining system. The adverse conditions of this high wall were well managed. Inspection of the mining rating categories indicates that most of the high walls are being managed by the design and mining methods used.

**CONCLUSIONS**

The use of the program has allowed site personnel to evaluate the potential for failure quickly and to prioritise high walls that may require additional monitoring controls. These controls may also include design revisions or revisions of mining methods. The program also highlights high walls with adverse geological or geotechnical conditions that require additional attention.

1) GEOLOGY			2) WATER		
1.1	Depth of weathering		2.1	Water coming out of face bedding or structure	
	0 - 5 m	1		NO	1
	5 - 10 m	5		YES	10
	10 - 20 m	10		Is there water accumulation at toe of slope	
	> 20 m	20	NO	1	
1.2	Discontinuities		YES	10	
	None		2.3 Water on top of highwall/benches within 30m of crest		
	1 (simple)	10	NO	1	
	2 (complex)	10	YES	10	
1.3	Direction of discontinuities		2.4 Rain		
	Not applicable		No rain in past 5 days		
	Same direction (<30 deg.)	10	Rained in the past 5 days	5	
1.4	Dipping structure / bedding		Has been raining for the past 5 days		
	Flat/dipping into the face		Head of water		
	Dipping into the cut		No water		
1.5	Clay material in bedding		Stable, no increase		
	NO	1	Increase in water head		
	YES	10	3) SPONTANEOUS COMBUSTION		
1.6	Length of structure		3.1 Is the toe of highwall burning		
	0 - 1 m		NO		
	1 - 5 m		YES		
	> 5 m		1		
1.7	Presence of floor rolls and dipping seam		3.2 Is the toe of lowwall/spoil or any layer burning		
	NO	1	NO		
1.8	Major dykes/faults/burnt coal		YES		
	NO		1		
	YES		10		
1.9	Cracks on highwall/benches within 10 m of crest		3) DRAGLINE		
	NO	1	4.1 Dragline bench built on		
	YES	20	Not applicable (truck and shovel operation)		
1.10	Highwall condition		Unweathered material		
	Stable		1		
	Loose/rock/blocks		Weathered material		
	Wedges/overhangs		5		
	Zone of weakness		Weathered material and water		
			10		

Figure 2 - Input sheet for the geotechnical risk section of open risk

1) GEOMETRY			1.9 Loose blocks at crest		
1.1	Batter back soft material		NO	1	
	Not Applicable		YES	20	
	Yes / minimum 50 deg.		2) MINING		
1.2	Height of highwall		2.1 Undercutting spoils		
	0 - 35 m		NO		
	35 - 50 m		YES		
	50 - 70 m		1		
1.3	Angle of highwall		2.2 Undercutting highwall		
	< 65 deg.		NO		
	65 - 75 deg.		YES		
1.4	Top bench width		2.3 Spoils in water		
	> 10 m		NO		
	0 - 10 m		YES		
1.5	Spoils on the highwall		2.4 Spoiling of weathered material at toe of spoils		
	Not applicable		NO		
	< 15 m high/>10 m from crest		YES		
	<15 m high/<10 m from crest		1		
	>15 m high/>10 m from crest		10		
1.6	Height of spoils on lowwall		3) BLASTING		
	Not applicable		3.1 Blasting method of highwall		
	0 - 40 m		Pre-split		
	40 - 95 m		No pre-split		
1.7	Cut width (deviation from standard)		Highwall condition due to blasting		
	Standard within 5 m		Straight H/W no loose material		
	Not standard (> 5 m deviation)		Straight highwall, some loose material		
1.8	Noses present		Frozen coal, overhangs, loose material		
	NO		10		
	YES		3.3 Pre-split barrels		
		Not applicable			
		Visible			
		Not visible			
		10			
		3.4 Blast holes			
		Visible			
		1			
		Not Visible			
		10			

Figure 3 - Input sheet for the mining risk section of open risk

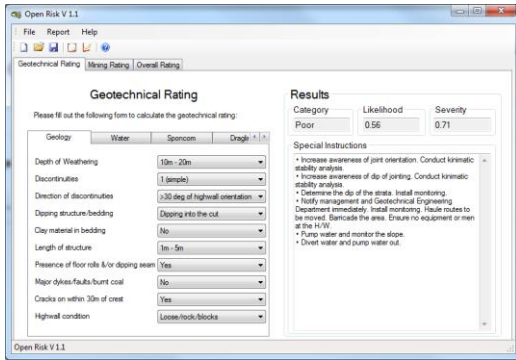


Figure 4 - Output of the geotechnical rating

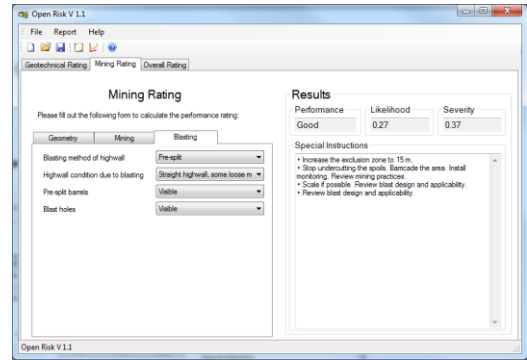


Figure 5 - Output of the mining rating

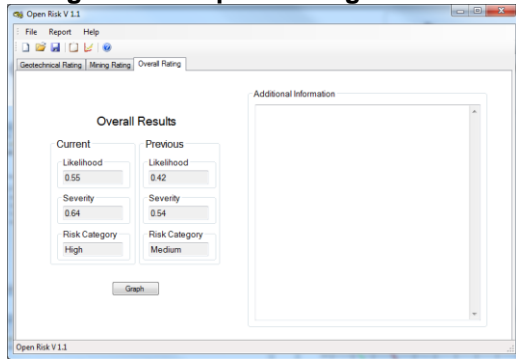


Figure 6 - Output of the overall results

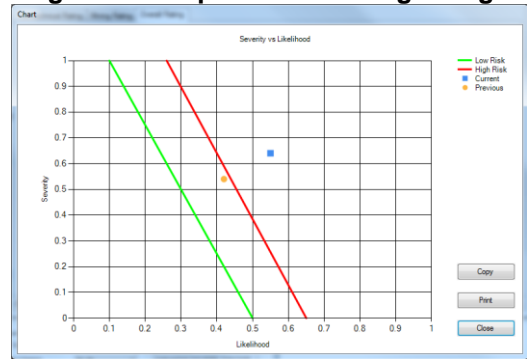


Figure 7 - Chart with the results of the initial and up-dated ratings

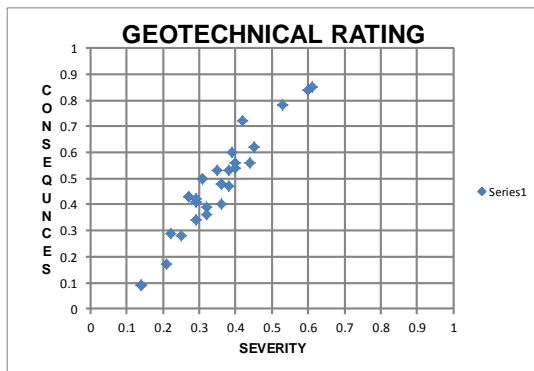


Figure 8 - The results of the geotechnical ratings from several high walls at the Anglo American mines

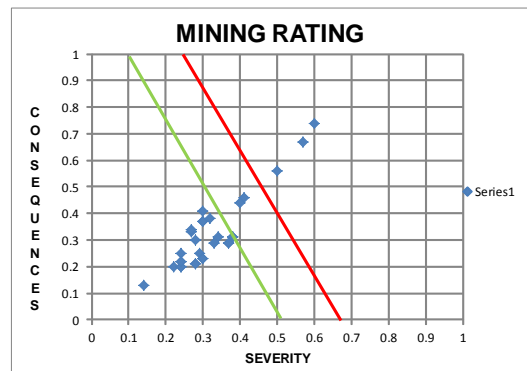


Figure 9 - The results of the mining ratings from several high walls at the Anglo American mines

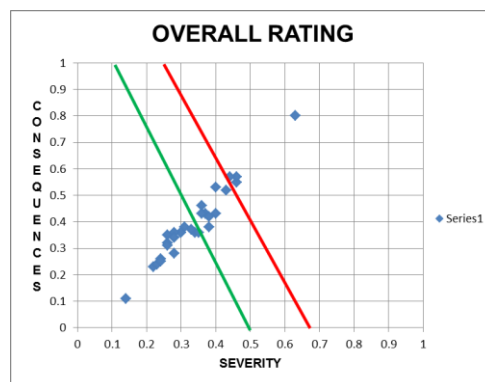


Figure 10 - The overall results from the high walls shown in Figures 8 and 9

---

**REFERENCES**

- Canbulat, I, Munsamy, L and Minney, D, 2004. A risk assessment tool for open cast mining In South Africa. Proceedings of 23rd International Conference on Ground Control in Mining. Morgantown, West Virginia. August. <http://icgcm.conferenceacademy.com/papers/detail.aspx?subdomain=icgcm&iid=575>.
- Hoelle, J, 2010. Proactive Strata Control Management at Anglo American Metallurgical Coal Australian Open Cut Operations. Proceedings of 2<sup>nd</sup> Australasian Ground Control Conference, Sydney. Nov. 23-24, Pp 159-162.
- Hoelle, J. and Canbulat, I, 2012 A risk rating system for Anglo American's open cut coal mines in Australia, in proceedings 12th Coal Operators' Conference, University of Wollongong and The Australasian Institute of Mining and Metallurgy, (Eds: Aziz Kininmonth, Nemcik, and Ren), pp 371-377, <http://ro.uow.edu.au/coal/428/>.
- Canbulat, I. Hoelle, J. and Emery, J., 2013, Risk Management in open cut coal mines. International Journal of Mining Science and Technology, 23, pp 369-374.

# OPTIMISATION OF OVERBURDEN BLASTS AT GLENCORE ULAN SURFACE COAL OPERATIONS

Daniel Thorn<sup>1</sup>, Bruno Cediél<sup>2</sup>, Sedat Esen<sup>3</sup> and Murali Nagarajan<sup>4</sup>

**ABSTRACT:** This paper presents the outcomes of a joint project carried out by Glencore Ulan Surface Operations and Orica, to reduce total mine cost by optimising overburden blasts. Typical overburden blasts are 60 m wide and 1000 m long with the blasts designed to cast. Ulan Surface operations has a Marion 8050 dragline operating using the traditional Key-Low wall combinations, High Wall Chopping and Extended Bench according with spoil profile balance with a dragline production rate of 2000 bcm/hr. The objectives of the project were to: optimise post blast muckpile profile to improve dragline advance; improve cast percentage (%); reduce coal roof damage and edge loss; and control blast emissions and their impact on neighbours. The aim of these objectives is to reduce the total cost of mining. The use of Orica's advanced blast modelling software, Distinct Motion Code (DMC), was essential in this as it allowed the analysis of alternative blast designs using the results from previous blasts in Strip 5 as the baseline. The results of the modelling indicated that there was scope to improve the cast % from a baseline of 23% to a range of 25-35% to final. In addition, the coal model was validated using touch coal and gamma logging data for each strip. From this information the blastholes were designed to stand-off from the coal seam and QA/QC approaches in the backfill and redrill tolerances were implemented. This paper also presents outcomes of this validation work.

## INTRODUCTION

Ulan Coal Mines Limited (UCML) is one of the most established coal mining operations in the Western Coal Fields of NSW. The mine is located 40km north of Mudgee in the state's central west region with operations only 3 km from the village of Ulan (Figure 1). The complex consists of two approved underground mining operations (Ulan No.3 and Ulan West) and an Open Cut coal reserve. There has been a rich history of open cut mining at Ulan dating back to the early 1980s with the current dragline in operation since that time. The operation has changed ownership several times over these years but most recently it was purchased by Xstrata to run in conjunction with the two underground operations. Ulan open Cut was brought to life in early 2012.

The Ulan Open Cut is set up as a 24x7 strip mine operation in which overburden is mined primarily using a dragline. Where possible the dragline removes all of the overburden material to ensure lower operating costs. Based around dragline techniques and efficiency, the blasting practices are to cast-blast an entire strip with several subsequent coal blasts as coal is uncovered and required (Figure 2). Currently the open cut produces approximately 2.0 Mtpa of coal with the flexibility to vary this significantly. Current life of mine plans extends out to 2019. This paper presents the outcomes of the joint project carried out by Glencore Ulan Surface Operations and Orica to reduce total mine cost by optimising overburden blasts. The paper also discusses the optimisation approach, enabling tools/software, Quality Assurance/ Quality Control (QA/QC), coal loss and blast emission controls to manage vibration, overpressure and fume.

## GEOLOGY

Borehole R834 was chosen to detail the geology of strip 6 which was being mined as of November 2013. The details of the geological description and core logs are given in Appendix 1. The overburden consists of interbedded, weathered sandstone and siltstone in the top 12 m above the base of weathering. The base of weathering is at around 12 m. Below the base of weathering is approximately 6 m of moderately soft, quartz lithic, fresh sandstone, light grey in colour. From 25 m to coal (30.83 m) is a moderately hard, lithic to quartz lithic, light grey sandstone.

<sup>1</sup> Graduate Engineer, Glencore Ulan Surface Operations, Australia

<sup>2</sup> Technical Services Superintendent, Glencore Ulan Surface Operations, Australia

<sup>3</sup> Principal Engineer, Orica, Australia, e: sedat.esen@orica.com. Tel: +61 478 401 108

<sup>4</sup> Specialist Engineer, Orica, Australia

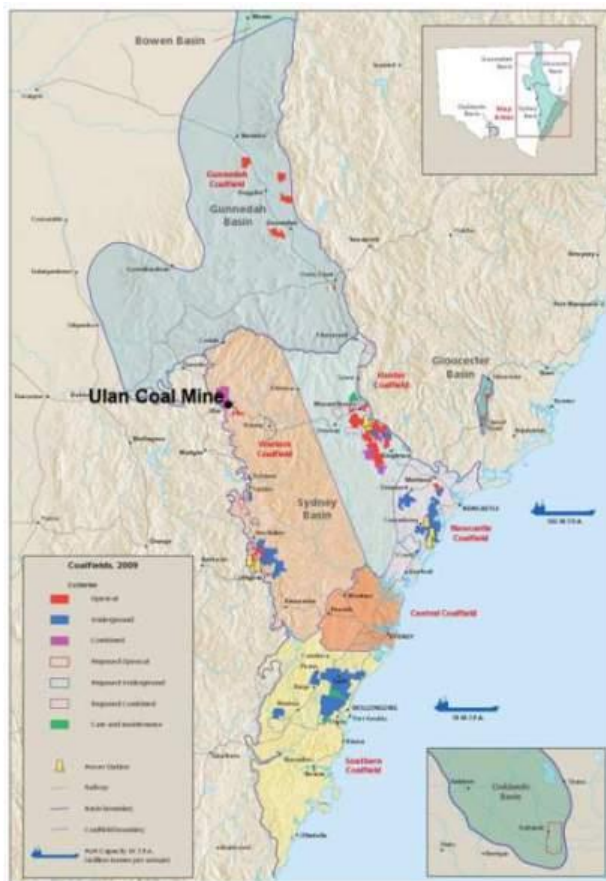


Figure 1 - Location of Glencore Ulan surface coal operations



Figure 2 - Pit layout for the strip mining

As shown in Appendix 1, there are two coal seams in the strips. The top seam is called the UAA Rider band which is approximately 0.58 m thick, of poor quality therefore not mined. The rock between the rider band and the main coal seam (ULA) is carbonaceous siltstone and the thickness of this band is 1.06 m. The Ulan Seam working section is 6.53 m thick.

Gamma logging was also carried out at Strip 6 to validate the top of coal seam obtained from driller's logs and the coal model. This would be discussed in detail in later section. Figure 3 shows the gamma log results of blasthole B11, Strip 6 showing both Rider band and Ulan main seam and is representative of the coal seams in this region.

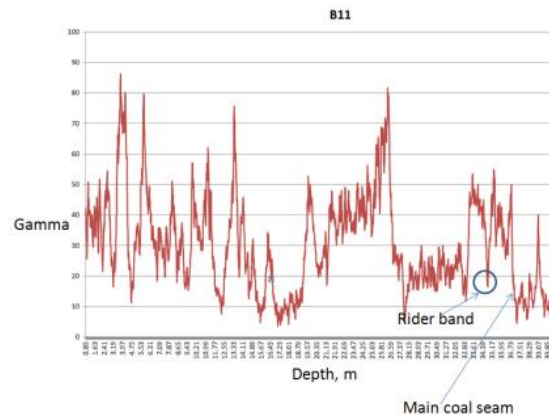


Figure 3 - Gamma log result for hole #B11

### STRIP MINING METHOD

Ulan Open Cut is a dragline open cut pit that recommenced mining in March 2012 with an estimate life of mine until 2019 at 2.0 Mt of ROM coal per year. It is a single coal seam operation (thermal – high ash) where coal seam is 7.5 m thick with a relatively flat floor. Overburden thickness varies from 28 up to 65 m. Pre-stripping operations are required to guarantee a blasting bench of not more than 50 m height.

The mine has got the following equipment: 1xMarion 8050 dragline, 1xHitachi EX3500 hydraulic excavator, 1xKomatsu WA1200 Loader, 5xCaterpillar 789 trucks and 7xCaterpillar D11T dozers.

Dragline dig methods used at Ulan Open Cut vary from traditional key-low wall combinations, high wall chopping and extended bench according with spoil profile balance and a planned dragline productivity of 2,000 bcm/h. Figure 4 shows the key-cut method used at the mine.



Figure 4 - Key-cut method used at Ulan Mine

### OVERBURDEN CAST BLASTING OPTIMISATION

#### Cast blast design parameters

Ulan surface operations commenced mining the first strip by firing Strip#1 on March 15<sup>th</sup> 2012. Currently Strip 6 is being mined out and Strip 7 is being drilled (Figure 5).

After the initial box cut each of the strips has essentially been blasted as a single cast blast with similar characteristics and blast parameters. In general the strips are 60 m wide, 30-50 m high and 800-1100 m long. The strip width is optimised for dragline efficiency. The pit profile is generally 30m from surface to top of coal in the middle and upwards of 50m on each end of the strip.

Previous strips used a variety of similar burdens and spacing with minor product variations in initiation systems (Exel™) and bulk products (Fortan™ 12) with a process of optimising the application of bulk products being applied for blast in Strips 2 to 4. For Strip 1 a spacing of 12 m was used with multiple decks to comply with site Maximum instantaneous charge (MIC) limits that resulted in a lower powder factor. The subsequent 4 strips used 14 m spacing with small variations in burden.

Strip 6 used a reduced spacing of 13 m and optimised burdens to aid an improved muckpile profile and optimised cast. Strip 6 had the following cast blast design parameters:

- 60 m wide
- 1 040 m long
- 644 holes, Depth: Average = 36 m, Min = 31 m, Max = 51 m.
- Hole diameter: 251 mm
- 13 m spacing, 6 m face burden, 6.5 m for the next row and 7.4m for remaining rows.
- 0.5 kg/m<sup>3</sup> design powder factor
- Blast volume: approximately 2.2 Mbcm
- 5 m stemming length
- 1800 kg/hole
- Initiation system: i-kon™ electronic blasting system
- Bulk explosives: Fortan™ Coal 12, Fortis™ Coal, Aquacharge™ Coal

Figure 5 shows the mine plan for Strip 6 and upcoming strips. To minimise coal edge loss the coal seam is buffered using imported coal rejects from the wash plant. Figure 6 shows Strip 6 buffering in process.

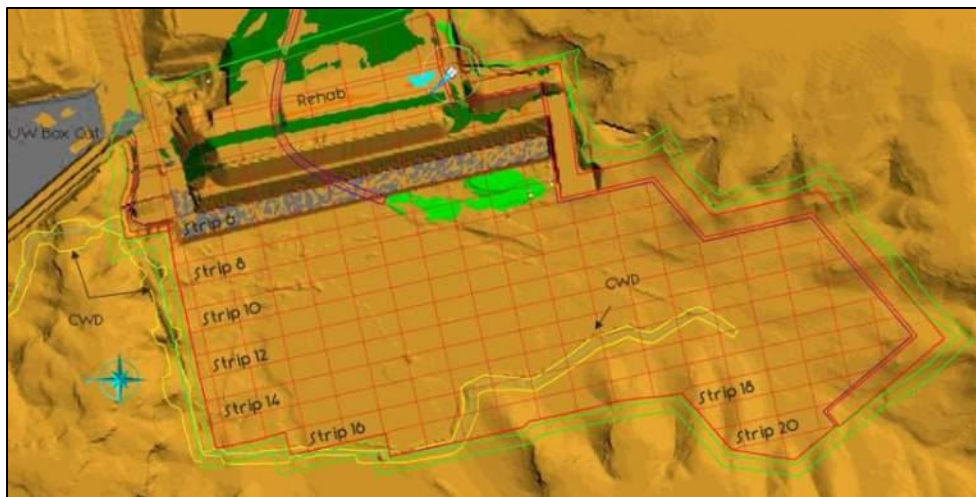


**Figure 5 - Strip 6 and other strips to be mined at Ulan surface operations**

### **Muckpile shaping for optimised dragline productivity**

A review of the drill and blast design was implemented after the firing of Strip 5 with final aim to reduce the overall cost of the dragline operation with the following key requirements:

- The post blast muckpile profile is required to have an optimum height of ~28 m to optimise the dragline performance by reducing rehandle and improving advance along strip;
- Optimise cast %;
- Identify the coal loss and implement methods to reduce coal loss; and
- Implement changes to drill and blast process with a continuous improvement imperative.



Figure 6 - Coal edge buffering process in Strip 6

#### ***Muckpile profile optimisation using blast modelling tools***

In the modelling process to meet the required muckpile profile the blast profile, blast parameter data from Strip 5 formed the base case. From this base case, alternative blast designs were modelled using Orica's advanced blast model, Distinct Motion Code (DMC). The base case and alternative blast designs are summarised in Table 1. The results of the alternative designs are detailed in Appendix 2.

Table 1 - Base case and alternative cases for blast modelling

	basecase	c1	c2	c3	c4
Row 1	7.1	6	6	6	5.5
Row 2	7.5	5.5	6	6	5.5
Row 3	7.5	7.5	6.5	6.5	5.5
Row 4	7.5	7.5	7	7	6
Row 5	7.5	7.5	7.5	7.5	6
Row 6	7.5	7.5	7.5	7.5	6.5
Row 7	6.7	7.5	8	8	7
Row 8	5.2	7.5	8	8	7
Row 9					7.5
Spacing	14	13	13	12	11
Burden(average)	7.1	7.1	7.1	7.1	6.3
PF (kg/m <sup>3</sup> )	0.49	0.53	0.53	0.57	0.7

The base case (Strip 5) delivered an actual cast of 23.1% and the modelled cast result for Case 1 was 25.5%. Using a step by step approach the team implemented the blast parameters as detailed in Case 1 for Strip 6.

To ensure optimum timing and the required emission control i-kon™ electronic blasting systems were implemented. Strip 6 loading required the use Aquacharge™ Coal due to rain events in the weeks prior to the loading making a large percentage of holes damp or having wet sides. This is discussed in more detail in Section 5.

The actual cast for Strip 6 was calculated to be 25.1%. The modelled prediction was 25.5%. Figure 5 shows the cast profiles before and after the optimisation work. As mentioned earlier prior to the start of the muckpile optimisation work the mine was using non-electric initiation and Fortan™ Coal 12. The use of these systems and associated blast parameters resulted in a cast of 21.1%. By the implementation of the muckpile profile project where the type of bulk product used was optimised, i-kon™ electronics blasting system implemented, blast patterns adjusted via DMC modelling and environmental emissions managed the team delivered an increased cast of 4% and an improved muckpile profile to reduce rehandle and improve the dragline rate of advance.

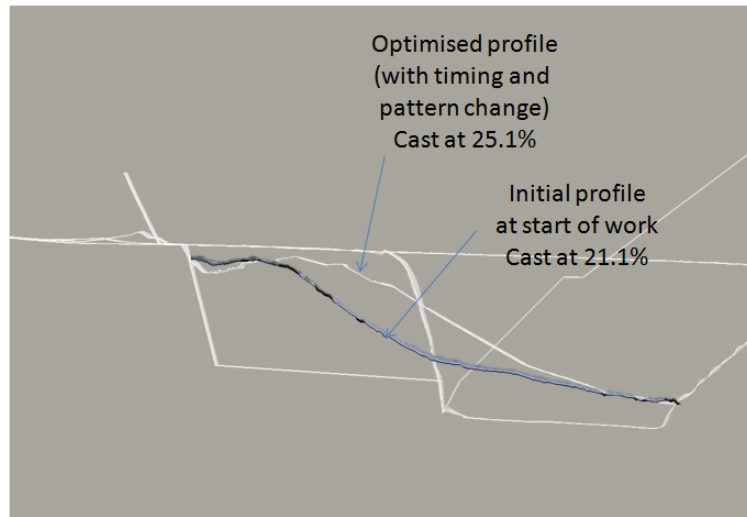


**Figure 7 - Comparison of the muckpile profiles**

Table 2 lists the cast % achieved in the last six strips. It is shown that cast % was gradually increased with the use of the continuous improvement process in the application of bulk products and the change to electronic detonators.

Table 3 shows the dragline productivity for October 2013 for Strip 6 and the productivity summary for Strip 5 for a similar time period. As can be seen the dragline productivity rates (bcm/h) are similar, swing angle has been reduced from 113 to 95 degrees and the cycle times reduced from 77 to 69 seconds. The combination of these factors indicates that the dragline advance along strip has improved.

**Table 2 - Cast % in strips mined to date**

Strip	Cast %
1	21.4
2	21.1
3	23.5
4	23.7
5	23.1
6	25.1

### **Quality Assurance/Quality Control**

Common practice at most coal mines is for drillers to be instructed to drill to coal every 5 to 10 holes and adjust the remainder of blastholes drilled to achieve the required standoff. This is primarily due to the variation between the modelled coal seam and the actual seam location. At Ulan the drillers used the rider coal band as the stand off line for blastholes that were not drilled to the main coal seam as a practical guide for drillers. For Strip 6 a change was implemented with every blasthole drilled to touch coal to ensure a consistency for all drillers and a QA/QC process implemented. This process required each drill hole to be measured and backfilled to achieve the required stand off and the depths recorded. The stand off used in Strip 5 was 3 m for the front row and 2 m for the remainder of the blastholes. When the holes were dipped it was found that majority of holes already had a backfill with cuttings of approximately 1-1.5 m due to a variety of factors such as drilling practice where air is turned off before hole has been completed, wind and rain. From the drill logs an actual coal surface was generated and

backfills applied during loading using drill cuttings. All blastholes that did not meet the required tolerance were redrilled. The implementation of this QA/QC process ensured improved control of blasthole depths and associated stand off from coal. Appendix 1 details an analysis of the blasthole depths and associated deviation.

**Table 3 - Dragline productivity analysis**

	Strip 5	Strip 6 (October report)
Cast %	23.1	25.1
Dragline bcm per operating hour	2113	2140
total cycles per cycling hour	47	52
Average Swing Angle (deg)	113	95
Average Cycle Time (secs)	77	69
Average Fill Time (secs)	15	15
Average Bucket Load (BCM's)	52.1	45.9
Total bcm/month	932,468	1,111,216

A review of the coal model and the actual coal surface from drill logs showed that the coal model was deeper by approximately 0.4 m with a 0.8 m standard deviation. The coal roof model when compared to the survey coal roof showed a standard deviation of 0.7 m (see Appendix 3).

When hole depths are compared for the strip 6's front row calculated from strip 5's survey coal data and touch coal data, it was shown that touch coal data was approximately 0.9 m shorter. This calculation was done for the front row as the coal seam dips slightly (-1.9°). There was limited survey coal information for Strip 6.

In addition to this analysis, five blastholes were gamma logged in Strip 6 to compare the coal surfaces obtained by touch coal, design coal and gamma log results. Table 4 summarises the results.

**Table 4 - Coal depths from design, touch coal and gamma logging**

Hole ID	Design coal depth, m	Touch Coal data_driller, m	Gamma Coal, m	Gamma vs design depths, m
B6	36.86	39.2	40.4	-3.5
B11	34.91	41.1	36.9	-2.0
D11	35.12	41	37.3	-2.2
E18	34.3	37.7	36.2	-1.9
G11	34.26	41.3	37.2	-2.9
average				-2.51

The following can be drawn from Table 4:

- Design depths are 2.5 m shorter when compared to the gamma coal depths for the zone that was logged.
- Design depths are shorter than Touch Coal (TC) depth by 0.8 m.
- When TC data is compared with the strip 5's last row's survey coal data, it was found that TC data is about 0.9 m shorter than actual survey coal.

### **Coal loss**

A post blast visual examination of the top of coal surface post dragline excavation showed, in general, minimal damage to the coal roof. It was noted that a 0.5 m shale band was left above coal roof after dragline excavation and the coal roof had limited to no damage. The second type of coal loss to be evaluated is edge loss which is relevant in cast blasts as at Ulan Coal Mine. An analysis of edge loss showed a loss of approximately 2 m for the top 1.5 m of coal which is consistent with the model (See Appendix 2) and observations (Figure 8).

A review of these results has led to changes for Strip 7 blast loading design with extra standoff and the use gravel for backfill in the front rows to minimise the coal edge. It is the opinion of the team that the

use of gravel for backfill in the front rows will assist in minimising the coal edge loss. By implementing this change the team is ensuring that all factors are evaluated before other options such as 'baby decking' are considered for future blast improvements.

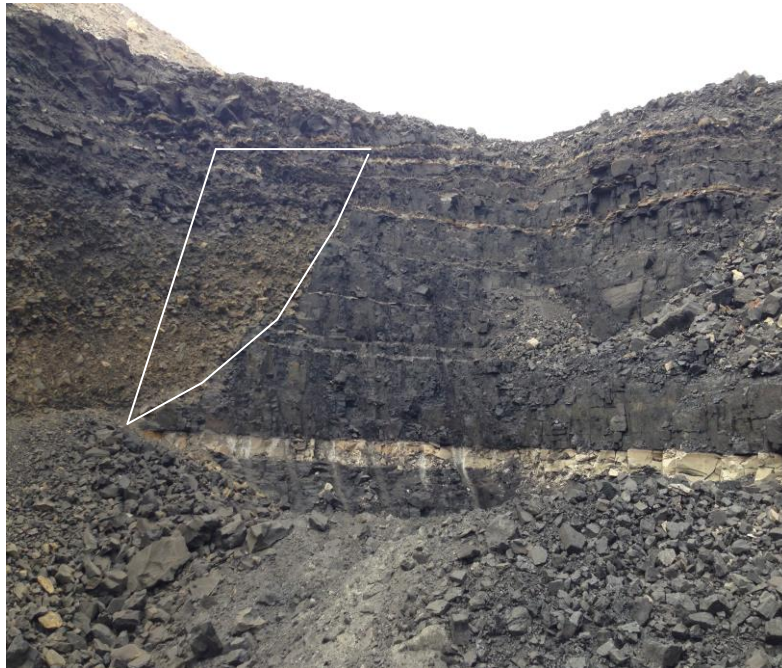


Figure 8 - Coal edge loss

## BLAST EMISSIONS

### Blast vibration and airblast

Despite its reasonably remote location, Ulan mine is faced with a number of blast emission constraints that restrict some blasting practices. As per project approval, Ulan mine is obligated to comply with the following:

- < 115 dBs and < 5 mm/s at closest neighbour (~2.5 km)
- < 115 dBs and < 5 mm/s at Ulan Public School (~3 km)
- < 100mm/s at archaeological sites
- 3000 kg MIC limit at site.
- Fume generation
- Fly rock

The 5 mm/s vibration limit is not an issue for the site at the current time as the blasts to date resulted in vibration values well below the limit (See Table 5).

The 115 dBover pressure limit is of concern due to the relatively close location of monitors, the large amounts of explosives detonated in a single blast event and the preferred firing direction to deliver the required blast profile is toward the monitors. To reduce the risk of an event Orica used its ShotPlus™ 5 Professional design program to determine the number of holes arriving at monitoring locations in a given time window, with this as a base a variety of timing options were evaluated whilst delivering the optimum blast profile.

The 3 tonne MIC is perhaps the most restricting of constraints as a single blast hole of a hole depth of 35 m contains 1.8 t alone. The constraint basically means that every hole needs to be fired within its own 4 ms window. This had an effect on options available for face row timings and variable burden timings, it proved quite difficult to achieve a face row faster than 4.2 ms/m without negative effects at monitors.

After the recent blast there has been a big effort to have the MIC limit lifted or removed. A late change was made to the timing in the northern end of the shot in an attempt to move the dirt in a more desirable position for the dragline which meant that precise timing was required to meet the blast emissions criteria. This would have been impossible without the use of electronic detonators.

**Table 5 - Blast vibration and airblast data from overburden blasts**

Shot ID	Distance		Actual Air Blast (dBL)		Actual Vibration (mm/s)	
	Ulan School	Cope Road	Ulan School	Cope Road	Ulan School	Cope Road
S6_Overburden	3314	2899	101.0	106.0	0.80	1.20
S5_Overburden	3306	2983	108.9	115.5	0.93	0.64
S4_Overburden	3485	3086	102.9	100.4	0.97	1.63
S4_Sth_Ext_OB	3217	2996	99.2	100.6	0.93	1.01
S3_Overburden	3496	3133	105.9	99.0	1.53	1.14
S3_Nth_Ext_OB	4204	3435	112.4	107.8	0.77	1.11
S2_Overburden	3820	3447	109.6	105.7	0.94	1.45
S2_Nth_Ext_OB	4262	3611	95.8	107.6	0.94	0.93
S1_Overburden_2	3630	3435	101.4	96.5	0.49	0.50
S1_Overburden	4007	3618	112.1	116.6	1.00	1.13

\*Yellow cells are high overpressure readings.

In the previous twelve months two of the overburden blasts caused airblast issues (>115 db). Investigations into the two events showed that the causes were stemming ejection due to cratering below the designed stem zone as a result of the increased explosive amount and/or stemming bridging. Another common cause for airblast is the face burst. The risk of this has been reduced at Ulan with the use of face scans to ensure sufficient burden exists for the front row with adjustments to the standard loading as required.

Presplit blasts were stemmed at Ulan with 4 m length. Initially, each hole was separated by 25 ms delay using the detonating cord on surface. After the introduction of i-kon electronic blasting system there was a change with four blastholes fired in a group with the similar delay time between groups. The change improved the presplit efficiency between blastholes. This configuration has resulted in a continuation of overpressure measurements less than 115 db.

### Fume

Typically the ground at Ulan is quite damp and varies from almost dry at the south to several meters of water at the north (the seam dips to the north east at  $\sim 2^\circ$ ). Wet holes are loaded with Fortis Coal product. The middle third of the blast is essentially dry with damp clays on the walls of the holes, this area of strip was loaded with mostly dry product (Fortan™ Coal 12) and some degree of slumping was observed through this section which resulted in small amount of fume. In Strip 4, a change in bulk product to Aquacharge™ Coal product was implemented with an improved blast result with no fume in the Aquacharge™ section. In Strips 5 and 6, the Aquacharge™ use increased due to unusual rain events prior to loading. For strip 6, due to rain a larger section of the loading used Aquacharge™ with good (no fume) results. To adjust for the changing ground conditions strip 6 comprised 40% dry (Fortan™ Coal 12), 40% Aquacharge™ Coal and 20% wet (Fortis Coal) products. The fume level in Strips 4 and 5 were recorded as Level 2. For Strip 6 the fume level was recorded as zero which can be attributed to the use of appropriate bulk products (Fortan™ Coal 12, Aquacharge™ Coal and Fortis™ Coal) for the blasthole conditions encountered.

All bulk products are blended to the same density to maintain powder factor and consistency of energy. Additionally there has been a reduction in sleep times from 3 weeks to 2 weeks with an improved team approach that has also reduced the risk of fume from extended sleep times. This approach has resulted in the blast in Strip 6 having a fume recorded as zero.

### Flyrock

Cast blasts, such as that being applied at Ulan Coal Mine, may result in an increased risk of fly rock. During the analysis process, it was found that a design of 6 m face burden does not cause flyrock. The blast face is affected by a variety of factors such as over dig by the dragline and/or excavator, weather events such as rain that lead to geological failures and damage from previous presplit blast especially at

the crest. As has already been mentioned to ensure the front row blastholes have the required face burdens and can contain the explosives being used the blast face is scanned. A profile is made for each blasthole and the loading is determined from this analysis. The analysis of Strip 6 has shown that there is a large amount of crest damage occurring that has required an increase in stem heights for the front to approximately 5.5 m. As part of the continuous improvement process this issue is assessed for improvement with changes to presplit loading for Strip 7 being implemented.

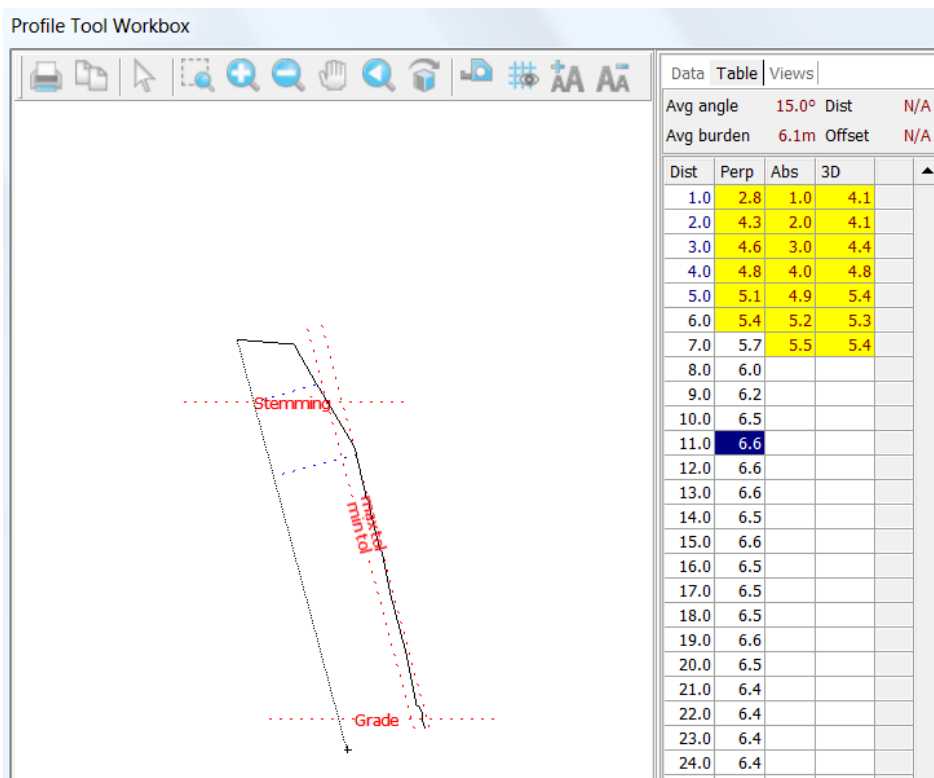


Figure 9 - One of the face row's hole position with respect to face

### CONCLUSIONS

The joint project carried out by Glencore-Xstrata at Ulan Surface Operations and Orica achieved the project objectives with a process for future continuous improvement using a team approach. The focus on QA/QC provided the means to analyse the changes being implemented, understanding the reasons for the results being achieved in coal damage, blast emissions and the final blast result. Orica's modelling programs, DMC and ShotPlus™ 5 Professional, were essential to analyse the variety of options to determine the optimum solution.

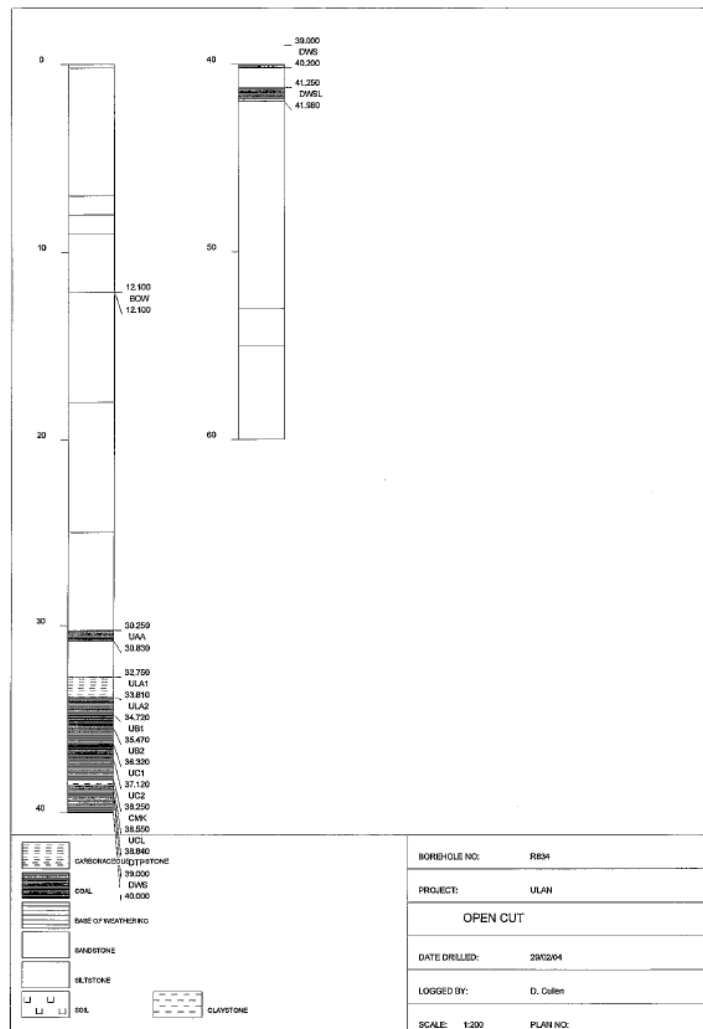
The achievements of this team were:

- The cast % increased from 21.1 to 25.1, which is 4% increase (19% improvement);
- Improved post blast profile improved the dragline's performance and operating method;
- Blast emissions managed;
- Fume managed by appropriate use of bulk product, blasthole determination and managing sleep time; and
- Coal loss has been reduced but coal edge loss is still an issue and options are being considered for implementation for Strip 7 to be fired in December 2013.

APPENDIX 1 - BOREHOLE R834 GEOLOGY

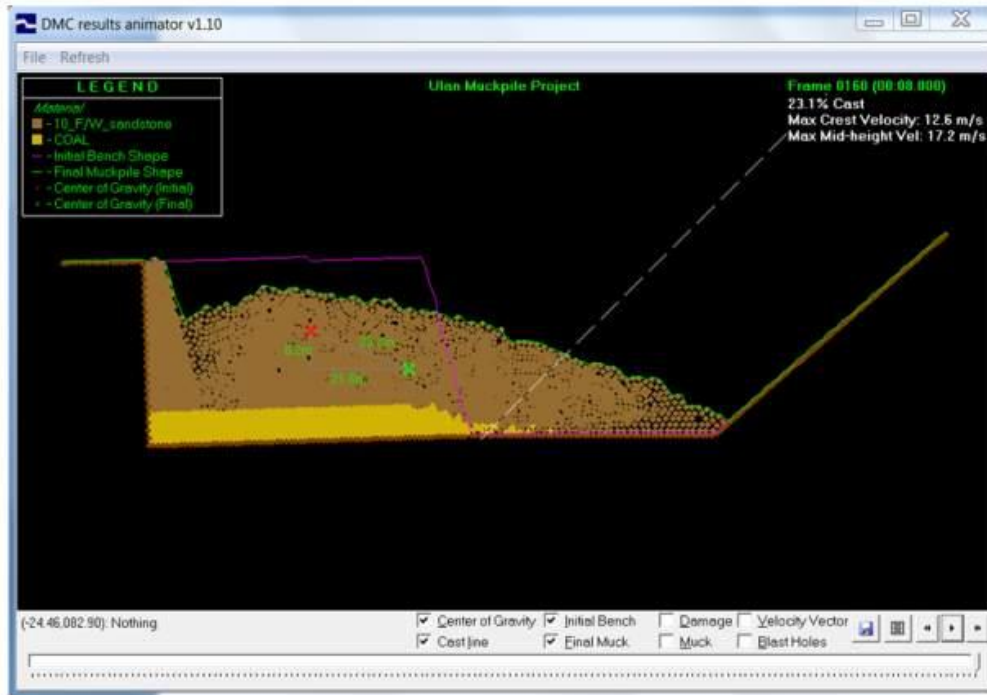
Geological strata description and core logging results for the borehole R834 in Strip 6 at Ulan Surface Operations

BORE NAME R834					
DEPTH	THICKNESS	RECOVERED	GEOLOGICAL DESCRIPTION OF STRATA		SEAM
0.200	0.200	0.200	SOIL	brown.	
7.000	6.800	6.800	SILTSTONE	brown orange, weathered, soft.	
8.000	1.000	1.000	SANDSTONE	light brown, medium to coarse grained, lithic, weathered, moderately soft.	
9.000	1.000	1.000	SILTSTONE	grey, slightly weathered, moderately soft.	
12.100	3.100	3.100	SANDSTONE	orange brown, coarse grained to granule sized, quartz-lithic, weathered, moderately soft.	
12.100	0.000	0.000	BASE OF WEATHERING		BOW
18.000	5.900	5.900	SANDSTONE	light grey, coarse grained to granule sized, quartz-lithic, fresh, moderately soft.	
25.000	7.000	7.000	SANDSTONE	light grey, fine grained, lithic, moderately hard.	
30.250	5.250	5.250	SANDSTONE	light grey, medium to coarse grained, quartz-lithic, moderately hard.	
30.830	0.580	0.580	COAL		UAA
32.750	1.920	1.920	SILTSTONE	grey dark grey, moderately soft.	
33.810	1.060	1.060	CARBONACEOUS SILTSTONE		ULAL
34.720	0.910	0.910	COAL		ULA2
35.470	0.750	0.750	COAL		UB1
36.320	0.850	0.850	COAL		UB2
37.120	0.800	0.800	COAL		UC1
38.250	1.130	1.130	COAL		UC2
38.550	0.300	0.300	CLAYSTONE		CMK
38.840	0.290	0.290	COAL		UC1
39.000	0.160	0.160	COAL		DTP
40.200	1.200	1.200	COAL		DWS
41.250	1.050	1.050	SANDSTONE	light grey, coarse grained, lithic, moderately hard.	
41.980	0.730	0.730	COAL		DWSL
53.000	11.020	11.020	SANDSTONE	light grey, medium to coarse grained, quartz-lithic, moderately hard.	
55.000	2.000	2.000	SILTSTONE	grey, moderately soft.	
60.000	5.000	5.000	SANDSTONE	light grey, coarse grained to granule sized, quartz-lithic, moderately hard.	



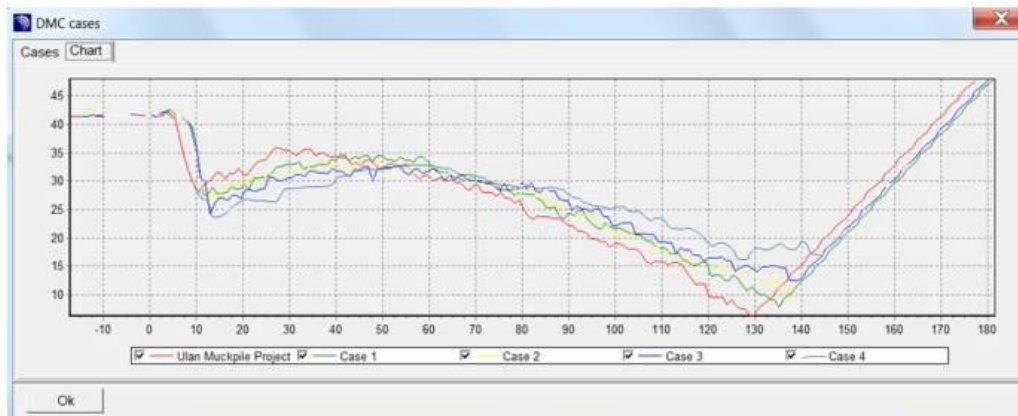
APPENDIX 2 - MODELLING RESULTS

Base case



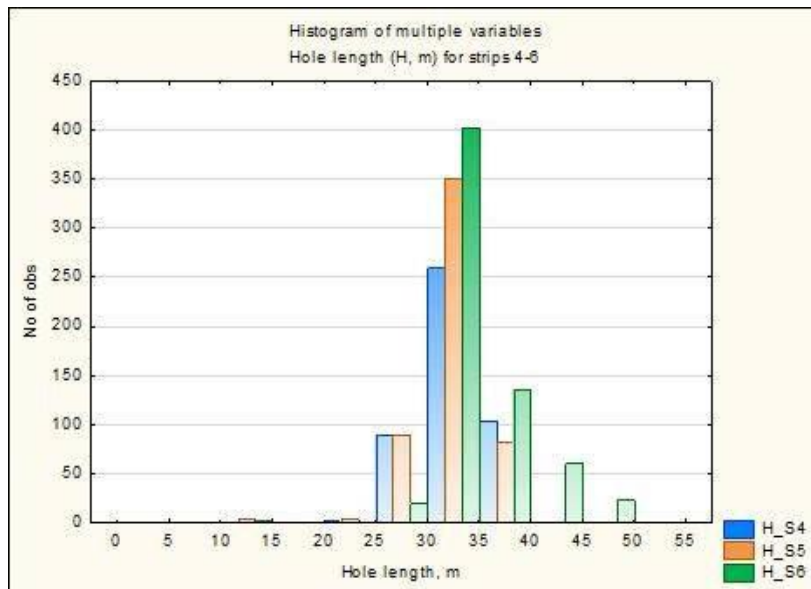
Summary

#	Description	Results	%Cast	CG movement X(m)	CG movement Y(m)	Max Crest Vel X(m/s)	Max Crest Vel Y(m/s)
1	Ulan Muckpile Project	Yes	23.1	21.6	-8.2	12.6	17.2
2	Case 1	Yes	25.5	24.6	-8.5	13.2	17
3	Case 2	Yes	27	26	-8.8	13.8	17.8
4	Case 3	Yes	29	28.4	-9	15.2	19.6
5	Case 4	Yes	34.7	34.5	-9.4	16.9	21.2



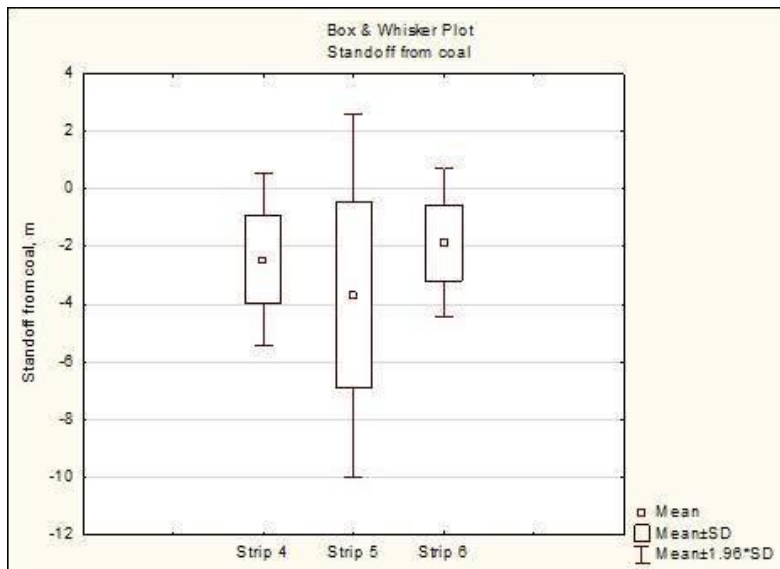
APPENDIX 3 - QA/QC

Hole depths at Strips 4,5,6:

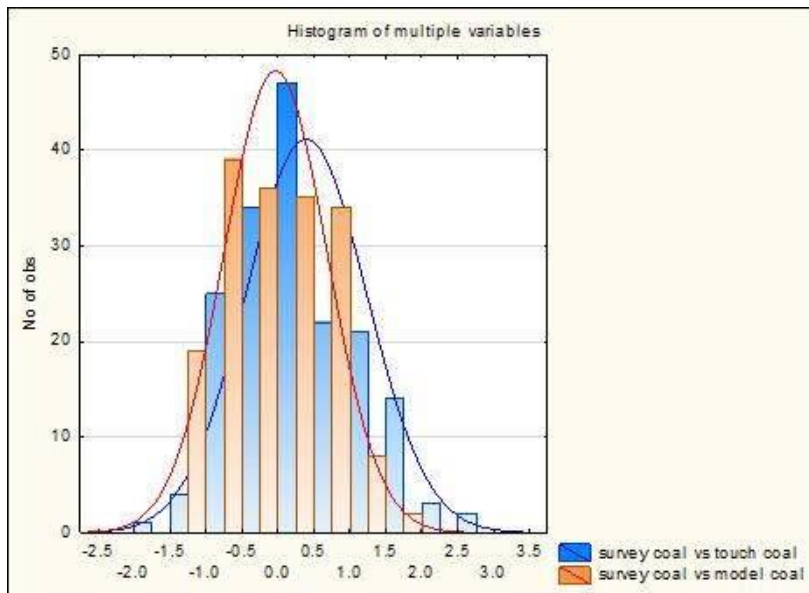


	Valid N	Mean	Minimum	Maximum	Std.Dev.
H_S4	454	32.9	25.0	42.0	3.0
H_S5	529	32.3	8.7	40.7	3.3
H_S6	644	34.7	10.0	49.3	4.6

Coal standoff at Strips 4-6 based on the coal model:



Comparison of standoffs - survey coal with touch coal and model:



	Valid N	Mean	Minimum	Maximum	Std.Dev.
survey coal vs touch coal	173	0.4	-1.7	3.0	0.8
survey coal vs model coal	173	0.0	-1.2	1.6	0.7

# OPTIMISATION OF WASTE-DUMP LIFT HEIGHTS FOR PRE-STRIP OPERATIONS

**Robert Lucas and Mehmet Siddiq Kizil**

**ABSTRACT:** The optimisation of waste dump design parameters is a vital aspect that has the potential to significantly influence operational costs within mining operations. This research study investigates the effects waste dump lift height has on a truck-shovel coal mining operation. The analysis focusses upon simulating various dump lift heights in a truck-shovel operation in order to determine the optimal overall dump lift height. The dump lift height is the height to which each dump level or lift is constructed. The optimal height will therefore be determined by plotting the simulated cost results for each height and undergoing a comparative study. Additional factors incorporated within the simulation results include the cost of haulage, and ancillary equipment works (dozers, graders and water carts to maintain the dump and construct haul roads to each new dump lift. Generating results from the research analysis to closely resemble real world applications, current mine data is incorporated within each simulation, including dig, dump and equipment data obtained from King 2 North pit of the Meandu mine located in Queensland.

## INTRODUCTION

Surface coal mining is a well-known mining method heavily utilised in Australia, most commonly implemented in Queensland and New South Wales as an abundance of coal deposits are located near to the surface. Queensland accommodates approximately 38% of Australian coal exploitation and New South Wales approximately 42% (Mitra and Saydam, 2012); these surface mining coal deposits contribute approximately 65% of Australia's total coal production (Scott, *et al.*, 2010). The implementation of truck-shovel operations within an Australian surface coal mining context is an extremely popular material extraction method. The truck-shovel mining operation generally constitutes approximately 50% to 60% of the total surface mining cost (Nel, *et al.*, 2011). The typical truck-shovel operation encompasses a loading unit which extracts/handles material, and a haulage unit for material transport. The truck-shovel mining method is popular due to increased flexibility and is capable of consistent high productivity in surface mining operations. The continual improvements and technological development of truck-shovel operations has resulted in increased utilisation of this extraction method within the Australian mining industry. The main benefit of running a truck-shovel operation is the improved flexibility of the mining system, resulting in better suitability and selective mining of complex ore deposits, varying ore depths, varying overburden thicknesses and is not restricted to ore deposit size. An additional benefit is that the initial capital investment required to employ a truck-shovel operation can be lower compared to other methods depending on operational scale, however truck-shovel includes higher operating costs per bank cubic m (Mitra and Saydam, 2012).

The transport and dumping of waste material is a substantial cost component of truck-shovel operations. Therefore a significant amount of research has been conducted regarding the optimisation of waste dump design standards and implementation aspects. However, the time constraints associated with the rapid expansion of surface mining operations does not allow for target waste dump design optimisation at specific locations. Hence a risk factor or compromise is generally associated with the development and costs of waste dump implementation. The ideal mining operation consists of optimal fleet productivity, utilisation and availability, along with the lowest attainable mining cost. The target mine for this research case study is the open cut coal mine, Meandu mine, located in Queensland. The mentioned factors are all influenced by incorrect design and staging of waste-dumps. Therefore indicating that analysing and optimisation of Meandu mine's dumps could improve potential for substantial operational cost savings within the King 2 North truck-shovel operation.

## WASTE DUMP DESIGN

Waste rock dumps, otherwise known as spoil piles are an integral part of surface mining. The waste rock dump is an area where surface mining operations dispose of low grade or barren material that has been

extracted from the pit in order to reach high grade ore (Kennedy, 1990). The construction of waste dumps in surface mining is unavoidable, whether they are built via haul truck or piled from dragline passes.

The overall aim of correct waste dump design is to plan a series of waste disposal stages that will effectively minimise the vertical and horizontal distances between the pit and potential waste dump site (Kennedy, 1990). The waste transport and dumping aspect of surface mining operations is one of the largest cost components of the mining cost constituting approximately 25-50% of mining operational costs (Adam and Bertinshaw, 1992). Therefore the designing and staging of waste dumps can significantly affect the total operational expenses. The two major parameters that dictate the overall design and staging of waste dumps are pit mining sequence and the production schedule, as these parameters influence the waste dump starting location, advancing rate and the ultimate dump volume (Kennedy, 1990).

There are various methods of waste disposal in surface mining operations, depending upon economics and safety. In-pit dumping is a common practice, as it is a practical method of waste disposal, especially when haul roads require establishment to new dump sites or new pit areas (Kennedy, 1990). However, waste dumps are often located outside the pit limits. As this minimises material rehandle, the waste material located at higher elevations must be hauled the longest distance in the dump design, whilst the lower elevated material must be hauled the shortest to improve the economics of truck-shovel productivity (Kennedy, 1990). Several external dump designs can be incorporated into surface mining including; valley fills, cross-valley fills, hillside wedges, fan and terrace dumps, ridge dumps and heaped dumps (Kennedy, 1990).

### **CASE STUDY- MEANDU MINE**

The Meandu coal mining operation commenced in 1978; 34 years later in January 2012 an approximate annual production of 7.6 million tonnes was extracted from the coal strip mining operation (Stanwell, 2013). The primary beneficiary for Meandu Mine is the Tarong power station which burns the majority of the thermal coal produced per annum. The later construction of Tarong North power station resulted in Meandu mine increasing the coal exploitation and productivity requirements in order to feed the new coal requirements of the combined Tarong power stations. The mine currently has five operational pits and geological surveys have identified six gently dipping coal seams of varying thicknesses on the project lease (Stanwell, 2013). Meandu Mine is owned by the Stanwell Corporation, an energy company that owns the Tarong power stations.

The King 2 pit operating at Meandu Mine is the primary focus of the research project, where equipment consists of a hydraulic excavator, and fleets of electric drive haul trucks. The primary equipment incorporated within the research case study includes a Hitachi EX8000 hydraulic excavator production unit, combined with a haul fleet of Komatsu 830E electric drive haul trucks. The additional ancillary equipment considered in the investigation includes the caterpillar D11T dozer, Caterpillar 777 water cart and 24M motor grader.

### **DETAILED HAULAGE ANALYSIS**

The analysis of the waste dump lift height influence on total operational costs at the Meandu mine truck-shovel operation contains several design factors that could influence the end results. Therefore to ensure sufficient realistic designs were modelled and simulated to closely resemble the operation, a detailed haulage analysis was conducted in the software packages *Minescape Dragline Module*, *Deswik CAD* and *Deswik Landform and Haulage Scheduler*.

The implementation of these software packages enabled realistic modelling of the truck-shovel operation by incorporating collected site data including surveyed topography files, pit and dump shells, current void profiles, planned haul routes, equipment specifications and accurate volume estimation. Therefore the detailed dumping reports generated via *Deswik Landform and Haulage Scheduler* conformed to the expected King 2 North truck-shovel operation. The detailed dumping report was generated for various lift height options to analyse the affect different lift construction heights have on operational costs. Therefore a range of scenarios are required to simulate the dump being constructed at different lift height increments.

## Scenarios

The modelling of the truck-shovel operation requires creation of various scenarios to differentiate between the different dump lift height options. However several key parameters are consistent between each scenario including utilisation of a single dig unit (Hitachi EX8000 excavator), unlimited trucking units (Komatsu 830E-AC), a single in-dump dozer unit (Caterpillar D11T), and a single haulage and dump route.

The purpose behind incorporating unlimited trucking units is that the case study operates under the assumption that the dig unit is fully trucked, thus avoiding any idle time. The reason behind this is that the exact trucking number for the King 2 North operation is unknown, and the optimal truck-shovel operation consists of a fully trucked digger to maximise productivity. The primary differing factor separating each scenario within the detailed haulage analysis is the pre-determined dump lift construction height (Figure 1), lift heights range from 2 to 24 m increasing in height by 2 m increments.

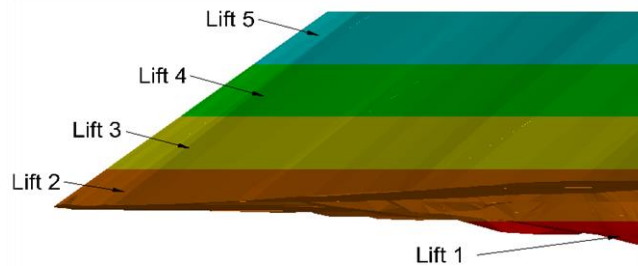


Figure 1 - Dump lift heights

## Scenario dependencies

The final conclusions of this study could potentially be implemented within surface mining operations. Therefore the importance of generating realistic and accurate results mimicking real world truck-shovel operations is an important aspect of the research project. Hence each scenario contains realistic dependencies designed to limit the haulage simulation within *Deswik Landform and Haulage Scheduler*.

The primary aspects of the haulage simulation that require dependency input are the truck and dump sections. Therefore the trucking dependencies input to limit the haulage model simulation include:

- Downhill speed limit of 15 kiloms per hour for grades -5% or more;
- Loaded rolling resistance factor of 3.4%;
- Unloaded rolling resistance factor of 2%;
- Truck spot and load time of approximately 2.83 minutes; and
- Truck spot and dump time of approximately 1 minute.

Dump dependencies are generated to limit the haulage model simulation to conform to realistic dump building practices incorporated in live surface mining operations, such as dump face angle and construction method. The dependencies and rules input into the dump design include:

- Vertical overlap of approximately 37° (angle of repose);
- Material swell factor of 25%;
- A unique dump lift height option ranging from 2 to 24 m;
- Dump limiting boundary (footprint);
- Maximum dump height (dump-shell);
- Single dump ramp at constant angle (haul road string); and
- Rule dictating the dump must be constructed at the minimum RL and minimum distance prior to proceeding.

## RESULTS AND DISCUSSION

### Dozer push analysis

The operational costs regarding the construction of waste dumps are commonly influenced by how effectively the ancillary and trucking resources are utilised. The most important ancillary equipment aspect of the research case study is the implementation of in-dump dozer push operations. The percentage of in-dump dozer push required for an operation is dictated by the dumping technique undertaken by the haul trucks. The two dumping methods commonly used include short and edge dumping.

The Meandu mine King 2 North operation intends to incorporate edge dumping as the waste material has proven in the past to contain geotechnical competency allowing this technique to be safely utilised. The basic process of edge dumping requires the truck to simply reverse to the edge of the dump and tip the waste material over the edge. Next an in-dump dozer unit pushes the remaining material that did not self-fall over the dump edge.

The safe performance of edge dumping limits the truck to dump away from the dump edge. Considering the haul unit implemented within the haulage analysis (Komatsu 830E-AC), the truck tray tipping point is estimated to be approximately 2 ms from the dump edge. The dumped waste material volume is dictated by the haul unit. Therefore the dumped volume is limited to the heaped tray capacity of approximately 126 cubic ms. The reason for fully loaded tray capacities is that realistically truck-shovel operations will fully load the haul units to maximise haulage and production.

The dozer push percentage is estimated for each lift height option via modelling the dumped material for each lift in *Minescape Dragline Module*, to determine how much dumped material volume is remaining above the dump level after freely flowing over the dump edge at an angle of 37 degrees, angle of repose. The material remaining above the dump lift is the waste material requiring dozer push (Figure 2).

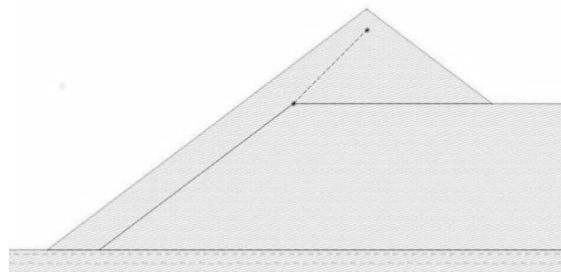


Figure 2 - Edge dumped waste material

The dozer push operations require a dozer to push the remaining dumped material over the dump edge (Figure 3). Therefore in the lower lift options the material requiring dozer push is much greater than high lift options.

The dozer push percentage results for each lift height (Figure 4) identifies that a 2 m lift requires approximately 85-90% dozer push, whereas a 20 m lift only requires approximately 30% dozer push. Therefore, a difference of 55-60% in dozer costs can be saved simply by incorporating a more optimal dump lift height into the final design. Furthermore the total dozer cost for each lift option is estimated within the cost model via multiplication of total hauled volume by dozer push percentage, the result is divided by the dozer production rate and finally multiplied by the hourly dozer operating cost.

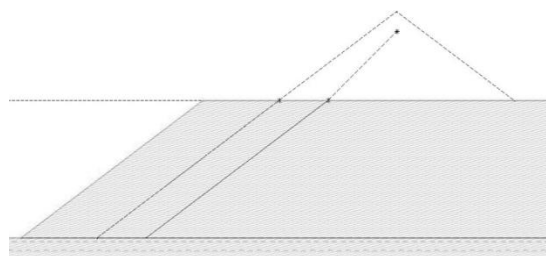


Figure 3 - Dozed dump material

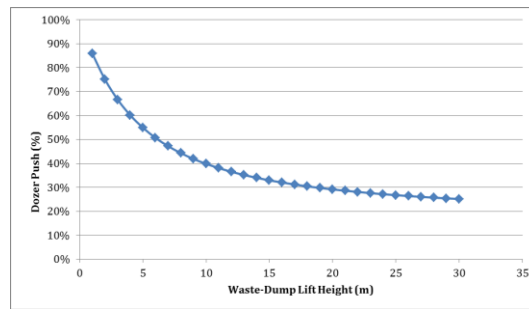


Figure 4 - Dozer push percentage Vs. lift height

### Haul road analysis

The haul road cost section is a combination of two vital components to truck-shovel operations, the construction and maintenance of the waste transportation roads. Therefore, an additional ancillary cost to consider is the construction and regular maintenance works required for each lift haul road. The assumptions incorporated into the haul road cost estimation include:

- Approximate haul road length of 250 ms per lift;
- Haul road width of 30 ms;
- Dozer blade width of 6.3 ms;
- Grader blade width of 7.3 ms; and
- Two cost components, construction and maintenance.

The equipment to construct and maintain the haul roads include a dozer (Caterpillar D11T), grader (Caterpillar 24M), and a water cart (Caterpillar 777). Analysing the detailed dumping report for each scenario, the number of lifts required to reach the maximum dump RL is determined for each individual lift height option.

### Road construction cost

The construction of waste transport roads is a key component to a successful truck-shovel mining operation, and estimation of haul road construction costs will assist in developing realistic and usable recommendations regarding optimal lift height for the King 2 dump. Hence as each dump lift requires a primary haul road and with each scenario the number of lifts change, an approximate cost per m of haul road construction is estimated. An assumption regarding the cost of haul road construction materials such as gravel (hardstand) and engineered fill, is made to keep a simplistic and generic construction cost. Therefore the material cost is not included in the analysis.

The estimation of machine cost per m of haul road construction (Equation 4) is calculated through a combination of various equations. The number of machine passes per m (Equation 1) requires calculation to determine how many passes are required to construct a 30 m width road based upon the machine blade or spray width.

$$\text{No. passes per metre} = \frac{\text{Road width}}{\text{Blade or spray width}} \quad (1)$$

The following stage is to calculate the total machine operation time per m (Equation 2), where the previously calculated number of passes per m is multiplied by the estimated time taken to complete each individual pass.

$$\text{Total time per metre} = \text{No. passes per m} * \text{time per pass} \quad (2)$$

The amount of time required for each machine to conduct a m of haul road construction is only a fraction of an hour. Therefore the hourly percentage taken to construct one m of haul road requires calculation (Equation 3). The calculation of the machine hourly percentage is simply the total time per m divided by 3,600 seconds.

$$\text{Hour Percentage (\%)} = \frac{\text{Total time per metre (s)}}{3600} \quad (3)$$

Calculating the estimated machine cost per m (Equation 4) is simply the multiplication of the machines hourly operating percentage by the individual machine rate of cost. Furthermore the estimated total haul road construction cost per m is the summarisation of each individual machines cost per m. The calculated total machine cost per m for the Caterpillar D11T dozer, 24M grader and Caterpillar 777 water cart is approximately \$16 per m.

$$\text{Machine cost per metre} = \text{Rate} \left( \frac{\$}{h} \right) * \text{Hour \%} \quad (4)$$

### Road maintenance cost

The regular maintenance of surface mine haul roads is a vital aspect in keeping productivity and costs at optimal levels. Without clean and well graded haul roads the trucking efficiencies and therefore productivity would considerably suffer. The cleanliness of haul roads also dictates the life of truck tyres, rolling resistance and safe speeds of the haulage units. Another factor to consider is how often road maintenance should be performed, as too often would suggest problems with the road construction material and increase the ancillary costs, and too few will result in road debris from overflowing trucks and increased rolling resistances due to road deterioration.

The estimation of machine cost per hour of road maintenance is calculated via Equation 7, however several additional parameters require calculation. The equipment considered for road maintenance includes the Caterpillar 24M motor grader and the 777 water cart. The initial parameter to estimate is the machine factor, which is an estimation of how much the machine is anticipated to work in an hour. The 24M grader is assumed to work 0.65 of an hour and the 777 water cart 0.5 of an hour. The total machinery operating hours can be determined using Equation 5, where the estimated machinery factor is multiplied via the total dig hours. The total dig hours limit the scheduled maintenance as the dig hours are simply the length of time taken to completely pre-strip King 2 North pit with the Hitachi EX8000 excavator.

$$\text{Machine hours} = \text{Machine factor} * \text{Total dig hours} \quad (5)$$

The machinery cost is the next parameter calculated through inputting the determined total machine hours for each piece of equipment into Equation 6, which is multiplied by the machines rate of cost.

$$\text{Total machine cost} = \text{Machine hours} * \text{Rate} \left( \frac{\$}{h} \right) \quad (6)$$

The total cost per hour of haul road maintenance (Equation 7) is estimated through the division of the calculated total machine cost by the estimated total dig hours for the King 2 North pre-strip. The calculated total cost per hour for the Caterpillar 24M grader and 777 water cart is approximately \$291 per hour of haul road maintenance.

$$\text{Total cost per hour} = \frac{\text{Total machine cost (\$)}}{\text{Total dig hours (h)}} \quad (7)$$

### Trucking fuel consumption

The transport and dumping of waste material is one of the largest cost components in a surface mining operation, in particular waste transport costs are significantly influenced by the efficient utilisation of trucking resources. Therefore when trucks are not efficiently utilised, the operational costs increase through aspects such as fuel consumption. Hence, the realistic modelling of a truck-shovel operation requires consideration of particular variables that could influence the final optimal lift height. The trucking aspect of fuel consumption is analysed via *Deswik CAD* detailed haulage reports generated from each scenario simulation to identify how the fuel consumption and cost changes with lift height. The detailed dumping reports contain a fuel algorithm per cycle. This combined with the number of cycles enables the litres of fuel consumed per trucking cycle to be estimated. The sum of the litres per cycle for the entire dump construction is multiplied using an assumed fuel cost of \$0.90 per litre to determine a total fuel consumption cost for each lift height option.

The plotted results (Figure 5) confirm that as greater lift heights are implemented within the dump design, additional fuel is consumed by the trucks through working harder when loaded and losing run-up

momentum whilst trying to reach the higher lift heights. The estimated difference solely in fuel consumption between the 2 and 24 m lift height is approximately \$180,000 (Figure 5). Therefore the optimisation of lift heights can provide a cost saving simply by reducing the amount of fuel consumed through waste transportation.

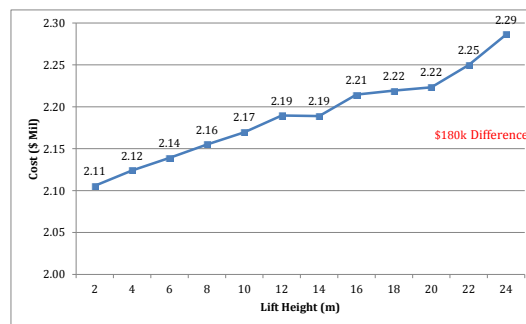


Figure 5 - Truck fuel consumption Vs. lift height

### Cost modelling

The process of cost estimation modelling is a common aspect associated within the mining industry, allowing easy estimation of project costs through mathematical algorithms and equations. The importance of cost modelling to the mining industry is to provide a realistic detailed result for budgets and financial planning in order to obtain approval for new designs or operational plans. Therefore the cost modelling stage of the research project will estimate the optimal waste dump lift height for the Meandu mine King 2 North operation. The estimate will be calculated through the collation of detailed dumping reports for each lift height option generated from *Deswik Landform and Haulage Scheduler*. The cost modelling process involves inputting mining cost rates. For the purpose of the research project, generic mining cost rates are adopted as site specific rates are unavailable. Furthermore the main benefit from utilising generic rates is the cost model, which is more applicable to the surface mining industry as opposed to being site specific. Concerns may arise through utilising generic costs to determine an optimal lift height for a specific mine site. However it is estimated that the difference in generic and Meandu mine rates is not great enough to significantly influence the total operational cost results or optimal waste dump lift height. Therefore the mining rates input into the cost model include:

- Digger cost per hour = \$1,370/h;
- Trucking cost per hour = \$270/h (ex. fuel);
- Trucking fuel cost per litre = \$0.9/L;
- Dozer cost per hour = \$340/h;
- Road construction cost = \$16.07/m;
- Road maintenance cost = \$291.25/h; and
- Prime (*in situ*) overburden blasting = \$1.15/bcm.

The cost model detailed dumping report input allows the estimation of equipment operating hours and costs, truck fuel consumption cost, haul road construction cost, haul road maintenance cost and the cost of prime (*in situ*) material requiring blasting for each waste dump lift height option. Therefore the total operational expenditure is simply the sum of these individual mining cost components.

### Operational cost results

The individual cost results determined from the cost modelling for each of the key components of the Meandu mine King 2 North truck-shovel operation identifies how each cost component trends with the various lift height increments (Figure 6). The trends provide valuable insight into which cost components are most susceptible to change resulting from lift height implementation and how it affects the total operational cost.

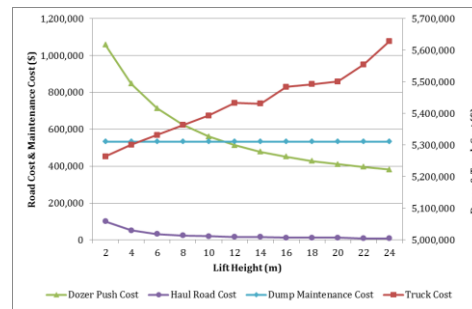


**Figure 6 - Operational cost results**

The major cost component in a truck-shovel surface mining operation is the cost of transporting and dumping the waste material. Hence the trucking costs in Figure 6 displays how as the lift height increases the cost of trucking will also increase. The reason behind why the trucking costs drastically increase as larger lift options are implemented is due to the extra trucking required, fuel consumption and longer cycle times. The trucking cost component is one of the more significant results that will affect the final optimal lift height selection.

The ancillary work is another major cost component influencing the optimal lift height for dump construction, specifically dozer push operations. Figure 6 displays how the dozer push costs are significantly higher in the lower lift heights, as more material requires dozing. Analysing the dozer push cost trend, the observation that the dozer cost closely resembles the previously estimated dozer push percentage plot, which indicates the resulting costing is estimated correctly. Through observing the plot it can be estimated that the optimal lift height is above the 10 m lift option as the dozer push costs plateau.

The construction and maintenance of haul roads is not a major cost component that will significantly influence the final optimal lift height. However including the trended costing for these additional ancillary operations provides more realistic results applicable to the Meandu mine King 2 North operation. As Figure 6 displays, the haul road construction cost is greater in the lower lift options due to the additional length of haul road requiring construction. However the haul road maintenance cost is uniform because it is calculated solely from hourly scheduled intervals. Therefore, as the amount of time taken to remove and transport the waste material does not significantly differ with lift height change, the haul road maintenance cost will not change.

### Total cost results

The total operational cost results output (Figure 7) from the cost modelling process identifies the cheapest lift height option for the Meandu mine truck-shovel operation and the optimal lift height. As modelling result generated within various software packages and between software versions is unpredictable a margin for error should be considered. Therefore the optimal lift height range for the Meandu mine is between 14 to 20 m. If a lift height option is implemented within the Meandu mine operation a potential saving of approximately \$500,000 is possible. This enables a significant operational cost saving for a single dump design aspect.

The optimal range is also applicable to most mining operations as the cost input within the cost model is the generic equipment rates. Furthermore if an operation incorporates a dump lift height of 8 m or less, or greater than 20 m the total operational cost will increase due to either an increase in ancillary equipment hours or trucking hours.

### Sensitivity analysis

The identification of what changes are expected when certain variables are modified is undertaken through a sensitivity analysis. Completing a sensitivity analysis is a vital aspect for determining the uncertainty of results generated from the modelling process via systematically manipulating specific scenario inputs. The scenario inputs manipulated within the cost modelling include the dozer push volume, dozer push production rates and the price of fuel regarding trucking.

An aspect influential to the total operational costs that is variable with different operations is the implementation of haulage units containing different capacities. Therefore a sensitivity analysis is

conducted targeting the dozer push volumes, basically identifying how the total operational cost will change in respect to different truck capacities.

The Figure 8 graph displays the trend of total operational cost dependent upon lift height. The results identify the lower lift height options are most susceptible to cost change when larger haul units are implemented. These results are accurate as logically an increase in truck capacity will result in less dumped waste volume, hence less dozer push hours are required, lowering the dozer push ancillary costs. The optimal lift height range reduces due to the dozed volume effect.

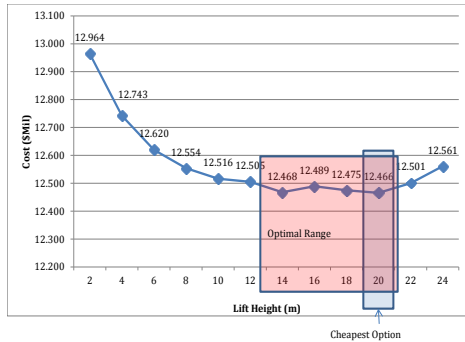


Figure 7 - Total cost results

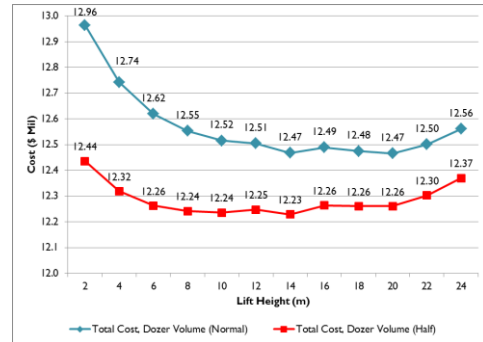


Figure 8 - Dozer volume sensitivity analysis

The selection of in-dump dozers is an operational aspect that can significantly influence the total operational costs of a surface mining operation. Hence a sensitivity analysis is conducted targeting the dozer push production rates predicting the changes expected when implementing dozers with different push production rates.

The Figure 9 graph displays the change in total operational cost with respect to an increase or decrease in dozer production rates. The change in production rates influences the total cost via increasing or decreasing the amount of hours required to perform dozer push operational in each lift. As the dozer push is a significant cost aspect the change in dozer hours can dramatically affect the total operational cost. As expected the lower lift height options are most susceptible to cost change when the dozer production rates are modified. If a larger dozer unit is implemented the optimal lift range reduces, however if a smaller dozer unit is selected the optimal lift height increases as more time is required to complete dozing operations.

An important aspect affecting the total operational cost of a truck-shovel mining operation that cannot be controlled is the fluctuation in fuel price. The trucking cost of waste transport is a significant contributor to the total operational cost. Therefore as fuel price fluctuates the cost of truck fuel consumption will also fluctuate.

Figure 10 identifies that the lift height options most susceptible to a fluctuation in fuel price are the higher value options. The reason for this is as the lift height increase, the trucks are required to work harder and burn additional fuel to reach the greater elevations. Unfortunately the fuel price cannot be controlled and fluctuates with the petroleum market. Hence it is important to predict what may occur if the price changes in order to compensate by implementing a different lift height during dump construction.

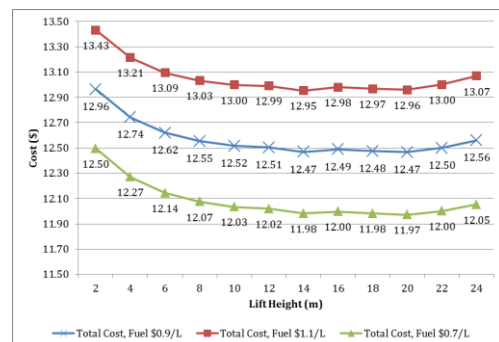
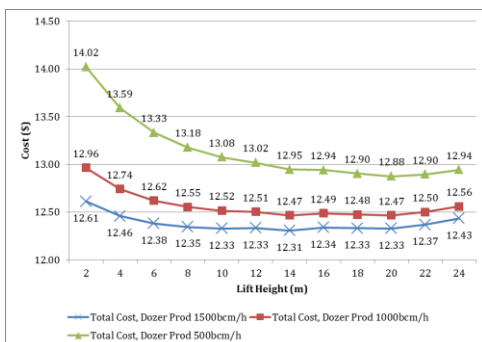


Figure 9 - Dozer production sensitivity analysis Figure 10 - Fuel price sensitivity analysis

## CONCLUSIONS

The research project aimed to optimise the fleet efficiency and utilisation through a detailed haulage analysis, and to identify any potential cost savings available within the Meandu mine King 2 truck-shovel operation. The detailed haulage analysis and cost modelling identified that by optimising the waste dump lift height design, cost savings of potentially \$500,000 is achievable. The two main contributing cost factors within the truck-shovel operation were identified as the trucking unit and the dozer push unit, with haul road costs being a minor contributor. Conducting a comparative study on the total operational expenses for each lift option, the cheapest lift option for the King 2 North works is identified as a 20 m lift height construction increment. However, due to the modelling methods utilised to determine this result, a margin for error within the modelling process should be considered. Hence the 'optimal' range for waste dump lift heights at King 2 North lies between 14 and 20 m lift height increments.

The main benefiting factors toward the mining industry that the research case study conveys, are dumps constructed at lift heights lower than 8 m, or greater than 20 m will see an unnecessary increase in operational costs due to inefficient utilisation of trucking and ancillary resources.

Aspects of the research project that could be researched in greater depth, thus improving the usability of results include more detailed dozer push analysis, consideration of trucking aspects such as tire consumption and maintenance costs, set number of trucks, truck queuing, bunching and digger idle times. Furthermore, as the research project primarily focused upon the Meandu Mine King 2 North pre-strip operation, future studies could be conducted targeting more generic data to produce a generic cost model applicable to general dump construction producing a ballpark cost estimate targeting any operation.

## ACKNOWLEDGEMENTS

The authors acknowledge the support and guidance provided by the industry professionals Tony O'Connell, Michael Hooper, Brett Ehler and Jacob Orbell.

## REFERENCES

- Adam, R A and Bertinshaw, R G, 1992. Waste dumps- the new frontier, in *Proceedings Third Large Open Pit Mining Conference*, Mackay, Australia, pp 255-259 (The Australasian Institute of Mining and Metallurgy).
- Kennedy, B A, 1990. SME surface mining second edition, pp 485-493 (Society for Mining, Metallurgy, and Exploration: United States).
- Mitra, R and Saydam, S, 2012. Surface coal mining methods in Australia, in *Mining Methods* (ed: T Onargan), pp 1-22 (InTech North America: New York).
- Nel, S, Kizil, M S and Knights, P, 2011. Improving truck-shovel matching, in *Proceedings 35th APCOM Symposium*, Wollongong, Australia, (eds: E Y Baafi, R J Kinimonth and I Porter) pp 381-391 (The Australasian Institute of Mining and Metallurgy).
- Scott, B, Ranjith, P G, Choi, S K and Khandelwal, M, 2010. A review on existing opencast coal mining methods within Australia [online]. *Journal of Mining Science*. 46: 280-297. Available from: <<http://link.springer.com/content/pdf/10.1007%2Fs10913-010-0036-3.pdf>> [Accessed: 9 May 2013].
- Stanwell, 2013. Meandu mine fact sheet [online]. Available from <[http://www.stanwell.com/Files/General\\_PDF\\_Files/Meandu\\_Mine\\_Fact\\_Sheet.pdf](http://www.stanwell.com/Files/General_PDF_Files/Meandu_Mine_Fact_Sheet.pdf)> [Accessed: 11 May 2013].

---

## INDEX OF AUTHORS

Amanzadeh, M. ....	369
Aminossadati, S. M. ....	369
Arora, D. ....	399
Atkins, A. S. ....	309
Aziz, N. ....	109, 156, 163, 202, 210, 252
Baafi, E. ....	193
Babjak, J. ....	34
Beamish, B. ....	324
Belle, B. ....	230
Black, D. J. ....	252
Brady, D. ....	330
Butel, N. ....	89
Cediel, B. ....	413
Chen, J. ....	137
Cliff, D. ....	330, 360, 389, 399
Craig, P. ....	109, 147
Daigle, L. ....	18
Darren Brady ....	ii
Donghi, M. ....	216
Donnelly, C. ....	216
ES, A. K. ....	399
Esen, O. ....	285
Esen, S. ....	413
Evans, D. ....	118
Evans, D. W. ....	177
Foldi, S. ....	163
Frith, R. ....	118
Gagrani, A. ....	399
Gale, W. ....	63
Ghojavand, H. ....	163
Gray, I. ....	301
Hagan, P. ....	128, 137, 186
Hajiantilaki, N. ....	224
Harris, J. ....	389, 399
Hatherly, P. ....	51
Heemann, K. ....	156
Hoelle, J. ....	408
Holden, M. ....	128, 147
Horberrry, T. ....	360
Hossack, A. ....	89
Hossaini, M. F. ....	224
Hoyer, D. ....	51
Hungerford, F. ....	293
Javanmard, H. ....	266
Joyce, D. ....	163
Kelly, M. ....	42
Kirsch, P. ....	389, 399
Kizil, M. S. ....	89, 369, 427
Kothandaraman, K. ....	399
Langham-Williams, J. ....	186

Levi, T. ....	324
Li, J. ....	399
Li, X. ....	163
Liu, T. ....	369
Lucas, R. ....	427
Ma, S. ....	163
Mayer, S. ....	156
McTyer, K. ....	118
Medhurst, T. ....	42, 51
Mendham, F. ....	360
Mirzaghobanali, A. ....	163, 202, 210
Mirzapour, B. ....	224
Mohammadi, M. ....	224
Morgan, Q. ....	274
Moslemi, A. ....	109, 163
Nagarajan, M. ....	413
Neels, B. ....	301
Nemcik, J. ....	82, 103, 109, 156, 163, 193, 210
Novák, P. ....	34
Olsen, M. ....	381
Ozer, S. C. ....	285
Pell, S. ....	25
Pinetown, K. ....	266
Plessis, J. J. L. d. ....	350
Pope, J. ....	274
Porter, I. ....	103, 193
Qiao, Q. ....	103
Ramage, G. ....	216
Ramsay, P. ....	274
Rankine, R. ....	42
Rasekh, H. ....	163, 202
Reed, G. ....	118
Ren, T. ....	293
Saghafi, A. ....	266
Sasaki, K. ....	339, 344
Saurat, J. ....	324
Saydam, S. ....	137
Seedsman, R. ....	25, 70
Shan, Z. ....	103, 193
Shi, M. ....	399
Singh, R. N. ....	309
Späth, H. ....	350
Sprott, D. ....	389
Stemp, C. ....	63
Straub, K. ....	25
Sugai, Y. ....	339, 344
Tabish, A. ....	399
Theiler, J. ....	324
Thorn, D. ....	413
Titheridge, D. ....	8
Torres, V. N. ....	309

Venticinque, G.....	82
Wang, Y. ....	339, 344
Watkinson, M. ....	330
Williams, R. ....	243
Zhang, X.....	339, 344